nutrients

High-Fat High-Saturated Diet

Edited by
Frederic Capel

Printed Edition of the Special Issue Published in *Nutrients*

www.mdpi.com/journal/nutrients

MDPI

High-Fat High-Saturated Diet

High-Fat High-Saturated Diet

Editor

Frederic Capel

MDPI • Basel • Beijing • Wuhan • Barcelona • Belgrade • Manchester • Tokyo • Cluj • Tianjin

Editor
Frederic Capel
INRAE, UNH, Unité de
Nutrition Humaine, CRNH
Auvergne, Université
Clermont Auvergne
France

Editorial Office
MDPI
St. Alban-Anlage 66
4052 Basel, Switzerland

This is a reprint of articles from the Special Issue published online in the open access journal *Nutrients* (ISSN 2072-6643) (available at: https://www.mdpi.com/journal/nutrients/special_issues/High_Fat_Saturated).

For citation purposes, cite each article independently as indicated on the article page online and as indicated below:

LastName, A.A.; LastName, B.B.; LastName, C.C. Article Title. *Journal Name* **Year**, *Volume Number*, Page Range.

ISBN 978-3-0365-5303-0 (Hbk)
ISBN 978-3-0365-5304-7 (PDF)

Contents

About the Editor

Frederic Capel

Frederic Capel is a senior scientist in the Human Nutrition Unit, part of the National Research Institute for Agriculture, Food and Environment (INRAE) and Clermont-Auvergne University (UCA). His research focuses on the identification of nutritional and sustainable strategies based on dietary lipids to prevent chronic diseases linked to excess body fat, such as metabolic syndrome or sarcopenia. It has been established that the quality of dietary lipids is crucial in the prevention of many human diseases. For his research activities, he develops, within a team of 20 people, both in vitro (cellular approaches) and in vivo/physiological (animal models, human interventions) studies to understand and regulate the relationship between lipid metabolism, adipose tissue, and skeletal muscle physiology. His work has contributed to new advances in the field of lipid nutrition, demonstrating the beneficial role of polyunsaturated fatty acids in both the prevention of the accumulation of deleterious lipid metabolites and also the progression of metabolic disorders and inflammation. He has recently developed interdisciplinary projects to propose healthy and sustainable lipid sources. He regularly supervises master's and PhD students, is a regular reviewer for several scientific journals indexed in Pubmed, and has obtained financial support to develop both national and international collaborations in the field.

Preface to "High-Fat High-Saturated Diet"

The quality of dietary fat is a major determinant of several physiological, biochemical and molecular processes in the body, tissues and cells. Lipids play a crucial biological role in an energy-balanced context, but a Westernized high-fat diet increases the risk of metabolic diseases. A typical Western diet is associated with a reduced intake of n-3 polyunsaturated fatty acids (PUFAs) and an increased consumption of saturated FAs (SFAs), n-6 PUFA and refined sugar. This situation leads to a positive energy balance, increasing the risk of obesity and related comorbidities, such as type 2 diabetes or hypertension. According to the most recent dietary guidelines, lipids should represent 30–35% of the daily energy intake in order to prevent the deleterious effects of a high glycaemic index in terms of carbohydrates and a deficiency in essential fatty acids. A focus on the quality of ingested lipids is necessary to better understand previous debates, misunderstandings and contradictory results in the field. If the beneficial role and essentiality of polyunsaturated fatty acids is demonstrated, an excess of SFAs has been described as contributing to the deleterious metabolic effect of the Western diet. FAs are mainly stored in fat cells and within lipid droplets (LDs) in other cell types to provide energy. Large amounts are also found in the cell membrane's phospholipids, where their structural role is crucial to the control of cellular functions. Differential effects were identified between different types of FAs on inflammatory and metabolic diseases during obesity or in response to physical exercise and chronic diseases. Hence, the prevalence of obesity could rise dramatically despite a fall in total fat intake. Although some controversies still exist, notably regarding cardiometabolic risk, most institutional dietary guidelines claim that the consumption of SFA should be limited to the expense of monounsaturated FA (MUFA) and PUFA. This Special Issue presents recent advances in the field, covering associations between dietary fat and cardiometabolic disorders, organ-specific alterations (brain, muscle, liver, etc.) using modern technics such as proteomic and transcriptomic analyses. We are grateful to the authors of these studies and hope that students, scientists and professionals involved in lipid and health sciences will learn about the topic and identify new research perspectives by reading the book. We also thank all reviewers of the published works. Scientific progress is strongly related to a rigorous methodology and data analysis process, but also to a careful and constructive reviewing of the submitted works.

Frederic Capel
Editor

nutrients

MDPI

Article

Short-Term Caloric Restriction Attenuates Obesity-Induced Pro-inflammatory Response in Male Rhesus Macaques

Hollis Wright [1], Mithila Handu [2], Allen Jankeel [3], Ilhem Messaoudi [3] and Oleg Varlamov [4,*]

1 Omics Data Automation Inc., Beaverton, OR 97005, USA; wrighth@omicsautomation.com
2 Knight Cancer Institute's Cancer Early Detection Advanced Research Center, Oregon Health & Science University, Portland, OR 97201, USA; handu@ohsu.edu
3 Department of Molecular Biology and Biochemistry, School of Biological Sciences, University of California–Irvine, Irvine, CA 92697, USA; allen.jankeel@uci.edu (A.J.); imessaou@uci.edu (I.M.)
4 Division of Cardiometabolic Health, Oregon National Primate Center, Beaverton, OR 97006, USA
* Correspondence: varlamov@ohsu.edu; Tel.: +1-503-346-5377

Received: 30 January 2020; Accepted: 14 February 2020; Published: 18 February 2020

Abstract: White adipose tissue (WAT) hypertrophy is an essential hallmark of obesity and is associated with the activation of resident immune cells. While the benefits of caloric restriction (CR) on health span are generally accepted, its effects on WAT physiology are not well understood. We previously demonstrated that short-term CR reverses obesity in male rhesus macaques exposed to a high-fat Western-style diet (WSD). Here, we analyzed subcutaneous WAT biopsies collected from this cohort of animals before and after WSD and following CR. This analysis showed that WSD induced adipocyte hypertrophy and inhibited β-adrenergic-simulated lipolysis. CR reversed adipocyte hypertrophy, but WAT remained insensitive to β-adrenergic agonist stimulation. Whole-genome transcriptional analysis revealed that β3-adrenergic receptor and de novo lipogenesis genes were downregulated by WSD and remained downregulated after CR. In contrast, WSD-induced pro-inflammatory gene expression was effectively reversed by CR. Furthermore, peripheral blood monocytes isolated during the CR period exhibited a significant reduction in the production of pro-inflammatory cytokines compared to those obtained after WSD. Collectively, this study demonstrates that short-term CR eliminates an obesity-induced pro-inflammatory response in WAT and peripheral monocytes.

Keywords: adipose tissue; caloric restriction; high-fat diet; nonhuman primates; obesity; transcriptome; western-style diet

1. Introduction

Consumption of a high-fat/calorie-dense Western-style diet (WSD) and physical inactivity are the main risk factors contributing to obesity characterized by a chronic low-grade pro-inflammatory state and insulin resistance [1]. A widely used approach for weight management is caloric restriction (CR). Studies in several organisms, including worms, flies, mice and nonhuman primates (NHPs), have shown that CR promotes survival [2] in part through the extension of health span [3,4]. In humans, CR decreases the risk of cardiovascular and metabolic diseases [5–9] and reduces obesity in older adults [10]. Furthermore, CR has been shown to decrease body weight and adiposity in postmenopausal women [11–13]. However, a significant fraction of these women regained weight soon after the termination of dietary intervention [14]. Moreover, we have shown that long-term CR initiated during early adulthood delayed T-cell senescence [15,16]. Specifically, CR initiated during early adulthood preserved circulating naïve CD8 and CD4 T-cells, maintained T-cell receptor diversity, and reduced T-cell production of pro-inflammatory cytokines.

Furthermore, we have previously demonstrated the beneficial effects of CR in obese middle-aged male rhesus macaques. In that study, animals consuming low-fat chow diet (15% calories from fat, 27% from protein, and 59% from carbohydrates) were switched to WSD (33% calories from fat, 17% from protein, 51% from carbohydrates) for six months. Following the WSD period, animals were subjected to a 70% calorically restricted chow diet for an additional four months. These studies showed that CR efficiently reversed WSD-induced obesity and insulin resistance, demonstrating the beneficial effects of short-term CR on metabolic health in NHPs [17,18]. These studies motivated us to further explore transcriptional and functional changes in white adipose tissue (WAT) following WSD-induced weight gain and after CR-induced weight loss. WAT plays a central role in regulating systemic glucose and lipid homeostasis and its dysfunction and the dysregulation of the central control of energy intake contributes to weight regain in obese patients [19]. Thus, we have described the functional and whole-genome RNA sequencing (RNA-Seq) analysis of subcutaneous (SC)-WAT biopsies collected before and after exposure to WSD, and at the end of CR [17,18]. Our study provides new evidence demonstrating that short-term CR is a highly efficient approach for mitigating an obesity-induced pro-inflammatory response and further emphasizes the beneficial effects of CR on immunometabolic health in NHPs.

2. Materials and Methods

2.1. Animal Characteristics and Diets

All procedures described in this study were approved by the Oregon National Primate Research Center (ONPRC) Institutional Animal Care and Use Committee. Study design and animal characteristics, including body composition, metabolic status, and cytokine profiles, have been described in our previous study [18]. Briefly, six male rhesus macaques (Indian origin) of 12–13 years of age were housed individually, with the cage size adjusted to animal weight according to the United States Department of Agriculture (USDA) Cage Size Guide, 8th Edition. Individual housing allowed us to mimic a sedentary lifestyle while accurately measuring physical activity and food intake. Chow diet consisted of two daily meals of the Fiber-balanced Monkey Diet (15% calories from fat, 27% from protein, and 59% from carbohydrates; no. 5052; Lab Diet, St. Louis, MO). WSD consisted of two daily meals of the TAD Primate Diet (5LOP) (36% calories from fat, 18% from protein, 45% from carbohydrates, 5A1F, Lab Diet). The Fiber-balanced Monkey Diet contains a lower fraction of high-glycemic carbohydrates and higher levels of low-glycemic carbohydrates compared to the TAD Primate Diet. The study design is outlined in Figure 1A. Before initiation of the study, all animals consumed ad libitum chow diet. Once the animals were individually housed, they were maintained for two months on ad libitum chow diet. During this baseline period, individual caloric intake was determined. After two months on chow diet, animals were switched to ad libitum WSD for six months. The WSD was discontinued after six months when HbA1c values reached prediabetic values [18]. CR was initiated using a chow diet, with the number of chow biscuits adjusted to 70% of individual baseline caloric intake values and continued for four months. CR was stopped after the average SC adipocyte size reached pre-WSD values (Figure 1B). During each dietary intervention, the animals received similar amounts of daily fruit supplements.

2.2. WAT Biopsies

Abdominal SC-WAT biopsies were performed by trained surgical personnel at ONPRC according to standard veterinary surgical procedures under sterile conditions and appropriate anesthesia with postoperative pain control, as described [17]. Tissue samples were cut into smaller fragments (explants) with the sharp surgical scissors and used for an ex vivo assay or frozen at −80 °C for RNA isolation.

2.3. Cell-Based Assays

Free fatty acid (FFA) uptake, adipocyte size and lipolysis was conducted as previously described [17,20–22]. For the lipolysis assay, ~200-mg SC-WAT explants were placed in M199 media (General Electric Company, Boston, MA, USA) at room temperature and transported to the laboratory. 50-mg SC-WAT explants (three basal and three isoproterenol-stimulated replicates) were placed in a 48-well plate containing 0.2 mL incubation medium (Hank's Salt (HBSS), 0.2% BSA (Sigma-Aldrich, St, Louis, MO, USA) and 5 mM glucose), and incubated at 37 °C for 2 h with or without 10 μM isoproterenol (Sigma-Aldrich, St. Louis, MO, USA). Glycerol release was determined using a glycerol detection kit (Sigma-Aldrich, St. Louis, MO, USA). Glycerol concentrations were normalized to wet tissue weight. For FFA uptake, 100 mg of SC-WAT were collected in M199 media at room temperature and separated into smaller explants. WAT explants were incubated floating in a 48-well plate filled with 0.4 mL incubation medium (M199 medium, 0.1% fatty acid-free BSA (Sigma-Aldrich, St. Louis, MO, USA), 20 mM HEPES (pH 7.4)). Fluorescently-labeled fatty acid BODIPY-500/510 C_1, C_{12} (BODIPY-C12; Life Technologies, Waltham, MA, USA) was prepared by diluting a 2.5 mM methanol stock solution in incubation medium to a final concentration of 10 μM and incubated for 15 min in a 37 °C water bath. One hundred μL of diluted BODIPY-C12 and 2 μL of live-cell staining dye Calcein Red-Orange AM (Life Technologies, Waltham, MA, USA) were added to each well and WAT explants were incubated for 15 min at 37 °C. Media was removed and explants were washed three times with incubation medium. WAT explants were fixed at room temperature in 4% paraformaldehyde (Sigma-Aldrich, St. Louis, MO, USA)/PBS for 20 min, washed with PBS and analyzed by confocal microscopy. WAT explants were placed into a 35-mm glass-bottom imaging culture dish (MatTek, Ashland, MA, USA) in PBS. Confocal microscopy was performed using a Leica SP5 AOBS spectral confocal system supplied with a ×20 objective. Adipocyte area and BODIPY fluorescence were measured using Fiji imaging software. The statistical analysis of adipocyte parameters was conducted using repeated measure one-way ANOVA followed by the Tukey's multiple comparison test using GraphPad Prism 8.2.0.

2.4. RNA-Seq Analysis

200 mg of frozen SC-WAT samples were homogenized with a TissueLyzer-II (QIAGEN, Hilden, Germany). RNA was isolated using the AllPrep DNA/RNA purification kit (QIAGEN). High-quality RNA (RIN >8) was used for library construction. RNA-Seq libraries were prepared using the TruSeq protocol (Illumina, San Diego, CA, USA) as described in [18]. Poly (A) + RNA was purified using oligo-dT coated magnetic beads and chemically fragmented followed by cDNA generation using random hexamer primers. The cDNA ends were repaired and ligated to library adaptors. Following purification with AMPure XP beads (Beckman Coulter Inc., Brea, CA, USA), libraries were amplified using 11 PCR cycles. Amplified libraries were cleaned using AMPure XP beads. Libraries were analyzed on a Bioanalyzer (Agilent, Santa Clara, CA, USA) and quantified using qRT-PCR (Kapa Biosystems, Wilmington, MA, USA) on a StepOnePlus qRT-PCR workstation (Life Technologies, Carlsbad, CA, USA). Libraries were multiplexed and final concentrations were determined by qRT-PCR. Multiplexed libraries were diluted to 1 nM for denaturation and then diluted to deliver optimal clustering on the flow cell. Flow cells were prepared on a cBot (Illumina, San Diego, CA, USA). Libraries were sequenced on a HiSeq 2000 (Illumina, San Diego, CA, USA). Data was assembled into standard fastq files using Bcl2Fastq (Illumina, San Diego, CA, USA). The quality of the raw reads was verified using FastQC (version 0.11.3). Low quality bases as well as any remaining Illumina adapters were trimmed. Reads with less than 25 bases remaining were discarded. The remaining reads were aligned to the rhesus macaque genome (genome assembly: Macaca mulatta 1.0) from ENSEMBL using the splice aware short read aligner suite Bowtie2/TopHat2 [23] in a strand-specific fashion allowing up to 5% mismatches. Reads were assigned to features using the featureCounts function of the Rsubread package [24] in R 3.4, using default parameters except for setting allowMultiOverlaps to TRUE. Transcripts were normalized and analyzed using the glm functionality of edgeR [25]; the

candidate differentially expressed genes (DEGs) were identified as those genes with a fold change (FC) ≥ 2 and a false discovery rate (FDR) ≤ 0.05.

2.5. Bioinformatic Analysis

Differential gene expression results (fold change, *p*-value, and FDR) were imported into the Ingenuity Pathway Analysis program (IPA, QIAGEN, Hilden, Germany). To facilitate this, ENSEMBL rhesus gene IDs were first mapped to human gene IDs using Ensembl's BioMart. Only high-confidence matches were used, and only the top match was chosen when one rhesus ID mapped to many human gene IDs. If no human gene ID was found, the rhesus gene ID was retained. Once imported into IPA, a fold-change cutoff of 1.5 and an FDR cutoff of 0.05 was applied to all comparisons to select differentially expressed genes. The STRING protein-protein interaction analysis (https://string-db.org/) was performed by pasting ENSEMBL IDs of DEGs into the STRING input window. The evidence-based STRING analysis was performed using the medium confidence value of 0.4.

2.6. Flow Cytometry Analysis

To measure frequencies of lymphocyte subsets, peripheral blood mononuclear cells (PBMCs) were surface-stained with antibodies against CD8β (Beckman Coulter, Brea, CA, USA), CD4 (eBioscience, San Diego, CA, USA), CD28 (BioLegend, San Diego, CA, USA), CD95 (BioLegend, San Diego, CA, USA), CCR7 (BD Pharmingen, San Diego, CA, USA), CD20 (BioLegend, San Diego, CA, USA), IgD (Southern Biotech, Birmingham, AL, USA), and CD27 (BioLegend, San Diego, CA, USA). This combination allowed for the delineation of central memory (CM; CD28 + CD95 + CCR7 +), transitional effector memory (TEM; CD28 + CD95 + CCR7 −), and effector memory (EM; CD28− CD95+ CCR7−), CD4 and CD8 T-cells (as well as marginal zone-like (MZ-like; IgD + CD27 +), memory (IgD − CD27 +), and double-negative (DN; IgD − CD27 −) B cell subsets). A second tube of PBMCs was stained with antibodies against CD3 (BD Pharmingen, San Diego, CA, USA), CD20 (Beckman Coulter, Brea, CA, USA), CD14 (BioLegend, San Diego, CA, USA), HLA-DR (BioLegend, San Diego, CA, USA), CD11c (BioLegend, San Diego, CA, USA), CD123 (BioLegend, San Diego, CA, USA), and CD8α (BD Pharmingen, San Diego, CA, USA) to delineate monocytes (CD3 − CD20 − CD14 + HLA-DR +), dendritic cells (DCs; CD3 − CD20 − CD14 − HLA-DR +), and natural killer (NK) cells (CD3 − CD20 − CD8a +). DCs were further defined into myeloid (mDCs; CD123 − CD11c +) and plasmacytoid (pDCs; CD123 + CD11c −) DCs. To measure inflammatory cytokine production by monocytes, PBMCs were stimulated with lipopolysaccharide (LPS) (100 μg/mL, PeproTech, Rocky Hill, NJ, USA) in the presence of brefeldin A (Sigma, St. Louis, MO, USA) for 6 h. After incubation, cells were stained with antibodies directed against CD4, CD8β, CD14, HLA-DR, and CD20. Samples were then fixed, permeabilized (permeabilization buffer, BioLegend, San Diego, CA, USA), and stained using antibodies against interferon γ (IFNγ, eBioscience, San Diego, CA, USA), tumor necrosis factor α (TNFα, eBioscience, San Diego, CA, USA), and interleukin-6 (IL-6, BioLegend, San Diego, CA, USA). All samples were analyzed using the Attune NxT Flow Cytometer (LIfeTech, Carlsbad, CA, USA) and FlowJo software (TreeStar, Ashland, OR, USA). The statistical analysis of flow cytometry data was conducted using the paired *t*-test.

3. Results

3.1. WSD-Induced Adipocyte Hypertrophy but not β-Adrenergic Resistance is Reversed by CR

In our previous studies, we demonstrated that adult male rhesus macaques exposed to six months of WSD exhibited a significant increase in fat mass. Furthermore, fat mass was decreased significantly following the subsequent CR period. We also determined that the consumption of a WSD induced systemic insulin resistance, while CR restored normal insulin sensitivity in rhesus macaques [17,18]. The analysis of SC-WAT biopsies collected during each dietary period showed that WSD led to a significant increase in the mean area of SC adipocytes, while subsequent CR reduced adipocyte area to the baseline levels (Figure 1B). To assess the effect of diet on lipolysis, SC-WAT explants derived from three longitudinal

biopsies were incubated ex vivo in basal media or in the presence of the β-adrenergic receptor agonist isoproterenol, and glycerol release in incubation media was quantified. SC-WAT collected during the WSD period exhibited a blunted β-adrenergic response compared to a chow diet, while the basal lipolysis remained unchanged. Interestingly, CR failed to restore a normal β-adrenergic response in SC-WAT despite a significant reduction in adipocyte area observed at the end of the CR period (Figure 1C). To assess the uptake of FFA in adipocytes, SC-WAT explants were incubated with the metabolizable fluorescent FFA analogue BODIPY-C12 [21,22,26–28] and single-cell fluorescence was quantified by confocal microscopy. SC adipocytes from WSD biopsies exhibited a trend to higher FFA uptake compared to the chow control and the CR conditions (Figure 1D,E). Collectively, this study shows that WSD induces SC adipocyte hypertrophy, which was efficiently reduced to a pre-obese level by CR. In contrast, WSD led to the inhibition of the β-adrenergic lipolytic response in SC adipocytes and this effect persisted even after adipocyte size, body weight and insulin sensitivity [17,18] were normalized by CR.

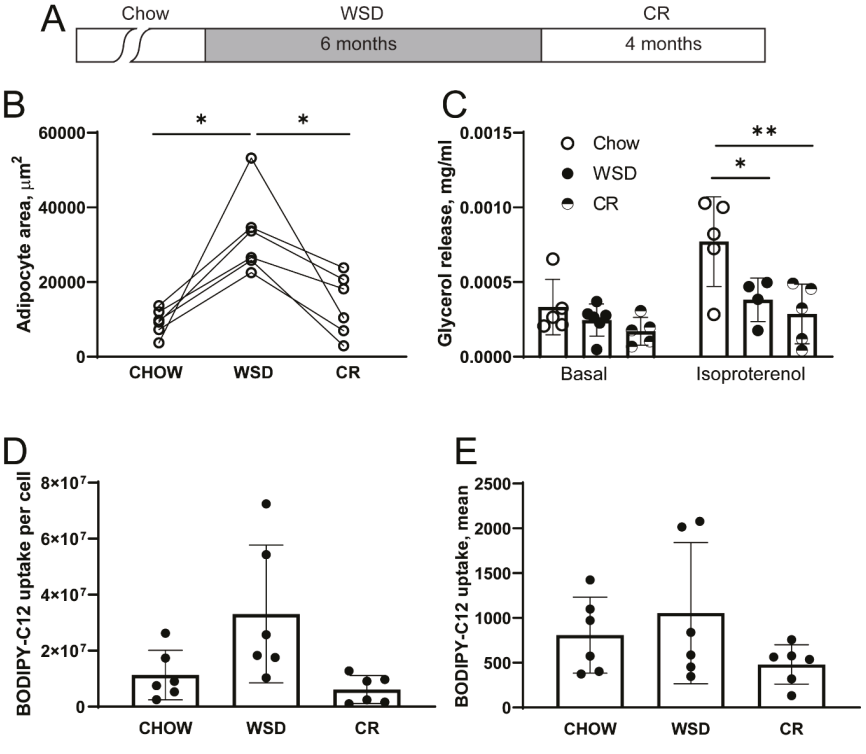

Figure 1. Western-style diet (WSD) induces sustained β-adrenergic resistance in adipocytes. (**A**) Study design. Animals were switched from a chow diet to WSD for six months followed by caloric restriction (CR) for an additional four months. Subcutaneous white adipose tissue (SC-WAT) collected at the end of each dietary intervention (chow, WSD and CR) were separated into small explants and used for lipolysis and free fatty acid (FFA) uptake assays. (**B**) Adipocyte area was determined using BODIPY-C12 labelled explants (see below); each data point is the average cell area per animal for n = 80–100 adipocytes; * $p < 0.05$, One-way ANOVA. (**C**) SC-WAT explants were incubated for 2 h under basal conditions, or in the presence of 10 μm isoproterenol and glycerol concentration in the media was determined as described in the "Materials and Methods;" * $p < 0.05$, ** $p < 0.01$, One-way ANOVA. (**D**,**E**) Basal BODIPY-C12 uptake was conducted as described in "Materials and Methods;" (**D**) total fluorescence per adipocyte; (**E**) mean fluorescence per area of adipocyte.

3.2. WSD-Induced Pro-Inflammatory Gene Expression in SC-WAT Is Reversed by CR

Three SC-WAT biopsies collected at the end of each dietary period were subjected to whole-genome RNA-Seq transcriptional analysis. DEGs were identified using three comparisons: WSD/CHOW, CR/WSD, and CR/CHOW (Supplementary Table S1). This experimental design allowed us to identify diet-specific DEGs, as well as genes whose expression did not change after the transition from WSD to CR. Functional enrichment was performed on WSD/CHOW, CR/WSD, and CR/CHOW subsets using IPA. Additionally, we identified 301 DEGs whose expression was significantly upregulated by WSD, then subsequently significantly downregulated by CR (Figure 2A and Supplementary Table S2). DEGs of this category with the highest fold change encoded pro-inflammatory factors such as *S100A7/8*, *CXCL1*, *CCL3*, *CCL5* and *MMD*; chemokine receptors e.g., *CCR1* and *CXCR2*, as well as proteins involved in the heme biosynthesis pathway, such as *ALAS2*, *HBB*, *HBA1* and *CYPE* (Table 1). WSD induced the upregulation of genes involved in granulocyte (p-value 4.2×10^{-12}) and agranulocyte (p-value 8.1×10^{-10}) migration and cell adhesion. The top upstream regulators identified by IPA included the pro-inflammatory cytokines *TNFα* (p-value 4.5×10^{-21}) and interleukin-1β (*IL-1*β, p-value 4.8×10^{-19}). To identify the functional interaction networks between proteins encoded by DEGs, we used the STRING Functional Protein Network Analysis. This analysis revealed the largest node of functional connectivity associated with immune response (n = 85; FDR 3.7×10^{-23}) and neutrophil activation (n = 34; FDR 3.3×10^{-11}) (Figure 2C, blue and yellow). Furthermore, we identified three functional nodes representing oxygen transport processes (n = 9; FDR 1.3×10^{-8}), the histone H3 network (n = 4, FDR 0.01), and lipoprotein metabolism (n = 23; FDR 0.02) (Figure 2C and Table 2, "LDLR"). Intriguingly, STRING identified a well-segregated node of functionally interacting proteins implicated in the regulation of cell cycle progression, DNA replication and intracellular signaling (Figure 2C, "Cell Cycle"). Collectively, this analysis suggests that WSD induces a pro-inflammatory transcriptional response in SC-WAT that is effectively reversed by subsequent CR.

Table 1. Top western-style diet (WSD)-induced genes whose expression was reversed by caloric restriction (CR).

		WSD/CHOW		CR/CHOW		CR/WSD	
Ensembl_ID	**Entrez Gene Name**	**LogFC**	**FDR**	**LogFC**	**FDR**	**LogFC**	**FDR**
ALAS2	5′-aminolevulinate synthase 2	3.56	3×10^{-52}	1.24	2×10^{-4}	−2.33	1×10^{-19}
HBZ	hemoglobin subunit zeta	3.35	7×10^{-49}	0.79	0.066	−2.56	5×10^{-23}
HBD	hypophosphatemic bone disease	3.14	2×10^{-47}	1.28	4×10^{-5}	−1.86	5.3×10^{-13}
HBB	hemoglobin subunit beta	3.11	1×10^{-46}	1.26	5×10^{-5}	−1.85	5.7×10^{-13}
HBA1	hemoglobin subunit alpha 1	3.09	1×10^{-46}	0.87	0.013	−2.21	1.7×10^{-18}
HBA2	hemoglobin subunit alpha 2	3.09	1×10^{-46}	0.87	0.013	−2.21	1.8×10^{-18}
HBE1	hemoglobin subunit epsilon 1	3.08	1.7×10^{-45}	1.23	9×10^{-5}	−1.85	5.6×10^{-13}
S100A9	S100 calcium binding protein A9	3.06	4×10^{-35}	0.54	0.516	−2.53	1.4×10^{-18}
PF4	platelet factor 4	2.98	4.8×10^{-22}	1.70	1×10^{-4}	−1.28	0.00054
GYPE	glycophorin E	2.87	4×10^{-32}	1.00	0.02	−1.87	2×10^{-10}
GYPA	glycophorin A	2.80	5.7×10^{-35}	1.11	0.002	−1.69	1.4×10^{-9}
HBBP1	hemoglobin subunit beta pseudogene 1	2.75	3.3×10^{-7}	−0.28	1	−3.03	1.1×10^{-6}
HBG1	hemoglobin subunit gamma 1	2.63	3.3×10^{-8}	1.05	0.021	−1.58	2.8×10^{-7}
HBG2	hemoglobin subunit gamma 2	2.63	3.6×10^{-23}	1.05	0.021	−1.58	2.8×10^{-7}
GYPB	glycophorin B (MNS blood group)	2.58	1×10^{-19}	0.46	0.84	−2.12	6.3×10^{-10}
CXCL1	C-X-C motif chemokine ligand 1	2.38	1.2×10^{-13}	1.13	0.095	−1.25	0.00614
S100A8	S100 calcium binding protein A8	2.28	1×10^{-20}	0.07	1	−2.21	3.7×10^{-13}
S100A7	S100 calcium binding protein A7	1.69	0.028	−0.03	1	−1.72	0.0441
MSR1	macrophage scavenger receptor 1	1.50	7.5×10^{-13}	0.51	0.231	−1.00	0.000509
CCL5	C-C motif chemokine ligand 5	1.44	3.3×10^{-7}	0.40	0.819	−1.03	0.010258
CCR1	C-C motif chemokine receptor 1	1.30	7×10^{-9}	0.25	0.901	−1.04	0.000282
CXCR2	C-X-C motif chemokine receptor 2	1.25	7.2×10^{-6}	0.23	0.995	−1.02	0.006017
CXCL10	C-X-C motif chemokine ligand 10	1.24	1.5×10^{-5}	0.10	1	−1.14	0.004538
CCL3	C-C motif chemokine ligand 3	1.14	4×10^{-6}	0.38	0.712	−0.77	0.040866
MMD	monocyte to macrophage differentiation associated	1.13	6.7×10^{-8}	−0.27	0.86	−1.41	4.3×10^{-8}

Differentially expressed genes (DEGs) were filtered using the following parameters. WSD/CHOW, Log_2 (fold change) > 1.0 and false discovery rate (FDR) < 0.05; CR/WSD, FDR < 0.05.

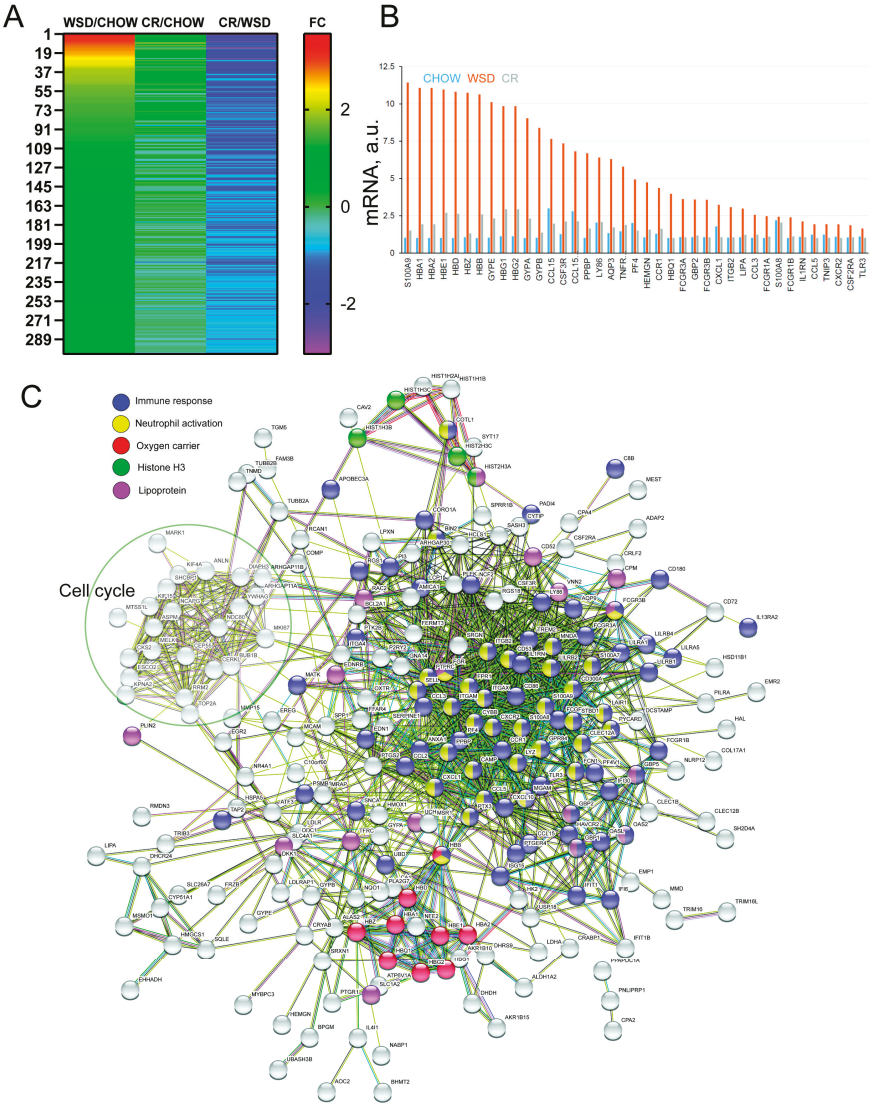

Figure 2. Western-style diet (WSD) induces and caloric restriction (CR) reverses pro-inflammatory gene expression in subcutaneous white adipose tissue (SC-WAT). Three SC-WAT biopsies collected at the end of each dietary period were subjected to the RNA-Seq transcriptional analysis. This figure describes only reversibly-induced differentially expressed genes (DEGs) that were significantly upregulated by WSD and then significantly downregulated by CR. (**A**) Heat map of DEGs (the number of genes is indicated); FC, log2fold changes in gene expression. (**B**) Top WSD-induced DEGs that were downregulated by CR; relative mRNA levels are shown in arbitrary units (a.u.). (**C**) STRING Functional Protein Network Analysis of DEGs reveals functional connectivity associated with immune response (blue), neutrophil activation (yellow), heme biosynthesis (red), histone H3 network (green), lipoprotein metabolism (magenta), and regulation of cell cycle progression (circled).

Table 2. Top metabolic genes differentially regulated by western-style diet (WSD) and caloric restriction (CR).

		WSD/CHOW		CR/CHOW		CR/WSD	
Ensembl_ID	**Entrez Gene Name**	**LogFC**	**FDR**	**LogFC**	**FDR**	**LogFC**	**FDR**
ELOVL6	ELOVL fatty acid elongase 6	−2.203	0.000	−2.959	0.000	−0.756	0.023
FASN	fatty acid synthase	−1.880	0.000	−2.139	0.000	−0.259	0.720
ACLY	ATP citrate lyase	−1.469	0.000	−2.310	0.000	−0.841	0.003
ACACA	acetyl-CoA carboxylase alpha	−1.384	0.000	−1.936	0.000	−0.552	0.133
ADCY10	adenylate cyclase 10 (soluble)	−1.251	0.000	−1.970	0.000	−0.719	0.044
GPR39	G protein-coupled receptor 39	−1.200	0.000	−1.208	0.000	−0.008	1.000
RUNX2	runt related transcription factor 2	−1.100	0.000	−0.771	0.021	0.329	0.621
PLIN2	perilipin 2	1.546	0.000	0.350	0.623	−1.196	0.000
LDLR	low density lipoprotein receptor	1.555	0.000	−0.491	0.284	−2.046	0.000

Differentially expressed genes (DEGs) were filtered using the following parameters. WSD/CHOW, Log_2 (fold change) < 1.0 and FDR < 0.05; CR/CHOW, Log_2 (fold change) < 1.0 and FDR < 0.05. PLIN2 and LDLR show the reversible pattern of regulation (upregulated by WSD and downregulated by CR).

3.3. De Novo Lipogenesis and β-Adrenergic Receptor Genes Remain Downregulated after CR

Gene expression analysis revealed a subset of 153 DEGs whose expression was significantly downregulated by WSD (FC < −1.5; FDR < 0.05) and remained significantly downregulated even after the CR period (FDR < 0.05; Figure 3A and Supplementary Table S3). The IPA pathway analysis showed that WSD caused the downregulation of genes encoding enzymes involved in de novo FFA biosynthesis from glucose (de novo lipogenesis, DNL), including ATP citrate lyase (*ACLY*), acetyl-coenzyme A carboxylase alpha (*ACACA*), FFA synthase (*FASN*), and elongation of very long chain FFAs protein 6 (*ELOVL6*) (Figure 3B and Table 2). In addition, carbohydrate metabolism genes of glucokinase (*GCK*), 6-phosphofructo-2-kinase/fructose-2, 6-bisphosphatase 1 (*PFKFB1*) and glycogen phosphorylase (*PYGM*) were also downregulated after WSD and remained downregulated even after CR (Figure 3B and Table 2). Changes in the expression of DNL genes correlated with the sustained downregulation of the gene encoding the master regulator of DNL, carbohydrate-responsive-element-binding protein (*ChREBP, MLXIPL*) [29,30] observed both after the WSD and following CR (WSD/Chow, 1.8 fold change, FDR 0.00067; Figure 3B,C). Furthermore, genes mediating the lipolytic function in adipocytes, including β_3-adrenergic receptor (*ADRB3*) [31] and G Protein-Coupled Receptor 39 (*GPR39*) [32,33] were significantly downregulated after WSD compared to chow (FDR 8.6×10^{-5}) and remained downregulated even after CR (Figure 3C and Table 2). The STRING Functional Protein Network Analysis revealed the downregulation of functional nodes related to FFA (n = 7; FDR 0.0033) and carbohydrate (n = 13; FDR 0.0012) metabolism and collagen biosynthesis (n = 22; FDR 1.0×10^{-11}) (Figure 3C). Collectively, our analysis shows that WSD induced the downregulation of DNL and lipolysis genes, which persisted even after CR-induced reduction in SC adipocyte size.

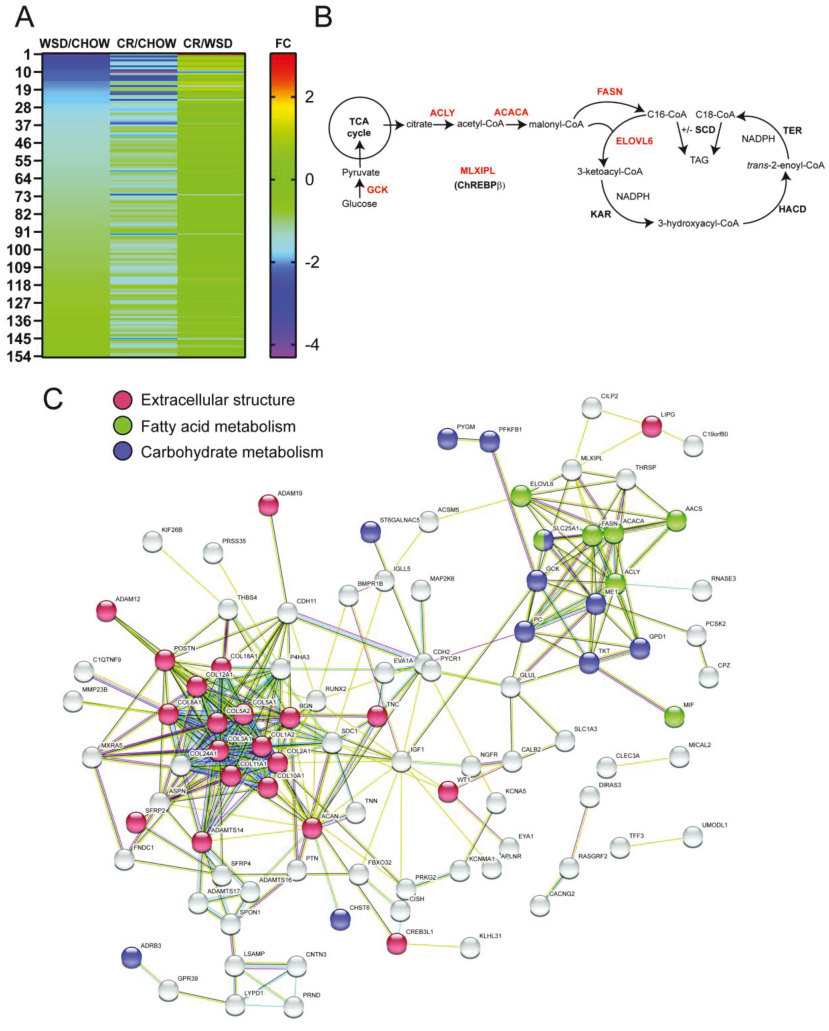

Figure 3. Western-style diet (WSD) causes sustained downregulation of de novo lipogenesis (DNL) genes in subcutaneous white adipose tissue (SC-WAT). Three SC-WAT biopsies collected at the end of each dietary period were subjected to the RNA-Seq transcriptional analysis. This figure describes a subset of differentially expressed genes (DEGs) that were downregulated after WSD and remained downregulated following caloric restriction (CR). (**A**) Heat map of DEGs (the number of genes of this category is indicated); FC, log2fold changes in gene expression. (**B**) DNL pathway; enzymes and transcription factors are in red: glucokinase (GCK), ATP-citrate lyase (ACLY), acetyl-CoA carboxylase (ACACA), fatty acid synthase (FASN), carbohydrate-responsive-element-binding protein-beta (MLXIPL/ChREBPβ, the transcriptional regulator of DNL). DNL-derived palmitate (C16) is elongated (C16– > C18) by elongation of very long chain fatty acids protein 6 (ELOVL6). C16 and C18 are desaturated by stearoyl-CoA desaturases (SCD). Additional enzymes regulating fatty acid elongation: 3-ketoacyl-CoA reductase (KAR), trans-2-enoyl-CoA reductase (TER), 3-hydroxyacyl ACP dehydrase (HACD); TAG, triacylglycerol. (**C**) STRING Functional Protein Network Analysis of downregulated DEGs reveals functional connectivity associated with fatty acid metabolism/DNL (green), carbohydrate metabolism (blue), and extracellular matrix structure (red).

3.4. CR Diminishes a Pro-Inflammatory Response in Circulating Monocytes

Obesity is associated with the development of a systemic pro-inflammatory state and the production of pro-inflammatory cytokines. In contrast, CR typically exerts the opposite effect on the immune system, leading to a reduced pro-inflammatory response [34], although the later has not been directly demonstrated in a NHP model of CR. To examine these dietary effects further, PBMCs isolated after exposure to WSD and at the end of CR were treated with the toll-like receptor-4 (TLR4) agonist LPS and the frequency of TNFα- producing monocytes was quantified using intracellular staining and flow cytometry. Approximately 10–40% of the total monocyte population isolated during the WSD period were TNFα-positive following LPS stimulation. In contrast, very few monocytes isolated at the end of the CR period expressed TNFα following LPS stimulation, suggesting that fasting supported the loss of obesity-induced pro-inflammatory phenotype in circulating monocytes (Figure 4A). Similar results were obtained using another pro-inflammatory cytokine IL-6, which was also downregulated in monocytes by CR (Figure 4B). In contrast to TNFα and IL-6, the percent of IFNγ + monocytes dramatically increased following a transition from WSD to CR (Figure 4C), suggesting that WSD suppressed and CR supported the production of a cytokine that is critical for antiviral and antibacterial immunity. Interestingly, a transition from WSD to CR did not cause significant changes in the proportion of total circulating monocytes or the ratio of classical (CD16−) to non-classical (CD16+) monocyte subtypes in peripheral blood (Figure 4D–F), suggesting that CR may modulate the functional capacity of the cells rather than cause major shifts in monocyte population frequencies.

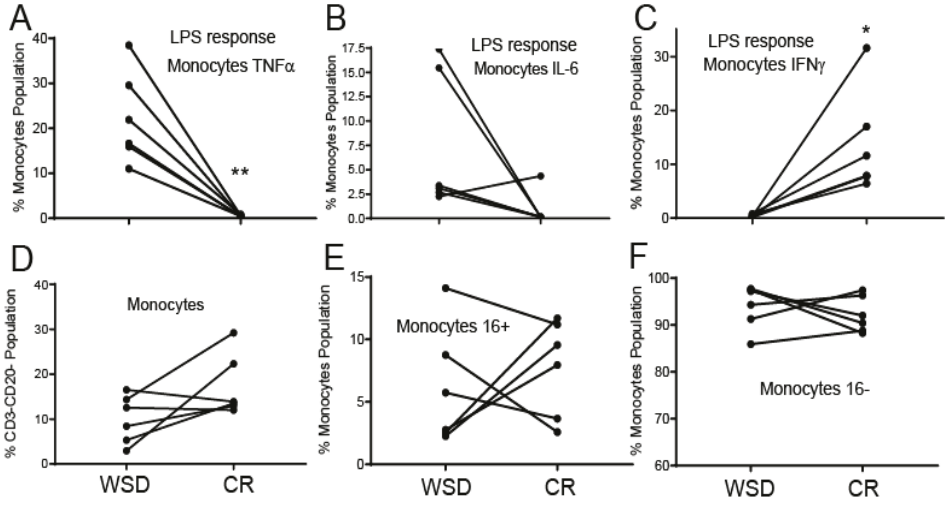

Figure 4. Caloric restriction (CR) suppresses a pro-inflammatory response in circulating monocytes. (**A**–**C**) Frequency of TNFα, IL-6, and IFNγ producing monocytes following 6 h liposaccharide (LPS) stimulation as measured by intracellular cytokine staining. (**D**) Frequency of monocytes within PBMCs. (**E**,**F**) Relative frequency of non-classical (CD16+) and classical (CD16-) monocytes within the monocyte population; * $p < 0.05$, ** $p < 0.01$, paired *t*-test.

4. Discussion

4.1. The Effects of WSD and CR on a Pro-Inflammatory Response

The main finding of the present report is that short-term CR efficiently reversed an obesity-induced pro-inflammatory transcriptional response in SC-WAT and reduced the production of pro-inflammatory cytokines in LPS-treated peripheral monocytes. The latter finding is consistent with the reported reduction in the cytokine levels in LPS-treated T-cell populations isolated from long-term calorically

restricted rhesus macaques [16,34], suggesting that fasting can have a beneficial effect on both adaptive and innate immune systems. It is important to emphasize that previous NHP studies were conducted using standard monkey chow low in saturated fats [16,34], while we used WSD matching the composition of a typical diet consumed in a modern society. Since WAT inflammation is strongly associated with insulin resistance [35], the present study suggests that a relatively short-term energy restriction can efficiently mitigate obesity-induced insulin resistance and reverse a pro-inflammatory phenotype in both SC-WAT and peripheral monocytes. Studies shows that the key pro-inflammatory cytokines driving insulin resistance are TNFα and IL1β secreted by local macrophages [36]. Furthermore, the suppression of a pro-inflammatory response by CR has been attributed to the production of ketone bodies and acetoacetate in the liver as alternative energy sources during nutrient deficiency [37]. The anti-inflammatory effect of ketogenic bodies has been linked to the direct inhibition of the NLRP3 inflammasome in human monocytes stimulated with LPS [38], which is consistent with the present and previous reports [16,34] that CR causes a significant reduction in the production of pro-inflammatory cytokines in rhesus monocytes and T-cells, respectively. The induction of erythroid-specific genes in SC-WAT by WSD reported here is a new phenomenon. Although the expression of *HBB* in mouse macrophages has been previously reported [39], the present study shows that WSD induces and CR reverses the expression of multiple erythroid-specific genes, including embryonic hemoglobin genes *HBZ* and *HBE1*. To our knowledge, this is the first report that shows a diet-specific regulation of erythroid genes in peripheral WAT. This may represent an increased production and/or bone marrow output of the erythroid progenitors in the presence of WSD. This hypothesis is consistent with our previous study demonstrating that WSD induced the expression of erythroid genes in the skeletal muscle of rhesus macaques [18].

4.2. The Effects of WSD and CR on Lipolysis

The present study demonstrates that male rhesus macaques transitioned from a low-fat diet to a WSD for six months exhibited SC adipocyte hypertrophy, a blunted β-adrenergic lipolytic response, and the downregulation of the *ADRB3* gene in SC-WAT. While CR efficiently reduced SC adipocyte size, it did not normalize the β-agonist lipolytic response and failed to restore *ADRB3* expression in SC-WAT. Several studies have shown that obese patients undergoing weight loss interventions experience weight regain [40–42], which coincides with functional changes in WAT [43]. Consistent with the present report, obesity has been shown to be associated with the development of lipolytic resistance of WAT to catecholamines [44]. A number of studies, however, have also demonstrated that CR increases the rate of catecholamine response and the density of β-adrenoceptors in WAT of obese patients [45–47], while others reported no significant effects of CR on lipolysis [48–52]. Interestingly, studies have shown that, during the weight-maintenance phase after the bariatric surgery, there was a marked decrease in the levels of hormone-sensitive lipase (HSL) in SC-WAT of women but not in men [53]. Similarly to the present study, it has been shown that the WAT lipolytic response of obese patients three years after initiation of a weight-reducing program was lower compared to the pre-diet conditions [54]. These studies demonstrate that the initial improvement of the lipolytic response after weight loss persists during the dynamic phase of energy restriction, but returns to lower values after adaptation to a new energy balance during the weight-maintenance phase. We also observed the sustained downregulation of *GPR39* in SC-WAT by WSD. *GPR39* deficiency has been reportedly associated with obesity and reduced lipolysis in adipocytes [32,33].

4.3. The Effects of WSD and CR on De Novo Lipogenesis Pathway

The present study demonstrates that DNL and *ChREBP* genes, whose expression in SC-WAT was suppressed by WSD, remained downregulated after CR. Previously, it has been shown that the WAT-specific isoform of the transcription factor ChREBP, ChREBPβ, is the central regulator of glucose-mediated activation of lipogenic genes, while its expression in WAT correlates with increased insulin sensitivity [29]. ChREBP activation in WAT is altered in obesity, resulting in the downregulation

of *ChREBP*β, *ACLY, ACACA, FASN,* and *ELOVL6* [55]. Activation of DNL in WAT has a positive effect both on direct glucose disposal [56,57] and metabolic homeostasis through the production of lipokines [58,59]. While the adipose-specific DNL pathway significantly contributes to body lipid reserves and thus directly regulates glucose homeostasis in humans [58], new studies have shown that it is also involved in the synthesis of biologically active branched FFAs that participate in the regulation of systemic insulin sensitivity and have anti-inflammatory properties [60,61]. The metabolic role of DNL-derived lipokines, in particular palmitoleate (C16: 1n−7), has been extensively described in a recent review [59]. The lipid biosynthesis pathway is dysregulated in obesity, which has been associated with the remodeling of lipid composition of adipocyte membranes [62] and the reduced presence of polyunsaturated fatty acids in high-BMI individuals [63]. Thus, we propose that WSD exerts a long-lasting effect on the lipolytic and DNL pathways in adipocytes, possibly through epigenetic modifications. Consistent with this hypothesis, we recently conducted the whole-genome gene expression and epigenetic analysis in visceral WAT of female rhesus macaques exposed to a WSD and excess androgens in combination or individually. This study demonstrated that testosterone could modulate the effects of WSD on transcription of lipid metabolism genes and DNA methylation in females WAT [64].

5. Conclusions

In summary, the present study advances our understanding of the functional and transcriptional response in SC-WAT associated with dynamic changes in fat mass in response to diet-induced obesity and weight loss and expands our previous studies in NHPs [17,18,20,64–66]. Our study has several limitations. In the present report, we used the RNA-Seq analysis of whole WAT. Further studies are needed to understand the immunophenotypic changes in WAT (in both SC and visceral depots) in the content of resident immune cells. While several previous reports addressed the metabolic adaptation of WAT to weight loss through energy restriction [67–69], sex-specific mechanisms that control WAT function in health, during the development of obesity and after weight loss are also not completely understood [31,70] and need to be further explored in a NHP model. Further studies are needed to understand the role of epigenetic factors, including DNA methylation and histone modifications, in programing WAT transcriptome in males and females.

Supplementary Materials: The following are available online at http://www.mdpi.com/2072-6643/12/2/511/s1, Table S1: Title: Diet-specific changes in gene expression, Table S2: Title: Top 200 WSD-induced genes whose expression was reversed by CR, and Table S3: Title: WSD-suppressed genes whose expression was not reversed by CR.

Author Contributions: H.W.: formal analysis; M.H.: formal analysis; A.J.: formal analysis; I.M.: formal analysis and writing—review and editing; O.V.: formal analysis and writing—original draft preparation. All authors have read and agreed to the published version of the manuscript.

Funding: This study was supported by NIH grants R21AG047543-01 to OV, and P51 OD01192 for operation of the Oregon National Primate Research Center.

Acknowledgments: We thank the ONPRC Division of Comparative Medicine for help with tissue collection, and the OHSU Massively Parallel Sequencing Shared Resource for DNA sequencing.

Conflicts of Interest: The authors declare no conflicts of interest.

Online Data Repository: Sequencing data are available at the Sequence Read Archive (accession no. PRJNA606903).

References

1. Kahn, S.E.; Hull, R.; Utzschneider, K.M. Mechanisms linking obesity to insulin resistance and type 2 diabetes. *Nature* **2006**, *444*, 840–846. [CrossRef] [PubMed]
2. Varlamov, O. Western-style diet, sex steroids and metabolism. *Biochim. et Biophys. Acta (BBA)-Mol. Basis Dis.* **2017**, *1863*, 1147–1155. [CrossRef] [PubMed]

3. Mirzaei, H.; Suarez, J.A.; Longo, V.D. Protein and amino acid restriction, aging and disease: From yeast to humans. *Trends Endocrinol. Metab.* **2014**, *25*, 558–566. [CrossRef] [PubMed]
4. Lee, C.; Longo, V.D. Dietary restriction with and without caloric restriction for healthy aging. *F1000Research* **2016**, *5*. [CrossRef] [PubMed]
5. Heilbronn, L.K.; de Jonge, L.; Frisard, M.I.; DeLany, J.P.; Larson-Meyer, D.E.; Rood, J.; Nguyen, T.; Martin, C.K.; Volaufova, J.; Most, M.M.; et al. Effect of 6-month calorie restriction on biomarkers of longevity, metabolic adaptation, and oxidative stress in overweight individuals: A randomized controlled trial. *JAMA* **2006**, *295*, 1539–1548. [CrossRef]
6. Larson-Meyer, D.E.; Heilbronn, L.K.; Redman, L.M.; Newcomer, B.R.; Frisard, M.I.; Anton, S.; Smith, S.R.; Maplstat, A.A.; Ravussin, E. Effect of Calorie Restriction With or Without Exercise on Insulin Sensitivity, β-Cell Function, Fat Cell Size, and Ectopic Lipid in Overweight Subjects. *Diabetes Care* **2006**, *29*, 1337–1344. [CrossRef]
7. Redman, L.M.; Heilbronn, L.K.; Martin, C.K.; Alfonso, A.; Smith, S.R.; Ravussin, E. Effect of Calorie Restriction with or without Exercise on Body Composition and Fat Distribution. *J. Clin. Endocrinol. Metab.* **2007**, *92*, 865–872. [CrossRef]
8. Fontana, L.; Villareal, D.T.; Weiss, E.P.; Racette, S.; Steger-May, K.; Klein, S.; Holloszy, J.O. Calorie restriction or exercise: Effects on coronary heart disease risk factors. A randomized, controlled trial. *Am. J. Physiol. Metab.* **2007**, *293*, E197–E202. [CrossRef]
9. Fontana, L. The scientific basis of caloric restriction leading to longer life. *Curr. Opin. Gastroenterol.* **2009**, *25*, 144–150. [CrossRef]
10. Villareal, D.T.; Chode, S.; Parimi, N.; Sinacore, D.R.; Hilton, T.; Armamento-Villareal, R.; Napoli, N.; Qualls, C.; Shah, K. Weight loss, exercise, or both and physical function in obese older adults. *New Engl. J. Med.* **2011**, *364*, 1218–1229. [CrossRef]
11. Katsoulis, K.; Blaudeau, T.E.; Roy, J.P.; Hunter, G.R. Diet-induced Changes in Intra-abdominal Adipose Tissue and CVD Risk in American Women. *Obesity (Silver Spring)* **2009**, *17*, 2169–2175. [CrossRef] [PubMed]
12. Camhi, S.M.; Stefanick, M.L.; Katzmarzyk, P.T.; Young, D.R. Metabolic syndrome and changes in body fat from a low-fat diet and/or exercise randomized controlled trial. *Obesity (Silver Spring)* **2010**, *18*, 548–554. [CrossRef] [PubMed]
13. Foster-Schubert, K.E.; Alfano, C.M.; Duggan, C.R.; Xiao, L.; Campbell, K.L.; Kong, A.; Bain, C.E.; Wang, C.Y.; Blackburn, G.L.; McTiernan, A. Effect of diet and exercise, alone or combined, on weight and body composition in overweight-to-obese postmenopausal women. *Obesity (Silver Spring)* **2012**, *20*, 1628–1638. [CrossRef] [PubMed]
14. Carels, R.A.; Darby, L.A.; Cacciapaglia, H.M.; Douglass, O.M. Reducing Cardiovascular Risk Factors in Postmenopausal Women through a Lifestyle Change Intervention. *J. Women's Heal.* **2004**, *13*, 412–426. [CrossRef] [PubMed]
15. Messaoudi, I.; Warner, J.; Fischer, M.; Park, B.; Hill, B.; Mattison, J.; Lane, M.A.; Roth, G.S.; Ingram, N.K.; Picker, L.J.; et al. Delay of T cell senescence by caloric restriction in aged long-lived nonhuman primates. *Proc. Natl. Acad. Sci. USA* **2006**, *103*, 19448–19453. [CrossRef] [PubMed]
16. Messaoudi, I.; Fischer, M.; Warner, J.; Park, B.; Mattison, J.; Ingram, N.K.; Totonchy, T.; Mori, M.; Nikolich-Zugich, J. Optimal window of caloric restriction onset limits its beneficial impact on T-cell senescence in primates. *Aging Cell* **2008**, *7*, 908–919. [CrossRef] [PubMed]
17. Cameron, J.L.; Jain, R.; Rais, M.; White, A.E.; Beer, T.M.; Kievit, P.; Winters-Stone, K.; Messaoudi, I.; Varlamov, O. Perpetuating effects of androgen deficiency on insulin resistance. *Int. J. Obes.* **2016**, *40*, 1856–1863. [CrossRef] [PubMed]
18. Messaoudi, I.; Handu, M.; Rais, M.; Sureshchandra, S.; Park, B.S.; Fei, S.; Wright, H.; White, A.E.; Jain, R.; Cameron, J.; et al. Long-lasting effect of obesity on skeletal muscle transcriptome. *BMC Genom.* **2017**, *18*, 411. [CrossRef]
19. MacLean, P.; Higgins, J.A.; Giles, E.D.; Sherk, V.D.; Jackman, M.R. The role for adipose tissue in weight regain after weight loss. *Obes. Rev.* **2015**, *16*, 45–54. [CrossRef]
20. Varlamov, O.; Bishop, C.; Handu, M.; Takahashi, D.; Srinivasan, S.; White, A.; Roberts, C.T. Combined androgen excess and Western-style diet accelerates adipose tissue dysfunction in young adult, female nonhuman primates. *Hum. Reprod.* **2017**, *32*, 1892–1902. [CrossRef]

21. Varlamov, O.; Chu, M.; Cornea, A.; Sampath, H.; Roberts, C.T., Jr. Cell-Autonomous Heterogeneity of Nutrient Uptake in White Adipose Tissue of Rhesus Macaques. *Endocrinology* **2014**. [CrossRef] [PubMed]
22. Chu, M.; Sampath, H.; Cahana, D.Y.; Kahl, C.A.; Somwar, R.; Cornea, A.; Roberts, C.T.; Varlamov, O. Spatiotemporal dynamics of triglyceride storage in unilocular adipocytes. *Mol. Boil. Cell* **2014**, *25*, 4096–4105. [CrossRef] [PubMed]
23. Kim, D.; Pertea, G.; Trapnell, C.; Pimentel, H.; Kelley, R.; Salzberg, S.L. TopHat2: Accurate alignment of transcriptomes in the presence of insertions, deletions and gene fusions. *Genome Boil.* **2013**, *14*, R36. [CrossRef] [PubMed]
24. Liao, Y.; Smyth, G.K.; Shi, W. featureCounts: An efficient general purpose program for assigning sequence reads to genomic features. *Bioinformatics* **2014**, *30*, 923–930. [CrossRef] [PubMed]
25. Robinson, M.D.; McCarthy, D.J.; Smyth, G.K. edgeR: A Bioconductor package for differential expression analysis of digital gene expression data. *Bioinformatics* **2010**, *26*, 139–140. [CrossRef]
26. Kolahi, K.; Louey, S.; Varlamov, O.; Thornburg, K. Real-Time Tracking of BODIPY-C12 Long-Chain Fatty Acid in Human Term Placenta Reveals Unique Lipid Dynamics in Cytotrophoblast Cells. *PLoS ONE* **2016**, *11*, e0153522. [CrossRef]
27. Varlamov, O.; Somwar, R.; Cornea, A.; Kievit, P.; Grove, K.L.; Roberts, J.C.T. Single-cell analysis of insulin-regulated fatty acid uptake in adipocytes. *Am. J. Physiol. Metab.* **2010**, *299*, E486–E496. [CrossRef]
28. Somwar, R.; Roberts, J.C.T.; Varlamov, O. Live-cell imaging demonstrates rapid cargo exchange between lipid droplets in adipocytes. *FEBS Lett.* **2011**, *585*, 1946–1950. [CrossRef]
29. Herman, M.; Peroni, O.D.; Villoria, J.; Schön, M.P.; Abumrad, N.A.; Blüher, M.; Klein, S.; Kahn, B.B. A novel ChREBP isoform in adipose tissue regulates systemic glucose metabolism. *Nature* **2012**, *484*, 333–338. [CrossRef]
30. Eissing, L.; Scherer, T.; Tödter, K.; Knippschild, U.; Greve, J.W.; Buurman, W.A.; Pinnschmidt, H.O.; Rensen, S.S.; Wolf, A.M.; Bartelt, A.; et al. De novo lipogenesis in human fat and liver is linked to ChREBP-β and metabolic health. *Nat. Commun.* **2013**, *4*, 1528. [CrossRef]
31. Varlamov, O.; Bethea, C.L.; Roberts, C.T., Jr. Sex-specific differences in lipid and glucose metabolism. *Front. Endocrinol. (Lausanne)* **2014**, *5*, 241. [CrossRef] [PubMed]
32. Catalan, V.; Gómez-Ambrosi, J.; Rotellar, F.; Silva, C.; Gil, M.J.; Rodríguez, A.; Cienfuegos, J.A.; Salvador, J.; Frühbeck, G. The obestatin receptor (GPR39) is expressed in human adipose tissue and is down-regulated in obesity-associated type 2 diabetes mellitus. *Clin. Endocrinol.* **2007**, *66*, 598–601. [CrossRef] [PubMed]
33. Petersen, P.S.; Jin, C.; Madsen, A.N.; Rasmussen, M.; Kuhre, R.E.; Egerod, K.L.; Nielsen, L.B.; Schwartz, T.W.; Holst, B. Deficiency of the GPR39 receptor is associated with obesity and altered adipocyte metabolism. *FASEB J.* **2011**, *25*, 3803–3814. [CrossRef] [PubMed]
34. Reilly, S.; Saltiel, A.R. Adapting to obesity with adipose tissue inflammation. *Nat. Rev. Endocrinol.* **2017**, *13*, 633–643. [CrossRef]
35. Olefsky, J.M.; Glass, C.K. Macrophages, Inflammation, and Insulin Resistance. *Annu. Rev. Physiol.* **2010**, *72*, 219–246. [CrossRef]
36. Hotamisligil, G.S. Inflammation, metaflammation and immunometabolic disorders. *Nature* **2017**, *542*, 177–185. [CrossRef]
37. Newman, J.C.; Verdin, E. Ketone bodies as signaling metabolites. *Trends Endocrinol. Metab.* **2014**, *25*, 42–52. [CrossRef]
38. Youm, Y.-H.; Nguyen, K.Y.; Grant, R.W.; Goldberg, E.L.; Bodogai, M.; Kim, D.; D'Agostino, D.; Planavsky, N.; Lupfer, C.; Kanneganti, T.-D.; et al. The ketone metabolite β-hydroxybutyrate blocks NLRP3 inflammasome–mediated inflammatory disease. *Nat. Med.* **2015**, *21*, 263–269. [CrossRef]
39. Liu, L.; Zeng, M.; Stamler, J.S. Hemoglobin induction in mouse macrophages. *Proc. Natl. Acad. Sci. USA* **1999**, *96*, 6643–6647. [CrossRef]
40. Johannsen, D.L.; Knuth, N.D.; Huizenga, R.; Rood, J.C.; Ravussin, E.; Hall, K.D. Metabolic slowing with massive weight loss despite preservation of fat-free mass. *J. Clin. Endocrinol. Metab.* **2012**, *97*, 2489–2496. [CrossRef]
41. Fothergill, E.; Guo, J.; Howard, L.; Kerns, J.C.; Knuth, N.D.; Brychta, R.; Chen, K.Y.; Skarulis, M.C.; Walter, M.; Walter, P.J.; et al. Persistent metabolic adaptation 6 years after "The Biggest Loser" competition. *Obesity* **2016**, *24*, 1612–1619. [CrossRef] [PubMed]

42. Greenway, F.L. Physiological adaptations to weight loss and factors favouring weight regain. *Int. J. Obes.* **2015**, *39*, 1188–1196. [CrossRef] [PubMed]
43. Rossmeislova, L.; Malisova, L.; Kracmerova, J.; Stich, V. Adaptation of human adipose tissue to hypocaloric diet. *Int. J. Obes. (Lond)* **2013**, *37*, 640–650. [CrossRef] [PubMed]
44. Reynisdottir, S.; Ellerfeldt, K.; Wahrenberg, H.; Lithell, H.; Arner, P. Multiple lipolysis defects in the insulin resistance (metabolic) syndrome. *J. Clin. Investig.* **1994**, *93*, 2590–2599. [CrossRef] [PubMed]
45. Stich, V.; Harant, I.; De Glisezinski, I.; Crampes, F.; Berlan, M.; Kunesova, M.; Hainer, V.; Dauzats, M.; Rivière, D.; Garrigues, M.; et al. Adipose Tissue Lipolysis and Hormone-Sensitive Lipase Expression during Very-Low-Calorie Diet in Obese Female Identical Twins1. *J. Clin. Endocrinol. Metab.* **1997**, *82*, 739–744.
46. Sengenes, C.; Stich, V.; Berlan, M.; Hejnova, J.; Lafontan, M.; Pariskova, Z.; Galitzky, J. Increased lipolysis in adipose tissue and lipid mobilization to natriuretic peptides during low-calorie diet in obese women. *Int. J. Obes.* **2002**, *26*, 24–32. [CrossRef]
47. Flechtner-Mors, M.; Ditschuneit, H.H.; Yip, I.; Adler, G. Sympathetic modulation of lipolysis in subcutaneous adipose tissue: Effects of gender and energy restriction. *J. Lab. Clin. Med.* **1999**, *134*, 33–41. [CrossRef]
48. Hellström, L.; Reynisdottir, S.; Langin, D.; Rössner, S.; Arner, P. Regulation of lipolysis in fat cells of obese women during long-term hypocaloric diet. *Int. J. Obes. Relat. Metab. Disord. : J. Int. Assoc. Study Obes.* **1996**, *20*, 745–752.
49. Presta, E.; Leibel, R.L.; Hirsch, J. Regional changes in adrenergic receptor status during hypocaloric intake do not predict changes in adipocyte size or body shape. *Metabolism* **1990**, *39*, 307–315. [CrossRef]
50. Berlan, M.; Dang-Tran, L.; Lafontan, M.; Denard, Y. Influence of hypocaloric diet on alpha-adrenergic responsiveness of obese human subcutaneous adipocytes. *Int. J. Obes.* **1981**, *5*, 145–153.
51. Rozen, R.; Banegas, E.; Davilla, M.; Apfelbaum, M. Effects of a very-low-calorie diet on adrenergic responsiveness in human adipose tissue. *Int. J. Obes.* **1984**, *8*, 141–149. [PubMed]
52. Kather, H.; Wieland, E.; Fischer, B.; Wirth, A.; Schlierf, G. Adrenergic regulation of lipolysis in abdominal adipocytes of obese subjects during caloric restriction: Reversal of catecholamine action caused by relief of endogenous inhibition. *Eur. J. Clin. Investig.* **1985**, *15*, 30–37. [CrossRef] [PubMed]
53. Kolehmainen, M.; Vidal, H.; Ohisalo, J.J.; Pirinen, E.; Alhava, E.; Uusitupa, M.I.J. Hormone sensitive lipase expression and adipose tissue metabolism show gender difference in obese subjects after weight loss. *Int. J. Obes.* **2002**, *26*, 6–16. [CrossRef] [PubMed]
54. Löfgren, P.; Hoffstedt, J.; Näslund, E.; Wirén, M.; Arner, P. Prospective and controlled studies of the actions of insulin and catecholamine in fat cells of obese women following weight reduction. *Diabetologia* **2005**, *48*, 2334–2342. [CrossRef] [PubMed]
55. Tang, Y.; Wallace, M.; Gurmaches, J.S.; Hsiao, W.-Y.; Li, H.; Lee, P.L.; Vernia, S.; Metallo, C.M.; Guertin, D.A. Adipose tissue mTORC2 regulates ChREBP-driven de novo lipogenesis and hepatic glucose metabolism. *Nat. Commun.* **2016**, *7*, 11365. [CrossRef] [PubMed]
56. Minehira, K.; Vega, N.; Vidal, H.; Acheson, K.; Tappy, L. Effect of carbohydrate overfeeding on whole body macronutrient metabolism and expression of lipogenic enzymes in adipose tissue of lean and overweight humans. *Int. J. Obes.* **2004**, *28*, 1291–1298. [CrossRef]
57. Strawford, A.; Antelo, F.; Christiansen, M.; Hellerstein, M.K. Adipose tissue triglyceride turnover, de novo lipogenesis, and cell proliferation in humans measured with 2H2O. *Am. J. Physiol. Metab.* **2004**, *286*, E577–E588. [CrossRef]
58. Solinas, G.; Borén, J.; Dulloo, A. De novo lipogenesis in metabolic homeostasis: More friend than foe? *Mol. Metab.* **2015**, *4*, 367–377. [CrossRef]
59. Yilmaz, M.; Claiborn, K.C.; Hotamisligil, G.S. De Novo Lipogenesis Products and Endogenous Lipokines. *Diabetes* **2016**, *65*, 1800–1807. [CrossRef]
60. Yore, M.M.; Syed, I.; Moraes-Vieira, P.M.; Zhang, T.; Herman, M.; Homan, E.A.; Patel, R.T.; Lee, J.; Chen, S.; Peroni, O.D.; et al. Discovery of a class of endogenous mammalian lipids with anti-diabetic and anti-inflammatory effects. *Cell* **2014**, *159*, 318–332. [CrossRef]
61. Moraes-Vieira, P.M.; Saghatelian, A.; Kahn, B.B. GLUT4 Expression in Adipocytes Regulates De Novo Lipogenesis and Levels of a Novel Class of Lipids with Antidiabetic and Anti-inflammatory Effects. *Diabetes* **2016**, *65*, 1808–1815. [CrossRef] [PubMed]

62. Pietiläinen, K.H.; Rog, T.; Seppänen-Laakso, T.; Virtue, S.; Gopalacharyulu, P.; Tang, J.; Rodríguez-Cuenca, S.; Maciejewski, A.; Naukkarinen, J.; Ruskeepää, A.-L.; et al. Association of lipidome remodeling in the adipocyte membrane with acquired obesity in humans. *PLoS Boil.* **2011**, *9*, e1000623. [CrossRef] [PubMed]
63. Würtz, P.; Wang, Q.; Kangas, A.; Richmond, R.; Skarp, J.; Tiainen, M.; Tynkkynen, T.; Soininen, P.; Havulinna, A.S.; Kaakinen, M.; et al. Metabolic Signatures of Adiposity in Young Adults: Mendelian Randomization Analysis and Effects of Weight Change. *PLoS Med.* **2014**, *11*, e1001765. [CrossRef] [PubMed]
64. Carbone, L.; Davis, B.A.; Fei, S.S.; White, A.; Nevonen, K.A.; Takahashi, D.; Vinson, A.; True, C.; Roberts, C.T., Jr.; Varlamov, O. Synergistic Effects of Hyperandrogenemia and Obesogenic Western-style Diet on Transcription and DNA Methylation in Visceral Adipose Tissue of Nonhuman Primates. *Sci. Rep.* **2019**, *9*, 19232. [CrossRef] [PubMed]
65. True, C.; Abbott, D.H.; Roberts, J.C.T.; Varlamov, O. Sex Differences in Androgen Regulation of Metabolism in Nonhuman Primates. *Adv. Exp. Med. Biol.* **2017**, *1043*, 559–574.
66. Varlamov, O.; Chu, M.P.; McGee, W.K.; Cameron, J.L.; O'Rourke, R.W.; Meyer, K.A.; Bishop, C.; Stouffer, R.L.; Roberts, J.C.T. Ovarian cycle-specific regulation of adipose tissue lipid storage by testosterone in female nonhuman primates. *Endocrinology* **2013**, *154*, 4126–4135. [CrossRef]
67. Viguerie, N.; Montastier, E.; Maoret, J.-J.; Roussel, B.; Combes, M.; Valle, C.; Villa-Vialaneix, N.; Iacovoni, J.S.; Martínez, J.A.; Holst, C.; et al. Determinants of Human Adipose Tissue Gene Expression: Impact of Diet, Sex, Metabolic Status, and Cis Genetic Regulation. *PLoS Genet.* **2012**, *8*, e1002959. [CrossRef]
68. Capel, F.; Klimčáková, E.; Viguerie, N.; Roussel, B.; Vítková, M.; Kováčiková, M.; Polak, J.; Kováčová, Z.; Galitzky, J.; Maoret, J.-J.; et al. Macrophages and Adipocytes in Human Obesity: Adipose Tissue Gene Expression and Insulin Sensitivity During Calorie Restriction and Weight Stabilization. *Diabetes* **2009**, *58*, 1558–1567. [CrossRef]
69. Giles, E.D.; Steig, A.J.; Jackman, M.R.; Higgins, J.A.; Johnson, G.C.; Lindstrom, R.C.; MacLean, P. Exercise Decreases Lipogenic Gene Expression in Adipose Tissue and Alters Adipocyte Cellularity during Weight Regain After Weight Loss. *Front. Physiol.* **2016**, *7*, 188. [CrossRef]
70. Wajchenberg, B.L. Subcutaneous and visceral adipose tissue: Their relation to the metabolic syndrome. *Endocr. Rev.* **2000**, *21*, 697–738. [CrossRef]

nutrients

MDPI

Article

The Role of High Fat Diets and Liver Peptidase Activity in the Development of Obesity and Insulin Resistance in Wistar Rats

Germán Domínguez-Vías [1,2], Ana Belén Segarra [1], Manuel Ramírez-Sánchez [1] and Isabel Prieto [1,*]

[1] Unit of Physiology, Department of Health Sciences, University of Jaén, Las Lagunillas, 23071 Jaén, Spain; germandv@go.ugr.es (G.D.-V.); asegarra@ujaen.es (A.B.S.); msanchez@ujaen.es (M.R.-S.)

[2] Department of Physiology, Faculty of Health Sciences, Ceuta, University of Granada, 18071 Granada, Spain

* Correspondence: iprieto@ujaen.es; Tel.: +34-953-212008

Received: 7 February 2020; Accepted: 25 February 2020; Published: 28 February 2020

Abstract: High-fat diets (HFD) have been widely associated with an increased risk of metabolic disorders and overweight. However, a high intake of sources that are rich in monounsaturated fatty acids has been suggested as a dietary agent that is able to positively influence energy metabolism and vascular function. The main objective of this study was to analyze the role of dietary fats on hepatic peptidases activities and metabolic disorders. Three diets: standard (S), HFD supplemented with virgin olive oil (VOO), and HFD supplemented with butter plus cholesterol (Bch), were administered over six months to male Wistar rats. Plasma and liver samples were collected for clinical biochemistry and aminopeptidase activities (AP) analysis. The expression of inducible nitric oxide synthase (iNOS) was also determined by Western blot in liver samples. The diet supplement with VOO did not induce obesity, in contrast to the Bch group. Though the VOO diet increased the time that was needed to return to the basal levels of plasma glucose, the fasting insulin/glucose ratio and HOMA2-%B index (a homeostasis model index of insulin secretion and valuation of β-cell usefulness (% β-cell secretion)) were improved. An increase of hepatic membrane-bound dipeptidyl-peptidase 4 (DPP4) activity was found only in VOO rats, even if no differences in fasting plasma glucagon-like peptide 1 (GLP-1) were obtained. Both HFDs induced changes in hepatic pyroglutamyl-AP in the soluble fraction, but only the Bch diet increased the soluble tyrosyl-AP. Angiotensinase activities that are implicated in the metabolism of angiotensin II (AngII) to AngIV increased in the VOO diet, which was in agreement with the higher activity of insulin-regulated-AP (IRAP) in this group. Otherwise, the diet that was enriched with butter increased soluble gamma-glutamyl transferase (GGT) and Leucyl-AP, iNOS expression in the liver, and plasma NO. In summary, VOO increased the hepatic activity of AP that were related to glucose metabolism (DPP4, angiotensinases, and IRAP). However, the Bch diet increased activities that are implicated in the control of food intake (Tyrosine-AP), the index of hepatic damage (Leucine-AP and GGT), and the expression of hepatic iNOS and plasma NO. Taken together, these results support that the source of fat in the diet affects several peptidases activities in the liver, which could be related to alterations in feeding behavior and glucose metabolism.

Keywords: obesity; high-fat diet; olive oil; aminopeptidase activity; renin–angiotensin-system

1. Introduction

Obesity is considered a serious chronic disease with adverse consequences due to the excessive accumulation of adipose tissue. Usually, obesity is caused by an imbalance between energy intake and energy expenditure [1]. The prevalence of obesity in the population has increased alarmingly in the past few decades, and it typically it is a part of a cluster of metabolic syndrome conditions that

increase the chance of developing several related disorders, such as type 2 diabetes, dyslipidemia, abnormal cholesterol levels, hypertension, stroke, heart disease, and cancer [2,3]. Several studies have documented a positive relationship between a high-fat diet (HFD) intake and obesity [4]. The efficacy of the current strategies of treatment for diseases that are caused by obesity is still not entirely satisfactory, and new approaches must be considered. Several studies have indicated relationships between the saturation of dietary fat and the concentrations of total plasma cholesterol and higher blood pressure [5], hepatic steatosis [6], adipose chronic inflammation [6], ectopic lipid deposition in the liver and brown fat [6], overweight [6,7], hyperinsulinemia [7], and hepatic insulin resistance [8]. However, high fat diets that are rich in monounsaturated fatty acids exert a protective role [9–15].

High monounsaturated fatty acids diets also have demonstrated an effect on the secretion of the insulinotropic peptide GLP-1 (glucagon-like peptide 1) [16,17]. GLP-1 is an incretin hormone with antidiabetic action that is capable of stimulating insulin secretion [18,19], increasing beta cell neogenesis [20], inhibiting beta cell apoptosis [20], inhibiting glucagon secretion [21], delaying gastric emptying, and inducing satiety [20,21]. However, the physiological inhibitory control of GLP-1 and its accelerated inactivation by plasma dipeptidyl-peptidase 4 (DPP4) hyperactivity [22] suggests that the impaired secretion and/or activity of GLP-1 may be involved in the pathogenesis of obesity [23].

The renin–angiotensin system (RAS) is an important regulator of blood pressure, electrolytes, and water balance. Until recently, angiotensin II (Ang II) was considered the main peptide that is involved in these homeostatic mechanisms. However, some of its metabolic derivatives such as angiotensin III (Ang III), angiotensin IV (Ang IV), and angiotensin 2-10 (Ang 2-10) have demonstrated important biological functions [24] (Figure 3A). The main peptides of the RAS (AngII and AngIII) bind to both AT1- and AT2-receptors with similar affinity [25,26]. In contrast, the affinity of Ang IV for the well-characterized AT1- and AT2-receptors is low [25], but it shows a high affinity to the AT4-receptor/insulin-regulated aminopeptidase (IRAP) [27]. Ang IV, which binds to IRAP (Figure 3A), appears to play a role in regulating local blood flow [28]. Local RASs could be altered by different degrees of saturation in dietary fat. Angiotensin peptides are metabolized by several angiotensinases, and we have previously demonstrated that those activities are affected by dietary fatty acids [5,29,30].

The local RAS in the liver plays an important role in the paracrine and autocrine regulation of hepatocyte metabolism [31], and all the components of this system have been described in hepatic cells [32–34]. Under pathological conditions, the role of the liver's RAS appears to be more important. Local angiotensin peptides increase cell proliferation, apoptosis, and the production of oxygen reactive species [35]. The Western diet induces liver steatosis and is also associated with the alteration of the local RAS in hepatocytes [36], and both renal and hepatic local RASs seem to be implicated in the development of chronic liver disease [37].

Lipids are recognized to be associated with the intracellular generation of reactive oxygen species (ROS) [38] as support for oxidative damage. The HFD, and subsequent dyslipidemia, are the major triggers for oxidative stress, and the increase of gamma-glutamyl transferase (GGT) like hepatic function biomarker [39]. Nitric oxide (NO) exerts a protective effect on liver diseases and hepatotoxicity that is associated with HFD [40,41]. The hepatic inducible isoform of the NO synthase (iNOS) functions as an adaptive response to minimize inflammatory injury [40,41].

The thyrotropin-released hormone (TRH)-degrading pyroglutamate aminopeptidase (pGluAP) activities convert TRH into cyclo His-Pro (cHP) [42], a potential hypoglycemic dipeptide that restores glucose metabolism, the blood insulin level, the lipid profile, and impaired β-cells in the pancreas [43]. Previous results suggested that the type of fat that is used in the diet may influence local pGluAP activity and modify its biological functions [44]. Other studies have implicated opioid transmission in the hedonic and metabolic control of feeding and diet-induced obesity [45]. Enkephalin (ENK) concentration changes in liver tissue and plasma during liver disorders [46,47], after a high-fat meal with an increased propensity to overeat [48], and with a higher systolic blood pressure [49]. ENK is hydrolyzed by specific enzymes, such as the ENK-degrading tyrosyl aminopeptidase (TyrAP) [50].

Then, hepatic TyrAP activity could be an index to evaluate the potential value of ENK degradation as a biological marker of the hedonic control and progression of obesity disorders.

In order to analyze the effects of HFD on liver peptide metabolism, we administered diets with different amounts and fat sources to rat groups in this study. We demonstrate that monounsaturated HFD is not related to metabolic manifestations because overweight, dyslipidemia, and high cholesterol levels were present in the animals that were fed with a saturated HFD. However, monounsaturated HFD mainly affects parameters that are related to glucose metabolism, probably in agreement with a greater use of fatty acids for energy. At the same time, the analyzed diets had a differential effect on several aminopeptidase activities with important roles in the development of metabolic syndromes.

2. Materials and Methods

2.1. Animals and Treatments

Adult male Wistar rats were purchased from Harlan Interfauna Ibérica S.A. (Barcelona, Spain). The rats had free access to experimental diets and water during 24 weeks, and they were maintained at a controlled temperature (20–25 °C) and humidity (50 ± 5%) environment in a 12 hours light/dark cycle. At the beginning of the study, the mean body weight and age were 495 g and six months, respectively. Experimental procedures for animal use and care were in accordance with European Communities Council Directive 2010/63/UE and Spanish regulation RD 53/2013, and the study was approved by the Institutional Animal Care and Use Committee of the University of Jaén. Rats were randomly assigned into three groups (n = 5 each): In the standard diet (S) group, rats were fed with a commercial chow for experimental animals. In HFDs, one group of rats was fed with a diet supplemented with 20% of virgin olive oil (VOO), and the second group of rats was fed with a diet supplemented with 20% butter plus cholesterol (0.1%) (Bch) in order to reach the average cholesterol content of the Western diet. The HFD diets were isocaloric. The food composition and nutritive value of different diets are shown in Supplemental Table S1. The food intake for each group was measured, and the animals were weighed once a week. At the end of the experimental period, a glucose tolerance test was performed. Animals were perfused with a saline solution through the left cardiac ventricle under Equithensin anesthesia (2 mL/kg Body Weight), and a sample of blood was collected for GLP-1, insulin, NO and other biochemical parameters. The blood samples were centrifuged for 10 min at 2000 *g* to obtain the plasma. Liver tissue samples were collected for angiotensinase activities, ENK- and TRH-degrading activities, hepatic damage markers, and immunoblot for hepatic iNOS.

2.2. Glucose Tolerance Test

A glucose tolerance test (GTT) was performed after overnight fasting. For the GTT, rats were i.p. injected (8 mL/kg BW) with a single dose of glucose that was dissolved in saline (2.0 g/kg BW). Blood glucose was measured by using a glucometer (Roche Accu-Check Inform.). A baseline (fasting) blood glucose measurement was taken before glucose administration, and further measurements were made at regular intervals thereafter (20, 40, 60 and 90 min).

2.3. Determination of Blood Parameters

Plasma insulin levels were determined by using an ELISA kit (#10-1113-01) that was purchased from Mercodia Developing Diagnostics (Winston Salem, NC, USA). Plasma GLP-1 concentrations were determined by using an ELISA kit (#107444-51-9) that was purchased from Cayman (Ann Arbor, MI, USA).

Plasma levels of NO were analyzed by the Griess method as a summation of NO2- and NO3- with an assay kit (Total Nitric Oxide and Nitrate/Nitrite Parameter#KGE001) that was purchased from R&D Systems (Minneapolis, MN, USA).

2.4. Determination of Insulin Resistance

A homeostasis model of insulin resistance (HOMA2-IR) was calculated by using the HOMA Calculator v.2.2.3 software [51]. HOMA-2 is an update and actualization of the HOMA equation, where a lineal regression is established between glucose and insulin by adjusting real physiology. It is possible, with this program, to calculate the HOMA2-%B, an index of insulin secretion and a valuation of β-cell usefulness (% β-cell secretion), and to know HOMA2-%S, an index for estimating sensitivity to insulin (% insulin sensitivity).

2.5. Sample Preparation for Aminopeptidase Activities Assay

Plasma samples were used for the peptidase activities assay. Samples from the liver were quickly removed and frozen in dry ice. To obtain a soluble fraction, tissue samples were homogenized in ten volumes of a 10 mM HCl-Tris buffer (pH 7.4) and ultracentrifuged (100,000 *g* for 30 min at 4 °C). The resulting supernatants were used to measure soluble (sol) enzymatic activity and protein content, assayed in triplicate. To solubilize membrane proteins, pellets were re-homogenized in an HCl-Tris buffer (pH 7.4) plus Triton X-100 (1%). After centrifugation (100,000 *g* for 30 min at 4 °C), supernatants were used to measure membrane-bound (mb) activity and proteins in triplicate. To ensure the complete recovery of activity, detergent (Triton X-100) was removed from the medium by adding the adsorbent polymeric SM-2 Biobeads (100 mg/mL), which were purchased form Bio-Rad (Richmond, VA, USA), to the samples and the shaking for 2 h at 4 °C [52].

2.6. Peptidase Activities Assay

The DPP4 family, GGT, LeuAP, pGluAP, TyrAP and angiotensinase (AspAP, GluAP, AlaAP, and IRAP) activities were determined in a fluorometric assay while using arylamidase as substrate according to the method of Ramírez et al. [53]. The substrate and substrate solution for each activity are listed in Supplemental Table S2. Briefly, 10 µL of each supernatant were incubated for 30 min at 37 °C with 100 µL of the substrate solution [54]. Later, enzymatic reactions were ceased after adding 100 µL of a 0.1 M acetate buffer (pH 4.2). The β-naphthylamine (β-NA) that was released as a product of proteolytic activity was fluorometrically assessed at 412 nm emission and at a 345 nm excitation wavelength. Specific peptidases activities were expressed as pmol of the β-NA that was hydrolyzed per minute and per milligram of protein. Fluorogenic assays were linear with respect to time of hydrolysis and protein concentration. The protein concentration was determined according to Bradford method [55] with BSA (Bovine Serum Albumin) as standard. All chemical products were supplied by Sigma (St. Louis, MO, USA).

2.7. Protein Extraction and Western Blot Analysis

For the Western blotting, total protein was isolated from the liver samples. The hepatic tissues were homogenized in a cooled protein extraction buffer (Tris-HCl, 0.1 M, pH 7.5; aprotinin, 0.1 mg/mL; sodium pyrophosphate, 0.1 M; sodium fluoride, 0.1 M; EDTA (Ethylene Diamine Tetraacetic Acid), 0.01 M; sodium orthovanadate, 0.01 M; and PMSF (Phenyl Methyl Sulfonyl Fluoride), 0.002 M), mixed with 10% Triton X-100 and centrifuged (12,000 *g* for 30 min at 4 °C). The supernatants were collected, and then the protein contents were analyzed with a micro Lowry reaction (DCTM Protein Assay #500-0116) purchased from Bio-Rad Laboratories (Hercules, CA, USA). A Western blot analysis was performed by using iNOS antibodies (BD Biosciences, CA, USA). The same amount of extracted protein from each sample (30~40 µg) was loaded for the sodium dodecyl sulphate-polyacrylamide gel electrophoresis (SDS-PAGE) immunoblot analysis. The separated proteins were electrophoretically transferred into a nitrocellulose membrane (Amersham), which was then blocked with 5% BSA and 0.1% Tween for 60 min at room temperature. The membranes were incubated with the primary antibody overnight at 4 °C. The regions containing proteins were visualized by using ECL (Amersham ECL prime Western blotting detection reagent # RPN2232) purchased from GE Healthcare Life Sciences (Buckinghamshire,

UK). Each band was normalized by the corresponding value of α1-tubulin as an internal control. A densitometric analysis was performed by Image J 1.36b (NIH) Software. The primary antibodies against the proteins are listed in Table S3.

2.8. Statistical Analysis

A statistical analysis was performed by one-way ANOVA followed by Tukey's post-hoc test for multiple comparisons. A comparison of parameters between two groups was performed with an unpaired Student's t-test. The relationship between variables were assessed by Pearson's correlation coefficient. The presence of significant difference was estimate with the Sigmaplot v11.0 software (Systat Software, Inc., San Jose, CA, USA), and p values below 0.05 ($p < 0.05$) were considered statistically significant. All the data are presented as mean ± standard error of the mean (SEM).

3. Results

3.1. Food and Energy Intakes

A significant difference was observed between the S and HFDs groups for daily food intake (g/100g BW), with the lowest values found for the Bch-fed rats (Figure 1A: Bch, 1.6 ± 0.3 g; VOO, 1.8 ± 0.2 g; S, 2.6 ± 0.3 g; $p < 0.05$). However, not significant differences for energy intake (kJ/day) were observed between the groups (Figure 1B: S, 181.8 ± 19.9; VOO, 178.2 ± 15.4; Bch, 171.4 ± 22.8), while the total weight gained was significantly higher in the Bch group (Bch, 151.9 ± 10.0 g; VOO, 101.6 ± 6.2 g; S, 73.6 ± 10.3 g; $p < 0.05$).

3.2. Glucose Tolerance Test (GTT) and Glycemic Control

No significant differences were found between groups in fasting plasma glucose (Figure 1E: S, 63.8 ± 7.6 mg/dL; VOO, 83 ± 13 mg/dL; Bch, 63 ± 2.5 mg/dL) and insulin (Figure 1C: S, 0.5 ± 0.1 ng/mL; VOO, 0.4 ± 0.1 ng/mL; Bch, 0.5 ± 0.1 ng/mL;). The effects of different diets on glucose tolerance were established at the end of the experimental period by using GGT (Figure 1D).

The highest levels of plasma glucose were achieved after 20 min of i.p. injection in the S and Bch groups (Figure 1E: S, 286.7 ± 34.9 mg/dL; VOO, 214.5 ± 43.4 mg/dL; Bch, 214.8 ± 15.7 mg/dL). Nevertheless, the VOO animals achieved the highest plasma glucose at 60 min after i.p. injection (S, 124.5 ± 11.7 mg/dL; VOO, 282.8 ± 58.5 mg/dL; Bch, 135 ± 12.3 mg/dL), and it remained elevated at 90 min.

Regarding the homeostasis model of insulin resistance, no significant differences were found between the diets in the fasting ration of insulin/glucose (Figure 1D: S, 25.8 ± 9.5 μIU/mg; VOO, 13.7 ± 5.0 μIU/mg; Bch, 26.3 ± 5.5 μIU/mg), HOMA-IR (Figure 1F: S, 1.7 ± 0.4; VOO, 1.3 ± 0.3; Bch, 1.9 ± 0.5), HOMA2-%S (Figure 1G: S, 74.8 ± 19.8; VOO, 86.6 ± 22.6; Bch, 60.7 ± 19.1) or HOMA2-%B (Figure 1H: S, 286.5 ±87.7; VOO, 159.6 ± 58.9; Bch, 317.2 ± 31.6).

3.3. Glucagon-Like-Peptide-1 and Dipeptidyl-Peptidase- 4 Activity

Though significant differences were not observed in circulating GLP-1 levels between the groups (Figure 1I: S, 4.3 ± 1.0 pmol/L; VOO, 6.0 ± 0.7 pmol/L; Bch, 7.4 ± 1.3 pmol/L), the hepatic DPP4 family activity (Figure 1J–K) was significantly higher in the high fat diets than in the control group. Namely, the hepatic membrane-bound fraction showed the significantly highest values in the VOO-fed rats compared with the S and Bch groups. (Figure 1K: S, 5.0 ± 0.5 pmol ($\times 10^2$)/min/mg protein; VOO, 7.8 ± 0.8 pmol ($\times 10^2$)/min/mg protein; Bch, 7.0 ± 0.4 pmol ($\times 10^2$)/min/mg protein) (Figure 1L: S, 0.8 ± 0.1 pmol ($\times 10^2$)/min/mg protein; VOO, 1.4 ± 0.2 pmol ($\times 10^2$)/min/mg protein).

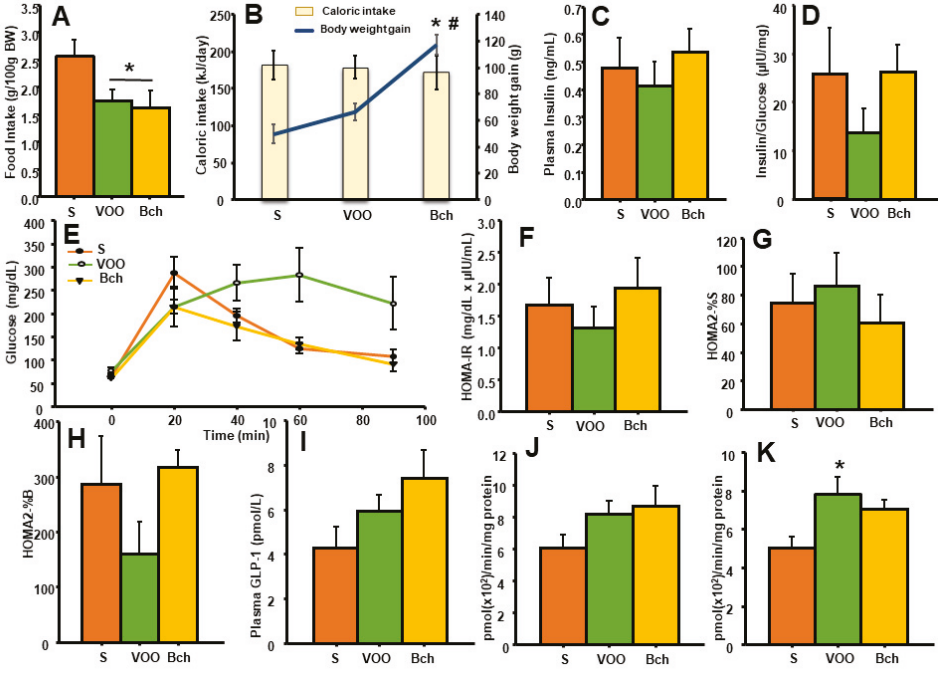

Figure 1. Means values ± standard errors of daily food intake, expressed as g/100 g Body Weight (**A**); the intake of energy, expressed as kJ/day and total body weight gain, expressed as g (**B**); values of plasma fasting insulin, expressed as ng/mL (**C**); ratio of plasma fasting insulin/glucose, expressed as µIU/mg (**D**); values of glucose during test tolerance (GTT), expressed as mg/dL (**E**); homeostasis model of insulin resistance (HOMA-IR), expressed as mg/dL x µIU/mL (**F**); an index for estimating sensitivity to insulin (% insulin sensitivity) (HOMA2-%S) (**G**); an index of insulin secretion and a valuation of β-cell usefulness (% β-cell secretion) (HOMA2%B) (**H**); plasma glucagon-like peptide 1 (GLP-1), expressed as pmol/L (**I**); and dipeptidyl-peptidase 4 (DPP4) activity in the liver-soluble fraction (**J**) and membrane-bound fraction (**K**), expressed as pmol/min/mg prot. S: standard diet, VOO: virgin olive oil diet, Bch: butter plus cholesterol diet. * indicates significant differences between VOO or Bch vs. S, * $p < 0.05$. # indicates significant differences between VOO and Bch, # $p < 0.05$.

3.4. Hepatic TRH-Degrading Pyroglutamate Aminopeptidase Activity and Tyrosine Aminopeptidase Activity

Previous studies have demonstrated that the effects of thyroid status on hepatic pGluAP and the release of endogenous peptides as cyclo His-Pro (cHP) are determinant in insulin sensitivity and body weight control [56,57]. In our results, HFDs significantly increased the soluble pGluAP activity in the liver (Figure 2A: S, 1.0 ± 0.1 pmol (×10^2)/min/mg protein; VOO, 1.5 ± 0.0 pmol (×10^2)/min/mg protein; Bch, 1.4 ± 0.0 pmol (×10^2)/min/mg protein). However, no differences were found in membrane-bound activity (Figure 2B).

On the other hand, enkephalins have been widely implicated in feeding behavior, and these endogenous opioid peptides are hydrolyzed by the tyrosine aminopeptidase activity (TyrAP). Our results showed higher levels of soluble tyrosyl aminopeptidase activity in the liver of rats that were fed with the Bch diet (Figure 2: S, 3.9 ± 0.5 pmol (×10^2)/min/mg protein; VOO, 4.5 ± 0.3 pmol (×10^2)/min/mg protein; Bch, 6.2 ± 0.5 pmol (×10^2)/min/mg protein), but no significant differences were found in the membrane-bound fraction.

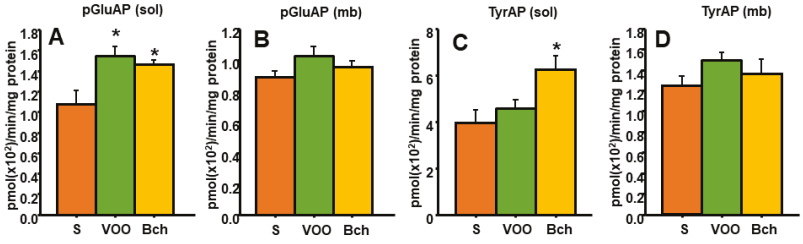

Figure 2. Means values ± standard errors of pyroglutamyl aminopeptidase activity (pGluAP) in liver-soluble (**A**) and membrane-bound (**B**) fractions, and tyrosine aminopeptidase activity (TyrAP) in liver-soluble (**C**) and membrane-bound (**D**) fractions, expressed as pmol/min/mg prot. S: standard diet, VOO: virgin olive oil diet, Bch: butter plus cholesterol diet. * indicates significant differences between VOO or Bch vs. S. * p <0.05.

3.5. Hepatic Angiotensinases Activities

Figure 3 shows the metabolism of angiotensin peptides in the local renin–angiotensin system, as well as the role of several aminopeptidases activities in soluble and membrane-bound fractions (AspAP, GluAP, AlaAP and CysAP/IRAP). Significant differences were not observed in soluble or membrane-bound fractions for aspartyl and glutamyl aminopeptidase activities between the diets (Figure 3B–E). However, the VOO diet significantly increased the activity of alanyl aminopeptidase activity (Figure 3G: S, 1.2 ± 0.1 pmol (×10^2)/min/mg protein; VOO, 2.4 ± 0.2 pmol (×10^2)/min/mg protein; Bch, 1.6 ± 0.2 pmol (×10^2)/min/mg protein) and cystinyl aminopeptidase activity (Figure 3I: S, 1.9 ± 0.3 pmol (×10^2)/min/mg protein; VOO: 3.9 ± 0.2 pmol (×10^2)/min/mg protein; Bch: 2.7 ± 0.4 pmol (×10^2)/min/mg protein) in the liver membrane-bound fraction.

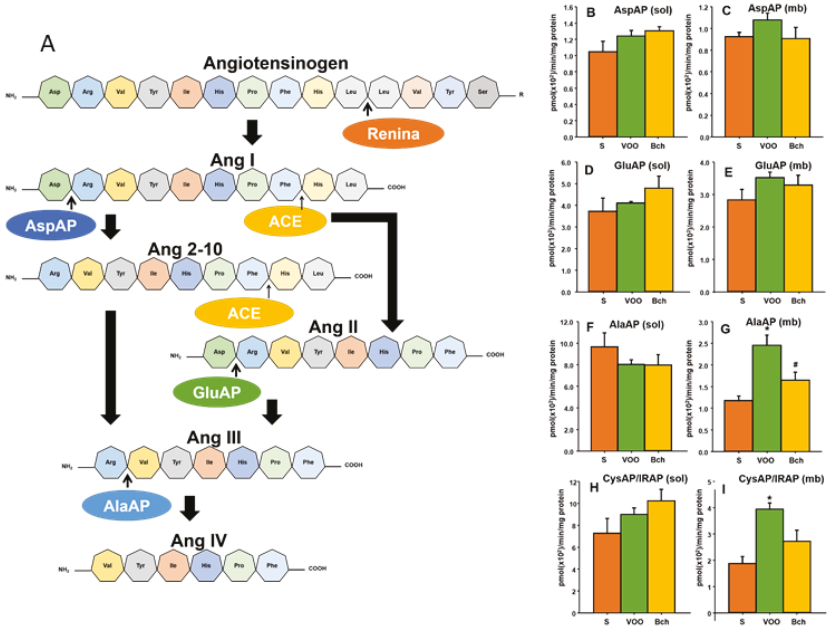

Figure 3. Partial representation of the renin–angiotensin system that shows the metabolic steps in which angiotensinase activities are involved (**A**); means values ± standard errors of aspartyl aminopeptidase activity (AspAP) in liver-soluble (**B**) and membrane-bound (**C**) fractions; glutamyl aminopeptidase

activity (GluAP) in liver-soluble (**D**) and membrane-bound (**E**) fractions; alanyl aminopeptidase activity (AlaAP) in liver-soluble (**F**) and membrane-bound (**G**) fractions; and cystinyl aminopeptidase activity (CysAP) in liver-soluble (**H**) and membrane-bound (**I**) fractions expressed as pmol/min/mg prot. S: standard diet, VOO: virgin olive oil diet, Bch: butter plus cholesterol diet. * indicates significant differences between VOO or Bch vs. S, * $p < 0.05$. # indicates significant differences between VOO and Bch, # $p < 0.05$. ACE: angiotensin converting enzyme; IRAP: insulin regulated aminopeptidase.

3.6. Leucine Aminopeptidase and Gamma Glutamyl Transferase

Several indicators of hepatic function, such as GGT and leucine aminopeptidase (LeuAP), were evaluated (Figure 4A–E). The butter plus cholesterol diet significantly increased hepatic membrane-bound GGT activity compared with the S and VOO diets (Figure 4B: S, 0.8 ± 0.0 pmol ($\times 10^2$)/min/mg protein; VOO, 09 ± 0.0 pmol ($\times 10^2$)/min/mg protein; Bch, 1.2 ± 0.1 pmol ($\times 10^2$)/min/mg protein). Furthermore, a significant relationship was established between GGT membrane-bound activity and the plasma lipid profile (total triglyceride) (Figure 4C).

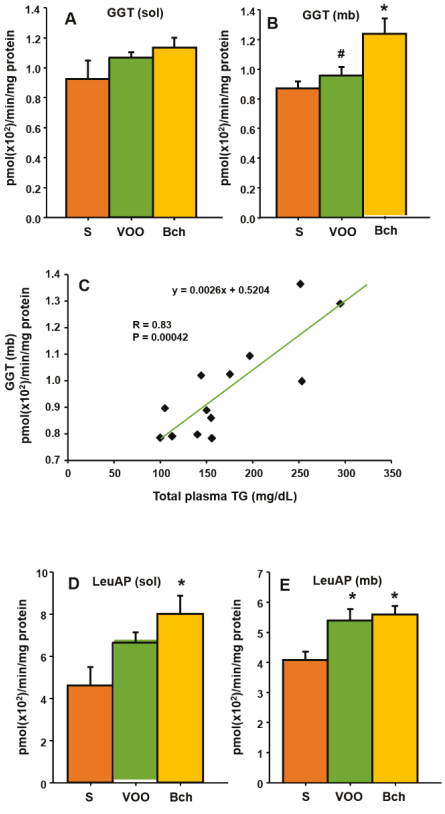

Figure 4. Means values ± standard errors of gamma glutamyl transferase activity (GGT) in liver-soluble (**A**) and membrane-bound (**B**) fractions, expressed as pmol/min/mg prot., linear regressions established between GGT and plasma triglycerides (TG) (**C**); and leucyl aminopeptidase activity (LeuAP) in liver-soluble (**D**) and membrane-bound (**E**) fractions, expressed as pmol/min/mg prot. S: standard diet, VOO: virgin olive oil diet, Bch: butter plus cholesterol diet. * indicates significant differences between VOO or Bch vs. S, * $p < 0.05$. # indicates significant differences between VOO and Bch, # $p < 0.05$.

Soluble LeuAP activity also increased in the Bch group (Figure 4D: S, 4.6 ± 0.8 pmol ($\times 10^2$)/min/mg protein; VOO, 6.6 ± 0.4 pmol ($\times 10^2$)/min/mg protein; Bch, 7.9 ± 0.8 pmol ($\times 10^2$)/min/mg protein), whereas membrane-bound LeuAP activity was higher in the two HFDs (Figure 4E: 4.0 ± 0.2 pmol ($\times 10^2$)/min/mg protein; VOO, 5.3 ± 0.3 pmol ($\times 10^2$)/min/mg protein; Bch, 5.5 ± 0.2 pmol ($\times 10^2$)/min/mg protein).

3.7. Plasma Nitric Oxide (NO) and Hepatic Inducible NO Synthase (iNOS)

In order to investigate the effects of HFDs on oxidative stress, the expression of hepatic iNOS was determined by using a Western blot assay (Figure 5A,B), and the plasma NO concentrations (NOx) were measured by the conversion of nitrate (NO3-) in to nitrite (NO2-) by nitrate reductase (Figure 5C). The Bch-fed rats exhibited a significant increase in iNOS expression (Figure 5B: S, 1.0 ± 0.2; VOO, 1.3 ± 0.1; Bch: 2.3 ± 0.5). Moreover, the concentration NOx was significantly higher in the Bch group compared with the S and VOO groups. Interestingly, the VOO group showed lower NOx levels than the S group (Figure 5C: S, 1.4 ± 0.1 µmol/L; VOO, 0.9 ± 0.0 µmol/L; Bch, 2.1 ± 0.2 µmol/L).

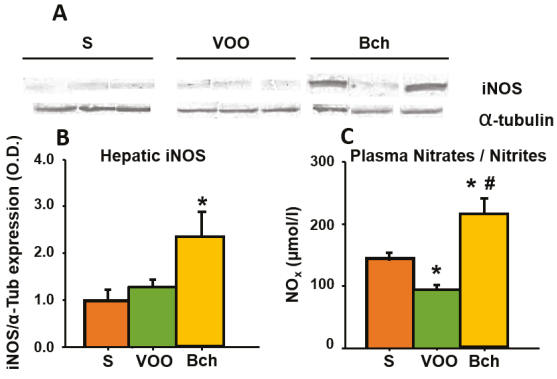

Figure 5. Hepatic inducible nitric oxide synthase (iNOS) measured by using by immunoblots (**A**), mean ±standard error of expression levels of iNOS that were quantified and normalized by the expression of α1-tubulin (**B**), and plasma NOx (NO2- and NO3-) concentration expressed as µmol/L (**C**). S: standard diet, VOO: virgin olive oil diet, Bch: butter plus cholesterol diet. * indicates significant differences between VOO or Bch vs. S, * $p < 0.05$. # indicates significant differences between VOO and Bch, # $p < 0.05$.

4. Discussion

High fat diets have demonstrated the ability to be a good model of obesity and metabolic syndrome in laboratory animals models [6–8,56,58,59]. However, the efficiency in the use of energy also influences the development of obesity in rodents. A study by Liu [7] demonstrated that obesity development was influenced by gender and the efficiency in the use of energy. In the current study, the animals were fed with two isoenergetic HFDs but with different degree of saturation in their fatty acids (mainly monounsaturated in the VOO group and saturated in the Bch group) and minor components (polyphenols in the VOO group and cholesterol in the Bch group). While the Bch animals achieved a significantly higher body weight than the control group, the VOO rats did not show significant differences with the control group (data not shown). Nevertheless, the greater gain of body weight in the Bch rats were not associated with a higher food intake. Indeed, daily food intakes (g/100g BW) were lower in the two HFDs at the end of the experimental period.

Regardless of the energetic-density of the diet, animals are usually able to adapt their food intake and get the same amount of energy [60]. The differences in body weight gain between the HFDs may be explained by the fact that saturated fatty acids show higher levels of energetic efficiency and are

able to decrease the mitochondrial oxidative capacity in the liver and the skeletal muscle [61]. However, the inclusion of VOO in the diet seems to have beneficial effects on body weight control [62,63], increase diet-induced thermogenesis [64], regulate UCP1 (uncoupling protein 1) expression in the adipose tissue [65], and enhance thermogenesis by increasing the UCP1 content in brown adipose tissue and increasing noradrenaline and adrenaline secretions [66]. These results suggest that the unsaturated dietary fatty acids and the quantity of dietary fat may have a significant effect on the regulation of thermogenic conditions. At the same time, these effects could be related to the polyphenols present in VOO [13,67].

The differences in final body weight do not seem to be associated with altered values of fasting plasma glucose and insulin in the three groups of animals. Nevertheless, our results showed differences in the intraperitoneal glucose tolerance test (GTT). During the GTT, the higher levels of plasma glucose were reached at 20 min after i.p. injection in the S and Bch groups. However, in VOO animals, the maximum values were delayed until 90 min after i.p. injection, and they remained high at 120 min. These results contradict with previous works [7,8,60], but the different index of insulin resistant that was calculated in our animals (HOMA-IR, HOMA-%S and HOMA-%B) were similar in the three diets. Still, mean values of fasting insulin/glucose and the HOMA2-%b were lower in the VOO group.

In the fed (postprandial) state, GLP-1 peptide has the ability to stimulate insulin secretion and the synthesis of glycogen in the liver, thus reducing postprandial hyperglycemia. On the other hand, the physiological inhibitory control of GLP-1 on gastric emptying and its contribution to the regulation of food intake and satiety suggests that impaired secretion and/or activity of GLP-1 may be involved in the pathogenesis of obesity. A previous study indicated that, in morbid obesity, the faster inactivation of circulating GLP-1 could result in lower plasma levels of this peptide and could contribute to eating behavior abnormalities [23]. Plasma DPP4 activity is the main factor that is implicated in the metabolism of GLP-1, as well as its main regulator [23,68]. In the present study, an increase of the hepatic DPP4 family activity was only found in the VOO-fed rats, even if no differences in fasting plasma GLP-1 levels were obtained between the three diets, probably because of the rapid inactivation of this peptide. Nevertheless, the high DPP4 activity in the VOO animals could have been related to high postprandial GLP-1 levels, which in agreement with other previous works [17,69,70]. During the GTT, the stimulation of the intestinal L cell did not take place, explaining the higher glucose values in the VOO group.

In addition to GLP-1, another peptide with important antidiabetic role able to improve insulin sensitivity and body weight control is cyclo-histidine-proline (cHP) [43,71]. Cyclo-histidine-proline can be found in hepatic cells [42,57], and it is a metabolic product of TRH by the activity of pyroglutamate aminopeptidase (pGluAP) [57].

The role of pGluAP and cHP in the obesity is not yet clear, but cHP plus zinc is effective in decreasing blood glucose concentrations in genetically obese (*ob*/*ob*), type 2 diabetic mice [72]. Moreover, it has been reported that HFDs raise TRH expression [73] and alter pGluAP activity, effects that seem to depend on the fat source [44]. Our results indicated that HFDs induced changes in hepatic TRH metabolism, increasing the pGluAP activity in the soluble fraction of liver, with the consequence of the overproduction of cHP.

Several orexigenic peptides, such as enkephalins (ENK), are able to modify the intake behavior and the energy metabolism in animals [48,49]. A high fat diet changes the hypothalamic expression of this peptide, increases the propensity to overeat, the gain of body weight, and the excess of white adipose tissue [48]. Enkephalin concentration changes in the hepatic tissue and plasma during liver disorders [47], and the liver cells can express Met-ENK immunoreactivity, suggesting that ENK is an endogenous opioid that is produced by the liver [74]. Ours results suggest an increase in soluble tyrosyl aminopeptidase activity (TyrAP), which was implicated in the degradation of ENK in the livers of the Bch group, which could have been related to the differences in food intake and body weight gain in these animals. In fact, ENK was recently proposed as a potential therapeutic peptide for HFD-induced obesity and metabolic disorders [75].

The renin–angiotensin system (RAS) is an important regulator of blood pressure and water balance. Beside the RAS, other local systems have been described in several tissues, including

the liver [24,74,76,77]. Changes in the balance of different angiotensin bioactive peptides (AngII, AngIII, AngIV, Ang2-10, and Ang1-7) have been implicated in different chronic diseases, such as liver fibrosis, portal hypertension, hepatic tumors [37,78,79], and metabolic alterations, whereas the blocking of angiotensin receptors has been shown to improve glycemic control and reduce hepatic triglyceride levels [80]. The relative amounts of angiotensines are regulated by the activity of several aminopeptidases, namely angiotensinases (Figure 3A). It is known that these activities are modulated by dietary fat [5,29,30,54,81,82]. Previous results have demonstrated that liver angiotensinases are altered by the thyroid status [83] and obesity [84,85]. The present results confirm the effect of a diet that is enriched with virgin olive oil on liver aminopeptidase activity, increasing the activity of alanyl and cystinyl aminopeptidase. Alanyl aminopeptidase (angiotensinase M) is implicated in the metabolism of AngIII to AngIV [86], whereas cystinyl aminopeptidase (IRAP/AT4) has been described as the insulin regulated aminopeptidase (IRAP) and also as the specific receptor to bind AngIV [83,85,87,88]. This result could indicate an increase of local levels of AngIV, the peptide that binds to the AT4 receptor that is colocalized with the glucose transporter GluT4 [27]. These changes were observed in the membrane-bound fraction, which suggest a more specific functional role for these enzymes [87].

Otherwise, the diet that was enriched with butter and cholesterol increased peptidase activities that have been widely proposed as hepatic biomarkers (GGT and LeuAP) [89,90]. Moreover, the activity levels of the GGT in the liver were significant and positively correlated with plasma triglycerides and total cholesterol. It has been reported that HFDs significantly increased GGT activity, whereas antioxidants (vitamin E) and hypocaloric diets decreased GGT levels [91,92]. Published data have shown that HFDs are the major triggers for oxidative stress [92], and both the cytoprotective role of NO in the liver and hepatic iNOS expression could be an adaptive response to minimize inflammatory injury, hepatic tumor, and cirrhosis [60]. Recently, studies that treated non-alcoholic fatty liver disease (NAFLD) showed that the hepatic expression of iNOS was markedly increased in HFD-fed mice [40,93]. In our results, only animals that were fed with the Bch diet significantly increased the plasmatic levels of nitrate, nitrites, and iNOS expression in the liver, probably as a response to the oxidative stress damage. The main effects of HFDs on peptidase activities are summarized in Figure 6.

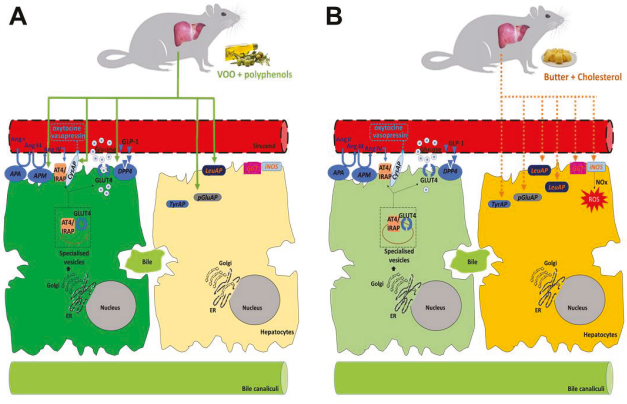

Figure 6. Schematic diagram modeling the role of the high-fat diets (HFDs) that are associated with changes in hepatic peptidases activities. (**A**) The virgin olive oil diet increased the hepatic aminopeptidase activities that are related to glucose metabolism (membrane-bound dipeptidyl peptidase 4 (DPP4), angiotensinase M (Alanine aminopeptidase), insulin-regulated-aminopeptidase (IRAP)/CysAP). (**B**) The butter plus cholesterol diet (Bch) increased soluble and/or membrane-bound activities that are implicated in the control of food intake (tyrosine aminopeptidase (TyrAP)), markers of hepatic damage (leucine aminopeptidase (LeuAP) and gamma glutamyl transferase (GGT)), and the expression of hepatic iNOS, which is involved the reactive oxidative stress (ROS) pathway and induces an increase of plasmatic nitrogen oxides (NOx) levels.

5. Conclusions

In conclusion, these results demonstrate that the metabolic response to a high fat diet that is enriched with different fat sources could be related to changes in hepatic peptidases that are implicated in the regulation of glucose metabolism and oxidative stress. The diet that was supplemented with butter plus cholesterol altered peptidases activities that are associated with the impaired in the control of food intake and hepatic damage, and it increased body weight. However, the diet that was supplemented with virgin olive oil affected peptidases that are involved in glucose homeostasis (DPP4 and angiotensinases), but it did not alter body weight. Taken together, these results support the beneficial effect of virgin olive oil on energy metabolism and body weight control. Further studies should be performed in order to analyze the expression of key enzymes in fatty acids metabolism, and its relation to peptidase activities.

Supplementary Materials: The following are available online at http://www.mdpi.com/2072-6643/12/3/636/s1, Table S1: Composition of diets; Table S2: Substrates for Aminopeptidases incubation media; Table S3: Antibodies used for Western-blotting.

Author Contributions: Conceptualization: G.D.-V., A.B.S. and I.P.; Data curation: G.D.-V. and A.B.S.; Funding acquisition: M.R.-S. and I.P.; Investigation: G.D.-V., A.B.S. and I.P.; Methodology: G.D.-V. and A.B.S.; Project administration: M.R.-S. and I.P.; Supervision: M.R.-S.; Writing—Original draft: G.D.-V. and I.P. Writing—Review & editing: G.D.-V., M.R.-S. and I.P. All authors have read and agreed to the published version of the manuscript.

Funding: This work was supported by grant code: ACCIÓN 1 PAIUJA 2019 2020: BIO221.

Acknowledgments: Technical and human support provided by CICT and CEPA of Universidad de Jaén (UJA, MINECO, Junta de Andalucía; FEDER) is gratefully acknowledged.

Conflicts of Interest: The authors declare no conflict of interest.

References

1. Guyenet, S.J.; Schwartz, M.W. Regulation of Food Intake, Energy Balance, and Body Fat Mass: Implications for the Pathogenesis and Treatment of Obesity. *J. Clin. Endocrinol. Metab.* **2012**, *97*, 745–755. [CrossRef]
2. Eckel, R.H.; Grundy, S.M.; Zimmet, P.Z. The metabolic syndrome. *Lancet* **2005**, *365*, 1415–1428. [CrossRef]
3. Pi-Sunyer, F.X. The Obesity Epidemic: Pathophysiology and Consequences of Obesity. *Obes. Res.* **2002**, *10*, 97S–104S. [CrossRef]
4. Hariri, N.; Thibault, L. High-fat diet-induced obesity in animal models. *Nutr. Res. Rev.* **2010**, *23*, 270–299. [CrossRef]
5. Villarejo, A.; Ramírez-Sánchez, M.; Segarra, A.B.; Martínez-Cañamero, M.; Prieto, I. Influence of Extra Virgin Olive Oil on Blood Pressure and Kidney Angiotensinase Activities in Spontaneously Hypertensive Rats. *Planta Medica* **2015**, *81*, 664–669. [CrossRef]
6. Gao, M.; Ma, Y.; Liu, D. High-Fat Diet-Induced Adiposity, Adipose Inflammation, Hepatic Steatosis and Hyperinsulinemia in Outbred CD-1 Mice. *PLoS ONE* **2015**, *10*, e0119784. [CrossRef]
7. Liu, X.J.; Wang, B.W.; Zhang, C.; Xia, M.Z.; Chen, Y.H.; Hu, C.Q.; Wang, H.; Chen, X.; Xu, D.X. Vitamin D Deficiency Attenuates High-Fat Diet-Induced Hyperinsulinemia and Hepatic Lipid Accumulation in Male Mice. *Endocrinology* **2015**, *156*, 2103–2113. [CrossRef]
8. Jiang, B.; Le, L.; Wan, W.; Zhai, W.; Hu, K.; Xu, L.; Xiao, P. The Flower Tea Coreopsis tinctoria Increases Insulin Sensitivity and Regulates Hepatic Metabolism in Rats Fed a High-Fat Diet. *Endocrinology* **2015**, *156*, 2006–2018. [CrossRef]
9. Carnevale, R.; Silvestri, R.; Loffredo, L.; Novo, M.; Cammisotto, V.; Castellani, V.; Bartimoccia, S.; Nocella, C.; Violi, F. Oleuropein, a component of extra virgin olive oil, lowers postprandial glycaemia in healthy subjects. *BJCP* **2018**, *84*, 1566–1574. [CrossRef]
10. Domínguez-Vías, G.; Segarra, A.; Martínez-Cañamero, M.; Ramírez-Sánchez, M.; Prieto, I. Influence of a virgin olive oil versus butter plus cholesterol-enriched diet on testicular enzymatic activities in adult male rats. *Int. J. Mol. Sci.* **2017**, *18*, 1701. [CrossRef]
11. Martínez, N.; Prieto, I.; Hidalgo, M.; Segarra, A.B.; Martínez-Rodríguez, A.; Cobo, A.; Ramírez, M.; Gálvez, A.; Martínez-Cañamero, M. Refined versus Extra Virgin Olive Oil High-Fat Diet Impact on Intestinal Microbiota of Mice and Its Relation to Different Physiological Variables. *Microorganisms* **2019**, *7*, 61. [CrossRef]

12. Nocella, C.; Cammisotto, V.; Fianchini, L.; D'Amico, A.; Novo, M.; Castellani, V.; Stefanini, L.; Violi, F.; Carnevale, R. Extra Virgin Olive Oil and Cardiovascular Diseases: Benefits for Human Health. *Endocr. Metab. Immune* **2017**, *18*, 4–13. [CrossRef]
13. Prieto, I.; Hidalgo, M.; Segarra, A.B.; Martínez-Rodríguez, A.M.; Cobo, A.; Ramírez, M.; Abriouel, H.; Gálvez, A.; Martínez-Cañamero, M. Influence of a diet enriched with virgin olive oil or butter on mouse gut microbiota and its correlation to physiological and biochemical parameters related to metabolic syndrome. *PLoS ONE* **2018**, *13*, e0190368. [CrossRef]
14. Romani, A.; Ieri, F.; Urciuoli, S.; Noce, A.; Marrone, G.; Nediani, C.; Bernini, R. Health Effects of Phenolic Compounds Found in Extra-Virgin Olive Oil, By-Products, and Leaf of *Olea europaea* L. *Nutrients* **2019**, *11*, 1776. [CrossRef]
15. Yubero-Serrano, E.M.; Lopez-Moreno, J.; Gomez-Delgado, F.; Lopez-Miranda, J. Extra virgin olive oil: More than a healthy fat. *Eur. J. Clin. Nutr.* **2019**, *72*, 8–17. [CrossRef]
16. Elias, S.; Wisam, S.; Luai, A.; Massad, B.; Nimer, A. Lipotoxicity in Obesity: Benefit of Olive Oil. *Adv. Exp. Med. Biol.* **2017**, *960*, 607–617. [CrossRef]
17. Prieto, P.; Cancelas, J.; Villanueva-Peñacarrillo, M.; Valverde, I.; Malaisse, W. Effects of an olive oil-enriched diet on plasma GLP-1 concentration and intestinal content, plasma insulin concentration, and glucose tolerance in normal rats. *Endocrine* **2005**, *26*, 107–115. [CrossRef] [PubMed]
18. Nauck, M.; Homberger, E.; Siegel, E.G.; Allen, R.C.; Eaton, R.P.; Ebert, R.; Creutzfeldt, W. Incretin Effects of Increasing Glucose Loads in Man Calculated from Venous Insulin and C-Peptide Responses*. *J. Clin. Endocrinol. Metab.* **1986**, *63*, 492–498. [CrossRef] [PubMed]
19. Nauck, M.; Stöckmann, F.; Ebert, R.; Creutzfeldt, W. Reduced incretin effect in type 2 (non-insulin-dependent) diabetes. *Diabetologia* **1986**, *29*, 46–52. [CrossRef] [PubMed]
20. Lovshin, J.A.; Drucker, D.J. Incretin-based therapies for type 2 diabetes mellitus. *Nat. Rev. Endocrinol.* **2009**, *5*, 262–269. [CrossRef] [PubMed]
21. Hare, K.J.; Vilsbøll, T.; Asmar, M.; Deacon, C.F.; Knop, F.K.; Holst, J.J. The glucagonostatic and insulinotropic effects of glucagon-like peptide 1 contribute equally to its glucose-lowering action. *Diabetes* **2010**, *59*, 1765–1770. [CrossRef]
22. Mentlein, R.; Gallwitz, B.; Schmidt, W.E. Dipeptidyl-peptidase IV hydrolyses gastric inhibitory polypeptide, glucagon-like peptide-1(7-36)amide, peptide histidine methionine and is responsible for their degradation in human serum. *Eur. J. Biochem.* **1993**, *214*, 829–835. [CrossRef]
23. Lugari, R.; Cas, A.D.; Ugolotti, D.; Barilli, A.L.; Camellini, C.; Ganzerla, G.C.; Luciani, A.; Salerni, B.; Mitternperger, F.; Nodari, S.; et al. Glucagon-like Peptide 1 (GLP-1) Secretion and Plasma Dipeptidyl Peptidase IV (DPP-IV) Activity in Morbidly Obese Patients Undergoing Biliopancreatic Diversion. *Horm. Metab. Res.* **2004**, *36*, 111–115. [CrossRef]
24. Barrett, A.J.; Rawlings, N.D.; Woessner, J.F. *Handbook of Proteolytic Enzymes*; Elsevier Academic Press: Amsterdam, The Netherlands, 2004.
25. de Gasparo, M.; Whitebread, S.; Bottari, S.P.; Levens, N.R. Heterogeneity of Angiotensin Receptor Subtypes. In *Medicinal Chemistry of the Renin-Angiotensin System*; Pbmwm, T., Wexler, R.R., Eds.; Elsevier: Amsterdam, The Netherlands, 1994; pp. 269–294.
26. García-Sáinz, J.A.; Martínez-Alfaro, M.; Romero-Avila, M.T.; González-Espinosa, C. Characterization of the AT1 angiotensin II receptor expressed in guinea pig liver. *J. Endocrinol.* **1997**, *154*, 133–138. [CrossRef]
27. Chai, S.Y.; Fernando, R.; Peck, G.; Ye, S.Y.; Mendelsohn, F.A.O.; Jenkins, T.A.; Albiston, A.L. What's new in the renin-angiotensin system? The angiotensin IV/AT4 receptor. *Cell. Mol. Life Sci.* **2004**, *61*, 2728–2737. [CrossRef]
28. Coleman, J.K.; Krebs, L.T.; Hamilton, T.A.; Ong, B.; Lawrence, K.A.; Sardinia, M.F.; Harding, J.W.; Wright, J.W. Autoradiographic identification of kidney angiotensin IV binding sites and angiotensin IV-induced renal cortical blood flow changes in rats. *Peptides* **1998**, *19*, 269–277. [CrossRef]
29. Segarra, A.B.; Ramirez, M.; Banegas, I.; Alba, F.; Vives, F.; de Gasparo, M.; Ortega, E.; Ruiz, E.; Prieto, I. Dietary Fat Influences Testosterone, Cholesterol, Aminopeptidase A, and Blood Pressure in Male Rats. *Horm. Metab. Res.* **2008**, *40*, 289–291. [CrossRef]

30. Segarra, A.B.; Ruiz-Sanz, J.I.; Ruiz-Larrea, M.B.; Ramírez-Sánchez, M.; de Gasparo, M.; Banegas, I.; Martínez-Cañamero, M.; Vives, F.; Prieto, I. The Profile of Fatty Acids in Frontal Cortex of Rats Depends on the Type of Fat Used in the Diet and Correlates with Neuropeptidase Activities. *Horm. Metab. Res.* **2011**, *43*, 86–91. [CrossRef]
31. de Macêdo, S.M.; Antunes-Guimarães, T.; Feltenberger, J.D.; Santos, S.H.S. The role of renin-angiotensin system modulation on treatment and prevention of liver diseases. *Peptides* **2014**, *62*, 189–196. [CrossRef]
32. Afroze, S.H.; Munshi, M.K.; Martínez, A.K.; Uddin, M.; Gergely, M.; Szynkarski, C.; Guerrier, M.; Nizamutdinov, D.; Dostal, D.; Glaser, S. Activation of the renin-angiotensin system stimulates biliary hyperplasia during cholestasis induced by extrahepatic bile duct ligation. *Am. J. Physiol. Gastrointest. Liver Physiol.* **2015**, *308*, G691–G701. [CrossRef]
33. Hayden, M.R.; Sowers, K.M.; Pulakat, L.; Joginpally, T.; Krueger, B.; Whaley-Connell, A.; Sowers, J.R. Possible Mechanisms of Local Tissue Renin-Angiotensin System Activation in the Cardiorenal Metabolic Syndrome and Type 2 Diabetes Mellitus. *Cardiorenal Med.* **2011**, *1*, 193–210. [CrossRef]
34. Takeshita, Y.; Takamura, T.; Ando, H.; Hamaguchi, E.; Takazakura, A.; Matsuzawa-Nagata, N.; Kaneko, S. Cross talk of tumor necrosis factor-alpha and the renin-angiotensin system in tumor necrosis factor-alpha-induced plasminogen activator inhibitor-1 production from hepatocytes. *Eur. J. Pharmacol.* **2008**, *579*, 426–432. [CrossRef]
35. Orlic, L.; Mikolasevic, I.; Lukenda, V.; Anic, K.; Jelic, I.; Racki, S. Nonalcoholic fatty liver disease and the renin-angiotensin system blockers in the patients with chronic kidney disease. *Wien. Klin. Wochenschr.* **2015**, *127*, 355–362. [CrossRef]
36. Tao, X.R.; Rong, J.B.; Lu, H.S.; Daugherty, A.; Shi, P.; Ke, C.L.; Zhang, Z.C.; Xu, Y.C.; Wang, J.A. Angiotensinogen in hepatocytes contributes to Western diet-induced liver steatosis. *J. Lipid Res.* **2019**, *60*, 1983–1995. [CrossRef]
37. Sansoè, G.; Aragno, M.; Wong, F. Pathways of hepatic and renal damage through non-classical activation of the renin-angiotensin system in chronic liver disease. *Liver Int.* **2019**, *40*, 18–31. [CrossRef]
38. Valko, M.; Leibfritz, D.; Moncol, J.; Cronin, M.T.; Mazur, M.; Telser, J. Free radicals and antioxidants in normal physiological functions and human disease. *Int. J. Biochem. Cell Biol.* **2007**, *39*, 44–84. [CrossRef]
39. Abbas, A.; Sakr, H.F. Simvastatin and vitamin E effects on cardiac and hepatic oxidative stress in rats fed on high fat diet. *J. Physiol. Biochem.* **2013**, *69*, 737–750. [CrossRef]
40. Pan, X.; Wang, P.; Luo, J.; Wang, Z.; Song, Y.; Ye, J.; Hou, X. Adipogenic changes of hepatocytes in a high-fat diet-induced fatty liver mice model and non-alcoholic fatty liver disease patients. *Endocrine* **2015**, *48*, 834–847. [CrossRef]
41. Taylor, B.S.; Alarcon, L.H.; Billiar, T.R. Inducible nitric oxide synthase in the liver: Regulation and function. *Biochemistry* **1998**, *63*, 766–781.
42. Scharfmann, R.; Aratan-Spire, S. Ontogeny of two topologically distinct TRH-degrading pyroglutamate aminopeptidase activities in the rat liver. *Regul. Pept.* **1991**, *32*, 75–83. [CrossRef]
43. Ra, K.S.; Suh, H.J.; Choi, J.W. Hypoglycemic effects of Cyclo (His-Pro) in streptozotocin-induced diabetic rats. *Biotechnol. Bioproc. E* **2012**, *17*, 176–184. [CrossRef]
44. Arechaga, G.; Prieto, I.; Segarra, A.B.; Alba, F.; Ruiz-Larrea, M.B.; Ruiz-Sanz, J.I.; de Gasparo, M.; Ramirez, M. Dietary fatty acid composition affects aminopeptidase activities in the testes of mice. *Int. J. Androl.* **2002**, *25*, 113–118. [CrossRef]
45. Mendez, I.A.; Ostlund, S.B.; Maidment, N.T.; Murphy, N.P. Involvement of Endogenous Enkephalins and β-Endorphin in Feeding and Diet-Induced Obesity. *Neuropsychopharmacology* **2015**, *40*, 2103–2112. [CrossRef]
46. Cieśla, A.; Mach, T.; Pierzchała-Koziec, K.; Skwara, P.; Szczepański, W. Met-enkephalin in the liver as a marker of hepatocellular damage in chronic viral hepatitis type B and C. *Adv. Med. Sci. Poland* **2006**, *51*, 261–264.
47. Owczarek, D.; Garlicka, M.; Pierzchała-Koziec, K.; Skulina, D.; Szulewski, P. Met-enkephalin plasma concentration and content in liver tissue in patients with primary biliary cirrhosis. *Przegl. Lek.* **2003**, *60*, 461–466.
48. Karatayev, O.; Gaysinskaya, V.; Chang, G.Q.; Leibowitz, S.F. Circulating triglycerides after a high-fat meal: Predictor of increased caloric intake, orexigenic peptide expression, and dietary obesity. *Brain. Res.* **2009**, *1298*, 111–122. [CrossRef]

49. Hill-Pryor, C.; Dunbar, J.C. The Effect of High Fat-Induced Obesity on Cardiovascular and Physical Activity and Opioid Responsiveness in Conscious Rats. *Clin. Exp. Hypertens.* **2006**, *28*, 133–145. [CrossRef]
50. Fernández, D.; Valdivia, A.; Irazusta, J.; Ochoa, C.; Casis, L. Peptidase activities in human semen. *Peptides* **2002**, *23*, 461–468. [CrossRef]
51. HOMA2 Calculator: Overview. The Oxford Centre for diabetes endocrinoly and metabolism. Diabetes Trials Unit, HOMA Calculator. (n.d.). Available online: https://www.dtu.ox.ac.uk/homacalculator/ (accessed on 14 December 2019).
52. Alba, F.; Arenas, J.C.; Lopez, M.A. Properties of rat brain dipeptidyl aminopeptidases in the presence of detergents. *Peptides* **1995**, *16*, 325–329. [CrossRef]
53. Ramírez, M.; Prieto, I.; Banegas, I.; Segarra, A.B.; Alba, F. Neuropeptidases. *Methods Mol. Biol.* **2011**, *789*, 287–294. [CrossRef]
54. Segarra, A.B.; Arechaga, G.; Prieto, I.; Ramirez-Exposito, M.J.; Martinez-Martos, J.M.; Ramirez, M.; Alba, F.; Ruiz-Larrea, M.B.; Ruiz-Sanz, J.I. Effects of dietary supplementation with fish oil, lard, or coconut oil on oxytocinase activity in the testis of mice. *Arch. Androl.* **2002**, *48*, 233–236. [CrossRef] [PubMed]
55. Bradford, M.M. A rapid and sensitive method for the quantitation of microgram quantities of protein utilizing the principle of protein-dye binding. *Anal. Biochem.* **1976**, *72*, 248–254. [CrossRef]
56. Prasad, C.; Imrhan, V.; Juma, S.; Maziarz, M.; Prasad, A.; Tiernan, C.; Vijayagopal, P. Bioactive Plant Metabolites in the Management of Non-Communicable Metabolic Diseases: Looking at Opportunities beyond the Horizon. *Metabolites* **2015**, *5*, 733–765. [CrossRef]
57. Scharfmann, R.; Ebiou, J.; Morgat, J.; Aratan-Spire, S. Thyroid status regulates particulate but not soluble TRH-degrading pyroglutamate aminopeptidase activity in the rat liver. *Acta Endocrinol.* **1990**, *123*, 84–89. [CrossRef] [PubMed]
58. Boozer, C.N.; Schoenbach, G.; Atkinson, R.L. Dietary fat and adiposity: A dose-response relationship in adult male rats fed isocalorically. *Am. J. Physiol. Endocrinol. Metab.* **1995**, *268*, E546–E550. [CrossRef]
59. Ghibaudi, L.; Cook, J.; Farley, C.; van Heek, M.; Hwa, J.J. Fat Intake Affects Adiposity, Comorbidity Factors, and Energy Metabolism of Sprague-Dawley Rats. *Obes. Res.* **2002**, *10*, 956–963. [CrossRef]
60. Blundell, J.E.; Gillett, A. Control of Food Intake in the Obese. *Obes. Res.* **2001**, *9*, S263–S270. [CrossRef]
61. Iossa, S.; Lionetti, L.; Mollica, M.P.; Crescenzo, R.; Botta, M.; Barletta, A.; Liverini, G. Effect of high-fat feeding on metabolic efficiency and mitochondrial oxidative capacity in adult rats. *Br. J. Nutr.* **2003**, *90*, 953–960. [CrossRef]
62. Pérez-Martínez, P.; García-Ríos, A.; Delgado-Lista, J.; Pérez-Jiménez, F.; López-Miranda, J. Mediterranean diet rich in olive oil and obesity, metabolic syndrome and diabetes mellitus. *Curr. Pharm. Des.* **2011**, *17*, 769–777. [CrossRef]
63. Soriguer, F.; Almaraz, M.C.; Ruiz-de-Adana, M.S.; Esteva, I.; Linares, F.; García-Almeida, J.M.; Morcillo, S.; García-Escobar, E.; Olveira-Fuster, G.; Rojo-Martínez, G. Incidence of obesity is lower in persons who consume olive oil. *Eur. J. Clin. Nutr.* **2009**, *63*, 1371–1374. [CrossRef]
64. Polley, K.R.; Miller, M.K.; Johnson, M.; Vaughan, R.; Paton, C.M.; Cooper, J.A. Metabolic responses to high-fat diets rich in MUFA v. PUFA. *Br. J. Nutr.* **2018**, *120*, 13–22. [CrossRef]
65. Shin, S.; Ajuwon, K.M. Effects of Diets Differing in Composition of 18-C Fatty Acids on Adipose Tissue Thermogenic Gene Expression in Mice Fed High-Fat Diets. *Nutrients* **2018**, *10*, 256. [CrossRef] [PubMed]
66. Oi-Kano, Y.; Kawada, T.; Watanabe, T.; Koyama, F.; Watanabe, K.; Senbongi, R.; Iwai, K. Extra virgin olive oil increases uncoupling protein 1 content in brown adipose tissue and enhances noradrenaline and adrenaline secretions in rats. *J. Nutr. Biochem.* **2007**, *18*, 685–692. [CrossRef] [PubMed]
67. Castro-Barquero, S.; Lamuela-Raventós, R.M.; Doménech, M.; Estruch, R. Relationship between Mediterranean Dietary Polyphenol Intake and Obesity. *Nutrients* **2018**, *10*, 1523. [CrossRef] [PubMed]
68. Pérez-Durillo, F.; Segarra, A.B.; Villarejo, A.; Ramírez-Sánchez, M.; Prieto, I. Influence of Diet and Gender on Plasma DPP4 Activity and GLP-1 in Patients with Metabolic Syndrome: An Experimental Pilot Study. *Molecules* **2018**, *23*, 1564. [CrossRef]
69. Cancelas, J.; Prieto, P.G.; Villanueva-Peñacarrillo, M.L.; Valverde, I.; Malaisse, W.J. Effects of an olive oil-enriched diet on glucagon-like peptide 1 release and intestinal content, plasma insulin concentration, glucose tolerance and pancreatic insulin content in an animal model of type 2 diabetes. *Horm. Metab. Res.* **2006**, *38*, 98–105. [CrossRef]

70. Rocca, A.S.; LaGreca, J.; Kalitsky, J.; Brubaker, P.L. Monounsaturated fatty acid diets improve glycemic tolerance through increased secretion of glucagon-like peptide-1. *Endocrinology* **2001**, *142*, 1148–1155. [CrossRef]
71. Song, M.K.; Rosenthal, M.J.; Song, A.M.; Yang, H.; Ao, Y.; Yamaguchi, D.T. Raw vegetable food containing high cyclo (his-pro) improved insulin sensitivity and body weight control. *Metabolism* **2005**, *54*, 1480–1489. [CrossRef]
72. Hwang, I.K.; Go, V.L.W.; Harris, D.M.; Yip, I.; Kang, K.W.; Song, M.K. Effects of cyclo (his-pro) plus zinc on glucose metabolism in genetically diabetic obese mice. *Diabetes Obes. Metab.* **2003**, *5*, 317–324. [CrossRef]
73. Araujo, R.L.; Andrade, B.M.; Padrón, A.S.; Gaidhu, M.P.; Perry, R.L.S.; Carvalho, D.P.; Ceddia, R.B. High-Fat Diet Increases Thyrotropin and Oxygen Consumption without Altering Circulating 3,5,3′-Triiodothyronine (T3) and Thyroxine in Rats: The Role of Iodothyronine Deiodinases, Reverse T3 Production, and Whole-Body Fat Oxidation. *Endocrinology* **2010**, *151*, 3460–3469. [CrossRef]
74. Bergasa, N.V.; Boyella, V.D. Liver derived endogenous opioids may interfere with the therapeutic effect of interferon in chronic hepatitis C. *Med. Hypotheses* **2008**, *70*, 556–559. [CrossRef]
75. Suo, J.; Zhao, X.; Guo, X.; Zhao, X. Met-enkephalin improves metabolic syndrome in high fat diet challenged mice through promotion of adipose tissue browning. *Toxicol. Appl. Pharm.* **2018**, *359*, 12–23. [CrossRef] [PubMed]
76. Fukasawa, K.M.; Fukasawa, K.; Kanai, M.; Fujii, S.; Harada, M. Molecular cloning and expression of rat liver aminopeptidase B. *J. Biol. Chem.* **1996**, *271*, 30731–30735. [CrossRef] [PubMed]
77. Nagasaka, T.; Nomura, S.; Okamura, M.; Tsujimoto, M.; Nakazato, H.; Oiso, Y.; Nakashima, N.; Mizutani, S. Immunohistochemical localization of placental leucine aminopeptidase/oxytocinase in normal human placental, fetal and adult tissues. *Reprod. Fertil. Dev.* **1997**, *9*, 747–753. [CrossRef] [PubMed]
78. Shim, K.Y.; Eom, Y.W.; Kim, M.Y.; Kang, S.H.; Baik, S.K. Role of the renin-angiotensin system in hepatic fibrosis and portal hypertension. *Korean J. Intern. Med.* **2018**, *33*, 453–461. [CrossRef]
79. van den Hoven, A.F.; Smits, M.L.J.; Rosenbaum, C.E.N.M.; Verkooijen, H.M.; van den Bosch, M.A.A.J.; Lam, M.G.E.H. The effect of intra-arterial angiotensin II on the hepatic tumor to non-tumor blood flow ratio for radioembolization: A systematic review. *PLoS ONE* **2014**, *9*, e86394. [CrossRef]
80. Graus-Nunes, F.; de Santos, F.O.; de Marinho, T.S.; Miranda, C.S.; Barbosa-da-Silva, S.; Souza-Mello, V. Beneficial effects of losartan or telmisartan on the local hepatic renin-angiotensin system to counter obesity in an experimental model. *World J. Hepatol.* **2019**, *11*, 359–369. [CrossRef]
81. Min, L.; Sim, M.K.; Xu, X.G. Effects of des-aspartate-angiotensin I on angiotensin II-induced incorporation of phenylalanine and thymidine in cultured rat cardiomyocytes and aortic smooth muscle cells. *Regul. Pept.* **2000**, *95*, 93–97. [CrossRef]
82. Reaux, A.; Fournie-Zaluski, M.C.; David, C.; Zini, S.; Roques, B.P.; Corvol, P.; Llorens-Cortes, C. Aminopeptidase A inhibitors as potential central antihypertensive agents. *Proc. Natl. Acad. Sci. USA* **1999**, *96*, 13415–13420. [CrossRef]
83. Segarra, A.B.; Prieto, I.; Martínez-Cañamero, M.; de Gasparo, M.; Luna, J.d.D.; Ramírez-Sánchez, M. Thyroid Disorders Change the Pattern of Response of Angiotensinase Activities in the Hypothalamus-Pituitary-Adrenal Axis of Male Rats. *Front. Endocrinol.* **2018**, *9*, 731. [CrossRef]
84. Gajdosechova, L.; Krskova, K.; Segarra, A.B.; Spolcova, A.; Suski, M.; Olszanecki, R.; Zorad, S. Hypooxytocinaemia in obese Zucker rats relates to oxytocin degradation in liver and adipose tissue. *J. Endocrinol.* **2014**, *220*, 333–343. [CrossRef]
85. Prieto, I.; Segarra, A.B.; de Gasparo, M.; Martínez-Cañamero, M.; Ramírez-Sánchez, M. Divergent profile between hypothalamic and plasmatic aminopeptidase activities in WKY and SHR. Influence of beta-adrenergic blockade. *Life Sci.* **2018**, *192*, 9–17. [CrossRef]
86. Villarejo, A.B.; Segarra, A.B.; Ramírez, M.; Banegas, I.; Wangensteen, R.; de Gasparo, M.; Cobo, J.; Alba, F.; Vives, F.; Prieto, I. Angiotensinase and vasopressinase activities in hypothalamus, plasma, and kidney after inhibition of angiotensin-converting enzyme: Basis for a new working hypothesis. *Horm. Metab. Res.* **2012**, *44*, 152–154. [CrossRef] [PubMed]
87. Prieto, I.; Villarejo, A.B.; Segarra, A.B.; Wangensteen, R.; Banegas, I.; de Gasparo, M.; Vanderheyden, P.; Zorad, S.; Vives, F.; Ramírez-Sánchez, M. Tissue distribution of CysAP activity and its relationship to blood pressure and water balance. *Life Sci* **2015**, *134*, 73–78. [CrossRef] [PubMed]

88. Segarra, A.B.; Prieto, I.; Martinez-Canamero, M.; Vargas, F.; De Gasparo, M.; Vanderheyden, P.; Zorad, S.; Ramirez-Sanchez, M. Cystinyl and pyroglutamyl-beta-naphthylamide hydrolyzing activities are modified coordinately between hypothalamus, liver and plasma depending on the thyroid status of adult male rats. *J. Physiol. Pharmacol.* **2018**, *69*, 197–204. [CrossRef]
89. Kanno, T.; Maekawa, M.; Kanda, S.; Kohno, H.; Sudo, K. Evaluation of Cytosolic Aminopeptidase in Human Sera: Evaluation in Hepatic Disorders. *Am. J. Clin. Pathol.* **1984**, *82*, 700–705. [CrossRef] [PubMed]
90. Porta, M.; Pumarega, J.; Guarner, L.; Malats, N.; Solà, R.; Real, F.X.; PANKRAS II Study Group. Relationships of hepatic and pancreatic biomarkers with the cholestatic syndrome and tumor stage in pancreatic cancer. *Biomarkers* **2012**, *17*, 557–565. [CrossRef]
91. Bezerra-Duarte, S.M.; Faintuch, J.; Stefano, J.T.; Sobral de Oliveira, M.B.; de Campos Mazo, D.F.; Rabelo, F.; Vanni, D.; Nogueira, M.A.; Carrilho, F.J.; Marques Souza de Oliveira, C.P. Hypocaloric high-protein diet improves clinical and biochemical markers in patients with nonalcoholic fatty liver disease (NAFLD). *Nutr. Hosp.* **2014**, *29*, 94–101. [CrossRef]
92. Li, Q.; Feenstra, M.; Pfaffendorf, M.; Eijsman, L.; van Zwieten, P.A. Comparative Vasoconstrictor Effects of Angiotensin II, III, and IV in Human Isolated Saphenous Vein. *J. Cardiovasc. Pharmacol.* **1997**, *29*, 451–456. [CrossRef]
93. Hassanin, A.; Malek, H.A.; Saleh, D. Heparin modulation on hepatic nitric oxide synthase in experimental steatohepatitis. *Exp. Ther. Med.* **2014**, *8*, 1551–1558. [CrossRef]

nutrients

MDPI

Article

The Effect of a High-Fat Diet on the Fatty Acid Composition in the Hearts of Mice

Alicja Pakiet [1], Agnieszka Jakubiak [2], Paulina Mierzejewska [3], Agata Zwara [1], Ivan Liakh [4], Tomasz Sledzinski [4] and Adriana Mika [1,4,*]

[1] Department of Environmental Analysis, Faculty of Chemistry, University of Gdansk, Wita Stwosza 63, 80-308 Gdansk, Poland; alicja.pakiet@phdstud.ug.edu.pl (A.P.); agata.zwara@phdstud.ug.edu.pl (A.Z.)
[2] Tri-City Academic Laboratory Animal Centre - Research & Services Centre, Medical University of Gdansk, 80-210 Gdansk, Poland; a.jakubiak@gumed.edu.pl
[3] Department of Biochemistry, Faculty of Medicine, Medical University of Gdansk, Debinki 1, 80-211 Gdansk, Poland; paulina.mierzejewska@gumed.edu.pl
[4] Department of Pharmaceutical Biochemistry, Faculty of Pharmacy, Medical University of Gdansk, Debinki 1, 80-211 Gdansk, Poland; liakh_ivan@mail.ru (I.L.); tsledz@gumed.edu.pl (T.S.)
* Correspondence: adrianamika@tlen.pl; Tel.: +48-585-230-810

Received: 24 February 2020; Accepted: 18 March 2020; Published: 20 March 2020

Abstract: The Western diet can lead to alterations in cardiac function and increase cardiovascular risk, which can be reproduced in animal models by implementing a high-fat diet (HFD). However, the mechanism of these alterations is not fully understood and may be dependent on alterations in heart lipid composition. The aim of this study was to evaluate the effect of an HFD on the fatty acid (FA) composition of total lipids, as well as of various lipid fractions in the heart, and on heart function. C57BL/6 mice were fed an HFD or standard laboratory diet. The FA composition of chow, serum, heart and skeletal muscle tissues was measured by gas chromatography–mass spectrometry. Cardiac function was evaluated by ultrasonography. Our results showed an unexpected increase in polyunsaturated FAs (PUFAs) and a significant decrease in monounsaturated FAs (MUFAs) in the heart tissue of mice fed the HFD. For comparison, no such effects were observed in skeletal muscle or serum samples. Furthermore, we found that the largest increase in PUFAs was in the sphingolipid fraction, whereas the largest decrease in MUFAs was in the phospholipid and sphingomyelin fractions. The hearts of mice fed an HFD had an increased content of triacylglycerols. Moreover, the HFD treatment altered aortic flow pattern. We did not find significant changes in heart mass or oxidative stress markers between mice fed the HFD and standard diet. The above results suggest that alterations in FA composition in the heart may contribute to deterioration of heart function. A possible mechanism of this phenomenon is the alteration of sphingolipids and phospholipids in the fatty acid profile, which may change the physical properties of these lipids. Since phospho- and sphingolipids are the major components of cell membranes, alterations in their structures in heart cells can result in changes in cell membrane properties.

Keywords: heart; high-fat diet; fatty acids; cell membrane; sphingolipids; phospholipids; polyunsaturated fatty acids

1. Introduction

The Western diet (WD) is characterized by overeating and an especially high intake of simple carbohydrates and saturated fats. Combined with a lack of physical activity, the WD can lead to obesity and related comorbidities, especially cardiovascular diseases (CVD) [1,2]. Recent data indicate that there is practically no organ or system that would not be affected by the WD [3]. The first target of the WD is the digestive system [4–6]. The WD leads to microbiome changes [7,8], which may be a

factor in the development of sporadic colon cancer [9,10] or inflammatory bowel disease [11]. The WD also affects the liver [12], which promotes the development of non-alcoholic fatty liver disease and [13] liver fibrosis [14] and disrupts bile acid synthesis [15]. Acting on the brain, the WD causes cognitive impairment [16–18], increases neuroinflammation and memory deficits [19], raises the risk of dementia [20], Alzheimer's disease [21], and autism spectrum disorders [22], and causes changes in the retina [23]. Changes in immune status, as a result of the WD, lead to sepsis [24], auto-inflammation [25], hypersensitivity [26], breast [27] and skin [28] inflammation, acne [29], and a decrease in infection control [30]. A WD leads to decreased fertility [31], foetal changes during pregnancy [32] and after childbirth [33,34], affects sex hormones [35] and causes negative effects on the kidneys [36,37].

However, in terms of mortality, the greatest danger to human health is the fact that the WD affects the cardiovascular system [2,38–40]. The World Health Organization claims that CVD is the leading cause of death in the world, with an estimated 17.9 million deaths per year (31% of all deaths in the world), which creates a huge burden on the health care system and the economy. The American Heart Association reports that 74% of the risk of stroke can be attributed to behavioural risk factors, including unhealthy diets [41]. A high-fat diet (HFD) is a well-established rodent model of the WD. Existing theories describing the relationship between HFDs and cardiovascular disorders mainly describe mechanisms for the development of structural and metabolic changes and the response to increased levels of inflammation during HFD in heart tissue [36,42–46]. An important role is attributed to intensified oxidative stress during HFD intake and subsequent activation of the inflammasome complex, which leads to activation and secretion of cytokines (IL-1β and IL-18), inducing sterile inflammation [47,48]. While the majority of studies suggested deterioration of cardiac contractility consequent to HFD [49–53], Mourmoura et al. [54] found an improvement of cardiac function after 3 months of feeding rats with HFD containing a high proportion of SFA. This underpins the importance of further studies to clarify this issue.

One theory explaining the adverse effects of a HFD on the heart is that decreased expression of genes of antioxidant enzymes, such as malic enzyme, and activation of caspase-3 in the heart leads to apoptosis due to oxidative stress and disruption of the anaplerotic flow of the Krebs cycle, respectively [55]. Additionally, enhanced β-oxidation of fatty acids (FAs) with HFD intake leads to the formation of reactive oxygen species and lipid peroxidation, which contributes to a change in mitochondrial function [56]. According to another theory, a HFD initiates cascading reactions in which increased carnitine palmitoyl transferase (CPT1) and uncoupling protein (UCP2) contents lead to reduced plasma membrane glucose transporter (GLUT4) and peroxisome proliferator-activated receptor gamma coactivator 1-alpha (PGC-1α) contents, which ultimately leads to reduced mitochondrial biogenesis and uncoupling of heart bioenergetic metabolism [57,58]. Overload, hypertrophy and a decrease in left ventricular conduction may be associated with exposure to free fatty acids (FFAs) and the accumulation of triglycerides in and around the myocardium, as well as a significant generalized excess of ectopic fat [59].

The harmful effects of a HFD on the heart are also associated with changes in cardiac mitochondrial membrane fluidity after a decrease in myocardial palmitoleoyl-CoA (16:1-CoA) content, wherein an enhanced activity of FA elongase and desaturase leads to increased hepatic lipogenic capacity [50]. Some authors described reduced 16:1-CoA after long-term HFD intake. Recent data also indicate that the FA composition of membrane phospholipids has a great influence on the properties of membranes and that the degree of unsaturation of membrane phospholipids correlates with contractile dysfunction [51]. Both exogenous saturated FAs (SFAs) and monounsaturated FAs (MUFAs) from the HFD cause different degrees of adverse myocardial changes as a consequence of the change in the levels of SFAs and MUFAs in the membrane phospholipids [51]. However, the authors of the above-mentioned paper did not study changes in polyunsaturated FA (PUFA) levels, although it is known that a high food intake of PUFAs reduces the risk of CVD [38,60]. Thus, the aim of this study was to evaluate the effect of an HFD on the whole FA composition, including PUFAs, in mouse hearts, both in all lipids and in specific lipid fractions.

2. Materials and Methods

2.1. Animals and Treatment

The animal study protocol was approved by the Local Ethics Committee for Experiments on Animals in Bydgoszcz (approval number 47/2016). Individually marked 6-week-old male mice (strain C57BL/6) from Tri-City Animal Laboratory Research and Service Center, Medical University of Gdansk, with an average body weight of 21.8 ± 1.1 g, were randomly assigned to two experimental groups (two cohorts—one for tissue collection and second for cardiac function assessment; 10 controls and 10 mice treated by HFD in each cohort). In each cohort, ten animals were fed a standard diet (SD) (Altromin C 1090 – 10) with energy from 11% fat, 24% protein and 65% carbohydrates (ME 14.6 MJ/kg), while the other 10 mice were provided a high-fat diet (HFD) (Altromin C 1090 – 60) containing 60% energy from fat, 16% protein, and 24% carbohydrates (ME 21.1 MJ/kg). The animals were housed in polysulfone cages in a room controlled for temperature (22 ± 2°C), humidity (55 ± 10%), and light cycle (12 h light/12 h dark). The air was exchanged ≥12 times per hour. The mice had access to chow and water *ad libitum*. Body weight and chow intake were measured weekly. After 19 weeks of experiments, the animals were sacrificed, and blood and organs/tissues were harvested. Hearts and sections of approximately 500 mg of skeletal muscle were immediately frozen in liquid nitrogen. Blood was centrifuged at 3000× *g* for 15 min at 4 °C, and serum was aliquoted. All samples were stored at –80 °C until analysis. Triacylglycerols (TAGs) and total protein levels were estimated using a laboratory analyser (XL-100, Erba Diagnostics Mannheim GmbH, Mannheim, Germany).

Plasma non-esterified fatty acid was measured using free fatty acid (FFA) Kit (MAK044, Sigma-Aldrich, St. Louis, MO, USA) according to the manufacturer's protocol. Briefly, 50 µL of a serum sample was added to individual plate wells. A quantity of 2 µL of Acyl-CoA synthase was added to each well and incubated at 37 °C for 30 min in the dark. Then, 50 µL of the master reaction mixture consisting of 44 µL of fatty acid assay buffer, 2 µL of fatty acid probe, 2 µL of enzyme mix and 2 µL of enhancer were added and incubated under the same conditions. After that, absorbances for individual wells were read at 570 nm using a Synergy HT multi-detection microplate reader (BioTek, Winooski, VT, USA).

2.2. Cardiac Function Assessment

At the age of 24 weeks, mice were anaesthetized with ketamine (100 mg/kg) and xylazine (10 mg/kg) intra-peritoneally. After chest hair removal, animals were placed on a heated platform to maintain the body temperature at 37 °C. Transthoracic echocardiography was performed with a Vevo 1100 (VisualSonics Inc, Toronto, Canada) equipped with a 40-MHz linear array transducer. Images were acquired at a frame rate consistently above 200 frames/s. The transducer was placed above the anterior chest wall and directed towards the ascending aorta in 2D mode, which was next switched to Doppler flow velocity mode. The readings were recorded and used directly or applied for aortic valve area (AVA) calculation. The AVA was determined with the continuity equation. Haemodynamic parameters, including stroke volume (SV), left ventricular (LV) ejection fraction (EF) and cardiac output (CO), were collected.

2.3. Lipid Analysis

2.3.1. Total Lipid Extraction

Lipids were extracted from tissue samples with a chloroform–methanol mixture (2:1, v/v) according to the method published by Folch et al. [61]. The chloroform phase was collected, divided into two parts, dried under a nitrogen stream and stored at −20°C for further analysis.

2.3.2. Solid Phase Extraction

Aliquots of total lipid extracts were fractionated on aminopropyl solid phase extraction (SPE) columns (Strata® NH2 500 mg, Phenomenex®, Torrance, CA, USA) in accordance with two procedures.

Method I, by Kaluzny et al. [62], allowed for the collection of FFAs, phospholipids (PLs) and acylglycerols (AGs). Two milligrams of dried extracts were reconstituted in chloroform and loaded onto SPE columns preconditioned with 2 × 2 mL of n-hexane. The phases were then eluted with 6 mL chloroform-isopropanol (2:1, v/v) to obtain neutral lipids (NLs), 6 mL 2% acetic acid in diethyl ether (v/v) to obtain FFAs, and 6 mL methanol to obtain PLs; all fractions were dried under a nitrogen stream. The NL fraction was dissolved in n-hexane and loaded onto a new SPE cartridge and fractionated with 6 mL n-hexane to obtain cholesteryl esters, which were discarded, 9 mL methylene chloride:diethyl ether-n-hexane (10:1:89, v/v/v) to obtain TAGs, 18 mL 5% ethyl acetate in n-hexane (v/v) to obtain cholesterol, which was discarded, 6 mL 15% ethyl acetate in n-hexane (v/v) to obtain diacylglycerols (DAGs) and 6 mL chloroform–methanol (2:1, v/v) to obtain monoacylglycerols (MAGs). The MAG, DAG and TAG phases were combined into an AG mixture, and all fractions were dried under a nitrogen stream.

Method II, by Bodennec et al. [63], used 1.5 mg lipid extract reconstituted in chloroform and loaded onto aminopropyl columns preconditioned with 5 mL of n-hexane. Samples were eluted with 5 mL 15% ethyl acetate in n-hexane (v/v) to obtain NLs without ceramides (Cer), MAGs and FFAs, 4 mL chloroform-methanol (23:1, v/v) to obtain Cer, 3 mL 5% acetic acid in diisopropyl ether (v/v) to obtain FFAs and α-hydroxy-FFAs, which were discarded, 11 mL acetone–methanol (9:1.35, v/v) to obtain glycosphingolipids (GSPLs), and 4 mL chloroform–methanol (2:1, v/v) to obtain sphingomyelins (SMs). All obtained fractions were evaporated to dryness under a nitrogen stream.

2.3.3. Fatty Acid Hydrolysis and Derivatization

All fractions collected after SPE and total lipid extracts were prepared for GC–MS analysis as follows. One millilitre 0.5 M KOH in methanol was added, and samples were hydrolysed at 90 °C for 3 h. Then, mixtures were acidified with 0.5 mL 5 M HCl, 1 mL of water was added, FAs were extracted with 3 × 1 mL of n-hexane, and the organic phase was evaporated to dryness. Derivatization to FA methyl esters (FAMEs) was achieved with a 10% boron trifluoride–methanol solution at 55 °C for 1.5 h. After incubation, 1 mL water was added, and FAMEs were extracted with 1 mL n-hexane thrice and dried under a nitrogen stream.

2.3.4. GC–MS Analysis

The FAME composition of the obtained samples was determined by using a QP-2010SE GC-EI-MS (Shimadzu, Kyoto, Japan). The chromatographic separation was conducted on a Zebron ZB-5MSi capillary column (30 m length × 0.25 mm i.d. × 0.25 μm film thickness, Phenomenex®, Torrance, CA, USA) with helium as the carrier gas (head pressure of 100 kPa). The GC oven temperature was programmed from 60 to 300°C (4°C/min) with an overall run time of 60 min. The electron impact source for mass spectrometric detection was operated at 70 eV. Acquisition of mass spectra was conducted in full scan mode with a mass scan range of m/z 45–700. 19-Methylarachidic acid was used as an internal standard. Peak identification was aided by the use of reference standards (37 FAME Mix, Sigma-Aldrich, St. Louis, MO, USA) and the NIST 2011 reference library.

2.4. Lipid Peroxidation

Lipid peroxidation was measured using the TBARS Assay Kit (cat. no. 10009055, Cayman Chemical Company, Ann Arbor, MI, USA). This method is based on the colorimetric determination of coloured adducts formed by the reaction of malondialdehyde (MDA) and thiobarbituric acid (TBA) at high temperatures (90–100 °C) under acidic conditions. Briefly, approximately 25 mg of heart tissue was added to 250 μL RIPA buffer (containing selected protease inhibitors), the tissues were homogenized on ice, and the tube was centrifuged at 1600× *g* for 10 min at 4 °C. One hundred microlitres of the supernatant were removed for analysis and mixed in a 5 mL vial with 100 μL SDS solution, after which 4 mL colour reagent was added, and the vials were placed in boiling water for 1 h. After an hour, the vials were placed in an ice bath and incubated for 10 min to stop the reaction. After centrifugation of

the vials for 10 min at 1600× *g* and 4 °C, 150 μL aliquots of the samples (in duplicate) were loaded from each vial into the plate, and the absorbance was read at 532 nm. Determination of concentration was carried out using a calibration curve, which was obtained using the standard provided in the kit.

2.5. Free Cholesterol Measurement

Free cholesterol content in mouse heart was measured using reagent for the quantitative in vitro determination of free, unesterified cholesterol in serum or plasma (Greiner Laboratories GmbH, Germany) according to the manufacturer's instructions. The colorimetric indicator is quinoneimine dye, which is formed from the catalytic action of peroxidase from 4-aminoantipyrine, phenol and hydrogen peroxide (Trinder reaction). Briefly, 10 μL of the supernatant is added to 1 mL of reagent, after which the samples are incubated for 20 min at 37 °C. After that, absorbance was determined spectrophotometrically at 546 nm using a Synergy HT multi-plate microplate reader (BioTek, Winooski, VT, USA).

2.6. Protein Carbonyl Groups Determination

Protein carbonyl content in mouse heart was measured using The Protein Carbonyl Content Assay Kit (Sigma-Aldrich, St. Louis, MO, USA, MAK094) according to the manufacturer's instructions. The method is based on the derivatization of protein carbonyl groups with 2,4-dinitrophenylhydrazine (DNPH), which leads to the formation of stable dinitrophenyl adducts (DNP) of hydrazone, which is further detected spectrophotometrically at 375 nm. Briefly, 100 μL of a DNPH solution was added to 100 μL of the homogenate and incubated for 10 min at room temperature. Then, 30 μL of a 100% TCA solution was added to each sample, shaken and incubated on ice for 5 min. After centrifugation, the pellet was washed twice with 500 μL of acetone. The resulting precipitate was dissolved in 200 μL of a 6 M guanidine solution and the absorbance was measured at 375 nm using a Synergy HT multi-plate microplate reader (BioTek, Winooski, VT, USA). In addition, the amount of total protein was determined using a laboratory analyser (XL-100, Erba Diagnostics Mannheim GmbH, Mannheim, Germany), and the results are presented as nmol/mg of total protein.

2.7. Statistical Analysis

The data are presented as the mean ± SD. Every sample was run in duplicate. For normally distributed data, the significance of differences between means was estimated with parametric Student's t-tests. The data that did not follow a normal distribution underwent a non-parametric Mann–Whitney U test. The statistical analysis was performed with Sigma-Plot 11 software (Systat Software, Inc. 2008, San Jose, CA, USA).

3. Results

3.1. Dietary-Induced Obesity

The 19-week-long treatment of mice resulted in a gradual, almost 30% increase ($p < 0.001$) in body weight of HFD-fed mice (final weight: 42 ± 5.3 g) compared to that of the SD-fed mice (final weight 30 ± 1.6 g) [64]. However, the mean weight of the animals' hearts did not differ significantly between the SD and HFD groups (218 ± 14 g and 214 ± 26 g, respectively). Likewise, the total protein concentration in the hearts was similar for HFD-fed mice (164 ± 31 g/g of wet tissue) and SD-fed mice (157 ± 12 g/g of wet tissue). To assess fat accumulation in the hearts, we measured the TAG content in tissue homogenates. The HFD-fed mice had 1.7 times more TAGs in the heart tissue (5.0 ± 1.7 mg/g of wet tissue) than that in the heart tissue of SD-fed mice (2.9 ± 0.5 mg/g of wet tissue) at $p < 0.01$. Moreover, mice fed with the HFD had significantly higher serum FFA concentrations than that of mice fed the SD (0.68 ± 0.34 vs 0.25 ± 0.12 mmol/L respectively, $p < 0.001$). We also measured free, non-esterified cholesterol in heart tissues and found no significant differences between HFD mice (3.62 ± 0.34 mg/g of wet tissue) and SD-fed mice (3.79 ± 0.51 mg/g of wet tissue, $p = 0.381$).

3.2. Cardiac Function Assessment

To characterise the implications of the HFD for cardiac function, we conducted two-dimensional echocardiographic measurements and examined the aortic valve flow velocity using Doppler ultrasound. These results are presented in Table 1. The in vivo analysis of the stroke volume and cardiac output did not differ between mice fed the two diets. However, the HFD caused a significant decrease in aortic valve area compared to that determined in the hearts of mice fed the SD. Furthermore, the aortic valve flow velocity (Vmax) tended to be higher in HFD group ($p = 0.056$), and a trend was observed for a decrease in the cell ventricular ejection fraction in comparison to that of the control (Table 1)

Table 1. Echocardiographic measurements in C57BL/6 mice fed a standard (SD) or high-fat diet (HFD).

Parameter	SD	HFD	*p*-Value
Left ventricular end-systolic volume (LVESV) (μL)	8.80 ± 2.00	10.8 ± 2.40	0.144
Left ventricular end-diastolic volume (LVEDV) (μL)	29.8 ± 4.60	31.1 ± 3.85	0.613
Stroke Volume (SV) (μL)	21.0 ± 2.70	20.3 ± 2.50	0.626
Cardiac Output (CO) (mL × min^{-1})	6.15 ± 0.99	6.10 ± 0.67	0.922
Left Ventricular Ejection Fraction (LVEF) (%)	70.8 ± 4.32	65.4 ± 5.50	0.090
Aortic Valve Area (AVA) (mm^2)	1.62 ± 0.45	1.34 ± 0.44	0.049
Vmax (m/s)	0.76 ± 0.27	0.98 ± 0.30	0.056

3.3. Changes in Total FA Profiles

A high-fat diet is one of the experimental models of the Western diet, and Table 2 shows that high-fat chow contains much higher levels of SFA than control chow, which is a characteristic feature of the Western diet. The HFD diet resulted in a significant elevation of the total FA concentration in the serum of HFD-fed mice compared to that in the serum of SD-fed mice (4.35 ± 0.77 and 2.65 ± 0.49 μg/mL, respectively; $p < 0.05$). The concentrations of all major FA groups in the sera of animals, namely, SFAs, MUFAs and PUFAs, and both *n*-3 and *n*-6, were increased in the HFD group, which corresponded to the higher overall concentrations of these groups in the HFD chow (Table 2). Among PUFAs, eicosapentaenoic acid (EPA, 20:5 *n*-3) was an exception, as its content in HFD serum was two-fold lower ($p < 0.001$), despite a high concentration of this acid in the HFD chow (Table 2). We also observed an expected increase in oleic acid (18:1), which was the most abundant MUFA, and surprisingly, an almost two-fold decrease in the serum palmitoleic acid (16:1) concentration in HFD-fed mice, even though this FA chow content was over eight times higher in the HFD chow (Table 2).

In both the hearts and skeletal tissues of HFD-fed mice, the changes in PUFAs followed similar trends as those observed in the serum; that is, the levels of total *n*-3 and *n*-6 PUFAs increased (Table 2). Interestingly, the changes in *n*-3 PUFA levels were much more pronounced in the heart than in the skeletal muscles. The *n*-3 PUFA content in the hearts of HFD-fed mice was 2.6 times greater than in the hearts of SD-fed mice ($p < 0.001$), whereas in the skeletal muscle, a nonsignificant difference of only 50% was observed. The increased content of particular FAs was significant in the hearts for almost all measured PUFAs, with the exception of EPA and eicosatetraenoic acid (ETA, 20:4 *n*-3), whereas in the skeletal muscles, only some PUFAs changed significantly. In both tissues, the n-6 PUFA levels were almost two-times higher for mice fed an HFD than for mice fed the SD ($p < 0.001$), and there was a slight decrease in the SFA content. Notably, only in the hearts was the MUFA content in HFD-fed mice significantly lowered (approximately 30%), which was in contrast to the trend observed for the MUFA content in serum (Table 2). Additionally, both palmitoleic acid and oleic acid in HFD hearts were significantly lowered. The changes of total SFA, total MUFA, total PUFA are presented in Figure 1a and PUFA/MUFA ratio in the hearts of control and HFD mice are presented in Figure 1b.

Table 2. Composition of selected fatty acids (FAs) in chow, serum and tissues.

	Chow (mg/g)		Serum (mg/L)		Heart (%)		Skeletal muscle (%)	
	10%	**60%**	**SD**	**HFD**	**SD**	**HFD**	**SD**	**HFD**
16:0	9.73 ± 0.46	74.3 ± 4.89 **	719 ± 210	1106 ± 244 *	21.01 ± 2.82	17.56 ± 2.77 *	23.17 ± 1.78	20.79 ± 1.15
18:0	4.59 ± 0.10	39.1 ± 19.2 **	228 ± 26.3	548 ± 90.4 #	23.88 ± 11.67	21.49 ± 6.64	6.07 ± 2.44	5.10 ± 0.68 **
Other SFAs	3.55 ± 0.10	22.8 ± 1.22 **	101 ± 51.3	201 ± 70.5 *	3.46 ± 0.98	3.01 ± 1.12	5.54 ± 0.35	5.04 ± 0.39
SFAs	**17.9 ± 0.64**	**136 ± 8.00** **	**1049 ± 286**	**1855 ± 397** **	**48.4 ± 10.1**	**42.1 ± 6.97**	**34.8 ± 3.50**	**31.0 ± 1.63**
16:1	0.75 ± 0.01	5.93 ± 0.33 **	222 ± 64.9	135 ± 23.7 *	4.07 ± 2.21	1.74 ± 0.87 **	10.8 ± 1.01	9.39 ± 1.02
18:1	9.63 ± 0.14	79.7 ± 3.65 #	920 ± 313	1127 ± 256	30.3 ± 9.60	21.9 ± 7.69 *	45.0 ± 3.03	45.6 ± 3.20
Other MUFAs	0.29 ± 0.01	2.28 ± 0.19 **	21.9 ± 12.0	27.5 ± 8.83	1.13 ± 0.48	0.77 ± 0.32	1.70 ± 0.28	1.03 ± 0.17 **
MUFAs	**10.7 ± 0.12**	**87.9 ± 4.15** #	**1164 ± 389**	**1289 ± 274**	**35.5 ± 12.1**	**24.4 ± 8.83** *	**57.5 ± 4.20**	**56.0 ± 2.65**
18:2 *n*-6 (LA)	2.04 ± 0.04	18.6 ± 0.70 #	356 ± 29.1	915 ± 114 #	6.32 ± 1.94	12.2 ± 3.11 #	4.29 ± 0.34	8.78 ± 0.14 #
20:4 *n*-6 (ARA)	0.037 ± 0.004	0.36 ± 0.01 #	152 ± 37.4	330 ± 59.2 #	4.14 ± 2.37	8.62 ± 3.24 **	1.30 ± 0.65	1.46 ± 0.47
22:4 *n*-6 (AdA)	0.008 ± 0.002	0.11 ± 0.02 *	1.48 ± 0.35	2.81 ± 0.60 #	0.18 ± 0.10	0.57 ± 0.27 #	0.12 ± 0.06	0.14 ± 0.03
Other *n*-6 PUFAs	0.073 ± 0.008	0.70 ± 0.08 **	42.0 ± 8.90	47.3 ± 14.2	1.75 ± 0.98	2.19 ± 0.82	0.68 ± 0.22	0.66 ± 0.09
***n*-6 PUFA**	**2.16 ± 0.03**	**19.7 ± 0.64** #	**552 ± 63.9**	**1295 ± 105** #	**12.4 ± 4.89**	**23.5 ± 7.17** #	**6.39 ± 1.02**	**11.0 ± 0.59** #
18:3 *n*-3 (ALA)	0.005 ± 0.002	0.049 ± 0.002 #	5.74 ± 2.18	9.97 ± 2.55 *	0.02 ± 0.01	0.02 ± 0.01	0.02 ± 0.01	0.03 ± 0.01
20:5 *n*-3 (EPA)	0.008 ± 0.002	0.074 ± 0.004 #	42.9 ± 11.7	20.1 ± 2.77 **	0.54 ± 0.27	0.16 ± 0.05 #	0.34 ± 0.10	0.08 ± 0.01 **
22:5 *n*-3 (DPA)	0.016 ± 0.003	0.15 ± 0.007 #	2.81 ± 0.53	7.87 ± 2.28 **	0.34 ± 0.23	1.87 ± 0.87 #	0.16 ± 0.08	0.36 ± 0.12 *
22:6 *n*-3 (DHA)	0.006 ± 0.003	0.06 ± 0.02	30.9 ± 8.24	72.1 ± 8.81	2.83 ± 1.93	7.91 ± 3.34 #	0.51 ± 0.29	1.10 ± 0.40 *
Other *n*-3 PUFAs	0.002 ± 0.001	0.01 ± 0.01	2.87 ± 0.56	3.44 ± 0.89	0.34 ± 0.23	1.87 ± 0.87 #	0.18 ± 0.09	0.38 ± 0.12 *
***n*-3 PUFA**	**0.04 ± 0.01**	**0.35 ± 0.007** #	**85.2 ± 21.7**	**114 ± 9.01** *	**3.77 ± 2.36**	**9.99 ± 4.24** #	**1.05 ± 0.47**	**1.59 ± 0.51**
PUFA	**2.20 ± 0.03**	**20.1 ± 0.64** #	**637 ± 82.3**	**1408 ± 112** #	**16.16 ± 7.14**	**33.53 ± 11.26** #	**7.44 ± 1.45**	**12.6 ± 1.09** #

p-value from *t*-tests: * $p < 0.05$, ** $p < 0.01$, # < 0.001; AdA–adrenic acid (22:4 *n*-6); ALA–α-linolenic acid (18:3 *n*-3); ARA–arachidonic acid (20:4 *n*-6); DGLA–dihomo-γ-linolenic acid (20:3 *n*-6); DHA–docosahexaenoic acid (22:6 *n*-3); DPA–docosapentaenoic acid (22:5 *n*-3); EPA–eicosapentaenoic acid (20:5 *n*-3); ETA–eicosatetraenoic acid (20:4 *n*-3); LA–linoleic acid (18:2 *n*-6); MUFA–monounsaturated fatty acids, PUFA–polyunsaturated fatty acids; SFA–saturated fatty acids. Bold represents main groups of fatty acids. SD – mice fed standard diet; HFD – mice fed high fat diet.

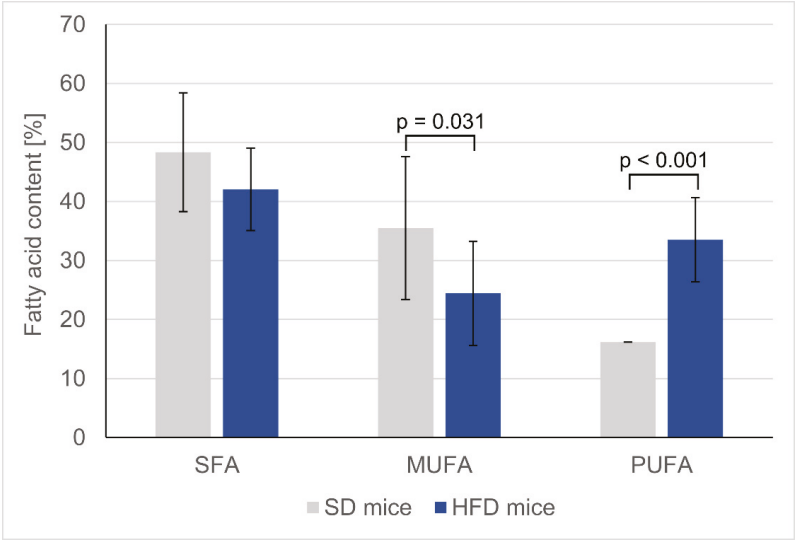

(a)

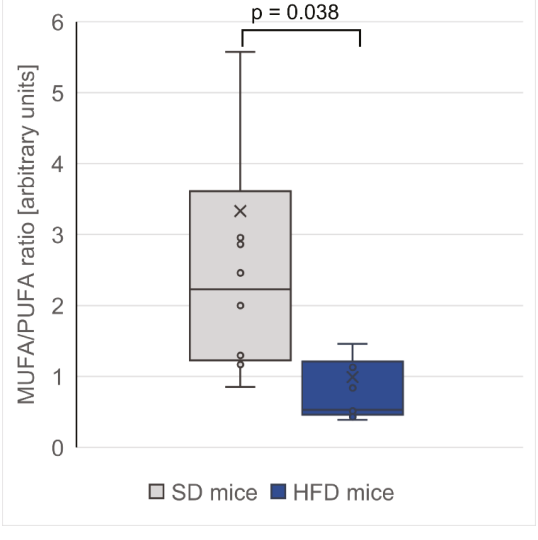

(b)

Figure 1. (**a**) Total saturated, monounsaturated and polyunsaturated fatty acids content in hearts. Values are mean ± SD. (**b**) Box-plot of monounsaturated to polyunsaturated fatty acid ratio in mice hearts. SD – mice fed standard diet; HFD – mice fed high fat diet.

3.4. Fatty Acid Alterations in Specific Lipid Fractions of the Hearts

The use of SPE allowed for us to obtain several fractions containing both polar and nonpolar lipid groups from the hearts of animals, which were then used for the analysis of the various FA contents among each group. The first method of fractionation followed the protocol established by Kaluzny

et al. [62], in which we separated lipids into FFAs, PLs and AGs. The second method of lipid separation by Bodennec et al. [63] yielded four fractions: NLs, Cer, GSPLs and SMs.

Phospholipids (PL fraction), which are the main component of the lipid bilayer [65], were characterized by a slight, albeit non-significant, increase in PUFAs after HFD treatment (Table 3, Figure 2A–C). Among the obtained sphingolipid fractions, namely, Cer, GSPLs and SMs, the upregulation of the n-3 PUFA level was the largest in the GSPL fraction (3.7 times higher in HFD-fed mice than in SD-fed mice), whereas the *n*-6 PUFA level increased the most in the Cer fraction (3.1 times higher in HFD-fed mice than in SD-fed mice) (Figure 2D-G). EPA was significantly downregulated in most polar lipid fractions (Table 3; Table 4) of the HFD-fed mice. Interestingly, arachidonic acid (ARA, 20:4 *n*-6) was the most abundant n-6 PUFA across all polar lipids except in the Cer fraction, where linoleic acid (LA, 18:2 *n*-6) predominated (Table 4), despite LA being supplied at higher concentrations in the diet. Both the Cer and GSPL fractions exhibited lower SFA contents in HFD-fed mice than in SD-fed mice, mostly due to the lowered stearic acid (18:0) content in the Cer fraction and the 16:0 decrease in the GSPL fraction (Table 4). On the other hand, SMs, an important component of lipid rafts [66], were characterized by a similar SFA content in both groups and a significant decrease in MUFA levels in the HFD-fed mice compared to those in the SD-fed mice (Table 4).

In both obtained non-polar groups, i.e., NLs and AGs, oleic acid was the most abundant FA, as MUFAs are major building blocks for AG synthesis [67], and the total MUFA percentage decreased in the hearts of HFD-fed mice (Tables 3 and 4). Similar to the polar lipids we gathered, PUFA accumulation in the hearts of HFD-fed mice was apparent in the AG and total NL fractions (Tables 3 and 4, Figure 2). Additionally, while we did not observe an increase in total SFAs, in the AG fraction, the stearic acid level increased almost two-fold in the HFD hearts.

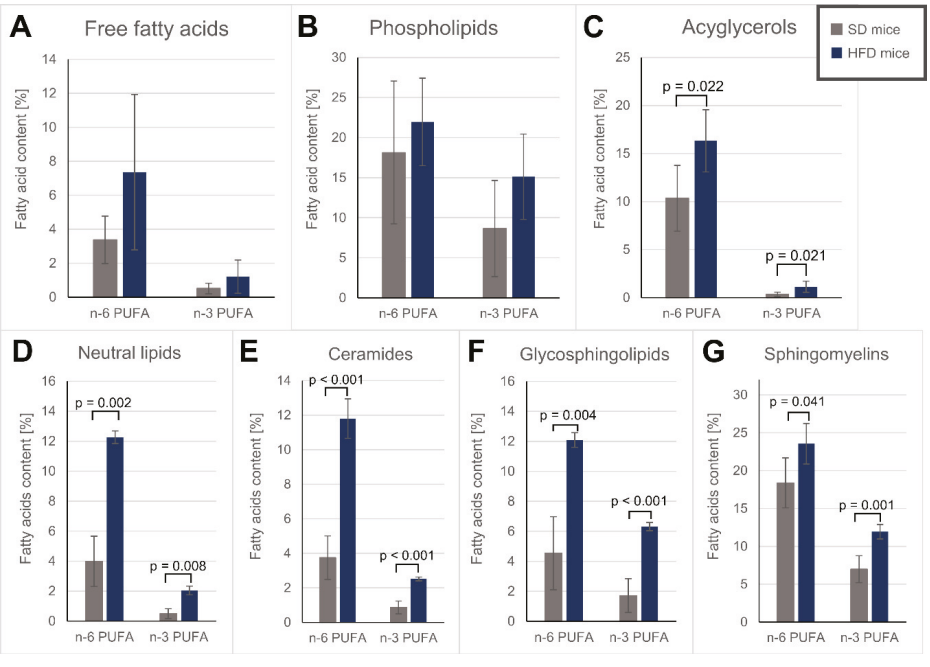

Figure 2. *n*-6 and *n*-3 polyunsaturated fatty acids content in different lipids fractions: (**A**) – free fatty acids; (**B**) – phospholipids; (**C**) – acylglycerols; (**D**) – neutral lipids; (**E**) – ceramides; (**F**) – glycosphingolipids; (**G**) - sphingomyelins; SD – mice fed standard diet; HFD – mice fed high fat diet.

Table 3. FA content (%) in heart fractions obtained with the Kaluzny et al. [62] method.

	Free fatty acids		Phospholipids		Acylglycerols	
	SD	**HFD**	**SD**	**HFD**	**SD**	**HFD**
16:0	45.2 ± 4.24	41.4 ± 8.53	21.0 ± 5.57	19.6 ± 4.32	23.6 ± 1.66	22.5 ± 0.64
18:0	28.4 ± 2.24	23.4 ± 3.01 **	27.4 ± 3.32	27.3 ± 3.95	5.30 ± 0.74	9.57 ± 1.25 #
Other SFAs	5.68 ± 1.08	6.19 ± 1.33	2.64 ± 0.83	1.92 ± 0.32	5.55 ± 0.71	6.57 ± 0.86
SFAs	**79.3 ± 3.40**	**71.1 ± 11.4**	**51.1 ± 9.40**	**48.8 ± 8.44**	**34.4 ± 1.92**	**38.7 ± 1.74** **
16:1	3.22 ± 1.42	3.00 ± 0.70	1.61 ± 0.73	0.65 ± 0.13 *	7.36 ± 1.64	3.84 ± 0.98 **
18:1	13.1 ± 2.80	16.6 ± 6.23	19.8 ± 4.75	13.0 ± 2.06 *	45.7 ± 1.07	38.5 ± 3.90 **
Other MUFAs	0.49 ± 0.19	0.79 ± 0.42	2.29 ± 0.87	1.10 ± 0.12 *	1.80 ± 0.17	1.61 ± 0.29
MUFAs	**16.8 ± 2.53**	**20.4 ± 5.94**	**22.2 ± 5.58**	**14.2 ± 2.17** *	**54.9 ± 2.20**	**43.9 ± 4.89** **
18:2 *n*-6 (LA)	2.48 ± 0.93	5.24 ± 3.00	4.47 ± 0.73	6.24 ± 1.40 *	9.61 ± 3.08	14.3 ± 3.39
20:4 *n*-6 (ARA)	0.53 ± 0.55	1.36 ± 1.08	9.75 ± 5.82	12.7 ± 3.62	0.28 ± 0.24	1.05 ± 0.65 *
22:4 *n*-6 (AdA)	0.11 ± 0.08	0.23 ± 0.19	0.40 ± 0.25	0.71 ± 0.21	0.08 ± 0.07	0.18 ± 0.12
Other *n*-6 PUFAs	0.26 ± 0.16	0.52 ± 0.34	3.52 ± 2.22	2.29 ± 0.61	0.37 ± 0.22	0.81 ± 0.34 *
18:3 *n*-3 (ALA)	0.03 ± 0.02	0.05 ± 0.02	0.03 ± 0.02	0.02 ± 0.01	0.02 ± 0.01	0.03 ± 0.01
20:5 *n*-3 (EPA)	0.18 ± 0.10	0.14 ± 0.07	1.09 ± 0.47	0.19 ± 0.04 **	0.10 ± 0.07	0.10 ± 0.02
22:5 *n*-3 (DPA)	0.12 ± 0.09	0.44 ± 0.43	0.94 ± 0.68	2.84 ± 1.13 *	0.11 ± 0.08	0.39 ± 0.24 *
22:6 *n*-3 (DHA)	0.17 ± 0.12	0.57 ± 0.51	6.51 ± 4.89	12.0 ± 4.20	0.11 ± 0.07	0.60 ± 0.36 *
Other *n*-3 PUFAs	0.001 ± 0.000	0.001 ± 0.000	0.08 ± 0.01	0.06 ± 0.02	0.009 ± 0.003	0.02 ± 0.01
PUFAs	**3.88 ± 1.61**	**8.56 ± 5.54**	**26.8 ± 14.9**	**37.1 ± 10.5**	**10.7 ± 3.56**	**17.5 ± 3.37** *

p-value from *t*-tests: * $p < 0.05$, ** $p < 0.01$, # $p < 0.001$; AdA–adrenic acid (22:4 *n*-6); ALA–α-linolenic acid (18:3 *n*-3); ARA–arachidonic acid (20:4 *n*-6); DHA–docosahexaenoic acid (22:6 *n*-3); DPA–docosapentaenoic acid (22:5 *n*-3); EPA–eicosapentaenoic acid (20:5 *n*-3); LA–linoleic acid (18:2 *n*-6); MUFA–monounsaturated fatty acids; PUFA–polyunsaturated fatty acids; SFA–saturated fatty acids. Bold represents main groups of fatty acids. SD – mice fed standard diet; HFD – mice fed high fat diet.

Table 4. Fatty acid content (%) in heart fractions obtained with the Bodennec et al. [63] method.

	Neutral lipids		Ceramides		Glycosphingolipids		Sphingomyelins	
	SD	HFD	SD	HFD	SD	HFD	SD	HFD
16:0	26.2 ± 2.02	24.1 ± 2.08	29.6 ± 4.12	24.3 ± 0.54	43.0 ± 4.14	33.7 ± 0.79 *	24.1 ± 2.13	22.3 ± 1.71
18:0	8.51 ± 1.38	8.59 ± 0.43	16.1 ± 2.74	11.9 ± 1.00 *	34.5 ± 2.80	31.2 ± 1.85	24.6 ± 1.34	25.6 ± 1.29
Other SFAs	6.38 ± 0.62	5.56 ± 0.42	12.9 ± 2.43	8.61 ± 1.81	6.02 ± 2.45	4.64 ± 0.25	2.11 ± 0.12	1.64 ± 0.16 **
SFAs	**41.1 ± 1.26**	**38.3 ± 2.33**	**58.6 ± 8.77**	**44.8 ± 2.91** *	**83.5 ± 4.68**	**69.6 ± 1.43** **	**50.8 ± 3.13**	**49.6 ± 2.97**
16:1	8.28 ± 0.99	3.99 ± 0.58 **	4.98 ± 0.58	4.19 ± 0.69	1.55 ± 0.38	1.53 ± 0.74	1.34 ± 0.09	0.54 ± 0.05 #
18:1	44.0 ± 1.14	42.7 ± 2.02	29.8 ± 7.31	35.5 ± 2.93	9.02 ± 1.70	10.6 ± 0.95	22.6 ± 1.85	14.4 ± 0.52 #
Other MUFAs	2.79 ± 0.63	1.59 ± 0.25	2.52 ± 0.52	1.53 ± 0.23 *	0.31 ± 0.11	0.17 ± 0.01	0.47 ± 0.08	0.28 ± 0.03 **
MUFAs	**55.1 ± 1.25**	**48.2 ± 2.00** *	**37.3 ± 7.89**	**41.2 ± 2.03**	**10.9 ± 1.32**	**12.3 ± 1.63**	**24.4 ± 1.90**	**15.2 ± 0.57** #
18:2 *n*-6 (LA)	3.43 ± 1.26	9.70 ± 0.10 **	2.71 ± 0.82	8.86 ± 1.27 #	1.74 ± 0.68	4.20 ± 0.30 **	6.00 ± 0.96	8.15 ± 1.55 *
20:4 *n*-6 (ARA)	0.30 ± 0.27	1.20 ± 0.14 *	0.75 ± 0.35	1.99 ± 0.29 **	2.21 ± 1.34	6.63 ± 0.21 **	9.07 ± 1.66	12.4 ± 1.09 *
22:4 *n*-6 (AdA)	0.07 ± 0.05	0.47 ± 0.06 **	0.05 ± 0.03	0.37 ± 0.02 #	0.07 ± 0.04	0.36 ± 0.01 #	0.33 ± 0.07	0.70 ± 0.07 #
Other *n*-6 PUFAs	0.19 ± 0.12	0.90 ± 0.17 **	0.23 ± 0.09	0.59 ± 0.11 **	0.50 ± 0.40	0.90 ± 0.10	2.98 ± 0.71	2.34 ± 0.14
18:3 *n*-3 (ALA)	0.02 ± 0.01	0.02 ± 0.01	0.06 ± 0.02	0.04 ± 0.01	0.04 ± 0.02	0.02 ± 0.01	0.01 ± 0.01	0.02 ± 0.01
20:5 *n*-3 (EPA)	0.22 ± 0.15	0.16 ± 0.04	0.4 ± 0.23	0.18 ± 0.06	0.43 ± 0.17	0.09 ± 0.02 *	1.39 ± 0.24	0.18 ± 0.02 #
22:5 *n*-3 (DPA)	0.12 ± 0.10	1.01 ± 0.14 **	0.08 ± 0.04	0.88 ± 0.07 #	0.15 ± 0.12	1.35 ± 0.16 #	0.72 ± 0.20	2.57 ± 0.39
22:6 *n*-3 (DHA)	0.12 ± 0.08	0.84 ± 0.12 **	0.32 ± 0.13	1.39 ± 0.07 #	1.07 ± 0.86	4.81 ± 0.23 #	4.75 ± 1.43	9.08 ± 0.64 #
Other *n*-3 PUFAs	0.013 ± 0.005	0.02 ± 0.01	0.010 ± 0.007	0.03 ± 0.01 *	0.02 ± 0.01	0.04 ± 0.01	0.10 ± 0.02	0.09 ± 0.03 #
PUFA	**4.47 ± 2.01**	**14.3 ± 0.70** **	**4.61 ± 1.61**	**14.3 ± 1.04** #	**6.24 ± 3.57**	**18.4 ± 0.37** **	**25.4 ± 5.05**	**35.5 ± 3.43** *

p-value from *t*-tests: * $p < 0.05$, ** $p < 0.01$, # $p < 0.001$; AdA–adrenic acid (22:4 *n*-6); ALA–α-linolenic acid (18:3 *n*-3); ARA–arachidonic acid (20:4 *n*-6); DHA–docosahexaenoic acid (22:6 *n*-3); DPA–docosapentaenoic acid (22:5 *n*-3); EPA–eicosapentaenoic acid (20:5 *n*-3); LA–linoleic acid (18:2 *n*-6); MUFA–monounsaturated fatty acids; PUFA–polyunsaturated fatty acids; SFA–saturated fatty acids. Bold represents main groups of fatty acids. SD – mice fed standard diet; HFD – mice fed high fat diet

3.5. Fatty Acid Oxidation and Protein Carbonylation Content

Lipid peroxidation in heart tissue, assessed on the basis of MDA formation, did not differ between the SD- and HFD-fed mice (8.41 ± 1.95 and 8.67 ± 1.29 μM MDA per g of total protein, respectively). Similarly, we did not find any difference in protein carbonyl groups level (1.59 ± 0.24 vs 1.52 ± 0.28 nmol/mg of total protein).

4. Discussion

Obesity is well known to be a risk factor for the development of cardiovascular diseases, in particular, coronary heart disease and heart failure [68,69]. Diet-induced obesity may lead to profound changes in heart lipid composition due to its limited capacity for de novo FA synthesis and, therefore, reliance on the exogenous supply of FAs [69]. Our study aimed to assess the influence of an HFD, a model of the Western diet, on heart function with regard to FA composition in different lipid groups. Opinion on the extent of the detrimental effect of HFD in the heart differs. Several studies imply that an HFD diet alone is not sufficient for inducing heart failure [44,70,71], while others report lipotoxic cardiomyopathy under long dietary regimens [49,50] or cardiac hypertrophy under specific FA contents of a HFD [72]. HFD treatment is also one of the established models for the induction of aortic valve disease [73–75]. HFD treatment altered aortic flow pattern [73]. Amendment of resting cardiac function did not identify significant deterioration consistent with earlier report [54]. Moreover, Mourmoura et al. [54] suggest an augmented inotropism after the 3-month HFD diet intake and increased cardiac output, resulting from an increased cardiac mechanical function. However, a trend for lower values in the HFD group may suggest that, in our study, under conditions of increased workload or with strain imaging, such dysfunction could manifest. We strived to explain the association of lipid alterations with observed changes in heart function considering 1) ectopic lipid accumulation, 2) oxidative stress and 3) FA content changes in different lipid groups.

Postnatal mammalian hearts depend on FA β-oxidation coupled with oxidative phosphorylation to generate ATP [76]. The heart uptakes FAs both in non-esterified form, as FFAs and as esterified, lipoprotein-bound species [77]. An increased consumption of fat causes the storage capacity of adipocytes to be exceeded, leading to the release of FFAs from adipose tissue and their elevated levels in serum [78], which was also confirmed in our study. The overabundance of circulating lipids may cause ectopic fat accumulation in the liver, skeletal muscle or heart [50,79], despite the heart's preference for lipids as the energy substrate rather than for storage [80]. In HFD-fed mice, we observed that excess dietary supplementation of fat caused a higher cardiac content of TAGs, which is representative of neutral lipid accumulation. This result is consistent with that of previous studies [50,78] and is indicative of possible lipotoxicity [80]. Although TAGs themselves might not be toxic, they can indicate accumulation of other lipotoxic species, such as DAGs, which were reported to be accumulated under HFD intake [77,81]. Elevated circulation of FFAs was also a feature found in our study and was described by other authors in mice fed an HFD [78,82]. FFAs are utilized by cells for energy production via oxidative pathways or as substrates for complex lipid synthesis [83]. Du et al. [84] reported that increased FFA levels contribute to the overproduction of superoxide, which activates proinflammatory signals in aortic endothelial cells. One of the obesity hallmarks is the increase in oxidative stress and inflammation [68]. However, we did not observe differences in lipid peroxidation, nor in protein carbonylation between the HFD and SD groups, which may be attributed to the composition of the mouse chow used [72] or the duration of our study [50]. Similarly, the protein carbonyl content in heart tissue did not differ between SD and HFD mice. Moreover, Leger et al. [85] found that HFD led to decrease of cardiac oxidative stress and apoptosis rate in rats. This was associated with increased arachidonic acid proportion in membrane phospholipids. We also observed a trend to increase arachidonic acid in heart phospholipids but it did not reach statistical significance (Table 3).

Although there are some studies investigating the effects of dietary fat on rodent cardiac functions, most of them do not report specific FA profiles or do so only for total lipid FA profiles in heart tissue [50,53,72]. Alternatively, only FA profiles for one selected group of lipid species are

presented [86–88]. Some studies focused mostly on SFAs and MUFAs [51], while PUFAs have not been widely reported. In contrast, in studies involving humans, the effects of PUFA supplementation on heart function were primarily considered [44].

In general, we found upregulation of both n-3 and n-6 PUFA series contents, as well as increased contents of most individual PUFAs in the heart muscle of mice fed an HFD, with the exception of significantly downregulated EPA (Table 2). This accumulation of specific PUFAs is consistent with previous studies; for example, mitochondrial phospholipids in hearts were shown to readily incorporate dietary DHA [89] or ARA [88]. One possible explanation for the elevated levels of long-chain PUFAs (ARA, DHA, etc.) is that these PUFAs can also be synthesized from exogenous 18-carbon PUFAs [90]. Another point worth considering is the different rates of FA oxidation (FAO). The readiness of cells for utilization of FA by β-oxidation, both mitochondrial and peroxisomal, seems to be dependent on both the degree of FA unsaturation and FA acyl chain length [91–93]. Experiments evaluating total body FAO [91,92] as well as FAO rates for different tissues, including the heart [93], point to a preference for unsaturated vs saturated FAs (oleic acid > stearic acid FAO rate). This may explain the significantly reduced MUFAs, which are preferred for β-oxidation over other FAs, in the hearts of HFD-fed mice. Among PUFAs, higher oxidation rates were observed for 18-carbon-chained PUFAs, especially for α-linolenic acid (ALA, 18:3 *n*-3), which is preferred for β-oxidation among other PUFAs [91] and may explain why we did not observe any ALA accumulation in hearts due to HFD treatment, in contrast to the observed accumulation of most other PUFAs (Tables 2–4). Another PUFA that did not accumulate in the hearts was EPA (Tables 2–4). However, it should be pointed out that the DPA content in the hearts of HFD-fed mice in our study increased three-fold (Table 2), and this FA is a metabolic intermediate between EPA and DHA, which may explain the depletion of EPA [90]. PUFAs can influence tissue function via their downstream metabolites. Moreover, *n*-3 PUFAs can exert positive effects on cardiac functions [94], which are mainly associated with anti-inflammatory metabolites of their enzymatic oxidation [95]. Increased arachidonic acid content in HFD-fed mouse serum and tissues may be explained both by the dietary supply and conversion of linoleic acid (LA, 18:2 *n*-6) [96] or, in the case of heart phospholipids, the preference of cardiac 1-acyl-sn-glycerol 3-phosphate acyltransferase (AGPAT) for ARA during phosphatidic acid synthesis [97]. While many ARA-derived eicosanoids have detrimental effects on cardiac health, some seem to be cardioprotective [98]. Keeping in mind that many LA-derived bioactive metabolites are, in fact, anti-inflammatory [96] and that an almost two-fold increase in the docosahexaenoic acid (DHA, 22:6 *n*-3) content was observed in HFD-fed mouse serum and heart, which is a precursor of anti-inflammatory docosanoids, the deleterious effects of EPA depletion may possibly be ameliorated by the increased content of these other PUFAs. Considering the association between inflammation and oxidative stress, the lack of oxidative stress in the hearts of HFD-fed mice found in our study may be the result of the accumulation of other anti-inflammatory *n*-3 PUFAs.

Since the changes in FA composition in various lipids can differentially impact cardiac function, we focused on trying to elucidate which lipid groups were most affected by an HFD. The SPE procedures allowed for us to obtain several lipid fractions, analysis of which revealed profound changes in polar lipids caused by HFD intake (Tables 3 and 4). While AGs and FFAs serve mainly as energy sources [77], alterations of polar lipids, which are the main components of cell membranes and membrane domains, can lead to changes in membrane fluidity, permeability and functions facilitated by the lipid bilayer [83,99]. In mammalian membranes, PUFAs are usually present in the *sn*-2 acyl chain position of PLs, e.g., phosphatidylcholine (PC) and phosphatidylethanolamine (PE) [100]. One consequence of PUFA incorporation into the side chains of membrane lipids is the enhanced fluidity, and this effect increases with the number of double bonds [100,101]. Nonetheless, this comes at the cost of PUFA susceptibility to autooxidation, resulting in damage to DNA or proteins by generation of reactive carbonyl species or induction of inflammation and apoptosis [101]. Our model did not display signs of increased oxidative stress; however, PUFA incorporation into polar lipids suggests a higher risk of membrane damage, which may not be apparent because of the short duration of the study. Moreover, these changes were found not only in phospholipids but also in sphingolipids

(Table 4 and Figure 2), which are responsible for cell–cell interactions (GSPL), apoptotic signalling and lipotoxicity (Cer, SM) [83]. PUFA incorporation reduces the thickness and disrupts the geometry of lipid membranes [102] and can disrupt the raft composition, causing displacement of membrane-bound proteins [103]. Since phospholipids are the main cell membrane components, PUFA contains more double bonds than MUFA, and PUFA are more numerous in phospholipids than MUFA (see Table 3), even when total MUFA decrease in heart phospholipids, the simultaneous increase of PUFA content (Table 3) may lead to increased membrane fluidity. Thus, one could speculate that a detrimental effect of increased PUFA content in membrane lipids may be a result of excessive cell membrane fluidity in heart after HFD. Yamamoto et al. [51] reported that an HFD rich in SFAs, but not MUFAs, causes a decrease in the expression of stearoyl-CoA desaturase 1 (SCD1), an enzyme that catalyses the rate-limiting step in MUFA synthesis. It is possible that the heart muscle compensates for the loss of saturation caused by the reduction of SCD1 expression and preferential MUFA β-oxidation by funnelling PUFAs into membrane lipids to alleviate this effect.

Among cardiac lipids, mitochondrial species are particularly worth considering. Heart tissue is rich in mitochondria; therefore, the mitochondrial lipidome accounts for a large portion of total heart lipids, with cardiolipin, a diphosphatidylglycerol PL species unique to mitochondrial membranes, present at approximately 15 nmol/mg protein in mice [104]. Cardiolipin is crucial for the proper function of many proteins in the mitochondrial membrane and is involved in electron flux during ATP production, and within it, the abundance of symmetrical species containing four LA side chains seems to be pivotal to maintaining proper membrane characteristics [105]. In our study, the content of LA in the heart PL fraction was significantly higher in HFD-fed mice (Table 3). However, there are suggestions that cardiolipin LA is readily replaced by longer chain PUFAs, especially DHA [106], which can affect mitochondrial functions [107]. We observed enrichment of DHA in the heart PL fraction (Table 3), but this result was not statistically significant. On the other hand, DPA can replace DHA in some membranes, where its additional bond may influence some membrane-bound protein functions [108]. Under HFD treatment, Sullivan et al. [65] reported the remodelling of some LA-containing cardiolipin species, as well as some mitochondrial phosphatidylcholines and phosphatidylethanolamines, with no significant impairment of mitochondrial supercomplex formation or respiratory enzymatic activity. Thus, the increase in PUFA incorporation in HFD-fed mice may explain the lack of severe cardiac dysfunction observed by us (Table 1).

5. Conclusions

In conclusion, the main value of our study was the determination of FA profiles in various lipid groups after HFD treatment of mice, which revealed severe changes in lipids of cell membranes. Considering the preferential β-oxidation of MUFAs in the heart described in the literature, one can expect that it leads to PUFA accumulation after HFD intake and excessive incorporation of PUFAs into membrane lipids. Although HFD caused mild heart dysfunction in our experimental conditions, excessive PUFA incorporation into the cell membrane might change the membrane properties and increase the risk of more serious damage during the progression of obesity. While our data clearly indicate a substantial impact of a high-fat diet on cardiac lipid composition its functional effects still should be treated as preliminary and we feel that work needs to be validated in different, preferably larger, animal cohorts.

Author Contributions: Conceptualization, A.M. and T.S.; investigation, A.J., A.M., A.Z., P.M., I.L., A.P.; resources, A.J.; writing—original draft preparation, A.P. and I.L., writing—review & editing, A.M. and T.S. All authors have read and agreed to the published version of the manuscript.

Funding: This research was funded by the National Science Centre of Poland, grant number NCN 2016/21/D/NZ5/00219.

Conflicts of Interest: The authors declare no conflict of interest. The funders had no role in the design of the study; in the collection, analyses, or interpretation of data; in the writing of the manuscript, or in the decision to publish the results.

References

1. Psaltopoulou, T.; Hatzis, G.; Papageorgiou, N.; Androulakis, E.; Briasoulis, A.; Tousoulis, D. Socioeconomic status and risk factors for cardiovascular disease: Impact of dietary mediators. *Hell. J. Cardiol.* **2017**, *58*, 32–42. [CrossRef]
2. Fung, T.T.; Stampfer, M.J.; Manson, J.E.; Rexrode, K.M.; Willett, W.C.; Hu, F.B. Prospective Study of Major Dietary Patterns and Stroke Risk in Women. *Stroke* **2004**, *35*, 2014–2019. [CrossRef]
3. Cordain, L.; Eaton, S.B.; Sebastian, A.; Mann, N.; Lindeberg, S.; Watkins, B.A.; O'Keefe, J.H.; Brand-Miller, J. Origins and evolution of the Western diet: Health implications for the 21st century. *Am. J. Clin. Nutr.* **2005**, *81*, 341–354. [CrossRef] [PubMed]
4. Zinöcker, M.; Lindseth, I. The Western Diet–Microbiome-Host Interaction and Its Role in Metabolic Disease. *Nutrients* **2018**, *10*, 365. [CrossRef] [PubMed]
5. Amato, K.R.; Yeoman, C.J.; Cerda, G.; Schmitt, C.A.; Cramer, J.D.; Miller, M.E.B.; Gomez, A.; Turner, T.R.; Wilson, B.A.; Stumpf, R.M.; et al. Variable responses of human and non-human primate gut microbiomes to a Western diet. *Microbiome* **2015**, *3*, 53. [CrossRef] [PubMed]
6. Martinez, K.B.; Leone, V.; Chang, E.B. Western diets, gut dysbiosis, and metabolic diseases: Are they linked? *Gut Microbes* **2017**, *8*, 130–142. [CrossRef]
7. Agus, A.; Denizot, J.; Thévenot, J.; Martinez-Medina, M.; Massier, S.; Sauvanet, P.; Bernalier-Donadille, A.; Denis, S.; Hofman, P.; Bonnet, R.; et al. Western diet induces a shift in microbiota composition enhancing susceptibility to Adherent-Invasive E. coli infection and intestinal inflammation. *Sci. Rep.* **2016**, *6*, 19032. [CrossRef]
8. Hyoju, S.K.; Zaborin, A.; Keskey, R.; Sharma, A.; Arnold, W.; van den Berg, F.; Kim, S.M.; Gottel, N.; Bethel, C.; Charnot-Katsikas, A.; et al. Mice Fed an Obesogenic Western Diet, Administered Antibiotics, and Subjected to a Sterile Surgical Procedure Develop Lethal Septicemia with Multidrug-Resistant Pathobionts. *mBio* **2019**, *10*, 263–271. [CrossRef]
9. Harris, K.L.; Pulliam, S.R.; Okoro, E.; Guo, Z.; Washington, M.K.; Adunyah, S.E.; Amos-Landgraf, J.M.; Ramesh, A. Western diet enhances benzo(a)pyrene-induced colon tumorigenesis in a polyposis in rat coli (PIRC) rat model of colon cancer. *Oncotarget* **2016**, *7*, 28947–28960. [CrossRef]
10. Mustafi, R.; Dougherty, U.; Mustafi, D.; Ayaloglu-Butun, F.; Fletcher, M.; Adhikari, S.; Sadiq, F.; Meckel, K.; Haider, H.I.; Khalil, A.; et al. ADAM17 is a Tumor Promoter and Therapeutic Target in Western Diet–associated Colon Cancer. *Clin. Cancer Res.* **2017**, *23*, 549–561. [CrossRef]
11. Laing, B.B.; Lim, A.G.; Ferguson, L.R. A Personalised Dietary Approach—A Way Forward to Manage Nutrient Deficiency, Effects of the Western Diet, and Food Intolerances in Inflammatory Bowel Disease. *Nutrients* **2019**, *11*, 1532. [CrossRef] [PubMed]
12. Ranjit, S.; Dvornikov, A.; Dobrinskikh, E.; Wang, X.; Luo, Y.; Levi, M.; Gratton, E. Measuring the effect of a Western diet on liver tissue architecture by FLIM autofluorescence and harmonic generation microscopy. *Biomed. Opt. Express* **2017**, *8*, 3143–3154. [CrossRef]
13. Gabbia, D.; Roverso, M.; Guido, M.; Sacchi, D.; Scaffidi, M.; Carrara, M.; Orso, G.; Russo, F.P.; Floreani, A.; Bogialli, S.; et al. Western Diet-Induced Metabolic Alterations Affect Circulating Markers of Liver Function before the Development of Steatosis. *Nutrients* **2019**, *11*, 1602. [CrossRef] [PubMed]
14. Lytle, K.A.; Depner, C.M.; Wong, C.P.; Jump, D.B. Docosahexaenoic acid attenuates Western diet-induced hepatic fibrosis in Ldlr −/− mice by targeting the TGFβ-Smad3 pathway. *J. Lipid Res.* **2015**, *56*, 1936–1946. [CrossRef] [PubMed]
15. Jena, P.K.; Sheng, L.; Di Lucente, J.; Jin, L.-W.; Maezawa, I.; Wan, Y.-J.Y. Dysregulated bile acid synthesis and dysbiosis are implicated in Western diet–induced systemic inflammation, microglial activation, and reduced neuroplasticity. *FASEB J.* **2018**, *32*, 2866–2877. [CrossRef]
16. Rutkowsky, J.M.; Lee, L.L.; Puchowicz, M.; Golub, M.S.; Befroy, D.E.; Wilson, D.W.; Anderson, S.; Cline, G.; Bini, J.; Borkowski, K.; et al. Reduced cognitive function, increased blood-brain-barrier transport and inflammatory responses, and altered brain metabolites in LDLr -/-and C57BL/6 mice fed a western diet. *PLoS ONE* **2018**, *13*, e0191909. [CrossRef] [PubMed]
17. Yokoyama, A.S.; Dunaway, K.; Rutkowsky, J.; Rutledge, J.C.; Milenkovic, D. Chronic consumption of a western diet modifies the DNA methylation profile in the frontal cortex of mice. *Food Funct.* **2018**, *9*, 1187–1198. [CrossRef] [PubMed]

18. Kanoski, S.E.; Davidson, T.L. Western diet consumption and cognitive impairment: Links to hippocampal dysfunction and obesity. *Physiol. Behav.* **2011**, *103*, 59–68. [CrossRef] [PubMed]
19. Maesako, M.; Uemura, K.; Iwata, A.; Kubota, M.; Watanabe, K.; Uemura, M.; Noda, Y.; Asada-Utsugi, M.; Kihara, T.; Takahashi, R.; et al. Continuation of Exercise Is Necessary to Inhibit High Fat Diet-Induced β-Amyloid Deposition and Memory Deficit in Amyloid Precursor Protein Transgenic Mice. *PLoS ONE* **2013**, *8*, e72796. [CrossRef] [PubMed]
20. Morris, M.C.; Tangney, C.C. Dietary fat composition and dementia risk. *Neurobiol. Aging* **2014**, *35*, S59–S64. [CrossRef] [PubMed]
21. Graham, L.C.; Harder, J.M.; Soto, I.; de Vries, W.N.; John, S.W.M.; Howell, G.R. Chronic consumption of a western diet induces robust glial activation in aging mice and in a mouse model of Alzheimer's disease. *Sci. Rep.* **2016**, *6*, 21568. [CrossRef] [PubMed]
22. Veniaminova, E.; Cespuglio, R.; Cheung, C.W.; Umriukhin, A.; Markova, N.; Shevtsova, E.; Lesch, K.-P.; Anthony, D.C.; Strekalova, T. Autism-Like Behaviours and Memory Deficits Result from a Western Diet in Mice. *Neural Plast.* **2017**, *2017*. [CrossRef] [PubMed]
23. Machado, M.V.; Michelotti, G.A.; Xie, G.; de Almeida, T.P.; Boursier, J.; Bohnic, B.; Guy, C.D.; Diehl, A.M. Mouse Models of Diet-Induced Nonalcoholic Steatohepatitis Reproduce the Heterogeneity of the Human Disease. *PLoS ONE* **2015**, *10*, e0127991. [CrossRef] [PubMed]
24. Napier, B.A.; Andres-Terre, M.; Massis, L.M.; Hryckowian, A.J.; Higginbottom, S.K.; Cumnock, K.; Casey, K.M.; Haileselassie, B.; Lugo, K.A.; Schneider, D.S.; et al. Western diet regulates immune status and the response to LPS-driven sepsis independent of diet-associated microbiome. *Proc. Natl. Acad. Sci. USA* **2019**, *116*, 3688–3694. [CrossRef]
25. Manzel, A.; Muller, D.N.; Hafler, D.A.; Erdman, S.E.; Linker, R.A.; Kleinewietfeld, M. Role of "Western Diet" in Inflammatory Autoimmune Diseases. *Curr. Allergy Asthma Rep.* **2014**, *14*, 404. [CrossRef]
26. Totsch, S.K.; Waite, M.E.; Tomkovich, A.; Quinn, T.L.; Gower, B.A.; Sorge, R.E. Total Western Diet Alters Mechanical and Thermal Sensitivity and Prolongs Hypersensitivity Following Complete Freund's Adjuvant in Mice. *J. Pain* **2016**, *17*, 119–125. [CrossRef]
27. Shively, C.A.; Register, T.C.; Appt, S.E.; Clarkson, T.B.; Uberseder, B.; Clear, K.Y.J.; Wilson, A.S.; Chiba, A.; Tooze, J.A.; Cook, K.L. Consumption of Mediterranean versus Western Diet Leads to Distinct Mammary Gland Microbiome Populations. *Cell Rep.* **2018**, *25*, 47–56.e3. [CrossRef]
28. Bedja, D.; Yan, W.; Lad, V.; Iocco, D.; Sivakumar, N.; Bandaru, V.V.R.; Chatterjee, S. Inhibition of glycosphingolipid synthesis reverses skin inflammation and hair loss in ApoE−/− mice fed western diet. *Sci. Rep.* **2018**, *8*, 11463. [CrossRef]
29. Lytle, K.A.; Jump, D.B. Is Western Diet-Induced Nonalcoholic Steatohepatitis in Ldlr-/- Mice Reversible? *PLoS ONE* **2016**, *11*, e0146942. [CrossRef]
30. Myles, I.A. Fast food fever: Reviewing the impacts of the Western diet on immunity. *Nutr. J.* **2014**, *13*, 61. [CrossRef]
31. Nazni, P. Association of western diet & lifestyle with decreased fertility. *Indian J. Med. Res.* **2014**, *140*, 78–81.
32. Sinclair, K.J.; Friesen–Waldner, L.J.; McCurdy, C.M.; Wiens, C.N.; Wade, T.P.; de Vrijer, B.; Regnault, T.R.H.; McKenzie, C.A. Quantification of fetal organ volume and fat deposition following in utero exposure to maternal Western Diet using MRI. *PLoS ONE* **2018**, *13*, e0192900. [CrossRef] [PubMed]
33. Perez, P.A.; DiPatrizio, N.V. Impact of maternal western diet-induced obesity on offspring mortality and peripheral endocannabinoid system in mice. *PLoS ONE* **2018**, *13*, e0205021. [CrossRef] [PubMed]
34. Frihauf, J.B.; Fekete, É.M.; Nagy, T.R.; Levin, B.E.; Zorrilla, E.P. Maternal Western diet increases adiposity even in male offspring of obesity-resistant rat dams: Early endocrine risk markers. *Am. J. Physiol. Integr. Comp. Physiol.* **2016**, *311*, R1045–R1059. [CrossRef]
35. Varlamov, O. Western-style diet, sex steroids and metabolism. *Biochim. Biophys. Acta Mol. Basis Dis.* **2017**, *1863*, 1147–1155. [CrossRef]
36. Hariharan, D.; Vellanki, K.; Kramer, H. The Western Diet and Chronic Kidney Disease. *Curr. Hypertens. Rep.* **2015**, *17*, 16. [CrossRef]
37. Odermatt, A. The Western-style diet: A major risk factor for impaired kidney function and chronic kidney disease. *Am. J. Physiol. Ren. Physiol.* **2011**, *301*, F919–F931. [CrossRef]
38. Houston, M.; Minich, D.; Sinatra, S.T.; Kahn, J.K.; Guarneri, M. Recent Science and Clinical Application of Nutrition to Coronary Heart Disease. *J. Am. Coll. Nutr.* **2018**, *37*, 169–187. [CrossRef]

39. Heidemann, C.; Schulze, M.B.; Franco, O.H.; van Dam, R.M.; Mantzoros, C.S.; Hu, F.B. Dietary Patterns and Risk of Mortality From Cardiovascular Disease, Cancer, and All Causes in a Prospective Cohort of Women. *Circulation* **2008**, *118*, 230–237. [CrossRef]
40. Hu, F.B.; Rimm, E.B.; Stampfer, M.J.; Ascherio, A.; Spiegelman, D.; Willett, W.C. Prospective study of major dietary patterns and risk of coronary heart disease in men. *Am. J. Clin. Nutr.* **2000**, *72*, 912–921. [CrossRef]
41. Benjamin, E.J.; Muntner, P.; Alonso, A.; Bittencourt, M.S.; Callaway, C.W.; Carson, A.P.; Chamberlain, A.M.; Chang, A.R.; Cheng, S.; Das, S.R.; et al. Heart Disease and Stroke Statistics—2019 Update: A Report From the American Heart Association. *Circulation* **2019**, *139*, e56–e66. [CrossRef] [PubMed]
42. Tikellis, C.; Thomas, M.C.; Harcourt, B.E.; Coughlan, M.T.; Pete, J.; Bialkowski, K.; Tan, A.; Bierhaus, A.; Cooper, M.E.; Forbes, J.M. Cardiac inflammation associated with a Western diet is mediated via activation of RAGE by AGEs. *Am. J. Physiol. Metab.* **2008**, *295*, E323–E330. [CrossRef] [PubMed]
43. Jia, G.; Habibi, J.; Bostick, B.P.; Ma, L.; DeMarco, V.G.; Aroor, A.R.; Hayden, M.R.; Whaley-Connell, A.T.; Sowers, J.R. Uric Acid Promotes Left Ventricular Diastolic Dysfunction in Mice Fed a Western Diet. *Hypertension* **2015**, *65*, 531–539. [CrossRef]
44. Stanley, W.C.; Dabkowski, E.R.; Ribeiro, R.F.; O'Connell, K.A. Dietary fat and heart failure: Moving from lipotoxicity to lipoprotection. *Circ. Res.* **2012**, *110*, 764–776. [CrossRef]
45. Libby, P.; Ridker, P.M.; Maseri, A. Inflammation and Atherosclerosis. *Circulation* **2002**, *105*, 1135–1143. [CrossRef] [PubMed]
46. Lopez-Garcia, E.; Schulze, M.B.; Fung, T.T.; Meigs, J.B.; Rifai, N.; Manson, J.E.; Hu, F.B. Major dietary patterns are related to plasma concentrations of markers of inflammation and endothelial dysfunction. *Am. J. Clin. Nutr.* **2004**, *80*, 1029–1035. [CrossRef]
47. Pavillard, L.E.; Marín-Aguilar, F.; Bullon, P.; Cordero, M.D. Cardiovascular diseases, NLRP3 inflammasome, and western dietary patterns. *Pharmacol. Res.* **2018**, *131*, 44–50. [CrossRef]
48. Pavillard, L.E.; Cañadas-Lozano, D.; Alcocer-Gómez, E.; Marín-Aguilar, F.; Pereira, S.; Robertson, A.A.B.; Muntané, J.; Ryffel, B.; Cooper, M.A.; Quiles, J.L.; et al. NLRP3-inflammasome inhibition prevents high fat and high sugar diets-induced heart damage through autophagy induction. *Oncotarget* **2017**, *8*, 99740–99756. [CrossRef]
49. Calligaris, S.D.; Lecanda, M.; Solis, F.; Ezquer, M.; Gutiérrez, J.; Brandan, E.; Leiva, A.; Sobrevia, L.; Conget, P. Mice Long-Term High-Fat Diet Feeding Recapitulates Human Cardiovascular Alterations: An Animal Model to Study the Early Phases of Diabetic Cardiomyopathy. *PLoS ONE* **2013**, *8*, e60931. [CrossRef]
50. Harmancey, R.; Wilson, C.R.; Wright, N.R.; Taegtmeyer, H. Western diet changes cardiac acyl-CoA composition in obese rats: A potential role for hepatic lipogenesis. *J. Lipid Res.* **2010**, *51*, 1380–1393. [CrossRef]
51. Yamamoto, T.; Endo, J.; Kataoka, M.; Matsuhashi, T.; Katsumata, Y.; Shirakawa, K.; Yoshida, N.; Isobe, S.; Moriyama, H.; Goto, S.; et al. Decrease in membrane phospholipids unsaturation correlates with myocardial diastolic dysfunction. *PLoS ONE* **2018**, *13*, e0208396. [CrossRef] [PubMed]
52. Raher, M.J.; Thibault, H.B.; Buys, E.S.; Kuruppu, D.; Shimizu, N.; Brownell, A.-L.; Blake, S.L.; Rieusset, J.; Kaneki, M.; Derumeaux, G.; et al. A short duration of high-fat diet induces insulin resistance and predisposes to adverse left ventricular remodeling after pressure overload. *Am. J. Physiol. Circ. Physiol.* **2008**, *295*, H2495–H2502. [CrossRef]
53. Park, S.-Y.; Cho, Y.-R.; Kim, H.-J.; Higashimori, T.; Danton, C.; Lee, M.-K.; Dey, A.; Rothermel, B.; Kim, Y.-B.; Kalinowski, A.; et al. Unraveling the Temporal Pattern of Diet-Induced Insulin Resistance in Individual Organs and Cardiac Dysfunction in C57BL/6 Mice. *Diabetes* **2005**, *54*, 3530–3540. [CrossRef] [PubMed]
54. Mourmoura, E.; Chaté, V.; Couturier, K.; Laillet, B.; Vial, G.; Rigaudiere, J.-P.; Morio, B.; Malpuech-Brugère, C.; Azarnoush, K.; Demaison, L. Body adiposity dictates different mechanisms of increased coronary reactivity related to improved in vivo cardiac function. *Cardiovasc. Diabetol.* **2014**, *13*, 54. [CrossRef]
55. Ballal, K.; Wilson, C.R.; Harmancey, R.; Taegtmeyer, H. Obesogenic high fat western diet induces oxidative stress and apoptosis in rat heart. *Mol. Cell. Biochem.* **2010**, *344*, 221–230. [CrossRef]
56. Boudina, S.; Sena, S.; Theobald, H.; Sheng, X.; Wright, J.J.; Hu, X.X.; Aziz, S.; Johnson, J.I.; Bugger, H.; Zaha, V.G.; et al. Mitochondrial Energetics in the Heart in Obesity-Related Diabetes: Direct Evidence for Increased Uncoupled Respiration and Activation of Uncoupling Proteins. *Diabetes* **2007**, *56*, 2457–2466. [CrossRef]

57. Sodhi, K.; Srikanthan, K.; Goguet-Rubio, P.; Nichols, A.; Mallick, A.; Nawab, A.; Martin, R.; Shah, P.T.; Chaudhry, M.; Sigdel, S.; et al. pNaKtide Attenuates Steatohepatitis and Atherosclerosis by Blocking Na/K-ATPase/ROS Amplification in C57Bl6 and ApoE Knockout Mice Fed a Western Diet. *Sci. Rep.* **2017**, *7*, 193. [CrossRef]
58. Neves, F.A.; Cortez, E.; Bernardo, A.F.; Mattos, A.B.M.; Vieira, A.K.; de Malafaia, T.O.; Thole, A.A.; de Rodrigues-Cunha, S.A.C.; Garcia-Souza, É.P.; Sichieri, R.; et al. Heart energy metabolism impairment in Western-diet induced obese mice. *J. Nutr. Biochem.* **2014**, *25*, 50–57. [CrossRef]
59. Kankaanpaa, M.; Lehto, H.-R.; Parkka, J.P.; Komu, M.; Viljanen, A.; Ferrannini, E.; Knuuti, J.; Nuutila, P.; Parkkola, R.; Iozzo, P. Myocardial Triglyceride Content and Epicardial Fat Mass in Human Obesity: Relationship to Left Ventricular Function and Serum Free Fatty Acid Levels. *J. Clin. Endocrinol. Metab.* **2006**, *91*, 4689–4695. [CrossRef]
60. Püschel, G.P.; Henkel, J. Dietary cholesterol does not break your heart but kills your liver. *Porto Biomed. J.* **2018**, *3*, e12. [CrossRef]
61. Folch, J.; Lees, M.; Sloane Stanley, G.H. A simple method for the isolation and purification of total lipides from animal tissues. *J. Biol. Chem.* **1957**, *226*, 497–509. [PubMed]
62. Kaluzny, M.A.; Duncan, L.A.; Merritt, M.V.; Epps, D.E. Rapid separation of lipid classes in high yield and purity using bonded phase columns. *J. Lipid Res.* **1985**, *26*, 135–140. [PubMed]
63. Bodennec, J.; Koul, O.; Aguado, I.; Brichon, G.; Zwingelstein, G.; Portoukalian, J. A procedure for fractionation of sphingolipid classes by solid-phase extraction on aminopropyl cartridges. *J. Lipid Res.* **2000**, *41*, 1524–1531.
64. Pakiet, A.; Jakubiak, A.; Czumaj, A.; Sledzinski, T.; Mika, A. The effect of western diet on mice brain lipid composition. *Nutr. Metab.* **2019**, *16*, 81. [CrossRef]
65. Sullivan, E.M.; Fix, A.; Crouch, M.J.; Sparagna, G.C.; Zeczycki, T.N.; Brown, D.A.; Shaikh, S.R. Murine diet-induced obesity remodels cardiac and liver mitochondrial phospholipid acyl chains with differential effects on respiratory enzyme activity. *J. Nutr. Biochem.* **2017**, *45*, 94–103. [CrossRef] [PubMed]
66. Silva, L.C.; Futerman, A.H.; Prieto, M. Lipid Raft Composition Modulates Sphingomyelinase Activity and Ceramide-Induced Membrane Physical Alterations. *Biophys. J.* **2009**, *96*, 3210–3222. [CrossRef] [PubMed]
67. Duarte, J.A.G.; Carvalho, F.; Pearson, M.; Horton, J.D.; Browning, J.D.; Jones, J.G.; Burgess, S.C. A high-fat diet suppresses de novo lipogenesis and desaturation but not elongation and triglyceride synthesis in mice. *J. Lipid Res.* **2014**, *55*, 2541–2553. [CrossRef]
68. Mika, A.; Sledzinski, T. Alterations of specific lipid groups in serum of obese humans: A review. *Obes. Rev.* **2017**, *18*, 247–272. [CrossRef]
69. Karlstaedt, A.; Schiffer, W.; Taegtmeyer, H. Actionable Metabolic Pathways in Heart Failure and Cancer—Lessons From Cancer Cell Metabolism. *Front. Cardiovasc. Med.* **2018**, *5*, 71. [CrossRef]
70. Rennison, J.H.; McElfresh, T.A.; Chen, X.; Anand, V.R.; Hoit, B.D.; Hoppel, C.L.; Chandler, M.P. Prolonged exposure to high dietary lipids is not associated with lipotoxicity in heart failure. *J. Mol. Cell. Cardiol.* **2009**, *46*, 883–890. [CrossRef]
71. Brainard, R.E.; Watson, L.J.; DeMartino, A.M.; Brittian, K.R.; Readnower, R.D.; Boakye, A.A.; Zhang, D.; Hoetker, J.D.; Bhatnagar, A.; Baba, S.P.; et al. High Fat Feeding in Mice Is Insufficient to Induce Cardiac Dysfunction and Does Not Exacerbate Heart Failure. *PLoS ONE* **2013**, *8*, e83174. [CrossRef] [PubMed]
72. Nguyen, S.; Shao, D.; Tomasi, L.C.; Braun, A.; de Mattos, A.B.M.; Choi, Y.S.; Villet, O.; Roe, N.; Halterman, C.R.; Tian, R.; et al. The effects of fatty acid composition on cardiac hypertrophy and function in mouse models of diet-induced obesity. *J. Nutr. Biochem.* **2017**, *46*, 137–142. [CrossRef] [PubMed]
73. Zukowska, P.; Kutryb-Zajac, B.; Jasztal, A.; Toczek, M.; Zabielska, M.; Borkowski, T.; Khalpey, Z.; Smolenski, R.T.; Slominska, E.M. Deletion of CD73 in mice leads to aortic valve dysfunction. *Biochim. Biophys. Acta Mol. Basis Dis.* **2017**, *1863*, 1464–1472. [CrossRef] [PubMed]
74. Drolet, M.-C.; Roussel, E.; Deshaies, Y.; Couet, J.; Arsenault, M. A High Fat/High Carbohydrate Diet Induces Aortic Valve Disease in C57BL/6J Mice. *J. Am. Coll. Cardiol.* **2006**, *47*, 850–855. [CrossRef]
75. Hofmann, B.; Yakobus, Y.; Indrasari, M.; Nass, N.; Santos, A.N.; Kraus, F.B.; Silber, R.E.; Simm, A. RAGE influences the development of aortic valve stenosis in mice on a high fat diet. *Exp. Gerontol.* **2014**, *59*, 13–20. [CrossRef] [PubMed]
76. Rajabi, M.; Kassiotis, C.; Razeghi, P.; Taegtmeyer, H. Return to the fetal gene program protects the stressed heart: A strong hypothesis. *Heart Fail. Rev.* **2007**, *12*, 331–343. [CrossRef]

77. Goldberg, I.J.; Trent, C.M.; Schulze, P.C. Lipid Metabolism and Toxicity in the Heart. *Cell Metab.* **2012**, *15*, 805–812. [CrossRef]
78. Kalaivanisailaja, J.; Manju, V.; Nalini, N. Lipid profile in mice fed a high-fat diet after exogenous leptin administration. *Pol. J. Pharmacol.* **2003**, *55*, 763–769.
79. Park, T.-S.; Hu, Y.; Noh, H.-L.; Drosatos, K.; Okajima, K.; Buchanan, J.; Tuinei, J.; Homma, S.; Jiang, X.-C.; Abel, E.D.; et al. Ceramide is a cardiotoxin in lipotoxic cardiomyopathy. *J. Lipid Res.* **2008**, *49*, 2101–2112. [CrossRef]
80. Drosatos, K.; Schulze, P.C. Cardiac Lipotoxicity: Molecular Pathways and Therapeutic Implications. *Curr. Heart Fail. Rep.* **2013**, *10*, 109–121. [CrossRef]
81. Schulze, P.C.; Drosatos, K.; Goldberg, I.J. Lipid Use and Misuse by the Heart. *Circ. Res.* **2016**, *118*, 1736–1751. [CrossRef] [PubMed]
82. Wilson, C.R.; Tran, M.K.; Salazar, K.L.; Young, M.E.; Taegtmeyer, H. Western diet, but not high fat diet, causes derangements of fatty acid metabolism and contractile dysfunction in the heart of Wistar rats. *Biochem. J.* **2007**, *406*, 457–467. [CrossRef] [PubMed]
83. Boini, K.M.; Xia, M.; Koka, S.; Gehr, T.W.B.; Li, P.L. Sphingolipids in obesity and related complications. *Front. Biosci.* **2017**, *22*, 96–116.
84. Du, X.; Edelstein, D.; Obici, S.; Higham, N.; Zou, M.-H.; Brownlee, M. Insulin resistance reduces arterial prostacyclin synthase and eNOS activities by increasing endothelial fatty acid oxidation. *J. Clin. Investig.* **2006**, *116*, 1071–1080. [CrossRef]
85. Leger, T.; Hininger-Favier, I.; Capel, F.; Geloen, A.; Rigaudière, J.-P.; Jouve, C.; Pitois, E.; Pineau, G.; Vaysse, C.; Chardigny, J.-M.; et al. Dietary canolol protects the heart against the deleterious effects induced by the association of rapeseed oil, vitamin E and coenzyme Q10 in the context of a high-fat diet. *Nutr. Metab.* **2018**, *15*, 15. [CrossRef]
86. Tepšic, V.; Ristic, V.; Ristic, D.; Vasiljevic, N.; Pecelj-Gec, M. Heart phospholipid content and fatty acid composition in the rat after feeding different lipid supplemented diets. *Physiol. Res.* **1998**, *47*, 413–418. [PubMed]
87. Duivenvoorde, L.P.M.; Van Schothorst, E.M.; Swarts, H.M.; Kuda, O.; Steenbergh, E.; Termeulen, S.; Kopecky, J.; Keijer, J. A Difference in fatty acid composition of isocaloric high-fat diets alters metabolic flexibility in male C57BL/6JOlaHsd mice. *PLoS ONE* **2015**, *10*, e0128515. [CrossRef]
88. Chen, B.; Huang, Y.; Zheng, D.; Ni, R.; Bernards, M.A. Dietary fatty acids alter lipid profiles and induce myocardial dysfunction without causing metabolic disorders in mice. *Nutrients* **2018**, *10*, 106. [CrossRef]
89. Watkins, S.M.; Lin, T.Y.; Davis, R.M.; Ching, J.R.; DePeters, E.J.; Halpern, G.M.; Walzem, R.L.; German, J.B. Unique phospholipid metabolism in mouse heart in response to dietary docosahexaenoic or α-linolenic acids. *Lipids* **2001**, *36*, 247–254. [CrossRef]
90. Tosi, F.; Sartori, F.; Guarini, P.; Olivieri, O.; Martinelli, N. Delta-5 and Delta-6 Desaturases: Crucial Enzymes in Polyunsaturated Fatty Acid-Related Pathways with Pleiotropic Influences in Health and Disease. In *Oxidative Stress and Inflammation in Non-communicable Diseases—Molecular Mechanisms and Perspectives in Therapeutics*; Camps, J., Ed.; Advances in Experimental Medicine and Biology; Springer: Cham, Switzerland, 2014; Volume 824, pp. 61–81.
91. DeLany, J.P.; Windhauser, M.M.; Champagne, C.M.; Bray, G.A. Differential oxidation of individual dietary fatty acids in humans. *Am. J. Clin. Nutr.* **2000**, *72*, 905–911. [CrossRef]
92. Leyton, J.; Drury, P.J.; Crawford, M.A. Differential oxidation of saturated and unsaturated fatty acids in vivo in the rat. *Br. J. Nutr.* **1987**, *57*, 383–393. [CrossRef]
93. Reubsaet, F.A.G.; Veerkamp, J.H.; Trijbels, J.M.F.; Monnens, L.A.H. Total and peroxisomal oxidation of various saturated and unsaturated fatty acids in rat liver, heart and m. quadriceps. *Lipids* **1989**, *24*, 945–950. [CrossRef] [PubMed]
94. Marventano, S.; Kolacz, P.; Castellano, S.; Galvano, F.; Buscemi, S.; Mistretta, A.; Grosso, G. A review of recent evidence in human studies of n-3 and n-6 PUFA intake on cardiovascular disease, cancer, and depressive disorders: Does the ratio really matter? *Int. J. Food Sci. Nutr.* **2015**, *66*, 611–622. [CrossRef] [PubMed]
95. Gabbs, M.; Leng, S.; Devassy, J.G.; Monirujjaman, M.; Aukema, H.M. Advances in Our Understanding of Oxylipins Derived from Dietary PUFAs. *Adv. Nutr.* **2015**, *6*, 513–540. [CrossRef] [PubMed]
96. Harris, W.S.; Shearer, G.C. Omega-6 Fatty Acids and Cardiovascular Disease. *Circulation* **2014**, *130*, 1562–1564. [CrossRef] [PubMed]

97. Shindou, H.; Shimizu, T. Acyl-CoA:Lysophospholipid Acyltransferases. *J. Biol. Chem.* **2009**, *284*, 1–5. [CrossRef]
98. Sonnweber, T.; Pizzini, A.; Nairz, M.; Weiss, G.; Tancevski, I. Arachidonic Acid Metabolites in Cardiovascular and Metabolic Diseases. *Int. J. Mol. Sci.* **2018**, *19*, 3285. [CrossRef]
99. Hatch, G.M. Cell biology of cardiac mitochondrial phospholipids. *Biochem. Cell Biol.* **2004**, *82*, 99–112. [CrossRef]
100. Stubbs, C.D.; Smith, A.D. The modification of mammalian membrane polyunsaturated fatty acid composition in relation to membrane fluidity and function. *Biochim. Biophys. Acta Rev. Biomembr.* **1984**, *779*, 89–137. [CrossRef]
101. Shchepinov, M.S.; Roginsky, V.A.; Brenna, J.T.; Molinari, R.J.; To, R.; Tsui, H.; Clarke, C.F.; Manning-Boğ, A.B. Deuterium Protection of Polyunsaturated Fatty Acids against Lipid Peroxidation. In *Omega-3 Fatty Acids in Brain and Neurological Health*; Academic Press: Cambridge, MA, USA, 2014; pp. 373–383.
102. Salmon, A.; Dodd, S.W.; Williams, G.D.; Beach, J.M.; Brown, M.F. Configurational Statistics of Acyl Chains in Polyunsaturated Lipid Bilayers from 2H NMR. *J. Am. Chem. Soc.* **1987**, *109*, 2600–2609. [CrossRef]
103. Stulnig, T.M.; Huber, J.; Leitinger, N.; Imre, E.-M.; Angelisová, P.; Nowotny, P.; Waldhäusl, W. Polyunsaturated Eicosapentaenoic Acid Displaces Proteins from Membrane Rafts by Altering Raft Lipid Composition. *J. Biol. Chem.* **2001**, *276*, 37335–37340. [CrossRef] [PubMed]
104. Han, X.; Yang, K.; Yang, J.; Cheng, H.; Gross, R.W. Shotgun lipidomics of cardiolipin molecular species in lipid extracts of biological samples. *J. Lipid Res.* **2006**, *47*, 864–879. [CrossRef] [PubMed]
105. Sparagna, G.C.; Lesnefsky, E.J. Cardiolipin Remodeling in the Heart. *J. Cardiovasc. Pharmacol.* **2009**, *53*, 290–301. [CrossRef] [PubMed]
106. Cortie, C.; Else, P. Dietary Docosahexaenoic Acid (22:6) Incorporates into Cardiolipin at the Expense of Linoleic Acid (18:2): Analysis and Potential Implications. *Int. J. Mol. Sci.* **2012**, *13*, 15447–15463. [CrossRef] [PubMed]
107. Yamaoka, S.; Urade, R.; Kito, M. Mitochondrial Function in Rats Is Affected by Modification of Membrane Phospholipids with Dietary Sardine Oil. *J. Nutr.* **1988**, *118*, 290–296. [CrossRef] [PubMed]
108. Eldho, N.V.; Feller, S.E.; Tristram-Nagle, S.; Polozov, I.V.; Gawrisch, K. Polyunsaturated docosahexaenoic vs docosapentaenoic acid—Differences in lipid matrix properties from the loss of one double bond. *J. Am. Chem. Soc.* **2003**, *125*, 6409–6421. [CrossRef]

nutrients

MDPI

Article

Interplay of Dietary Fatty Acids and Cholesterol Impacts Brain Mitochondria and Insulin Action

Mareike Schell [1,2,†], Chantal Chudoba [1,2,†], Antoine Leboucher [1,2], Eugenia Alfine [1], Tanina Flore [1], Katrin Ritter [1], Katharina Weiper [1,3], Andreas Wernitz [4], Janin Henkel [3,‡] and André Kleinridders [1,2,5,*,‡]

1 Junior Research Group Central Regulation of Metabolism, German Institute of Human Nutrition, D-14558 Nuthetal, Germany; Mareike.Schell@dife.de (M.S.); Chantal.Chudoba@dife.de (C.C.); Antoine.Leboucher@dife.de (A.L.); Eugenia.Alfine@dife.de (E.A.); Tanina.Flore@dife.de (T.F.); Katrin.Ritter@dife.de (K.R.); weiper@uni-potsdam.de (K.W.)
2 German Center for Diabetes Research (DZD), D-85764 München-Neuherberg, Germany
3 Department of Nutritional Biochemistry, Institute of Nutritional Science, University of Potsdam, D-14558 Nuthetal, Germany; jhenkel@uni-potsdam.de
4 Department of Molecular Epidemiology, German Institute of Human Nutrition, D-14558 Nuthetal, Germany; Andreas.Wernitz@dife.de
5 Department of Molecular and Experimental Nutritional Medicine, Institute of Nutritional Science, University of Potsdam, D-14558 Nuthetal, Germany
* Correspondence: kleinridders@uni-potsdam.de; Tel.: +49-33200-885230
† Equally contributed.
‡ Equally contributed last authors.

Received: 24 April 2020; Accepted: 21 May 2020; Published: 23 May 2020

Abstract: Overconsumption of high-fat and cholesterol-containing diets is detrimental for metabolism and mitochondrial function, causes inflammatory responses and impairs insulin action in peripheral tissues. Dietary fatty acids can enter the brain to mediate the nutritional status, but also to influence neuronal homeostasis. Yet, it is unclear whether cholesterol-containing high-fat diets (HFDs) with different combinations of fatty acids exert metabolic stress and impact mitochondrial function in the brain. To investigate whether cholesterol in combination with different fatty acids impacts neuronal metabolism and mitochondrial function, C57BL/6J mice received different cholesterol-containing diets with either high concentrations of long-chain saturated fatty acids or soybean oil-derived poly-unsaturated fatty acids. In addition, CLU183 neurons were stimulated with combinations of palmitate, linoleic acid and cholesterol to assess their effects on metabolic stress, mitochondrial function and insulin action. The dietary interventions resulted in a molecular signature of metabolic stress in the hypothalamus with decreased expression of occludin and subunits of mitochondrial electron chain complexes, elevated protein carbonylation, as well as c-Jun N-terminal kinase (JNK) activation. Palmitate caused mitochondrial dysfunction, oxidative stress, insulin and insulin-like growth factor-1 (IGF-1) resistance, while cholesterol and linoleic acid did not cause functional alterations. Finally, we defined insulin receptor as a novel negative regulator of metabolically stress-induced JNK activation.

Keywords: cholesterol; insulin signaling; mitochondria; brain; inflammation; fatty acids; JNK; insulin receptor

1. Introduction

The growing obesity pandemic is nowadays a global health concern and affects all age classes. Obesity is a major determinant for the establishment of insulin resistance and can lead to metabolic

disorders, such as non-alcoholic fatty liver disease, type 2 diabetes and metabolic syndrome [1]. The development of obesity is mainly due to a lack of physical exercise with disproportional food intake. Feeding mice high caloric diets containing either high-fructose or high-fat concentrations induces obesity and insulin resistance [2]. In line with this, increased portion sizes with concomitant increased caloric intake cause obesity in humans [3]. Though high-fat diets (HFDs) have been shown to be instrumental for the induction of obesity and insulin resistance, it is of importance to differentiate between the quality of consumed fatty acids and their potential interplay with other nutrients. Not every high-fat diet has to exert only negative effects on metabolism. Feeding mice a HFD containing 45%–60% of calories derived mainly from lard is sufficient to induce obesity and insulin resistance. Yet, obese mice fed a HFD supplemented with the ω3 poly-unsaturated fatty acid, eicosapentaenoic acid, exhibit improved glucose tolerance and insulin sensitivity but did not decrease food intake [4]. These data indicate that the different HFDs exert diet-specific effects on insulin sensitivity, which also depends on genetic predispositions. In addition, feeding mice cholesterol-containing HFDs, containing either increased amounts of long-chain saturated fatty acids (LCSFA) or poly-unsaturated fatty acids (PUFA), induces body weight gain, fat mass accumulation and insulin resistance. Mice fed a cholesterol-containing low-fat diet developed hepatic steatosis, although they did not become obese [5].

The brain occupies a pivotal role in the regulation of body weight and insulin sensitivity. We have recently shown that feeding mice a HFD induces brain insulin resistance with a reduced mitochondrial stress response as early as three days of dietary exposure, while activation of brain insulin signaling counteracted these HFD-induced metabolic alterations [6]. This HFD contained high amounts of LCSFA, suggesting that an increased consumption of LCSFA is a potential mediator of brain insulin resistance. Indeed, the LCSFA palmitate is sufficient to induce hypothalamic insulin resistance [7,8], whereas long-chain mono-unsaturated fatty acids do not alter insulin sensitivity [9]. In addition, palmitate induces cell stress and activates cellular stress kinases, such as inhibitor of κB kinase, c-Jun N-terminal kinase (JNK) or protein kinase C. As these kinases have been linked to insulin resistance, it indicates that palmitate induces an inflammatory response with reduced insulin action in neurons [7,9,10]. Yet, humans do not consume exclusively only one fatty acid species but ingest a mixture of fatty acids, lipids, cholesterol and other nutrients, which modulate each other's effects on metabolism. In line with this, it has been shown that oleate or, e.g., the PUFA docosahexaenoic acid, reverse palmitate-induced insulin resistance [11,12], highlighting the importance of understanding the interplay of fatty acids on cellular metabolism. An interplay of different fatty acids with cholesterol might also modulate insulin action. Cholesterol-containing diets have been shown to induce insulin resistance in peripheral tissues [13,14], but reduced cholesterol levels cause brain insulin resistance [15]. Although the brain is independent of dietary cholesterol, as it synthesizes its own cholesterol pool, high-fat/high-cholesterol intake has been shown to affect barrier integrity [16], which might cause altered neuronal homeostasis and metabolism [17]. Decreased mitochondrial cholesterol content deteriorates mitochondrial function [18]. In contrast, elevated cholesterol levels in mitochondrial membranes impair mitochondrial function [19] and mitochondrial cholesterol loading exacerbates inflammation [20]. These data indicate that increased as well as decreased cholesterol levels within mitochondria worsen their function, pointing to an important role of precise cholesterol regulation for brain health. Interestingly, insulin is a key regulator of brain cholesterol metabolism and reduced brain cholesterol synthesis is a consequence of impaired insulin sensitivity [21]. Conversely, reducing cholesterol levels in neurons induces insulin resistance [22], highlighting the interplay of cholesterol metabolism, insulin action and mitochondrial function. We have recently shown that mitochondrial dysfunction is cause and consequence of hypothalamic insulin resistance and can be induced by feeding mice a HFD [6,23]. It seems plausible that altered cholesterol levels with increased concentrations of LCSFAs might further deteriorate mitochondrial function and insulin signaling in the brain.

Increased dietary intake of PUFAs, especially ω3-PUFA, correlates with metabolic health [24], whereas an increased ω6- to ω3-PUFA ratio raises the risk for obesity [25]. We were able to show

that a Western-type HFD containing soybean oil-derived PUFAs and cholesterol caused obesity with hepatic steatosis, massive liver inflammation, mitochondrial dysfunction and hepatic insulin resistance in mice, displaying many clinical parameters of patients with non-alcoholic steatohepatitis suffering from metabolic syndrome [5,26]. Interestingly, this diet was more detrimental for liver function than a combination of conventional HFD (containing mainly lard) with cholesterol. As soybean oil consists of high amounts of the ω6-PUFA linoleic acid, these data implicate that the interplay of ω6-PUFA with cholesterol is particularly harmful for metabolism, especially for liver function. Up to now, it is unclear how these diets affect brain metabolism, inflammation and mitochondrial function.

In this study, we investigated the effect of a standard chow diet (STD), 0.75% cholesterol in a standard diet (CHO + STD), 0.75% cholesterol in a HFD containing ω6-PUFA-rich soybean oil (CHO + SOY), 0.75% cholesterol in a HFD containing mainly lard as a fat source (CHO + LAR) or a HFD (containing mainly lard as a fat source, LAR) on hypothalamic stress responses and homeostasis in mice. Further, we tested whether cholesterol, the LCSFA palmitate or ω6-PUFA linoleic acid, or a combination of these fatty acids with cholesterol, impairs mitochondrial function and insulin action in hypothalamic neurons.

All tested dietary interventions cause a molecular signature of metabolic stress in the hypothalamus with decreased markers of blood–brain barrier integrity, mitochondrial function, elevated protein carbonylation and JNK activation. Palmitate causes mitochondrial dysfunction, oxidative stress and insulin as well as insulin-like growth factor-1 (IGF-1) resistance in vitro, while cholesterol and linoleic acid do not cause functional alterations. Overall, using in vivo and in vitro models, we (A) detect palmitate as a negative regulator of hypothalamic insulin receptor (IR) and insulin-like growth factor-1 receptor (IGF-1R) signaling, as well as of mitochondrial function, (B) reveal that cholesterol and ω6-PUFA treatment of hypothalamic neurons is not detrimental for insulin action or mitochondrial activity and (C) identify IR as a novel modulator of palmitate-induced JNK activation.

2. Materials and Methods

All chemicals were of analytical or higher grade and obtained from local providers, unless otherwise stated.

2.1. Animals and Experimental Design

Male C57BL/6JRj mice were group-housed in type II cages at 20 ± 2 °C with a 12 h light/dark-cycle and fed a standard chow diet (STD), 0.75% cholesterol in a standard diet (CHO + STD), 0.75% cholesterol in a high-fat diet containing ω6-PUFA-rich soybean oil (CHO + SOY), 0.75% cholesterol in a high-fat diet containing mainly lard as a fat source (CHO + LAR) or a high-fat diet containing mainly lard without additional cholesterol (LAR) for 20 weeks. Detailed diet composition is shown in Supplementary Table S1, as previously described [5]. Animal experiments were performed according to the ARRIVE guidelines. Treatment of the animals followed the German animal protection laws and was performed with the approval of the state animal welfare committee (LAVG, Brandenburg). The study was conducted in accordance with the Declaration of Helsinki, and the protocol was approved by the Ethics Committee of the state of Brandenburg (TVA 2347-18-2013).

2.2. In Vitro Stimulations

For all stimulations, immortalized hypothalamic CLU183 (mHypoA-2/23 CLU183) cells were cultivated in Dulbecco's Modified Eagle's Medium (DMEM) GlutaMAX high-glucose (Gibco), supplemented with 1 mM sodium pyruvate (Gibco), 10% fetal bovine serum (Pan, South Africa) and 1% penicillin-streptomycin (Gibco). CLU183 insulin receptor knockout (IR KO) cells were generated as previously described [6]. All cell cultures were maintained at 37 °C with 5% CO_2. For all experiments, cells were seeded one day before the stimulation. CLU183 cells were incubated for 16 h with 5 μM cholesterol (complexed with 50 μM methyl-β-cyclodextrin (MβCD)), 250 μM linoleic acid or palmitic acid (LA or PA, both hydrolyzed under alkaline conditions and coupled to bovine serum

albumin (BSA), as described previously [27]), or respective controls (5 μM MβCD and/or 125 μM BSA). The used concentrations were consistent through all in vitro experiments.

For insulin stimulation, CLU183 cells were first stimulated with cholesterol and/or fatty acids for 16 h, and were then serum-deprived for 3 h with DMEM GlutaMAX high-glucose, 1 mM sodium pyruvate and 1% penicillin-streptomycin, and subsequently stimulated with 100 nM insulin (Sigma-Aldrich, Taufkirchen, Germany) for 5 min.

For inhibition of the IR, CLU183 cells were first stimulated with palmitate with and without cholesterol for 16 h, were then serum-deprived for 3 h in the presence of 100 nM IR antagonist S961 (Novo Nordisk), and finally stimulated with 100 nM insulin (Sigma-Aldrich, Taufkirchen, Germany) for 5 min.

For inhibition of JNK, CLU183 cells were stimulated with 10 μM JNK-inhibitor SP600125 (Sigma-Aldrich, Taufkirchen, Germany) and with cholesterol and/or fatty acids for 16 h, and were then serum-deprived for 3 h in the presence of SP600125 and additionally stimulated with 100 nM insulin for 5 min. Dimethyl sulfoxide (Sigma-Aldrich, Taufkirchen, Germany) was used as a solvent control for SP600125 (= –SP600125).

2.3. Ex Vivo Stimulations

Cholesterol and fatty acid stimulation experiments were performed on coronal slices of eight 19–21 weeks old male C57BL/6N mice, which were killed by cervical dislocation. After carefully removing the brain from the skull, the brain was placed into a brain matrix (Zivic Instruments, Pittsburgh, PA, United States) to isolate the hypothalamus (bregma -1.34 mm to bregma -1.74 mm). Consecutive coronal slices of 300 μm were cut using a vibration microtome (Leica, Wetzlar, Germany), and were then placed in artificial cerebrospinal fluid [28] and oxygenized with 5% CO_2/95% O_2. Following 1 h recovery, slices were stimulated for 5 h with either 5 μM cholesterol, 250 μM LA, 250 μM PA, or a combination of cholesterol and fatty acids, as well as their respective control BSA with MβCD, and were subsequently stimulated with 100 nM insulin for 15 min. The protocol was approved by the Ethics Committee of the state of Brandenburg (T-07-19-CRM).

2.4. Serum Analysis

Insulin levels were measured using an insulin (ELISA) kit (Crystal Chem; Downers Grove, IL, United States). Analysis of fatty acid spectra of serum phospholipids (PL) was performed with a strongly modified method using extraction with tert-butyl methyl ether/methanol, solid-phase separation, hydrolysis and methylation with trimethyl sulfonium hydroxide, and subsequent analysis by gas chromatography [29–31] and a flame ionization detector. Modifications of the analysis method were previously published [32]. In this study, 50 μL serum samples were processed as described and were then subjected to a bonded phase column separation after redissolving the dried lipids in chloroform. Fatty acid composition of serum PL was expressed as area percentage of each fatty acid relative to total area of all detected fatty acids: C12:0, C14:0, C15:0, C16:0, C16:1n7c, C17:0, C18:0, C18:1n9c, C18:1n7c, C18:2n6c, C20:0, C18:3n6, C18:3n3, C20:1n9, C20:2n6, C20:3n6, C20:4n6, C20:5n3, C22:4n6, C22:5n6, C22:5n3, C22:6n3.

2.5. Cholesterol Assay

Total and free cholesterol in hypothalamic tissue and cell culture experiments were determined as described previously [5], with minor modifications. Briefly, frozen tissue or cell homogenates homogenized in lysis buffer using a pestile mixer or sonicator were heated, centrifuged and supernatants were subsequently incubated with an assay buffer containing 100 mmol/L phosphate buffer (pH 7.4), 0.026% Triton X-100, 1 mmol/L sodium cholate, 0.63 mg/mL p-hydroxyphenylacetic acid, 0.5 U/mL cholesterol oxidase and 0.2 U/mL peroxidase without or with 0.5 U/mL cholesterol esterase. Fluorescence was detected after 40 min incubation at 37 °C with 325 nm (excitation) and 415 nm (emission). The esterified cholesterol was quantified by the difference between total and free cholesterol.

2.6. Western Blot and Protein Carbonylation Assay

Western blot analysis was performed as described previously [5,6] using anti-occludin (NBP1-87402) obtained from Novusbio, Total OXPHOS Rodent WB Antibody Cocktail (ab110413) and anti-PGC-1α (ab54481) obtained from Abcam (Cambridge, UK), anti-HSP60 (sc-376240) obtained from Santa Cruz and anti-phospho-SAPK/JNK (Thr183/Tyr185) (#9251), anti-JNK2 (#9258), anti-SOD2 XP (#13141), anti-SIRT3 (#5490), anti-phospho-AKT (Ser473) (#9271), anti-AKT (#9272), anti-IRβ (#3025) and anti-IGF-1Rβ (#3027) antibodies, as well as the secondary antibodies anti-rabbit antibody (#7074) and anti-mouse antibody (#7076) obtained from Cell Signaling (Cambridge, UK). Ponceau staining served as a loading control. Oxyblot analysis was carried out as previously published [33] with anti-DNP antibody after membrane derivatization (D9656, Sigma-Aldrich, Taufkirchen, Germany). Specific bands were detected by using a chemiluminescence reagent in the ChemiDoc™ Imaging System with ImageLab software (Bio-Rad, Munich, Germany). Band intensities were quantified via densitometric analysis using Image Lab 5.2.1 and Image J software and were normalized to protein content exemplified by Ponceau staining or total unphosphorylated proteins (JNK and AKT phosphorylation).

2.7. Gene Expression Analysis

Total RNA was extracted from 3–4 × 10^5 cells with QIAzol Lysis Reagent (Qiagen, Hilden, Germany) or RNeasy Kit (Qiagen). Overall, 1 μg of RNA from cells was reverse transcribed in 20 μL using Random hexamer primers (11034731001, Hoffmann-La Roche, Basel, Switzerland), Thermo Scientific™ dNTP-Set, and M-MLV Reverse Transcriptase (Promega GmbH, Walldorf, Germany). Real-time PCR was performed and analyzed as previously published [6] and primer sequences are listed in Supplementary Table S2. Gene expression was calculated according to the ΔΔCT method using Tbp (TATA-box binding protein) or β-Actin as a reference gene. The specificity of SYBR Green primers was confirmed by melting curve analysis.

2.8. Genomic DNA Isolation

DNA from cells was extracted using the Invisorb Spin Tissue Mini Kit (Invitek Molecular GmbH, Berlin, Germany) following the manufacturer's manual.

2.9. Mitochondrial Respiration

Differences in mitochondrial respiration were determined using the Seahorse XF Mito Stress Test Kit and the Seahorse XF96 extracellular Bioflux analyzer (Agilent, Santa Clara, CA, United States), measuring oxygen consumption rate (OCR) and extracellular acidification rate (ECAR) of adherent cells to test mitochondrial function. All compound concentrations were tested and optimized before the assay and were consistent through all Seahorse runs for all experimental setups [6]. Final concentrations for the compounds were 2 μM for Oligomycin (Port A), 0.5 μM for carbonyl cyanide-4-(trifluoromethoxy)phenylhydrazone (FCCP) (Port B) and 1 μM for Rotenone/2 μM for Antimycin A (Port C). Cells were seeded at a density of 5000 cells/well two days prior to the experiment within a 96-well microplate. Four wells were prepared without cells as background signal ('blank'). On the following day, cells were stimulated with cholesterol and/or fatty acids as well as the respective controls for 16 h overnight. For IR inhibition, cells were stimulated with palmitate with or without cholesterol for 13 h and with 100 nM S961 for an additional 3 h. Prior to the assay, cells were washed once with Seahorse Medium (XF base Minimum DMEM supplemented with 1 mM sodium pyruvate, 2 mM glutamine and 10 mM glucose, pH 7.4) and then incubated in the final amount of assay medium in a non-CO_2 incubator at 37 °C to maintain pH levels. After calibration, the microplate was placed in the Seahorse Bioflux analyzer and the experiment was performed according to manufacturer's instructions (3 min mix, 3 min measure; 3 cycles for each port). OCR data were normalized to protein content and were analyzed using Wave 2.4.0 software (Agilent, Santa Clara, CA, USA).

2.10. Statistical Analysis

Two groups were compared using the unpaired two-tailed Student's *t*-test or the Mann–Whitney test when necessary. The statistical significance between differences of more than two groups was determined by one-way analysis of variance (ANOVA) or two-way ANOVA with Tukey's post hoc test for multiple comparisons, or the Kruskal–Wallis test for non-parametric samples, as detailed in the legends to the figures using GraphPad Prism version 8 for Windows (GraphPad Software, La Jolla, CA, USA). Differences with a p-value ≤ 0.05 were considered statistically significant.

3. Results

3.1. Cholesterol/PUFA Diet Increases Both Cholesterol and Metabolic Stress in the Brain

Mice were divided into five groups and were fed different diets with altered fat composition. For this purpose, 6-week-old mice were either fed a STD, CHO + STD, CHO + SOY (contains high amounts of soybean oil-derived PUFAs), CHO + LAR (contains high amounts of LCSFAs) or LAR for 20 weeks, as reported previously [5]. Animals on all high-fat diets gained more weight than animals fed either a chow diet or cholesterol-enriched chow diet (already published in Reference [5] and Figure 1A). Despite similar weight gain between mice fed a CHO + SOY, CHO + LAR or LAR diet, animals fed the LAR diet were significantly more insulin resistant than other groups, as evidenced by four-fold increased fasting serum insulin levels and higher blood glucose levels in response to glucose or insulin administration compared to STD control, confirming the detrimental effect of LCSFA-containing diets on insulin sensitivity (Figure 1B, Supplementary Figure S1A–C).

As the CHO + SOY compared to CHO + STD and CHO + LAR diet groups had an enormous effect on liver function and caused massive hepatic inflammation [5], we assessed their effects on brain homeostasis and mitochondrial dysfunction. To exemplarily validate the SOY feeding regime, we determined the relative abundance of ω6-PUFA linoleic acid (LA) in serum of mice fed a CHO + SOY diet compared to the STD diet group. Indeed, feeding mice a CHO + SOY diet increased LA abundance by ~37% compared to STD control, identifying a successful enrichment of LA in the serum in CHO + SOY-fed mice (Supplementary Figure S2A). Overall, the CHO + SOY diet caused a general altered profile of fatty acids in the serum, showing the extensive impact of the diet on serum fatty acid abundance (Supplementary Figure S2B).

We then assessed whether cholesterol-supplemented diets were able to increase cholesterol content in the hypothalamus. This analysis revealed that, unexpectedly, only the CHO + SOY diet, but not CHO + STD or CHO + LAR diets, increased cholesterol levels in the hypothalamus, with a 61% increase of esterified cholesterol and about a 20% increase of free and total cholesterol compared to the STD group (Figure 1C). The majority of dietary cholesterol is not able to penetrate the blood–brain barrier in healthy conditions [34] and thus, can only enter the brain via a disruption of the blood–brain barrier (BBB). Interestingly, occludin protein expression, which is a marker for BBB integrity, was decreased in the hypothalamus of all mice fed a cholesterol-containing diet compared to STD control (Figure 1D). Yet, cholesterol levels were only increased in the CHO + SOY group (Figure 1C), suggesting that an interaction of soybean oil-derived PUFAs with cholesterol is responsible for the elevated cholesterol levels in the hypothalamus. As the deterioration of the BBB can harm the brain, we further investigated the activation of the serine/threonine stress kinase JNK in hypothalamic samples of the different mouse groups. Only mice fed a LAR, CHO + LAR or CHO + SOY diet caused increased JNK activation with elevated Thr183/Tyr185 phosphorylation, while a CHO + STD diet did not affect JNK activation. In detail, LAR-fed mice exhibited a 3.7-fold increase in JNK activation, whereas CHO + LAR- and CHO + SOY-fed mice showed a ~2.3-fold increase compared to STD control. Interestingly, p46 JNK was more strongly activated by LAR, CHO + LAR and CHO + SOY than p54, which was barely detectable (Figure 1E).

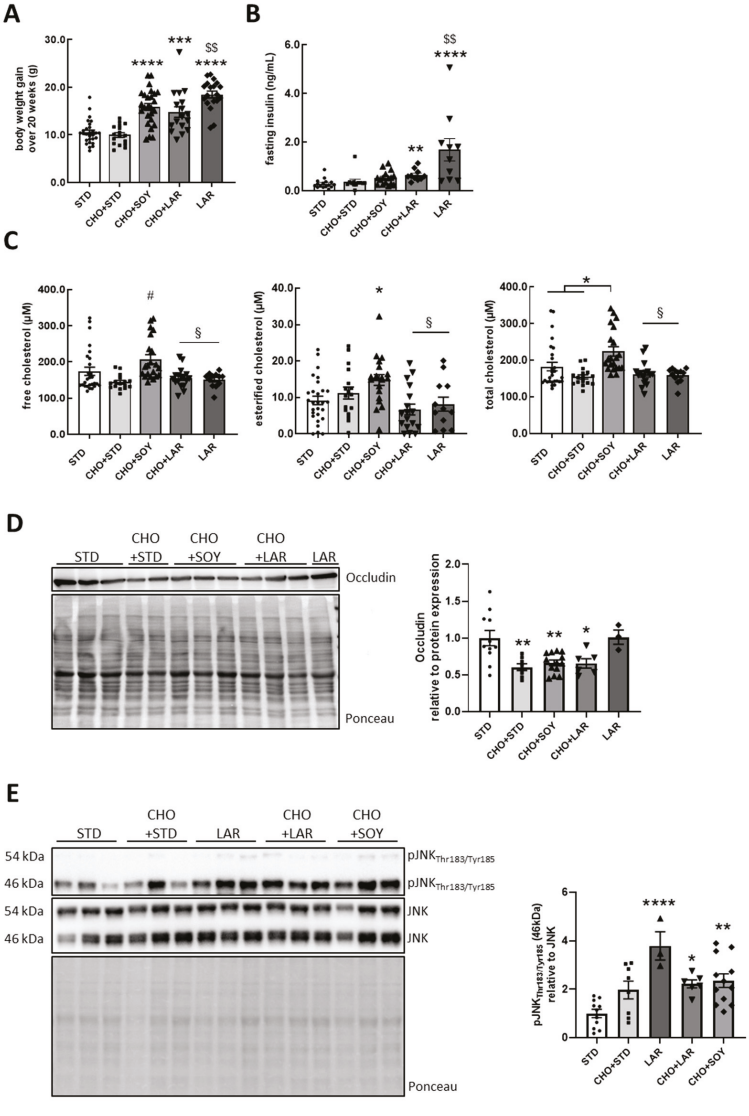

Figure 1. Cholesterol/Poly-unsaturated fatty acids increases cholesterol and metabolic stress in the brain. (**A**) Cumulative body weight change and (**B**) fasting insulin levels measured after a 16 h fast. (**C**) Levels of free, esterified and total cholesterol in hypothalamus. (**D**) Protein expression of tight junction protein occludin and (**E**) of phosphorylated stress kinase c-Jun N-terminal kinase (JNK) Thr183/Tyr185 in the hypothalamus. Dense intensity of occludin was normalized to Ponceau staining and pJNK Thr183/Tyr185 to total JNK protein, which was verified on the same Western blot membrane as a loading control and calculated relative to the standard chow diet (STD) group in each gel. A representative blot is shown. All values are displayed as median ± SEM with a total n of (**A**,**B**) 17–28, (**C**) 12–27, (**D**,**E**) 3–13 mice per group. Statistics: One-way ANOVA with Tukey's post hoc test for multiple comparisons (**A–E**). * $p < 0.05$, ** $p < 0.01$, *** $p < 0.001$, **** $p < 0.0001$. *: versus STD; #: versus CHO + STD; $$: versus CHO + LAR; §: versus CHO + SOY.

3.2. Specific Alterations of Mitochondrial Protein Expression Due to Cholesterol-Containing Diets

As elevated concentrations of both LCSFAs and ω6-PUFAs correlate with metabolic alterations and impaired insulin action in obesity, we further investigated hypothalamic mitochondrial protein homeostasis, which is under the control of insulin [6]. First, we investigated the expression pattern of subunits of the electron transport chain complexes I, II, III, IV and V (ATP synthase), and the mitochondrial antioxidative enzyme superoxide dismutase 2 (SOD2). This analysis revealed that mice fed either LAR- or cholesterol-containing diets showed reduced protein expression of subunit ATP5A (ATP synthase subunit alpha) of complex V (Figure 2A,B). A similar phenotype was also observed for complex III regulation with decreased expression of its subunit UQCRC2 (Cytochrome b-c1 complex subunit 2), while the LAR diet did not affect its expression. Interestingly, protein expression of NDUFB8 (NADH:Ubiquinone Oxidoreductase Subunit B8) and SDHB (succinate dehydrogenase complex subunits B), subunits of complex I and II, were increased in the hypothalamus of mice fed a LAR diet, indicating that each diet causes a unique alteration of the hypothalamic mitochondrial proteome (Figure 2A,B). In contrast, protein levels of the mitochondrial antioxidative enzyme SOD2 were indistinguishable between all tested groups (Figure 2A,B).

Next, we assessed protein levels of regulators of mitochondrial function, the master regulator of mitochondrial biogenesis peroxisome proliferator-activated receptor-gamma coactivator 1α (PGC1α), the main mitochondrial matrix chaperone heat-shock protein 60 (HSP60), as well as the mitochondrial deacetylase sirtuin 3 (SIRT3)—all proteins whose dysregulations affect insulin action [23,35,36]. PGC1α was reduced in all tested groups, whereas HSP60 or SIRT3 were only reduced in mice fed a LAR or CHO + LAR diet, confirming that different HFDs induce distinct alterations of mitochondrial protein expression (Figure 2C,D). As alterations in the mitochondrial proteome can cause cellular stress [37], we further assessed protein carbonylation—a marker of oxidative stress—in the hypothalamus of these mice. Total protein carbonylation was only slightly altered in the hypothalamus, yet with a significant increase in mice fed a LAR diet when comparing to STD, and surprisingly, a minor decrease in CHO + SOY-fed mice compared to STD and CHO + STD control (Figure 2E,F). Furthermore, feeding mice a CHO + LAR, as well as LAR diet, caused increased protein carbonylation compared to the CHO + STD and CHO + SOY diets. As the majority of carbonylated proteins seemed to be larger than 150 kDa, we additionally only analyzed proteins with high molecular weight, confirming our previous observation that both the CHO + LAR and LAR diets show an increase in carbonylated proteins compared to CHO + SOY (Figure 2E,F). Overall, this analysis revealed that each feeding regime elicits distinct alterations in mitochondrial protein expression with reduced expression of subunits of complex III and V in cholesterol-containing diets and slightly elevated protein carbonylation, especially in the hypothalamus of mice fed LAR-containing diets.

3.3. Palmitate but not Cholesterol or Linoleate Decreases Mitochondrial Function

To gain detailed insights into metabolic effects of fatty acids enriched in these diets cholesterol, or the combination of cholesterol with these fatty acids, we treated the hypothalamic cell line CLU183 with 5 μM cholesterol, 250 μM of palmitic acid (PA) and linoleic acid (LA), or a combination of cholesterol with these fatty acids, for 16 h and assessed mitochondrial function. 5 μM of cholesterol was chosen, as this lowest concentration did not decrease cell viability (Supplementary Figure S3). We used methyl-β-cyclodextrin (MβCD) to complex cholesterol and achieve cholesterol uptake in vitro. As MβCD per se reduces cholesterol levels in neurons [22], we used only 5 μM MβCD as solvent control for cholesterol-treated cells to avoid artificial cholesterol depletion in our control conditions [38,39]. In comparison with 50 μM, 5 μM MβCD did not alter gene expression of the cholesterol biosynthesis pathway or insulin sensitivity (data not shown). LA and PA were coupled to bovine serum albumin (BSA) and thus, we used BSA as a control for these conditions.

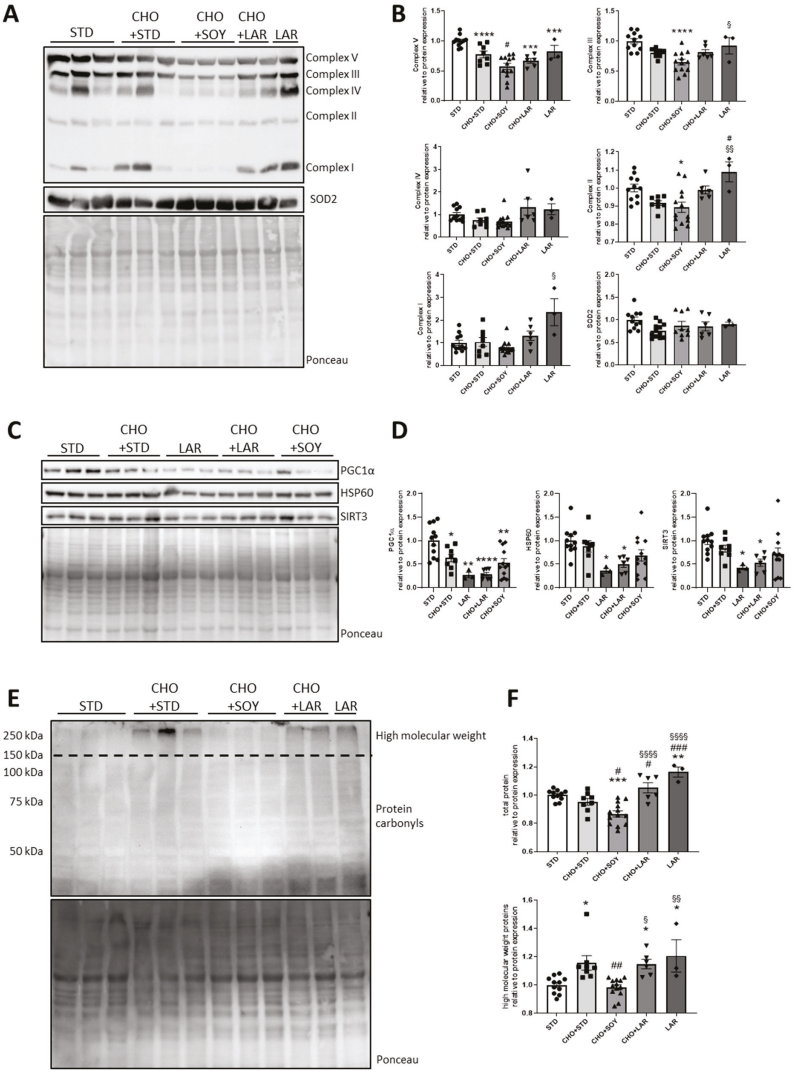

Figure 2. Specific alterations of mitochondrial protein expression due to cholesterol-containing diets. (**A**) Protein expression of subunits of the oxidative phosphorylation complexes (I–V) and SOD2 (Superoxide dismutase 2) in the hypothalamus and (**B**) densitometric analysis. (**C**) Protein expression of PGC1α (Peroxisome proliferator-activated receptor gamma coactivator 1-alpha), SIRT3 (Sirtuin 3) and HSP60 (Heat shock protein 60) and (**D**) densitometric analysis. (**E**) Protein carbonylation as a marker of oxidative stress in the hypothalamus and (**F**) densitometric analysis. Dense intensity was normalized to Ponceau staining, which was verified on the same Western blot membrane as a loading control and calculated relative to the STD group in each gel. Representative blots are shown. All values are displayed as median ± SEM with a total n of 3–13 mice per group. Statistics: One-way ANOVA with Tukey's post hoc test for multiple comparisons. * $p < 0.05$, ** $p < 0.01$, *** $p < 0.001$, **** $p < 0.0001$. *: versus STD, #, ##, ###: versus CHO + STD and §, §§, §§§§: versus CHO + SOY.

To confirm successful cholesterol treatment, we analyzed cholesterol accumulation and cholesterol-regulated gene expression in cholesterol-treated CLU183 cells. In line with our in vivo data, this analysis revealed that only the combination of LA with cholesterol was sufficient to cause a significant ~30% and 41% increase of free and total cholesterol levels in neurons, while esterified cholesterol levels were unchanged (Figure 3A). As elevated cholesterol concentrations are able to inhibit endogenous cholesterol biosynthesis, we assessed gene expression levels of the cholesterol biosynthesis pathway. This analysis revealed reduced gene expression of sterol regulatory element-binding protein 2 (*Srebp2*), farnesyl diphosphate synthase (*Fdps*) and squalene epoxidase (*Sqle*) in cholesterol-treated cells, whereas 3-hydroxy-3-methylglutaryl-CoA reductase (*Hmgcr*), the rate-controlling enzyme of the mevalonate pathway, was not affected (Supplementary Figure S4). These data indicate that CLU183 cells were able to take up and metabolize extracellular cholesterol, as evidenced by increased intracellular cholesterol accumulation and reduced expression levels of cholesterol-regulated genes. Following this, we determined mitochondrial function using a Seahorse Bioflux analyzer. Interestingly, only PA and the CHO + PA treatment reduced basal respiration by 65% (PA) and 52% (CHO + PA), reduced maximal respiration by 59% and 55% respectively, with an additional 52% and 44% reduction in ATP production (Figure 3B) and with overall reduced energy metabolism, as both PA and CHO + PA also decreased extracellular acidification rate (ECAR) (data not shown). Cholesterol treatment did not affect mitochondrial function nor did it change the combination of cholesterol with PA or LA effect of these fatty acids on mitochondrial function (Figure 3B).

To understand why PA caused mitochondrial dysfunction, we performed a detailed mitochondrial analysis of subunits of the electron transport chain complexes, SOD2, as well as gene expression of *Pgc1α*, *Hsp60* and *Sirt3*, similar to our in vivo study. This analysis revealed that neither cholesterol, LA, PA, nor a combination affected protein expression of the electron transport chain complexes along with unaltered SOD2 protein expression (Figure 3C,D). In addition, mitochondrial DNA content was unaltered, indicating that PA does not affect mitochondrial function by decreasing mitochondrial mass (Supplementary Figure S5A). In line with this, neuronal *Hsp60* mRNA levels were unaffected by different treatments, while *Sirt3* and *Pgc1α* gene expression were significantly reduced by cholesterol treatment (Supplementary Figure S5B). As cholesterol did not change mitochondrial function, the reduction of *Sirt3* and *Pgc1α* mRNA levels in any CHO-treated cells, including CHO + PA treatment, could not account for the observed decreased mitochondrial function in CLU183 cells treated with PA. Next, we assessed markers of mitochondrial dynamics. While PA treatment did not change the gene expression of *Mfn1* (*Mitofusin-1*) or *Drp1* (*Dynamin-related protein 1*) (Supplementary Figure S5C), PA treatment decreased *Opa1* (*OPA1 mitochondrial dynamin-like GTPase*) expression (Supplementary Figure S5C), suggesting that PA treatment induces mitochondrial fission along with reduced mitochondrial activity. Surprisingly, CHO + PA reduced mitochondrial respiration but did not affect mitochondrial dynamics.

Based on these findings, we investigated oxidative stress by assessing protein carbonylation. Similar to our observed protein carbonylation results in vivo, PA, but also both PA and LA with cholesterol treatment, caused increased total protein carbonylation as well as carbonylated proteins at high molecular weight (>150 kDa) in CLU183 neurons compared to control-treated neurons (Figure 3E,F). In summary, PA causes oxidative stress and mitochondrial dysfunction, while cholesterol does not affect mitochondrial activity in these experimental setups.

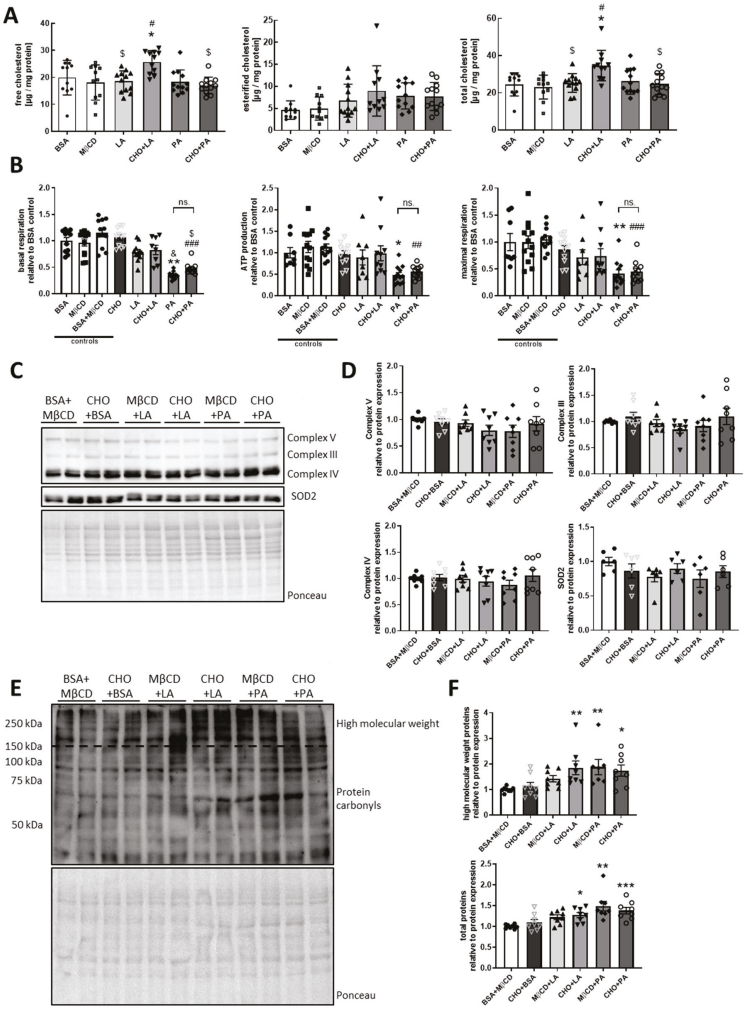

Figure 3. Palmitate, but not cholesterol or linoleate, decreases mitochondrial function. (**A**) Levels of free, esterified and total cholesterol in stimulated CLU183 hypothalamic neurons. (**B**) Relative oxygen consumption rate (basal respiration, ATP production and maximal respiration) in stimulated neurons. A representative experiment is shown. (**C**) Protein expression of subunits of the oxidative phosphorylation complexes (III–V) and SOD2 in stimulated neurons and (**D**) densitometric analysis. (**E**) Protein carbonylation as a marker of oxidative stress in stimulated neurons (high molecular weight proteins > 150 kDa) and (**E**) and (**F**) densitometric analysis. Dense intensity was normalized to Ponceau staining, which was verified on the same Western blot membrane as a loading control and calculated relative to the control (BSA + MβCD) group in each gel. Representative blots are shown. All values are displayed as median ± SEM with a total n of (**A**) 11–12, (**B**) 8–12 and (**C**–**F**) 6–8 per group. Statistics: One-way ANOVA with Tukey's post hoc test for multiple comparisons. * $p < 0.05$, ** $p < 0.01$, *** $p < 0.001$. Separate depiction of statistics for cholesterol (A) *: versus BSA, #: versus MβCD, $: CHO + LA. Separate depiction of statistics for mitochondrial respiration (B) *: versus BSA, #, ##, ###: versus BSA + MβCD, $: versus CHO + LA, &: versus LA, n.s: not significant. Separate depiction of statistics for (F) *: versus BSA + MβCD.

3.4. Palmitate, but not Cholesterol or Linoleic Acid, Induces Insulin and IGF-1 Resistance with Increased Inflammation in Hypothalamic Neurons

We have previously shown that dietary intake of soybean oil-derived PUFAs with cholesterol caused hepatic inflammation and insulin resistance [5]. In addition, our in vitro data show that palmitate treatment causes mitochondrial dysfunction in hypothalamic neurons, a phenomenon that can cause insulin resistance [23]. By performing in vitro insulin stimulation experiments, we tested whether PA or LA affected insulin sensitivity. As IR and IGF-1R signaling is difficult to distinguish [40], we investigated the effects of fatty acids in control and CLU183 cells deficient for the insulin receptor (IR KO) (Supplementary Figure S6A). To activate IR and IGF-1R, we used 100 nM insulin, which is sufficient to potently cross-activate the IGF-1 receptor [40]. Thus, we treated control and IR KO CLU183 cells with PA, LA or BSA as control, followed by insulin stimulation. These experiments showed that PA, but not LA, caused insulin resistance in control cells, as evidenced by a ~49% reduction in Ser473 phosphorylation of AKT (Figure 4A). Unexpectedly, control and IR KO cells exhibited the same degree of insulin-induced AKT phosphorylation under all tested conditions, suggesting a compensatory mechanism in IR KO cells. Indeed, IR KO cells exhibited an almost 7-fold increase in IGF-1R gene and protein expression compared to control, explaining the lack of reduced insulin-induced AKT activation in these cells (Supplementary Figure S6B,C). Interestingly, IR KO cells exhibited a similar reduction of insulin-induced AKT phosphorylation after PA treatment, showing that palmitate also reduces insulin-induced IGF-1R activation or causes IGF-1 resistance (Figure 4A).

We further tested the effect of PA, LA, cholesterol and their combination on mitochondrial function in IR KO cells using the Seahorse Bioflux analyzer. This analysis revealed that IR KO cells exhibited increased basal respiration compared to control cells, which was presumably due to elevated IGF-1R expression. Yet, PA or CHO + PA treatment caused a similar reduced basal respiration with a stronger suppression of mitochondrial activity in IR KO cells (Supplementary Figure S6D), confirming that IR expression is a crucial modulator of hypothalamic mitochondrial function [6] and suggesting that IR is vital to counteract the negative effects of PA on cellular homeostasis. Furthermore, neuronal *Pgc1α* and *Hsp60* mRNA levels were unaffected, while gene expression of *Mfn1*, *Opa1* and *Drp1* was significantly increased in IR KO cells (Supplementary Figure S6E), pointing to increased mitochondrial dynamics.

Overconsumption of HFD with high amounts of palmitate causes neuroinflammation. We identified increased activation of the stress kinase JNK in our in vitro settings (Figure 4B, Supplementary Figure S7A). We were able to identify a 5.4-fold increase of palmitate-induced p54 JNK Thr183/Tyr185 phosphorylation in control cells, which was not altered by short-term insulin stimulation (Figure 4B). Yet, comparing JNK activation between control and IR KO cells revealed a significant almost 2-fold enhanced palmitate-induced JNK activation in IR KO cells, indicating that the presence of IR is anti-inflammatory and cannot be compensated by endogenous IGF-1R overexpression (Figure 4B).

Next, we investigated whether cholesterol or a combination of cholesterol with PA or LA affected neuronal insulin sensitivity. To enable the comparison of all tested combinations, we examined the effect of used control substances (BSA for PA or LA, MβCD for cholesterol, BSA and MβCD for cholesterol with PA or LA) on insulin sensitivity, showing that controls exhibited similar insulin sensitivity (Supplementary Figure S8). Subsequently, control and IR KO CLU183 cells were treated with cholesterol and fatty acids, followed by insulin stimulation. CHO treatment did not alter insulin sensitivity, but CHO + LA increased insulin sensitivity in control and IR KO cells compared to control-treated cells, whereas CHO + PA reduced insulin sensitivity compared to CHO + LA-treated cells, as evidenced by a 1.7-fold increase and a ~50% decrease in Ser473 phosphorylation of AKT, respectively (Figure 4C). In line with the effect of PA on JNK activation, we only identified increased JNK activation in CHO + PA-treated neurons (Figure 4D, Supplementary Figure S7B) with a 3.9-fold increase of p54 JNK Thr183/Tyr185 phosphorylation. Additionally, these data confirmed the protective effect of IR on aberrant JNK activation, as IR KO cells revealed elevated CHO + PA-induced JNK phosphorylation compared to control, with an overall significant genotype effect (Figure 4D). Interestingly, CHO + LA treatment enhanced insulin sensitivity, while LA treatment did not alter insulin action.

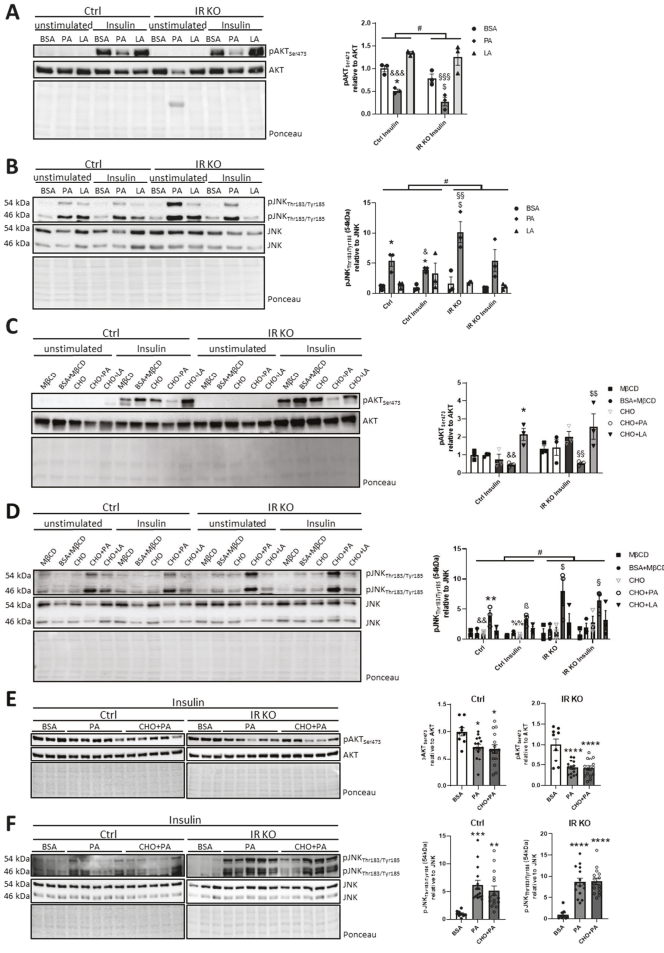

Figure 4. Palmitate, but not cholesterol, induces insulin and IGF-1R resistance with increased inflammation. (**A,C,E**) Protein expression in stimulated control or insulin receptor knockout (IR KO) CLU183 cells of phospho-protein kinase B (pAKT) Ser473, AKT and densitometric analysis. (**B,D,F**) Protein expression in stimulated control (Ctrl) or IR KO CLU183 cells of pJNK Thr183/Tyr185, JNK and densitometric analysis. All values are displayed as median ± SEM. (**A**–**D**) Data of three independent experiments with a total n = 3. (**F**) Data of three independent experiments with a total n = 9–15. Dense intensity of pAKT Ser473 was normalized to total AKT protein, and for pJNK Thr183/Tyr185 to total JNK protein, which was verified on the same Western blot membrane as a loading control and calculated relative to the respective control (BSA or BSA + MβCD) group in each gel. Representative blots are shown. Statistics: Two-way ANOVA with Tukey's post hoc test for multiple comparisons of Ctrl versus IR KO and one-way ANOVA with Tukey's post hoc test for multiple comparisons. * $p < 0.05$, ** $p < 0.01$, *** $p < 0.001$, **** $p < 0.0001$. Separate depiction of statistics for A–C *: versus BSA (Ctrl) or BSA + MβCD (Ctrl), &, &&, &&&: versus LA (Ctrl) or CHO + LA (Ctrl), $, $$: versus BSA (IR KO) or BSA + MβCD (IR KO), §§ §§§: versus LA (IR KO) or CHO + LA (IR KO), Separate depiction of statistics for D *: versus BSA + MβCD (Ctrl), &&: versus CHO + PA (Ctrl), ß: versus BSA + MβCD (Ctrl Insulin), %%: versus CHO + PA (Ctrl Insulin), $: versus BSA + MβCD (IR KO), §: versus BSA + MβCD (IR KO Insulin), #: Ctrl versus IR KO. Separate depiction of statistics for **E**–**F** *: versus BSA.

To investigate whether CHO + PA compared to PA treatment had an additive effect on insulin resistance and JNK activation, we directly compared PA with the CHO + PA treatment. These experiments revealed that the addition of cholesterol had no further effect on the PA-induced insulin resistance with similar Ser473 AKT- and Thr183/Tyr185 JNK-phosphorylation (Figure 4E,F, Supplementary Figure S7C).

3.5. Palmitate- and Palmitate/Cholesterol-Induced Insulin Resistance is Independent of JNK Activation

Next, we tested whether the PA- and CHO + PA-induced JNK activation was responsible for the observed insulin resistance phenotype in CLU183 cells using JNK inhibitor SP600125. While SP600125 successfully inhibited PA-induced JNK activation in both control and IR KO cells, JNK inhibition was not able to reverse PA- or CHO + PA-induced reduction of insulin-stimulated AKT-phosphorylation in both cell lines (Supplementary Figure S9A,B). Interestingly, JNK inhibition was more potent in control cells compared to IR KO cells, confirming that decreased IR signaling results in enhanced palmitate-induced JNK activation and cellular stress.

To further investigate a potential, differential effect of PA and CHO + PA on IGF-1R signaling in hypothalamic neurons, we inhibited IR action using the high-affinity IR peptide antagonist S961 at a concentration of 100 nM [41,42]. This analysis revealed that both PA and CHO + PA reduced insulin-induced Ser473 AKT phosphorylation, which was aggravated by the inhibition of the IR (Figure 5A). These data clearly show that PA and CHO + PA potently reduce IR and IGF-1R signaling and that the observed similar insulin sensitivity of control and IR KO cells was presumably based on the compensatory upregulation of IGF-1R (Figure 4C, Supplementary Figure S6B,C).

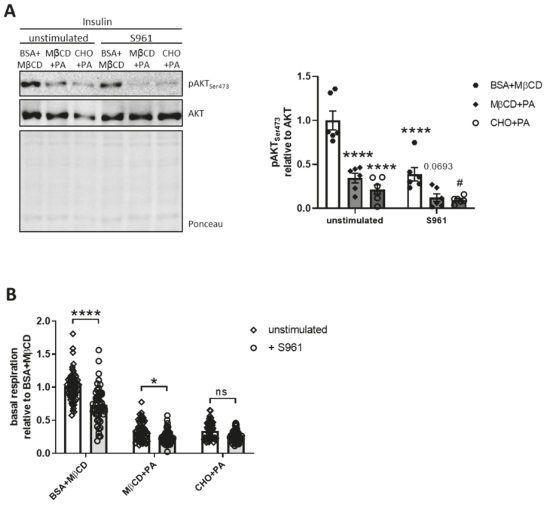

Figure 5. Inhibition of insulin receptor (IR) further increases palmitate-induced IR and insulin-like growth factor-1 receptor resistance. (**A**) Protein expression of pAKT Ser473 and AKT in stimulated neurons and densitometric analysis. (**B**) Relative oxygen consumption rate (basal respiration) in stimulated neurons. Dense intensity was normalized for pAKT Ser473 to total AKT, which was verified on the same Western blot membrane as a loading control and calculated relative to the control (BSA + MβCD) group in each gel. A representative blot is shown. All values are displayed as median ± SEM. (A) Data of three independent experiments with a total n = 6. (B) Pooled data of four independent experiments with a total n = 51–58. Statistics: One-way ANOVA with Tukey's post hoc test for multiple comparisons., * $p < 0.05$, **** $p < 0.0001$. *: versus unstimulated BSA + MβCD, #: versus S961 BSA + MβCD, 0.0693 versus S961 BSA + MβCD.

To investigate the effect of IR inhibition on mitochondrial function in cells without compensatory elevated IGF-1R expression, we treated cells with PA or CHO + PA and added S961. As shown earlier (Figure 3B), PA and CHO + PA caused a decrease in mitochondrial respiration. Surprisingly, S961 significantly reduced basal respiration only in control-treated cells and cells treated with PA but not with CHO + PA (Figure 5B), suggesting that proper IR action is important for mitochondrial activity.

3.6. Only Palmitate Induces Insulin Resistance on Hypothalamic Brain Slices

In the brain, there is a functional and metabolic interplay of neurons with astrocytes and microglia, which might cause different sensitivities to fatty acids and cholesterol-induced effects on insulin signaling. To assess this interplay in the hypothalamus, we cultivated coronal brain slices in oxygenated, artificial cerebrospinal fluid and added cholesterol, PA, LA or the combination of fatty acids with cholesterol to this medium. This treatment was followed by a 15 min insulin stimulation and Western blot analysis of Ser473 AKT phosphorylation. This experimental setup should reveal whether the interplay of different cell populations might modulate the effect of tested fatty acids and cholesterol on insulin action. This analysis showed that PA treatment was sufficient to induce brain insulin resistance with a reduction in insulin-induced Ser473 phosphorylation of AKT by 43%, while, unexpectedly, CHO + PA treatment did not result in a markedly decreased phosphorylation of AKT (Figure 6A,B). These data confirm the detrimental effect of palmitate on hypothalamic insulin signaling, while the CHO + PA treatment did not cause a significant decrease in insulin-induced Ser473 AKT phosphorylation, indicating that cholesterol treatment differentially regulates insulin action on brain slices compared to neuronal stimulations in vitro.

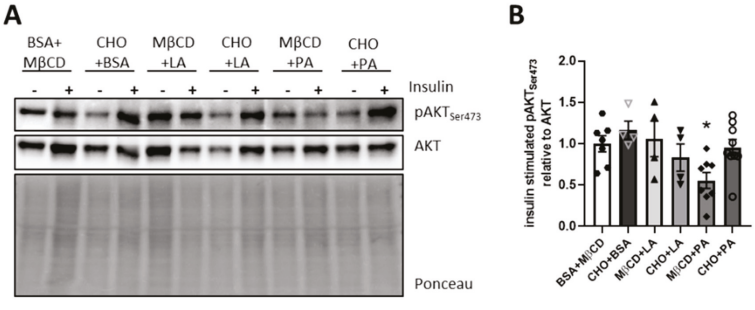

Figure 6. Only palmitate induces insulin resistance in hypothalamic coronal slices. (**A**) Protein expression of pAKT Ser473 and AKT in unstimulated and insulin-stimulated hypothalamic coronal slices and (**B**) densitometric analysis. Dense intensity of insulin-stimulated samples was normalized for pAKT Ser473 to total AKT, which was verified on the same Western blot membrane as a loading control and calculated relative to the control (BSA + MβCD) group in each gel. A representative blot is shown. All values are displayed as median ± SEM. Data of two independent experiments with a total n = 4–9. Statistics: One-way ANOVA with Tukey's post hoc test for multiple comparisons. * $p < 0.05$ versus BSA + MβCD.

4. Discussion

This study investigated the effect of different fatty acids and cholesterol on metabolic stress, mitochondrial function and insulin signaling in hypothalamic neurons. Our data revealed that the investigated cholesterol-containing diets (CHO + STD and CHO + LAR), as well as the conventional high-fat diet (LAR) increased oxidative stress in the brain with slightly increased protein carbonylation. In addition, all HFD treatments reduced protein expression of PGC1α and HSP60 (Figure 2). Further, only cholesterol-containing diets reduced the expression of occludin (Figure 1D), a marker of BBB integrity. As the activation of the stress kinase JNK was only enhanced in hypothalamic samples of

mice fed a LAR, CHO + LAR or a CHO + SOY diet, but not a CHO + STD diet, these data indicate that overall, increased inflammation is not the causal factor for the reduction of occludin (Figure 1E) and other yet undefined mechanisms cause an altered BBB integrity [43].

Treating neurons with PA, the most frequent saturated fatty acid in lard, or the combination of PA and cholesterol, intensified JNK activation and caused insulin resistance in vitro (Figure 4E,F). Interestingly, PA-induced insulin resistance was independent of JNK-activation as the inhibition of JNK did not reverse insulin resistance. The present study further showed that cholesterol might even be protective against palmitate-induced hypothalamic insulin resistance ex vivo, as CHO + PA was not as detrimental as PA treatment to insulin action on hypothalamic brain slices (Figure 6A,B). But, cholesterol treatment per se did not alter mitochondrial function, insulin action and palmitate-induced insulin resistance in vitro. Similarly, LA and a combination of LA and cholesterol were not detrimental for mitochondrial function or insulin signaling. Importantly, we demonstrated that the presence of IR is a crucial negative modulator of PA-induced JNK activation. This suggests that one important aspect of brain insulin signaling is to fine-tune brain function and ensure a balanced metabolism.

4.1. Impact of Cholesterol on Brain Insulin Resistance and Mitochondrial Function

In contrast to peripheral cholesterol metabolism, nearly all brain cholesterol is independently regulated and synthesized by de novo synthesis [44]. The cholesterol movement in and out of the central nervous system is controversially discussed. Due to the lack of direct experimental evidence, it is expected to be very unlikely that cholesterol-containing lipoproteins cross the BBB (Reference [45] and references therein). We showed that only the combination of CHO + SOY elevates cholesterol levels in the hypothalamus (Figure 1C), whereas all cholesterol-containing diets led to decreased protein expression of occludin (Figure 1D), indicating that prolonged excessive dietary intake of cholesterol might harm brain physiology by reducing BBB integrity [46]. Still, it is unclear whether this reduction is due to the presence of increased cholesterol concentrations, and it might be due to overall increased inflammation or other yet undefined mechanisms that might cause an altered BBB integrity [43]. Interestingly, only neurons treated with LA and cholesterol exhibited increased cholesterol levels (Figure 3A), but cholesterol treatment in general decreased expression levels of genes involved in endogenous cholesterol biosynthesis (Supplementary Figure S4).

Cholesterol is an essential structural component for cell membranes and modulates membrane fluidity. While the central nervous system accounts for only 2%–3% of the whole body mass, it contains ~25% of the whole body's cholesterol [44]. Cholesterol homeostasis is strictly regulated. Deficiency as well as aberrant storage of brain cholesterol can have profound consequences on neuronal survival, causing neurodegeneration [47]. Brain insulin resistance associates with neurodegenerative diseases and a reduction of white matter, which contains high cholesterol levels, and is linked to decreased cognitive function and insulin resistance [48,49]. In line with this, neuronal insulin resistance reduces cholesterol synthesis and diabetes impairs cholesterol biosynthesis [21]. Conversely, a reduction of cholesterol induces neuronal insulin resistance [22], indicating that a reduction rather than a surplus of cholesterol deteriorates insulin signaling. Our study supports this hypothesis, showing that cholesterol does not exert a negative impact on brain insulin signaling (Figure 4C–F, (Figure 5A,B and Figure 6A,B). It may even be protective against palmitate-induced hypothalamic insulin resistance ex vivo, as CHO + PA was not as detrimental to insulin action as PA treatment on hypothalamic brain slices (Figure 6A,B). Supporting this observation, mice fed a LAR diet were more insulin-resistant compared to STD-fed mice, whereas feeding of CHO + LAR caused lower insulin levels compared to the LAR group (Figure 1B).

Proper neuronal insulin signaling is closely related to mitochondrial homeostasis [6]. In this study, we did not observe altered mitochondrial activity in cells treated with cholesterol (Figure 3B), although cholesterol treatment reduced the expression of mitochondrial genes and mitochondria-regulating genes, such as *Sirt3* and *Pgc1α*, and combined treatment of cholesterol with linoleic acid slightly induced protein carbonylation (Figure 3E,F, Supplementary Figure S5B,C). So far, it remains unclear why the

combined treatment of cholesterol with linoleic acid causes oxidative stress. But, long-term treatment of cholesterol may exert negative effects on mitochondrial activity. It has been shown that reducing cholesterol levels in mitochondria of Niemann-Pick Type C1 mice improves mitochondrial function, suggesting that reducing cholesterol levels in certain conditions can be beneficial for mitochondria [19].

4.2. Impact of Fatty Acids on Brain Insulin Resistance

We showed that palmitate is also able to induce insulin and IGF-1 resistance in neurons (Figure 4). Although this observation is not surprising, given the close homology between IR and IGF-1R signaling, it reveals that constant, elevated palmitate concentrations in the brain can be detrimental for brain function, as a reduction of IGF-1R signaling causes massive growth retardation of the brain and induces brain oxidative damage [50,51]. Palmitate induces JNK activation in hypothalamic neurons (Reference [7] and Figure 4) and JNK activation can cause insulin resistance [52], but palmitate-induced JNK activation in neurons does not seem to be a major cause for neuronal insulin resistance (Supplementary Figure S9A,B). As JNK deficiency in the brain improves insulin sensitivity [53], palmitate presumably induces other kinases in hypothalamic neurons, which are instrumental for palmitate-induced neuronal insulin resistance [7,9]. Interestingly, PA-induced JNK activation was aggravated by the lack of IR (Figure 4B) and IR KO cells showed unaltered insulin sensitivity compared to control cells, presumably due to elevated IGF-1R expression (Figure 4C). To avoid a compensatory upregulation of IGF-1R and to differentiate between IR and IGF-1R signaling (Supplementary Figure S6B,C), we used the IR inhibitor S961. This experimental design revealed that PA and CHO + PA treatment caused insulin and IGF-1 resistance, highlighting the detrimental impact of the LCSFA palmitate on two key hormones for neuronal homeostasis (Figure 5).

It is still unclear why JNK is increased in IR KO cells. Previous studies have demonstrated that insulin acts as an anti-inflammatory [54,55]. In addition, it has been shown that JNK enhances IR expression in flies [56], suggesting an internal self-regulatory mechanism of neurons to counteract reduced IR expression and action. Although JNK is known to cause serine phosphorylation of IRS1, which is linked to insulin resistance [52], loss of the described JNK-induced Ser307 IRS1 phosphorylation actually deteriorates insulin action and metabolism [57], questioning direct negative effects of JNK activation on insulin action. In line with this, a constitutive active form of JNK overexpressed in hypothalamic Agrp neurons does not impair hypothalamic insulin action [58] and JNK inhibition did not affect PA- and CHO + PA-induced insulin resistance in our study (Supplementary Figure S9).

It remains uncertain whether LA is good or detrimental for brain function [59]. Most human data originated from epidemiological studies identify associations rather than causations, with contradicting results showing benefits but also risks for metabolism with regards to LA levels [59]. One prospective cohort study revealed that high dietary intake of PUFAs was inversely associated with higher mortality risk, which was mainly driven by LA [60]. LA is incorporated in cardiolipin's acyl chain, a crucial mitochondrial lipid species [61], and decreased cardiolipin biosynthesis reduces mitochondrial function [62,63]. Therefore, LA seems to be beneficial for mitochondrial function. Yet, LA treatment did not affect mitochondrial respiration in neurons, suggesting that increasing LA levels above normal does not further improve mitochondrial function under basal conditions (Figure 3B). Analyzing mitochondrial respiration with a focus on different substrates and cellular pathways might help to better understand the role of LA in neuronal metabolism. In contrast, it has been previously shown that LA stimulation is sufficient to reduce mitochondrial respiration and increase cell death in hepatoma 1C1 cells [64]. We have observed that combined cholesterol and LA treatment enhances protein carbonylation, suggesting that LA under certain metabolic conditions might be detrimental for neuronal health (Figure 3E–F). Since mitochondria reveal cell- and tissue-specific functions [65], it might explain different results with regards to the influence of LA on cellular homeostasis. We showed that LA in contrast to PA does not induce neuronal insulin resistance (Figure 4A), but in combination with cholesterol can even enhance insulin signaling (Figure 4C). As neurons and glia cells differ in metabolism and interact functionally in vivo, we tested these stimulations on brain slices. We

confirmed our in vitro data showing that LA or LA in combination with cholesterol are not detrimental for insulin action in these settings (Figure 6A,B). Yet, further research is clearly needed to investigate whether overall ω6-PUFA levels affect insulin signaling and whether our observation is specific for the ω6-PUFA LA.

4.3. Interplay of Cholesterol and Fatty Acids in the Brain and the Periphery

In peripheral tissues, cholesterol can be acquired from endogenous synthesis and from exogenous lipoproteins that deliver sterols from the circulation [47]. Mice challenged with high-cholesterol diets accumulated high levels of cholesterol esters in the liver [5], while only dietary cholesterol in combination with soybean oil-derived fatty acids like the ω6-PUFA linoleic acid in the CHO + SOY diet induced massive oxidative stress, a reduction in mitochondrial protein content and severe inflammation in the liver, demonstrating an interaction of cholesterol and ω6-PUFAs in peripheral tissues [5].

Investigating the brains of mice fed high-cholesterol diets in combination with chow (CHO + STD) or HFDs (CHO + SOY, CHO + LAR) revealed only minor effects on protein carbonylation in the brain (Figure 2E,F) compared to the liver [5], suggesting that the brain is broadly protected by the BBB at a young age. As cholesterol-containing diets reduce the expression of the tight junction protein occludin and reduce the protein expression of some mitochondrial electron transport chain subunits (Figures 1D and 2A,B), it suggests that long-term intake of high-cholesterol diets might harm the brain by increasing BBB permeability. Therefore, our studies (this study and Reference [5]) disclose that tissues react differently to increased dietary intake of fat and cholesterol. In contrast to the brain, the CHO + SOY diet, but not the CHO + STD or CHO + LAR diets, caused hepatic dysfunction [5]. Furthermore, our own unpublished data of this in vivo study revealed that soybean- and lard-based HFDs, independent of cholesterol, impair insulin signaling in muscle, whereas only the LAR diet, but not the high-cholesterol-containing diets, triggered inflammation in white adipose tissue. The liver is able to secrete factors, so-called hepatokines, which are beneficial for metabolism and health. As a stress response, the liver secretes, among others, FGF21 [66,67], which modulates metabolism via acting in the brain [68]. Thus, the mild effect of the different tested diets on brain function might also be explained by regulatory signals from peripheral tissues impacting the brain. Consequently, it is important to assess the effect of dietary components on neuronal and brain function in vitro and ex vivo, to avoid compensatory effects which might mask the consequences of organ-specific nutrient exposure.

Overall, our data have revealed that palmitate and palmitate with cholesterol harm neuronal mitochondrial activity, IR and IGF-1R sensitivity. Importantly, we showed that IR expression is important to mitigate the detrimental effect of PA and CHO + PA on mitochondrial function, insulin signaling and JNK activation. In addition, cholesterol-containing HFDs affect BBB integrity, and cause altered mitochondrial protein expression and metabolic stress in vivo, highlighting the importance of balanced dietary intake of different fatty acids for brain function.

Supplementary Materials: The following are available online at http://www.mdpi.com/2072-6643/12/5/1518/s1, Table S1: Diet composition, Table S2: Primer pairs specific for each gene used in the study, Figure S1: High-fat diets decrease insulin sensitivity, Figure S2: Changes in relative abundance of fatty acids in serum due to dietary intervention, Figure S3: Determination of concentration for MβCD and cholesterol in hypothalamic neurons, Figure S4: Cholesterol regulates endogenous cholesterol biosynthesis in hypothalamic neurons, Figure S5: Cholesterol regulates mitochondrial function and dynamics in hypothalamic neurons, Figure S6: Characterization of insulin receptor-deficient hypothalamic neurons, Figure S7: Palmitate, but not cholesterol, induces JNK activation, Figure S8: Investigating different control stimulations on insulin sensitivity in hypothalamic neurons, Figure S9: Palmitate-and palmitate/cholesterol-induced insulin resistance is independent of JNK activation.

Author Contributions: Conceptualization, J.H. and A.K.; Methodology, M.S., C.C., A.L., E.A., T.F., K.R., K.W., A.W. and J.H.; Validation, M.S., C.C., J.H. and A.K.; Formal analysis, M.S. and C.C.; Investigation, J.H. and A.K.; Resources, J.H. and A.K.; Data curation, M.S. and C.C.; Writing—original draft preparation, A.K.; Writing—review and editing, M.S., C.C. and J.H.; Visualization, M.S., C.C. and J.H.; Supervision, J.H. and A.K.; Funding acquisition, J.H. and A.K. All authors have read and agreed to the published version of the manuscript.

Funding: This research was funded by Deutsche Forschungsgemeinschaft (DFG), grant project KL 2399/4-1 (to A.K.) and by grants from the German Ministry of Education and Research (BMBF) and the State of Brandenburg (DZD grant 82DZD00302 and BMBF grant 031B0569). Additionally, this work was supported by the Deutsche Forschungsgemeinschaft (DFG), grant project HE-7032/1-1 (to J.H.).

Acknowledgments: We thank Michael Schupp for providing plasmids (insulin receptor gRNA plasmid). We further thank Robert Hauffe for critical discussions and technical support. We acknowledge the support of Open Access Publication Fund of the University of Potsdam.

Conflicts of Interest: The authors declare no conflict of interest.

References

1. Fabbrini, E.; Sullivan, S.; Klein, S. Obesity and nonalcoholic fatty liver disease: Biochemical, metabolic, and clinical implications. *Hepatology* **2010**, *51*, 679–689. [CrossRef]
2. Kleinert, M.; Clemmensen, C.; Hofmann, S.M.; Moore, M.C.; Renner, S.; Woods, S.C.; Huypens, P.; Beckers, J.; de Angelis, M.H.; Schürmann, A.; et al. Animal models of obesity and diabetes mellitus. *Nat. Rev. Endocrinol.* **2018**, *14*, 140–162. [CrossRef]
3. Steenhuis, I.; Poelman, M. Portion Size: Latest Developments and Interventions. *Curr. Obes. Rep.* **2017**, *6*, 10–17. [CrossRef]
4. Pinel, A.; Pitois, E.; Rigaudiere, J.-P.; Jouve, C.; de Saint-Vincent, S.; Laillet, B.; Montaurier, C.; Huertas, A.; Morio, B.; Capel, F. EPA prevents fat mass expansion and metabolic disturbances in mice fed with a Western diet. *J. Lipid Res.* **2016**, *57*, 1382–1397. [CrossRef]
5. Henkel, J.; Alfine, E.; Saín, J.; Jöhrens, K.; Weber, D.; Castro, J.P.; König, J.; Stuhlmann, C.; Vahrenbrink, M.; Jonas, W.; et al. Soybean Oil-Derived Poly-Unsaturated Fatty Acids Enhance Liver Damage in Nafld Induced by Dietary Cholesterol. *Nutrients* **2018**, *10*, 1326. [CrossRef]
6. Wardelmann, K.; Blümel, S.; Rath, M.; Alfine, E.; Chudoba, C.; Schell, M.; Cai, W.; Hauffe, R.; Warnke, K.; Flore, T.; et al. Insulin action in the brain regulates mitochondrial stress responses and reduces diet-induced weight gain. *Mol. Metab.* **2019**, *21*, 68–81. [CrossRef]
7. Mayer, C.M.; Belsham, D.D. Palmitate Attenuates Insulin Signaling and Induces Endoplasmic Reticulum Stress and Apoptosis in Hypothalamic Neurons: Rescue of Resistance and Apoptosis through Adenosine 5? Monophosphate-Activated Protein Kinase Activation. *Endocrinology* **2010**, *151*, 576–585. [CrossRef] [PubMed]
8. Posey, K.A.; Clegg, D.J.; Printz, R.L.; Byun, J.; Morton, G.J.; Vivekanandan-Giri, A.; Pennathur, S.; Baskin, D.G.; Heinecke, J.W.; Woods, S.C.; et al. Hypothalamic proinflammatory lipid accumulation, inflammation, and insulin resistance in rats fed a high-fat diet. *Am. J. Physiol. Metab.* **2008**, *296*, 1003–1012. [CrossRef] [PubMed]
9. Benoit, S.C.; Kemp, C.J.; Elias, C.F.; Abplanalp, W.; Herman, J.P.; Migrenne, S.; Lefevre, A.-L.; Cruciani-Guglielmacci, C.; Magnan, C.; Yu, F.; et al. Palmitic acid mediates hypothalamic insulin resistance by altering PKC-theta subcellular localization in rodents. *J. Clin. Investig.* **2009**, *119*, 2577–2589. [CrossRef] [PubMed]
10. Boucher, J.; Kleinridders, A.; Kahn, C.R. Insulin Receptor Signaling in Normal and Insulin-Resistant States. *Cold Spring Harb. Perspect. Boil.* **2014**, *6*, a009191. [CrossRef] [PubMed]
11. Coll, T.; Eyre, E.; Rodriguez-Calvo, R.; Palomer, X.; Sánchez, R.M.; Merlos, M.; Laguna, J.C.; Vázquez-Carrera, M. Oleate Reverses Palmitate-induced Insulin Resistance and Inflammation in Skeletal Muscle Cells. *J. Boil. Chem.* **2008**, *283*, 11107–11116. [CrossRef] [PubMed]
12. Benzler, M.; Benzler, J.; Stoehr, S.; Hempp, C.; Rizwan, M.Z.; Heyward, P.; Tups, A. "Insulin-like" effects of palmitate compromise insulin signalling in hypothalamic neurons. *J. Comp. Physiol. B* **2019**, *189*, 413–424. [CrossRef] [PubMed]
13. Lang, P.; Hasselwander, S.; Li, H.; Xia, N. Effects of different diets used in diet-induced obesity models on insulin resistance and vascular dysfunction in C57BL/6 mice. *Sci. Rep.* **2019**, *9*, 19556–19614. [CrossRef] [PubMed]
14. Püschel, G.P.; Henkel, J. Dietary cholesterol does not break your heart but kills your liver. *Porto Biomed. J.* **2018**, *3*, e12. [CrossRef] [PubMed]

15. Martín-Segura, A.; Ahmed, T.; Casadomé-Perales, Á.; Palomares-Perez, I.; Palomer, E.; Kerstens, A.; Munck, S.; Balschun, D.; Dotti, C.G. Age-associated cholesterol reduction triggers brain insulin resistance by facilitating ligand-independent receptor activation and pathway desensitization. *Aging Cell* **2019**, *18*, e12932. [CrossRef] [PubMed]
16. Freeman, L.R.; E Granholm, A.-C. Vascular Changes in Rat Hippocampus following a High Saturated Fat and Cholesterol Diet. *Br. J. Pharmacol.* **2011**, *32*, 643–653. [CrossRef] [PubMed]
17. Hsu, T.M.; Kanoski, S.E. Blood-brain barrier disruption: Mechanistic links between Western diet consumption and dementia. *Front. Aging Neurosci.* **2014**, *6*, 88. [CrossRef]
18. Ziolkowski, W.; Szkatuła, M.; Nurczyk, A.; Wakabayashi, T.; Kaczor, J.J.; Olek, R.A.; Knap, N.; Antosiewicz, J.; Wieckowski, M.R.; Woźniak, M. Methyl-beta-cyclodextrin induces mitochondrial cholesterol depletion and alters the mitochondrial structure and bioenergetics. *FEBS Lett.* **2010**, *584*, 4606–4610. [CrossRef]
19. Yu, W.; Gong, J.-S.; Ko, M.; Garver, W.S.; Yanagisawa, K.; Michikawa, M. Altered Cholesterol Metabolism in Niemann-Pick Type C1 Mouse Brains Affects Mitochondrial Function. *J. Boil. Chem.* **2005**, *280*, 11731–11739. [CrossRef]
20. Fernandez, A.; Llacuna, L.; Fernández-checa, J.C.; Colell, A. Mitochondrial cholesterol loading exacerbates amyloid beta peptide-induced inflammation and neurotoxicity. *J. Neurosci.* **2009**, *29*, 6394–6405. [CrossRef]
21. Suzuki, R.; Lee, K.; Jing, E.; Biddinger, S.B.; McDonald, J.G.; Montine, T.J.; Craft, S.; Kahn, C.R. Diabetes and Insulin in Regulation of Brain Cholesterol Metabolism. *Cell Metab.* **2010**, *12*, 567–579. [CrossRef] [PubMed]
22. Fukui, K.; Ferris, H.A.; Kahn, C.R. Effect of Cholesterol Reduction on Receptor Signaling in Neurons. *J. Boil. Chem.* **2015**, *290*, 26383–26392. [CrossRef] [PubMed]
23. Kleinridders, A.; Lauritzen, H.P.; Ussar, S.; Christensen, J.H.; Mori, M.A.; Bross, P.; Kahn, C.R. Leptin regulation of Hsp60 impacts hypothalamic insulin signaling. *J. Clin. Investig.* **2013**, *123*, 4667–4680. [CrossRef] [PubMed]
24. Linn, T.; Noke, M.; Woehrle, M.; Kloer, H.U.; Hammes, H.P.; Litzlbauer, D.; Bretzel, R.G.; Federlin, K. Fish oil-enriched diet and reduction of low-dose streptozocin-induced hyperglycemia. Inhibition of macrophage activation. *Diabetes* **1989**, *38*, 1402–1411. [CrossRef]
25. Simopoulos, A.P. An increase in the omega-6/omega-3 fatty acid ratio increases the risk for obesity. *Nutrients* **2016**, *8*, 128. [CrossRef]
26. Henkel, J.; Coleman, C.D.; Schraplau, A.; Jöhrens, K.; Weber, D.; Castro, J.P.; Hugo, M.; Schulz, T.; Krämer, S.; Schürmann, A.; et al. Induction of Steatohepatitis (NASH) with Insulin Resistance in Wild-type B6 Mice by a Western-type Diet Containing Soybean Oil and Cholesterol. *Mol. Med.* **2017**, *23*, 70–82. [CrossRef]
27. Listenberger, L.L.; Ory, D.S.; Schaffer, J.E. Palmitate-induced Apoptosis Can Occur through a Ceramide-independent Pathway. *J. Boil. Chem.* **2001**, *276*, 14890–14895. [CrossRef]
28. Mielke, J.G.; Taghibiglou, C.; Liu, L.; Zhang, Y.; Jia, Z.; Adeli, K.; Wang, Y.T. A biochemical and functional characterization of diet-induced brain insulin resistance. *J. Neurochem.* **2005**, *93*, 1568–1578. [CrossRef]
29. Baylin, A.; Kim, M.K.; Donovan-Palmer, A.; Siles, X.; Dougherty, L.; Tocco, P.; Campos, H. Fasting Whole Blood as a Biomarker of Essential Fatty Acid Intake in Epidemiologic Studies: Comparison with Adipose Tissue and Plasma. *Am. J. Epidemiol.* **2005**, *162*, 373–381. [CrossRef]
30. A Kaluzny, M.; Duncan, L.; Merritt, M.V.; Epps, D. Rapid separation of lipid classes in high yield and purity using bonded phase columns. *J. Lipid Res.* **1985**, *26*, 135–140.
31. Metges, C.C.; Lehmann, L.; Boeuf, S.; Jetzke, K.J.; Müller, A.; Rickert, R.; Franke, W.; Steinhart, H.; Nürnberg, G.; Klaus, S. Cis-9, trans-11 and trans-10, cis-12 Cla affect lipid metabolism differently in primary white and brown adipocytes of djungarian hamsters. *Lipids* **2003**, *38*, 1133–1142. [CrossRef] [PubMed]
32. Gohlke, S.; Zagoriy, V.; Inostroza, A.C.; Méret, M.; Mancini, C.; Japtok, L.; Schumacher, F.; Kuhlow, R.; Graja, A.; Stephanowitz, H.; et al. Identification of functional lipid metabolism biomarkers of brown adipose tissue aging. *Mol. Metab.* **2019**, *24*, 1–17. [CrossRef] [PubMed]
33. Castro, J.P.; Ott, C.; Jung, T.; Grune, T.; Almeida, H. Carbonylation of the cytoskeletal protein actin leads to aggregate formation. *Free. Radic. Boil. Med.* **2012**, *53*, 916–925. [CrossRef]
34. Pitas, R.; Boyles, J.K.; Lee, S.H.; Hui, D.; Weisgraber, K.H. Lipoproteins and their receptors in the central nervous system. Characterization of the lipoproteins in cerebrospinal fluid and identification of apolipoprotein B,E(LDL) receptors in the brain. *J. Boil. Chem.* **1987**, *262*, 14352–14360.

35. Kleiner, S.; Mepani, R.J.; Laznik, D.; Ye, L.; Jurczak, M.J.; Jornayvaz, F.R.; Estall, J.L.; Bhowmick, D.C.; Shulman, G.I.; Spiegelman, B.M. Development of insulin resistance in mice lacking PGC-1α in adipose tissues. *Proc. Natl. Acad. Sci. USA* **2012**, *109*, 9635–9640. [CrossRef] [PubMed]
36. Lantier, L.; Williams, A.S.; Williams, I.M.; Yang, K.K.; Bracy, D.P.; Goelzer, M.; James, F.D.; Gius, D.; Wasserman, D.H. Sirt3 Is Crucial for Maintaining Skeletal Muscle Insulin Action and Protects Against Severe Insulin Resistance in High-Fat–Fed Mice. *Diabetes* **2015**, *64*, 3081–3092. [CrossRef] [PubMed]
37. Castro, J.P.; Wardelmann, K.; Grune, T.; Kleinridders, A. Mitochondrial Chaperones in the Brain: Safeguarding Brain Health and Metabolism? *Front. Endocrinol.* **2018**, *9*. [CrossRef]
38. Christian, A.; Haynes, M.P.; Phillips, M.C.; Rothblat, G.H. Use of cyclodextrins for manipulating cellular cholesterol content. *J. Lipid Res.* **1997**, *38*, 2264–2272.
39. Widenmaier, S.; Snyder, N.A.; Nguyen, T.B.; Arduini, A.; Lee, G.Y.; Arruda, A.P.; Saksi, J.; Bartelt, A.; Hotamisligil, G.S. Nrf1 Is an ER Membrane Sensor that Is Central to Cholesterol Homeostasis. *Cell* **2017**, *171*, 1094–1109.e15. [CrossRef]
40. Kleinridders, A. Deciphering Brain Insulin Receptor and Insulin-Like Growth Factor 1 Receptor Signalling. *J. Neuroendocr.* **2016**, *28*. [CrossRef]
41. Knudsen, L.; Hansen, B.F.; Jensen, P.; Pedersen, T.A.; Vestergaard, K.; Schäffer, L.; Blagoev, B.; Oleksiewicz, M.B.; Kiselyov, V.V.; de Meyts, P. Agonism and Antagonism at the Insulin Receptor. *PLoS ONE* **2012**, *7*, e51972. [CrossRef] [PubMed]
42. Schäffer, L.; Brand, C.L.; Hansen, B.F.; Ribel, U.; Shaw, A.C.; Slaaby, R.; Sturis, J. A novel high-affinity peptide antagonist to the insulin receptor. *Biochem. Biophys. Res. Commun.* **2008**, *376*, 380–383. [CrossRef] [PubMed]
43. Ballabh, P.; Braun, A.; Nedergaard, M. The blood-brain barrier: An overview: Structure, regulation, and clinical implications. *Neurobiol. Dis.* **2004**, *16*, 1–13. [CrossRef] [PubMed]
44. Dietschy, J.M.; Turley, S.D. Cholesterol metabolism in the brain. *Curr. Opin. Lipidol.* **2001**, *12*, 105–112. [CrossRef] [PubMed]
45. Dietschy, J.M.; Turley, S.D. Thematic review series: Brain Lipids.Cholesterol metabolism in the central nervous system during early development and in the mature animal. *J. Lipid Res.* **2004**, *45*, 1375–1397. [CrossRef]
46. Kim, S.Y.; Buckwalter, M.S.; Soreq, H.; Vezzani, A.; Kaufer, D. Blood-brain barrier dysfunction-induced inflammatory signaling in brain pathology and epileptogenesis. *Epilepsia* **2012**, *53*, 37–44. [CrossRef]
47. Vance, J.E. Dysregulation of cholesterol balance in the brain: Contribution to neurodegenerative diseases. *Dis. Model. Mech.* **2012**, *5*, 746–755. [CrossRef]
48. De Groot, J.C.; de Leeuw, F.-E.; Oudkerk, M.; Hofman, A.; Jolles, J.; Breteler, M. Cerebral white matter lesions and subjective cognitive dysfunction: The Rotterdam Scan Study. *Neurology* **2001**, *56*, 1539–1545. [CrossRef]
49. Ryu, S.Y.; Coutu, J.-P.; Rosas, H.D.; Salat, D.H. Effects of insulin resistance on white matter microstructure in middle-aged and older adults. *Neurology* **2014**, *82*, 1862–1870. [CrossRef]
50. Kappeler, L.; Filho, C.D.M.; Dupont, J.; Leneuve, P.; Cervera, P.; Perin, L.; Loudes, C.; Blaise, A.; Klein, R.; Epelbaum, J.; et al. Brain igf-1 Receptors Control Mammalian Growth and Lifespan through a Neuroendocrine Mechanism. *PLoS Boil.* **2008**, *6*, e254. [CrossRef]
51. Puche, J.; Muñoz, U.; García-Magariño, M.; Sádaba, M.C.; Castilla-Cortázar, I. Partial igf-1 deficiency induces brain oxidative damage and edema, which are ameliorated by replacement therapy. *BioFactors* **2016**, *42*, 60–79. [PubMed]
52. Aguirre, V.; Uchida, T.; Yenush, L.; Davis, R.; White, M.F. The c-Jun NH(2)-terminal kinase promotes insulin resistance during association with insulin receptor substrate-1 and phosphorylation of Ser(307). *J. Boil. Chem.* **2000**, *275*, 9047–9054. [CrossRef] [PubMed]
53. Belgardt, B.F.; Mauer, J.; Wunderlich, F.T.; Ernst, M.B.; Pal, M.; Spohn, G.; Brönneke, H.S.; Brodesser, S.; Hampel, B.; Schauss, A.C.; et al. Hypothalamic and pituitary c-Jun N-terminal kinase 1 signaling coordinately regulates glucose metabolism. *Proc. Natl. Acad. Sci. USA* **2010**, *107*, 6028–6033. [CrossRef] [PubMed]
54. Dandona, P.; Aljada, A.; Mohanty, P.; Ghanim, H.; Hamouda, W.; Assian, E.; Ahmad, S. Insulin inhibits intranuclear nuclear factor kappab and stimulates ikappab in mononuclear cells in obese subjects: Evidence for an anti-inflammatory effect? *J. Clin. Endocrinol. Metab.* **2001**, *86*, 3257–3265.
55. Dandona, P.; Chaudhuri, A.; Mohanty, P.; Ghanim, H. Anti-inflammatory effects of insulin. *Curr. Opin. Clin. Nutr. Metab. Care* **2007**, *10*, 511–517. [CrossRef]

56. Wang, Z.-H.; Liu, Y.; Chaitankar, V.; Pirooznia, M.; Xu, H. Electron transport chain biogenesis activated by a Jnk-insulin-Myc relay primes mitochondrial inheritance in Drosophila. *eLife* **2019**, *8*. [CrossRef]
57. Copps, K.D.; Hancer, N.J.; Opare-Ado, L.; Qiu, W.; Walsh, C.; White, M.F. Irs1 Serine 307 Promotes Insulin Sensitivity in Mice. *Cell Metab.* **2010**, *11*, 84–92. [CrossRef]
58. Tsaousidou, E.; Paeger, L.; Belgardt, B.F.; Pál, M.; Wunderlich, C.M.; Brönneke, H.; Collienne, U.; Hampel, B.; Wunderlich, F.T.; Schmidt-Supprian, M.; et al. Distinct Roles for Jnk and Ikk Activation in Agouti-Related Peptide Neurons in the Development of Obesity and Insulin Resistance. *Cell Rep.* **2014**, *9*, 1495–1506. [CrossRef]
59. Taha, A.Y. Linoleic acid–good or bad for the brain? *NPJ Sci. Food* **2020**, *4*, 1–6. [CrossRef]
60. Wang, D.D.; Li, Y.; Chiuve, S.E.; Stampfer, M.J.; Manson, J.E.; Rimm, E.B.; Willett, W.C.; Hu, F.B. Association of specific dietary fats with total and cause-specific mortality. *JAMA Intern. Med.* **2016**, *176*, 1134–1145. [CrossRef]
61. Chicco, A.J.; Sparagna, G.C. Role of cardiolipin alterations in mitochondrial dysfunction and disease. *Am. J. Physiol. Physiol.* **2007**, *292*, 33–44. [CrossRef] [PubMed]
62. Dudek, J.; Cheng, I.-F.; Balleininger, M.; Vaz, F.M.; Streckfuss-Bömeke, K.; Hübscher, D.; Vukotic, M.; Wanders, R.; Rehling, P.; Guan, K. Cardiolipin deficiency affects respiratory chain function and organization in an induced pluripotent stem cell model of Barth syndrome. *Stem Cell Res.* **2013**, *11*, 806–819. [CrossRef] [PubMed]
63. Gohil, V.M.; Hayes, P.; Matsuyama, S.; Schägger, H.; Schlame, M.; Greenberg, M.L. Cardiolipin Biosynthesis and Mitochondrial Respiratory Chain Function Are Interdependent. *J. Boil. Chem.* **2004**, *279*, 42612–42618. [CrossRef] [PubMed]
64. Penzo, D.; Tagliapietra, C.; Colonna, R.; Petronilli, V.; Bernardi, P. Effects of fatty acids on mitochondria: Implications for cell death. *Biochim. Biophys. Acta Bioenerg.* **2002**, *1555*, 160–165. [CrossRef]
65. Brandt, T.; Mourier, A.; Tain, L.S.; Partridge, L.; Larsson, N.-G.; Brandt, T. Changes of mitochondrial ultrastructure and function during ageing in mice and Drosophila. *eLife* **2017**, *6*. [CrossRef]
66. Henkel, J.; Buchheim-Dieckow, K.; Castro, J.; Laeger, T.; Wardelmann, K.; Kleinridders, A.; Jöhrens, K.; Püschel, G. Reduced Oxidative Stress and Enhanced Fgf21 Formation in Livers of Endurance-Exercised Rats with Diet-Induced NASH. *Nutrients* **2019**, *11*, 2709. [CrossRef]
67. Dushay, J.; Chui, P.C.; Gopalakrishnan, G.S.; Varela–Rey, M.; Crawley, M.; Fisher, F.M.; Badman, M.K.; Martínez-Chantar, M.L.; Maratos-Flier, E. Increased fibroblast growth factor 21 in obesity and nonalcoholic fatty liver disease. *Gastroenterology* **2010**, *139*, 456–463. [CrossRef]
68. Liang, Q.; Zhong, L.; Zhang, J.; Wang, Y.; Bornstein, S.R.; Triggle, C.R.; Ding, H.; Lam, K.S.L.; Xu, A. FGF21 Maintains Glucose Homeostasis by Mediating the Cross Talk Between Liver and Brain During Prolonged Fasting. *Diabetes* **2014**, *63*, 4064–4075. [CrossRef]

nutrients

MDPI

Article

Lipotoxic Injury Differentially Regulates Brain Microvascular Gene Expression in Male Mice

Saivageethi Nuthikattu [1,†], Dragan Milenkovic [1,2,†], John C. Rutledge [1] and Amparo C. Villablanca [1,*]

[1] Division of Cardiovascular Medicine, Department of Internal Medicine, University of California, One Shields Ave., The Grove, Rm 1159, Davis, CA 95616, USA; snuthikattu@ucdavis.edu (S.N.); dragan.milenkovic@inra.fr (D.M.); jcrutledge@ucdavis.edu (J.C.R.)

[2] INRA, UNH, Université Clermont Auvergne, 63000 Clermont-Ferrand, France

* Correspondence: avillablanca@ucdavis.edu; Tel.: +1-530-752-0718; Fax: +1-530-752-3264

† Authors Contributed Equally.

Received: 7 May 2020; Accepted: 12 June 2020; Published: 13 June 2020

Abstract: The Western diet (WD) and hyperlipidemia are risk factors for vascular disease, dementia, and cognitive impairment. However, the molecular mechanisms are poorly understood. This pilot study investigated the genomic pathways by which the WD and hyperlipidemia regulate gene expression in brain microvessels. Five-week-old C57BL/6J wild type (WT) control and low-density lipoprotein receptor deficient (LDL-R−/−) male mice were fed the WD for eight weeks. Differential gene expression, gene networks and pathways, transcription factors, and non-protein coding RNAs were evaluated by a genome-wide microarray and bioinformatics analysis of laser-captured hippocampal microvessels. The WD resulted in the differential expression of 1972 genes. Much of the differentially expressed gene (DEG) was attributable to the differential regulation of cell signaling proteins and their transcription factors, approximately 4% was attributable to the differential expression of miRNAs, and 10% was due to other non-protein coding RNAs, primarily long non-coding RNAs (lncRNAs) and small nucleolar RNAs (snoRNAs) not previously described to be modified by the WD. Lipotoxic injury resulted in complex and multilevel molecular regulation of the hippocampal microvasculature involving transcriptional and post-transcriptional regulation and may provide a molecular basis for a better understanding of hyperlipidemia-associated dementia risk.

Keywords: genomics; microvascular; brain; dementia; hyperlipidemia; Western diet; males

1. Introduction

Alzheimer's disease (AD) is a progressive disease characterized by a decline in cognitive function and loss of memory, and its etiology includes both environmental and genetic factors [1]. The strongest genetic risk factor for AD is the ε4 variant of apolipoprotein E (ApoE), yet the most common cause of vascular dementia (VaD) is cerebral small vessel disease [2]. Risk factors for cardiovascular disease (CVD) are known to overlap with risk factors of AD and VaD [1], still the mechanistic links have not been clearly established [3]. As a result, understanding the effect of CVD risk factors in dementia provides potential important therapeutic targets for the prevention of cognitive dysfunction.

The global increase in obesity has been linked to a decline in complex carbohydrate and fiber intake, diets with fewer fruits and vegetables, and a shift towards diets high in fat and refined sugars—otherwise known as the Western-type diet (WD). An association has been reported between obesity and cognitive dysfunction and reduced neural integrity (e.g., grey and white matter atrophy) [4]. One consequence of the WD is hyperlipidemia. A greater risk of AD is correlated with high concentrations of low-density lipoprotein cholesterol (LDL-C) and total cholesterol (TC) [5] and increased consumption of saturated

fat is linked to compromised cognitive function, working memory, and attention [6]. We have also recently shown that the WD results in cognitive dysfunction in hyperlipidemic male mice [7].

High dietary fat and cholesterol also have functional sequelae in the brain. The blood–brain barrier (BBB) plays a key role in many cognitive dysfunction and neurodegenerative disorders, presumably leading to increased movement of immune cells and immune intermediaries into the brain, which contribute to neuro-inflammation and consequently, neuro-degeneration [8,9]. The BBB function is regulated by brain endothelial cells, which together with neurons and non-neuronal cells (e.g., pericytes, astrocytes, and microglia), form a functional unit known as the neurovascular unit. Injury of the endothelial cell layer can have adverse consequences on brain function. Our prior work has shown that when the endothelial cell function is disrupted in wild type C57BL/6J mice fed the WD, there is a significant increase in BBB permeability associated with cognitive dysfunction and impaired memory [7]. Further, we have shown that exposure of endothelial cells to triglyceride-rich lipoproteins (TGRL) lipolysis products induces significant endothelial cell injury related to BBB dysfunction [10]. Others have similarly shown that hyperlipidemia induces changes in the expression of the vascular endothelial growth factor and tight junction protein Claudin-5 that affects the permeability of the BBB [11].

In vivo studies have been performed on whole brains or specific regions of the brain, thus obscuring the specific effects of a hyperlipidemic diet on endothelial cells. In addition, it is known that lipids are central to the pathogenesis of dementia, yet the multifactorial mechanisms by which they contribute to cognitive dysfunction in the brain are not entirely understood. Several studies have employed genomic approaches to assess for molecular level effects following the Western-type diet or hyperlipidemia induced by the low-density lipoprotein receptor-deficient (LDLR−/−) genotype. For example, high-fat diets can modulate the expression of genes related to neuronal projections and synaptic transmission corresponding to significant deterioration of neurite morphology and cognition [12]. In addition to changes in the expression of protein-coding genes, diets rich in lipids can modulate the expression of several miRNAs [13].

More recently, it has also been shown that a high-fat diet can also regulate long non-coding RNAs (ncRNAs) [14]. LncRNAs are non-protein-coding transcripts with at least 200 nucleotides in length. They have a broad range of functions in diverse biologic processes, including having a potential role in brain function and disease [15]. LncRNAs have also been found to recruit transcription factors and chromatin-modifying complexes to specific genomic sites, thereby contributing to the transcriptional and epigenetic regulation of gene expression. These studies suggest that lipotoxic injury can induce significant changes at the genome level in the brain. However, these studies were performed on whole brain or brain regions, and the specific response of different cell types, specifically brain microvascular endothelial cells, is not well understood.

LDL-R-deficient mice are widely used as models for the investigation of atherosclerosis and diet-associated lipotoxic injury because the LDL receptor is essential to the removal of ApoE-containing lipoproteins from the blood [16]. Deficiency of LDL receptors extends the residence of LDL in the blood, making LDL-R-deficient mice a particularly useful model for examining the association between lipid metabolism and inflammatory processes [16]. This, in turn, is of importance to understanding neurovascular inflammation and the vascular determinants of dementia. In our recently published work, we used whole genome transcriptomic analysis to study how hyperlipidemia affects the microvasculature in the hippocampus, a key memory center in the brain, in female low-density lipoprotein receptor-deficient (LDL-R−/−) mice fed the Western diet (WD) [17]. We showed for the first time that hyperlipidemic stress modulates the differential expression of the hippocampal microvascular genome in the females by 7%, including for protein-coding and non-coding genes (microRNAs, small nucleolar RNAs, and long non-coding RNAs). These differentially expressed genes (DEGs) were associated with the differential regulation of a number of important cellular pathways such as the regulation of the actin cytoskeleton, cell adhesion amyloid proteins, regulation of angiogenesis, Rap-1 signaling pathway, and transcription factors such as CREB1 (cAMP responsive element binding protein),

ESR1 (estrogen receptor 1), and YY1 (Yin Yang 1) [17]. However, how hyperlipidemic stress and the WD affect the entire hippocampal microvascular genome in male mice is currently unknown. As women have more rapid cognitive decline after a diagnosis of dementia than men [18] and these differences do not appear to be solely explainable by the longer life expectancy of women when compared with men, it is important to fully characterize the nutrigenomic response in males to better understand the effect of the WD on the male brain microvasculature. We hypothesized that the WD would induce complex genomic effects that lead to the differential gene expression of previously unreported protein-coding and non-protein-coding genes in the male brain hippocampal microvasculature.

Thus, the goal of our study was to determine and characterize the molecular mechanisms for the genomic effects of a high-fat diet and experimental hyperlipidemia on brain endothelium of LDL-R-deficient male mice, by performing global transcriptomic analyses on laser-captured isolated microvessels from the hippocampal regions of the brain. In addition, most prior studies have evaluated the impact of lipids on one type of RNA but have not ventured beyond that or looked at potential interactions, and therefore, a secondary goal was to perform integrated omics analyses to better understand the complexity of genetic regulation by non-protein-coding RNAs in response to the WD in males.

2. Methods

2.1. Experimental Animals

Low-density lipoprotein receptor-deficient (LDL-R−/−; strain B6.129S7-Ldlr tm1Her/J, Jackson Laboratories, Bar Harbor, ME, USA) and C57BL/6J wild type (WT; Jackson Laboratories, stock 000664) male mice were fed either a standard chow control diet (CD = Chow, Nestlé Purina PetCare Co., St. Louis, MO, USA) or a Western diet (WD, catalog no. 88137, Harlan Laboratories, Madison, WI, USA) composed of 21% fat and 0.2% cholesterol (*w*/*w*) for 8 weeks. There were four experimental treatment groups randomly assigned to the diets: WT fed CD = WT-CD, WT fed WD = WT-WD, LDL-R −/− fed CD = LR-CD, and LDL-R fed WD = LR-WD; n = 7 mice/group. Animals were housed in single cages in a temperature- and humidity-controlled environment with a 12 h light/dark cycle in the University of California, Davis Mouse Biology Program. Body weight was measured at baseline and at the completion of the dietary intervention period, and activity and food intake monitored daily by vivarium staff. Research was conducted in conformity with the Public Health Service Policy on Humane Care and Use of Laboratory Animals. The institutional review board of the University of California, Davis, the Institutional Animal Care and Use Committee (IACUC) approved this project protocol number 19750 on 7 February 2017.

2.2. Blood Metabolic and Hormone Assays

Fasting lipid levels were measured in serum samples that were stored at −80 °C until assayed. Triglyceride (TG), total cholesterol (TC), high-density lipoprotein cholesterol (HDL), and low-density lipoprotein cholesterol (LDL) were measured using enzymatic assays from Fisher Diagnostics (Middleton, VA, USA), and precipitation separation from AbCam (Cambridge, MA, USA) adapted to a microplate format. Fasting glucose and insulin levels were also measured on serum samples. Glucose was measured using enzymatic assays from Fisher Diagnostics (Middleton, VA, USA), and insulin was determined by electrochemiluminescence from Meso Scale Discovery (Rockville, MD, USA) according to the manufacturer's instructions. All assays were performed by the UC Davis Mouse Metabolic Phenotyping Center (MMPC) in triplicate, on non-pooled plasma samples.

2.3. Isolation and Cryosection of Murine Brain Hippocampus

Following completion of the dietary feeding period, mice were anesthetized by intraperitoneal xylazine/ketamine and euthanized by exsanguination during the light phase of their light/dark cycle, then intravascularly perfused with DEPC-treated PBS. Intact brains were rapidly removed under

RNAse free conditions, cut into regions including the temporal lobe segment, and embedded using HistoPrep Frozen Tissue Embedding Media (Fisher Scientific, Pittsburgh, PA, USA). To identify the hippocampus and hippocampal neurons, brain sections in the medial aspect of the temporal lobe were stained with hematoxylin and visualized with microscopy by a histopathology expert at UC Davis (Dr. Dennis Wilson). The hippocampus was then coronally cryosectioned (8 μm, Leica Frigocut 2800 n Cryostat, Leica Biosystems, Buffalo Grove, IL, USA). Hippocampal cryosections were placed on charged RNA-free PEN membrane glass slides, treated with RNA*later*®-ICE (Life Technologies, Grand Island, NY, USA) to prevent RNA degradation, and stored at −80 °C until use. When ready for use, cryosections from the hippocampal segments were submerged in nuclease-free water and dehydrated in desiccant.

2.4. Laser Capture Microdissection (LCM) of Hippocampal Microvessels

For the analysis of the gene transcriptome of the hippocampal brain microvessels, endothelial microvessels (<20μm) were first identified in the hippocampal brain cryosections by alkaline phosphatase staining utilizing 5-bromo-4-chloro-3-indolyl phosphate/nitro blue tetrazolium chloride (BCIP/NBT) substrate as previously described [19]. Laser capture microdissection (LCM) was then used to isolate the endothelium of the microvessels within the hippocampal sections by capture of the entire vessel wall under direct microscopic visualization using a Leica LMD6000 Laser Microdissection Microscope (Leica Microsystems, Wetzlar, Germany), Supplemental Figure S1. Microvessels were not categorized by the hippocampal region or subregion, although they primarily corresponded to endothelial-enriched sections in the hippocampus dorsal segments that would have included the CA1 and CA3 regions.

2.5. RNA Extraction from Laser Captured Brain Microvessels

Total RNA was extracted from the laser-captured hippocampal brain microvessels (100 microvessels/sample) from each of the four experimental animal groups using an Arcturus PicoPure™ RNA Isolation Kit (Thermo Fisher Scientific, Santa Clara, CA, USA) according to the manufacturer's instructions. The quality of the RNA from the LCM-derived vessels was assessed by Nanodrop, and RNA integrity verified by qRT-PCR of the control gene transcription (GAPDH). RNA quantification was performed according to Affymetrix RNA quantification kit with the SYBR Green I and ROX™ Passive Reference Dye protocol (Affymetrix, Santa Clara, CA, USA).

2.6. Microarray Hybridization and Transcriptome Analysis

For the transcriptomics analysis, we used Affymetrix GeneChip Mouse Gene 2.0 ST Array (~28,000 coding transcripts and ~7000 non-coding transcripts, Affymetrix, Santa Clara, CA, USA). RNA (125 pg) was used to prepare cRNA and sscDNA using an Affymetrix GeneChip ® WT Pico Kit. SscDNA (5.5 μg) was fragmented by uracil-DNA glycosylase (UDG) and apurinic/apyrimidinic endonuclease 1 (APE 1) and labeled by terminal deoxynucleotidyl transferase (TdT) using the DNA labeling reagent that is covalently linked to biotin. Fragmented and labelled ssCDNA samples in triplicate were then submitted to the UC Davis Genome Center shared resource core for hybridization, staining, and scanning using the Affymetrix WT array hybridization protocol following the manufacturer's protocol. Hybridization of the fragmented and labelled ssCDNA samples was done using GeneChip ™Hybridization Oven 645, and samples then washed and stained using GeneChip ™ Fluidics Station 450. The arrays were scanned using a GeneChip™ Scanner 3000 7G (Thermo Fisher Scientific, Santa Clara, CA, USA). Quality control of the microarrays was done using the Affymetrix Expression Console software version 1.4.1 and data analysis performed using the Affymetrix Transcriptome Analysis Console software version 3.1.0.5.

2.7. qRT-PCR Analysis of Gene Expression in Murine Hippocampal Microvessels

To corroborate the microarray analysis results, we performed qRT-PCR on 11 randomly selected differentially expressed RNA transcripts. For these experiments, RNA (75 ng) from the laser-captured brain microvessels was reverse-transcribed into cDNA using iScript Reverse Transcription Supermix for RT-Qpcr (Biorad, Hercules, CA, USA). qRT-PCR for selected genes was performed in the ABI Vii7 Sequence detection system (PE Applied Biosystems, Foster City, CA, USA). Reactions were carried out in 384-well optical plates containing 25 ng cDNA/well and SsoAdvanced™ Universal SYBR ® Green Supermix as the fluorescent reporter (Biorad, Hercules, CA, USA). Specific primers were designed with the Primer3 software [20] using the gene sequences obtained from the Affymetrix transcript IDs. The sequences of the primers used are listed in the Table S1. The PCR amplification parameters were as follows: initial denaturation step at 95 °C for 10 min followed by 40 cycles, each at 95 °C for 15 s (melting) and 60 °C for 1 min (annealing and extension). Gene expression was normalized to the glyceraldehyde-3-phosphate dehydrogenase (GAPDH) transcription. Relative gene expression was calculated using the delta–delta comparative threshold cycle (Ct) method and expressed as a fold change compared with the wild type (WT) mice fed with the control diet (CD).

2.8. Bioinformatic Analysis

Bioinformatics analysis of differentially expressed genes was performed by two of the study investigators (SN and DM) using multiple software tools. We compared each study group (LR-WD, LR-CD, and WT-WD) to the control (WT-CD). For the fold change calculations, it was also necessary to input the experimental group data and compare them to the control group data. This information is required by the microarray software (Affymetrix Transcriptome Analysis Console, version 3.1.0.5, Santa Clara, CA) used in the project.

Gene ontology of identified differentially expressed genes was done using the David bioinformatics database (https://david.ncifcrf.gov/home.jsp) [21,22], and a treemap was constructed using Revigo (http://revigo.irb.hr/) [23]. Canonical pathway analysis was conducted using the GeneTrial2 online database (https://genetrail2bioinfuni-sbde) [24] and the Metacore software package (https://portalgenegocom) to identify significantly over represented pathways. Enrichment statistics were calculated for these data sets assuming a hypergeometric distribution to identify significantly over represented pathways. Gene network and transcription factor analyses were performed using Metacore™. MicroRNA validated targets were searched using the miRWalk database (http://zmf.umm.uni-heidelberg.de/apps/zmf/mirwalk2/index.html) [25] that enables the retrieval of experimentally verified miRNA–gene target interactions. Hierarchical clustering and heat map representations of miRNA profiles were performed using the PermutMatrix software (http://www.atgc-montpellier.fr/permutmatrix/) [26]. Venn diagrams were generated using Venny (http://bioinfogp.cnb.csic.es/tools/venny/). Network analysis of interactions between functional groups was identified using Metascape (http://metascape.org/) [27], and obtained networks were visualized using the Cytoscape platform (https://cytoscape.org/) [28]. OmicsNet from MetaboAnalyst (http://wwwmetaboanalystca/MetaboAnalyst/faces/homexhtml) [29] was used for the integrated analyses of the protein–protein network with miRNAs and transcription factors. To identify potential target genes and miRNAs of lncRNAs, we used several databases, including starBase (http://starbase.sysu.edu.cn/index.php) [30], starBase v2.0: decoding miRNA–mRNA, miRNA–ncRNA and protein–RNA interaction networks from large-scale CLIP-Seq data; miRcode (http://www.mircode.org/index.php) [31], and the RNAcentral database (https://rnacentral.org) [32].

2.9. Statistical Methods

For the microarray, a two-way ANOVA (Affymetrix Transcriptome Analysis Console software, Santa Clara, CA) was used for the statistical analysis of the microvessel transcriptome of the WT-WD, LR-CD mice, and LR-WD, each compared with the WT-CD mice. All genes from the microarray with $p < 0.05$ and a ±2.0-fold change were considered as significantly differentially expressed. Mean body

weight and plasma lipid levels of all diet/genotype groups (WT-CD, WT-WD, LR-CD, LR-WD) were expressed as means ± standard error of the mean (SEM), and significance was determined at $p \leq 0.05$ using unpaired student's *t*-tests (GraphPad software, La Jolla, CA, USA). qRT-PCR determined the gene expression in the hippocampal microvessels of the experimental mice, compared with WT-CD, and was expressed as a log2-fold change, and statistical significance was determined by unpaired student's *t*-tests (GraphPad software, La Jolla, CA, USA).

3. Results

3.1. Model of Hyperlipidemia

The dietary treatment resulted in the expected weight gain in the study mice as follows: mean weight for WT mice at baseline was 21 g and increased by an average of 24% when fed with CD and 39% when fed with WD; mean weight of LR mice at baseline was 17.25 g and increased by an average of 62% when fed with CD and 74% when fed with WD ($p < 0.05$ respectively for all group comparisons): Supplemental Figure S2.

After eight weeks on the experimental diets, the mean total cholesterol levels in the CD- and WD-fed WT mice were 89.3 and 252.8 mg/dL ($p < 0.05$), respectively, and 285.6 and 1151.8 mg/dL ($p < 0.05$) for the LR-CD and LR-WD-fed mice, respectively: Supplemental Table S2A. We also determined the blood glucose and insulin levels in our study mice. Compared with WT-CD, glucose levels were highest and significantly greater ($p < 0.05$) in the LR-WD-fed groups: Supplemental Table S2B. Insulin levels were highest and significantly greater ($p < 0.05$) in the LDL-R−/− genotype and WD-fed mice compared with the WT mice on the CD. These results are consistent with what has been published previously for these experimental models [33,34].

3.2. Effect of the Western Diet on Brain Hippocampal Microvessel Gene Expression

To define the molecular mechanisms in the brain hippocampal microvessels in response to the WD, we began by assessing the effect of the WD on the global gene expression in the hippocampal microvessels of the CD-fed and WD-fed WT and LDL-R−/− male mice. These studies showed that among the 34,472 genes studied in the microarrays, 1972 genes (5.7%) were differentially expressed (DE). Volcano plots of the significantly up- or down-regulated genes in the brain microvessels of WT-WD showed up-regulation of two genes and down-regulation of eight genes compared with the microvessels of the WT-CD mice: Supplemental Figure S3A (see Supplemental Table S3 for a complete listing of the DE genes). The effect of the WD was contrasted to the effect of genotype by comparing the differential gene expression in LR-CD to WT-CD, which revealed up-regulation of 961 genes and down regulation of 2 genes: Supplemental Figure S3B (see Supplemental Table S4 for a complete listing of the DE genes). In contrast, in the microvessels of LR-WD, there was up-regulation of 1012 genes and down-regulation of 5 genes compared with the WT-CD mice: Supplemental Figure S3C (see Supplemental Table S5 for a complete listing of the DE genes). Although over 85% of the differential gene expression in the brain microvessels of male mice was for protein-coding genes, to our knowledge, we show for the first time that the WD also regulated the expression of protein-non-coding genes in the male brain microvessels: long non-coding RNAs (lncRNA), microRNAs (miRNAs), and small nucleolar RNAs (snoRNAs). The total number of differentially expressed non-protein-coding genes was greatest (153 total) for LR-WD, and for lncRNAs (113) compared with the other ncRNA (83 miRNAs and 97 snoRNAs).

A random sample of eleven differentially expressed protein-coding and ncRNA, representative of each of the experimental genotype/diet groups, was tested by qRT-PCR and confirmed to have the same direction of change in gene expression (up- or down-regulation) as observed with the microarrays (Figure 1). These data suggest a significant effect of the consumption of the WD on the differential gene expression in brain microvessels, attributable to both the WD and the LR genotype.

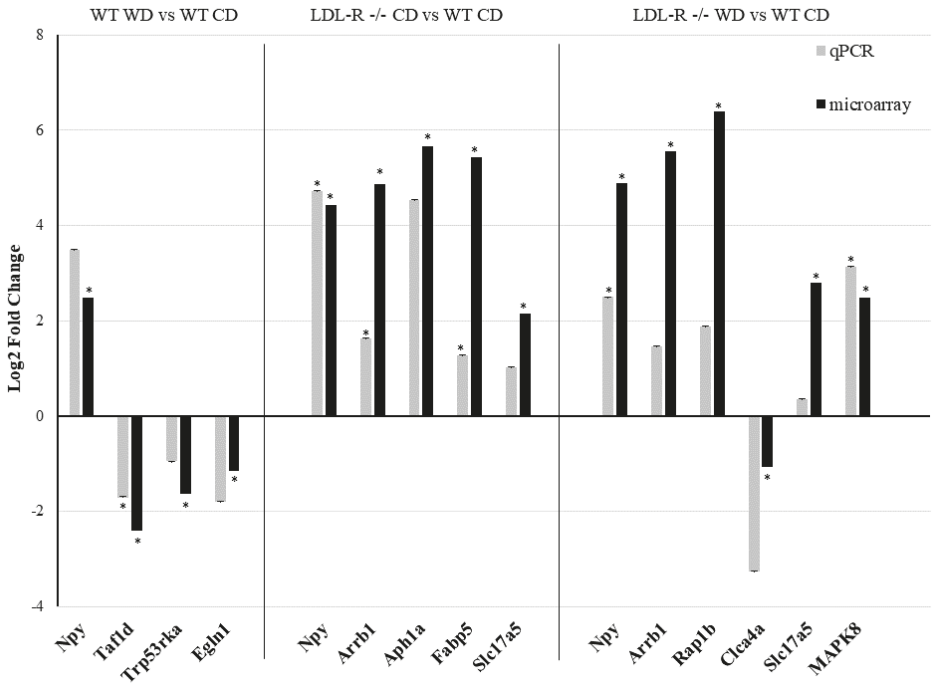

Figure 1. Gene expression by qRT-PCR of genes identified by microarray analysis in hippocampal microvessels. Eleven genes (Npy, Taf1d, Trp53rka, Egln1, Arrb1, Aph1a, Fabp5, Slc17a5, Rap1b, Clca4a, MAPK8) were tested by qRT-PCR in the hippocampal microvessels isolated from wild type (WT) and LDL-R−/− mice fed with the control diet (CD) and Western diet (WD) and showed the same trend in gene expression as the microarray. Expression levels were expressed as a log2-fold change (* $p \leq 0.05$ for WT-WD, LDL-R−/− CD, and LDL-R−/− WD when compared with WT-CD).

3.3. Effect of the Western Diet on Expression of Protein-coding Genes in Brain Hippocampal Microvessels

To identify the biological functions of differentially expressed protein-coding genes, and consequently the potential cellular processes which could be affected by changes in their expression, we performed a series of bioinformatic analyses. Our first analysis was to identify the gene ontologies of the differentially expressed genes. The genes identified as differentially expressed are involved in many biological functions: Supplemental Figure S4. These functions include angiogenesis (cellular response to insulin stimulus, triglyceride metabolism regulation of reactive oxygen species, or G protein-coupled receptor internalization), apoptotic processes (leukocyte chemotaxis, regulation of vasodilation, regulation of endothelial cell migration, angiogenesis), gene regulation and RNA biogenesis (mRNA splicing via spliceosomes, ubiquitin-dependent protein catabolism, regulation of Nf-kB transcription factor activity), and cell adhesion. This observation suggests that the cellular functions primarily affected by lipid-associated vascular injury are involved in angiogenesis, apoptosis, immune cell interaction, and gene regulation and RNA biogenesis.

Next, we performed gene network analyses using a text-mining algorithm (MetaCore) to identify the functional groups of the gene networks (Figure 2). Using this approach, we identified gene networks involved in cell adhesion (cell–matrix interactions and cadherins), cytoskeleton (cytoplasmic microtubules, intermediate filaments, macropinocytosis and its regulation), proliferation, proteolysis, transcription (nuclear receptors transcriptional regulation, chromatin modification), development, and signal transduction (Wingless and Int-1 (WNT) signaling, Notch signaling or neuropeptide signaling pathways). The gene network analysis suggests that lipid injury can principally affect

the expression of genes involved in cellular network processes that participate in cell adhesion, development, or signal transduction.

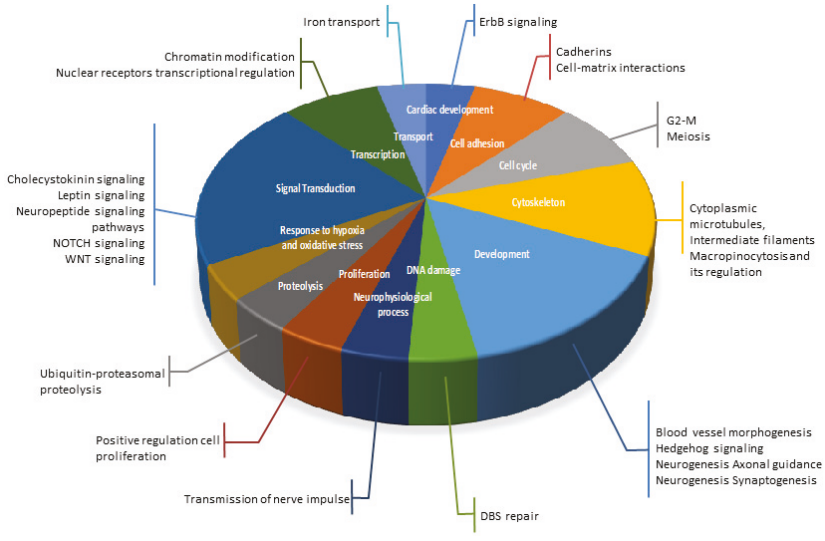

Figure 2. Gene Network Analysis of differentially expressed protein-coding genes in hippocampal microvessels. A text-mining algorithm (Metacore) was used to perform the gene network analyses and identify functional groups of the differentially expressed protein-coding genes in the hippocampus microvessels from Western diet (WD)-fed C57BL/6J (WT) mice compared with control diet (CD)-fed WT mice, CD-fed LDL-R−/− mice compared with CD-fed WT mice, and WD-fed LDL-R −/− mice compared with CD-fed WT mice. These gene networks represented in the pie chart were involved in cell adhesion (orange), cytoskeleton (yellow), proliferation (brown), proteolysis (grey), transcription (dark green), development (light blue), and signal transduction (dark blue).

Following the gene network analyses, we used KEGG and MetaCore to identify the cellular pathways for the differentially expressed genes. We observed the differential regulation of a number of important cellular pathways including those for neurological function-related pathways (axon guidance, long-term depression, or neuroactive ligand–receptor interaction), cellular metabolism (fatty acid metabolism, ABC transporters, glutathione metabolism, or oxidative phosphorylation), cell signaling (Nf-kB signaling, p53 signaling, Raps1/Ras signaling, insulin signaling, cAMP signaling, or MAPK signaling pathways), endothelial function (focal adhesion, gap junction, or tight junction), and a few other cellular processes (Figure 3). In general, when compared with the WT-CD mice, the LDL-R−/− genotype showed a larger number of genes involved in the differential expression of cellular pathways. The gene network analyses showed a similar trend to the pathway analyses for the LDL-R−/− genotype.

Using the ClueGo tool on Cytoscape, we also searched cellular pathways that form networks to identify the function of the groups of pathways of differentially expressed genes. Using this approach, we identified over 50 pathways in a network. These networks of pathways formed functional groups involved in cell signaling, oxidative stress, endothelial cell function, and neurofunction.

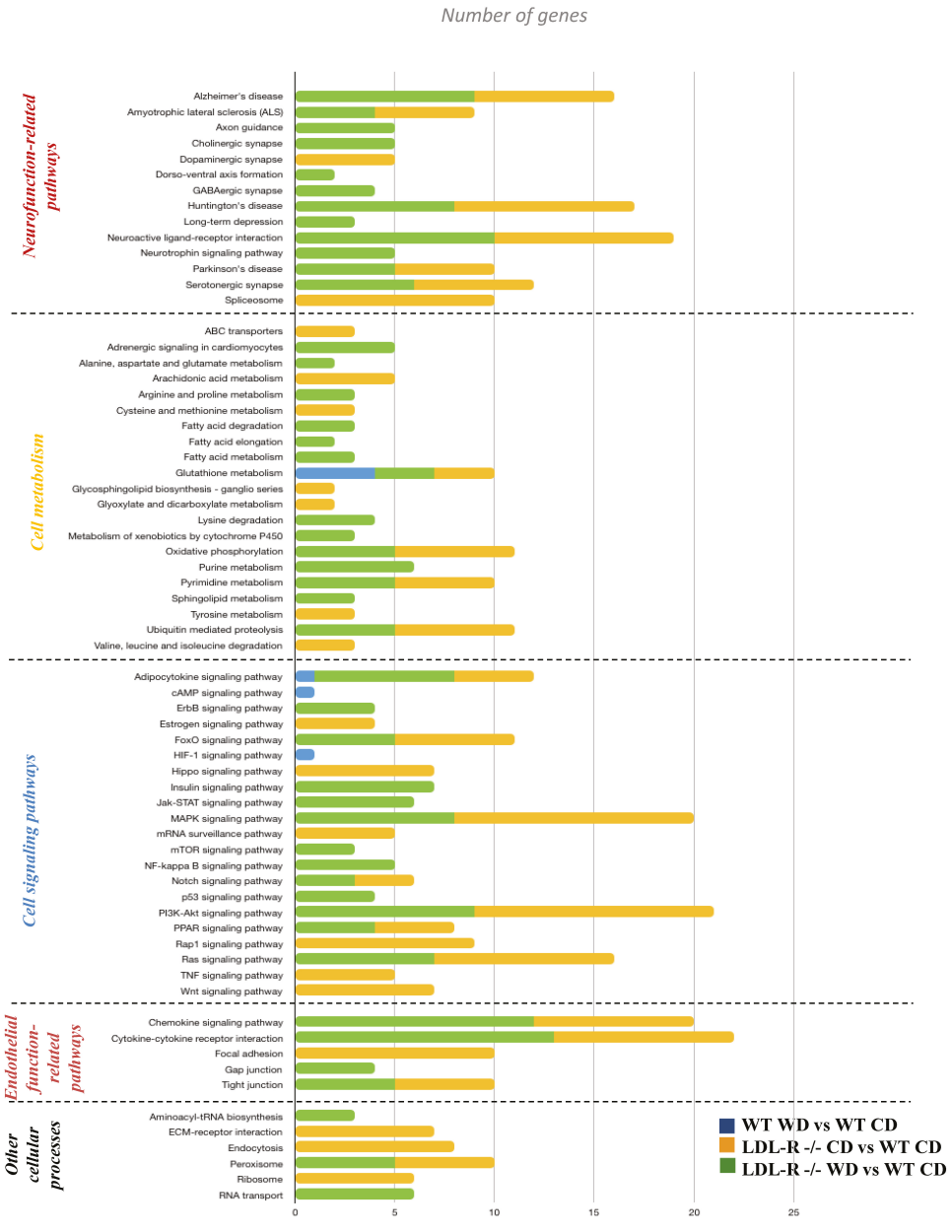

Figure 3. Pathway analyses of the pathways of differentially expressed protein-coding genes in hippocampal microvessels. Histogram of the significant cellular pathways of differentially expressed protein-coding genes in hippocampal microvessels. Cellular pathways of differentially expressed genes in hippocampus microvessels from Western diet (WD)-fed C57BL/6J (WT) mice compared with control diet (CD)-fed WT mice, CD-fed LDL-R−/− mice compared with CD-fed WT mice, and WD-fed LDL-R−/− mice compared with CD-fed WT mice were identified using KEGG and MetaCore.

3.4. Potential Transcription Factors Involved in the Genomic Effects of the Western Diet on Brain Hippocampal Microvessels

We also performed bioinformatics analyses of the gene expression data to identify potential transcription factors (TF) whose activity could be modulated by lipid injury and be involved in mediating the observed genomic effects. The most statistically significant transcription factors were ETS1 (ETS proto-oncogene 1), c-Myc (cellular myelocytomatosis), FOXP3 (forkhead box P3), and GABPalpha (GA binding protein transcription factor) (Supplemental Table S6). Comparisons of the top 30 transcription factors (TFs) identified in our study groups are shown in Venn diagrams in Figure 4. Among the top TFs, 17 were in common for the 3 diet and genotype groups. Eleven TFs were in common between the LDLR−/− mice on the CD and the LDLR−/− mice on the WD compared with the WT mice on the CD, while no common TFs were identified between LDLR−/− on the CD and WT on the WD. One TF (YY1) was in common between LDLR−/− on the WD and WT on the WD.

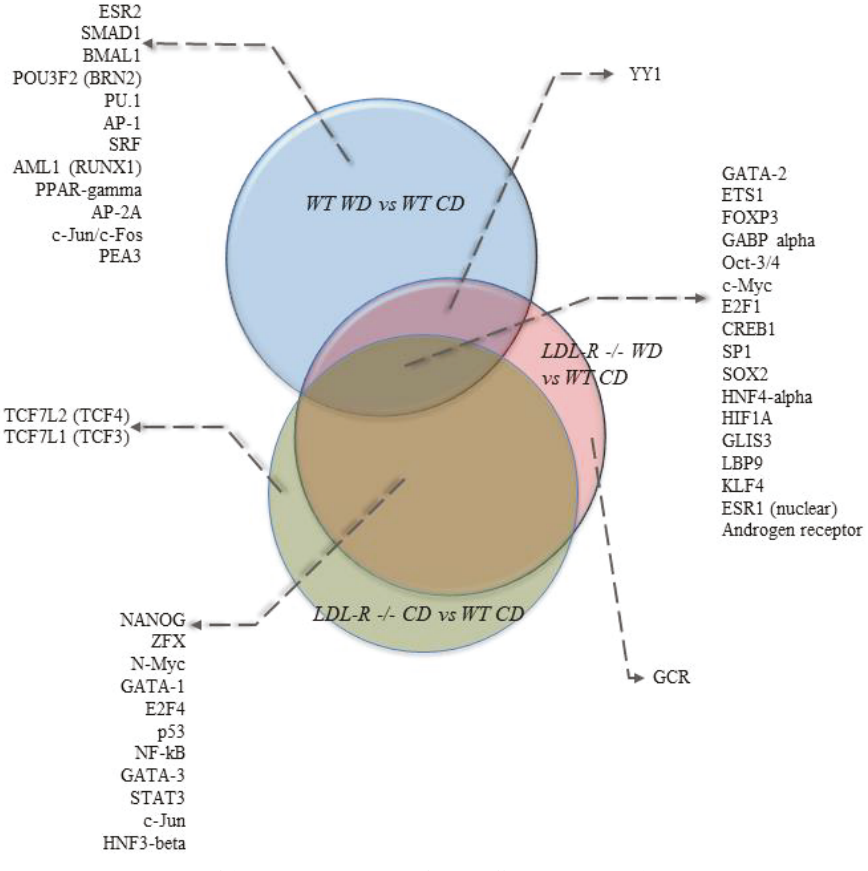

Figure 4. Venn diagram of the top 30 transcription factors affected by diet and genotype in hippocampal microvascular endothelium. Transcription factors potentially modulated by lipid injury were identified using a MetaCore transcription regulation algorithm. Venn diagram shows 17 transcription factors (TFs) in common for the Western diet (WD)-fed C57BL/6J (WT) mice, control diet (CD)-fed LDL-R−/− mice, and WD-fed LDL-R−/− mice, when compared with the CD-fed WT mice.

3.5. Impact of the Western Diet on Expression of miRNA, their Targets and Pathways in Brain Microvessels

Our microarray analysis allowed us to study not only protein-coding but also miRNAs. Using this approach, we identified that lipotoxic injury can modulate the expression of miRNAs in brain endothelial cells (Supplemental Table S7). We identified that the WD in WT mice increased the expression of one miRNA, miR-1954. On the other hand, lipotoxic injury induced by the LDL-R−/− genotype on the WD resulted in the increased expression of 42 miRNAs, including miR692, miR-196a, miR-210 or miR-486, and 39 miRNAs. In comparing the differentially expressed miRNAs for the three study conditions, only one miRNA was in common, miR-1954. On the other hand, 15 miRNAs were identified in common between the LDLR −/− mice on the CD and the WD when compared with the WT mice, including miR-375, miR-210, or miR-678.

To identify potential target genes for the differentially expressed miRNAs in the study groups, we used the miRWalk database (Supplemental Figure S5A). When compared with the WT-CD mice, the miRNA target gene analysis identified 554 differentially expressed gene targets for miRNA in WT-WD, 6844 gene targets for miRNA in LR-CD, and 6153 gene targets for miRNA in LR-WD. The comparison of the target genes of the differentially expressed miRNAs revealed relatively little overlap (a total of 1 gene, 269 genes, and 189 genes, in common for WT-WD, LR-CD, and LR-WD, respectively, when compared with the WT-CD mice).

Our next step was to identify the pathways of the target genes of the differentially expressed miRNAs. We used the miRWalk online tool to search for the pathways in the KEGG database. Using this approach, we showed that compared with the WT-CD mice, there were 6, 68, and 25 pathways of miRNA target genes in the WT-WD, LR-CD, and WD-fed LDL-R−/− mice, respectively (Supplemental Figure S5B). Among the pathways were those involved in the regulation of cGMP-PKG signaling, Ras/Rap signaling, regulation of the actin cytoskeleton, chemokine signaling, insulin resistance, PI3K-Akt signaling, focal adhesion, cytokine–cytokine receptor interaction, and the NF-kappa B signaling pathway.

The comparisons of the pathways identified with the differentially expressed genes and pathways identified using the target genes of miRNAs revealed a group of pathways in common between the two modes of gene regulation (Figure 5). Among the pathways in common were the chemokine signaling pathway, focal adhesion, gap junction, insulin signaling, Nf-kB signaling or Gap junctions, and pathways that regulate endothelial cell interaction and permeability. The integrated analyses of focal adhesion or the Rap1 signaling pathway showed that most of the genes were either differentially expressed following lipotoxic injury or were potential target genes of differentially expressed miRNAs. This observation suggests a potential dual mode of action of lipotoxic injury in brain endothelial cells—both at the transcriptional and post-transcriptional levels of regulation.

We used the OmicsNet tool to incorporate the data obtained by the individual analyses and integrate it with the data obtained on the effect of lipotoxic injury on the expression of protein-coding genes, potential transcription factors involved in the observed genomic response, and potential post-transcriptional regulation of gene expression (Figure 6). We observed a large inter-connecting network between the three levels of genomic regulation of cell function. The transcription factors identified were associated with a large number of genes identified as differentially expressed. These genes were also connected to the expression of miRNAs identified as modulated by lipotoxic injury. Taken together, this analysis suggests a very complex and multilevel genomic effect of lipotoxic injury on hippocampal microvascular endothelial cells.

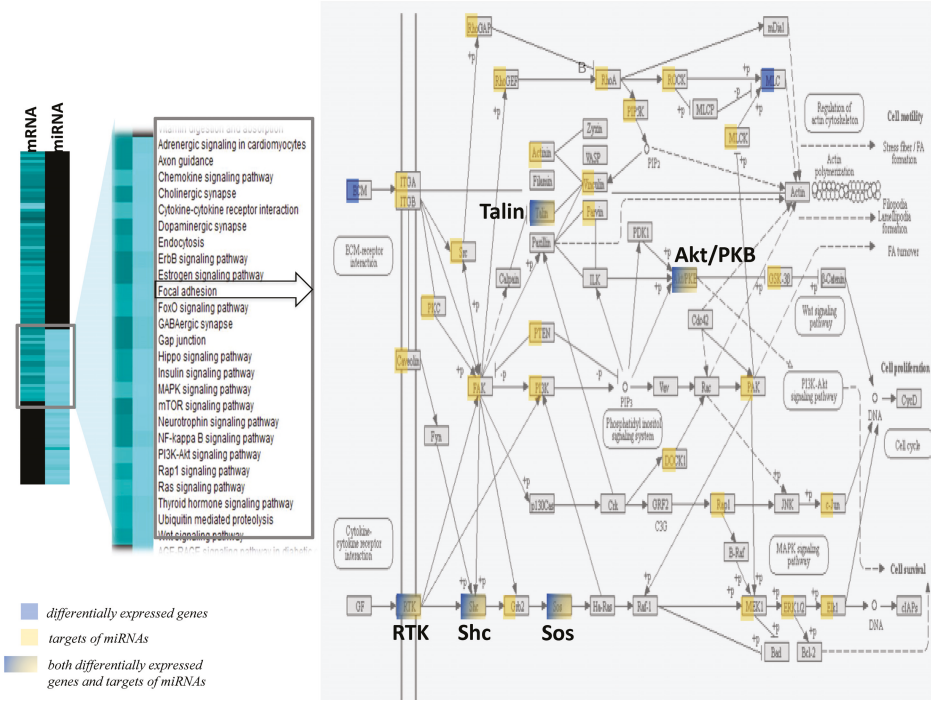

Figure 5. Effect of lipid injury on microRNA target differentially expressed gene pathways expression in hippocampal microvessels. Heat map of differentially expressed gene pathways and miRNA target gene pathways. Comparisons of pathways of differentially expressed genes and pathways of miRNA target genes identified a group of pathways such as the chemokine signaling pathway, focal adhesion, gap junction, insulin signaling, Nf-kB signaling or Gap junctions, and pathways that regulate endothelial cell interaction and permeability in common. The representative integrated analysis of the differentially expressed genes, and target genes of differentially expressed miRNAs for the focal adhesion signaling pathway is detailed. Blue = differentially expressed genes; yellow = target genes of differentially expressed miRNAs; color gradation from blue to yellow = genes identified to be both differentially expressed and to be targets of differentially expressed miRNAs.

3.6. Impact of the Western Diet on Expression of snoRNAs and lncRNAs in Brain Microvessels

As detailed above, most of the differential gene expression in our study system was attributable to the differential regulation of cell signaling proteins and their transcription factors. However, approximately 4% of the differential expression was attributable to the differential expression of miRNAs, and 10% was due to other ncRNA, primarily long non-coding RNAs (lncRNAs) and small nucleolar RNAs (snoRNAs).

Regarding non-coding RNAs, we identified the differential expression of a total of 109 lncRNAs and 97 snoRNAs in the experimental groups when compared with the control WT-CD mice: Table 1. The differential expression for snoRNAs and lncRNAs consisted almost exclusively of their up-regulation, and only a few snoRNAs, like Snord61, Gm25443, and Snord61, were identified as down-regulated. This analysis shows for the first time that lipotoxic injury modulates the expression of ncRNA in the brain microvasculature in vivo, revealing a new mode of biological regulation via snoRNAs and lncRNAs.

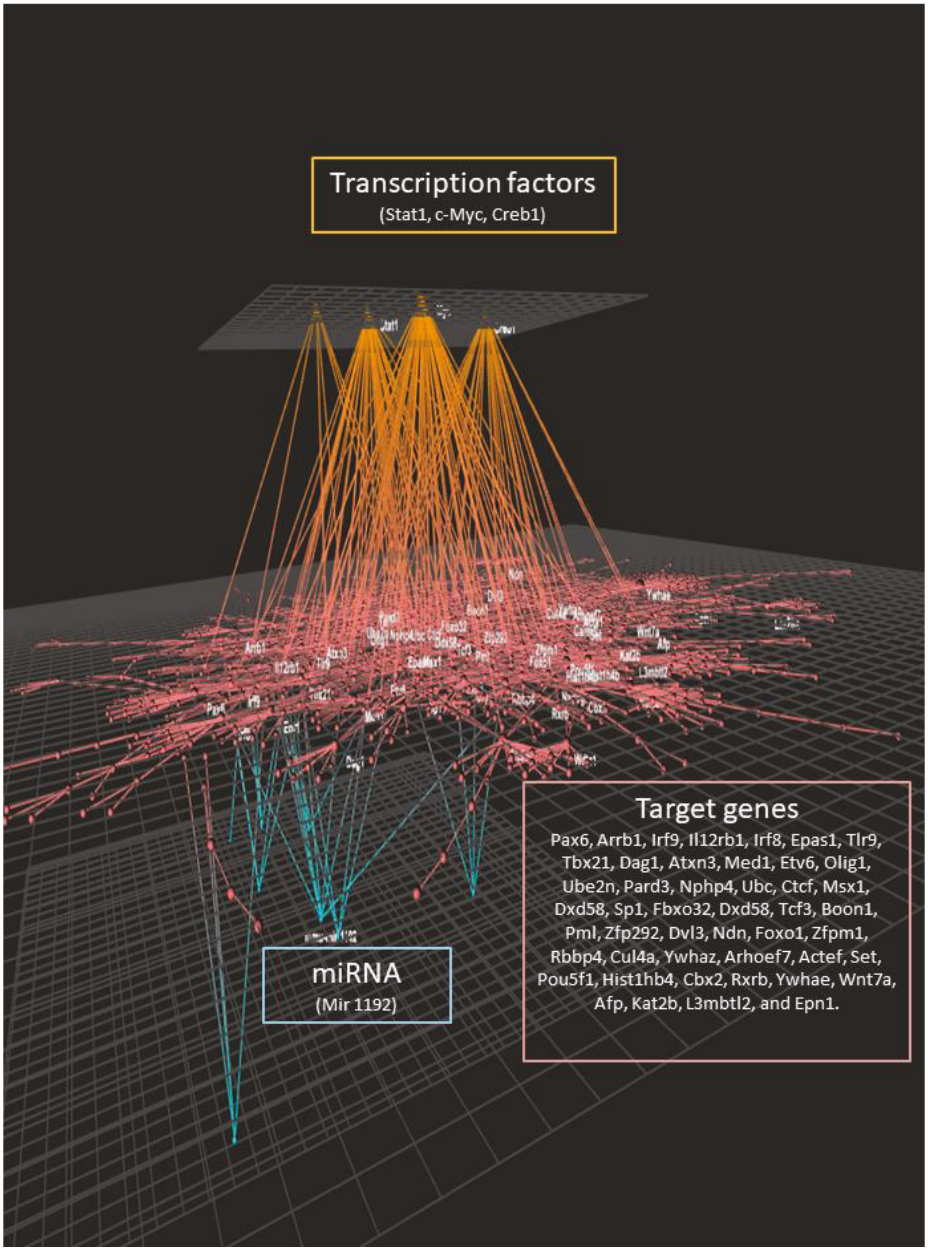

Figure 6. Protein–protein network enriched with transcription factors and miRNA regulation. Protein–protein interactions were identified using the STRING database from differentially expressed genes. Interactions between the protein–protein network, differentially expressed miRNAs (Mir 1192), and potential transcription factors (Stat1, c-Myc, Creb1) were constructed using the OmicsNet online tool. Target genes are: Pax6, Arrb1, Irf9, Il12rb1, Irf8, Epas1, Tlr9, Tbx21, Dag1, Atxn3, Med1, Etv6, Olig1, Ube2n, Pard3, Nphp4, Ubc, Ctcf, Msx1, Dxd58, Sp1, Fbxo32, Dxd58, Tcf3, Boon1, Pml, Zfp292, Dvl3, Ndn, Foxo1, Zfpm1, Rbbp4, Cul4a, Ywhaz, Arhoef7, Actef, Set, Pou5f1, Hist1hb4, Cbx2, Rxrb, Ywhae, Wnt7a, Afp, Kat2b, L3mbtl2, and Epn1.

3.7. Integration of Multiomics Data

The next step in our bioinformatic analyses was to integrate the different omic analyses together. Using a heat map tool, we first compared the pathways identified from the three omic analyses, i.e., from differentially expressed protein-coding genes, targets of differentially expressed miRNAs, and targets of lncRNAs (Figure 7). Using this approach, we identified a set of 12 pathways in common for the three analyses. Among these pathways was the pathway involved in the regulation of cytoskeletal organization. In Figure 8A,B, we present differentially expressed genes implicated in cytoskeletal organization (shown in detail in Supplemental Figure S6A), miRNAs with identified target genes in cytoskeletal organization (shown in detail in Supplemental Figure S6B), as well as lncRNA in this pathway with their target genes (shown in detail in Supplemental Figure S6C). We also identified that differentially expressed lncRNAs can regulate differentially expressed miRNAs. In addition, certain target genes of differentially expressed genes were identified to themselves be differentially expressed. Using the pathway of cytoskeletal organization as an example, these observations exemplify the interactions between the different modes of genomic regulation and indicate that lipotoxic injury can modulate the expression of genes involved in cytoskeletal organization at the level of transcription, but also post-transcription via miRNAs and lncRNAs.

Table 1. Effect of the Western diet on the expression of small nucleolar RNAs (snoRNAs) and long non-coding RNAs (lncRNAs) in male hippocampal microvessels.

SnoRNAs	WTWD vs. WTCD	LDL-R−/− CD vs. WTCD	LDL-R−/− CD vs. WTCD	lncRNAs	WTWD vs. WTCD	LDL-R−/− CD vs. WTCD	LDL-R−/− CD vs. WTCD
Snord61	−39.34			AI504432		56.21	
Gm25443	−2.32			Cep83os		49.06	
AF357355		123.27		Zfp91Cntf		19.36	27.1
Gm25635		90.8		D4Ertd617e		12.6	
Gm25856		55.53		2810049E08Rik		11.51	
Gm22289		45.23		Mir124-1		10.4	
Snord95		27.98		Ftx *		6.43	
Gm25607		12.59		F420014N23Rik		5.55	6.86
Snora17		11.93	64.98	1700110C19Rik		4.07	
Gm23123		9.93	6.21	AI314278		2.98	
Snora23 *		8.96		2310069G16Rik		2.4	
Snord88c		7.89		1700027J07Rik		2.27	2.5
Gm24013		6.77		1700009J07Rik		2.23	
Gm24336		6.38	33.24	1700024B18Rik		2.23	
Gm25125		6.24		D130017N08Rik		2.08	
Gm24770		5.9	6.8	C130071C03Rik *		2.87	
Gm23456		5.32	11.45	Gm10010		4.65	
Gm24844		5.3		Gm13411		3.58	3.32
Gm25092		3.89		Gm15409		2.92	
Snord107		3.77		Gm26593		2.84	
Snord16a *		3.73		Gm26643		2.68	
Gm22546		3.59		Gm14254		2.06	
Gm24284		3.07		AU022754		2.22	
Snord72		2.99		1700016L21Rik		2.2	
Gm26070		2.72		Snhg7os		2.1	
Gm23722		2.4		1700027H10Rik		2.08	
Snora5c		2.38		Pcsk2os2		2.11	2.03
Gm25410		2.24		Plet1os		2.15	

Table 1. *Cont.*

SnoRNAs	WTWD vs. WTCD	LDL-R−/− CD vs. WTCD	LDL-R−/− CD vs. WTCD	lncRNAs	WTWD vs. WTCD	LDL-R−/− CD vs. WTCD	LDL-R−/− CD vs. WTCD
Gm22531		2.21		Gldnos		2.15	
Gm24429		2.09		Sp3os		2.31	
Gm26272		2.09		4921534H16Rik		2.24	
Gm25860		2.05		4930405O22Rik		2.21	
Gm26387		2.04		5330413P13Rik		2.19	2.3
Snord61		−27.1	−29.61	6330415B21Rik		5.62	
Gm23199		32.34		Mhrt *		3.72	
Gm24400		20.1		Med9os		3.15	
Gm23121		17.62		9530082P21Rik		2.75	
Gm22935		11.9		A930024E05Rik *		2.52	
Gm24878		9.74		9430083A17Rik		2.45	
Gm25401		9.05		Gm26583		2.22	
Gm25720		6.28	67.3	Gm14061		2.13	
Gm22378		6.25		Gm26777		15.18	
Gm24449		5.46		Gm15323		3.28	
Gm22485		3.66		Gm15322		3.28	
Gm25371		3.12		Gm12121		2.7	
Gm24504		2.57		Gm22		2.03	
Gm25982		2.14		Atcayos			5.91
Gm24678		2.03	3.88	Gm10790			5.16
Gm24682		3.65		Chn1os3			3.42
Snhg7		11.93		5730420D15Rik			3.27
Snord66 *			70.95	Gm16793			3.2
Gm23546			66.56	Gm10390			3.07
Gm25777			36.23	Arhgap33os			3
Gm25788			29.72	B230312C02Rik			2.98
Gm23734			18.87	4632428C04Rik			2.96
Gm24916			11.99	4933424G05Rik			2.65
Gm22144			11.18	Gm19784			2.59
Gm24771			11.03	Gm12603 *			2.59
Gm22504			8.42	D5Ertd605e			2.54
Snord14a *			7.54	9330102E08Rik			2.51
Gm23527			5.66	9230105E05Rik			2.43
Gm26148			4.58	9630013K17Rik			2.43
Gm25376			4.27	4933432I03Rik			2.36
Gm25432			3.18	4930565D16Rik			2.35
Gm25715			3.1	Gm16548			2.33
Gm23534			2.94	Gm13985			2.31
Gm26047			2.88	Gm10007			2.24
Gm25526			2.81	Gm10619			2.23
Rnu3a			2.76	4930568E12Rik			2.2
Snord53 *			2.72	C130080G10Rik *			2.19
Gm24127			2.67	4930522O17Rik			2.19
Gm24581			2.26	Gm13003			2.14
Gm24648			2.23	4930444M15Rik			2.12
Gm25945			2.17	4931403G20Rik			2.11
Gm23136			2.16	4930488L21Rik			2.11

Table 1. *Cont.*

SnoRNAs	WTWD vs. WTCD	LDL-R−/− CD vs. WTCD	LDL-R−/− CD vs. WTCD	lncRNAs	WTWD vs. WTCD	LDL-R−/− CD vs. WTCD	LDL-R−/− CD vs. WTCD
Gm23129			2.13	1700113A16Rik			2.1
Gm24252			2.13	Gm5144			2.09
Gm22840			2.11	Lincred1 *			2.09
Gm24313			2.07	4933433G08Rik			2.08
Gm22269			2.05	A930019D19Rik			2.07
AF357425 *			−22.59	1700047A11Rik			2.07
ScaRNA15			8.54	2500002B13Rik			2.07
Gm24668			167.27	4930455F16Rik			2.05
Gm22940			75.5	Hoxaas3 *			2.05
Gm23970			14.37	1700045H11Rik			2.04
Gm23000			4.21	Gm15413			2.04
Gm22883			2.56	1700064J06Rik			2.02
Gm23031			2.21	5430434I15Rik			2.02
Gm24524			2.03	1700066N21Rik			2.01
Gm23119			63.09	C530044C16Rik			2.01
				Snhg7 *			64.98
				Gm12590			28.43
				Gm26906			4.55
				Gm26675			4.4
				Gm6410			3.92
				Gm9898			2.58
				Gm10425			2.45
				Gm13790			2.42
				Gm28890			2.36
				Gm26542			2.26
				Gm16295			2.19
				Gm14684			2.17
				Gm26656			2.1
				Gm15556			2.07
				Gm12148			2.05
				Gm12637			2.05

* denotes snoRNAs and LncRNAs of a known function.

Figure 7. Heatmap of pathway analyses of differentially expressed genes, miRNA target genes, and lncRNA targets. Heat map of the pathways identified using the KEGG database using differentially expressed genes, target genes of differentially expressed miRNA, and targets of lncRNA. The color intensity is proportional to the number of genes in the pathway.

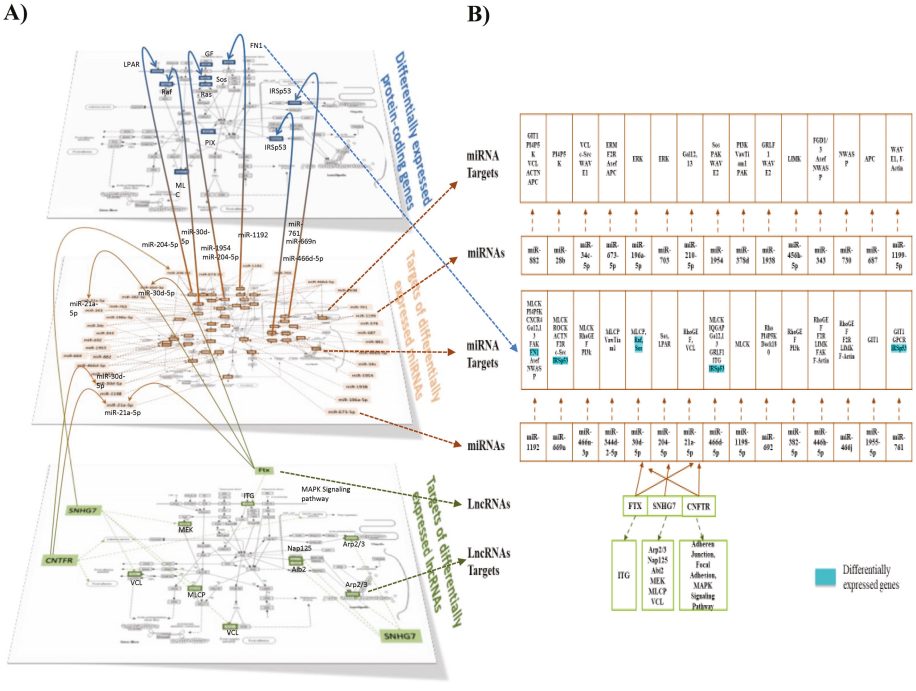

Figure 8. Regulation of the actin cytoskeleton pathway by differentially expressed genes, miRNA, and lncRNA. **(A)** Integration analysis showing differentially expressed genes (blue squares), differentially expressed miRNAs (brown squares) and their targets (brown broken arrows), and differentially expressed lncRNAs (green squares) and their targets (green broken arrows). Potential interactions between genes, miRNA, and lncRNAs are also shown. (**B**) Amplification of the list of differentially expressed genes (highlighted in blue), miRNAs and their targets, and lncRNAs and their targets, regulating the actin cytoskeleton pathway.

4. Discussion

This pilot study was a large-scale transcriptome gene-profiling of the male mice hippocampal microvasculature in relation to lipotoxic injury from two different sources, diet and genetics, using the Western diet (WD) and/or LDL-R−/− (LR) genotype, respectively. Our study focused on the molecular mechanisms of differential gene expression in the brain microvessels due to their significance in the pathogenesis of vascular dementia, and also due to our recently published work demonstrating that the WD results in increased blood–brain barrier (BBB) permeability and cognitive impairment [7], providing a functional correlation to the molecular pathways indicated in this experimental study. Although we describe hippocampal injury induced by the WD and the LR mouse as lipotoxic injury, we cannot omit potential glycemic injury associated with the WD and further studies are needed to make this distinction.

Our main findings are as follows:

- The WD resulted in the differential expression (primarily up-regulation) of a large number of genes (1972), representing 5.7% of the genome of microvessels in the hippocampus of male mice;
- Overall, the differential gene expression was associated with the differential regulation of cell signaling proteins and their transcription factors, with complex mechanisms of action for genes that regulate increased endothelial dysfunction following lipid stress as the main disruption,

particularly via pathways that serve to increase permeability, consistent with the previously reported increase in BBB permeability following the WD;

- ➢ There were some differences in the differential gene expression for diet and genotype. Differentially expressed genes involved in focal adhesion, ECM–receptor interaction, and signaling pathways (such as PI3K-Akt, TNF, Jak-STAT, and Ras) were up-regulated with lipid injury in the LR genotype while down-regulated by the WD in the wild type mice;
- ➢ Most of the differential gene expression was attributable to protein-coding genes (85%), but approximately 4% was due to the differential expression of miRNAs, and 10% was due to other non-protein-coding RNAs not previously found to be affected by the WD, including mostly long non-coding RNAs (lncRNAs) and small nucleolar RNAs (snoRNAs). The targets of lncRNAs included genes involved in NF-kB signaling, Ras/Rap signaling, focal adhesion, actin cytoskeleton organization, cell adhesion, chemokine signaling, tight junctions, and adherent junctions;
- ➢ Lipotoxic injury resulted in previously unreported complex and multilevel molecular regulation of the hippocampal microvasculature involving transcriptional and post-transcriptional regulation. Post-transcriptional regulation accounted for up to a third of the differential gene expression;
- ➢ Specific detailed examples of this complex regulation for the representative genes, pathways, transcription factors, and non-coding RNAs are provided below.

4.1. Lipotoxic Injury Up-Regulates Hippocampal Microvascular Gene Expression

Our study demonstrated the expected significant differences in cholesterol and lipid levels between the control diet (CD) and the high-fat LR-WD in male mice. The LR-CD mice spontaneously demonstrated hyperlipidemia because of the absence of the LDL receptor. While the physiological implications of severe hyperlipidemia are a topic of further study, it has been shown to correlate with accelerated atherosclerosis and vascular injury in other systems [16]. We decided to carry out our studies in the LR phenotype and recognize that the outcomes may differ in other murine models of hyperlipidemia. We also found in our experimental models serum glucose and insulin changes that were consistent with those previously published [33,34].

However, it was previously unknown how a high-fat diet affects the transcriptome of the brain hippocampal microvessels in males. Using a candidate gene approach in our previous work, we identified activating transcription factor 3 (ATF3) as an important regulator of neuro-inflammation in male mice [10]. The present study significantly extends our prior work and demonstrates for the first time that the WD and LR genotype significantly modulate the differential expression of approximately 5.7% of the hippocampal microvasculature genome of male mice, including protein-coding genes as well as ncRNA (miRNAs, snoRNAs, and LncRNAs), and the analysis suggests a separation between diet and genotype. Analyses of the global expression profile of the genes differentially expressed in at least one of the three comparison study groups showed that the majority of genes were modulated in a similar manner by lipotoxicity, up-regulated. We also identified four clusters of genes containing genes that were down-regulated by the WD in the WT mice compared with the CD, while their expression was up-regulated in the LR mice (Supplemental Figure S7**)**. This observation suggests that lipotoxicity induced by the LR genotype has a potentially greater impact on differential gene expression than the WD and could mask the effect of the WD in the LR genotype.

4.2. Regulation of Gene Networks and Pathways for Endothelial Permeability, Neurofunction and Serotonergic Pathways

It has previously been suggested that consumption of fatty acids can modulate gene expression in rat brain [35] and that a high-fat diet can modulate the brain transcriptome in a mouse model of Alzheimer's disease [12]. These studies suggest that lipotoxic injury can induce changes in different cell types in the brain or in specific brain regions. We have previously shown that exposure of brain microvascular endothelial cells to lipid induces significant modification in the target gene expression profiles [10]. Bioinformatic analyses of protein-coding genes in the present study revealed

that lipotoxic injury can also modulate the expression of genes involved in a variety of key cellular processes including gene networks and pathways that regulate endothelial cell adhesion, cytoskeletal organization, neurofunction, cell junctions and chemotaxis, and focal adhesion—all mechanisms involved in the regulation of endothelial permeability [36]. This is of significance because a disruption of endothelial permeability in the brain, where endothelial cells are part of a neurovascular unit, results in BBB dysfunction which may be a significant contributor to the pathogenesis of cognitive impairment, amyotrophic lateral sclerosis, or Alzheimer's disease [37]. We also found various differentially expressed gene networks that contribute to inflammation, oxidative stress, and Alzheimer's dementia.

Amongst the differentially expressed genes controlling BBB specifically was GTPase HRas, a GTP-binding protein that plays an important role in cytoskeletal reorganization, cell polarity, cell cycle progression, or angiogenesis [38]. Inadequate angiogenic signaling results in malformed vessels with reduced investiture by pericytes, which results in increased vascular permeability, vascular instability, greater endothelial cell apoptosis and proliferation, and inflammation processes implicated in neurovascular disease [39]. Furthermore, over-expression of HRas results in dilated proliferative blood vessels in the brain, or in blood–brain barrier break-down [39]. Therefore, an increased expression of HRas by lipotoxic injury could lead to an increase in BBB permeability, consistent with our previous work demonstrating increased BBB permeability by fMRI in vivo following a high-fat diet [7].

We also observed that lipotoxic injury differentially regulates the expression of genes involved in pathways related to neurofunction and serotonergic pathways. Among these genes is MOAB, which encodes for Monoamine oxidases isoform B, important in oxidative deamination and thus vascular oxidative stress and endothelial dysfunction [40]. In our study, a lipid injury-induced increased expression of MOAB could therefore lead to increased oxidative stress and brain endothelial dysfunction. The serotonergic synapse pathway was also identified to be differentially expressed and includes genes such as 5-Hydroxytryptamine Receptor 1A (HTR1A) and 5-Hydroxytryptamine Receptor 1B (HTR1B). Interestingly, serotonin/5-hydroxytryptamine (5-HT) and its receptors are known to contribute to atherosclerosis-associated conditions, are associated with chronic inflammation, leukocyte activation, recruitment of leukocytes to endothelial cells [41], and cognition impairment [42]. Taken together, a modulation of the expression of these genes by chronic lipotoxic injury could be associated with cognitive dysfunction and present novel molecular mechanisms of action of lipotoxic injury on brain endothelial cells.

4.3. Differential Regulation of Transcription Factors for Endothelial Dysfunction: HNF4a, KLF4, CREB1

Using bioinformatic tools, we identified from the list of differentially expressed genes potential transcription factors (TFs) that could have their activity modulated by lipotoxic injury and be involved in the observed genomic effect. Among the TFs identified, 17 were in common between the study groups. Among them was hepatocyte nuclear factor 4 alpha (HNF4a), whose activity is known to be modulated by fatty acids [43]. HNF4a can in turn modulate both mRNA and the protein expression levels in the brain where it plays a role in depression and physiological homeostasis [44]. Krüppel-like factor 4 (KLF4) is another transcription factor we identified. KLF4 activity is known to be modulated in endothelial cells by a high-fat diet leading to endothelial cell dysfunction, including increased monocyte endothelial adhesion and increased endothelial permeability [45]. This finding suggests another mechanism whereby lipotoxic injury induced by the WD or the LR genotype could induce endothelial dysfunction and increased permeability in the brain. Moreover, several studies indicate that KLF4 is linked to multiple neurological disorders, including Alzheimer's disease [46]. Other TFs we identified to be differentially expressed by lipid injury, such as CREB1, have also previously been implicated to play a role in vascular dementia [47].

4.4. Novel Lipotoxic Injury-Mediated Differential Expression of non-Coding RNAs (miRNA, sno RNA, lncRNA), and their Targets: Implications for Cognitive Dysfunction

In addition to assessing the effect of chronic consumption of the WD on the expression of protein-coding genes, we also identified a previously unknown effect of lipid injury on the expression of ncRNA in the male hippocampal microvasculature. These included microRNAs (miRNAs), small nucleolar RNAs (snoRNAs), and long non-coding RNAs (lncRNAs). This is of significance as ncRNAs have been previously reported to play a vital role in cognition and the vasculature, but the mechanisms have not been defined.

Following a high-fat diet, miRNAs have been reported to be involved in neural function and in metabolic and inflammatory pathways that play a role in atherogenesis [48]. In our study, we observed that lipotoxic injury regulates the expression of a number of microRNAs including up-regulation of mir-678 and mir-210. Mir-678 is known to be regulated by a high-fat diet [13]. Mir-210 has been shown to be up-regulated in the hippocampus and increase cognitive dysfunction in a rat model of vascular dementia (VD) [49]. Mir-210 expression is also important for endothelial cell survival and migration [50]. This suggests that lipotoxic injury-activated mir-210 could impair cognitive function and play a role in endothelial cell migration. Thus, the differential expression of miRNAs mediated by lipotoxic injury could be a mechanism for cognitive dysfunction.

Additionally, some several hundred target genes were identified for each dietary experimental group from the analyses of the predicted miRNA target genes. Interestingly, we observed that 28% of the miRNA target genes overlapped with differentially expressed genes (DEG), suggesting that nearly one-third of the gene expression could be regulated at the post-transcriptional level by lipid injury, while the remaining can be regulated at the level of transcription. The target genes of the differentially expressed miRNAs were involved in pathways related to endothelial cell permeability and function, cell signaling, insulin signaling/resistance, apoptosis, and dementia. Insulin dysregulation has been linked with cognitive dysfunction [51] and endothelial cell dysfunction [52]. It was therefore interesting that among the target DEG miRNAs induced by lipotoxic injury was NGFR, also known as p75NTR (low affinity neurotrophin receptor), which is a target of miRNA-882. p75NTR is known to promote apoptosis of endothelial cells and disrupt angiogenesis in type-1 diabetic mice [53]. In addition, the NGFR levels are low in the hippocampus of learning-impaired aged rats [54]. This suggests that the lipotoxic injury-induced expression of miRNA-882 targets NGFR, which could play a role in apoptosis of endothelial cells and affect cognitive function. Lipotoxic injury also activated miRNA-678 which targets the differentially expressed gene platelet endothelial cell adhesion molecule-1 (PECAM-1). Increased expression of PECAM-1 is found in endothelial cell junctions and plays a role in the BBB [55]. This suggests that miRNA-678 could target the PECAM-1 mRNA expression which could affect endothelial cell adhesion and migration. Taken together, these results are consistent with lipotoxic injury effects on the expression of miRNAs, which post-transcriptionally regulate the expression of mRNA, with functional implications consistent with endothelial cell dysfunction and cognitive dysfunction.

Our microarray analysis also identified the differential expression of other ncRNA other than miRNAs, including snoRNAs and lncRNAs. SnoRNAs play a key role in the regulation of gene expression, post-transcriptional modification of other RNAs, and in stabilizing the genome [56]. We observed that up-regulation in the expression of the brain-specific snoRNA AF357425 (MBII-48) occurred following lipotoxic injury. In the hippocampus, AF357425 is down-regulated following contextual fear memory consolidation [57], a component of memory that is diminished in patients with early-stage AD. Therefore, the observed up-regulation of the AF357425 expression implies that it could contribute to impaired memory consolidation. However, most of the snoRNAs we identified do not currently have known functions, allowing the possibility for the future identification of additional important functional sequelae for the differential expression of snoRNAs following lipid injury.

This study also revealed that lipotoxic injury can control the expression of several lncRNAs. LncRNAs are regulatory RNAs involved in the transcriptional, post-transcriptional, and translational

modulation of genes. As such, lncRNAs function in several aging-related processes, including apoptosis, neuronal differentiation, and immune or stress responses [58,59]. We observed an increased expression of the lncRNA A930024E05Rik, also known as LncKdm2b, which positively regulates the transcription of Kdm2b, a histone demethylase that is important for neural development [60] and plays a role in autism and syndromic intellectual disability [61]. Single nucleotide polymorphisms (SNPs) in Kdm2b have been found to increase AD incidence and interact with the APOE e4 gene, a key genetic risk factor in AD [62]. We also observed an increased expression of the lncRNA Ftx, which has been shown to decrease the phosphorylation of vimentin [63], which plays a role in integrin-mediated signal transduction in endothelial cells and is a crucial regulator of focal adhesion organization and endothelial sprouting [64]. This suggests that the inhibition of vimentin by up-regulated Ftx due to lipotoxic injury may lead to defects in endothelial cell adhesion, migration, and signaling. In addition, we observed an increased expression of the lncRNA SNHG7 (small nucleolar RNA host gene 7). GRN is found to be up-regulated in neurodegenerative diseases such as AD and multiple sclerosis and may also function in neuro-inflammation [65–67]. Another lncRNA whose expression was increased by lipotoxic injury in male hippocampal microvessels was Gm12603 (WINCR1), important in collective cell migration and collagen contraction [68], suggesting that lipotoxic injury-activated WINCR1 might affect endothelial cell migration and contractibility, and also potentially endothelial permeability.

In summary, to our knowledge, these findings are novel indicators that lipotoxic injury modulates the expression of non-coding RNAs (miRNAs, snoRNAs, and lncRNAs) in the male hippocampal microvasculature via targets that may play an important role in lipotoxic injury-associated brain microvascular disease and vascular dementia.

4.5. An Integrated Multi-omics Approach Reveals a Complex and Integrated Transcriptional and Post Transcriptional Response to Lipid Injury in Brain Microvessels

Integrative analyses of the genomic data allowed us to identify the full complexity of the genomic effects of lipotoxicity in the brain microvasculature. Bioinformatic analyses of the genes allowed us to identify the cellular functional pathways in which they were involved, including angiogenesis, apoptosis, and immune cell interactions as well as functional networks, including for cell adhesion and signal transduction. The comparison of the pathways identified separately for the different types of RNAs showed that a third of them were in common for at least two different RNA types and 12 of them were identified for the three different RNA types studied (Figure 7). This observation suggests that cellular processes, including networks of pathways that formed functional groups encompassing cell signaling, oxidative stress, endothelial cell function, and neurologic function, could be affected by lipotoxicity through the regulation of different types of RNAs, providing novel and deeper knowledge regarding the mechanisms of action of lipid injury on brain microvascular molecular regulation. The integrated analysis shown in Figures 7 and 8, revealed for the first time the complex genomic response of the brain microvascular endothelium to lipotoxic injury in vivo in mice. It also demonstrated interactions between different levels of cellular regulators and the need to use systems biology approaches to study lipotoxic injury on cellular function in order to decipher as precisely as possible the underlying molecular mechanisms of action.

Our study is one of a few studies that have analyzed multi-omic regulation simultaneously and integrated different types of RNAs in the brain microvasculature [69,70], and to our knowledge, ours is the only study that has used a multi-omics approach to show the role of various RNA types in the brain microvasculature following lipid injury in male mice. As presented in the example of the regulation of the cytoskeleton pathways, we identified differentially expressed protein-coding genes and also target genes of miRNAs and lncRNAs (Figure 8A,B). Interestingly, important interactions were observed as some of the targets of differentially expressed miRNAs were also identified as differentially expressed, and could also be targets of lncRNAs. Therefore, by regulating the expression of lncRNAs, lipid injury can impact miRNAs and consequently their target genes, but also the differential expression of protein-coding genes. In this manner, our integrated analysis revealed a large interconnecting

cascade between the three levels of genomic regulation of cell function (protein-coding genes, possible transcription factors, and potential post-transcriptional regulation via non-protein-coding mechanisms involving primarily miRNAs and lncRNAs) (Supplemental Figure S8), especially for the WD-fed LR mice, our experimental model with the highest degree of lipid stress. The novel, complex, and substantial multilevel genomic effect of lipotoxic injury on the brain microvasculature could help explain the deleterious impact of the Western diet on brain microvascular function and cognitive performance.

4.6. Summary and Implications for Future Research

In alignment with our hypothesis, our results showed profound transcriptome changes in response to the WD in the hippocampal microvasculature of male mice including the modulation of protein-coding genes, miRNAs, snoRNAs, and lncRNAs, as well as the corresponding cellular functional pathways, and the mechanism of regulation by transcription factors. Integrative analyses of the genomic data also identified the cellular functions primarily affected by lipid-associated vascular injury to include angiogenesis, apoptosis, immune cell interactions, and gene regulation and RNA biogenesis, which could be related to vascular injury or response to lipid injury. Among these gene networks and pathways, endothelial cell adhesion, cytoskeleton organization, neurofunction, cell junctions and chemotaxis, and focal adhesion are regulated—mechanisms involved in the regulation of endothelial permeability. This is of significance because a disruption to the endothelial permeability in the brain, where endothelial cells are part of a neurovascular unit, results in BBB dysfunction, which may be a significant contributor to the pathogenesis of cognitive impairment, Alzheimer's disease, and other related dementias. As such, our work helps to significantly advance the field and elucidate the molecular mechanisms whereby the Western diet disrupts brain microvascular endothelial function and how that may predispose to vascular dementia. Future work will need to address whether and how the high-glycemic component of a Western diet contributes to microvascular lipid injury in the brain, the reversibility of diet associated vascular dementia, and the interaction of genetic factors and diet on vascular dementia.

Supplementary Materials: The following are available online at http://www.mdpi.com/2072-6643/12/6/1771/s1. Figure S1: Representative images of hippocampal neurons and microvessels dissected by laser capture microdissection. Figure S2: Mean body weight of wild type (WT) and LDL-R −/− mice pre- and post-feeding with the control (CD) and Western (WD) diets. Figure S3: Volcano plot of gene expression changes in hippocampal microvessels. A) WT-WD vs. WT-CD, B) LDL-R −/− CD vs. WT-CD and C) LDL-R −/− WD vs. WT-CD. Figure S4: Gene ontology biological processes tree map of differentially expressed protein coding genes in hippocampal microvessels. Figure S5: (A) Venn diagrams representing the number of differentially expressed (DE) genes, compared to miRNA target genes, affected by diet and genotype in hippocampal microvessels. (B) Venn diagrams representing the pathways of differentially expressed (DE) genes, compared to pathways of miRNA target genes, affected by diet and genotype in hippocampal microvessels. Figure S6: Regulation of actin cytoskeleton pathway. (A) Differentially expressed genes. (B) Differentially expressed miRNAs and their targets. (C) Differentially expressed LncRNAs and their targets. Figure S7: Effect of the Western diet and LDL-R −/− genotype on differentially expressed protein-coding genes in hippocampal microvessels. Figure S8: Schematic presentation of genomic modifications and interactions in brain hippocampal microvascular following Western diet consumption of LDR knock-out. Table S1: Primer sequences for genes tested by qRT-PCR were prepared by the Primer3 software using Affymetrix transcript ID sequences. Table S2: (A) Plasma lipid levels of wildtype (WT) and LDL-R−/− mice fed with control (CD) and Western (WD) diet. B) Plasma glucose and insulin levels of wildtype (WT) and LDL-R−/− mice fed with control (CD) and Western (WD) diet. Table S3: Differentially expressed genes in Western diet (WD)-fed WT mice when compared to control diet (CD)-fed WT mice. Table S4: Differentially expressed genes in control diet (CD)-fed LDL-R−/− mice when compared to control diet (CD)-fed WT mice. Table S5: Differentially expressed genes in Western diet (WD)-fed LDL-R−/− mice when compared to control diet (CD)-fed WT mice. Table S6: Transcription factors affected by Western diet and LDL-R−/− in hippocampal microvascular endothelium. Table S7: Effect of the Western diet on the expression of microRNAs (miRNAs) in male hippocampal microvessels.

Author Contributions: Individual contributions of the authors were as follows. Conceptualization, A.C.V. and J.C.R.; methodology, S.N., A.C.V.; software, S.N., A.C.V., D.M.; validation, A.C.V., S.N. and D.M.; formal analysis, S.N., D.M., A.C.V.; investigation, S.N.; resources, A.C.V. and J.C.R.; data curation, A.C.V., D.M., S.N.; writing—original draft preparation, A.C.V. and S.N.; writing—review and editing, A.C.V., S.N., D.M.; visualization, A.C.V., S.N., D.M.; supervision, A.C.V., J.C.R., D.M.; project administration, S.N.; funding acquisition, A.C.V. and J.C.R. All authors have read and agreed to the published version of the manuscript.

Funding: This work was supported by an NIH RO1 (AG045541), the Richard A. and Nora Eccles Harrison Endowed Chair in Diabetes Research (J.C.R.), and the Frances Lazda Endowed Chair in Women's Cardiovascular Medicine (A.C.V).

Acknowledgments: Laser Capture Microdissection and Cryo-Sectioning were conducted at the Cellular and Molecular Imaging core facility at the University of California Davis (UC Davis) Center for Health and the Environment. Microarray Scanning and Hybridization was done by the Genomics Shared Resource at the UC Davis Medical Center. We thank Robin Altman, Sindhu Addepalli, Theresa Pasion, Janeet Dhauna, Ryan Borden, Natalia Brennan, Lauren Saputo, Ryan Vinh, Nejma Wais, Corey Buckley, Nikita Patel, Anthony Pham and Taarini Hariharan for technical assistance in this project. We are also grateful for the technical support and/or services provided to our research by the UC Davis MMPC which assisted with performance of the metabolic assays and is supported by U24 DK092993.

Conflicts of Interest: The authors declare no conflict of interest.

References

1. Reitz, C.; Brayne, C.; Mayeux, R. Epidemiology of Alzheimer disease. *Nat. Rev. Neurol.* **2011**, *7*, 137–152. [CrossRef] [PubMed]
2. Kalaria, R.N.; Erkinjuntti, T. Small vessel disease and subcortical vascular dementia. *J. Clin. Neurol.* **2006**, *2*, 1–11. [CrossRef] [PubMed]
3. Cohen, A.D. Distinct pathways for cognitive decline in the presence of Alzheimer's disease pathology or cerebrovascular disease. *Brain A J. Neurol.* **2016**, *139*, 2340–2341. [CrossRef] [PubMed]
4. Dye, L.; Boyle, N.B.; Champ, C.; Lawton, C. The relationship between obesity and cognitive health and decline. *Proc. Nutr. Soc.* **2017**, *76*, 443–454. [CrossRef] [PubMed]
5. Schilling, S.; Tzourio, C.; Soumaré, A.; Kaffashian, S.; Dartigues, J.F.; Ancelin, M.L.; Samieri, C.; Dufouil, C.; Debette, S. Differential associations of plasma lipids with incident dementia and dementia subtypes in the 3C Study: A longitudinal, population-based prospective cohort study. *PLoS Med.* **2017**, *14*, e1002265. [CrossRef] [PubMed]
6. Francis, H.; Stevenson, R. The longer-term impacts of Western diet on human cognition and the brain. *Appetite* **2013**, *63*, 119–128. [CrossRef] [PubMed]
7. Rutkowsky, J.M.; Lee, L.L.; Puchowicz, M.; Golub, M.S.; Befroy, D.E.; Wilson, D.W.; Anderson, S.; Cline, G.; Bini, J.; Borkowski, K.; et al. Reduced cognitive function, increased blood-brain-barrier transport and inflammatory responses, and altered brain metabolites in LDLr-/-and C57BL/6 mice fed a western diet. *PLoS ONE* **2018**, *13*, e0191909. [CrossRef]
8. Palmer, A.M. The role of the blood brain barrier in neurodegenerative disorders and their treatment. *J. Alzheimers Dis.* **2011**, *24*, 643–656. [CrossRef]
9. Montagne, A.; Barnes, S.R.; Sweeney, M.D.; Halliday, M.R.; Sagare, A.P.; Zhao, Z.; Toga, A.W.; Jacobs, R.E.; Liu, C.Y.; Amezcua, L.; et al. Blood-brain barrier breakdown in the aging human hippocampus. *Neuron* **2015**, *85*, 296–302. [CrossRef] [PubMed]
10. Aung, H.H.; Altman, R.; Nyunt, T.; Kim, J.; Nuthikattu, S.; Budamagunta, M.; Voss, J.C.; Wilson, D.; Rutledge, J.C.; Villablanca, A.C. Lipotoxic brain microvascular injury is mediated by activating transcription factor 3-dependent inflammatory and oxidative stress pathways. *J. Lipid Res.* **2016**, *57*, 955–968. [CrossRef]
11. Yang, W.; Shi, H.; Zhang, J.; Shen, Z.; Zhou, G.; Hu, M. Effects of the duration of hyperlipidemia on cerebral lipids, vessels and neurons in rats. *Lipids Health Dis.* **2017**, *16*, 26. [CrossRef] [PubMed]
12. Nam, K.N.; Mounier, A.; Wolfe, C.M.; Fitz, N.F.; Carter, A.Y.; Castranio, E.L.; Kamboh, H.I.; Reeves, V.L.; Wang, J.; Han, X.; et al. Effect of high fat diet on phenotype, brain transcriptome and lipidome in Alzheimer's model mice. *Sci. Rep.* **2017**, *7*, 4307. [CrossRef]
13. Labouesse, M.A.; Polesel, M.; Clementi, E.; Muller, F.; Markkanen, E.; Mouttet, F.; Cattaneo, A.; Richetto, J. MicroRNA Expression Profiling in the Prefrontal Cortex: Putative Mechanisms for the Cognitive Effects of Adolescent High Fat Feeding. *Sci. Rep.* **2018**, *8*, 8344. [CrossRef]
14. Yoon, G.; Cho, K.A.; Song, J.; Kim, Y.-K. Transcriptomic Analysis of High Fat Diet Fed Mouse Brain Cortex. *Front. Genet.* **2019**, *10*, 83. [CrossRef] [PubMed]
15. Andersen, R.E.; Lim, D.A. Forging our understanding of lncRNAs in the brain. *Cell Tissue Res.* **2018**, *371*, 55–71. [CrossRef] [PubMed]

16. Bieghs, V.; Van Gorp, P.J.; Wouters, K.; Hendrikx, T.; Gijbels, M.J.; van Bilsen, M.; Bakker, J.; Binder, C.J.; Lutjohann, D.; Staels, B.; et al. LDL receptor knock-out mice are a physiological model particularly vulnerable to study the onset of inflammation in non-alcoholic fatty liver disease. *PLoS ONE* **2012**, *7*, e30668. [CrossRef] [PubMed]
17. Nuthikattu, S.; Milenkovic, D.; Rutledge, J.; Villablanca, A. The Western Diet Regulates Hippocampal Microvascular Gene Expression: An Integrated Genomic Analyses in Female Mice. *Sci. Rep.* **2019**, *9*, 19058. [CrossRef]
18. Kochanek, K.D.; Murphy, S.L.; Xu, J.; Tejada-Vera, B. Deaths: Final Data for 2014. *Cent. Dis. Control Prev.* **2016**, *65*, 1–122.
19. Ball, H.J.; McParland, B.; Driussi, C.; Hunt, N.H. Isolating vessels from the mouse brain for gene expression analysis using laser capture microdissection. *Brain Res. Brain Res. Protoc.* **2002**, *9*, 206–213. [CrossRef]
20. Untergasser, A.; Cutcutache, I.; Koressaar, T.; Ye, J.; Faircloth, B.C.; Remm, M.; Rozen, S.G. Primer3–new capabilities and interfaces. *Nucleic Acids Res.* **2012**, *40*, e115. [CrossRef]
21. Huang da, W.; Sherman, B.T.; Lempicki, R.A. Systematic and integrative analysis of large gene lists using DAVID bioinformatics resources. *Nat. Protoc.* **2009**, *4*, 44–57. [CrossRef] [PubMed]
22. Huang da, W.; Sherman, B.T.; Lempicki, R.A. Bioinformatics enrichment tools: Paths toward the comprehensive functional analysis of large gene lists. *Nucleic Acids Res.* **2009**, *37*, 1–13. [CrossRef]
23. Supek, F.; Bosnjak, M.; Skunca, N.; Smuc, T. REVIGO summarizes and visualizes long lists of gene ontology terms. *PLoS ONE* **2011**, *6*, e21800. [CrossRef] [PubMed]
24. Stockel, D.; Kehl, T.; Trampert, P.; Schneider, L.; Backes, C.; Ludwig, N.; Gerasch, A.; Kaufmann, M.; Gessler, M.; Graf, N.; et al. Multi-omics enrichment analysis using the GeneTrail2 web service. *Bioinformatics* **2016**, *32*, 1502–1508. [CrossRef] [PubMed]
25. Dweep, H.; Sticht, C.; Pandey, P.; Gretz, N. miRWalk–database: Prediction of possible miRNA binding sites by "walking" the genes of three genomes. *J. Biomed. Inform.* **2011**, *44*, 839–847. [CrossRef] [PubMed]
26. Caraux, G.; Pinloche, S. PermutMatrix: A graphical environment to arrange gene expression profiles in optimal linear order. *Bioinformatics* **2005**, *21*, 1280–1281. [CrossRef] [PubMed]
27. Zhou, Y.; Zhou, B.; Pache, L.; Chang, M.; Khodabakhshi, A.H.; Tanaseichuk, O.; Benner, C.; Chanda, S.K. Metascape provides a biologist-oriented resource for the analysis of systems-level datasets. *Nat. Commun.* **2019**, *10*, 1523. [CrossRef]
28. Shannon, P.; Markiel, A.; Ozier, O.; Baliga, N.S.; Wang, J.T.; Ramage, D.; Amin, N.; Schwikowski, B.; Ideker, T. Cytoscape: A software environment for integrated models of biomolecular interaction networks. *Genome Res.* **2003**, *13*, 2498–2504. [CrossRef]
29. Chong, J.; Soufan, O.; Li, C.; Caraus, I.; Li, S.; Bourque, G.; Wishart, D.S.; Xia, J. MetaboAnalyst 4.0: Towards more transparent and integrative metabolomics analysis. *Nucleic Acids Res.* **2018**, *46*, W486–W494. [CrossRef]
30. Li, J.H.; Liu, S.; Zhou, H.; Qu, L.H.; Yang, J.H. starBase v2.0: Decoding miRNA-ceRNA, miRNA-ncRNA and protein-RNA interaction networks from large-scale CLIP-Seq data. *Nucleic Acids Res.* **2014**, *42*, D92–D97. [CrossRef]
31. Jeggari, A.; Marks, D.S.; Larsson, E. miRcode: A map of putative microRNA target sites in the long non-coding transcriptome. *Bioinformatics* **2012**, *28*, 2062–2063. [CrossRef]
32. RNAcentral: A hub of information for non-coding RNA sequences. *Nucleic Acids Res.* **2019**, *47*, D1250–D1251. [CrossRef] [PubMed]
33. Gruben, N.; Funke, A.; Kloosterhuis, N.J.; Schreurs, M.; Sheedfar, F.; Havinga, R.; Houten, S.M.; Shiri-Sverdlov, R.; van de Sluis, B.; Kuivenhoven, J.A.; et al. Cholesterol-induced hepatic inflammation does not underlie the predisposition to insulin resistance in dyslipidemic female LDL receptor knockout mice. *J. Diabetes Res.* **2015**, *2015*, 956854. [CrossRef] [PubMed]
34. Ngai, Y.F.; Quong, W.L.; Glier, M.B.; Glavas, M.M.; Babich, S.L.; Innis, S.M.; Kieffer, T.J.; Gibson, W.T. Ldlr-/-mice display decreased susceptibility to Western-type diet-induced obesity due to increased thermogenesis. *Endocrinology* **2010**, *151*, 5226–5236. [CrossRef] [PubMed]
35. Mehus, A.A.; Dickey, A.M.; Smith, T.P.L.; Yeater, K.M.; Picklo, M.J. Next-Generation Sequencing Identifies Polyunsaturated Fatty Acid Responsive Genes in the Juvenile Rat Cerebellum. *Nutrients* **2019**, *11*, 407. [CrossRef] [PubMed]
36. Sukriti, S.; Tauseef, M.; Yazbeck, P.; Mehta, D. Mechanisms Regulating Endothelial Permeability. *Pulm. Circ.* **2014**, *4*, 535–551. [CrossRef]

37. Rosenberg, G.A. Neurological Diseases in Relation to the Blood–Brain Barrier. *J. Cereb. Blood Flow Metab.* **2012**, *32*, 1139–1151. [CrossRef]
38. Song, S.; Cong, W.; Zhou, S.; Shi, Y.; Dai, W.; Zhang, H.; Wang, X.; He, B.; Zhang, Q. Small GTPases: Structure, biological function and its interaction with nanoparticles. *Asian J. Pharm. Sci.* **2019**, *14*, 30–39. [CrossRef]
39. Li, Q.-F.; Decker-Rockefeller, B.; Bajaj, A.; Pumiglia, K. Activation of Ras in the Vascular Endothelium Induces Brain Vascular Malformations and Hemorrhagic Stroke. *Cell Rep.* **2018**, *24*, 2869–2882. [CrossRef]
40. Sturza, A.; Popoiu, C.M.; Ionica, M.; Duicu, O.M.; Olariu, S.; Muntean, D.M.; Boia, E.S. Monoamine Oxidase-Related Vascular Oxidative Stress in Diseases Associated with Inflammatory Burden. *Oxidative Med. Cell. Longev.* **2019**, *2019*, 8954201. [CrossRef]
41. Kataoka, H.; Ariyama, Y.; Deushi, M.; Osaka, M.; Nitta, K.; Yoshida, M. Inhibitory Effect of Serotonin Antagonist on Leukocyte-Endothelial Interactions In Vivo and In Vitro. *PLoS ONE* **2016**, *11*, e0147929. [CrossRef]
42. Morgan, J.A.; Singhal, G.; Corrigan, F.; Jaehne, E.J.; Jawahar, M.C.; Breen, J.; Pederson, S.; Baune, B.T. Ceasing exercise induces depression-like, anxiety-like, and impaired cognitive-like behaviours and altered hippocampal gene expression. *Brain Res. Bull.* **2019**, *148*, 118–130. [CrossRef] [PubMed]
43. Ceccarelli, V.; Nocentini, G.; Riccardi, C.; Ayroldi, E.; Di Nardo, P.; Roberti, R.; Binaglia, L.; Vecchini, A. Effect of dietary saturated fatty acids on HNF-4alpha DNA binding activity and ApoCIII mRNA in sedentary rat liver. *Mol. Cell. Biochem.* **2011**, *347*, 29–39. [CrossRef] [PubMed]
44. Yamanishi, K.; Doe, N.; Sumida, M.; Watanabe, Y.; Yoshida, M.; Yamamoto, H.; Xu, Y.; Li, W.; Yamanishi, H.; Okamura, H.; et al. Hepatocyte nuclear factor 4 alpha is a key factor related to depression and physiological homeostasis in the mouse brain. *PLoS ONE* **2015**, *10*, e0119021. [CrossRef] [PubMed]
45. Hartmann, P.; Zhou, Z.; Natarelli, L.; Wei, Y.; Nazari-Jahantigh, M.; Zhu, M.; Grommes, J.; Steffens, S.; Weber, C.; Schober, A. Endothelial Dicer promotes atherosclerosis and vascular inflammation by miRNA-103-mediated suppression of KLF4. *Nat. Commun.* **2016**, *7*, 10521. [CrossRef]
46. Cheng, Z.; Zou, X.; Jin, Y.; Gao, S.; Lv, J.; Li, B.; Cui, R. The Role of KLF4 in Alzheimer's Disease. *Front. Cell. Neurosci.* **2018**, *12*, 12. [CrossRef]
47. Han, X.-R.; Wen, X.; Wang, Y.-J.; Wang, S.; Shen, M.; Zhang, Z.-F.; Fan, S.-H.; Shan, Q.; Wang, L.; Li, M.-Q.; et al. Effects of CREB1 gene silencing on cognitive dysfunction by mediating PKA-CREB signaling pathway in mice with vascular dementia. *Mol. Med.* **2018**, *24*, 18. [CrossRef]
48. Bao, M.H.; Luo, H.Q.; Chen, L.H.; Tang, L.; Ma, K.F.; Xiang, J.; Dong, L.P.; Zeng, J.; Li, G.Y.; Li, J.M. Impact of high fat diet on long non-coding RNAs and messenger RNAs expression in the aortas of ApoE (-/-) mice. *Sci. Rep.* **2016**, *6*, 34161. [CrossRef]
49. Ren, Z.; Yu, J.; Wu, Z.; Si, W.; Li, X.; Liu, Y.; Zhou, J.; Deng, R.; Chen, D. MicroRNA-210-5p Contributes to Cognitive Impairment in Early Vascular Dementia Rat Model Through Targeting Snap25. *Front. Mol. Neurosci.* **2018**, *11*, 388. [CrossRef]
50. Fasanaro, P.; D'Alessandra, Y.; Di Stefano, V.; Melchionna, R.; Romani, S.; Pompilio, G.; Capogrossi, M.C.; Martelli, F. MicroRNA-210 modulates endothelial cell response to hypoxia and inhibits the receptor tyrosine kinase ligand Ephrin-A3. *J. Biol. Chem.* **2008**, *283*, 15878–15883. [CrossRef]
51. McNay, E.C.; Recknagel, A.K. Brain insulin signaling: A key component of cognitive processes and a potential basis for cognitive impairment in type 2 diabetes. *Neurobiol. Learn. Mem.* **2011**, *96*, 432–442. [CrossRef] [PubMed]
52. Rask-Madsen, C.; Li, Q.; Freund, B.; Feather, D.; Abramov, R.; Wu, I.H.; Chen, K.; Yamamoto-Hiraoka, J.; Goldenbogen, J.; Sotiropoulos, K.B.; et al. Loss of insulin signaling in vascular endothelial cells accelerates atherosclerosis in apolipoprotein E null mice. *Cell Metab.* **2010**, *11*, 379–389. [CrossRef] [PubMed]
53. Caporali, A.; Pani, E.; Horrevoets, A.J.; Kraenkel, N.; Oikawa, A.; Sala-Newby, G.B.; Meloni, M.; Cristofaro, B.; Graiani, G.; Leroyer, A.S.; et al. Neurotrophin p75 receptor (p75NTR) promotes endothelial cell apoptosis and inhibits angiogenesis: Implications for diabetes-induced impaired neovascularization in ischemic limb muscles. *Circ. Res.* **2008**, *103*, e15–e26. [CrossRef]
54. Henriksson, B.G.; Söderström, S.; Gower, A.J.; Ebendal, T.; Winblad, B.; Mohammed, A.H. Hippocampal nerve growth factor levels are related to spatial learning ability in aged rats. *Behav. Brain Res.* **1992**, *48*, 15–20. [CrossRef]

55. Wimmer, I.; Tietz, S.; Nishihara, H.; Deutsch, U.; Sallusto, F.; Gosselet, F.; Lyck, R.; Muller, W.A.; Lassmann, H.; Engelhardt, B. PECAM-1 Stabilizes Blood-Brain Barrier Integrity and Favors Paracellular T-Cell Diapedesis Across the Blood-Brain Barrier During Neuroinflammation. *Front. Immunol.* **2019**, *10*, 711. [CrossRef]
56. Stepanov, G.A.; Filippova, J.A.; Komissarov, A.B.; Kuligina, E.V.; Richter, V.A.; Semenov, D.V. Regulatory role of small nucleolar RNAs in human diseases. *BioMed Res. Int.* **2015**, *2015*, 206849. [CrossRef]
57. Rogelj, B.; Hartmann, C.E.; Yeo, C.H.; Hunt, S.P.; Giese, K.P. Contextual fear conditioning regulates the expression of brain-specific small nucleolar RNAs in hippocampus. *Eur. J. Neurosci.* **2003**, *18*, 3089–3096. [CrossRef]
58. Kim, C.; Kang, D.; Lee, E.K.; Lee, J.S. Long Noncoding RNAs and RNA-Binding Proteins in Oxidative Stress, Cellular Senescence, and Age-Related Diseases. *Oxidative Med. Cell. Longev.* **2017**, *2017*, 2062384. [CrossRef]
59. Montes, M.; Lund, A.H. Emerging roles of lncRNAs in senescence. *FEBS J.* **2016**, *283*, 2414–2426. [CrossRef]
60. Li, W.; Shen, W.; Zhang, B.; Tian, K.; Li, Y.; Mu, L.; Luo, Z.; Zhong, X.; Wu, X.; Liu, Y.; et al. Long Non-Coding RNA LncKdm2b Regulates Cortical Neuronal Differentiation by Cis-Activating Kdm2b. *bioRxiv* **2018**, *11*, 161–186. [CrossRef] [PubMed]
61. Labonne, J.D.J.; Lee, K.-H.; Iwase, S.; Kong, I.-K.; Diamond, M.P.; Layman, L.C.; Kim, C.-H.; Kim, H.-G. An atypical 12q24.31 microdeletion implicates six genes including a histone demethylase KDM2B and a histone methyltransferase SETD1B in syndromic intellectual disability. *Hum. Genet.* **2016**, *135*, 757–771. [CrossRef] [PubMed]
62. Jiang, S.; Yang, W.; Qiu, Y.; Chen, H.Z. Identification of novel quantitative traits-associated susceptibility loci for APOE epsilon 4 non-carriers of Alzheimer's disease. *Curr. Alzheimer Res.* **2015**, *12*, 218–227. [CrossRef] [PubMed]
63. Yang, Y.; Zhang, J.; Chen, X.; Xu, X.; Cao, G.; Li, H.; Wu, T. LncRNA FTX sponges miR-215 and inhibits phosphorylation of vimentin for promoting colorectal cancer progression. *Gene Ther.* **2018**, *25*, 321–330. [CrossRef] [PubMed]
64. Dave, J.M.; Bayless, K.J. Vimentin as an integral regulator of cell adhesion and endothelial sprouting. *Microcirculation* **2014**, *21*, 333–344. [CrossRef] [PubMed]
65. Baker, M.; Mackenzie, I.R.; Pickering-Brown, S.M.; Gass, J.; Rademakers, R.; Lindholm, C.; Snowden, J.; Adamson, J.; Sadovnick, A.D.; Rollinson, S.; et al. Mutations in progranulin cause tau-negative frontotemporal dementia linked to chromosome 17. *Nature* **2006**, *442*, 916–919. [CrossRef] [PubMed]
66. Vercellino, M.; Grifoni, S.; Romagnolo, A.; Masera, S.; Mattioda, A.; Trebini, C.; Chiavazza, C.; Caligiana, L.; Capello, E.; Mancardi, G.L.; et al. Progranulin expression in brain tissue and cerebrospinal fluid levels in multiple sclerosis. *Mult. Scler.* **2011**, *17*, 1194–1201. [CrossRef]
67. Pickford, F.; Marcus, J.; Camargo, L.M.; Xiao, Q.; Graham, D.; Mo, J.R.; Burkhardt, M.; Kulkarni, V.; Crispino, J.; Hering, H.; et al. Progranulin is a chemoattractant for microglia and stimulates their endocytic activity. *Am. J. Pathol.* **2011**, *178*, 284–295. [CrossRef]
68. Mullin, N.K.; Mallipeddi, N.V.; Hamburg-Shields, E.; Ibarra, B.; Khalil, A.M.; Atit, R.P. Wnt/beta-catenin Signaling Pathway Regulates Specific lncRNAs That Impact Dermal Fibroblasts and Skin Fibrosis. *Front. Genet.* **2017**, *8*, 183. [CrossRef] [PubMed]
69. Mao, C.X.; Yin, J.Y.; Zhang, Y.; Wang, Z.B.; Yang, Z.Q.; He, Z.W.; Li, X.M.; Mao, X.Y.; Cui, R.T.; Li, X.J.; et al. The molecular classification of astrocytic tumors. *Oncotarget* **2017**, *8*, 96340–96350. [CrossRef]
70. Chen, X.; Ma, C.; Chen, C.; Lu, Q.; Shi, W.; Liu, Z.; Wang, H.; Guo, H. Integration of lncRNA-miRNA-mRNA reveals novel insights into oviposition regulation in honey bees. *PeerJ* **2017**, *5*, e3881. [CrossRef]

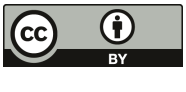

nutrients

MDPI

Article

Obese Adipose Tissue Secretion Induces Inflammation in Preadipocytes: Role of Toll-Like Receptor-4

Mariana Renovato-Martins [1,*,†], Catharina Moreira-Nunes [2,†], Georgia C. Atella [3,4], Christina Barja-Fidalgo [5] and João Alfredo de Moraes [2]

1 Departamento de Biologia Celular e Molecular, Instituto de Biologia, Universidade Federal Fluminense, Niterói 24020-140, Brazil
2 Programa de Pesquisa em Farmacologia e Inflamação, Instituto de Ciências Biomédicas, Universidade Federal do Rio de Janeiro, Rio de Janeiro 21941-902, Brazil; catharinanunes@hotmail.com (C.M.-N.); joaomoraes@icb.ufrj.br (J.A.d.M.)
3 Instituto de Bioquímica Médica Leopoldo De Meis, Universidade Federal do Rio de Janeiro, Rio de Janeiro 21941-902, Brazil; atella@bioqmed.ufrj.br
4 Instituto Nacional de Ciência e Tecnologia em Entomologia Molecular- INCT-EM, Universidade Federal do Rio de Janeiro, Rio de Janeiro 21940-590, Brazil
5 Departamento de Biologia Celular, IBRAG, Universidade do Estado do Rio de Janeiro, Rio de Janeiro 20551-030, Brazil; barja-fidalgo@uerj.br
* Correspondence: marianarenovato@id.uff.br; Tel.: +55-219-714-14811
† These authors contributed equally to this work.

Received: 30 July 2020; Accepted: 14 September 2020; Published: 16 September 2020

Abstract: In obesity, the dysfunctional adipose tissue (AT) releases increased levels of proinflammatory adipokines such as TNFα, IL-6, and IL-1β and free fatty acids (FFAs), characterizing a chronic, low-grade inflammation. Whilst FFAs and proinflammatory adipokines are known to elicit an inflammatory response within AT, their relative influence upon preadipocytes, the precursors of mature adipocytes, is yet to be determined. Our results demonstrated that the conditioned medium (CM) derived from obese AT was rich in FFAs, which guided us to evaluate the role of TLR4 in the induction of inflammation in preadipocytes. We observed that CM derived from obese AT increased reactive oxygen species (ROS) levels and NF-kB nuclear translocation together with IL-6, TNFα, and IL-1β in 3T3-L1 cells in a TLR4-dependent manner. Furthermore, TLR4 signaling was involved in the increased expression of C/EBPα together with the release of leptin, adiponectin, and proinflammatory mediators, in response to the CM derived from obese AT. Our results suggest that obese AT milieu secretes lipokines, which act in a combined paracrine/autocrine manner, inducing inflammation in preadipocytes via TLR4 and ROS, thus creating a paracrine loop that facilitates the differentiation of adipocytes with a proinflammatory profile.

Keywords: adipose tissue; preadipocyte; TLR4; inflammation; free fatty acid; obesity

1. Introduction

The obese state is described as the expansion of fat depots causing adipose tissue (AT) dysfunctionality, which is often characterized by low-grade inflammation in situ. This condition is highly correlated with the onset of obesity-related comorbidities including type 2 diabetes, insulin resistance, and several types of cancers [1]. It is consensual that AT-resident immune cells play a role in the regulation of this obesity-induced inflammation. Although different types of immune cells are found in AT, macrophages play a pivotal role in the establishment of inflammation, as they produce the most cytokines in response to obesity [2,3]. Despite the lack of information about the

precise mechanism of the inflammatory response in expanding AT, it is suggested that adipocyte death, impairment of adipogenesis, fibrosis, hypoxia, oxidative stress, endoplasmic reticulum stress, and the dysregulation in free fatty acid (FFA) release contribute to this effect [4]. Once in a proinflammatory state, mature adipocytes secrete adipokines, such as TNFα, IL-6, and IL-1β [4] with visceral AT releasing high amounts of FFAs. Low-grade inflammation and the high rate of lipolysis are responsible for the negative metabolic consequences of fat accumulation in the body, such as insulin resistance, dyslipidemia, and lipotoxicity [5,6]. Even though the release of FFAs by AT ensures survival during prolonged food deprivation, it can be further augmented in obesity as a result of the spillover of lipoprotein lipase, an enzyme that processes triglyceride-rich proteins to release FFAs [7]. AT-derived cytokines, i.e., TNFα and IL-6, are known to stimulate lipolysis and promote the release of FFAs [6]. This can be further augmented when enlarged adipocytes release more FFAs together with a reduced FFA clearance [8].

The plasma FFA concentrations in obese individuals are commonly correlated with AT expansion [9,10], which can lead to the activation of TLR2 and TLR4, increasing NF-kB activity [11], eliciting the generation of proinflammatory cytokines [12]. TLRs are major upstream molecules in the activation of the IKKβ/NF-κB pathway, and their role in the development of obesity-induced inflammation has been studied. According to Shi et al., TLR4 is the molecular link between FFAs, inflammation, and the innate immune system [13]. In obese animal models, inhibition of the IKKβ/NF-κB pathway by pharmacological inhibitors of IKKβ, or by the genetic deletion of IKKβ, improves insulin resistance [14,15].

Recent studies have shown that the stromal vascular fraction (SVF) regulates the release of inflammatory mediators. Among the SVF, preadipocytes, the precursors of mature adipocytes, account for 15 to 50% of cells in human AT [5]. However, even though FFAs are known to elicit an inflammatory response in AT, the precise mechanism of how these FFAs act together in a paracrine manner on preadipocytes still needs to be determined.

Thus, we hypothesized that in response to obesity, there is an increased release of inflammatory mediators, as well as FFAs, which would act in a paracrine manner on preadipocytes to generate an inflammatory response, contributing to the establishment of a positive feedback loop in the low-grade inflammation of AT. We conducted this study to investigate whether the inflammatory mediators, as well and FFAs produced by the obese AT could act in a paracrine manner on preadipocytes to generate an inflammatory response, contributing to the establishment of a positive feedback loop in the low-grade inflammation of the AT. Understanding how the endocrine and immune functions interconnect in AT may pave the way for the development of new strategies for the treatment of obesity and its associated comorbidities.

2. Materials and Methods

2.1. Reagents

Benzamidine, bovine serum albumin (BSA), EDTA, HEPES, leupeptin, phenylmethylsulfonyl fluoride (PMSF), soybean trypsin inhibitor, and trypsin were obtained from Sigma-Aldrich (St. Louis, MO, USA). TLR4 antagonist TAK-242 (TAK) was obtained from the Cayman Chemical Company (Ann Arbor, MI, USA). Dulbecco's modified Eagle's medium (DMEM) and fetal bovine serum (FBS) were acquired from GIBCO (Carlsbad, CA, USA). Ready-To-Glow pNF-κB-secreted luciferase reporter system was obtained from Clontech (Mountain View, CA, USA). Antibodies anti-C/EBPα and anti-PPARγ were purchased from Santa Cruz Biotechnology (Dallas, TX, USA). Antibody anti-actin was purchased from Abcam (Cambridge, UK). Enzyme-linked immunosorbent assay (ELISA) kits (IL-6, IL-1β, Leptin, and TNFα) were purchased from Peprotech (Rocky Hill, NJ, USA). The adiponectin ELISA kit was purchased from R&D systems (Minneapolis, MN, USA). CM-H_2DCFDA (DCF) was from Life Technologies (Carlsbad, CA, USA). The enhanced chemiluminescence (ECL) and BCA protein assay kit were purchased from Pierce Biotechnology (Waltham, MA, USA).

2.2. Obesity Animal Model

Animal experiments were performed in strict accordance with the recommendations of the 1964 Declaration of Helsinki. The animal study was approved by the Committee on the Ethics of Animal Experiments of the Federal University of Rio de Janeiro (UFRJ) (CEUA 042/2016). We obtained C57BL/6J mice from the animal facilities of CEMIB/UNICAMP (São Paulo, Brazil). Animals were housed (four mice per cage) in a temperature-controlled room (25 ± 1 °C) and 12 h artificial light-dark-cycle. Upon weaning, male mice were randomly divided into two groups and fed according to AIN-93M recommendations: Standard chow (control group: 3.9 kcal/g of chow; 13% of energy derived from fat) or high-fat diet chow (high-fat diet group (HFD): 4.7 kcal/g, calorically enhanced by lard; 45% of energy derived from fat) until 90 days of age, when they were euthanized. Further information about the diet composition is shown in Table S1. The body weight of each animal was evaluated at 90 days of age.

2.3. AT Explant Culture

Epididymal AT obtained from control and obese mice was rinsed and cleaned with a phosphate-buffered saline. The explant culture was performed as previously described [16]. Briefly, 100 mg of AT explants obtained from mouse AT was incubated in 1 mL of DMEM supplemented with 1% FBS at 37 °C for 24 h. After this time, supernatants (conditioned medium [CM]) were aspirated on ice and centrifuged at 350× *g* for 10 min at 4 °C. The supernatants were collected (CM) and stored at −80 °C for further experiments.

2.4. Gas Chromatography-Mass Spectrometry (GC–MS)

The content of long-chain fatty acids in the CM was analyzed in a volume corresponding to 500 µg of proteins using GC–MS, as previously described [17]. Lipid samples were dissolved in 1 mL toluene, and to this was added 2 mL of 1% sulfuric acid in methanol. After 24 h in a stoppered tube at 50 °C, 1 mL of 5% NaCl was added, and the required esters were extracted (2X) with 2 mL hexane and then removed in a stream of nitrogen. Dried fatty acid methyl esters (FAME) were suspended in 100 µL heptane. GC/MS analyses were carried out on a Shimadzu GCMS-QP2010 Plus system, using an HP Ultra 2 (5% phenyl-methylpolysiloxane) and Agilent (25 m × 0.20 mm × 0.33 µm). The splitless injector was set at 250 °C. Column temperature was programmed to increase from 40–160 °C at 30 °C/min, 160–233 °C at 1 °C/min, 233–300 °C at 3 °C/min, and held at 300 °C for 10 min. We used helium as the carrier gas with a linear velocity of 36.0 cm/s. Then, a volume of 2 mL of the sample was injected into the chromatograph. Electron ionization (EI-70 eV) and a quadrupole mass analyzer performed the analysis in scans from 40 to 440 amu. The interface was set at 240 °C and the ion source at 240 °C. The components were identified by comparing their mass spectra with those of the library NIST05 contained in the computer of the mass spectrometer. To confirm the identity of the peaks in the chromatogram by Supelco 37 Component FAME Mix (Sigma-Aldrich), we used retention indices. FFAs were quantified by determining peak-area ratios with the internal standards 9:0 and 19:0.

2.5. Cell Culture

3T3-L1 preadipocytes were obtained from the American Type Culture Collection (Rockville, MD, USA). The cells were cultured in DMEM containing 10% FBS, 100 µg/mL streptomycin, and 50 U/mL penicillin. The cells were incubated at 37 °C in a 5% CO_2 atmosphere. The cells were passaged following dissociation with 0.1%/0.01% trypsin/EDTA, and after this process, the cells were seeded into new culture flasks for a maximum of five passages.

2.6. Reactive Oxygen Species (ROS) Production

3T3-L1 cells (5×10^3 cells/well) were seeded in 96-well black plates overnight in DMEM containing 10% FBS. The cells were washed three times with PBS, then the medium was removed, and cells were incubated with DMEM containing 1% FBS and incubated for 1 h. To detect intracellular ROS, 3T3-L1

cells were loaded with DCF (10 μM) for 1 h and then washed to remove the excess probe. Cells were pretreated or not with TAK (1 μM) for 15 min and then incubated with Lean CM, Obese CM, or LPS 1 μg/mL for 2 h at 37 °C in a 5% CO_2 atmosphere. CM-H_2DCFDA fluorescence was monitored at an excitation of 495 nm and emission of 530 nm wavelengths. Fluorescence was quantified using the Flexstation™ multilabel plate reader (Molecular Devices, San Jose, CA, USA).

2.7. NF-kB Activation

3T3-L1 cells (2×10^5 cells/well) were seeded in 24-well plates in DMEM containing 10% FBS overnight. The cells were washed three times with PBS, then the medium was removed, and cells were incubated with DMEM containing 1% FBS and incubated for 1 h. The cells were then washed three times with PBS and transfected with the NF-kB-responsive luciferase reporter construct (NF-kB pMetLuc 2) and its control plasmid (pMetLuc 2) in DMEM containing 1% FBS and incubated for 24 h. Cells were pretreated or not with TAK (1 μM) for 15 min and then incubated with Lean CM, Obese CM, or LPS 1 μg/mL for 2 h at 37 °C in a 5% CO_2 atmosphere. The medium containing luciferase was collected for each treatment and was incubated with luciferin. Luminescence emitted from the luciferin cleavage was monitored using the Flexstation™ multilabel plate reader (Molecular Devices, San Jose, CA, USA).

2.8. Immunofluorescence Microscopy

3T3-L1 cells were plated (5×10^4 cells) on glass coverslips in DMEM containing 10% FBS and grown on glass coverslips at 37 °C in a 5% CO_2 atmosphere. The next day, the cells were washed with PBS, then cells were incubated with a serum-free medium, and after 30 min, the cells were stimulated with Lean CM, Obese CM, or LPS 1 μg/mL for 2 h. The monolayers were washed with PBS, and the cells were fixed with 4% paraformaldehyde/4% sucrose in PBS. After 20 min, the cells were blocked with 5% BSA in PBS for 30 min. Then, cells were washed three times with PBS and incubated with phalloidin-TRITC (1:1000) at room temperature. After 2 h, 3T3-L1 cells were washed three times with PBS and incubated for 24 h with anti-NF-κB (1:200) at 4 °C. The cells were rinsed with 0.1% Tween in TBS and incubated for 1 h at room temperature with a FITC-conjugated secondary antibody (1:200). Coverslips were mounted on a slide with the use of DAPI Prolong for nuclear staining before examination under an epifluorescence microscope (BX40 Olympus). The images were analyzed using ImageJ (NIH).

2.9. ELISA

3T3-L1 cells (2×10^5 cells/well) were seeded in 24-well plates in DMEM containing 10% FBS overnight. The cells were washed three times with PBS, and the medium was replaced with DMEM containing 1% FBS and incubated for 1 h. Cells were pretreated or not with TAK (1 μM) for 15 min and then incubated with Lean CM, Obese CM, or LPS 1 μg/mL at 37 °C in a 5% CO_2 atmosphere for 3 h. The medium was then replaced with DMEM containing 1% FBS and incubated for 24 h to quantify IL-6, IL-1β, and TNF-α levels. To quantify adiponectin, IL-6, IL-1β, leptin, and TNF-α levels after differentiation, cells were pretreated or not with TAK (1 μM) for 15 min and then incubated with Lean CM, Obese CM, or Differentiation Medium (dexamethasone 1 μM, isobutylmethylxanthine 0.5 mM, and insulin 5 μg/mL) at 37 °C in a 5% CO_2 atmosphere for six days. The medium was then replaced with DMEM containing 1% FBS and incubated for 24 h. These adipokines were quantified in supernatants using a sandwich ELISA kit. All procedures were performed according to the manufacturer's instructions.

2.10. Cellular Extract

3T3-L1 cells (1×10^6 cells/well) were cultured on 6-well plates with DMEM 10% FBS for 24 h. Then, the cells were washed with PBS and incubated with serum-free DMEM for 1 h. Groups were pretreated or not with TAK (1 μM) for 15 min and then incubated with Lean CM, Obese CM, or Differentiation

Medium (dexamethasone 1 μM, isobutylmethylxanthine 0.5 mM, and insulin 5 μg/mL) for 48 h at 37 °C in a 5% CO_2 atmosphere. Then, 3T3-L1 cells were lysed in a lysis buffer (benzamidine 1 mM, EDTA 10 mM, HEPES 50 mM, pH 6.4, $MgCl_2$ 1 mM, 1 % Triton X-100, DNase 1 μg/mL, Rnase 0.5 μg/mL, PMSF 1 mM, leupeptin 1 μg/mL, and soybean trypsin inhibitor 1 μg/mL).

2.11. Western Blot Analysis

The total protein in the cell extracts was determined by the BCA method. Cell lysates were denatured in a sample buffer (Tris·HCl 50 mM, 10% glycerol, pH 6.8, 1% SDS, 5% 2-ME, and 0.001% bromophenol blue) and heated in a boiling water bath for 3 min. We loaded 30 μg of proteins from each sample onto electrophoresis gels. Next, the proteins were electroblotted from the gels to nitrocellulose membranes and blocked with 5% BSA containing 0.1% Tween in TBS. The blocked membranes were incubated overnight at 4 °C with primary antibodies. After washing in Tween-TBS, the membranes were incubated for 2 h with a peroxidase-conjugated secondary antibody. The bands were visualized using ECL and quantified by densitometry using the ImageJ software (NIH). The results are expressed as fold increase compared to the control after normalization with the housekeeping protein actin.

2.12. Adipogenesis Quantification

3T3-L1 cells (1×10^3 cells/well) were seeded in 96-well plates in DMEM containing 10% FBS overnight. The cells were washed three times with PBS, and the medium was replaced with DMEM containing 1% FBS and incubated for 1 h. Cells were pretreated or not with TAK (1 μM) for 15 min and then incubated with Lean CM, Obese CM, or Differentiation Medium (dexamethasone 1 μM, isobutylmethylxanthine 0.5 mM, and insulin 5 μg/mL) at 37 °C in a 5% CO_2 atmosphere. The medium was replaced every three days. After seven days, the medium was removed and cells were fixed with formalin 10%. After 30 min, the cells were washed and incubated with oil red O for 20 min. Then, the cells were washed and treated with 70% isopropanol, and the absorbance was quantified at 492 nm using the Flexstation™ multilabel plate reader (Molecular Devices, San Jose, CA, USA).

2.13. Statistical Analysis

The data are expressed as means ± standard error. Statistical significance was assessed by ANOVA, followed by the Bonferroni t-test. For all analyses, a p-value < 0.05 was considered statistically significant.

3. Results

3.1. AT from Obese Animals Released Increased Amounts of FFAs

Our results demonstrated that, compared to controls (lean), the 90-day-old obese mice showed a 45.7% increase in body weight (Figure 1A) and a 75% increase in epididymal fat pad weight (Figure 1B). The expansion in adiposity was accompanied by dramatic changes in the quality of FFAs released by the AT of obese mice. The analysis of FFAs present in the CM harvested from cultures of visceral AT showed that the AT from obese mice, but not lean mice, released myristic (14:0), palmitic (16:0), and arachidonic (20:4) acids. Furthermore, the AT from obese mice secreted increased quantities of linoleic (18:2; 36-fold), oleic (18:1; 33-fold), and stearic (18:2; 9-fold) acids in the CM, when compared to the AT from control mice (Figure 1C).

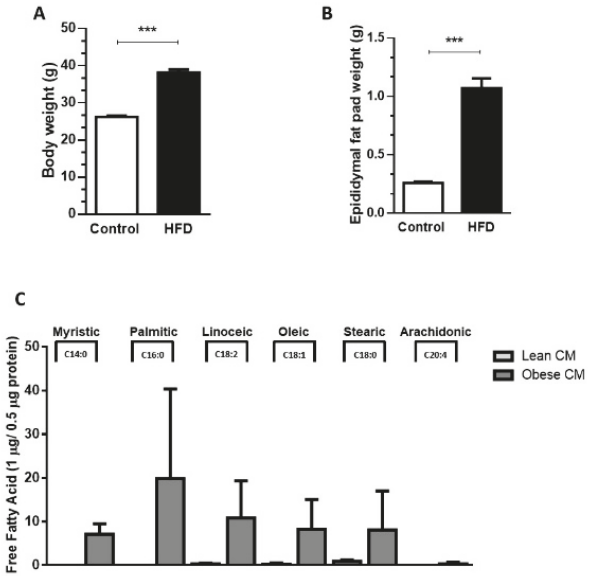

Figure 1. Male mice were randomly housed in cages (n = 4 animal per cage) and, after weaning were fed either with regular control chow (CTL; 13% of energy derived from fat) or high-fat-diet (HFD; 45% of energy derived from fat) until 90 days of age. (**A**) Body weight and epididymal fat pad (**B**) were measured after 90 days. Results are representative of 28 at least 30 mice. Data are expressed as means ± SEM. *** $p < 0.005$ vs. control. (**C**). Epididymal adipose tissue depots were collected and maintained in culture in Dulbecco's modified Eagle's medium (DMEM) 1% FBS for 24 h. Then, the supernatant was collected, and free fatty acids were analyzed in gas chromatography-mass spectrometry (GC-MS). Results are representative of three different experiments.

3.2. FFAs Released by Obese AT Induce ROS Production and NF-kB Translocation in Preadipocytes in a TLR4-Dependent Manner

Once the CM from cultures of AT from obese animals was enriched with FFAs, we determined the cytotoxic potential of the CM from lean and obese AT, analyzing the viability of 3T3-L1 cells after 24 h of incubation with different concentrations of CM (10, 20, and 30% *v*/*v*) (Supplementary Materials Figure S1). Based on these results, the concentration of CM at 20% was utilized in all assays throughout the study. FFAs play a role in the recruitment of macrophages into AT [18]. Although the paracrine/autocrine effects of FFAs on adipocytes have been demonstrated [19], no experimental data on the effects of AT secretion on preadipocytes are available yet. We analyzed the ROS production in 3T3-L1 cells stimulated with CM derived from AT. It was observed that the CM derived from obese AT induced a 1.65-fold-increase in ROS production by 3T3-L1 cells when compared to that of control AT. As expected, LPS, used as a positive control, induced a greater increase in ROS levels in the preadipocytes. Additionally, we observed that when TLR4 was selectively inhibited by TAK, ROS production induced by obese AT CM or by LPS, significantly decreased to the control levels (Figure 2A).In order to prove that the CM was not free from LPS, we performed one experiment in the presence of polymyxin, which blocks the effects of LPS by binding to lipid A [20,21], and the results were similar to the CM itself (Figure S2A). We observed an increase in the expression of TLR4 mRNA in 3T3-L1 cells stimulated by CM derived from obese AT (Figure S3), suggesting that TLR4-dependent signaling may be increased in the preadipocytes.

In agreement with the data, we demonstrated that the CM derived from obese AT induced the nuclear translocation of NF-kB (Figure 2B) in 3T3-L1 cells, indicative of the activation of this pathway. This effect was eradicated by TLR4 signaling inhibition (Figure 2C).

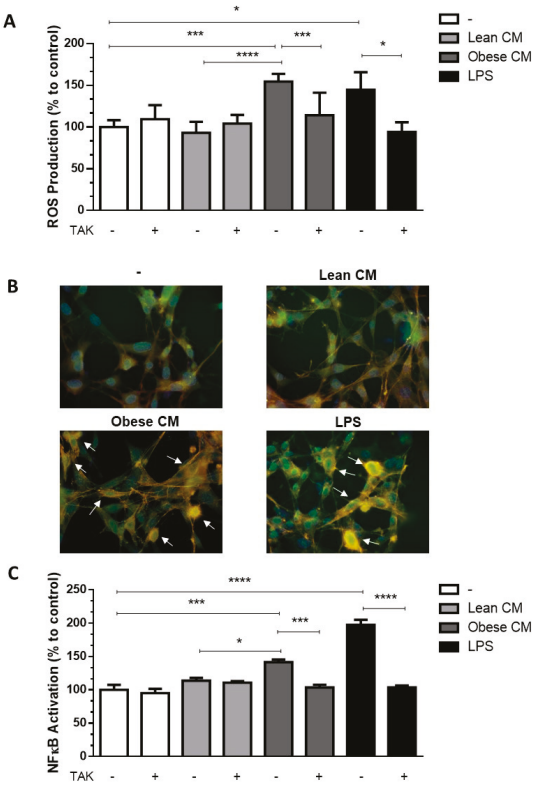

Figure 2. 3T3-L1 cells were left untreated or were pre-incubated with TAK-242 (TAK) 1 μM for 15 min, at 37 °C/5% CO_2. After pre-treatment, 3T3-L1 cells were treated or not with Lean Conditioned Medium (CM), Obese Conditioned Medium, or LPS 1 μg/mL for 2 h. (**A**). Reactive oxygen species (ROS) production was assessed using CM-H_2DCFDA probe. (**B**). NF-κB translocation to nucleus was evaluated by immunofluorescence staining with anti-NF-κB-FITC (green), actin was visualized using phalloidin-rodhamin (red) and nuclei was visualized using DAPI (blue). Arrows indicate the NF-κB presence in nucleus. Results are representative of three different experiments. (**C**). NF-κB activation was evaluated by luciferase activity. (**A**,**C**). Results are representative of three independent experiments. Data are expressed as means ± SEM. * Represents $p < 0.05$, *** represents $p < 0.005$, **** represents $p < 0.001$. LPS—Lipopolysaccharide.

3.3. Stimulation of Preadipocytes with CM Derived from Obese AT Increased Inflammatory Cytokines Released via TLR4 Signaling

Adipocytes within AT are known to contribute to the low-grade inflammation apparent in obesity, by secreting increased amounts of proinflammatory cytokines [22]. To investigate whether preadipocytes may also contribute to this inflammatory profile in the obese AT microenvironment, we incubated 3T3-L1 cells with the CM derived from AT for 3 h and then analyzed the cytokines released by these cells in a CM-free medium. The results depicted in Figure 3 show that the cells primed with obese AT released increased amounts of IL6 (Figure 3A), TNF-α (Figure 3B), and IL-1β (Figure 3C) for the subsequent 24 h. The release of cytokines was prevented in the presence of TAK, a TLR4 signaling inhibitor (Figure 3A–C). Altogether, these results indicate that the contact of preadipocytes with the secretion released from obese AT induced, in a paracrine manner, a proinflammatory phenotype in preadipocytes within the AT, which is mediated by TLR4 signaling.

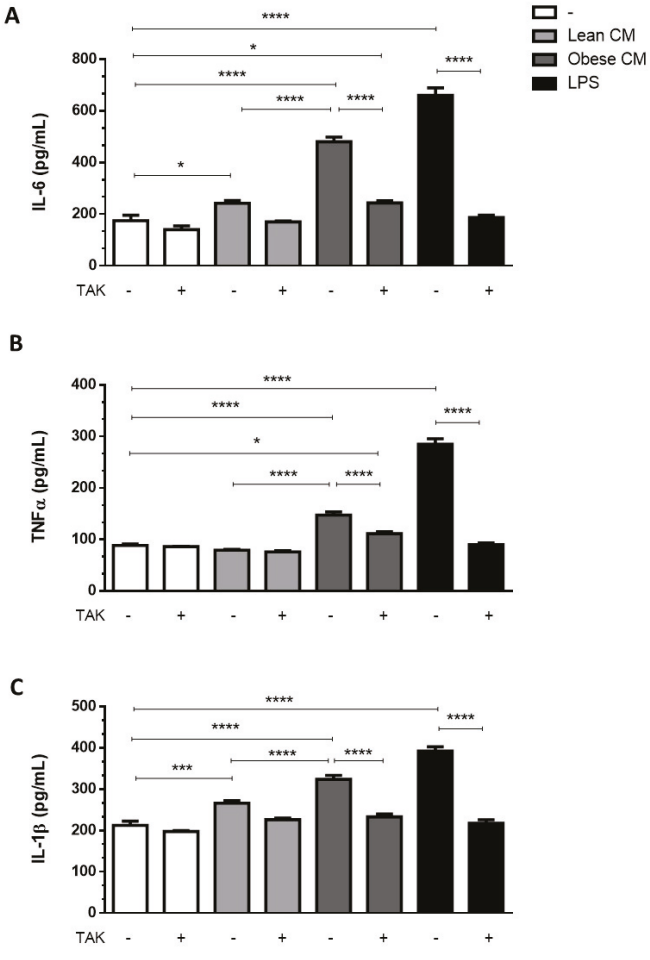

Figure 3. 3T3-L1 cells were left untreated or were pre-incubated with TAK-242 (TAK) 1 μM for 15 min, at 37 °C/5% CO_2. After pre-treatment, 3T3-L1 cells were treated or not with Lean Conditioned Medium (CM), Obese Conditioned Medium or LPS 1 μg/mL for 3 h. Then, the medium was removed, and cells were incubated with DMEM 1% FBS, for 21 h (to complete 24 h). IL-6 (**A**), TNFα (**B**), and IL-1β (**C**) were measured in supernatants using a sandwich enzyme-linked immunosorbent assay kit. Results are representative of three independent experiments. Data are expressed as means ± SEM. * Represents $p < 0.05$, *** represents $p < 0.005$, **** represents $p < 0.001$.

3.4. CM Derived from Obese AT Increased C/EBPα Expression in Preadipocytes via TLR4 Signaling

The transcription factors C/EBPα and PPARγ are key activators of adipogenesis reported to cooperate in the activation of a few adipocyte genes directly associated with the maturation of the adipocyte phenotype [23]. Most of the FFAs are among the compounds that are able to activate all three members of the PPAR family [24]. We have investigated the effect of CM derived from obese AT, rich in saturated and unsaturated FFAs, on the expression of adipogenic genes in 3T3-L1 cells. We showed that the stimulation of 3T3-L1 cells with the CM derived from obese AT increased the expression of C/EBPα (Figure 4A) and induced a trend of increase in PPARγ (Figure 4B) at levels comparable to those induced by the differentiation cocktail.

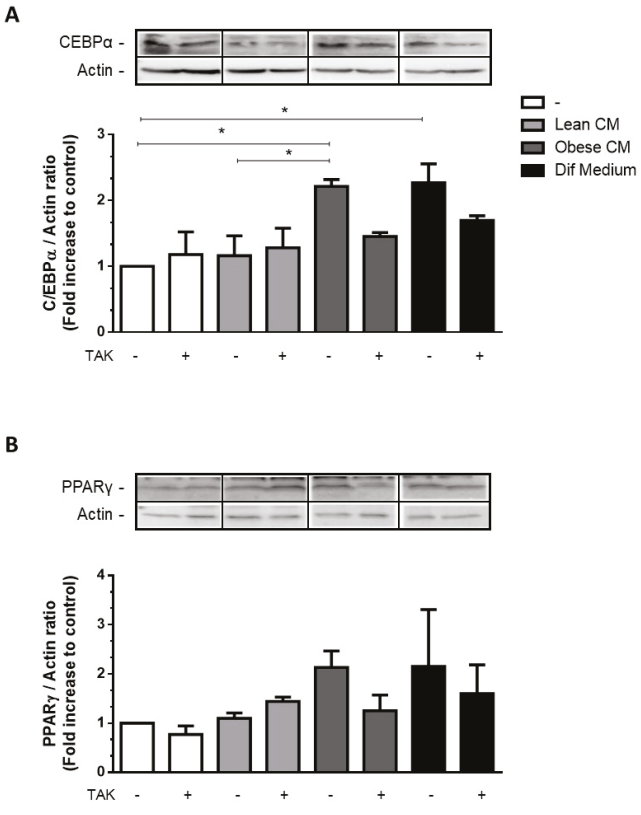

Figure 4. 3T3-L1 cells were left untreated or were pre-incubated with TAK-242 (TAK) 1 μM for 15 min, at 37 °C/5% CO_2. After pre-treatment, 3T3-L1 cells were treated or not with Lean Conditioned Medium (CM), Obese Conditioned Medium, or differentiation mix for 48 h. Thirty μg of proteins from cell lysates were subjected to Western blotting for C/EBPα (**A**) and PPARγ (**B**). Results are representative of three independent experiments. Data are expressed as means ± SEM. * Represents $p < 0.05$.

3.5. Preadipocytes Stimulated with the CM Derived from Obese AT Underwent Morphologic Changes and Lipid Accumulation in a TLR4-Dependent Manner

Having observed increased levels of C/EBPα, we analyzed whether the CM derived from obese AT could induce in 3T3-L1 preadipocytes the morphologic changes required for the differentiation process. In Figure 5A, we show that 3T3-L1 preadipocytes treated with CM derived from obese AT underwent morphologic changes toward a round shape that was similar to the shape of the completely differentiated adipocytes found in the positive control cells (treated with the differentiation cocktail). No changes in morphology were observed in the preadipocytes that were treated with CM derived from lean AT (Figure 5A). To investigate if TLR4 would play a role in the effect of obese AT secretion on the adipocyte differentiation, 3T3-L1 cells were treated with CM derived from obese AT or with the differentiation cocktail, and lipid accumulation was evaluated by oil red O staining. We observed that both treatments increased lipid accumulation within the cells. However, the inhibition of TLR4 signaling by TAK prevented lipid accumulation induced by the CM from obese AT, but no effect was detected in 3T3-L1 cells treated with the differentiation cocktail (Figure 5B). Furthermore, to better characterize the profile of differentiated 3T3-L1, we evaluated the release of proinflammatory and anti-inflammatory adipokines. We observed that the treatment of 3T3-L1 preadipocytes with the CM derived from obese AT, for seven days, stimulated the release of increased levels of TNF-α, IL-6,

and IL-1β (Figure 5C–E, respectively), which were eradicated by TAK pre-treatment. Furthermore, we also observed an increase in the release of leptin and adiponectin, both markers of mature adipocytes, which was abolished in the presence of TAK (Figure 5F,G, respectively). Importantly, the treatment with TAK did not inhibit the release of leptin and adiponectin by adipocytes differentiated in the presence of the differentiation cocktail (Figure 5F,G, respectively), indicating that independent pathways may be triggered by the CM and differentiation cocktail.

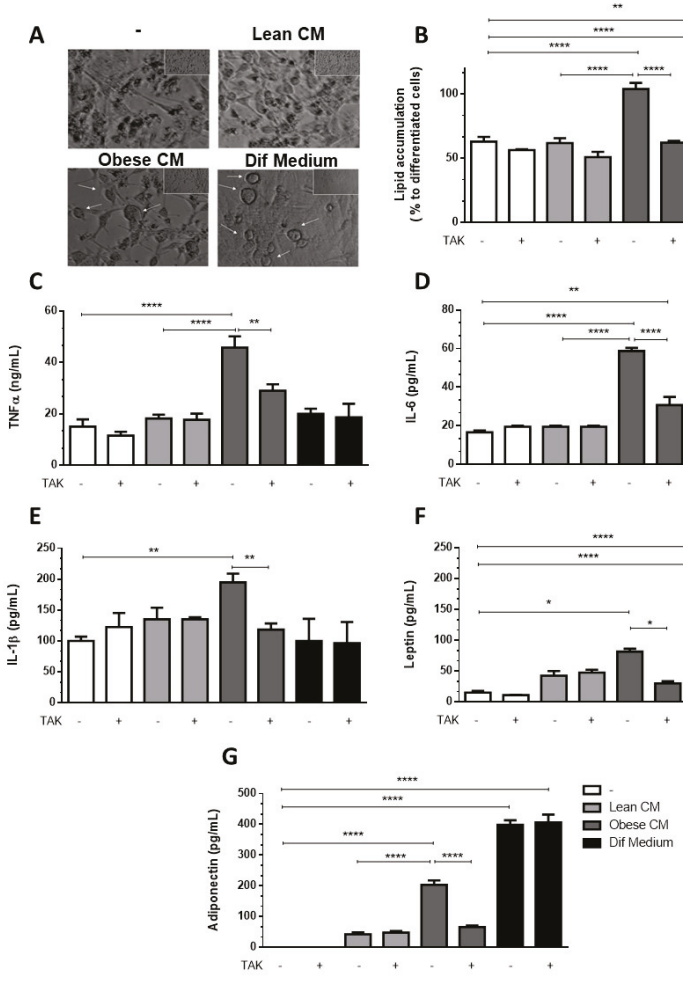

Figure 5. 3T3-L1 cells were left untreated or were pre-incubated with TAK-242 (TAK) 1 μM for 15 min, at 37 °C/5% CO_2. After pre-treatment, 3T3-L1 cells were treated or not with Lean Conditioned Medium (CM), Obese Conditioned Medium, or differentiation mix. After seven days, the images were registered in an optical microscope (**A**) or lipid were stained with Oil red O which was quantified in a plate cell reader (**B**). D-H. After six days the medium was removed, and cells were incubated with DMEM 1% FBS, for 24 h (to complete seven days). TNFα (**C**), IL-6 (**D**), IL-1β (**E**), leptin (**F**), and adiponectin (**G**) were measured in supernatants using a sandwich enzyme-linked immunosorbent assay kit. Results are representative of three independent experiments. B-H. Data are expressed as means ± SEM. * Represents $p < 0.05$, ** represents $p < 0.01$, **** represents $p < 0.001$.

4. Discussion

Inflammation due to dysfunctional AT is a central process involved in the etiopathogenesis of obesity as a hallmark of various metabolic syndrome-associated chronic pathologies [25].

Here, we provide evidence of how the secretion released by obese AT act directly (in a paracrine/autocrine manner) in establishing inflammation on preadipocytes. It should be noted that 15–50% of the cells in AT are preadipocytes [5], which, in obesity, can express increased proinflammatory protein levels [26]. Furthermore, they play a role in the release of inflammatory adipokines involved in the pathogenesis of obesity [27]. Preadipocytes have an inflammatory nature; they became inflamed in response to stimuli such as LPS [28,29] and factors secreted by macrophages [30,31]. Despite evidence that saturated FFAs give rise to inflammation in AT, the contribution of preadipocytes to this effect has yet to be elucidated. Dordevic et al. demonstrated that the FFA exposure for 2 h induced an inflammatory gene expression response, leading to MCP-1 release by preadipocytes [32]. This is an interesting study; however, their study does not mimic the whole pathophysiological process established in obese AT, given the fact that both saturated and unsaturated FFAs are released by obese AT and act in a paracrine manner. Palmitate, oleate, and linoleate are described as the most common FFAs in human fat tissue [5]. Here, we demonstrated that the AT of obese mice releases a wide range of FFAs, such as myristic, palmitic, linoleic, oleic, stearic, and arachidonic acids. Thus, it is crucial to observe the effect of this secretion on the inflammatory profile of preadipocytes. Some studies have already demonstrated the role of some FFAs acting individually on preadipocytes; however, as "adipogenic" cocktails, they do not reflect the conditions in which enlarged fat tissues exist. Guo et al. demonstrated that palmitate increases apoptosis in 3T3-L1 preadipocytes, which is attenuated by the co-treatment with unsaturated fatty acids (oleate and linoleate) [5]. Herein, we aimed to mimic the synergistic pathophysiological role triggered by the total FFAs together with the adipokines released by obese AT on preadipocytes.

Studies have demonstrated that NF-kB activation has a role to play in the inflammatory processes in 3T3-L1 preadipocytes. Moreover, NF-kB is a key molecule of the TLR4 signaling pathway. Once we had established that FFAs can activate TLR4, we examined the NF-kB activation in 3T3-L1 preadipocytes after treatment with the CM derived from obese AT. The results showed that the CM derived from obese AT, which contains several saturated and unsaturated FFAs, enhances the NF-kB activation to the same extent as the TLR4 agonist LPS. This effect was blocked when the cells were pretreated with TAK, demonstrating the pivotal role of TLR4 in this process. TLR4 mediates lipid-induced insulin resistance, even though some studies on TLR4-deficient mouse models report controversial results, and TLR4 seems to play an essential role in AT inflammation and insulin sensitivity [33]. Accordingly, it was demonstrated that deletion of the TLR4 gene protects mice from diet-induced insulin resistance, despite an increase in weight gain compared to the control [13]. In contrast, a study conducted in C3H/HeJ mice, which have a spontaneous TLR4 loss-of-function mutation, demonstrated that these mice are protected from diet-induced insulin resistance and weight gain [34]. Similarly, TLR4 mediates ceramide-mediated insulin resistance [35] and inhibition of TLR4 eliminates oxidative stress induced by palmitic acid in endothelial cells [36]. Since these studies used total body knockout or mutant mice, it was not clear whether it was TLR4 on hematopoietic cells or in the AT that promoted the development of insulin resistance. Conversely, a study demonstrated that total body TLR4 knockout or the deletion of TLR4 in non-hematopoietic or hematopoietic cells further enhanced insulin resistance [37]. In our study, the mRNA expression of TLR4 was 4.6-fold higher in preadipocytes treated with the CM derived from obese AT than in the preadipocytes treated with the CM derived from lean AT (Figure S3).

We demonstrated that preadipocytes stimulated with 20% of the CM derived from obese AT presented increased ROS production, which was eliminated by the pre-treatment with TAK, reinforcing the role of TLR4 in the impaired response of preadipocytes in the obese AT milieu. The use of 20% of CM is capable of triggering responses in both primary [16] and immortalized cells [38]. Despite the action of inflammatory cytokines in increasing oxidative stress in obese AT [39], we suggest that the combination of proinflammatory cytokines with FFAs increases ROS observed in obese AT.

Asehnoune et al. demonstrated that events in TLR4 signaling are ROS dependent, indicating that ROS can modulate NF-kB-dependent transcription via TLR4-mediated responses [40]. Long-chain saturated fatty acids such as palmitic, stearic, and lauric acids are capable of stimulating an inflammatory response through the TLR4 signaling pathway [41,42]. However, according to Lancaster et al., TLR4 is not a receptor for palmitic acid; nevertheless, despite not being a TLR4 agonist, its signaling is TLR4 dependent [43]. Here, we demonstrated that several FFAs are released by obese AT, and considering that both ROS production and NF-kB activation were prevented when TLR4 signaling was blocked in 3T3-L1 cells, we reiterate the pivotal role of TLR4 under the inflammatory response in preadipocytes in an obese milieu. Our results further demonstrated that TLR4-dependent signaling is needed to increase the release of IL-1β, IL-6, and TNF-α by preadipocytes stimulated with the CM derived from obese AT.

This study has some limitations. Despite the wide applicability and reliability of 3T3-L1 cells as an in vitro model of adipogenesis, not all signaling pathways are shared with primary preadipocytes. Palmitate itself was not able to induce adipogenic genes in preadipocytes without adipogenic stimuli [5]. FFAs and peroxisome proliferators do not act alone but induce adipogenesis by a shared mechanism, acting synergistically with other inducers to activate adipocyte differentiation [44]. Our results demonstrated that stimulation of preadipocytes with the CM from obese AT induces an increase in C/EBPα levels, as well as leptin and adiponectin release in preadipocytes. We believe that this increase in adipogenic transcription factors is because the CM derived from obese AT is rich in FFAs, which are structurally similar to peroxisome proliferators. Our results strongly suggest that most of the effects observed here were attributable to FFAs, as the denaturation of proteins and the blockade of LPS action with polymyxin induced no changes in lipid accumulation (Figure S2A). However, we cannot rule out that the CM has other participants that may be involved in these processes. Different studies have shown that the obese adipose tissue is capable of releasing adipokines with inflammatory properties [2,4,6,16], which could induce a proinflammatory profile in 3T3-L1 or amplify the FFA effects.

Our data suggest that the secretions released by obese AT act through TLR4, increasing NF-kB activity and proinflammatory factors in preadipocytes. Short-term HFD may trigger an acute inflammatory response in AT since it was demonstrated that within three days of HFD feeding, the inflammatory responses are altered in AT [45]. However, macrophages were not crucial in this initial acute inflammatory response as the depletion of macrophages with clodronate did not affect insulin sensitivity in a rodent model of HFD [41]. These results strongly suggest that non-esterified fatty acids are potentially taken up by other cell types in the near vicinity of mature adipocytes, including preadipocytes. Some studies have shown that FFAs induce NF-kB in adipocytes [18,19]. In contrast, Cullberg et al. found neither pro- nor anti-inflammatory effects of different FFAs in 3T3-L1 adipocytes [46].

Limited data are available on the differences in inflammatory cytokine expression and activation of NF-κB signaling in preadipocytes, compared with mature adipocytes, following exposure to FFAs, and there are no data showing the paracrine effects of obese AT secretion on preadipocytes. Thus, we propose that inflamed preadipocytes may sustain and exacerbate the low-grade inflammation in obese AT. Recently, Kumar et al. demonstrated that macrophages can be modulated in vitro, by using the CM of senescent or proliferative preadipocytes. While the treatment of proliferative preadipocytes with CM upregulated arginase-1 and mannose receptor genes toward an M2 phenotype, a suppression of these genes was observed when macrophages were cultured in the presence of secretory metabolites of senescent preadipocytes [47]. Preadipocytes from omental fat depots, which possess a high inflammatory profile, induce more monocyte/macrophage infiltration than those from subcutaneous AT [48]. In addition to the inflammatory profile assumed by preadipocytes, we observed an increase in adipogenic transcription factors such as C/EBPα after treatment (for 48 h) with the CM derived from obese AT. These results, together with the increased accumulation of lipids and release of leptin and adiponectin, suggest that these cells differentiated into adipocytes. It is known that adipogenesis is a healthier process than hypertrophy of adipocytes [18,49,50]; however, adipogenesis can lead to inflammation and the release of dangerous FFAs [51]. We observed that even though the

CM derived from obese AT induces adipogenesis, these cells are able to secrete increased levels of proinflammatory cytokines TNF-α, IL-6, IL-1β, and leptin in a TLR4-dependent manner, showing that the CM derived from obese AT induces inflammation in preadipocytes, which remains even after differentiation. Our results demonstrated that lipid accumulation in preadipocytes is diminished when cells are pretreated with the antioxidant Trolox (Figure S2B), corroborating the pro-oxidant effects of the obese AT milieu. However, we also observed that seven days after treatment, the differentiated preadipocytes also release increased levels of adiponectin, an anti-inflammatory adipokine [52]. Nevertheless, differentiated adipocytes stimulated with FFAs (oleic, palmitic, palmitoleic, and stearic acids) release increased levels of adiponectin [19,53].

In conclusion, our results demonstrate that in the CM derived from obese AT act in a combined paracrine/autocrine manner inducing inflammation in preadipocytes via increased TLR4 signaling and ROS production, thus creating a paracrine loop, which facilitates the differentiation of preadipocytes to adipocytes with a proinflammatory profile (Figure 6).

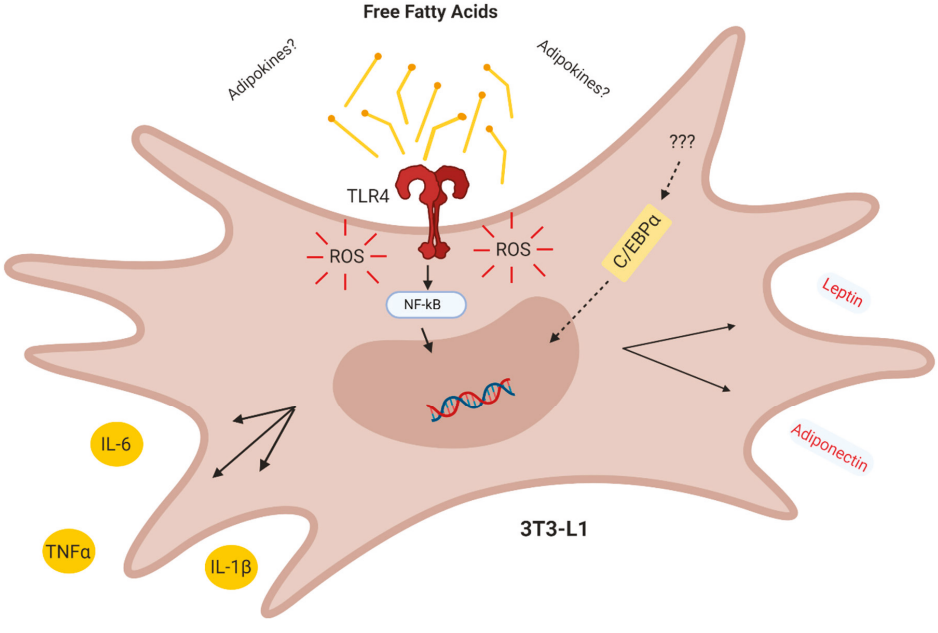

Figure 6. Conclusion. The obese adipose tissue secretes lipokines which act in a combined paracrine/autocrine manner inducing inflammation in preadipocytes via TLR4 and increased ROS, thus creating a paracrine loop which facilitates the differentiation of adipocytes with a proinflammatory profile.

Supplementary Materials: The following are available online at http://www.mdpi.com/2072-6643/12/9/2828/s1, Figure S1: 3T3-L1 cells were treated or not with Lean Conditioned Medium (CM), Obese CM, LPS 1 μg/mL or DMEM 10% FBS at 37 °C/5% CO_2. Figure S2: 3T3-L1 cells were left untreated or were pre-incubated with A. Polymyxin or B. Trollox 100 μM at 37 °C/5% CO_2. Figure S3: 3T3-L1 cells were treated or not with Lean Conditioned Medium (CM), Obese CM or LPS 1 μg/mL for 24 h at 37 °C/5% CO_2. Table S1: Composition of the diets.

Author Contributions: Conceptualization, M.R.-M. and J.A.d.M.; methodology, M.R.-M., C.M.-N., and G.C.A.; formal analysis, J.A.d.M., M.R.-M., and C.M.-N.; investigation, M.R.-M. and C.M.-N.; resources, J.A.d.M.; data curation, M.R.-M.; writing—original draft preparation, M.R.-M.; writing—review and editing, C.B.-F. and J.A.d.M.; visualization, C.B.-F.; supervision, J.A.d.M.; project administration, M.R.-M.; funding acquisition, J.A.d.M. All authors have read and agreed to the published version of the manuscript.

Funding: This research was funded by Coordenação de Aperfeiçoamento de Pessoal de Nível Superior (CAPES), Conselho Nacional de Desenvolvimento Científico e Tecnológico (CNPq), and Fundação de Amparo à Pesquisa do Estado do Rio de Janeiro (FAPERJ).

Acknowledgments: We thank Mileane S Busch for the technical support, and Biorender.com for figure editing.

Conflicts of Interest: The authors declare no conflict of interest.

References

1. Hotamisligil, G.S. Inflammation and Metabolic Disorders. *Nature* **2006**, *444*, 860–867. [CrossRef] [PubMed]
2. Weisberg, S.P.; McCann, D.; Desai, M.; Rosenbaum, M.; Leibel, R.L.; Ferrante, A.W., Jr. Obesity Is Associated with Macrophage Accumulation in Adipose Tissue. *J. Clin. Investig.* **2003**, *112*, 1796–1808. [CrossRef] [PubMed]
3. Xu, H.; Barnes, G.T.; Yang, Q.; Tan, G.; Yang, D.; Chou, C.J.; Sole, J.; Nichols, A.; Ross, J.S.; Tartaglia, L.A.; et al. Chronic Inflammation in Fat Plays a Crucial Role in the Development of Obesity-Related Insulin Resistance. *J. Clin. Investig.* **2003**, *112*, 1821–1830. [CrossRef]
4. Blüher, M. Adipose Tissue Dysfunction in Obesity. *Exp. Clin. Endocrinol. Diabetes.* **2009**, *117*, 241–250. [CrossRef] [PubMed]
5. Guo, W.; Wong, S.; Xie, W.; Lei, T.; Luo, Z. Palmitate Modulates Intracellular Signaling, Induces Endoplasmic Reticulum Stress, and Causes Apoptosis in Mouse 3t3-l1 and Rat Primary Preadipocytes. *Am. J. Physiol. Endocrinol. Metab.* **2007**, *293*, E576–E586. [CrossRef] [PubMed]
6. Makki, K.P.; Wolowczuk, I. Adipose Tissue in Obesity-Related Inflammation and Insulin Resistance: Cells, Cytokines, and Chemokines. *ISRN Inflamm.* **2013**, 139239. [CrossRef]
7. Bartelt, A.; Merkel, M.; Heeren, J. A New, Powerful Player in Lipoprotein Metabolism: Brown Adipose Tissue. *J. Mol. Med.* **2012**, *90*, 887–893. [CrossRef]
8. Bjorntorp, P.; Bergman, H.; Varnauskas, E. Plasma Free Fatty Acid Turnover in Obesity. *Acta Med. Scand.* **1969**, *185*, 351–356. [CrossRef]
9. Karpe, F.; Dickmann, J.R.; Frayn, K.N. Fatty Acids, Obesity, and Insulin Resistance: Time for a Reevaluation. *Diabetes* **2011**, *60*, 2441–2449. [CrossRef]
10. Ferrante, A.W., Jr. Obesity-induced inflammation: A metabolic dialogue in the language of inflammation. *J. Intern. Med.* **2007**, *262*, 408–414. [CrossRef]
11. Carlsen, H.; Haugen, F.; Zadelaar, S.; Kleemann, R.; Kooistra, T.; Drevon, C.A.; Blomhoff, R. Diet-Induced Obesity Increases NF-κB Signaling in Reporter Mice. *Genes Nutr.* **2009**, *4*, 215–222. [CrossRef] [PubMed]
12. Dasu, M.R.; Jialal, I. Free fatty acids in the presence of high glucose amplify monocyte inflammation via Toll-like receptors. *Am. J. Physiol. Endocrinol. Metab.* **2011**, *300*, E145–E154. [CrossRef] [PubMed]
13. Shi, H.; Kokoeva, M.V.; Inouye, K.; Tzameli, I.; Yin, H.; Flier, J.S. TLR4 links innate immunity and fatty acid-induced insulin resistance. *J. Clin. Investig.* **2006**, *116*, 3015–3025. [CrossRef] [PubMed]
14. Kim, J.K.; Kim, Y.J.; Fillmore, J.J.; Chen, Y.; Moore, I.; Lee, J.; Yuan, M.; Li, Z.W.; Karin, M.; Perret, P.; et al. Prevention of fat-induced insulin resistance by salicylate. *J. Clin. Investig.* **2001**, *108*, 437–446. [CrossRef] [PubMed]
15. Yuan, M.; Konstantopoulos, N.; Lee, J.; Hansen, L.; Li, Z.W.; Karin, M.; Shoelson, S.E. Reversal of obesity- and diet-induced insulin resistance with salicylates or targeted disruption of Ikkbeta. *Science* **2001**, *293*, 1673–1677. [CrossRef]
16. Renovato-Martins, M.; Matheus, M.E.; de Andrade, I.R.; Moraes, J.A.; da Silva, S.V.; Citelli dos Reis, M.; de Souza, A.A.; Bouskela, E.; Barja-Fidalgo, C. Microparticles derived from obese adipose tissue elicit a pro-inflammatory phenotype of CD16 +, CCR5 + and TLR8 + monocytes. *Biochim. Biophys. Acta Mol. Bas. Dis.* **2017**, *1863*, 139–151. [CrossRef]
17. Christie, W.W. *Gas Chromatography and Lipids: A Practical Guide. Bridgwater*; The Oily Press Ltd.: Dundee, Scotland, UK, 1989.
18. Han, C.J.; Kargi, A.Y.; Omer, M.; Chan, C.K.; Wabitsch, M.; O'Brien, K.D.; Wight, T.N.; Chait, A. Differential effect of saturated and unsaturated free fatty acids on the generation of monocyte adhesion and chemotactic factors by adipocytes: Dissociation of adipocyte hypertrophy from inflammation. *Diabetes* **2010**, *59*, 386–396. [CrossRef]

19. Schaeffler, A.; Gross, P.; Buettner, R.; Bollheimer, C.; Buechler, C.; Neumeier, M.; Kopp, A.; Schoelmerich, J.; Falk, W. Fatty acid-induced induction of Toll-like receptor-4/nuclear factor-kappaB pathway in adipocytes links nutritional signalling with innate immunity. *Immunology* **2009**, *126*, 233–245. [CrossRef]
20. Palmer, J.D.; Rifkind, D. Neutralization of the hemodynamic effects of endotoxin by polymyxin B. *Surg. Gynecol. Obs.* **1974**, *138*, 755–759.
21. Lindemann, R.A. Bacterial activation of human natural killer cells: Role of cell surface lipopolysaccharide. *Infect. Immun.* **1988**, *56*, 1301–1308. [CrossRef]
22. Longo, M.; Zatterale, F.; Naderi, J.; Parrillo, L.; Formisano, P.; Alexander, G.; Beguinot, F.; Miele, C. Adipose Tissue Dysfunction as Determinant of Obesity-Associated Metabolic Complications. *Int. J. Mol. Sci.* **2019**, *20*, 2358. [CrossRef] [PubMed]
23. MacDougald, A.O.; Lane, M.D. Transcriptional regulation of gene expression during adipocyte differentiation. *Annu. Rev. Biochem.* **1995**, *64*, 345–373. [CrossRef]
24. Madsen, L.; Petersen, R.K.; Kristiansen, K. Regulation of adipocytes differentiation and function by polyunsaturated fatty acids. *Biochim. Biophys. Acta* **2005**, *1740*, 266–286. [CrossRef] [PubMed]
25. Unamuno, X.; Gómez-Ambrosi, J.; Rodríguez, A.; Becerril, S.; Frühbeck, G.; Catalán, V. Adipokine dysregulation and adipose tissue inflammation in human obesity. *Eur. J. Clin. Investig.* **2018**, e1299. [CrossRef] [PubMed]
26. Cousin, B.; André, M.; Casteilla, L.; Pénicaud, L. Altered macrophage-like functions of preadipocytes in inflammation and genetic obesity. *J. Cell. Physiol.* **2001**, *186*, 380–386. [CrossRef]
27. O'Hara, A.; Lim, F.L.; Mazzattim, D.J. Trayhurn P Stimulation of inflammatory gene expression in human preadipocytes by macrophage-conditioned medium: Upregulation of IL-6 production by macrophage-derived IL-1beta. *Mol. Cell. Endocrinol.* **2012**, *349*, 239–247. [CrossRef]
28. Chung, S.; Lapoint, K.; Martinez, K.; Kennedy, A.; Boysen Sandberg, M.B.; McIntosh, M.K. Preadipocytes mediate lipopolysaccharide-induced inflammation and insulin resistance in primary cultures of newly differentiated human adipocytes. *Endocrinology* **2006**, *147*, 5340–5351. [CrossRef]
29. Poulain-Godefroy, O.; Froguel, P. Preadipocyte response and impairment of differentiation in an inflammatory environment. *Biochem. Biophys. Res. Commun.* **2007**, *356*, 662–667. [CrossRef]
30. Keophiphath, M.; Achard, V.; Henegar, C.; Rouault, C.; Clement, K.; Lacasa, D. Macrophage-secreted factors promote a profibrotic phenotype in human preadipocytes. *Mol. Endocrinol.* **2009**, *23*, 11–24. [CrossRef]
31. Lacasa, D.; Taleb, S.; Keophiphath, M.; Miranville, A.; Clement, K. Macrophage-secreted factors impair human adipogenesis: Involvement of proinflammatory state in preadipocytes. *Endocrinology* **2007**, *148*, 868–877. [CrossRef]
32. Dordevic, A.L.; Konstantopoulos, N.; Cameron-Smit, D. 3T3-L1 Preadipocytes Exhibit Heightened Monocyte-Chemoattractant Protein-1 Response to Acute Fatty Acid Exposure. *PLoS ONE* **2014**, *9*, e99382. [CrossRef] [PubMed]
33. Shengyi, S.; Yewei, J.; Sander, K.; Ling, Q. Mechanisms of Inflammatory Responses in Obese Adipose Tissue. *Annu. Rev. Nutr.* **2012**, *21*, 261–286.
34. Tsukumo, D.M.; Carvalho-Filho, M.A.; Carvalheira, J.B.; Prada, P.O.; Hirabara, S.M.; Schenka, A.A.; Araújo, E.P.; Vassallo, J.; Curi, R.; Velloso, L.A.; et al. Loss-of-function mutation in Toll-like receptor 4 prevents diet-induced obesity and insulin resistance. *Diabetes* **2007**, *56*, 1986–1998. [CrossRef] [PubMed]
35. Holland, W.L.; Bikman, B.T.; Wang, L.P.; Yuguang, G.; Sargent, K.M.; Bulchand, S.; Knotts, T.A.; Shui, G.; Clegg, D.J.; Wenk, M.R.; et al. Lipid-induced insulin resistance mediated by the proinflammatory receptor TLR4 requires saturated fatty acid-induced ceramide biosynthesis in mice. *J. Clin. Investig.* **2011**, *121*, 1858–1870. [CrossRef]
36. Kramer, B.; França, L.M.; Zhang, Y.; Paes, A.M.A.; Gerdes, A.M.; Carrillo-Sepulveda, M.A. Western diet triggres toll-like receptor 4 signaling -induces endothelial discfunction in female Wistar rats. *Am. J. Physiol. Heart Circ. Physiol.* **2018**, *315*, H1735–H1747. [CrossRef]
37. Orr, J.S.; Puglisi, M.J.; Ellacott, K.L.; Lumeng, C.N.; Wasserman, D.H.; Hasty, A.H. Toll-like receptor 4 deficiency promotes the alternative activation of adipose tissue macrophages. *Diabetes* **2012**, *61*, 2718–2727. [CrossRef]
38. Ramos-Andrade, I.; Moraes, J.; Brandão-Costa, R.M.; Vargas da Silva, S.; de Souza, A.; da Silva, C.; Renovato-Martins, M.; Barja-Fidalgo, C. Obese adipose tissue extracellular vesicles raise breast cancer cell malignancy. *Endocr. Relat. Cancer* **2020**, *27*, 571–582. [CrossRef]

39. Hauck, A.K.; Huang, Y.; Hertzel, A.V.; Bernlohr, D.A. Adipose oxidative stress and protein carbonylation. *J. Biol. Chem.* **2019**, *294*, 1083–1088. [CrossRef]
40. Asehnoune, K.; Strassheim, D.; Mitra, S.; Kim, J.Y.; Abraham, E. Involvement of Reactive Oxygen Species in Toll-Like Receptor 4-Dependent Activation of NF-κB. *J. Immunol.* **2004**, *172*, 2522–2529. [CrossRef]
41. Lee, Y.S.; Li, P.; Huh, J.Y.; Hwang, I.J.; Lu, M.; Kim, J.I.; Ham, M.; Talukdar, S.; Chen, A.; Lu, W.J.; et al. Inflammation is necessary for long-term but not short-term high-fat diet-induced insulin resistance. *Diabetes* **2011**, *60*, 2474–2483. [CrossRef]
42. Hwang, D.H.; Kim, J.A.; Lee, J.Y. Mechanisms for the activation of Toll-like receptor 2/4 by saturated fatty acids and inhibition by docosahexaenoic acid. *Eur. J. Pharmacol.* **2016**, *785*, 24–35. [CrossRef] [PubMed]
43. Lancaster, G.I.; Langley, K.G.; Berglund, N.A.; Kammoun, H.L.; Reibe, S.; Estevez, E.; Weir, J.; Mellett, N.A.; Pernes, G.; Conway, J.R.W.; et al. Evidence that TLR4 is not a receptor for saturated fatty acids but mediates lipid-induced inflammation by reprogramming macrophage metabolism. *Cell Metab.* **2018**, *27*, 1096–1110. [CrossRef] [PubMed]
44. Mac Dougald, O.A.; Lane, M.D. When precursors are also regulators. *Curr. Biol.* **1995**, *5*, 618–621. [CrossRef]
45. Kleemann, R.; van Erk, M.; Verschuren, L.; van den Hoek, A.M.; Koek, M.; Wielinga, P.Y.; Jie, A.; Pellis, L.; Bobeldijk-Pastorova, I.; Kelder, T.; et al. Time-resolved and tissue-specific systems analysis of the pathogenesis of insulin resistance. *PLoS ONE* **2010**, *21*, e8817. [CrossRef]
46. Cullberg, K.B.; Larsen, J.Ø.; Pedersen, S.B.; Richelsen, B. Effects of LPS and dietary free fatty acids on MCP-1 in 3T3-L1 adipocytes and macrophages in vitro. *Nutr. Diabetes* **2014**, *4*, e113. [CrossRef]
47. Kumar, R.; Sharma, A.; Padwad, Y.; Sharma, R. Preadipocyte secretory factors differentially modulate murine macrophage functions during aging which are reversed by the application of phytochemical EGCG. *Biogerontology* **2020**, *21*, 325–343. [CrossRef]
48. Zhu, Y.; Tchkoniam, T.; Stout, M.B.; Giorgadze, N.; Wang, L.; Li, P.W.; Heppelmann, C.J.; Bouloumié, A.; Jensenm, M.D.; Bergen, H.R., 3rd; et al. Inflammation and the Depot-Specific Secretome of Human Preadipocytes. *Obesity* **2015**, *23*, 989–999. [CrossRef]
49. McLaughlin, T.; Craig, C.; Liu, L.F.; Perelman, D.; Allister, C.; Spielman, D.; Cushman, S.W. Adipose Cell Size and Regional Fat Deposition as Predictors of Metabolic Response to Overfeeding in Insulin-Resistant and Insulin-Sensitive Humans. *Diabetes* **2016**, *65*, 1245–1254. [CrossRef]
50. Woo, C.H.; Jang, J.E.; Lee, S.E.; Koh, E.H.; Lee, K.U. Mitochondrial Dysfunction in Adipocytes as a Primary Cause of Adipose Tissue Inflammation. *Diabetes Metab.* **2019**, *43*, 247–256. [CrossRef]
51. El Hafidi, M.; Buelna-Chontal, M.; Sánchez-Muñoz, F.; Carbó, R. Adipogenesis: A Necessary but Harmful Strategy. *Int. J. Mol. Sci.* **2019**, *20*, 3657. [CrossRef]
52. Frühbeck, G.; Catalán, V.; Rodríguez, A.; Gómez-Ambrosi, J. Adiponectin-leptin ratio: A promising index to estimate adipose tissue dysfunction. Relation with obesity-associated cardiometabolic risk. *Adipocyte* **2018**, *7*, 57–62. [CrossRef] [PubMed]
53. Kadowaki, T.; Yamauchi, T.; Kubota, N.; Hara, K.; Ueki, K.; Tobe, K. Adiponectin and adiponectin receptors in insulin resistance, diabetes, and the metabolic syndrome. *J. Clin. Investig.* **2006**, *116*, 1784–1792. [CrossRef] [PubMed]

nutrients

MDPI

Article

Beneficial Role of Replacing Dietary Saturated Fatty Acids with Polyunsaturated Fatty Acids in the Prevention of Sarcopenia: Findings from the NU-AGE Cohort

Diego Montiel-Rojas [1,†], Aurelia Santoro [2,3,†], Andreas Nilsson [1,*], Claudio Franceschi [2,4], Miriam Capri [2,3], Alberto Bazzocchi [5], Giuseppe Battista [2], Lisette C. P. G. M. de Groot [6], Edith J. M. Feskens [6], Agnes A. M. Berendsen [6], Agata Bialecka-Debek [7], Olga Surala [7], Barbara Pietruszka [7], Susan Fairweather-Tait [8], Amy Jennings [8], Frederic Capel [9] and Fawzi Kadi [1]

1 School of Health Sciences, Örebro University, 702 81 Örebro, Sweden; diego.montiel@oru.se (D.M.-R.); fawzi.kadi@oru.se (F.K.)
2 Department of Experimental, Diagnostic and Specialty Medicine, Alma Mater Studiorum, University of Bologna, 40138 Bologna, Italy; aurelia.santoro@unibo.it (A.S.); claudio.franceschi@unibo.it (C.F.); miriam.capri@unibo.it (M.C.); g.battista@unibo.it (G.B.)
3 Alma Mater Research Institute on Global Challenges and Climate Change (Alma Climate), University of Bologna, 40126 Bologna, Italy
4 Department of Applied Mathematics, Institute of Information Technology, Mathematics and Mechanics (ITMM), Lobachevsky State University of Nizhny Novgorod-National Research University (UNN), Nizhny Novgorod 603950, Russia
5 Diagnostic and Interventional Radiology, IRCCS Istituto Ortopedico Rizzoli, 40136 Bologna, Italy; alberto.bazzocchi@ior.it
6 Department of Human Nutrition and Health, Wageningen University, 6708WE Wageningen, The Netherlands; lisette.degroot@wur.nl (L.C.P.G.M.d.G.); edith.feskens@wur.nl (E.J.M.F.); agnes.berendsen@wur.nl (A.A.M.B.)
7 Department of Human Nutrition, Warsaw University of Life Sciences-SGGW, 02-776 Warsaw, Poland; agata_bialecka_debek@sggw.edu.pl (A.B.-D.); olga.surala@insp.waw.pl (O.S.); barbara_pietruszka@sggw.edu.pl (B.P.)
8 Norwich Medical School, University of East Anglia, Norwich NR4 7TJ, UK; S.Fairweather-Tait@uea.ac.uk (S.F.-T.); Amy.Jennings@uea.ac.uk (A.J.)
9 Unité de Nutrition Humaine (UNH), Institut National de Recherche pour L'agriculture, L'alimentation et L'environnement (INRAE), Université Clermont Auvergne, CRNH Auvergne, 63000 Clermont-Ferrand, France; frederic.capel@inrae.fr
* Correspondence: andreas.nilsson@oru.se; Tel.: +46-19-303553
† These authors contributed equally to this work.

Received: 8 September 2020; Accepted: 4 October 2020; Published: 9 October 2020

Abstract: Dietary fat subtypes may play an important role in the regulation of muscle mass and function during ageing. The aim of the present study was to determine the impact of isocaloric macronutrient substitutions, including different fat subtypes, on sarcopenia risk in older men and women, while accounting for physical activity (PA) and metabolic risk. A total of 986 participants, aged 65–79 years, completed a 7-day food record and wore an accelerometer for a week. A continuous sex-specific sarcopenia risk score (SRS), including skeletal muscle mass assessed by dual-energy X-ray absorptiometry (DXA) and handgrip strength, was derived. The impact of the isocaloric replacement of saturated fatty acids (SFAs) by either mono- (MUFAs) or poly-unsaturated (PUFAs) fatty acids on SRS was determined using regression analysis based on the whole sample and stratified by adherence to a recommended protein intake (1.1 g/BW). Isocaloric reduction of SFAs for the benefit of PUFAs was associated with a lower SRS in the whole population, and in those with a protein intake below 1.1 g/BW, after accounting for age, smoking habits, metabolic disturbances, and adherence to PA

guidelines. The present study highlighted the potential of promoting healthy diets with optimised fat subtype distribution in the prevention of sarcopenia in older adults.

Keywords: ageing; muscle mass; dietary fats; macronutrients; isocaloric substitution; muscle strength; physical activity; metabolic syndrome

1. Introduction

Population ageing is accompanied by an increased risk of sarcopenia, a chronic condition characterised by a loss of muscle mass and strength, and associated with several adverse outcomes, including physical disability and a poor quality of life [1,2]. Fortunately, the rate of muscle mass and function decline in older adults can be reduced by appropriate nutrition and physical activity behaviours, making these modifiable lifestyle behaviours important non-pharmacological approaches for the prevention of sarcopenia [3,4].

While nutritional habits have the potential of readily impacting sarcopenia risk, the complex relationship between macronutrient composition and the regulation of muscle health is not fully established. To date, a large number of studies has focused on adequate protein intake for the maintenance of muscle mass and function, where an intake of around 1.1 g/BW has been recommended for older adults [5]. In addition to proteins, it has been hypothesized that lipid intake in general, and fat subtypes in particular, may have further influence on age-related loss of muscle mass and function [6]. For example, it has been reported that a high dietary intake of saturated fatty acids (SFAs) may exacerbate the development of sarcopenia [7].

Alongside absolute intakes of single macronutrients, the isocaloric distribution of different macronutrients and their related subtypes likely influences the regulation of muscle mass and function in older adults [8,9]. Therefore, to disentangle the interactive effect of macronutrients on muscle health, isocaloric substitution models offer the opportunity to explore the effects on health outcomes of replacing one macronutrient with another, whilst keeping the remaining relative macronutrient intakes constant. This approach accounts for the fact that an isocaloric change of one macronutrient inevitably alters the relative intakes of other macronutrients. Based on isocaloric substitution models, associations with metabolic health outcomes were previously reported in relation to different macronutrient distributions [10–12], and the replacement of fatty acids by either carbohydrates or proteins has previously been linked to a lower cardiovascular disease incidence [13]. Currently, there are limited data on the impact of macronutrient replacement on muscle mass and function in older adults, which is unfortunate considering the demographic shift accompanied by the increased prevalence of people with a physical disability. Importantly, given the existing protein intake recommendations for older adults, the impact of macronutrient replacement on muscle mass in older adults below and above this threshold is warranted. Notably, there is a well-established relationship between physical activity (PA) of at least moderate intensity and muscle quantity and quality. Therefore, to clarify the relationships between macronutrient distribution and muscle mass in older adults, the confounding effects of PA need also to be considered.

The aim of the present study was to explore the impact of isocaloric macronutrient substitutions, including different fat subtypes, on sarcopenia risk in a cohort of older European men and women from the NU-AGE study (New dietary strategies addressing the specific needs of elderly population for an healthy ageing in Europe).

2. Materials and Methods

2.1. Participants

The present study included 986 older men and women, aged 65–79 years, recruited within the frame of the NU-AGE project (Clinicaltrials.gov, NCT01754012) at baseline (April 2012–January 2014). A detailed description of the recruitment process and study design has been described elsewhere [14,15]. Participants fulfilling the frailty criteria [16], with a disability or overt disease at screening, were excluded. Local ethical approval was provided by the Independent Ethics Committee of the Sant'Orsola-Malpighi Hospital Bologna (Italy-03/2011/U/Sper), the National Research Ethics Committee East of England (UK-12/EE/0109), the Wageningen University Medical Ethics Committee (Netherlands-11/41 NU-AGE), and the Bioethics Committee of the Polish National Food and Nutrition Institute (Poland). Written informed consent was obtained, and the study was conducted in accordance with the standards set by the Declaration of Helsinki.

2.2. Dietary Intake

Dietary intake was assessed using a food record as previously described [14,17]. Participants completed a 7-day food record and had an interview with a trained dietician/research nutritionist to review the records. Consumed foods were coded according to standardised procedures and translated into nutrients by the use of software exploiting local food composition tables [14,17,18]. Macronutrient intakes of carbohydrates, proteins, and fats, including saturated fatty acids (SFAs), monounsaturated fatty acids (MUFAs), and polyunsaturated fatty acids (PUFAs), were derived. Energy intake from macronutrients was normalised against body weight (kcal/BW).

2.3. Body Composition

Height and weight were measured using standardised procedures, and body composition was assessed using dual-energy X-ray absorptiometry (DXA), as described previously [19,20]. DXA scans were performed by trained personnel. The analytical program defined six corporeal regions, where total and regional fat and lean masses were derived. Skeletal muscle mass index (SMI, %) was calculated as previously described [19–22].

2.4. Handgrip Strength and Physical Limitations

Handgrip strength, adjusted by body weight, was determined with a Jamar handheld dynamometer (Patterson Medical, Warrenville, IL, United States) using standardised procedures. Participants were also classified as having or not having physical function (PF) limitations by the 10-item PF subscale of the 36-item Short Form Health Survey (SF-36) [23], as described elsewhere [24].

2.5. Sarcopenia Risk Score

A continuous clustered sarcopenia risk score (SRS) was created based on SMI and handgrip strength, according to the most recent operational definition of sarcopenia [1]. First, sex-specific standardised values of SMI and handgrip strength were calculated and averaged into composite z-scores, where higher scores indicated a higher sarcopenia risk.

2.6. Adherence to Physical Activity Guidelines

Time spent in moderate-to-vigorous PA (MVPA) was assessed using a waist-worn Actigraph accelerometer (GT3x activity monitor, Actigraph, Pensacola, FL, USA) for a week. As previously described [25], the monitor had to be worn for at least 4 days, with at least 10 h per day for inclusion, and non-wear time was defined as 60 min of continuous zero counts. The count cut-point used to determine MVPA time was based on previous work [26]. Adherence to PA guidelines (≥150 weekly minutes of MVPA) was approximated to a daily average of ≥22 min in MVPA.

2.7. Assessment of Metabolic Risk

Participants were classified as with or without metabolic syndrome (MetS) based on sex-specific definitions set by the International Diabetes Federation [27]. In brief, waist circumference (WC) was determined at the midpoint between the iliac crest and lower costal margin to the nearest 0.1 cm. Systolic and diastolic blood pressures were assessed using an automated electronic blood pressure monitor as previously described [20]. All biochemical analyses, including blood glucose and blood lipids (triglycerides, high-density lipoprotein (HDL) and low-density lipoprotein (LDL) cholesterol), were performed in one centre based on standard methodologies.

2.8. Statistical Analysis

The data are presented as arithmetic mean and standard deviation unless otherwise indicated. Differences between male and female participants were determined by either independent sample *t*-tests or chi-square tests. Partial correlation was used to investigate the relationship between macronutrient intake and SRS, adjusting for total energy intake. Linear regression modelling was used to assess the hypothetical change in SRS by an isocaloric replacement of macronutrients. First, the effects of altering macronutrient distribution were achieved by including the total energy intake together with energy intakes from two macronutrients, while leaving out the third. Second, the effects of reducing intakes of SFAs were achieved by including energy from MUFAs and PUFAs, while keeping the remaining energy-providing nutrients unchanged. All models were adjusted by age, recruiting centre, smoking habit, fibre intake (g/day), the prevalence of MetS, and adherence to PA guidelines. Given the likely influence of protein intake on SRS, isocaloric substitution modelling of SFAs by other fat subtypes (MUFAs and PUFAs) was further stratified based on a protein intake of 1.1 g/BW. All assumptions behind regression analyses including normality, linearity, homoscedasticity, and multicollinearity were checked. Based on our sample size, a priori power calculation revealed that small-to-moderate effect sizes were detectable in SRS with a power of >80% and alpha set to 0.05. All analyses were conducted using SPSS, version 26.

3. Results

The general characteristics of the study population are presented in Table 1. Male participants had significantly higher handgrip strength and SMI compared to females (Table 1). Further, a significantly higher proportion of males adhered to PA guidelines, with a lower proportion reporting a physical function limitation compared to females (Table 1). There were no significant sex differences in body mass index (BMI), or MetS prevalence (Table 1).

Table 1. General characteristics of the study population.

	Total	Male	Female
n	986	417	569
Basic Characteristics			
Age (years)	71 ± 4	71 ± 4	71 ± 4
Weight (kg)	74.7 ± 13.4	82.4 ± 12	69.1 ± 11.3 *
Height (cm)	165 ± 9	173 ± 6	160 ± 7 *
BMI (kg/m^2)	27.0 ± 4.0	27.2 ± 3.7	26.8 ± 4.2
SMI (%)	27.0 ± 4.3	30.6 ± 3.2	24.4 ± 2.8 *
Full Education (years)	13 ± 4	13 ± 4	12 ± 3 *
Smoking (% never)	51.3	37.6	61.3 *
Medication (% yes)	77.6	77.5	77.7
PA Guidelines (% yes)	54.1	63.8	46.9 *
Physical Function			
Handgrip Strength (kg/BW)	0.42 ± 0.11	0.49 ± 0.09	0.38 ± 0.09 *
Physical Limitation (% yes)	33.8	22.1	42.4 *

Table 1. *Cont.*

	Total	Male	Female
Metabolic Risk Factors			
MetS (% yes)	41.7	44.6	39.5
Waist Circumference (cm)	92.4 ± 11.7	98.0 ± 10.6	88.3 ± 10.8 *
SBP (mmHg)	140 ± 20	141 ± 18	139 ± 21
DBP (mmHg)	75 ± 11	77 ± 10	74 ± 11 *
Glucose (mmol/L)	5.57 ± 0.83	5.75 ± 0.94	5.43 ± 0.71 *
Triglycerides (mmol/L)	1.07 ± 0.47	1.08 ± 0.49	1.06 ± 0.45
HDL-cholesterol (mmol/L)	1.53 ± 0.47	1.32 ± 0.36	1.71 ± 0.47 *
LDL-cholesterol (mmol/L)	3.31 ± 0.96	3.13 ± 0.93	3.47 ± 0.98 *

Continuous data are expressed as mean ± SD, or are otherwise indicated. BMI: body mass index; SMI: skeletal muscle mass index; BW: body weight; PA: physical activity; MetS: metabolic syndrome; DBP: diastolic blood pressure; SBP: systolic blood pressure; HDL: high-density lipoprotein; LDL, low-density lipoprotein. * $p < 0.05$ vs. male.

Total energy intake in the whole population was 1809 ± 419 kcal/day (Table 2), with an average of 49% of energy derived (E%) from carbohydrates, 17 E% from protein, and 31 E% from fat (12 E%, 13 E%, and 6 E% for SFAs, MUFAs, and PUFAs, respectively). After adjustment by body weight, total energy and carbohydrate intake were significantly higher in the male participants ($p < 0.05$), whereas no corresponding differences were observed for protein, total fat, or its subtypes. Approximately two-thirds (66%) of all participants had a protein intake less than 1.1 g/BW, and 75% had an energy intake of SFAs above 10 E%.

Table 2. Daily energy and macronutrient intake of the study population.

	Total	Male	Female
n	986	417	569
Nutritional Intake			
Total Energy (kcal)	1809 ± 419	2037 ± 433	1642 ± 319 *
Carbohydrates (g)	221.1 ± 61.5	250.0 ± 66.6	200.0 ± 47.6 *
Fat (g)	62.7 ± 19.1	69.4 ± 20.4	57.8 ± 16.4 *
SFAs (g)	24.9 ± 9.4	27.1 ± 10.0	23.3 ± 8.7 *
MUFAs (g)	26.1 ± 8.4	29.5 ± 9.2	23.7 ± 6.9 *
PUFAs (g)	11.7 ± 5.1	12.8 ± 5.4	10.8 ± 4.7 *
Protein (g)	74.5 ± 17.7	82.1 ± 19.2	68.9 ± 14.2 *

Continuous data are expressed as mean ± SD. SFAs: saturated fatty acids; MUFAs: monounsaturated fatty acids; PUFAs: polyunsaturated fatty acids. * $p < 0.05$ vs. male.

Partial correlation analysis showed inverse associations between energy intake from all macronutrients and SRS ($p < 0.05$), after controlling for total energy intake.

Isocaloric substitution models showed that replacing total fat by a given amount of either protein or carbohydrates was significantly associated with a reduced risk of sarcopenia (Table 3). However, an isocaloric substitution of total carbohydrates by protein was not associated with SRS (β-Coeff. −0.037, 95% CI (−0.108 to 0.034), $p = 0.305$).

Table 3. Effect of isocaloric substitution of fat with either protein or carbohydrates on sarcopenia risk score in older European adults.

	Sarcopenia Risk Score		
Model	**β-Coeff.**	**95% CI**	***p*-Value**
Protein	−0.077	−0.152 to −0.003	0.042
Carbohydrates	−0.040	−0.07 to −0.008	0.015

CI: confidence interval. Substitution model contains total energy intake (Kcal/BW), protein intake (Kcal/BW), carbohydrates intake (Kcal/BW), alcohol intake (Kcal/BW), and fibre intake (g/day). Models were additionally adjusted for age, recruiting centre, smoking habits, meeting the recommendations of physical activity (yes/no), and prevalence of metabolic syndrome (yes/no). Estimates were interpreted as the association of the SRS with a 1 Kcal/BW increase of the substituent macronutrients (protein or carbohydrates) to the detriment of fat, while keeping the remaining constant. Analysed based on n = 986.

Further analysis revealed a reduced SRS when replacing SFAs by PUFAs in isocaloric models, whereas no corresponding effect was evident when substituting SFAs by MUFAs (Table 4). Additionally, we sought to investigate whether meeting the recommended daily amount of 1.1 g/BW of protein may alter the associations between SRS and the distribution of fat subtypes. Interestingly, an isocaloric substitution of SFAs by PUFAs resulted in lower SRS only in participants with a protein intake below 1.1 g/BW (Table 4).

Table 4. Effect of the isocaloric substitution of saturated fatty acids by unsaturated fatty acids on sarcopenia risk score in the whole population of older European adults and stratified by meeting the recommendation of 1.1 g/BW of protein intake.

	Sarcopenia Risk Score		
Model	**β-Coeff.**	**95% CI**	***p*-Value**
Whole Population			
MUFAs	−0.012	−0.121 to 0.097	0.829
PUFAs	−0.152	−0.253 to −0.051	0.003
Protein Intake < 1.1 kg/BW			
MUFAs	−0.012	−0.168 to 0.144	0.879
PUFAs	−0.162	−0.303 to −0.020	0.025
Protein Intake ≥ 1.1 kg/BW			
MUFAs	−0.067	−0.227 to 0.094	0.417
PUFAs	−0.093	−0.241 to 0.056	0.221

CI: confidence interval; MUFAs: monounsaturated fatty acids; PUFAs: polyunsaturated fatty acids; BW: body weight. Substitution model contains total energy intake (Kcal/BW), protein intake (Kcal/BW), carbohydrates intake (Kcal/BW), MUFAs intake (Kcal/BW), PUFAs intake (Kcal/BW), alcohol intake (Kcal/BW), and fibre intake (g/day). Models were additionally adjusted for age, recruiting centre, smoking habits, meeting the recommendations of physical activity (yes/no), and prevalence of metabolic syndrome (yes/no). Estimates were interpreted as the association of the SRS with a 1 Kcal/BW increase of the substituent macronutrients (MUFAs or PUFAs) to the detriment of SFAs while keeping the remaining constant. Analysed based on n = 986.

4. Discussion

The present study highlighted the beneficial impact of replacing SFAs with PUFAs on the risk of sarcopenia in older European adults. This is of particular importance in older men and women with a protein intake below the recommended amount of 1.1 g/BW. Furthermore, the impact of dietary fat quality on sarcopenia risk was evident regardless of adherence to PA guidelines and metabolic risk status, which suggests that dietary fat quality plays a pivotal role in the prevention of sarcopenia in older adults.

Our study revealed that the replacement of total fat intake at the expense of other macronutrients is related to a lower sarcopenia risk. Recent reports have shown that high-fat diets are associated with an increased sarcopenia risk in ageing populations [28,29], suggesting that the distribution of fat subtypes may explain the increased sarcopenia risk. To test this hypothesis, we further analysed

the impact of the replacement of SFAs by either MUFAs or PUFAs on sarcopenic risk using isocaloric modelling. A major finding was that the replacement of SFAs with PUFAs, but not MUFAs, was related to a significant reduction in sarcopenia risk, which supports that the type of fat, as well as the relative distribution, should be emphasized in dietary strategies against sarcopenia progression. In accordance with our findings, previous studies investigating the influence of fat subtypes on single components of sarcopenia risk (e.g., muscle mass and function) showed that SFA intake is linked to a higher risk of functional impairment [30] and lower physical function [31]. Furthermore, positive associations of higher intakes of PUFA-rich food and muscle mass and function have been shown in a population of ≥60-year-old men and women [32,33]. At the cellular level, several molecular pathways leading to muscle wasting may explain the detrimental action of SFAs. For example, exposure of muscle cells to SFAs induced reduction in cell size and suppression in insulin signalling, together with an increased expression of pro-atrophic genes [34,35]. Another pathway by which SFAs may modulate muscle mass is their ability to downregulate the activity of key nutrient transporters, which can impair amino acid uptake and thus facilitate muscle mass loss [36]. In parallel, PUFAs may promote muscle hypertrophy through enhanced activation of the mammalian target of rapamycin (mTOR) growth pathway and downregulation of the pro-inflammatory mediator IL-1β [37,38]. To date, the effects of MUFAs on muscle mass and function are inconclusive. For instance, positive, negative, and no relationships were reported between intakes of MUFAs and indices of muscle health [6,30,39]. In light of our results and previous literature, further investigations including experimental designs are warranted.

Given the well-established role of adequate protein intake on the maintenance of muscle mass, we further investigated whether the impact of fat subtype distribution on sarcopenia risk is moderated by adherence to a recommended protein intake of 1.1 g/BW. Interestingly, while the detrimental impact of SFAs was suppressed in older men and women meeting the recommended intake, it was still observed at protein intakes below this quantity. In our sample of older European adults, approximately two-thirds had a protein intake below 1.1 g/BW, which is in line with a recent report on the prevalence of older adults with inadequate protein intake [40]. Thus, given that a substantial proportion of older adults do not consume recommended protein intakes, our findings strengthen the need to consider diets with favourable fat subtype distribution in order to reduce sarcopenia risk.

Together with healthy dietary patterns, PA is regarded as a key lifestyle factor that can readily have an impact on muscle mass and function, where 150 weekly minutes of MVPA is the guideline endorsed by major health organizations [41]. Therefore, adherence to this PA guideline should be considered when exploring diet-related health effects. The present study demonstrated that the detrimental impact of SFAs on sarcopenia risk is evident regardless of adherence to the PA guidelines. This finding has important implications in terms of public health strategies, where efforts need to include optimization of dietary fat intakes alongside adequate protein intake and health-enhancing PA behaviours.

The population sample of the present study comprised older men and women of diverse geographical and cultural origins and with different metabolic health status (with or without MetS). Interestingly, the beneficial impact of replacing SFAs with PUFAs on sarcopenia risk occurred regardless of these study sample variations, which strengthens the need to optimize dietary fat intake irrespective of culturally related dietary differences or stages of metabolic disease progression.

The main findings of the present study were strengthened by the use of objective assessment of PA together with a food record-based assessment of macronutrient intakes. Sarcopenia risk was assessed by incorporating single elements (SMI and handgrip strength) into one composite score according to recent operational definitions of sarcopenia [1], which is likely to better capture different stages of sarcopenia progression than separate single parameters of muscle mass and strength. The present study was not without limitations. The cross-sectional design prevented conclusions about causality. Further experimental work is warranted to confirm the findings of this study. While food records are regarded as valid for determining energy intakes, over- and under-reporting likely occur. The data on macronutrient intakes were in line with data from previous reports in older adults [3,28,42], and general over- or under-reporting in this population would not affect the validity of the study conclusions.

Although several covariates were included in the main analyses, residual confounding from other variables cannot be ruled out.

5. Conclusions

The present study suggested a beneficial impact of replacing SFAs with PUFAs, but not MUFAs, on the sarcopenia risk score in non-frail older men and women, especially in those with a protein intake below the current recommendation. Efforts to promote healthy diets with optimised fat subtype distribution should be emphasised regardless of adherence to PA guidelines.

Author Contributions: Conceptualization, D.M.-R., A.N., F.K., A.S. and C.F.; methodology, D.M.-R., A.N., F.K., A.S. and C.F.; validation, D.M.-R.; formal analysis, D.M.-R., A.S., A.N. and F.K.; investigation, D.M.-R., A.N., A.S., C.F., M.C., A.B., G.B., L.C.P.G.M.d.G., E.J.M.F., A.A.M.B., A.B.-D., O.S., B.P., S.F.-T., A.J., F.C. and F.K.; writing—original draft preparation, D.M.-R., A.S., A.N. and F.K.; writing—review and editing, D.M.-R., A.N., A.S., C.F., M.C., A.B., G.B., L.C.P.G.M.d.G., E.J.M.F., A.A.M.B., A.B.-D., O.S., B.P., S.F.-T., A.J., F.C. and F.K.; supervision, A.N. and F.K.; project administration, A.S.; funding acquisition, C.F. All authors have read and agreed to the published version of the manuscript.

Funding: This research was supported by the European Union's Seventh Framework Program under agreement no. 266486 (NU-AGE: New dietary strategies addressing the specific needs of the elderly population for healthy ageing in Europe).

Acknowledgments: We would like to thank all principal investigators and collaborators. We also express our gratitude to the participants and staff involved in data collection and management in NU- AGE research centres. We would like to thank the EU HORIZON 2020 Research and Innovation Programme (European Joint Programming Initiative "A healthy diet for a healthy life" "JPI HDHL" and the ERA-NET co-fund HDHL-INTIMIC) for supporting three authors (A.S., A.N. and F.K.).

Conflicts of Interest: The authors declare no conflict of interest.

References

1. Cruz-Jentoft, A.J.; Bahat, G.; Bauer, J.; Boirie, Y.; Bruyère, O.; Cederholm, T.; Cooper, C.; Landi, F.; Rolland, Y.; Sayer, A.A.; et al. Sarcopenia: Revised European consensus on definition and diagnosis. *Age Ageing* **2019**, *48*, 16–31. [CrossRef] [PubMed]
2. Dodds, R.M.; Roberts, H.C.; Cooper, C.; Sayer, A.A. The Epidemiology of Sarcopenia. *J. Clin. Densitom.* **2015**, *18*, 461–466. [CrossRef] [PubMed]
3. Nilsson, A.; Montiel Rojas, D.; Kadi, F. Impact of Meeting Different Guidelines for Protein Intake on Muscle Mass and Physical Function in Physically Active Older Women. *Nutrients* **2018**, *10*, 1156. [CrossRef] [PubMed]
4. Fontana, L.; Hu, F.B. Optimal body weight for health and longevity: Bridging basic, clinical, and population research. *Aging Cell* **2014**, *13*, 391–400. [CrossRef] [PubMed]
5. Bauer, J.; Biolo, G.; Cederholm, T.; Cesari, M.; Cruz-Jentoft, A.J.; Morley, J.E.; Phillips, S.; Sieber, C.; Stehle, P.; Teta, D.; et al. Evidence-Based Recommendations for Optimal Dietary Protein Intake in Older People: A Position Paper From the PROT-AGE Study Group. *J. Am. Med. Dir. Assoc.* **2013**, *14*, 542–559. [CrossRef] [PubMed]
6. Welch, A.A.; MacGregor, A.J.; Minihane, A.-M.; Skinner, J.; Valdes, A.A.; Spector, T.D.; Cassidy, A. Dietary Fat and Fatty Acid Profile Are Associated with Indices of Skeletal Muscle Mass in Women Aged 18–79 Years. *J. Nutr.* **2014**, *144*, 327–334. [CrossRef] [PubMed]
7. Granic, A.; Mendonça, N.; Sayer, A.A.; Hill, T.R.; Davies, K.; Siervo, M.; Mathers, J.C.; Jagger, C. Effects of dietary patterns and low protein intake on sarcopenia risk in the very old: The Newcastle 85+ study. *Clin. Nutr.* **2020**, *39*, 166–173. [CrossRef]
8. Welch, A.A. Nutritional influences on age-related skeletal muscle loss. *Proc. Nutr. Soc.* **2014**, *73*, 16–33. [CrossRef] [PubMed]
9. Jyväkorpi, S.K.; Urtamo, A.; Kivimäki, M.; Strandberg, T.E. Macronutrient composition and sarcopenia in the oldest-old men. *Clin. Nutr.* **2020**. [CrossRef]

10. Campmans-Kuijpers, M.J.E.; Sluijs, I.; Nöthlings, U.; Freisling, H.; Overvad, K.; Weiderpass, E.; Fagherazzi, G.; Kühn, T.; Katzke, V.A.; Mattiello, A.; et al. Isocaloric substitution of carbohydrates with protein: The association with weight change and mortality among patients with type 2 diabetes. *Cardiovasc. Diabetol.* **2015**, *14*, 39. [CrossRef]
11. Skilton, M.R.; Laville, M.; Cust, A.E.; Moulin, P.; Bonnet, F. The association between dietary macronutrient intake and the prevalence of the metabolic syndrome. *Br. J. Nutr.* **2008**, *100*, 400–407. [CrossRef] [PubMed]
12. Hernández-Alonso, P.; Salas-Salvadó, J.; Ruiz-Canela, M.; Corella, D.; Estruch, R.; Fitó, M.; Arós, F.; Gómez-Gracia, E.; Fiol, M.; Lapetra, J.; et al. High dietary protein intake is associated with an increased body weight and total death risk. *Clin. Nutr.* **2016**, *35*, 496–506. [CrossRef] [PubMed]
13. Flock, M.R.; Fleming, J.A.; Kris-Etherton, P.M. Macronutrient replacement options for saturated fat. *Curr. Opin. Lipidol.* **2014**, *25*, 67–74. [CrossRef]
14. Berendsen, A.; Santoro, A.; Pini, E.; Cevenini, E.; Ostan, R.; Pietruszka, B.; Rolf, K.; Cano, N.; Caille, A.; Lyon-Belgy, N.; et al. Reprint of: A parallel randomized trial on the effect of a healthful diet on inflammageing and its consequences in European elderly people: Design of the NU-AGE dietary intervention study. *Mech. Ageing Dev.* **2014**, *136–137*, 14–21. [CrossRef] [PubMed]
15. Santoro, A.; Pini, E.; Scurti, M.; Palmas, G.; Berendsen, A.; Brzozowska, A.; Pietruszka, B.; Szczecinska, A.; Cano, N.; Meunier, N.; et al. Combating inflammaging through a Mediterranean whole diet approach: The NU-AGE project's conceptual framework and design. *Mech. Ageing Dev.* **2014**, *136–137*, 3–13. [CrossRef] [PubMed]
16. Fried, L.P.; Tangen, C.M.; Walston, J.; Newman, A.B.; Hirsch, C.; Gottdiener, J.; Seeman, T.; Tracy, R.; Kop, W.J.; Burke, G.; et al. Frailty in Older Adults: Evidence for a Phenotype. *J. Gerontol. Biol. Sci.* **2001**, *56*, 808–813. [CrossRef] [PubMed]
17. Ostan, R.; Guidarelli, G.; Giampieri, E.; Lanzarini, C.; Berendsen, A.A.M.; Januszko, O.; Jennings, A.; Lyon, N.; Caumon, E.; Gillings, R.; et al. Cross-Sectional Analysis of the Correlation Between Daily Nutrient Intake Assessed by 7-Day Food Records and Biomarkers of Dietary Intake Among Participants of the NU-AGE Study. *Front. Physiol.* **2018**, *9*, 1–12. [CrossRef] [PubMed]
18. Berendsen, A.; van de Rest, O.; Feskens, E.; Santoro, A.; Ostan, R.; Pietruszka, B.; Brzozowska, A.; Stelmaszczyk-Kusz, A.; Jennings, A.; Gillings, R.; et al. Changes in Dietary Intake and Adherence to the NU-AGE Diet Following a One-Year Dietary Intervention among European Older Adults—Results of the NU-AGE Randomized Trial. *Nutrients* **2018**, *10*, 1905. [CrossRef]
19. Santoro, A.; Guidarelli, G.; Ostan, R.; Giampieri, E.; Fabbri, C.; Bertarelli, C.; Nicoletti, C.; Kadi, F.; de Groot, L.C.P.G.M.; Feskens, E.; et al. Gender-specific association of body composition with inflammatory and adipose-related markers in healthy elderly Europeans from the NU-AGE study. *Eur. Radiol.* **2019**, *29*, 4968–4979. [CrossRef]
20. Santoro, A.; Bazzocchi, A.; Guidarelli, G.; Ostan, R.; Giampieri, E.; Mercatelli, D.; Scurti, M.; Berendsen, A.; Surala, O.; Jennings, A.; et al. A Cross-Sectional Analysis of Body Composition among Healthy Elderly from the European NU-AGE Study: Sex and Country Specific Features. *Front. Physiol.* **2018**, *9*, 9. [CrossRef]
21. Kim, K.M.; Jang, H.C.; Lim, S. Differences among skeletal muscle mass indices derived from height-, weight-, and body mass index-adjusted models in assessing sarcopenia. *Korean J. Intern. Med.* **2016**, *31*, 643–650. [CrossRef]
22. Guglielmi, G.; Ponti, F.; Agostini, M.; Amadori, M.; Battista, G.; Bazzocchi, A. The role of DXA in sarcopenia. *Aging Clin. Exp. Res.* **2016**, *28*, 1047–1060. [CrossRef] [PubMed]
23. Syddall, H.E.; Martin, H.J.; Harwood, R.H.; Cooper, C.; Sayer, A.A. The SF-36: A simple, effective measure of mobility-disability for epidemiological studies. *J. Nutr. Heal. Aging* **2009**, *13*, 57–62. [CrossRef] [PubMed]
24. Montiel Rojas, D.; Nilsson, A.; Ponsot, E.; Brummer, R.J.; Fairweather-Tait, S.; Jennings, A.; de Groot, L.C.P.G.M.; Berendsen, A.; Pietruszka, B.; Madej, D.; et al. Short Telomere Length Is Related to Limitations in Physical Function in Elderly European Adults. *Front. Physiol.* **2018**, *9*, 1–6. [CrossRef] [PubMed]
25. Nilsson, A.; Wåhlin-Larsson, B.; Kadi, F. Physical activity and not sedentary time per se influences on clustered metabolic risk in elderly community-dwelling women. *PLoS ONE* **2017**, *12*, e0175496. [CrossRef]
26. Troiano, R.P.; Berrigan, D.; Dodd, K.W.; Masse, L.C.; Tilert, T.; McDowell, M. Physical Activity in the United States Measured by Accelerometer. *Med. Sci. Sport. Exerc.* **2008**, *40*, 181–188. [CrossRef]

27. Alberti, K.G.M.M.; Zimmet, P.; Shaw, J. Metabolic syndrome-a new world-wide definition. A Consensus Statement from the International Diabetes Federation. *Diabet. Med.* **2006**, *23*, 469–480. [CrossRef]
28. Isanejad, M.; Sirola, J.; Mursu, J.; Rikkonen, T.; Kröger, H.; Tuppurainen, M.; Erkkilä, A.T. Association of the Baltic Sea and Mediterranean diets with indices of sarcopenia in elderly women, OSPTRE-FPS study. *Eur. J. Nutr.* **2018**, *57*, 1435–1448. [CrossRef]
29. Ganapathy, A.; Nieves, J.W. Nutrition and Sarcopenia—What Do We Know? *Nutrients* **2020**, *12*, 1755. [CrossRef]
30. Arias-Fernández, L.; Struijk, E.A.; Rodríguez-Artalejo, F.; Lopez-Garcia, E.; Lana, A. Habitual dietary fat intake and risk of muscle weakness and lower-extremity functional impairment in older adults: A prospective cohort study. *Clin. Nutr.* **2020**. [CrossRef]
31. Abbatecola, A.M.; Cherubini, A.; Guralnik, J.M.; Lacueva, C.A.; Ruggiero, C.; Maggio, M.; Bandinelli, S.; Paolisso, G.; Ferrucci, L. Plasma Polyunsaturated Fatty Acids and Age-Related Physical Performance Decline. *Rejuvenation Res.* **2009**, *12*, 25–32. [CrossRef] [PubMed]
32. Gedmantaite, A.; Celis-Morales, C.A.; Ho, F.; Pell, J.; Ratkevicius, A.; Gray, S.R. Associations between diet and handgrip strength: A cross-sectional study from UK Biobank. *Mech. Ageing Dev.* **2020**, *189*, 111269. [CrossRef] [PubMed]
33. Witard, O.C.; Combet, E.; Gray, S.R. Long-chain *n*-3 fatty acids as an essential link between musculoskeletal and cardio-metabolic health in older adults. *Proc. Nutr. Soc.* **2020**, *79*, 47–55. [CrossRef] [PubMed]
34. Bryner, R.W.; Woodworth-Hobbs, M.E.; Williamson, D.L.; Alway, S.E. Docosahexaenoic Acid Protects Muscle Cells from Palmitate-Induced Atrophy. *ISRN Obes.* **2012**, *2012*, 1–14. [CrossRef]
35. Woodworth-Hobbs, M.E.; Hudson, M.B.; Rahnert, J.A.; Zheng, B.; Franch, H.A.; Price, S.R. Docosahexaenoic acid prevents palmitate-induced activation of proteolytic systems in C2C12 myotubes. *J. Nutr. Biochem.* **2014**, *25*, 868–874. [CrossRef]
36. Hyde, R.; Hajduch, E.; Powell, D.J.; Taylor, P.M.; Hundal, H.S. Ceramide down-regulates System A amino acid transport and protein synthesis in rat skeletal muscle cells. *FASEB J.* **2005**, *19*, 1–24. [CrossRef] [PubMed]
37. Smith, G.I.; Atherton, P.; Reeds, D.N.; Mohammed, B.S.; Rankin, D.; Rennie, M.J.; Mittendorfer, B. Dietary omega-3 fatty acid supplementation increases the rate of muscle protein synthesis in older adults: A randomized controlled trial. *Am. J. Clin. Nutr.* **2011**, *93*, 402–412. [CrossRef]
38. Strandberg, E.; Ponsot, E.; Piehl-Aulin, K.; Falk, G.; Kadi, F. Resistance Training Alone or Combined With N-3 PUFA-Rich Diet in Older Women: Effects on Muscle Fiber Hypertrophy. *J. Gerontol. Ser. A* **2019**, *74*, 489–494. [CrossRef]
39. Gerling, C.J.; Whitfield, J.; Mukai, K.; Spriet, L.L. Variable effects of 12 weeks of omega-3 supplementation on resting skeletal muscle metabolism. *Appl. Physiol. Nutr. Metab.* **2014**, *39*, 1083–1091. [CrossRef]
40. Hengeveld, L.M.; Boer, J.M.A.; Gaudreau, P.; Heymans, M.W.; Jagger, C.; Mendonça, N.; Ocké, M.C.; Presse, N.; Sette, S.; Simonsick, E.M.; et al. Prevalence of protein intake below recommended in community-dwelling older adults: A meta-analysis across cohorts from the PROMISS consortium. *J. Cachexia. Sarcopenia Muscle* **2020**, jcsm.12580. [CrossRef]
41. U.S. Department of Health and Human Service. *Physical Activity Guidelines Advisory Committee Scientific Report 2018*; U.S. Department of Health and Human Service: Washington, DC, USA, 2018.
42. Machado-Fragua, M.D.; Struijk, E.A.; Ballesteros, J.-M.; Ortolá, R.; Rodriguez-Artalejo, F.; Lopez-Garcia, E. Habitual coffee consumption and risk of falls in 2 European cohorts of older adults. *Am. J. Clin. Nutr.* **2019**, *109*, 1431–1438. [CrossRef] [PubMed]

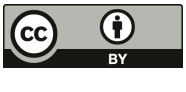

nutrients

MDPI

Review

High Fat Rodent Models of Type 2 Diabetes: From Rodent to Human

Nicole L. Stott and Joseph S. Marino *

Laboratory of Systems Physiology, Department of Kinesiology, The University of North Carolina at Charlotte, Charlotte, NC 28223, USA; Nstott1@uncc.edu

* Correspondence: jmarin10@uncc.edu

Received: 26 October 2020; Accepted: 23 November 2020; Published: 27 November 2020

Abstract: Poor dietary habits contribute to increased incidences of obesity and related co-morbidities, such as type 2 diabetes (T2D). The biological, genetic, and pathological implications of T2D, are commonly investigated using animal models induced by a dietary intervention. In spite of significant research contributions, animal models have limitations regarding the translation to human pathology, which leads to questioning their clinical relevance. Important considerations include diet-specific effects on whole organism energy balance and glucose and insulin homeostasis, as well as tissue-specific changes in insulin and glucose tolerance. This review will examine the T2D-like phenotype in rodents resulting from common diet-induced models and their relevance to the human disease state. Emphasis will be placed on the disparity in percentages and type of dietary fat, the duration of intervention, and whole organism and tissue-specific changes in rodents. An evaluation of these models will help to identify a diet-induced rodent model with the greatest clinical relevance to the human T2D pathology. We propose that a 45% high-fat diet composed of approximately one-third saturated fats and two-thirds unsaturated fats may provide a diet composition that aligns closely to average Western diet macronutrient composition, and induces metabolic alterations mirrored by clinical populations.

Keywords: high-fat diet; metabolism; type 2 diabetes; insulin resistance; obesity; rodent models of type 2 diabetes

1. Introduction

High fat diet (HFD) animal models utilize a variety of fat sources to mimic the typical Western diet, which in the U.S. population consists of ~70% more saturated fat than the recommended dietary guidelines [1]. A twelve-year National Health and Nutrition Examination Study (NHANES) study demonstrated that individuals consuming high amounts of carbohydrates, cholesterol, saturated fatty acids, polyunsaturated fats, monounsaturated fats, and protein have a greater propensity to develop glucose intolerance when compared to individuals with dietary patterns high in vitamin, mineral, and fiber content [2]. Saturated fatty acids (SFA), which are stored more readily in rodents and humans compared to monounsaturated and polyunsaturated fats, increase the risk of obesity [3]. Therefore, it is important to work towards the uniform formulation of a rodent diet that best represents human consumption, while promoting a similar type 2 diabetes (T2D) phenotype.

HFD consumed *ab libitum* results in rodents exceeding typical daily caloric intake [4], and animal-based fats promote diet-induced obesity and insulin resistance better than vegetable-based fats in rats [5]. Commonly used saturated fatty acid sources include hydrogenated coconut oil, corn oil, lard, palmitic acid, and stearic acid [6,7]. Unsaturated fats, such as oleic acid and linoleic acid, are also utilized in some nutritional animal models [8]. HFD, even when isocalorically matched with a standard purified control diet, induces obesity in rodents through alterations in metabolic homeostasis and

reduced physical activity levels [9]. HFD-induced phenotypes of T2D in rodents and humans share weight gain, hyperglycemia, hyperinsulinemia, insulin resistance, inflammatory cytokine secretion, and ectopic lipid accumulation [10]. However, diet-induced animal models employ marked differences in micronutrient and macronutrient composition, including a variety of saturated fats, resulting in significant inter-study variability [11–13].

Despite these variables, the chronic consumption of a HFD by rodents alters a variety of genes and/or receptors involved in metabolism, inflammation, oxidative stress, substrate transport, protein synthesis and modification, and transcriptional regulation [6,7,14–16]. Notably, the modification of such genes is tissue-specific [6]. A better understanding of tissue specific effects in response to dietary composition will provide guidance into the most appropriate HFD-induced animal model(s) to study the pathogenesis of T2D and associated phenotypic changes.

Thorough review articles addressing the value and limitations of T2D animal models have been published [10,17,18]. Variable diet composition, rodent strain, intervention time-points, and duration of protocols further complicate the translatability of animal-based findings to the human disease state. Here, we summarize how the combination of percentage and type of fat with varying durations of intervention, affect the major insulin responsive tissues. These are important considerations to get closer to an animal model with high clinical relevance to the human disease.

2. Tissue-Specific Effects of HFD Models

2.1. Liver

Mice. The composition of saturated fatty acids in a HFD differentially affects adipose deposition within the liver and subsequently cellular and molecular signaling. Examples of saturated fats that adversely affect the liver of C57BL/6 male mice include corn oil, lard, and hydrogenated coconut oil (Table 1). The composition of HFD is responsible for the different effects in hepatic lipid storage. For example, a 45% HFD containing palm oil (high in saturated fat) or olive oil (low in saturated fat) increased hepatic triacylglycerol (TAG) content following an 8-week intervention in C57BL/6 mice [19]. In male and female C57BL/6 mice, 18 to 20 weeks of a 60% lard-based diet increased lipid accumulation and steatosis in the liver [20–22]. Other studies showed hepatic inflammation and fibrosis following only 8 weeks of a similar diet [23].

On a whole organism level, male and female mice developed insulin resistance and glucose intolerance in response to 45% [19] and 60% HFD [20–22]. However, the source of the fat must be considered [19] (Table 1).

Table 1. Liver.

Source	Fat Source	Macronutrients (% kcal)	Duration	Strain; Sex	Tissue Findings	T2D Status
[19]	(a) Cocoa butter (b) Palm oil (c) Olive oil (d) Safflower oil	45% fat 20% protein 35% carbohydrate All diet formulations maintained same ratio	8 weeks	C57BL/6 mice; Male	↑ Liver TAG in palm and olive oil groups	↑ Body weight in palm oil compared to cocoa butter. ↓ Glucose tolerance: cocoa, palm and safflower oils
[6]	Hydrogenated coconut oil	59% fat 15% protein 26% carbohydrate	20 weeks	C57BL/6 mice; Male	↑ FABP mRNA ↑ Inflammation ↑ Increased BTNL2	↑ Fat mass ↓ Insulin sensitivity ↑ Plasma insulin
[22]	Lard and Soybean oil	60% fat 20% protein 20% carbohydrate	20 weeks	C57BL/6 mice; Female	↑ Lipid accumulation ↑ Hepatic steatosis	↑ Body weight ↓ Glucose tolerance ↑Serum insulin ↑ Serum glucose
[20,21,23,24]	Lard and Soybean oil	60% fat ~20% protein ~20% carbohydrate	8 weeks [23] 15 weeks [24] 18 weeks [20] 20 weeks [21]	C57BL/6 mice; Male	↑ Inflammation ↑ Lipid accumulation ↑ Fibrosis	↑ Body weight ↑ Serum glucose ↑ Serum insulin ↑ HOMA-IR
[25]	Lard	45% fat 30% protein 25% carbohydrate	4 weeks	Wister rats; Male	↑ Liver mass ↑ Liver TAG ↑ Hepatic steatosis	↑ Body weight ↓Insulin sensitivity ←→ Plasma glucose
[26]	Lard and Soybean oil	45% fat 20% protein 35% carbohydrate	12 weeks	Sprague-Dawley rats; Male	↑ Lipid accumulation ↑ Lipogenic gene and protein expression	↑ Body weight
[27]	Butter	58% fat 25% protein 17% carbohydrate	18 weeks	Sprague-Dawley rats; Male	↑ Inflammation ↑ Lipid accumulation ↓ Insulin signaling ↑ Hepatic necrosis ↑ Oxidative stress	↑ Body weight ↑ Serum glucose ↑ Serum insulin ↑ HOMA-IR

Studies cited in this table were limited to those that included macronutrient composition. The direction of arrows indicate change when compared to a standard diet control group within that study. Triacylglycerol (TAG), butyrophilin-like Protein 2 (BTNL2), fatty acid binding protein (FABP), major histocompatibility complex I and II (MHC I and II), and homeostatic model assessment of insulin resistance (HOMA-IR).

Inflammatory responses and β-oxidation gene changes in mice have been reported, particularly as a result of a HFD containing more than 45% fat. Inflammatory responses are a known etiology of T2D development in rodents and humans [16,28]. However, establishing similarities between species is difficult when models vary in the percentage of fat, 59% to 82%, and duration, 12 to 36 weeks [6,29]. Eighteen to 20 weeks of a 60% lard-based diet increased cellular and biochemical markers of hepatic inflammation in male [20,21], but not female mice [22]. As the percentage of saturated fat increases, so does liver dysfunction. Interestingly an extremely HFD, 82% lard, caused hepatic lipid deposition accompanied by a transient increase in the expression of genes regulating fatty acid oxidation and synthesis after just 2 weeks [29]. By 4 weeks of consuming such a diet, gene expression patterns changed to reflect 2 to 4-fold increases adipogenesis (PPARγ and fatty acid binding protein) and lipid deposition (CD36) [29]. Not surprisingly, as the percentage of HFD increased, the inflammatory response followed the same trend. These studies suggest that excessive high fat content may cause a rapid transient pattern in hepatic fatty acid metabolism. Due to the rapid changes, it is plausible that many of the cellular and molecular events that alter hepatic lipid accumulation may be missed by studies focusing on prolonged consumption, especially when employing very high fat content. Due to the more progressive phenotype of lipid accumulation in human liver, such studies may contribute little to the understanding of the human phenotype.

Rats. Four weeks of a 45% lard-based diet caused hepatic steatosis, increased liver mass and increased hepatic TAG content in Wister rats [25] (Table 1). Changes in liver characteristics were accompanied by obesity and reduced insulin sensitivity, despite no evidence of hyperglycemia [25]. This more mild phenotype may be the result of a short diet intervention period and/or modest concentration of fat. In response to diets containing higher concentrations of SFA, a more severe phenotype emerges. Sprague–Dawley rats developed hepatic insulin resistance, fatty liver, inflammation, and necrosis following consumption of a 58% butter [27] or 65% lard-based diet [30]. Under both dietary conditions, a severer whole body T2D phenotype emerged [27,30] (Table 1).

The composition of fat within a diet may be just as important as the percentage and treatment duration. While a 45.5% HFD composed of SFA, monounsaturated fatty acids (MUFA), and polyunsaturated fatty acids (PUFA) did not cause an increase in body mass compared to control fed animals, liver mass and blood glucose were elevated after 15 weeks [31]. Such findings are similar to those reported in mice, such that higher concentrations of MUFA and PUFA mixtures produce a more mild phenotype [19] (Table 1).

2.2. Adipose

Mice. Insulin promotes lipogenesis in adipose tissue, reducing glycerol and fatty acid availability. Insulin resistant adipose tissue impairs glucose disposal and increases lipolysis, promoting fatty acid and glycerol availability for hepatic gluconeogenesis [32]. When unable to regulate hepatic glucose production properly, hyperglycemia coincides with lipid accumulation in adipose depots and peripheral tissues.

Saturated and unsaturated fat differentially effect the metabolic and immune responses in adipose tissue. A 45% HFD enriched with palmitic acid (SFA) induced adipose tissue hypertrophy, but a 45% HFD, enriched with oleic acid (MUFA), caused adipose tissue hyperplasia [33] (Table 2). Insulin sensitivity was improved, but not normalized, in mice fed monounsaturated fat [34]. Improved insulin sensitivity was partially a result of adipose-mediated inflammatory signaling. Adipose tissue macrophages secrete pro-inflammatory mediators, such as tumor necrosis factor-alpha (TNF-α), interleukin-6 (IL-6), and monocyte chemoattractant protein-1 (MCP-1), which correlate with adipocyte cell death [35] (Table 2). A 45% HFD enriched with saturated fats exacerbated the inflammatory response within adipose tissue, evidenced by increased TNF-α and IL-6 gene expression and reduced insulin sensitivity [36]. Furthermore, 31 weeks of a 42% HFD composed of SFA and MUFA caused white adipose tissue inflammation, reduced insulin signaling, and reduced the capacity for mitochondrial biogenesis and function in male mice [34]. However, when the fat source was based on mono or polyunsaturated fats, the inflammatory response was mitigated, and insulin responsiveness restored [36].

Table 2. Adipose.

Source	Fat Source	Macronutrients (% kcal)	Duration	Strain; Sex	Findings	T2D Status
[38]	Lard and Soybean oil	45% fat 20% protein 35% carbohydrate	12 weeks	C57BL/6; Male	↑ Body weight ↑ Epididymal fat mass and adipocyte size ↑ Inflammation	↑ Body weight ↑ Blood glucose
[33]	(1) Palm oil (2) Sunflower oil	(1) 45% fat 20% protein 35% carbohydrate (2) 45% fat 20% protein35% carbohydrate	24 weeks	C57BL/6; Male	↓ SFA: Adipose insulin signaling ↑ SFA: Inflammation ↑ SFA: Adipocyte size ↑ SFA and MUFA: Epididymal, visceral, subcutaneous, and perirenal fat pad mass	↓ Palm and sunflower oils: Glucose tolerance ↑ Sunflower oil: Hyperinsulinemia ↑ Palm oil: Hyperinsulinemia above sunflower oil
[37,39]	Lard and Soybean oil	60% fat 20% protein 20% carbohydrate	7 to 8 weeks	C57BL/6; Male	↑ Subcutaneous fat ↑ Visceral fat ↑ Adipocyte size ↑ Lipogenic gene expression	↑ Body weight ↑ Serum glucose
[40]	Lard and Soybean oil	60% fat 20% protein 20% carbohydrate	12 weeks	C57BL/6; female	↑ Perirenal fat ↑ Gonadal fat ↑ Mesenteric fat	↑ Body weight ←→ Glucose tolerance
[35]	Lard and Soybean oil	60% fat 20% protein20% carbohydrate	20 weeks	C57BL/6; Male	↑ Adipose weight ↑ Adipocyte size peaks at 12 weeks ↑ Adipocyte death peaks at 16 weeks ↑ Inflammation	↑ Body weight ↑ Serum insulin by 8 weeks ↑ Insulin resistance by 8 weeks ↑ HOMA-IR by 8 weeks
[41]	Lard and Soybean oil	45% fat 20% protein 35% carbohydrate	13 weeks	Sprague-Dawley rats; Male	↑ Retroperitoneal and epididymal fat mass ↑ Adipocyte size ↑ Adipogenic gene expression ↑ Macrophage accumulation ↑ Inflammation	↑ Body weight
[42]	Unknown	57% fat 10% protein 31% carbohydrate	11 weeks	Wister rats; Male and Female	↑ Subcutaneous and retroperitoneal fat mass and adipocyte diameter in males and females ↑ Oxidative stress in males only ↑ Subcutaneous fat inflammation in males only	↑ Body weight males only
[43]	Lard and Soybean oil	60% fat 20% protein 20% carbohydrate	8 weeks	Wister rats; Male	↑ Ceramide content ↑ DAG content ↑ Plasma free fatty acids	←→ Body weight ↑ Plasma glucose ↑ Plasma insulin ↑ HOMA-IR
[44]	UFA Mix: Sheep rump fat	62.1% fat 16% protein 28.2% fat	20 weeks	Wister rats; Males	↑ Inguinal, mesenteric, epididymal, retroperitoneal, and perirenal fat mass ↓ Capillary density ↑ Increased macrophage crown-like structures	↑ Body weight ↑ Blood glucose ↑ HOMA-IR ←→ Insulin

Studies cited in this table were limited to those that included macronutrient composition. The direction of arrows indicate change when compared to a standard diet control group within that study. Homeostatic model assessment of insulin resistance (HOMA-IR), saturated fatty acid (SFA), monounsaturated fatty acid (MUFA, and diacylglycerol (DAG).

An HFD of 60% caused a more severe inflammatory response [35]. Progressive increases in adipocyte size were followed by cell death with increased fat pad weight through 20 weeks [35]. This phase of adipose tissue remolding was largely driven by macrophage infiltration [35] and may be associated with adipose hyperplasia to account for adipocyte death. Following as little as 1 week of a 60% lard-based HFD, pro-inflammatory macrophages (M1-like macrophages) were significantly increased and remained elevated through 7 weeks [37]. However, consumption of a 45% HFD for 12 weeks led to a similar phenotype [38] (Table 2).

Rats. Diets ranging from 45% to 62% fat caused adipocyte dysfunction and a T2D-like phenotype [41,43,44] (Table 2). Thirteen weeks of a 45% lard-based diet increased fat pad mass, adipocyte size and inflammation, but markers of T2D were not reported [41]. Diets of ~60% fat induced similar characteristics of adipose dysfunction with insulin and glucose intolerance, despite different fat sources [43,44]. Specifically, 62% mixed unsaturated fat caused significant adipose inflammation, accompanied by increased fasting glucose and homeostatic model assessment of insulin resistance (HOMA-IR) [44]. Diets composed of lower [41] and similar [43] percentages of fat from lard, reported comparable cellular and phenotypic changes in adipose. However, the duration of HFD consumption varied greatly in such studies, making it difficult to distinguish the importance of the fat concentration or source, from the duration of consumption (Table 2).

Changes in adipose integrity are influenced by sex, supporting the necessity for inclusion of female subjects. Following 11 weeks of a 57% HFD, only male rats developed oxidative stress and inflammation in subcutaneous adipose [42]. In female rats, increased subcutaneous and retroperitoneal fat mass was not associated with increased inflammatory cytokines or evidence of immune cell accumulation [42]. Notably, the source of fat and markers of T2D were not reported. However, in female mice, a similar diet increased adiposity without a change in glucose tolerance [40].

2.3. Pancreas

Mice. The pancreas serves as a critical regulator of insulin and glucose homeostasis. Under low energy availability, glucagon could stimulate hepatic glucose production, while under energy surplus, insulin could facilitate glucose uptake. A better understanding of how different dietary models affect the pancreas will facilitate the development of a model that aligns with alterations in pancreatic function in the progression of human T2D.

Six weeks of a 45% lard-based diet increased β-cell proliferation and mass, in the splenic region, contributing to the onset of insulin resistance in C57BL/6 male mice [45]. Following 12 weeks of the same diet, β-cell expression of adipose differentiation-related protein (ADFP) was increased, and pancreatic lipid accumulation was evident [46]. As a result, mice were hyperglycemic and hyperinsulinic. Human pancreatic β-cells treated with fatty acids showed a similar trend in ADFP expression [46].

In response to a 60% lard-based diet, reduced glucose tolerance and hyperinsulinemia were evident within 1 week, but insulin resistance did not manifest until 11 weeks [47]. At the onset, pancreatic cells compensated for increased glucose levels by doubling insulin secretion (detectable within 2 weeks), but insulin secretion became significantly impaired as insulin resistance developed and β-cell mass continued to increase [47]. Genes associated with hyperinsulinemia and β-cell proliferation were significantly elevated by week 8, which was 3 weeks prior to measurable insulin resistance [47]. More recently, a 60% HFD for 8 weeks, caused obesity, hyperglycemia, hyperlipidemia, and pancreatic β-cell hypertrophy in C57BL/6 mice [48] (Table 3). Metabolic profiling revealed that global metabolite changes of bioactive lipids associated with β-cell expansion and β-cell proliferation increased 1.75-fold [49].

Rats. Pancreatic inflammation in 60% HFD fed male Sprague–Dawley rats was associated with pancreatic atrophy, hyperinsulinemia, hyperglycemia, increased HOMA-IR, and pancreatic triglyceride (TG) accumulation following 24 weeks [50]. A similar dietary composition (66% fat), increased β-cell autophagy and glucagon production after 16 weeks [51] (Table 3). Elevated glucagon production is likely the cause for hyperglycemia reported at 16 weeks and at later time points in other

studies [51,52]. However, 46% HFD for 12 weeks reduced glucose tolerance, indicating progression of the diabetic phenotype with a lower fat load [53]. Taken together, 46% and 66% HFD elicit β and α cell expansion, hyperinsulinemia, and reduced glucose tolerance [51,53]. Importantly, the source of fat in the aforementioned studies was not reported. Nonetheless, these similarities suggest that a fat content closer to a Western-based diet provides a sufficient stimulus to study HFD-induced pancreatic dysfunction.

Identifying the concentration and composition that best relates to pancreatic alterations in the human T2D population should be the priority, rather than adjusting the percentage of fat for the greatest tissue insult. Indeed, species-specific differences exist, such as primarily β-cell proliferation in rodents and β-cell apoptosis in humans prior to insulin resistance [49,54]. Therefore, if the pancreas is the tissue of interest, it may be beneficial to combine a moderate HFD model with low dose streptozotocin to reduce β-cell mass and allow for insulin levels to decline throughout T2D progression [55].

Table 3. Pancreas.

Source	Fat Source	Macronutrients (% kcal)	Duration	Strain; Sex	Findings	T2D Status
[45]	Lard and Soybean oil	45% fat 20% protein 35% carbohydrate	6 weeks	C57BL/6; Male	↑ Beta cell proliferation in splenic region ↑ Increased insulin secretion from isolated islets	↑ Body weight ↑ Plasma insulin ↓ Glucose tolerance ↓ Insulin tolerance
[46]	Lard and Soybean oil	45% fat 20% protein 35% carbohydrate	12 weeks	C57BL/6; Male	↑ Lipid accumulation in acinar cells ↑ Adipose differentiation-related protein (ADFP)	↑ Body weight ↑ Serum insulin ↑ Blood glucose
[48]	Lard and Soybean oil	60% fat 20% protein 20% carbohydrate	8 weeks	C57BL/6; Male	↑ Islet size ↑ Islet Insulin	↑ Body weight ↑ Blood glucose ↑ HbA1c ↑ Serum Insulin ↑ HOMA-IR
[53]	Not reported	46% fat 20.3% protein 24% carbohydrate	12 weeks	Sprague-Dawley rats; Male	↑ Mast cell accumulation ↑ Islet area and proliferation ↑ β and α cell area	↑ Plasma insulin ↓ Glucose tolerance
[56]	Not reported	60% fat 18% protein 22% carbohydrate	8 weeks	Sprague-Dawley rats; Male	Glucose-stimulated islet insulin secretion	Glucose tolerance
[51]	Not reported	66.43% fat 18.08% protein 15.48% carbohydrate	8 and 16 weeks	Sprague-Dawley rats; Male	↑ Islet cell insulin at 8 and 16 weeks ↑ Glucagon at 16 weeks ↑ β and α cell area at 16 weeks ↑ β cell autophagy at 16 weeks	↑ Body weight at 16 weeks ↑ Plasma glucose at 16 weeks ↑ Serum insulin at 8 and 16 weeks ↑ HOMA-IR at 8 and 16 weeks

Studies cited in the table were limited to those that included macronutrient composition. The direction of arrows indicate change when compared to a standard diet control group within that study. Homeostatic model assessment of insulin resistance (HOMA-IR) and hemoglobin A1c (HbA1c).

2.4. Brain

Mice. Chronic consumption of a HFD significantly impairs cognitive function by altering neuronal activity in the hippocampus of humans and rodents [57–59]. Altered hippocampal function is likely a result of chronic inflammation associated with obesity, with more severe outcomes from saturated fatty acids [59–61]. Furthermore, peripheral insulin and glucose homeostasis is largely regulated by hypothalamic insulin responsiveness [62]. Therefore, HFD-induced neuroinflammation, mitochondrial dysfunction, cognitive impairment, and whole-body glucose and insulin resistance highlight the brain as a critical organ in the pathogenesis of the T2D phenotype.

Lard-based diets of 45% and 60% increased the microglial and astrocyte activity in the hypothalamus, the primary regulatory region of energy balance [63,64]. Furthermore, both fat concentrations caused hyperinsulinemia, hyperglycemia, and reduced glucose tolerance, though this was more severe in response to 60% fat [63] (Table 4). Only the 60% HFD altered the hypothalamic, hippocampal, and cortex metabolite profile, showing a shift in cellular energy and metabolism. Similar metabolic dysfunction was reported following 4 weeks of HFD, accompanied by reduced insulin signaling in hypothalamic and hippocampal neurons [65] (Table 4). HFD also induces

changes in the neuropeptide milieu to account for high nutrient density. In response to 60% HFD, the population of anorexigenic proopiomelanocortin (POMC) increased [64], and the expression of orexigenic neuropeptide-Y (NPY) decreased [66] (Table 4).

Table 4. Brain.

Source	Fat Source	Macronutrients (% kcal)	Duration	Strain; Sex	Findings	T2D Status
[63]	Lard and soybean oil	10, 45, or 60% fat 20% protein 70, 35, or 20 % carbohydrates	24 weeks	C57BL/6; Male	45% and 60% fat ↓ Spontaneous activity ↓ Locomotion ↑ Neuroinflammation 60% fatAltered metabolite profile	45% and 60% fat ↑ Body weight: 60% > 45% ↑ Plasma glucose: 60% > 45% ↑ Plasma insulin ↑ Plasma Leptin ↓ Glucose tolerance: 60% > 45% at 2 h
[65]	Lard and soybean oil	60% fat 20% protein 20% carbohydrates	4 weeks	C57BL/6; Male	↓ Insulin signaling in isolated hypothalamic and hippocampal neurons ↓ Mitochondrial function ↑ Oxidative stress	↑ Body weight ↑ Fat mass ↑ Plasma glucose ↑ Plasma insulin ↑ HOMA-IR
[66]	Palm oil	60% fat 16% protein 24% carbohydrates	8 weeks	C57BL/6; Male	↓ Socialization behavior ↑ Disruption of normal circadian feeding Hypothalamic NPY expression	↑ Body weight
[64]	Lard and soybean oil	60% fat 20% protein 20% carbohydrates	12 weeks	C57BL/6; Female	↑ Microglia in hypothalamic arcuate nucleus ↑ Trend in neurogenesis of POMC neurons	↑ Body weight ↑ Fat mass
[67]	Lard	10 % added to standard diet	3 days	Sprague-Dawley Rats; Male	↓ Hypothalamic insulin sensitivity ↓ Hypothalamic insulin-stimulated adipose lipolysis ↓ Hypothalamic insulin-stimulated hepatic glucose production	←→ Body weight ←→ Plasma glucose ←→ Plasma insulin
[68]	Not reported	45% fat 20% protein 35% carbohydrates	20 weeks	Wistar-Han Rats; Male	←→ CSF glucose ↓ CSF glucose tolerance	↑ Body weight Plasma glucose ↓ Glucose tolerance
[69]	Lard and soybean oil	60% fat 20% protein 20% carbohydrates	24 weeks	Sprague-Dawley Rats; Male	↓ Cognitive function ↓ Insulin-stimulated hippocampal perfusion ↓ Hippocampal insulin signaling ↓ Hippocampal eNOS	↓ Whole body glucose disposal ↑ Plasma insulin

Studies cited in the table were limited to those that included macronutrient composition. The direction of arrows indicate change when compared to a standard diet control group within that study. Cerebrospinal fluid (CSF), proopiomelanocortin (POMC), endothelial nitric oxide synthase (eNOS), and homeostatic model assessment of insulin resistance (HOMA-IR).

Rats. Impaired hypothalamic insulin signaling occurred following just three days of a low saturated fat diet (10% lard) in male Sprague–Dawley rats [67] (Table 4). The ability for hypothalamic insulin signaling to suppress white adipose lipolysis and hepatic glucose production was significantly impaired. Such hypothalamic insulin resistance was likely the cause of acute increases in plasma free fatty acids [67]. Diets slightly higher in saturated fats (20%) impaired learning and memory function when compared to standard diet (~4.5% fat) and diets higher in polyunsaturated fat (soybean oil) [70]. Following 18 weeks of a 39% HFD, Wistar rats developed glucose intolerance and increased body weight without hyperglycemia, hyperinsulinemia, or insulin resistance [71]. These rats displayed distinct neurometabolic alterations in the hippocampus and caudate-putamen, including glutamine and N-acetylaspartate (NAA), two prominent amino acids in the brain that play a role in energy metabolism via lipid turnover and the citric acid cycle [52,71,72]. These data do contradict previous studies that showed no alterations in hippocampus metabolic profiles, particularly in genetically modified obese rats [73]. Male Wistar–Han rats fed a 40% HFD for 20 weeks demonstrated reductions in glucose tolerance in both plasma and cerebrospinal fluid following glucose challenge, suggesting that HFD induced changes in both central and peripheral glucose tolerance [68] (Table 4).

Six months of a 60% lard and soybean oil-based HFD impaired insulin-mediated microvascular perfusion and hippocampal cognitive function in Sprague–Dawley rats [74]. A similar response was reported in C57BL/6J mice [63,66,75].

Collectively, the literature supports moderate (45%) and high (60%) saturated fat concentrations as perturbing central and peripheral glucose and insulin sensitivity. While a 60% diet produces a more severe phenotype [63], we must consider whether the increased severity in a rodent model recapitulates the pathogenesis of T2D in humans. A 45% HFD, more in line with a Western-based diet, produces similar central and peripheral metabolic dysfunction, and may align more with the progressive development of human T2D.

2.5. Skeletal Muscle

Mice. Chronic HFD consumption results in intramyocellular lipid storage in skeletal muscle, one of the largest contributors to glucose disposal in the body [24,74,76]. Excess intramyocellular lipid storage, particularly in sedentary populations promotes DAG accretion, protein kinase C activity, AMP-activated protein kinase (AMPK) inhibition, and attenuated glucose uptake [77,78]. The amount of saturated fatty acid in HFD differentially effects lipid deposition within skeletal muscle, potentially promoting differences in metabolism and oxidative capacity.

When consumed for 8 weeks, a 45% cocoa butter (saturated fat), olive oil (monounsaturated fat), or palm oil (a combination of fats), but not safflower oil (polyunsaturated fat)-based HFD, increased TAG and DAG content in skeletal muscle of C57BL/6J mice [19] (Table 5). All cohorts, except the 45% olive oil, demonstrated similar reductions in systemic glucose clearance, despite no changes in insulin-glucose transporter type 4 (GLUT4) expression [19]. β-oxidative remained unchanged, suggesting lipid accumulation occurred without a compensatory increase in oxidation [19].

One week of a 60% lard-based HFD reduced carbohydrate metabolism within skeletal muscle without insulin resistance [49]. When consumed for 15 to 20 weeks, a 60% lard-based diet causes significant dysfunction within skeletal muscle [6,14,30]. Such a diet caused skeletal muscle lipid accumulation, increased fasting glucose levels, and increased peroxisome proliferator-activated receptor gramma coactivator 1alpha (PGC-1α) protein expression [24]. Elevated PGC-1α expression is a characteristic of lipid accumulation in human muscle cells [79]. Furthermore, 191 skeletal muscle genes were altered following 20 weeks of the 60% lard-based HFD, favoring adipogenesis [6]. In agreement, 8 weeks of a similar diet reduced fatty acid oxidation and mitochondrial function [80] (Table 5). In human skeletal muscle, ectopic lipid accumulation, led to insulin resistance [81,82], similarly to that observed in rodent studies [19,24,83]. Subcellular localization of DAG in human skeletal muscle suggests that mitochondrial DAG is elevated in individuals with low insulin sensitivity and may be contributing to alterations in mitochondrial function [84].

Female mice are seldom studied in metabolic research; however, it is naive to assume that male and female rodents respond similarly to HFD models. A 58% coconut oil-based diet caused obesity only in male mice [85]. While muscle insulin sensitivity was reduced in both sexes, only males showed reduced whole-body glucose and insulin tolerance [85] (Table 5).

Table 5. Skeletal Muscle.

Source	Fat Source	Macronutrients (%kcal)	Duration	Strain; Sex	Findings	T2D Status
[19]	(a) Cocoa butter (b) Palm oil (c) Olive oil (d) Safflower oil	45% fat 20% protein 35% carbohydrateAll diet formulations maintained same ratio	8 weeks	C57BL/6; Male	↑ Gastrocnemius TAG and DAG: cocoa butter, palm oil, and olive oil	↑ Body weight in palm oil compared to cocoa butter. ↑ Glucose tolerance: cocoa, palm and safflower oils
[85]	Coconut oil and soybean oil	58% fat 17% protein 25% carbohydrate	16 weeks	FVB; B6;Male and Female	↓ Muscle insulin sensitivity: Males and Females	↑ Body weight: Males only ↑ Plasma glucose: Males only ↓ Glucose and insulin tolerance: Males only
[6,80]	Hydrogenated coconut oil	59% fat 15% protein 26% carbohydrate	8 weeks [83] 20 weeks [6]	C57BL/6; Male	↑ Fatty acid transport ↑ Lipogenesis ↑ Muscle Adipocyte differentiation ↓ Fatty acid oxidation ↓ Mitochondrial function	↑ Body weight ↑ Blood glucose ↑ Plasma insulin ↓ Insulin sensitivity
[86]	Lard and soybean oil	60% fat 20% protein 20% carbohydrate	15 weeks	C57BL/6; Male	↓ Insulin sensitivity ↑ Muscle weight ↑ Inflammatory mRNA profile	↑ Body weight ↑ Serum insulin ↕ Glucose tolerance
[87]	Lard	45% fat 20% protein 35% carbohydrate	15 weeks	Sprague-Dawley rats; Male	↑ Soleus lipid accumulation ↑ Protein and mRNA supporting fatty acid transport and lipogenesis	↑ Body weight ↑ Plasma glucose ↑ Serum insulin ↑ HOMA-IR ↓ Insulin sensitivity
[88,89]	Lard and soybean oil	60% fat 20% protein 20% carbohydrate	2 weeks	Wister rats; Male	←→ Soleus and extensor digitorum longus weight ←→ Soleus and extensor digitorum longus insulin signaling ↓ Soleus force production ↓ Soleus glutathione ↑ Soleus IL-6 mRNA ↑ Lipid droplet size in soleus ↑ Percentage of large lipid droplets in soleus ↑ Lipogenic mRNA in soleus	←→ Body weight
[90,91]	Lard and soybean oil	60% fat 20% protein 20% carbohydrate	2 weeks	Wister rats; Male	↓ Glucose uptake by isolated type IIAX, IIX, IIBX, and IIB fibers ↑ Lipid droplet density in type I, IIA, and IIAX fibers ↑ Lipid droplet size in type I and IIA fibers ↓ Insulin-stimulated glucose uptake in whole muscle ↓ Insulin-stimulated glucose uptake in isolated type IIA, IIAX, and IIB fibers	←→ Body weight

Studies cited in the table were limited to those that included macronutrient composition. The direction of arrows indicate change when compared to a standard diet control group within that study. Diacylglycerol (DAG), triacylglycerol (TAG), interleukin 6 (IL-6), and homeostatic model assessment of insulin resistance (HOMA-IR).

Rats. Within a short exposure to 60% HFD, skeletal muscle metabolism and function are altered. These effects are fiber-type specific with increased lipid accumulation in type I and II intermediate fibers and reduced insulin-stimulated glucose uptake in a spectrum of type II fibers [88–91] (Table 5). Increased lipid accumulation in the soleus is associated with increase inflammatory signaling, evidenced by changes in IL-6 mRNA, and decreased control of oxidative stress [88].

A moderate 45% HFD also increased soleus lipid accumulation, as determined after 15 weeks [87]. Lipid accumulation was supported by increases in plasma membrane fatty acid binding protein (FABPpm), fatty acid transporter protein 1 (FATP1), fatty acid transporter protein 4 (FATP4), and CD36 [87] (Table 5). This diet was also associated with significant changes in whole-body insulin and glucose homeostasis. Hyperglycemia, hyperinsulinemia, and increased HOMA-IR were evident by 8 weeks of dietary consumption and persisted for 15 weeks [87]. Therefore, these data support the suitability of a macronutrient composition more closely aligned to a Western-based diet for studying the effects of HFD on skeletal muscle metabolism.

3. Choosing the Most Appropriate Model

As the percentage of fat in a diet increases, the metabolic changes become more significant, demonstrated by a 60% HFD animal model decreasing glucose sensitivity more rapidly (within one week) than a 45% HFD [92]. Furthermore, using a fat percentage that is 1.7-fold greater than a typical Western diet (~35% HFD) may induce pathology that is not characteristic of the T2D-like phenotype found in humans. Challenges with data interpretation and translatability to human studies include animal strain-specific responses, dietary variation, and the metabolic differences between humans and murine models [93]. A rodent's heart rate ranges from 350–550 beats·min^{-1}, but a human's resting heart is approximately 70 beats·min^{-1} [93]. A mouse's basal metabolic rate is ~7.5-fold greater than a human's, suggesting the metabolic demand on a mouse is significantly greater [94]. Hepatic glycogen storage in a mouse is depleted every 16–24 h, and gluconeogenesis provides the majority of endogenous glucose, demonstrated by over 80% of glucose supplied via gluconeogenesis following a 4-h fasting period [94,95]. In contrast, humans utilize hepatic glycogen at approximately half that rate, even after an overnight (~12 h) fasting period [94]. Due to the faster depletion of glycogen stores and increased metabolic rate, mice consumed food and water more frequently throughout a 24-h period than humans. On average, mice consumed ~4.5 g food across 36 feedings and ~5.8 mL of water across 32 drinking times per day [96]. Feeding habit variability between rodents and humans may also contribute to dissimilarities in metabolism. As nocturnal animals, rodents consume the majority of their food in the evenings, but humans primarily eat during the day [97]. Further complicating this comparison is the treatment of rodents as diurnal rather than using a reverse light cycle to create a more natural rodent living environment. Circadian clocks are involved in many biological processes, including glucose metabolism and insulin secretion, particularly within pancreatic β-cells [98–100]. Disruptions in circadian rhythms could alter disease pathology or data interpretation, making translatability further challenging. Obesity and insulin resistance induced by a 60% high-fat diet caused alterations in circadian rhythm patterns in the hypothalamus [101]. Exogenous dopamine administration during appropriate peaks of circadian rhythm stimulated a physiological response mirroring a non-obese and an insulin sensitive rodent [101].

The full etiology of T2D cannot be accurately assessed and entirely translated to clinical practice because rodents experience β-cell proliferation or increased β-cell mass, rather than the loss of β-cell mass or β-cell failure [54]. To most effectively translate findings to the human population, an optimal animal model or a combination of a few select models may be most appropriate. Although the Western diet is known for excess fats, carbohydrates, and sugars, a longitudinal study over 17 years concluded that less than 35% of the average adult's diet actually comes from fats [102]. According to the National Health and Nutrition Examination Survey, the mean dietary intake for adults (≥20 years) is composed of ~16% protein, ~47% carbohydrates, and ~35% fat. Nearly one-third of the total fat intake is saturated fat, demonstrating that there is a combination of fat sources in the typical Western

diet. This data suggests that including a variety of fat sources (saturated, monounsaturated and polyunsaturated fats) would more accurately mimic the diet macronutrient composition seen in the average population. Based on this literature review, a 45% HFD with a combination of fat sources (monounsaturated, polyunsaturated, and saturated fats) induces pathological changes in rodents that closely resembles the T2D-like phenotype etiology in human populations. For example, adipose tissue becomes inflamed with a 45% high-fat model, but adipose tissue undergoes severe inflammation, remodulation, and adipocytosis following a 60% high-fat diet [35,103]. Commonly used 60% HFDs also contain more than nine times the amount of saturated fat (lard) when compared to unsaturated fat (soybean oil), suggesting that there are fat composition variables that need continued refinement to improve mirroring the human diet composition and translatability to target populations. Based on the literature reviewed here, we propose a 45% HFD composed of one-third saturated fats and two-thirds unsaturated fat closely aligns with the typical human Western diet and disease progression (Figure 1). Utilizing such a composition may provide better alignment between rodent and human T2D phenotypes and more inter-study agreement.

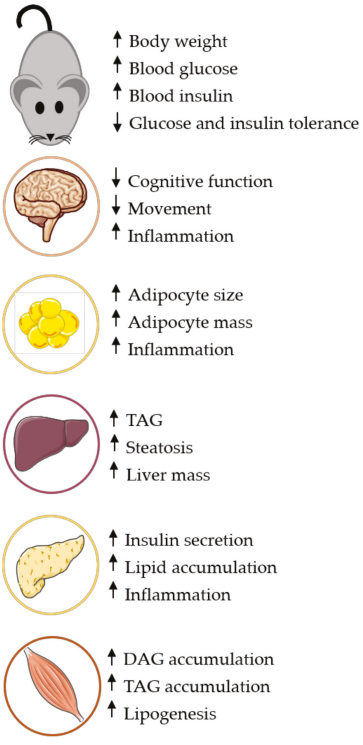

Figure 1. Rodent tissue responses to Western-like diet. A 45% HFD provides a progressive development of tissue and whole-body changes consistent with the T2D-like phenotype. Using higher fat percentages may create a greater magnitude of tissue dysfunction or accelerate the process, resulting in missed opportunity to study key aspects of disease progression. Detailed tissue responses could be found in Table 1 through Table 5. High-fat diet (HFD), Type 2 Diabetes (T2D), Triacylglycerol (TAG) and Diacylglycerol (DAG).

It is important to acknowledge limitations to this review. While we attempted to use an un-biased review of the literature that used non-genetically altered rodents, we were not able to include all relevant publications. Those chosen provided sufficient methodological detail regarding dietary composition,

intervention duration, and comprehensive sets of data. Moreover, only studies that compared HFD to a standard diet groups were included. Those in which the HFD served as the control against a pharmacological treatment were excluded. Mouse studies were focused on the C57BL/6 background because it is the most common. However, because the inclusion for female mice was rare, we included studies that investigated sexual dimorphism using other strains. Sprague–Dawley and Wister strains were targeted for rat studies because of their predominance in the literature. We attempted to narrow our literature to the last 5 years, particularly for studies included in the tables; however, in some cases we had to expand our search to accommodate for our inclusion criteria. Furthermore, this review focuses exclusively on HFD composition and concentration. Other dietary concerns, such as sugar, cholesterol, fiber, vitamin, and mineral composition and their combination with pharmacological strategies should be considered but are beyond the scope of this review. Additionally, numerous transgenic models exist, such as Ob/Ob, db/db, and KKAy, which cause metabolic dysfunction. Likewise, genetic models alone and in combination with dietary and pharmacological intervention are commonly used, particularly in the study of central insulin and glucose homeostasis. Lastly, animal models often include one gender, typically males, to avoid complications with the estrous cycle in female rodents, but diet-induced animal models can exhibit sexual dimorphisms [104]. Future studies should make every effort to include male and female rodents to comprehensively enhance our understanding of HFD models of T2D and associated phenotypes.

Author Contributions: Conceptualization, N.L.S. and J.S.M.; writing—original draft preparation, N.L.S. and J.S.M.; writing—review and editing, J.S.M. All authors have read and agreed to the published version of the manuscript.

Funding: This research received no external funding.

Acknowledgments: The authors would like to thank the Laboratory of Systems Physiology group for their support and feedback during the writing of this manuscript.

Conflicts of Interest: The authors have nothing to disclose.

References

1. Agriculture, USA. *2015–2020 Dietary Guidelines for Americans*; U.S. Department of Health and Human Services and U.S. Department of Agriculture: Washington, DC, USA, 2015; pp. 1–144.
2. Mazidi, M.; Kengne, A.-P.; Mikhailidis, D.P.; Toth, P.P.; Ray, K.K.; Banach, M. Dietary food patterns and glucose/insulin homeostasis: A cross-sectional study involving 24,182 adult Americans. *Lipids Health Dis.* **2017**, *16*, 192. [CrossRef]
3. Hariri, N.; Gougeon, R.; Thibault, L. A highly saturated fat-rich diet is more obesogenic than diets with lower saturated fat content. *Nutr. Res.* **2010**, *30*, 632–643. [CrossRef]
4. Licholai, J.A.; Nguyen, K.P.; Fobbs, W.C.; Schuster, C.J.; Ali, M.A.; Kravitz, A.V. Why Do Mice Overeat High-Fat Diets? How High-Fat Diet Alters the Regulation of Daily Caloric Intake in Mice. *Obesity (Silver Spring)* **2018**, *26*, 1026–1033. [CrossRef]
5. Kubant, R.; Poon, A.N.; Sanchezhernandez, D.; Domenichiello, A.F.; Huot, P.S.P.; Pannia, E.; Cho, C.E.; Hunschede, S.; Bazinet, R.P.; Anderson, G.H. A comparison of effects of lard and hydrogenated vegetable shortening on the development of high-fat diet-induced obesity in rats. *Nutr. Diabetes* **2015**, *5*, e188. [CrossRef]
6. Lee, R.K.; Hittel, D.S.; Nyamandi, V.Z.; Kang, L.; Soh, J.; Sensen, C.W.; Shearer, J. Unconventional microarray design reveals the response to obesity is largely tissue specific: Analysis of common and divergent responses to diet-induced obesity in insulin-sensitive tissues. *Appl. Physiol. Nutr. Metab.* **2012**, *37*, 257–268. [CrossRef]
7. De Fourmestraux, V.; Neubauer, H.; Poussin, C.; Farmer, P.; Falquet, L.; Burcelin, R.; Delorenzi, M.; Thorens, B. Transcript Profiling Suggests That Differential Metabolic Adaptation of Mice to a High Fat Diet Is Associated with Changes in Liver to Muscle Lipid Fluxes. *J. Biol. Chem.* **2004**, *279*, 50743–50753. [CrossRef]
8. Tajima, K.; Shirakawa, J.; Okuyama, T.; Kyohara, M.; Yamazaki, S.; Togashi, Y.; Terauchi, Y. Effects of metformin on compensatory pancreatic β-cell hyperplasia in mice fed a high-fat diet. *Am. J. Physiol. Endocrinol. Metab.* **2017**, *313*, E367–E380. [CrossRef]

9. Moretto, T.L.; Benfato, I.D.; De Carvalho, F.P.; Barthichoto, M.; Le Sueur-Maluf, L.; De Oliveira, C.A.M. The effects of calorie-matched high-fat diet consumption on spontaneous physical activity and development of obesity. *Life Sci.* **2017**, *179*, 30–36. [CrossRef]
10. Kleinert, M.; Clemmensen, C.; Hofmann, S.M.; Moore, M.C.; Renner, S.; Woods, S.C.; Huypens, P.; Beckers, J.; De Angelis, M.H.; Schürmann, A.; et al. Animal models of obesity and diabetes mellitus. *Nat. Rev. Endocrinol.* **2018**, *14*, 140–162. [CrossRef]
11. Islam, S.; Wilson, R.D. Experimentally Induced Rodent Models of Type 2 Diabetes. *Animal Models Diabetes Res.* **2012**, *933*, 161–174. [CrossRef]
12. Kanuri, G.; Bergheim, I. In Vitro and in Vivo Models of Non-Alcoholic Fatty Liver Disease (NAFLD). *Int. J. Mol. Sci.* **2013**, *14*, 11963–11980. [CrossRef]
13. Warden, C.H.; Fisler, J.S. Comparisons of Diets Used in Animal Models of High-Fat Feeding. *Cell Metab.* **2008**, *7*, 277. [CrossRef]
14. Bullen, J.W.; Bluher, S.; Kelesidis, T.; Mantzoros, C.S. Regulation of adiponectin and its receptors in response to development of diet-induced obesity in mice. *Am. J. Physiol. Endocrinol. Metab.* **2007**, *292*, E1079–E1086. [CrossRef]
15. Kim, S.; Sohn, I.; Ahn, J.-I.; Lee, K.-H.; Lee, Y.S.; Lee, Y.S. Hepatic gene expression profiles in a long-term high-fat diet-induced obesity mouse model. *Gene* **2004**, *340*, 99–109. [CrossRef]
16. Flanagan, A.M.; Brown, J.L.; Santiago, C.A.; Aad, P.Y.; Spicer, L.J.; Spicer, M.T. High-fat diets promote insulin resistance through cytokine gene expression in growing female rats. *J. Nutr. Biochem.* **2008**, *19*, 505–513. [CrossRef]
17. Xavier, G.D.S.; Hodson, D.J. Mouse models of peripheral metabolic disease. *Best Pr. Res. Clin. Endocrinol. Metab.* **2018**, *32*, 299–315. [CrossRef]
18. Hintze, K.J.; Benninghoff, A.D.; Cho, C.E.; Ward, R.E. Modeling the Western Diet for Preclinical Investigations. *Adv. Nutr.* **2018**, *9*, 263–271. [CrossRef]
19. Timmers, S.; Bosch, J.D.V.-V.D.; De Wit, N.; Schaart, G.; Van Beurden, D.; Hesselink, M.K.C.; Van Der Meer, R.; Schrauwen, P. Differential effects of saturated versus unsaturated dietary fatty acids on weight gain and myocellular lipid profiles in mice. *Nutr. Diabetes* **2011**, *1*, e11. [CrossRef]
20. An, X.; Liu, J.; Li, Y.; Dou, Z.; Li, N.; Suo, Y.; Ma, Y.; Sun, M.; Tian, Z.; Xu, L. Chemerin/CMKLR1 ameliorates nonalcoholic steatohepatitis by promoting autophagy and alleviating oxidative stress through the JAK2-STAT3 pathway. *Peptides* **2020**, *135*, 170422. [CrossRef]
21. Lu, Z.; Li, Y.; Syn, W.-K.; Li, A.-J.; Ritter, S.; Wank, S.A.; Lopes-Virella, M.F.; Huang, Y. GPR40-Deficiency Is Associated with Hepatic FAT/CD36 Upregulation, Steatosis, Inflammation and Cell Injury in C57BL/6 Mice. *Am. J. Physiol. Endocrinol. Metab.* **2020**. [CrossRef]
22. Sardi, C.; Martini, E.; Mello, T.; Camelliti, S.; Sfondrini, L.; Marcucci, F.; Kallikourdis, M.; Sommariva, M.; Rumio, C. Effect of acetylsalicylic acid on inflamed adipose tissue. Insulin resistance and hepatic steatosis in a mouse model of diet-induced obesity. *Life Sci.* **2020**, 118618. [CrossRef]
23. Shen, H.H.; Alex, R.; Bellner, L.; Raffaele, M.; Licari, M.; Vanella, L.; Stec, D.E.; Abraham, N.G. Milk thistle seed cold press oil attenuates markers of the metabolic syndrome in a mouse model of dietary-induced obesity. *J. Food Biochem.* **2020**, e13522. [CrossRef] [PubMed]
24. Peck, B.; Huot, J.; Renzi, T.; Arthur, S.; Turner, M.J.; Marino, J.S. Mice Lacking PKCtheta in Skeletal Muscle Have Reduced Intramyocellular Lipid Accumulation and Increased Insulin Responsiveness in Skeletal Muscle. *Am. J. Physiol. Regul. Integr. Comp. Physiol.* **2017**, *314*, 468–477. [CrossRef]
25. Bezan, P.; Holland, H.; De Castro, G.S.; Cardoso, J.; Ovidio, P.; Calder, P.C.; Jordão, A. High Dose of A Conjugated Linoleic Acid Mixture Increases Insulin Resistance in Rats Fed Either A Low Fat or A High Fat Diet. *Exp. Clin. Endocrinol. Diabetes* **2018**, *126*, 379–386. [CrossRef]
26. Baek, K.-W.; Gim, J.-A.; Park, J.-J. Regular moderate aerobic exercise improves high-fat diet-induced nonalcoholic fatty liver disease via monoacylglycerol O-acyltransferase 1 pathway suppression. *J. Sport Health Sci.* **2020**, *9*, 472–478. [CrossRef]
27. Abdulmalek, S.A.; Fessal, M.; El-Sayed, M. Effective amelioration of hepatic inflammation and insulin response in high fat diet-fed rats via regulating AKT/mTOR signaling: Role of Lepidium sativum seed extracts. *J. Ethnopharmacol.* **2021**, *266*, 113439. [CrossRef] [PubMed]
28. Saltiel, A.R.; Olefsky, J.M. Inflammatory mechanisms linking obesity and metabolic disease. *J. Clin. Investig.* **2017**, *127*, 1–4. [CrossRef]

29. Inoue, M.; Ohtake, T.; Motomura, W.; Takahashi, N.; Hosoki, Y.; Miyoshi, S.; Suzuki, Y.; Saito, H.; Kohgo, Y.; Okumura, T. Increased expression of PPARgamma in high fat diet-induced liver steatosis in mice. *Biochem. Biophys. Res. Commun.* **2005**, *336*, 215–222. [CrossRef]
30. Wikan, N.; Tocharus, J.; Sivasinprasasn, S.; Kongkaew, A.; Chaichompoo, W.; Suksamrarn, A.; Tocharus, C. Capsaicinoid nonivamide improves nonalcoholic fatty liver disease in rats fed a high-fat diet. *J. Pharmacol. Sci.* **2020**, *143*, 188–198. [CrossRef]
31. Ramalho, L.; Da Jornada, M.N.; Antunes, L.D.C.; Hidalgo, M.P.L. Metabolic disturbances due to a high-fat diet in a non-insulin-resistant animal model. *Nutr. Diabetes* **2017**, *7*, e245. [CrossRef]
32. Erion, D.M.; Park, H.-J.; Lee, H.-Y. The role of lipids in the pathogenesis and treatment of type 2 diabetes and associated co-morbidities. *BMB Rep.* **2016**, *49*, 139–148. [CrossRef] [PubMed]
33. Finucane, O.M.; Lyons, C.L.; Murphy, A.M.; Reynolds, C.M.; Klinger, R.; Healy, N.P.; Cooke, A.A.; Coll, R.C.; McAllan, L.; Nilaweera, K.N.; et al. Monounsaturated Fatty Acid–Enriched High-Fat Diets Impede Adipose NLRP3 Inflammasome–Mediated IL-1β Secretion and Insulin Resistance Despite Obesity. *Diabetes* **2015**, *64*, 2116–2128. [CrossRef] [PubMed]
34. Shen, H.H.; Peterson, S.J.; Bellner, L.; Choudhary, A.; Levy, L.; Gancz, L.; Sasson, A.; Trainer, J.; Rezzani, R.; Resnick, A.; et al. Cold-Pressed Nigella Sativa Oil Standardized to 3% Thymoquinone Potentiates Omega-3 Protection against Obesity-Induced Oxidative Stress, Inflammation, and Markers of Insulin Resistance Accompanied with Conversion of White to Beige Fat in Mice. *Antioxidants* **2020**, *9*, 489. [CrossRef]
35. Strissel, K.J.; Stancheva, Z.; Miyoshi, H.; Perfield, J.W.; DeFuria, J.; Jick, Z.; Greenberg, A.S.; Obin, M.S. Adipocyte death, adipose tissue remodeling, and obesity complications. *Diabetes* **2007**, *56*, 2910–2918. [CrossRef] [PubMed]
36. Lyons, C.L.; Kennedy, E.B.; Roche, H.M. Metabolic Inflammation-Differential Modulation by Dietary Constituents. *Nutrition* **2016**, *8*, 247. [CrossRef] [PubMed]
37. Liu, Y.; Lu, X.; Li, X.; Du, P.; Qin, G. High-fat diet triggers obesity-related early infiltration of macrophages into adipose tissue and transient reduction of blood monocyte count. *Mol. Immunol.* **2020**, *117*, 139–146. [CrossRef] [PubMed]
38. Hu, Q.; Lu, Y.; Hu, F.; He, S.; Xu, X.; Niu, Y.; Zhang, H.; Li, X.; Su, Q. Resistant dextrin reduces obesity and attenuates adipose tissue inflammation in high-fat diet-fed mice. *Int. J. Med Sci.* **2020**, *17*, 2611–2621. [CrossRef]
39. Eom, J.; Thomas, S.S.; Sung, N.-Y.; Kim, D.-S.; Cha, Y.-S.; Kim, K.-A. *Abeliophyllum distichum* Ameliorates High-Fat Diet-Induced Obesity in C57BL/6J Mice by Upregulating the AMPK Pathway. *Nutrients* **2020**, *12*, 3320. [CrossRef]
40. Liang, H.; Jiang, F.; Cheng, R.; Luo, Y.; Wang, J.; Luo, Z.; Li, M.; Shen, X.; He, F. A high-fat diet and high-fat and high-cholesterol diet may affect glucose and lipid metabolism differentially through gut microbiota in mice. *Exp. Anim.* **2020**, 20. [CrossRef]
41. Kim, S.-Y.; Lee, M.-S.; Chang, E.; Jung, S.; Ko, H.; Lee, E.; Lee, S.; Kim, C.-T.; Kim, I.-H.; Kim, Y. Tartary Buckwheat Extract Attenuated the Obesity-Induced Inflammation and Increased Muscle PGC-1a/SIRT1 Expression in High Fat Diet-Induced Obese Rats. *Nutrition* **2019**, *11*, 654. [CrossRef]
42. Vasconcelos, R.P.; Peixoto, M.S.; De Oliveira, K.A.; Ferreira, A.C.F.; Coelho-De-Souza, A.N.; Carvalho, D.P.; De Oliveira, A.C.; Fortunato, R.S. Sex differences in subcutaneous adipose tissue redox homeostasis and inflammation markers in control and high-fat diet fed rats. *Appl. Physiol. Nutr. Metab.* **2019**, *44*, 720–726. [CrossRef] [PubMed]
43. Grycel, S.; Markowski, A.R.; Hady, H.R.; Zabielski, P.; Kojta, I.; Imierska, M.; Górski, J.; Błachnio-Zabielska, A. Metformin treatment affects adipocytokine secretion and lipid composition in adipose tissues of diet-induced insulin-resistant rats. *Nutrition* **2019**, *63*, 126–133. [CrossRef] [PubMed]
44. Kolahdouzi, S.; Talebi-Garakani, E.; Hamidian, G.; Safarzade, A. Exercise training prevents high-fat diet-induced adipose tissue remodeling by promoting capillary density and macrophage polarization. *Life Sci.* **2019**, *220*, 32–43. [CrossRef]
45. Ellenbroek, J.H.; Töns, H.A.; De Graaf, N.; Loomans, C.J.; Engelse, M.A.; Vrolijk, H.; Voshol, P.J.; Rabelink, T.J.; Carlotti, F.; De Koning, E.J.P. Topologically Heterogeneous Beta Cell Adaptation in Response to High-Fat Diet in Mice. *PLoS ONE* **2013**, *8*, e56922. [CrossRef]

46. Faleck, D.M.; Ali, K.; Roat, R.; Graham, M.J.; Crooke, R.M.; Battisti, R.; Garcia, E.; Ahima, R.S.; Imai, Y. Adipose differentiation-related protein regulates lipids and insulin in pancreatic islets. *Am. J. Physiol. Endocrinol. Metab.* **2010**, *299*, E249–E257. [CrossRef] [PubMed]
47. Gupta, D.; Jetton, T.L.; LaRock, K.; Monga, N.; Satish, B.; Lausier, J.; Peshavaria, M.; Leahy, J.L. Temporal characterization of beta cell-adaptive and -maladaptive mechanisms during chronic high-fat feeding in C57BL/6NTac mice. *J. Biol. Chem.* **2017**, *292*, 12449–12459. [CrossRef]
48. Li, H.; Park, H.-M.; Ji, H.-S.; Han, J.; Kim, S.K.; Park, H.-Y.; Jeong, T.-S. Phenolic-enriched blueberry-leaf extract attenuates glucose homeostasis, pancreatic β-cell function, and insulin sensitivity in high-fat diet–induced diabetic mice. *Nutr. Res.* **2020**, *73*, 83–96. [CrossRef]
49. Seferovic, M.D.; Beamish, C.A.; Mosser, R.E.; Townsend, S.; Pappan, K.; Poitout, V.; Aagaard, K.M.; Gannon, M.A. Increases in bioactive lipids accompany early metabolic changes associated with β-cell expansion in response to short-term high-fat diet. *Am. J. Physiol. Endocrinol. Metab.* **2018**, *315*, E1251–E1263. [CrossRef]
50. Ye, T.; Chen, Y.-H.; Gao, J.-H.; Wang, X.-X.; Qiang, O.; Tang, C.-W.; Liu, R. Effect of octreotide on pancreatic fibrosis in rats with high-fat diet-induced obesity. *Int. J. Clin. Exp. Pathol.* **2018**, *11*, 4784–4794. [CrossRef]
51. Sun, Q.; Nie, S.; Wang, L.; Yang, F.; Meng, Z.; Xiao, H.; Xiang, B.; Li, X.; Fu, X.; Wang, S. Factors that Affect Pancreatic Islet Cell Autophagy in Adult Rats: Evaluation of a Calorie-Restricted Diet and a High-Fat Diet. *PLoS ONE* **2016**, *11*, e0151104. [CrossRef]
52. Teleman, A. Faculty Opinions recommendation of Glutamine oxidation maintains the TCA cycle and cell survival during impaired mitochondrial pyruvate transport. *Fac. Opin.* **2015**, *56*, 414–424. [CrossRef]
53. Abdel-Hamid, A.A.M.; Firgany, A.E.-D.L. Correlation between pancreatic mast cells and the low grade inflammation in adipose tissue of experimental prediabetes. *Acta Histochem.* **2019**, *121*, 35–42. [CrossRef] [PubMed]
54. Butler, A.E.; Janson, J.; Bonner-Weir, S.; Ritzel, R.A.; Rizza, R.A.; Butler, P.C. Cell Deficit and Increased -Cell Apoptosis in Humans With Type 2 Diabetes. *Diabetes* **2003**, *52*, 102–110. [CrossRef] [PubMed]
55. Parilla, J.H.; Willard, J.R.; Barrow, B.M.; Zraika, S. A Mouse Model of Beta-Cell Dysfunction as Seen in Human Type 2 Diabetes. *J. Diabetes Res.* **2018**, *2018*, 6106051. [CrossRef]
56. Lu, B.; Wu, H.; Gu, P.; Du, H.; Shao, J.; Wang, J.; Zou, D. Improved glucose-stimulated insulin secretion by intra-islet inhibition of protein-tyrosine phosphatase 1B expression in rats fed a high-fat diet. *J. Endocrinol. Investig.* **2011**, *35*, 63–70.
57. Cordner, Z.A.; Tamashiro, K.L. Effects of high-fat diet exposure on learning & memory. *Physiol. Behav.* **2015**, *152 Pt B*, 363–371. [CrossRef]
58. Kanoski, S.E.; Davidson, T.L. Western diet consumption and cognitive impairment: Links to hippocampal dysfunction and obesity. *Physiol. Behav.* **2011**, *103*, 59–68. [CrossRef]
59. Beilharz, J.E.; Maniam, J.; Morris, M.J. Diet-Induced Cognitive Deficits: The Role of Fat and Sugar, Potential Mechanisms and Nutritional Interventions. *Nutrients* **2015**, *7*, 6719–6738. [CrossRef]
60. Chesnokova, V.; Pechnick, R.N.; Wawrowsky, K. Chronic peripheral inflammation, hippocampal neurogenesis, and behavior. *Brain Behav. Immun.* **2016**, *58*, 1–8. [CrossRef]
61. Kowiański, P.; Lietzau, G.; Czuba, E.; Waśkow, M.; Steliga, A.; Moryś, J. BDNF: A Key Factor with Multipotent Impact on Brain Signaling and Synaptic Plasticity. *Cell. Mol. Neurobiol.* **2018**, *38*, 579–593. [CrossRef]
62. Marino, J.S.; Xu, Y.; Hill, J.W. Central insulin and leptin-mediated autonomic control of glucose homeostasis. *Trends Endocrinol. Metab.* **2011**, *22*, 275–285. [CrossRef] [PubMed]
63. Lizarbe, B.; Soares, A.F.; Larsson, S.; Duarte, J.M.N.; Lizarbe, B.; Soares, A.F.; Larsson, S.; Duarte, J.M.N. Neurochemical Modifications in the Hippocampus, Cortex and Hypothalamus of Mice Exposed to Long-Term High-Fat Diet. *Front. Neurosci.* **2019**, *12*, 985. [CrossRef] [PubMed]
64. Klein, C.; Jonas, W.; Wiedmer, P.; Schreyer, S.; Akyüz, L.; Spranger, J.; Hellweg, R.; Steiner, B. High-fat Diet and Physical Exercise Differentially Modulate Adult Neurogenesis in the Mouse Hypothalamus. *Neuroscience* **2019**, *400*, 146–156. [CrossRef]
65. Ruegsegger, G.N.; Vanderboom, P.M.; Dasari, S.; Klaus, K.A.; Kabiraj, P.; McCarthy, C.B.; Lucchinetti, C.F.; Nair, K.S. Exercise and metformin counteract altered mitochondrial function in the insulin-resistant brain. *JCI Insight* **2019**, *4*. [CrossRef] [PubMed]

66. Hassan, A.M.; Mancano, G.; Kashofer, K.; Fröhlich, E.E.; Matak, A.; Mayerhofer, R.; Reichmann, F.; Olivares, M.; Neyrinck, A.M.; Delzenne, N.M.; et al. High-fat diet induces depression-like behaviour in mice associated with changes in microbiome, neuropeptide Y, and brain metabolome. *Nutr. Neurosci.* **2019**, *22*, 877–893. [CrossRef]
67. Scherer, T.; Lindtner, C.; Zielinski, E.; O'Hare, J.; Filatova, N.; Buettner, C. Short Term Voluntary Overfeeding Disrupts Brain Insulin Control of Adipose Tissue Lipolysis*. *J. Biol. Chem.* **2012**, *287*, 33061–33069. [CrossRef]
68. Top, M.V.D.; Zhao, F.-Y.; Viriyapong, R.; Michael, N.J.; Munder, A.C.; Pryor, J.T.; Renaud, L.P.; Spanswick, D. The impact of ageing, fasting and high-fat diet on central and peripheral glucose tolerance and glucose-sensing neural networks in the arcuate nucleus. *J. Neuroendocr.* **2017**, *29*, e12528. [CrossRef]
69. Fu, Z.; Wu, J.; Nesil, T.; Li, M.D.; Aylor, K.W.; Liu, Z. Long-term high-fat diet induces hippocampal microvascular insulin resistance and cognitive dysfunction. *Am. J. Physiol. Endocrinol. Metab.* **2017**, *312*, E89–E97. [CrossRef]
70. Greenwood, E.C.; Winocur, G. Cognitive impairment in rats fed high-fat diets: A specific effect of saturated fatty-acid intake. *Behav. Neurosci.* **1996**, *110*, 451–459. [CrossRef]
71. Ribeiro, M.; Castelhano, J.; Petrella, L.; Sereno, J.; Rodrigues, T.; Neves, C.; Letra, L.; Baptista, F.I.; Seiça, R.; Matafome, P.; et al. High-fat diet induces a neurometabolic state characterized by changes in glutamate and N-acetylaspartate pools associated with early glucose intolerance: An in vivo multimodal MRI study. *J. Magn. Reson. Imaging* **2018**, *48*, 757–766. [CrossRef]
72. Moffett, J.R.; Arun, P.; Ariyannur, P.S.; Namboodiri, A.M.A. N-Acetylaspartate reductions in brain injury: Impact on post-injury neuroenergetics, lipid synthesis, and protein acetylation. *Front. Neuroenerg.* **2013**, *5*, 11. [CrossRef] [PubMed]
73. van der Graaf, M.; Janssen, S.W.; van Asten, J.J.; Hermus, A.R.; Sweep, C.G.; Pikkemaat, J.A.; Martens, G.J.; Heerschap, A. Metabolic profile of the hippocampus of Zucker Diabetic Fatty rats assessed by in vivo 1H magnetic resonance spectroscopy. *NMR Biomed.* **2004**, *17*, 405–410. [CrossRef] [PubMed]
74. Bouchard-Mercier, A.; Rudkowska, I.; Lemieux, S.; Couture, P.; Vohl, M.-C. The metabolic signature associated with the Western dietary pattern: A cross-sectional study. *Nutr. J.* **2013**, *12*, 158. [CrossRef] [PubMed]
75. Tsai, S.-F.; Chen, Y.-W.; Kuo, Y.-M. High-fat diet reduces the hippocampal content level of lactate which is correlated with the expression of glial glutamate transporters. *Neurosci. Lett.* **2018**, *662*, 142–146. [CrossRef]
76. Krssak, M.; Petersen, K.F.; Dresner, A.; DiPietro, L.; Vogel, S.M.; Rothman, D.L.; Shulman, G.I.; Roden, M. Intramyocellular lipid concentrations are correlated with insulin sensitivity in humans: A 1 H NMR spectroscopy study. *Diabetology* **1999**, *42*, 113–116. [CrossRef]
77. Jiang, L.Q.; de Castro Barbosa, T.; Massart, J.; Deshmukh, A.S.; Löfgren, L.; Duque-Guimaraes, D.E.; Ozilgen, A.; Osler, M.E.; Chibalin, A.V.; Zierath, J.R. Diacylglycerol kinase-delta regulates AMPK signaling, lipid metabolism, and skeletal muscle energetics. *Am. J. Physiol. Endocrinol. Metab.* **2016**, *310*, E51–E60. [CrossRef]
78. Gao, Z.; Wang, Z.; Zhang, X.; Butler, A.A.; Zuberi, A.; Gawronska-Kozak, B.; Lefevre, M.; York, D.; Ravussin, E.; Berthoud, H.R.; et al. Inactivation of PKCtheta leads to increased susceptibility to obesity and dietary insulin resistance in mice. *Am. J. Physiol. Endocrinol. Metab.* **2007**, *292*, E84–E91. [CrossRef]
79. Mormeneo, E.; Jimenez-Mallebrera, C.; Palomer, X.; De Nigris, V.; Vázquez-Carrera, M.; Orozco, A.; Nascimento, A.; Colomer, J.; Lerin, C.; Gómez-Foix, A.M. PGC-1α Induces Mitochondrial and Myokine Transcriptional Programs and Lipid Droplet and Glycogen Accumulation in Cultured Human Skeletal Muscle Cells. *PLoS ONE* **2012**, *7*, e29985. [CrossRef]
80. De Mendonça, M.; De Sousa, É.; Da Paixão, A.O.; Dos Santos, B.A.; Spagnol, A.R.; Murata, G.M.; Araújo, H.N.; De Lima, T.I.; Guimarães, D.S.P.S.F.; Silveira, L.R.; et al. MicroRNA miR-222 mediates pioglitazone beneficial effects on skeletal muscle of diet-induced obese mice. *Mol. Cell. Endocrinol.* **2019**, *501*, 110661. [CrossRef]
81. Gao, Z.; Wang, Z.; Zhang, X.; Butler, A.A.; Zuberi, A.; Gawronska-Kozak, B.; Lefevre, M.; York, D.; Ravussin, E.; Berthoud, H.R.; et al. Role of diacylglycerol activation of PKCtheta in lipid-induced muscle insulin resistance in humans. *Proc. Natl. Acad. Sci. USA* **2014**, *111*, 9597–9602.
82. Bergman, B.C.; Hunerdosse, D.M.; Kerege, A.; Playdon, M.C.; Perreault, L. Localisation and composition of skeletal muscle diacylglycerol predicts insulin resistance in humans. *Diabetology* **2012**, *55*, 1140–1150. [CrossRef] [PubMed]

83. Kim, J.K.; Fillmore, J.J.; Sunshine, M.J.; Albrecht, B.; Higashimori, T.; Kim, D.-W.; Liu, Z.-X.; Soos, T.J.; Cline, G.W.; O'Brien, W.R.; et al. PKC knockout mice are protected from fat-induced insulin resistance. *J. Clin. Investig.* **2004**, *114*, 823–827. [CrossRef] [PubMed]
84. Perreault, L.; Newsom, S.A.; Strauss, A.; Kerege, A.; Kahn, D.E.; Harrison, K.A.; Snell-Bergeon, J.K.; Nemkov, T.; D'Alessandro, A.; Jackman, M.R.; et al. Intracellular localization of diacylglycerols and sphingolipids influences insulin sensitivity and mitochondrial function in human skeletal muscle. *JCI Insight* **2018**, *3*. [CrossRef] [PubMed]
85. Rudnicki, M.; Abdifarkosh, G.; Rezvan, O.; Nwadozi, E.; Roudier, E.; Haas, T.L. Female Mice Have Higher Angiogenesis in Perigonadal Adipose Tissue Than Males in Response to High-Fat Diet. *Front. Physiol.* **2018**, *9*, 1452. [CrossRef] [PubMed]
86. Kim, B.; Kwon, J.; Kim, M.-S.; Park, H.; Ji, Y.; Holzapfel, W.; Hyun, C.-K. Protective effects of Bacillus probiotics against high-fat diet-induced metabolic disorders in mice. *PLoS ONE* **2018**, *13*, e0210120. [CrossRef] [PubMed]
87. Cao, Y.; Chang, S.; Dong, J.; Zhu, S.; Zheng, X.; Li, J.; Long, R.; Zhou, Y.; Cui, J.; Zhang, Y. Emodin ameliorates high-fat-diet induced insulin resistance in rats by reducing lipid accumulation in skeletal muscle. *Eur. J. Pharmacol.* **2016**, *780*, 194–201. [CrossRef]
88. Andrich, D.E.; Melbouci, L.; Ou, Y.; Auclair, N.; Mercier, J.; Grenier, J.-C.; Lira, F.S.; Barreiro, L.B.; Danialou, G.; Comtois, A.-S.; et al. A Short-Term High-Fat Diet Alters Glutathione Levels and IL-6 Gene Expression in Oxidative Skeletal Muscles of Young Rats. *Front. Physiol.* **2019**, *10*, 372. [CrossRef]
89. Andrich, D.E.; Ou, Y.; Melbouci, L.; Leduc-Gaudet, J.-P.; Auclair, N.; Mercier, J.; Secco, B.; Tomaz, L.M.; Gouspillou, G.; Danialou, G.; et al. Altered Lipid Metabolism Impairs Skeletal Muscle Force in Young Rats Submitted to a Short-Term High-Fat Diet. *Front. Physiol.* **2018**, *9*. [CrossRef]
90. Pataky, M.W.; Wang, H.; Yu, C.S.; Arias, E.B.; Ploutz-Snyder, R.J.; Zheng, X.; Cartee, G.D. High-Fat Diet-Induced Insulin Resistance in Single Skeletal Muscle Fibers is Fiber Type Selective. *Sci. Rep.* **2017**, *7*, 13642. [CrossRef]
91. Pataky, M.W.; Yu, C.S.; Nie, Y.; Arias, E.B.; Singh, M.; Mendias, C.L.; Ploutz-Snyder, R.J.; Cartee, G.D. Skeletal muscle fiber type-selective effects of acute exercise on insulin-stimulated glucose uptake in insulin-resistant, high-fat-fed rats. *Am. J. Physiol. Endocrinol. Metab.* **2019**, *316*, E695–E706. [CrossRef]
92. Soares, A.F.; Duarte, J.M.N.; Gruetter, R. Increased hepatic fatty acid polyunsaturation precedes ectopic lipid deposition in the liver in adaptation to high-fat diets in mice. *MAGMA* **2017**, *31*, 341–354. [CrossRef]
93. Lai, M.; Chandrasekera, P.C.; Barnard, N.D. You are what you eat, or are you? The challenges of translating high-fat-fed rodents to human obesity and diabetes. *Nutr. Diabetes* **2014**, *4*, e135. [CrossRef] [PubMed]
94. Kowalski, G.M.; Bruce, C.R. The regulation of glucose metabolism: Implications and considerations for the assessment of glucose homeostasis in rodents. *Am. J. Physiol. Endocrinol. Metab.* **2014**, *307*, E859–E871. [CrossRef] [PubMed]
95. Burgess, S.M.; Jeffrey, F.M.H.; Storey, C.; Milde, A.; Hausler, N.; Merritt, M.E.; Mulder, H.; Holm, C.; Sherry, A.D.; Malloy, C.R. Effect of murine strain on metabolic pathways of glucose production after brief or prolonged fasting. *Am. J. Physiol. Endocrinol. Metab.* **2005**, *289*, E53–E61. [CrossRef] [PubMed]
96. Gannon, K.S.; Smith, J.C.; Henderson, R.; Hendrick, P. A system for studying the microstructure of ingestive behavior in mice. *Physiol. Behav.* **1992**, *51*, 515–521. [CrossRef]
97. Ellacott, K.L.; Morton, G.J.; Woods, S.C.; Tso, P.; Schwartz, M.W. Assessment of Feeding Behavior in Laboratory Mice. *Cell Metab.* **2010**, *12*, 10–17. [CrossRef]
98. Perelis, M.; Ramsey, K.M.; Marcheva, B.; Bass, J. Circadian Transcription from Beta Cell Function to Diabetes Pathophysiology. *J. Biol. Rhythm.* **2016**, *31*, 323–336. [CrossRef]
99. Qian, J.; Yeh, B.; Rakshit, K.; Colwell, C.S.; Matveyenko, A.V. Circadian Disruption and Diet-Induced Obesity Synergize to Promote Development of β-Cell Failure and Diabetes in Male Rats. *Endocrinology* **2015**, *156*, 4426–4436. [CrossRef]
100. Johnston, J.D.; Ordovás, J.M.; Scheer, F.A.; Turek, F.W. Circadian Rhythms, Metabolism, and Chrononutrition in Rodents and Humans. *Adv. Nutr.* **2016**, *7*, 399–406. [CrossRef]
101. Luo, S.; Zhang, Y.; Ezrokhi, M.; Li, Y.; Tsai, T.-H.; Cincotta, A.H. Circadian peak dopaminergic activity response at the biological clock pacemaker (suprachiasmatic nucleus) area mediates the metabolic responsiveness to a high-fat diet. *J. Neuroendocr.* **2018**, *30*, e12563. [CrossRef]

102. Vadiveloo, M.; Scott, M.; Quatromoni, P.; Jacques, P.; Parekh, N. Trends in dietary fat and high-fat food intakes from 1991 to 2008 in the Framingham Heart Study participants. *Br. J. Nutr.* **2014**, *111*, 724–734. [CrossRef] [PubMed]
103. Kalupahana, N.S.; Voy, B.H.; Saxton, A.M.; Moustaid-Moussa, N. Energy-Restricted High-Fat Diets Only Partially Improve Markers of Systemic and Adipose Tissue Inflammation. *Obesity (Silver Spring)* **2011**, *19*, 245–254. [CrossRef] [PubMed]
104. Salinero, A.E.; Anderson, B.M.; Zuloaga, K.L. Sex differences in the metabolic effects of diet-induced obesity vary by age of onset. *Int. J. Obes.* **2018**, *42*, 1088–1091. [CrossRef] [PubMed]

nutrients

MDPI

Article

An Integrated Analysis of miRNA and Gene Expression Changes in Response to an Obesogenic Diet to Explore the Impact of Transgenerational Supplementation with Omega 3 Fatty Acids

Karla Fabiola Corral-Jara [1], Laura Cantini [2], Nathalie Poupin [3], Tao Ye [4], Jean Paul Rigaudière [1], Sarah De Saint Vincent [1], Alexandre Pinel [1], Béatrice Morio [5] and Frédéric Capel [1,*]

[1] Unité de Nutrition Humaine (UNH), Université Clermont Auvergne, Institut National de Recherche pour L'agriculture, L'alimentation et L'environnement (INRAE), Faculté de Médecine, F-63000 Clermont-Ferrand, France; karla-fabiola.corral-jara@inrae.fr (K.F.C.-J.); jean-paul.rigaudiere@inrae.fr (J.P.R.); sarah.de_saint_vincent@uca.fr (S.D.S.V.); alexandre.pinel@uca.fr (A.P.)

[2] Computational Systems Biology Team, Institut de Biologie de l'Ecole Normale Supérieure, CNRS, INSERM, Ecole Normale Supérieure, Université PSL, 75005 Paris, France; cantini@bio.ens.psl.eu

[3] Toxalim (Research Centre in Food Toxicology), Université de Toulouse, INRAE, ENVT, INP-Purpan, UPS, 31027 Toulouse, France; nathalie.poupin@inrae.fr

[4] GenomEast Platform, Institut de Génétique et de Biologie Moléculaire et Cellulaire (IGBMC), 1 rue Laurent Fries/BP 10142/, 67404 Illkirch, France; yetao@igbmc.fr

[5] CarMeN Laboratory, INSERM U1060, INRAE U1397, Université Lyon 1, 69310 Pierre Bénite, France; beatrice.morio@inrae.fr

* Correspondence: frederic.capel@inrae.fr; Tel.: +33-4-731-78-262

Received: 20 November 2020; Accepted: 15 December 2020; Published: 17 December 2020

Abstract: Insulin resistance decreases the ability of insulin to inhibit hepatic gluconeogenesis, a key step in the development of metabolic syndrome. Metabolic alterations, fat accumulation, and fibrosis in the liver are closely related and contribute to the progression of comorbidities, such as hypertension, type 2 diabetes, or cancer. Omega 3 (*n*-3) polyunsaturated fatty acids, such as eicosapentaenoic acid (EPA), were identified as potent positive regulators of insulin sensitivity in vitro and in animal models. In the current study, we explored the effects of a transgenerational supplementation with EPA in mice exposed to an obesogenic diet on the regulation of microRNAs (miRNAs) and gene expression in the liver using high-throughput techniques. We implemented a comprehensive molecular systems biology approach, combining statistical tools, such as MicroRNA Master Regulator Analysis pipeline and Boolean modeling to integrate these biochemical processes. We demonstrated that EPA mediated molecular adaptations, leading to the inhibition of miR-34a-5p, a negative regulator of Irs2 as a master regulatory event leading to the inhibition of gluconeogenesis by insulin during the fasting–feeding transition. Omics data integration provided greater biological insight and a better understanding of the relationships between biological variables. Such an approach may be useful for deriving innovative data-driven hypotheses and for the discovery of molecular–biochemical mechanistic links.

Keywords: metabolic syndrome; transcriptome; microRNA; liver; omega 3 fatty acids; obesity

1. Introduction

Weight gain and abnormal lipid metabolism are major determinants of whole body insulin resistance, leading to the appearance of cardiovascular diseases, type 2 diabetes, cancer, etc. [1]. Insulin resistance corresponds to the decreased ability of insulin to stimulate glucose uptake in muscle, adipose, and other tissue, and to inhibit hepatic gluconeogenesis. Under normal conditions,

a fasted state is characterized because glucagon can activate hepatic gluconeogenesis, lipolysis, and the oxidation of fatty acids (FA). Upon feeding, insulin released from pancreatic B cells reaches hepatocytes to inhibit gluconeogenesis and promote glycolysis and de novo lipogenesis [2]. With insulin resistance, these mechanisms are dysregulated, as no more glucose enters the cell, gluconeogenesis and lipolysis are increased. Inhibition of insulin signaling may arise from the deposition of FA or other lipid mediators in the peripheral tissues, proteins secreted by dysfunctional/inflamed adipose tissue through intracellular mechanism which remain partially characterized [3]. Several reports have suggested that metabolic abnormalities and alterations of adipose tissue biology could be prevented by increasing the intake of omega-3 (*n*-3) polyunsaturated fatty acids (PUFAs), especially those of marine origin such as eicosapentaenoic acid (EPA) or docosahexaenoic acid (DHA) [4–6].

Promising and higher effects of EPA compared to DHA were described against obesity and insulin resistance, but the molecular mechanisms leading to a differential effect are not yet fully clarified and the long term or transgenerational effects are unknown [7]. Hence, metabolic adaptations during pregnancy may be influenced by the lipid quality of the diet, inducing a differential response to a nutritional stress, probably linked to epigenetic modifications [8]. The integration of multi-omic data can provide deeper biological insights, a better understanding of relationships between biometric, biological, molecular variables. Innovative data-driven hypotheses paving the way to the discovery of mechanistic links could then be proposed. Recently, an integration of multi-omic data allowed the study of calorie restriction-induced changes in insulin sensitivity and the identification of diverse biomarkers [9]. On the other hand, the analysis of large data sets generated by metabolomics and lipidomics has shed new light on the roles of metabolites, such as lipids, amino acids and bile acids, in modulating insulin sensitivity. Metabolites can regulate insulin sensitivity directly by modulating components of the insulin signaling pathway, such as insulin receptor substrates (Irs) and AKT, and indirectly by altering the flux of substrates through multiple metabolic pathways, including lipogenesis, lipid oxidation, protein synthesis and degradation and hepatic gluconeogenesis [10].

In this study, we used a systems biology approach to explore hepatic metabolic and regulatory networks in response to an obesogenic diet in mice supplemented with EPA during three generations. We extracted cues of the underlying molecular mechanisms from transcriptomic and miRomic high-throughput data, using statistical methods, such as MicroRNA Master Regulator Analysis (MMRA) pipeline, and Boolean modelling. We were able to predict microRNA (miRNA)–gene interactions and simulate hepatic metabolic pathways of glucose flux in silico. From this analysis, we were able to extract new regulations between Irs2 gene and miR-34a-5p linked to transgenerational intake of EPA as a master controller of hepatic gluconeogenesis to prevent insulin resistance

2. Materials and Methods

2.1. Dietary Intervention and Sample Collection

The present study was approved by the Animal Care and Use Committee of Auvergne (CEMEA Auvergne) and the Ministère de l'Enseignement Supérieur et de la Recherche (01276.01). C57bl/6J mice were bred for 3 generations in the animal facility the INRAE research center of Theix (63122 Saint-Genes Champanelle, France) with a growing diet (A03 diet from Safe diets, Augy, France) supplemented with 1% (*w*/*w*) of fish oil (Polaris Omegavie 70 TG, EPA) containing 75% of omega 3 FA (omega 3 lineage), mainly in the form of EPA which represented 8% of the fatty acids in the final diet or 1% (*w*/*w*) of high oleic sunflower oil (control lineage) containing 83.5% of oleic acid (Lesieur, Coudekerque Branche, France) as a control group. The supplementation of the control group with 1% of sunflower oil aimed at matched the caloric supplementation related to the addition of fish oil in the omega 3 lineage with a marginal impact on metabolic parameters. The details of the breeding strategy and lipid composition of the diets are described in Supplementary Figure S1. F3 male mice from control and omega 3 lineages were matched for body weight ($n = 8$ per group) and fed with a high-fat, high-sucrose diet (HFD, 24% of fat, 20% of sucrose) providing 45% of energy from fat (RD 12,451 from Research

diet, Brogaarden Gentofte, Denmark) for 17 weeks. These animals constituted the HFoleic and HFepa groups, respectively. A reference group of F3 male mice (n = 9) from the control lineage was fed with a low-fat diet (LFD) providing 10% of energy from fat (RD 12450H from Research diet) during the challenge as a reference group. Animals were maintained under a temperature-controlled environment and 12 h–12 h light-dark cycle throughout the study. All the procedures were followed to reduce the number and manipulation of the animals in the study.

At the end of the feeding period, during the fasting period, the animals were sacrificed under anesthesia with 4% isoflurane. Liver was harvested, snap-frozen in liquid nitrogen and stored at −80 °C until use. Total RNA was extracted from the liver using TRIzol® reagent (Thermo Scientific, Courtaboeuf, France) according to the manufacturer's instructions. Each total RNA sample was assessed for quantification and integrity using the Agilent Bioanalyzer (Agilent, Santa Clara, CA, USA).

2.2. Gene Expression and miRNA Analysis

2.2.1. Microarray Gene Expression Analysis

Gene expression profiles were performed at the GeT-TRiX facility (INRAE, GénoToul, Génopole Toulouse Midi-Pyrénées, Toulouse, France) using Agilent Sureprint G3 Mouse GE v2 microarrays (8 × 60 K, design 074809) following the manufacturer's instructions. For each sample, 200 ng of total RNA were prepared for hybridization using the One-Color Quick Amp Labeling kit (Agilent Technologies, Les Ulis, France) following the manufacturer's instruction. All samples had an RNA integrity number above 7.5. The slides were scanned on Agilent G2505C Microarray Scanner (Agilent Technologies, Les Ulis, France) using Agilent Scan Control A.8.5.1 software (Agilent Technologies, Les Ulis, France) and fluorescence signal extracted using Agilent Feature Extraction software v10.10.1.1 (Agilent Technologies, Les Ulis, France). Raw data (median signal intensity) were filtered; log2 transformed and normalized using quantile method [11]. A model was fitted using the limma lmFit function [12]. Microarray data and experimental details are available in NCBI's Gene Expression Omnibus [13] and are accessible through GEO Series accession number GSE145620 (https://www.ncbi.nlm.nih.gov/geo/query/acc.cgi?acc=GSE145620).

2.2.2. Small RNA Sequencing (Small RNA-Seq) Analysis

Small RNA-seq were performed at the IGBMC GenomEast Platform (Strasbourg, France), small RNA-seq libraries were generated from 2000 ng of total RNA using TruSeq Small RNA Library Prep Kit (Illumina, San Diego, CA, USA), according to manufacturer's instructions. Briefly, during the first step, RNA adapters were sequentially ligated to each end of the RNA, firstly the 3′ RNA adapter (5′-TGGAATTCTCGGGTGCCAAGG-3′) which is specifically designed to target miRNAs and other small RNAs, then the 5′ RNA adapter (5′-GTTCAGAGTTCTACAGTCCGACGATC-3′). Small RNA ligated with 3′ and 5′ adapters were reverse transcribed, and PCR amplified (30 s at 98 °C; (10 s at 98 °C, 30 s at 60 °C, 15 s at 72 °C) × 13 cycles; 10 min at 72 °C) to obtain cDNA. Acrylamide gel purifications of 140–160 nt amplified cDNA (corresponding to cDNA obtained from small RNA +120 nt from adapters) were performed. The final cDNA libraries were checked for quality and quantified using capillary electrophoresis. Libraries were loaded in the flow cell at 2.8 nM and clusters were generated using Cbot and sequenced on HiSeq 4000 (Illumina) as single-end 50 base reads, according to manufacturer's instructions. Adapters were removed using FASTX-Toolkit (http://hannonlab.cshl.edu/fastx_toolkit/index.html). The trimmed sequencing reads of each library were then mapped and annotated with ncPRO-seq [14] onto the mus musculus genome GRCm38.p6 genome (mm9). Briefly, read alignment was performed using Bowtie v0.12.8, allowing a sum of qualities of mismatching bases lower than 50 (denoted –e 50). Aligned reads were then annotated accordingly against ortholog miRNAs in mice (miRBase release 22.1). MiRNA data were Log2 transformed and normalized using the quantile method [11]. MiRNA data and experimental details are described in GEO accession GSE146445 (https://www.ncbi.nlm.nih.gov/geo/query/acc.cgi?acc=GSE146445).

2.3. Bioinformatic and Statistical Analysis

2.3.1. Gene Differential Expression between Biological Conditions

Pair-wise comparisons between biological conditions (reference, HFoleic, HFepa) were performed using T-test and Fold Change (FC). A correction for multiple testing was applied using the Benjamini–Hochberg procedure [15] to control the false discovery rate (FDR). Genes with FDR-adjusted $p < 0.05$ were considered to be differentially expressed between conditions. For the combination of gene and miRNA expression data (see Section 2.3.3), we defined as "up signature genes", those with log2 FC > 0 and FDR-adjusted $p < 0.05$, and as "down signature genes" those with log2 FC < 0 and FDR-adjusted $p < 0.05$ in each biological comparison (HFepa vs. reference, HFoleic vs. reference and HFepa vs. HFoleic).

2.3.2. Testing Gene Signature Performances with Partial Least-Squares Discriminant Analysis and Hierarchical Clustering

In order to verify the classification group (condition) of our samples, we performed a partial least squares regression-discriminant analysis (PLS-DA). PLS-DA was performed from differentially expressed genes and miRNA using Mixomics R [16]. In addition, hierarchical clustering of samples and gene expression data was performed using Euclidean distance and Ward's method.

2.3.3. Application of MicroRNA Master Regulator Analysis (MMRA)

The four steps of the MicroRNA Master Regulator Analysis (MMRA) pipeline [17] was applied to identify miRNA-gene interactions possibly involved in the differential biological regulations in each comparison (HFepa vs. reference and HFoleic vs. reference). MMRA consists of four sequential steps, each aimed at progressively reducing the number of candidate miRNAs: (i) differential expression analysis to highlight miRNAs with subtype-specific expression; (ii) target gene transcript enrichment analysis, to further select those miRNAs whose predicted targets are enriched in the associated subtype gene signature; (iii) network analysis, in which an mRNA network is constructed around each miRNA and tested for enrichment in signature genes; and (iv) identification of miRNAs whose expression "explains" the expression of subtype signature genes.

- MMRA step1: MiRNA differential expression analysis

Pair-wise comparisons between biological conditions in miRNA expression data were performed using the Bioconductor package DEGseq [18] to capture the differentially expressed miRNAs. miRNAs with FC > 0.25, $p < 0.01$ (corresponding to an FDR < 0.05) [15] were defined as differentially expressed between biological conditions and retained for further analysis.

- MMRA step2: target genes enrichment analysis

For each miRNA differentially expressed in a biological condition, miRNA target genes were predicted by combining the results of three miRNA-target databases (miRTarBase [19], miRDB [20], and TargetScan [21]). Only miRNA-target interactions predicted by at least two databases were included as putative targets in our analysis. We performed a target enrichment analysis in the "up" and "down" gene signature of the biological condition in which the miRNA was found differentially expressed. The enrichment analysis was performed with a Fisher's exact test. The miRNAs whose targets were enriched with a Fisher's $p < 0.05$ were retained for the following steps of the pipeline.

- MMRA step3: network analysis

ARACNE information-theoretic algorithm (http://wiki.c2b2.columbia.edu/califanolab/index.php/Software/ARACNE) was used to infer interactions between each miRNA selected in the previous step and any gene from the paired dataset. The software was available through the Cyni Toolbox panel under

the Infer Network tab, implemented in Cytoscape (https://cytoscape.org/). Quantile normalization was performed as standard ARACNE pre-processing. Only edges connecting miRNA to genes were considered, thus having the miRNA as the only hub of the network. A mutual information (MI) *p*-value significance threshold fixed at 10^{-7} was used as recommended. Each of the consensus networks was tested for significant enrichment in "up" and "down" gene signature of each biological condition with Fisher's exact test. A threshold of $p < 0.05$ was used in the enrichment test.

- MMRA step4: Step-wise Linear Regression (SLR) analysis

SLR is here used to filter out weak miRNA-gene interactions identified in the previous steps. In the SLR analysis, the gene log2-expression levels were considered as response variables, and the log2-expression levels of miRNAs linked by ARACNE or by databases to the gene were considered as the explanatory variables. Akaike information criterion was used as the stop criterion. At the end of this step, for each biological condition, we obtained a list of miRNAs with their associated signature genes.

2.4. Pathways Analysis

In order to gain mechanistic insight into gene lists generated from our previous analysis, we performed a pathway enrichment analysis, and we identified related biological pathways.

2.4.1. Molecular Pathway Analysis with GeneTrail2

Molecular signatures from HFepa vs. reference, HFoleic vs. reference and HFepa vs. HFoleic comparisons were explored using gene set enrichment analysis (GSEA) implemented in GeneTrail2 [22,23]. In order to limit the effect of outliers, the unweighted version of GSEA implemented in GeneTrail2 evaluated whether the genes of different biological categories from KEGG-, Reactome- and Wiki-pathway datasets were randomly distributed or accumulated on top or bottom of the list. To this aim, a Kolmogorov–Smirnov test was applied on FC of genes with a differential expression between 2 groups at $p < 0.05$ with no FDR adjustment. As recommended by the GeneTrail2 algorithm, only sets of genes identified at $p < 0.05$ after adjustment for multiple testing using the Benjamini–Yekutieli method were considered.

2.4.2. Metabolic Pathways Analysis with MetExplore

The list of genes exhibiting a differential expression and regulated by at least one miRNA was used for visualization and exploration of metabolic pathways using MetExplore [24] (https://metexplore.toulouse.inra.fr/metexplore2/). This list of genes was mapped on the mouse metabolic network iSS1393 [25] (biosource Id #2893 in MetExplore) to find the associated metabolic reactions. The identified reactions were assigned a different numerical attribute if they were associated with differentially expressed genes in the HFoleic condition (1), HFepa condition (2) or in both conditions (3) compared to reference group. The whole list of reactions with their numerical attributes was then mapped on the metabolic network to locate them in the whole metabolic network and visualize associated metabolic pathways of interest. Pathway enrichment analyses were performed over the sets of reactions associated with the HFoleic condition, the HFepa condition and common to both condition, respectively, to assess whether the given reactions were significantly over-represented in a metabolic pathway. Pathway enrichment statistics were performed using one-tailed exact Fisher test, with a Benjamini–Hochberg correction for multiple tests, using the metabolic pathways defined in the iSS1393 network.

2.5. Logical Modeling of Gene Regulatory and Metabolic Networks

A Boolean modelling approach implemented in GINsim software (v3.0.0b, http://ginsim.org) was used to build a dynamic model of the associations between the highlighted signaling pathways

and the metabolic phenotypes related to obesity and insulin resistance [26]. This approach consisted in a simplified reconstruction of biochemical networks to connect metabolic components based on prior knowledge. The model inherently provided links of causality and an input–output relationship at the molecular level, allowing the in silico analysis of the dynamical behavior of the network (presence/activation, absence/deactivation of the different components) under different combinations of inputs or perturbations in the system [27].

Each node in the graph was represented by a single Boolean variable which exhibited two possible levels, 0 (OFF) if the element was absent/inactive or 1 (ON) if the element was present/active. For some exceptions, this two-state representation may be biologically too restrictive and 3 levels should be necessary, 0 (OFF), 1 (LOW), and 2 (HIGH), representing high or low activation of this node regulator in the network [28]. The model was represented on a regulatory graph where each node represented a component of the network. Edges represented the regulatory positive or negative influences between nodes. Next, we defined logical rules to determine the level of activity of each target node depending on the levels of regulators. Computational modeling through in silico simulations and perturbations revealed dynamical properties of the network. The model was then used to test and predict biological hypotheses. The model was built using input information from the literature, the KEGG database [29], and the present experiment.

2.6. Validation of Gene Expression

For microarray validation purposes, cDNAs were synthesized from 2 µg of total RNA using the High Capacity cDNA Reverse Transcription Kit from Applied Biosystem (Thermo Scientific, Courtaboeuf, France). The products of reverse transcription were used for Quantitative Real Time Polymerase Chain Reaction (qRT-PCR) using specific primers and Rotor-Gene SYBR Green PCR master mix on a Rotor-Gene Q system (Qiagen, Courtaboeuf, France). Quantification of mRNA of selected genes was assayed using the ddCT method using Hprt as housekeeping gene. Differential expression between reference, HFoleic and HFepa conditions were analyzed using pairwise T-test and a correction for multiple testing [15] using a cut-off for significance fixed at $p < 0.05$. Primer sequences and PCR conditions are available upon request (frederic.capel@inrae.fr).

3. Results

3.1. Effect of High Fat Diet and Transgenerational Supplementation with EPA in Gene and miRNAs Expression

The impact of the obesogenic diet on fat mass accumulation, increase in liver weight, plasma glucose, and insulin levels was reduced in mice that received a transgenerational supplementation with EPA as compared to the oleic/control lineage (Table 1).

The global workflow of our study was based on an integration of bioinformatic and statistical blocks, including the use of R packages, and software applications such as Cytoscape and GINsim (Figure 1). In order to go into the molecular mechanisms that could mediate the positive effect of supplementation with omega 3 FA in mice challenged with an obesogenic HFD; we characterized the adaptations at the level of miRNA and gene in the liver. We then analyzed differential expression between 3 biological conditions (HFepa, HFoleic and reference) as described in Sections 2.3.1 and 2.3.3.

Table 1. Metabolic characteristics of mice after the dietary intervention.

Parameter-	Reference	HFoleic	HFepa
Body Weight (g)	26.7 ± 0.9	36.1 ± 1 ***	33.8 ± 2.7 **
Fat %	16 ± 1	32 ± 1 ***	24 ± 3 ** †
Lean %	79 ± 1	64 ± 1 ***	72 ± 3 ** ††
Liver (gram)	0.87 ± 0.04	1.11 ± 0.04 *	0.99 ± 0.09
AUCglucose (a.u.)	171 ± 6	207 ± 11 *	196 ± 8
Glucose (mg/dL)	195.6 ± 13.1	274.2 ± 13.1 **	228.1 ± 14.0 †
Insulin (pg/mL)	68.6 ± 8.3	182.8 ± 18.8 ***	109.4 ± 25.9 †
TAG (g/L)	0.310 ± 0.013	0.366 ± 0.024	0.378 ± 0.039
T Cholesterol (g/L)	0.926 ± 0.034	1.116 ± 0.050 *	1.166 ± 0.068 *
Glycerol (µM)	213.1 ± 11.9	237.2 ± 19.0	257.1 ± 24.0
Nefa (mM)	0.350 ± 0.038	0.228 ± 0.029	0.404 ± 0.081

Data are mean ± SEM (n = 9, 8 and 7 mice in Ref, HFoleic and HFepa, respectively). * $p < 0.05$ vs. Ref; ** $p < 0.01$ vs. Ref; *** $p < 0.001$ vs. Ref; † $p < 0.05$ vs. HFoleic; †† $p < 0.01$ vs. HFoleic. TAG, triacylglycerols; Nefa, non-esterified fatty acids.

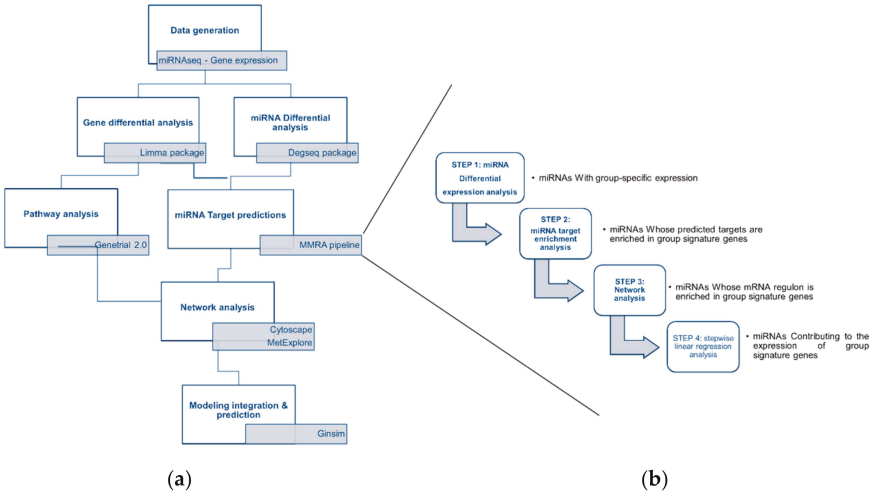

Figure 1. Bioinformatic workflow. (**a**) Bioinformatic analysis of microarray and microRNA-seq data was performed through a series of bioinformatic blocks: differential expression analysis, prediction of miRNA targets, analysis and visualization of interaction networks and computational modeling to predict cellular metabolic behaviors and phenotypes. (**b**) The four-step MMRA (microRNA Master Regulator Analysis) pipeline was followed to obtain the putative miRNA targets and included miRNA target enrichment analysis, network analysis and stepwise linear regression analysis.

As illustrated on the Venn diagrams showing the overlap of differentially expressed genes and miRNAs between comparisons (Figure 2a,b), a considerable difference in the number of genes regulated in HFepa and HFoleic groups, compared to the reference group was observed, whereas no significant differential expression of genes were detected between HFoleic and HFepa. Sixty-six genes were commonly regulated when HFepa and HFoleic were compared to reference group.

On the contrary, the number of differentially expressed miRNAs showed a balance between the biological conditions. Of these, 74 differentially expressed miRNAs were shared between HFepa and HFoleic conditions as compared to reference group. Thirty and twenty eight differentially expressed miRNAs were shared between HFepa vs. reference-HFepa vs. HFoleic comparisons and HFoleic vs. reference-HFepa vs. HFoleic comparisons respectively. The PLS-DA analysis showed a clear separation of the expression profiles in genes and miRNAs between groups (Figure 2c,d) but the expression profile of the HFepa group presented a similarity to the reference group.

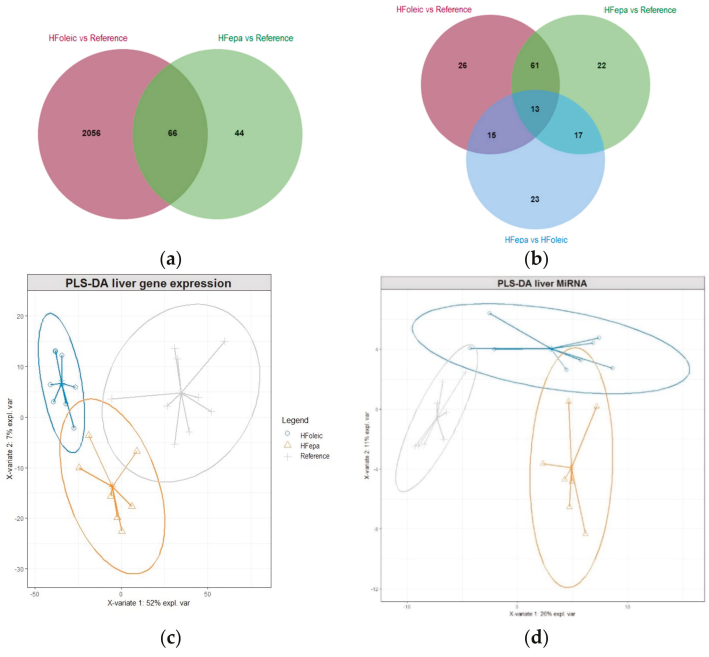

Figure 2. Effect of High Fat Diet and transgenerational supplementation with EPA in gene and miRNAs expression. (**a**) Venn diagram showing the relationships in the number of genes differentially expressed between HFepa vs. reference and HFoleic vs. reference biological condition. (**b**) Venn diagram showing the relationships in the number of miRNAs differentially expressed between three biological conditions, HFepa vs. reference, HFoleic vs. reference and HFepa vs. HFoleic. (**c**) Differentially expressed genes from three group biological condition, HFepa vs. reference, HFoleic vs. reference, HFepa vs. HFoleic were used to perform a partial least squares regression-discriminant analysis (PLS-DA). (**d**) PLS-DA analysis of differentially expressed miRNAs from three biological conditions, HFepa vs. reference, HFoleic vs. reference, HFepa vs. HFoleic.

3.2. MiRNAs Significantly Contribute to the Expression of Phenotype Signature Gene

The four-step sequential MMRA pipeline was applied to look over the regulation mediated by miRNAs on the differentially expressed genes. MMRA aims at progressively reduce the number of candidate miRNAs which could regulate one gene (Figure 1b). The four steps of the pipeline were differential expression analysis, target/transcript enrichment analysis, network analysis and Stepwise linear regression analysis as described in Section 2.3.3. As a result, miRNA-gene interactions were obtained with a strong statistical support. We performed a MMRA analysis for HFepa vs. reference and HFoleic vs. reference separately, showing, respectively, 12 and 32 potential miRNAs regulating the phenotype signature (Supplementary Tables S1 and S2). Table 2 shows down and up regulated target gene with the highest FC in the HFepa vs. reference comparison. Only seven of these genes were exclusively differentially expressed in the HFepa group compared to the Reference group. All the others were regulated after the obesogenic diet whatever the lineage. In the case of miRNAs, which could regulate the transcription of these genes, few of them were specific to each biological condition. Globally, downregulated genes are regulated by upregulated miRNAs and vice versa, although some exceptions were observed. Likewise, some differentially expressed genes in the HFepa group were regulated by miRNAs that were differentially expressed exclusively in the HFoleic group compared to the reference group.

Table 2. Differentially expressed genes are regulated by miRNAs.

Gene	Associated Signature in HFepa	Associated Signature in HFoleic	miRNA Regulation	microRNA Regulation in HFepa	microRNA Regulation in HFoleic
Sigmar1	Down		mmu.miR.32.5p		up
Xpa	Down	Down	mmu.miR.150.5p		down
Xpa	Down	Down	mmu.miR.335.3p	up	up
Xpa	Down	Down	mmu.miR.1948.3p	up	up
Rai1	Down		mmu.miR.7052.3p		down
Zfp777	Down	Down	mmu.miR.335.3p	up	up
Txn2	Down	Down	mmu.miR.18a.3p		up
Txn2	Down	Down	mmu.miR.98.3p	down	
Trpt1	Down	Down	mmu.miR.148a.3p	up	
Agpat6	Down	Down	mmu.miR.195a.3p	down	down
Leng9	Down	Down	mmu.miR.7052.3p		down
Plekhf1	up	up	mmu.miR.150.5p		down
Plekhf1	up	up	mmu.miR.335.3p	up	up
Stard4	up	up	mmu.miR.32.5p		up
Stard4	up	up	mmu.miR.7052.3p		down
Dnajb1	up		mmu.miR.19a.3p		down
Dnajb1	up		mmu.miR.7068.3p	down	down
Hspb1	up	up	mmu.miR.128.3p	down	down
Hspb1	up	up	mmu.miR.150.5p		down
Hspb1	up	up	mmu.miR.7068.3p	down	down
Pcp4l1	up	up	mmu.miR.1948.3p	up	up
A_55_P2525368	Down		miRNA regulation not significant		
Ptpmt1	Down	Down	miRNA regulation not significant		
Magohb	Down		miRNA regulation not significant		
A130022F02Rik	Down	Down	miRNA regulation not significant		
Gm13547	Down	Down	no regulated by a miRNA		
Lrrfip1	Down	Down	no regulated by a miRNA		
Rabl3	Down	Down	no regulated by a miRNA		
Kansl1l	up	up	miRNA regulation not significant		
P4ha1	up		miRNA regulation not significant		
Inhbb	up		miRNA regulation not significant		
Mtss1	up	up	miRNA regulation not significant		
Hyou1	up	up	miRNA regulation not significant		
Gbe1	up	up	miRNA regulation not significant		
Slc5a3	up	up	miRNA regulation not significant		
Ints6	up	up	miRNA regulation not significant		
0610031O16Rik	up	up	no regulated by a miRNA		

Fifteen upregulated genes and 15 downregulated genes with the highest FC value (>0.25) in the HFepa condition were selected to demonstrate its regulation mediated by miRNAs. The four-step sequential MMRA pipeline was applied to obtain miRNA-gene regulations. The Table shows the regulatory pattern of genes and miRNAs in HFepa vs. Reference or HFoleic vs. Reference biological condition.

3.3. Identification of Differentially Regulated Cellular and Signaling Pathways

Global pathway enrichment analysis on the three biological comparisons (HFoleic vs. reference, HFepa vs. reference and HFepa vs. HFoleic) using significant gene expression regulations ($p < 0.05$) with no FDR correction was performed with GSEA to relate genes and their biological functions. Enriched pathways were identified using the Wiki, Reactome, and KEGG databases. Pathways were mostly enriched in the HFoleic condition compared to the reference condition for which 8, 11 and 7 enriched pathways were found respectively (Figure 3a and Supplementary Table S3). Figure 3a exhibited a summary of this analysis, illustrating an enrichment of pathways related to oxidative phosphorylation, cholesterol metabolism, peroxisome proliferator-activated receptor (PPAR) signaling pathway, eicosanoid metabolism. Fewer pathways were enriched when HFepa and reference conditions were compared (Figure 3b, Supplementary Table S4). Enriched biological processes in this comparison were related to cholesterol metabolism, PPAR signaling pathway, sulfur-containing amino acid metabolism and adipocytokine signaling pathway. Comparison between the HFepa and HFoleic conditions showed a regulation of FA metabolism and PPAR signaling pathway (Figure 3c, Supplementary Table S5). Hierarchical clustering of expression data of genes related to PPAR and Cholesterol pathways identified in the HFepa vs. HFoleic biological conditions showed a well separation of samples according to their group, except for minor exceptions (Figure 3d).

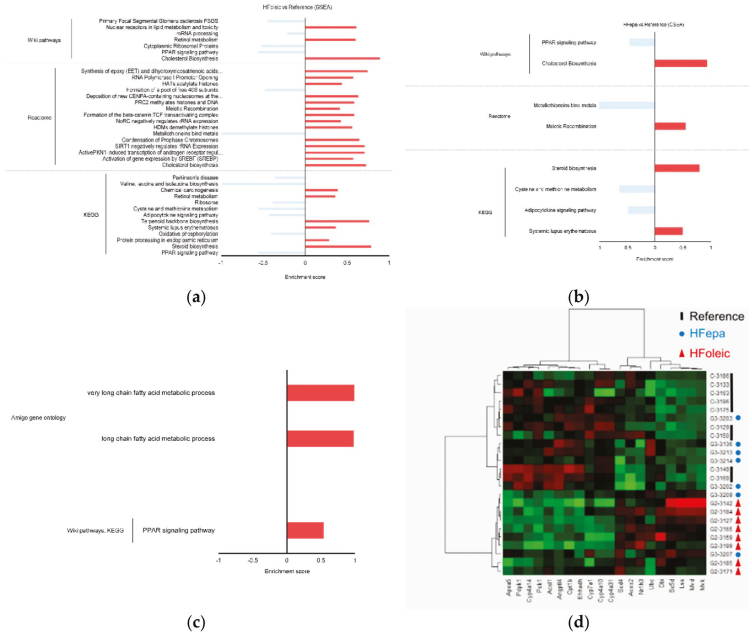

Figure 3. Gene set enrichment analysis of differentially expressed genes between conditions. (**a**) Histogram showing the enriched pathways in HFoleic condition vs. reference. (**b**) Histogram showing the enriched pathways in HFepa condition vs. reference. (**c**) Histogram showing the enriched pathways in HFepa condition vs. HFoleic condition. In panels (**a**)–(**c**), the red bars represent over representation of corresponding pathway or reaction; blue bars represent under representation of corresponding pathway or reaction. (**d**) Heat map visualization of expression data of the genes involved in peroxisome proliferator-activated receptor (PPAR) and Cholesterol pathways. The color code indicates the expression level of each genes and for each sample (green, low expression level; red, high expression level). The genes are represented as columns and the samples with the identification of group correspondence as rows.

3.4. Differential Enrichment of Metabolic Pathways in HFepa and HFoleic Groups

An identification of all potentially regulated enzymatic reactions using the MetExplore tool allowed a detailed extraction and visualization of metabolic sub-networks associated with differentially expressed genes in the HFepa and HFoleic groups compared to the reference condition (Figure 4a,b). As illustrated in Figure 4, all identified enriched metabolic pathways were represented as a network of reactions and metabolites (nodes) interactions (edges). Most of the reactions identified as enriched in the HFepa vs. Reference comparison were also enriched in the HFoleic vs. reference comparison (Figure 4b). The lists of metabolic pathways linked to all identified reactions and specifically enriched in each set of reactions from the different comparisons or shared between them can be found in Supplementary Table S6. Significant enrichment in the HFepa vs. Reference comparison concerned the metabolism of biotin and of blood group biosynthesis (Figure 4b). The most significantly enriched enzymatic reactions when HFoleic and reference groups were compared belonged to mitochondrial activity, fatty acid transport, and cholesterol. Enrichment in cysteine, arginine and proline metabolisms was shared between the two comparisons versus reference group. Carbohydrate metabolism (Glycolysis/gluconeogenesis) also strongly tended to be enriched ($p = 0.06$, Supplementary Table S6) and was identified to be connected to biotin and cysteine metabolisms (Supplementary Figure S2A and Figure S2B).

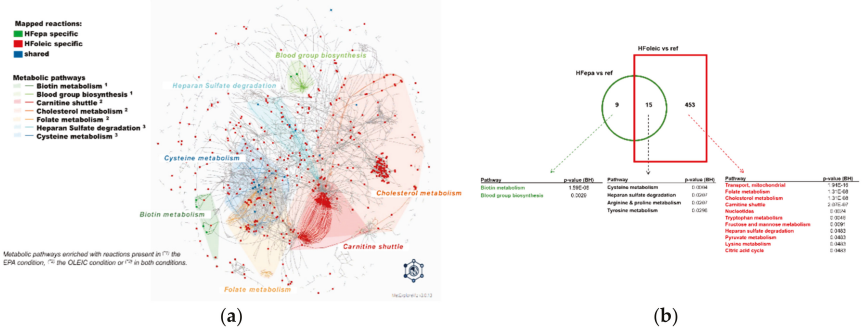

(**a**) (**b**)

Figure 4. Connections between regulated metabolic pathways in HFoleic and HFepa goups. Genes differentially expressed from HFepa vs. reference and HFoleic vs. reference biological conditions were used to identify related metabolic reactions in MetExplore allowing a complementary exploration of enriched metabolic pathways. Metabolic reactions associated with modulated genes in both HFepa and HFoleic conditions were mapped in the Mus musculus metabolic network. (**a**) The Figure shows a global network of mapped metabolic reactions. Reactions in red are HFoleic-related; reactions in green are HFepa-related; blue reactions are both regulated in HFoleic and HFepa groups. Represented metabolic pathways correspond to metabolic pathways enriched with reactions present in the EPA condition (1), in the oleic condition (2) or in both conditions (3). (**b**) Representation of the number of identified reactions and the significantly enriched related metabolic pathways according to the MetExplore analysis in the two comparisons that exhibited significant differential gene expression (HFoleic vs. reference and HFepa vs. reference).

As illustrated in Supplementary Figure S2A,B, changes in one of the genes encoding the catalysts of a HFepa-specific reaction may be connected with reactions enriched in the HFoleic vs. reference-specific and vice versa. As an example, a connection between the biotin- (acetyl-CoA-carboxylase) ligase reaction (R_BACCL) and holocarboxylase synthetase's reaction (R_BTNPL), both catalyzed by the HFepa-specific holocarboxylase synthetase (Hlcs) gene with the synthetase's reaction (R_BTND1) catalyzed by the HFoleic-specific Biotinidase (Btd) gene was found (Supplementary Figure S2A). Interestingly, these reactions from biotin metabolism were connected by AMP with the glycolysis/gluconeogenesis and FA metabolism pathways (R_ACS, R_HEX1, R_PEPCK, R_ENO and R_ALDD2x). Likewise, the Glutamic-Oxaloacetic Transaminase 1 (Got1) gene, was differentially expressed in both HFepa

and HFoleic groups compared to reference group. This enzyme is involved in L-Cysteate 2-oxoglutarate aminotransferase (R_LCYSTAT) and 3-sulfino-alanine transaminase (R_3SALATAi) reactions with 2-oxoglutanate as a common metabolite (Supplementary Figure S2B). These reactions from cysteine metabolism, could constitute a link between the changes in FA metabolism and glycolysis/gluconeogenesis through pyruvate and acetyl CoA in the control/oleic lineage.

3.5. MiRNAs Regulated Genes Involved in the Integration of Insulin Signaling, PPAR Signaling, Glucose Metabolism, and FA Metabolism

We explored the possible mechanisms linking miRNA and gene expression in the modulation of insulin resistance and the development of obesity using the MMRA pipeline. Based on the pathways identified in the GeneTrial2 analysis (see part 3) and the exploration of metabolic reactions (see part 4) as differentially affected between the three biological conditions, four cellular regulation layouts were selected. One signaling pathway: insulin signaling, one gene regulatory networks: PPAR signaling, and two metabolic networks: Glycolysis/Gluconeogenesis, and FA metabolism. These selected pathways were also highlighted in our GSEA analysis of the conditions between the HFepa and HFoleic groups (Supplementary Table S5). We extracted the list of genes that participated in each of the selected pathways and differentially expressed in our study and we identified the genes that were common in two or more of these pathways (Figure 5a). As a validation of this approach, the differential expression of several of these genes was confirmed by RT-qPCR (Supplementary Table S7). Subsequently, the mentioned genes with at least one miRNA regulation identified in the MMRA pipeline were presented in Figure 5b. This Figure shows a network of these recurrent genes and their regulation by miRNAs. As can be seen, Ppargc1a (or Pgc-1α), G6pc, Pck1, are genes that participate in two or more of the selected pathways, and could be regulated by two or more miRNAs, indicating that they are highly connected.

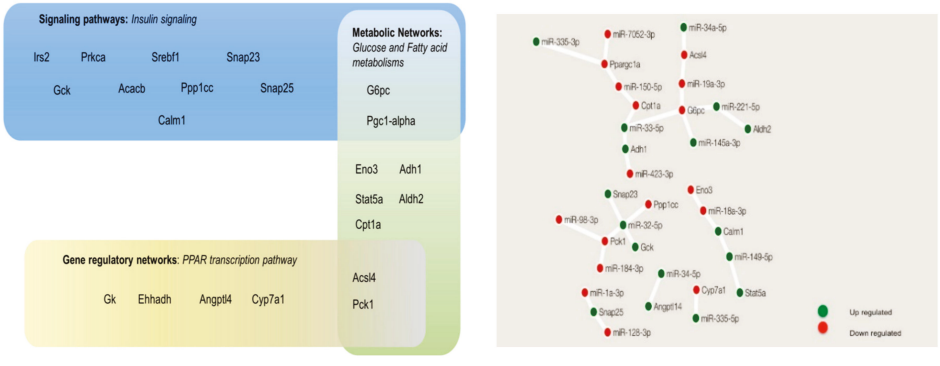

(**a**) (**b**)

Figure 5. Interactions between miRNAs and genes in pathways related to insulin signaling, PPAR signaling, glucose and fatty acid metabolism. (**a**) Representation and compartmentalization of master genes involved in the selected pathways. (**b**) miRNAs-genes interactions of the genes represented in (**a**), obtained following the MMRA pipeline; green circles represented upregulated network components and red circles were downregulated network components. Construction of the network in (**b**) was done using Cytoscape software.

3.6. Computational Modeling Predicts that Dynamism in Genes and miRNAs Expression Leads to Specific Cell Metabolic Phenotypes

To achieve an integrated comprehension of our results and the dynamic of gene expression regulations involved in the mechanisms of insulin resistance and obesity, a logical bioinformatics model was built using the software GINsim (Figure 6). Our model included three inputs which

could not be affected by other components of the network: glucagon, glucose, and FA; five outputs: gluconeogenesis, glycolysis, lipogenesis, lipolysis, and adipogenesis; and several internal elements like Irs2, Pck1, G6pc, Pgc-1α, Pparγ, and Pparα. The model was based on the observation that a high level of Pgc-1α expression during fasting shifts the ratio of Irs1:Irs2 toward a higher Irs2 expression to prime the insulin receptor response toward a more efficient inhibition of gluconeogenesis after feeding [30]. Pgc-1α was then considered with three possible activation levels (0,1,2) to simulate the regulation of metabolic pathways under diverse input conditions, such as the exposure to glucose during feeding. PPARs were introduced as activators of lipolysis, gluconeogenesis (through Ppar-α) and lipogenesis (through Ppar-γ), respectively.

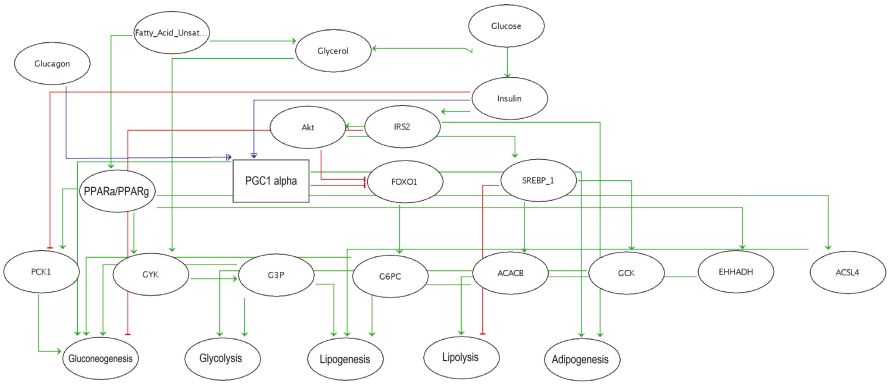

Figure 6. Computational modeling predicts that dynamism in genes expression leads to specific cell metabolic phenotypes. A Boolean modeling of glycolysis, gluconeogenesis, lipolysis, lipogenesis, and adipogenesis metabolic processes in the liver was obtained to create a logical regulatory graph of hepatic metabolism. The model encompassed 24 components (represented as ellipses) and 37 interactions (green edges = activation, red blunt = inhibition). A rectangle denoted a ternary component.

As calibration controls of the modeling and in agreement with prior knowledge, the presence of glucose lead to insulin, Irs2 and Akt activation, and consequently to glycolysis, lipogenesis, and adipogenesis (Figure 7, environment 4). On the contrary, when glucose was considered low, glucagon production was increased, while Akt and Irs2 remained inactivated, leading to the activation of lipolysis and gluconeogenesis (not shown).

	Environment
1	High glucose, Pgc1-a knock-out
2	Low glucose, Pgc1-a knock-out
3	Low glucose, Irs2 ectopic expression
4	High glucose, no perturbation

	1	2	3	4
Foxo1				
Ppars				
Pck1				
Pgc1-alpha				
AKT				
G6pc				
Irs2				
Adipogenesis				
Glycolysis				
Lipogenesis				
Lipolysis				
Gluconeogenesis				

OFF	
LOW	
HIGH	

Figure 7. Model simulations in scenarios with perturbations. Context-dependent stable states computed for the model. Blank cell = inactivation of the corresponding component; blue cell = maximal activation (1 for Boolean components, 2 for Pgc-1α); green cell = intermediate level (1 for Pgc-1α only).

Then, a series of in silico perturbations were performed to find a metabolic profile that could correspond to our experimental observations. Simulations were focused on Pgc-1α and Irs2 activation levels and compared to our experimental results. In the present study, we observed a stable expression of Pgc-1α and an upregulation of Irs2 expression in the HFepa group compared to the HFoleic condition in the context of a low level of circulating glucose (fasting state). Microarray data showed that both genes were downregulated in the HFoleic compared to reference mice. In the fasting state, simulation of a knockout of Pgc-1α (Figure 7, environment 2) resulted in the activation of lipolysis but not gluconeogenesis nor adipogenesis. Irs2 expression was null in this condition. In the context of environment 1, the simulation of a fed state (elevation of glucose in plasma), glycolysis and lipogenesis were still activated, even if Pgc-1α expression was absent (Figure 7). Finally, an ectopic expression of Irs2 was simulated when glucose level was low (Figure 7, environment 3), resulting in the inhibition of gluconeogenesis, but a maintained activation of glycolysis and lipogenesis. In this condition, Pgc-1α reached an intermediate expression value. This last condition probably best fitted to our experimental conditions.

No differential expression of Pgc-1α was observed between HFepa and HFoleic conditions. This may imply an adaptive mechanism to control glucose homeostasis independently of Pgc-1α after transgenerational supplementation with EPA and allowing an improvement of glucose homeostasis and insulin resistance. It raised the hypothesis that Irs2 protein was a master regulator of the differential molecular and biological adaptations between the two groups of mice receiving the obesogenic HFD diet. The MMRA pipeline was used to investigate how Irs2 gene could be regulated. It identified miR-34a-5p as a regulator of Irs2 expression. miR-34a-5p was downregulated in the HFepa condition compared to the HFoleic condition and upregulated in the HFoleic and HFepa conditions compared to the reference condition. Integrally, these data suggested that a new regulation between EPA-mediated miR-34a-5p-Irs2 and an inhibition of gluconeogenesis during fasting states through Irs2 overexpression could be clue mechanisms to modulate glucose flux and improve insulin resistance in an obesogenic environment.

4. Discussion

The omega-3 (*n*-3) long-chain polyunsaturated FAs (LC-PUFA), eicosapentaenoic (EPA, 20:5*n*-3) and docosahexaenoic (DHA, 22:6*n*-3) acids, are essential components of a healthy, balanced diet, having beneficial effects on development and in mitigating a range of pathological conditions [31]. LC-PUFAs control some key molecular cell mechanisms, resulting in a beneficial role in obesity and inflammatory diseases. Such mechanisms are complex and reflect the diversity of their functions, mainly as modulators of the dynamic properties of membranes, regulators of gene expression, and precursors of active mediators [32]. The development of obesity involved alterations in many biochemical processes and a pro-inflammatory state in insulin-sensitive tissues, leading to an increased risk of developing cardiovascular disease, type 2 diabetes, and cancer. The transgenerational modulation of the fatty acid profile of the diet was found to affect the susceptibility of the descendants [8] but the molecular adaptations remained to be elucidated. The liver has a key role in glucose and lipid homeostasis. Then, liver diseases are closely associated to these obesity-related morbidities. Transgenerational supplementation with EPA alleviated the metabolic impact of the HFD and limited fat mass accumulation in this early stage of weight gain. Beneficial effects were also observed against muscle metabolic disorders and energy expenditure [33]. In order to obtain further insights into the molecular mechanisms that contribute to the beneficial effects mediated by EPA, we integrated an analysis of hepatic gene and miRNA expression data using the statistically based MMRA pipeline. We implemented systems biology methodologies, such as Boolean modeling to simulate the metabolic processes of a cell under specific conditions. We were able to extract a new regulation between gene and miRNAs, which could play a key role in the inhibition of hepatic gluconeogenesis and the improvement of insulin resistance.

Transgenerational supplementation with EPA modulated hepatic gene expression and the related regulation by miRNAs in response to an obesogenic challenge in mice as compared to animals receiving a mixture of mono and saturated FA provided by a "high oleic" sunflower oil as a control condition. The diet supplemented with 1% of "high-oleic" sunflower oil was used to match the addition of energy provided by 1% of fish oil in the EPA lineage with a marginal metabolic impact. Most of the differentially expressed miRNAs and genes in the liver from mice exposed to a HFD were shared between the animals from the EPA and the control lineages. However, some of the genes were exclusive of the control/oleic or omega 3 lineage and could be involved in the differential metabolic response. Likewise, differentially expressed genes were analyzed to extract their miRNA regulation. Among the 30 mostly affected genes when HFepa and Reference groups were compared, some genes were regulated by miRNAs identified as differentially expressed in both HFepa or HFoleic groups, even some of these miRNAs were exclusive to the HFoleic lineage. Some genes had no known regulation by the identified miRNA and for which the mechanisms controlling their expression were not identified in our statistical analysis. Then, we performed a GeneTrial and MetExplore analysis to find the relations between our differentially expressed genes with general pathways or specific metabolic pathways, respectively. Our results provided new biological links between PPAR signaling, glucose metabolism, and FA metabolism as crucial determinants of the health effect of the transgenerational supplementation with EPA. We highlighted pathways related to amino acids, cholesterol, adipogenesis, biotin metabolism that converged on glucose and FA flux metabolism. Regulation of these pathways were related to pathologies mediated by obesity or metabolic syndrome. For instance, biotin is involved in gluconeogenesis, FA synthesis, amino acids catabolism by acting as a prosthetic group for pyruvate carboxylase, propionyl-CoA carboxylase, beta-methylcrotinyl-CoA carboxylase, and acetyl-CoA carboxylase [34]. On the other hand, oxoglutarate is at the intersection between carbon and nitrogen metabolic pathways [35]. Although experimental models should be developed to validate these links, our approach provided new potential targets for future therapeutic or preventive assays.

The integration of all our data suggested that the PPAR pathway appeared as a central axis in the differential adaptions to the obesogenic diet between the two lineages. The PPAR subfamily of nuclear receptors controls many different target genes involved in lipid metabolism, FA oxidation and glucose homeostasis [36,37]. PPARγ has a central role in adipogenesis and lipogenesis [38,39]. Heterozygous PPARγ-null mice exhibited greater insulin sensitivity than wild-type littermates and were protected from the development of insulin resistance and glucose intolerance mediated by a HFD [39]. As natural ligands for PPARs, could bind and activate PPARα to stimulate the expression of genes involved in FA oxidation and repress inflammation [40,41]. Omega-3 FA could also interact with PPARγ, but the impact of omega-3 FA binding to PPARγ on lipid metabolism remains controversial. An acute exposure to omega-3 FA had a stimulatory effect on PPARγ and adipogenesis, although a chronic exposure had a repressive effect [5]. Discrepancies between studies about the effect of EPA on PPAR transcription factors may have been linked to differences in the dose and time effect which should be considered to achieve a comprehension of modifications in insulin resistance and fat mass gain. Furthermore, it would be of scientific relevance to explore if similar adaptations occurred in the adipose tissue of these mice as PPARs are master regulators of adipose tissue biology.

Despite no differential expression of Pgc-1α gene between HFepa and HFoleic group, our results underscored the importance of Pgc-1α in glucose homeostasis in mice from the EPA lineage during the obesogenic diet. Pgc-1α is a member of a family of transcription coactivators which could interact with PPARγ in a ligand-independent manner. Pgc-1α was described to be highly abundant in tissues with high capacity for mitochondrial FA oxidation such as the brown adipose tissue, the heart, and skeletal muscle [42]. Hepatic Pgc-1α expression is induced in the liver during fasting and elevated during diabetes, causing an uncontrolled gluconeogenesis [43]. It was found that Pgc-1α promoted insulin resistance in the liver through a PPARα-dependent activation of the mammalian tribbles homolog TRB-3 [44], a fasting-inducible inhibitor of the serine-threonine kinase Akt/PKB [45]. A recent report

showed that Pgc-1α had a crucial role in the control of gluconeogenesis during the fasting-to-fed transition [30] through the regulation of the balance between Irs1 and Irs2 expression, two major elements of the insulin-signaling pathway, during the fasting-to-fed transition to quickly modulate gluconeogenesis. Sensitization of the liver to insulin by Pgc-1α represented a necessary priming of the liver to shut down gluconeogenesis immediately after the rise of insulin during feeding [30], allowing a fine-tuning of plasma glucose level. Muscle-specific transgenic overexpression of Pgc-1α contributed to the development of diet-induced insulin resistance, probably due to an increase in FA and reduced glucose uptake, inducing intramuscular lipid accumulations and then the alteration of insulin signaling [46]. Altogether, these studies suggested that strong Pgc-1α overexpression, but not physiologic Pgc-1α overexpression, would induce harmful metabolic effects.

To help the interpretation of our observations, we used a model in silico of the cellular metabolic behavior under different scenarios by the integration of key variables or components which modulate glycolysis, gluconeogenesis, lipolysis, lipogenesis and adipogenesis processes as key modulator of metabolic homeostasis.

Our modeling analysis confirmed that an adequate expression level of Pgc-1α was required after feeding and that an intermediate level of Pgc-1α during the fasting state, resulted in the activation of lipolysis and gluconeogenesis. The simulation of Pgc-1α knockout resulted in the inhibition of both gluconeogenesis and adipogenesis, but an activation of lipolysis. This simulated state was likely to mimic the hepatic environment in mice from the omega 3 lineage during the obesogenic challenge as mechanisms to control glucose homeostasis and the accumulation of fat mass. In agreement with this, a recent report concluded that an inhibition of the FOXO1/Pgc-1α pathway regulated hepatic gluconeogenesis and improved insulin resistance in rats fed with a HFD and insulin-resistant cells [47].

As Pgc-1α gene level did not differ between control and EPA lineages, other factors, linked to the co-activator could modulate its activity. Our data and bioinformatics analysis suggested a contribution of insulin receptor substrate 2 (Irs2) in the effect of Pgc-1α against insulin resistance. Irs proteins are directly phosphorylated by the insulin receptor, leading to the recruitment and activation of additional signaling proteins [48]. Irs1 and Irs2 are crucial determinant of gluconeogenesis and lipogenesis in the liver and decreased hepatic Irs2 gene level was observed with hepatosteatosis [49–51]. These data strongly suggested that Irs2 is a key to achieve an understanding. Our data confirmed that Irs2 was a key element within the network of molecular mechanisms linked to insulin resistance. We showed differences in the levels of individual expression of the Irs2 gene between the HFepa vs. HFoleic conditions. Irs2 gene was upregulated in the HFepa group, while a downregulation of Irs2 expression was observed in the HFoleic group as compared to the reference group. Although it was proposed that Pgc-1α stimulated Irs2 expression [30], our data suggested that Irs2 could also be controlled by other mechanisms.

The expression of the Irs2 gene could be directly regulated by fixation of insulin, Srebp-1c and TF3 proteins to its promoter [52–54]. A negative control by miRNAs was also demonstrated in pancreatic beta cells [55]. A crucial role for miRNAs was described in the control of the integration of metabolism and mitochondrial functions during the fed-fasted transitions [56] to prevent hepatic dysfunction and metabolic or aging-associated diseases.

We hypothesized that Irs2 was, at least partly regulated by miRNA-34a (miR-34a-5p). MiR-34a is a part of the p53 tumor suppressor network [57] and one of the major miRNAs involved in the production of insulin, pancreatic development and glucose homeostasis [58].

In agreement with the downregulation of miR-34a-5p in HFepa group compared to HFoleic group, the expression level of this miRNA was increased in the fatty liver in mouse models of obesity [59]. Increased circulating levels of miR-34a were also correlated with the severity of hepatic disease in patients with non-alcoholic fatty-liver disease (NAFLD) or type 2 diabetes [60,61].

5. Conclusions

Our integrative analysis allowed the extraction of information about the molecular events and gene–protein networks modulated by manipulating of the diet across generations and which could affect metabolic and physiologic susceptibility to nutritional stress. We concluded that mice from the EPA lineage exhibited an improved response against fat accumulation, insulin resistance through a regulatory axis involving Pgc-1α, Irs2, and miR-34a-5p. This hypothesis must now be validated using invalidation or overexpression models targeting these proteins.

Supplementary Materials: The following are available online at http://www.mdpi.com/2072-6643/12/12/3864/s1, Figure S1: Schematic representation of the dietary intervention, Figure S2: MetExplore pathways representation, Table S1: miRNAs regulating HFepa vs. reference phenotype signature (MMRA Analysis), Table S2: miRNAs regulating HFoleic vs. reference phenotype signature (MMRA Analysis), Table S3: Enriched pathways resulted from an overrepresentation analysis in GeneTrial 2.0. in HFoleic vs. reference, Table S4: Enriched pathways resulted from an overrepresentation analysis in GeneTrial 2.0. in HFepa vs. reference, Table S5: Enriched pathways resulted from a GSEA analysis in GeneTrial 2.0. in HFepa vs. HFoleic biological conditions, Table S6: Metabolic enriched pathways from MetExplore analysis in each group, Table S7: RT-qPCR validation of microarray data.

Author Contributions: Conceptualization, A.P., B.M., and F.C.; methodology, K.F.C.-J., L.C., A.P., and F.C.; software, K.F.C.-J., T.Y., and N.P.; validation, K.F.C.-J., L.C., N.P., and S.D.S.V.; formal analysis, S.D.S.V., A.P., and J.P.R.; investigation, K.F.C.-J., A.P., J.P.R., S.D.S.V., and F.C.; resources, B.M. and F.C.; data curation, K.F.C.-J., T.Y., and F.C.; writing—original draft preparation, K.F.C.-J.; writing—review and editing, K.F.C.-J., L.C., N.P., T.Y., A.P., B.M., and F.C.; visualization, K.F.C.-J., N.P., and F.C.; supervision, F.C.; project administration, F.C.; funding acquisition, B.M. and F.C. All authors have read and agreed to the published version of the manuscript.

Funding: This research was funded by Avril in partnership with Lesieur and a grant from the European Regional Development Fund (ERDF) operational programme, la Région Auvergne-Rhône-Alpes (CPER 2017 AUDACE: ICARES).

Acknowledgments: We are grateful to the staff of the Installation Expérimentale de Nutrition (INRAE of Saint Genès Champanelle-Theix) for providing everyday care to the animals; Elodie Pitois for her expert technical assistance to the study. We thank Claire Naylies and Yannick Lippi for their contribution to microarray fingerprints acquisition and microarray data analysis carried out at GeT-TRiX Genopole Toulouse Midi-Pyrénées facility (Toxalim (Research Centre in Food Toxicology), Université de Toulouse, INRA, ENVT, INP-Purpan, UPS, Toulouse, France). We also thank Dragan Milenkovic for its critical reading of the manuscript.

Conflicts of Interest: The authors declare no conflict of interest.

References

1. de Ferranti, S.; Mozaffarian, D. The perfect storm: Obesity, adipocyte dysfunction, and metabolic consequences. *Clin. Chem.* **2008**, *54*, 945–955. [CrossRef]
2. Hatting, M.; Tavares, C.D.J.; Sharabi, K.; Rines, A.K.; Puigserver, P. Insulin regulation of gluconeogenesis. *Ann. N.Y. Acad. Sci.* **2018**, *1411*, 21–35. [CrossRef] [PubMed]
3. Samuel, V.T.; Shulman, G.I. The pathogenesis of insulin resistance: Integrating signaling pathways and substrate flux. *J. Clin. Investig.* **2016**, *126*, 12–22. [CrossRef]
4. Albracht-Schulte, K.; Kalupahana, N.S.; Ramalingam, L.; Wang, S.; Rahman, S.M.; Robert-McComb, J.; Moustaid-Moussa, N. Omega-3 fatty acids in obesity and metabolic syndrome: A mechanistic update. *J. Nutr. Biochem.* **2018**, *58*, 1–16. [CrossRef] [PubMed]
5. Martinez-Fernandez, L.; Laiglesia, L.M.; Huerta, A.E.; Martinez, J.A.; Moreno-Aliaga, M.J. Omega-3 fatty acids and adipose tissue function in obesity and metabolic syndrome. *Prostaglandins Other Lipid Mediat.* **2015**, *121*, 24–41. [CrossRef] [PubMed]
6. Pinel, A.; Morio-Liondore, B.; Capel, F. n-3 Polyunsaturated fatty acids modulate metabolism of insulin-sensitive tissues: Implication for the prevention of type 2 diabetes. *J. Physiol. Biochem.* **2014**, *70*, 647–658. [CrossRef] [PubMed]
7. Pinel, A.; Pitois, E.; Rigaudiere, J.P.; Jouve, C.; De Saint-Vincent, S.; Laillet, B.; Montaurier, C.; Huertas, A.; Morio, B.; Capel, F. EPA prevents fat mass expansion and metabolic disturbances in mice fed with a Western diet. *J. Lipid Res.* **2016**, *57*, 1382–1397. [CrossRef] [PubMed]
8. Massiera, F.; Barbry, P.; Guesnet, P.; Joly, A.; Luquet, S.; Moreilhon-Brest, C.; Mohsen-Kanson, T.; Amri, E.Z.; Ailhaud, G. A Western-like fat diet is sufficient to induce a gradual enhancement in fat mass over generations. *J. Lipid Res.* **2010**, *51*, 2352–2361. [CrossRef] [PubMed]

9. Dao, M.C.; Sokolovska, N.; Brazeilles, R.; Affeldt, S.; Pelloux, V.; Prifti, E.; Chilloux, J.; Verger, E.O.; Kayser, B.D.; Aron-Wisnewsky, J.; et al. A Data Integration Multi-Omics Approach to Study Calorie Restriction-Induced Changes in Insulin Sensitivity. *Front. Physiol.* **2018**, *9*, 1958. [CrossRef]
10. Yang, Q.; Vijayakumar, A.; Kahn, B.B. Metabolites as regulators of insulin sensitivity and metabolism. *Nat. Rev. Mol. Cell Biol.* **2018**, *19*, 654–672. [CrossRef]
11. Bolstad, B.M.; Irizarry, R.A.; Astrand, M.; Speed, T.P. A comparison of normalization methods for high density oligonucleotide array data based on variance and bias. *Bioinformatics* **2003**, *19*, 185–193. [CrossRef] [PubMed]
12. Ritchie, M.E.; Phipson, B.; Wu, D.; Hu, Y.; Law, C.W.; Shi, W.; Smyth, G.K. limma powers differential expression analyses for RNA-sequencing and microarray studies. *Nucleic Acids Res.* **2015**, *43*, e47. [CrossRef] [PubMed]
13. Edgar, R.; Domrachev, M.; Lash, A.E. Gene Expression Omnibus: NCBI gene expression and hybridization array data repository. *Nucleic Acids Res.* **2002**, *30*, 207–210. [CrossRef] [PubMed]
14. Chen, C.J.; Servant, N.; Toedling, J.; Sarazin, A.; Marchais, A.; Duvernois-Berthet, E.; Cognat, V.; Colot, V.; Voinnet, O.; Heard, E.; et al. ncPRO-seq: A tool for annotation and profiling of ncRNAs in sRNA-seq data. *Bioinformatics* **2012**, *28*, 3147–3149. [CrossRef]
15. Benjamini, Y.; Hochberg, Y. Controlling the False Discovery Rate: A Practical and Powerful Approach to Multiple Testing. *J. R. Stat. Soc. Ser. B (Methodol.)* **1995**, *57*, 289–300. [CrossRef]
16. Rohart, F.; Gautier, B.; Singh, A.; Le Cao, K.A. mixOmics: An R package for 'omics feature selection and multiple data integration. *PLoS Comput. Biol.* **2017**, *13*, e1005752. [CrossRef]
17. Cantini, L.; Isella, C.; Petti, C.; Picco, G.; Chiola, S.; Ficarra, E.; Caselle, M.; Medico, E. MicroRNA-mRNA interactions underlying colorectal cancer molecular subtypes. *Nat. Commun.* **2015**, *6*, 9878. [CrossRef]
18. Wang, L.; Feng, Z.; Wang, X.; Zhang, X. DEGseq: An R package for identifying differentially expressed genes from RNA-seq data. *Bioinformatics* **2010**, *26*, 136–138. [CrossRef]
19. Hsu, S.D.; Lin, F.M.; Wu, W.Y.; Liang, C.; Huang, W.C.; Chan, W.L.; Tsai, W.T.; Chen, G.Z.; Lee, C.J.; Chiu, C.M.; et al. miRTarBase: A database curates experimentally validated microRNA-target interactions. *Nucleic Acids Res.* **2011**, *39*, D163–D169. [CrossRef]
20. Chen, Y.; Wang, X. miRDB: An online database for prediction of functional microRNA targets. *Nucleic Acids Res.* **2020**, *48*, D127–D131. [CrossRef]
21. Agarwal, V.; Bell, G.W.; Nam, J.W.; Bartel, D.P. Predicting effective microRNA target sites in mammalian mRNAs. *eLife* **2015**, *4*. [CrossRef] [PubMed]
22. Stockel, D.; Kehl, T.; Trampert, P.; Schneider, L.; Backes, C.; Ludwig, N.; Gerasch, A.; Kaufmann, M.; Gessler, M.; Graf, N.; et al. Multi-omics enrichment analysis using the GeneTrail2 web service. *Bioinformatics* **2016**, *32*, 1502–1508. [CrossRef] [PubMed]
23. Subramanian, A.; Tamayo, P.; Mootha, V.K.; Mukherjee, S.; Ebert, B.L.; Gillette, M.A.; Paulovich, A.; Pomeroy, S.L.; Golub, T.R.; Lander, E.S.; et al. Gene set enrichment analysis: A knowledge-based approach for interpreting genome-wide expression profiles. *Proc. Natl. Acad. Sci. USA* **2005**, *102*, 15545–15550. [CrossRef] [PubMed]
24. Cottret, L.; Wildridge, D.; Vinson, F.; Barrett, M.P.; Charles, H.; Sagot, M.F.; Jourdan, F. MetExplore: A web server to link metabolomic experiments and genome-scale metabolic networks. *Nucleic Acids Res.* **2010**, *38*, W132–W137. [CrossRef]
25. Heinken, A.; Sahoo, S.; Fleming, R.M.; Thiele, I. Systems-level characterization of a host-microbe metabolic symbiosis in the mammalian gut. *Gut Microbes* **2013**, *4*, 28–40. [CrossRef]
26. Gonzalez, A.G.; Naldi, A.; Sanchez, L.; Thieffry, D.; Chaouiya, C. GINsim: A software suite for the qualitative modelling, simulation and analysis of regulatory networks. *Bio Syst.* **2006**, *84*, 91–100. [CrossRef]
27. Yugi, K.; Kubota, H.; Hatano, A.; Kuroda, S. Trans-Omics: How to Reconstruct Biochemical Networks Across Multiple 'Omic' Layers. *Trends Biotechnol.* **2016**, *34*, 276–290. [CrossRef]
28. Miskov-Zivanov, N.; Turner, M.S.; Kane, L.P.; Morel, P.A.; Faeder, J.R. The duration of T cell stimulation is a critical determinant of cell fate and plasticity. *Sci. Signal.* **2013**, *6*, ra97. [CrossRef]
29. Kanehisa, M.; Goto, S. KEGG: Kyoto encyclopedia of genes and genomes. *Nucleic Acids Res.* **2000**, *28*, 27–30. [CrossRef]

30. Besse-Patin, A.; Jeromson, S.; Levesque-Damphousse, P.; Secco, B.; Laplante, M.; Estall, J.L. PGC1A regulates the IRS1:IRS2 ratio during fasting to influence hepatic metabolism downstream of insulin. *Proc. Natl. Acad. Sci. USA* **2019**, *116*, 4285–4290. [CrossRef]
31. Tocher, D.R.; Betancor, M.B.; Sprague, M.; Olsen, R.E.; Napier, J.A. Omega-3 Long-Chain Polyunsaturated Fatty Acids, EPA and DHA: Bridging the Gap between Supply and Demand. *Nutrients* **2019**, *11*, 89. [CrossRef] [PubMed]
32. Rodriguez-Cruz, M.; Serna, D.S. Nutrigenomics of omega-3 fatty acids: Regulators of the master transcription factors. *Nutrition* **2017**, *41*, 90–96. [CrossRef] [PubMed]
33. Pinel, A.; Rigaudiere, J.P.; Jouve, C.; Montaurier, C.; Jousse, C.; LHomme, M.; Morio, B.; Capel, F. Transgenerational supplementation with eicosapentaenoic acid reduced the metabolic consequences on the whole body and skeletal muscle in mice receiving an obesogenic diet. *Eur. J. Nutr.* **2020**. under review.
34. Rodriguez Melendez, R. Importance of biotin metabolism. *Rev. Investig. Clin.* **2000**, *52*, 194–199.
35. Huergo, L.F.; Dixon, R. The Emergence of 2-Oxoglutarate as a Master Regulator Metabolite. *Microbiol. Mol. Biol. Rev. Mmbr.* **2015**, *79*, 419–435. [CrossRef] [PubMed]
36. Hardwick, J.P.; Osei-Hyiaman, D.; Wiland, H.; Abdelmegeed, M.A.; Song, B.J. PPAR/RXR Regulation of Fatty Acid Metabolism and Fatty Acid omega-Hydroxylase (CYP4) Isozymes: Implications for Prevention of Lipotoxicity in Fatty Liver Disease. *PPAR Res.* **2009**, *2009*, 952734. [CrossRef] [PubMed]
37. Dubois, V.; Eeckhoute, J.; Lefebvre, P.; Staels, B. Distinct but complementary contributions of PPAR isotypes to energy homeostasis. *J. Clin. Investig.* **2017**, *127*, 1202–1214. [CrossRef]
38. Booth, A.D.; Magnuson, A.M.; Cox-York, K.A.; Wei, Y.; Wang, D.; Pagliassotti, M.J.; Foster, M.T. Inhibition of adipose tissue PPARgamma prevents increased adipocyte expansion after lipectomy and exacerbates a glucose-intolerant phenotype. *Cell Prolif.* **2017**, *50*. [CrossRef]
39. Jones, J.R.; Barrick, C.; Kim, K.A.; Lindner, J.; Blondeau, B.; Fujimoto, Y.; Shiota, M.; Kesterson, R.A.; Kahn, B.B.; Magnuson, M.A. Deletion of PPARgamma in adipose tissues of mice protects against high fat diet-induced obesity and insulin resistance. *Proc. Natl. Acad. Sci. USA* **2005**, *102*, 6207–6212. [CrossRef]
40. Sethi, S.; Ziouzenkova, O.; Ni, H.; Wagner, D.D.; Plutzky, J.; Mayadas, T.N. Oxidized omega-3 fatty acids in fish oil inhibit leukocyte-endothelial interactions through activation of PPAR alpha. *Blood* **2002**, *100*, 1340–1346. [CrossRef]
41. Zuniga, J.; Cancino, M.; Medina, F.; Varela, P.; Vargas, R.; Tapia, G.; Videla, L.A.; Fernandez, V. N-3 PUFA supplementation triggers PPAR-alpha activation and PPAR-alpha/NF-kappaB interaction: Anti-inflammatory implications in liver ischemia-reperfusion injury. *PLoS ONE* **2011**, *6*, e28502. [CrossRef] [PubMed]
42. Puigserver, P.; Wu, Z.; Park, C.W.; Graves, R.; Wright, M.; Spiegelman, B.M. A cold-inducible coactivator of nuclear receptors linked to adaptive thermogenesis. *Cell* **1998**, *92*, 829–839. [CrossRef]
43. Yoon, J.C.; Puigserver, P.; Chen, G.; Donovan, J.; Wu, Z.; Rhee, J.; Adelmant, G.; Stafford, J.; Kahn, C.R.; Granner, D.K.; et al. Control of hepatic gluconeogenesis through the transcriptional coactivator PGC-1. *Nature* **2001**, *413*, 131–138. [CrossRef]
44. Koo, S.H.; Satoh, H.; Herzig, S.; Lee, C.H.; Hedrick, S.; Kulkarni, R.; Evans, R.M.; Olefsky, J.; Montminy, M. PGC-1 promotes insulin resistance in liver through PPAR-alpha-dependent induction of TRB-3. *Nat. Med.* **2004**, *10*, 530–534. [CrossRef]
45. Du, K.; Herzig, S.; Kulkarni, R.N.; Montminy, M. TRB3: A tribbles homolog that inhibits Akt/PKB activation by insulin in liver. *Science* **2003**, *300*, 1574–1577. [CrossRef]
46. Choi, C.S.; Befroy, D.E.; Codella, R.; Kim, S.; Reznick, R.M.; Hwang, Y.J.; Liu, Z.X.; Lee, H.Y.; Distefano, A.; Samuel, V.T.; et al. Paradoxical effects of increased expression of PGC-1alpha on muscle mitochondrial function and insulin-stimulated muscle glucose metabolism. *Proc. Natl. Acad. Sci. USA* **2008**, *105*, 19926–19931. [CrossRef]
47. Gu, L.; Ding, X.; Wang, Y.; Gu, M.; Zhang, J.; Yan, S.; Li, N.; Song, Z.; Yin, J.; Lu, L.; et al. Spexin alleviates insulin resistance and inhibits hepatic gluconeogenesis via the FoxO1/PGC-1alpha pathway in high-fat-diet-induced rats and insulin resistant cells. *Int. J. Biol. Sci.* **2019**, *15*, 2815–2829. [CrossRef]
48. White, M.F. IRS proteins and the common path to diabetes. *Am. J. Physiol. Endocrinol. Metab.* **2002**, *283*, E413–E422. [CrossRef]
49. Honma, M.; Sawada, S.; Ueno, Y.; Murakami, K.; Yamada, T.; Gao, J.; Kodama, S.; Izumi, T.; Takahashi, K.; Tsukita, S.; et al. Selective insulin resistance with differential expressions of IRS-1 and IRS-2 in human NAFLD livers. *Int. J. Obes.* **2018**, *42*, 1544–1555. [CrossRef]

50. Nandi, A.; Kitamura, Y.; Kahn, C.R.; Accili, D. Mouse models of insulin resistance. *Physiol. Rev.* **2004**, *84*, 623–647. [CrossRef]
51. Valverde, A.M.; Burks, D.J.; Fabregat, I.; Fisher, T.L.; Carretero, J.; White, M.F.; Benito, M. Molecular mechanisms of insulin resistance in IRS-2-deficient hepatocytes. *Diabetes* **2003**, *52*, 2239–2248. [CrossRef] [PubMed]
52. Zhang, J.; Ou, J.; Bashmakov, Y.; Horton, J.D.; Brown, M.S.; Goldstein, J.L. Insulin inhibits transcription of IRS-2 gene in rat liver through an insulin response element (IRE) that resembles IREs of other insulin-repressed genes. *Proc. Natl. Acad. Sci. USA* **2001**, *98*, 3756–3761. [CrossRef]
53. Ide, T.; Shimano, H.; Yahagi, N.; Matsuzaka, T.; Nakakuki, M.; Yamamoto, T.; Nakagawa, Y.; Takahashi, A.; Suzuki, H.; Sone, H.; et al. SREBPs suppress IRS-2-mediated insulin signalling in the liver. *Nat. Cell Biol.* **2004**, *6*, 351–357. [CrossRef]
54. Nakagawa, Y.; Shimano, H.; Yoshikawa, T.; Ide, T.; Tamura, M.; Furusawa, M.; Yamamoto, T.; Inoue, N.; Matsuzaka, T.; Takahashi, A.; et al. TFE3 transcriptionally activates hepatic IRS-2, participates in insulin signaling and ameliorates diabetes. *Nat. Med.* **2006**, *12*, 107–113. [CrossRef] [PubMed]
55. Tao, H.; Wang, M.M.; Zhang, M.; Zhang, S.P.; Wang, C.H.; Yuan, W.J.; Sun, T.; He, L.J.; Hu, Q.K. MiR-126 Suppresses the Glucose-Stimulated Proliferation via IRS-2 in INS-1 beta Cells. *PLoS ONE* **2016**, *11*, e0149954. [CrossRef] [PubMed]
56. Maniyadath, B.; Chattopadhyay, T.; Verma, S.; Kumari, S.; Kulkarni, P.; Banerjee, K.; Lazarus, A.; Kokane, S.S.; Shetty, T.; Anamika, K.; et al. Loss of Hepatic Oscillatory Fed microRNAs Abrogates Refed Transition and Causes Liver Dysfunctions. *Cell Rep.* **2019**, *26*, 2212–2226. [CrossRef] [PubMed]
57. He, L.; He, X.; Lim, L.P.; de Stanchina, E.; Xuan, Z.; Liang, Y.; Xue, W.; Zender, L.; Magnus, J.; Ridzon, D.; et al. A microRNA component of the p53 tumour suppressor network. *Nature* **2007**, *447*, 1130–1134. [CrossRef]
58. Chakraborty, C.; Doss, C.G.; Bandyopadhyay, S.; Agoramoorthy, G. Influence of miRNA in insulin signaling pathway and insulin resistance: Micro-molecules with a major role in type-2 diabetes. *Wiley Interdiscip. Rev. RNA* **2014**, *5*, 697–712. [CrossRef] [PubMed]
59. Lee, J.; Padhye, A.; Sharma, A.; Song, G.; Miao, J.; Mo, Y.Y.; Wang, L.; Kemper, J.K. A pathway involving farnesoid X receptor and small heterodimer partner positively regulates hepatic sirtuin 1 levels via microRNA-34a inhibition. *J. Biol. Chem.* **2010**, *285*, 12604–12611. [CrossRef]
60. Cheung, O.; Puri, P.; Eicken, C.; Contos, M.J.; Mirshahi, F.; Maher, J.W.; Kellum, J.M.; Min, H.; Luketic, V.A.; Sanyal, A.J. Nonalcoholic steatohepatitis is associated with altered hepatic MicroRNA expression. *Hepatology* **2008**, *48*, 1810–1820. [CrossRef]
61. Kong, L.; Zhu, J.; Han, W.; Jiang, X.; Xu, M.; Zhao, Y.; Dong, Q.; Pang, Z.; Guan, Q.; Gao, L.; et al. Significance of serum microRNAs in pre-diabetes and newly diagnosed type 2 diabetes: A clinical study. *Acta Diabetol.* **2011**, *48*, 61–69. [CrossRef] [PubMed]

nutrients

MDPI

Article

Intermittent Fasting Ameliorated High-Fat Diet-Induced Memory Impairment in Rats via Reducing Oxidative Stress and Glial Fibrillary Acidic Protein Expression in Brain

Suzan M. Hazzaa [1], Mabrouk A. Abd Eldaim [2,*], Amira A. Fouda [3], Asmaa Shams El Dein Mohamed [3], Mohamed Mohamed Soliman [4,5] and Eman I. Elgizawy [1]

[1] Medical Physiology Department, Faculty of Medicine, Menoufia University, Shebeen Elkom 32511, Egypt; suzanhazzaa@med.menofia.edu.eg (S.M.H.); eman.elgizawi@med.menofia.edu.eg (E.I.E.)
[2] Department of Biochemistry and Chemistry of Nutrition, Faculty of Veterinary, Medicine, Menoufia University, Shebeen Elkom 32511, Egypt
[3] Pathology Department, Faculty of Medicine, Menoufia University, Shebeen Elkom 32511, Egypt; aamf8296@gmail.com (A.A.F.); asmaashams@rocketmail.com (A.S.E.D.M.)
[4] Clinical Laboratory Sciences Department, Turabah University College, Taif University, Taif 21995, Saudi Arabia; mmsoliman@tu.edu.sa
[5] Biochemistry Department, Faculty of Veterinary Medicine, Benha University, Benha 13736, Egypt
* Correspondence: mabroukattia@vet.menofia.edu.eg

Abstract: Intermittent fasting (IF) plays an important role in the protection against metabolic syndrome-induced memory defects. This study aimed to assess the protective effects of both prophylactic and curative IF against high-fat diet (HFD)-induced memory defects in rats. The control group received a normal diet; the second group received a HFD; the third group was fed a HFD for 12 weeks and subjected to IF during the last four weeks (curative IF); the fourth group was fed a HFD and subjected to IF simultaneously (prophylactic IF). A high-fat diet significantly increased body weight, serum lipids levels, malondialdehyde (MDA) concentration, glial fibrillary acidic protein (GFAP) and H score in brain tissue and altered memory performance. In addition, it significantly decreased reduced glutathione (GSH) concentration in brain tissue and viability and thickness of pyramidal and hippocampus granular cell layers. However, both types of IF significantly decreased body weight, serum lipids, GFAP protein expression and H score and MDA concentration in brain tissue, and improved memory performance, while it significantly increased GSH concentration in brain tissue, viability, and thickness of pyramidal and granular cell layers of the hippocampus. This study indicated that IF ameliorated HFD-induced memory disturbance and brain tissue damage and the prophylactic IF was more potent than curative IF.

Keywords: high fat diet; intermittent fasting; GFAP

Citation: Hazzaa, S.M.; Eldaim, M.A.A.; Fouda, A.A.; Mohamed, A.S.E.D.; Soliman, M.M.; Elgizawy, E.I. Intermittent Fasting Ameliorated High-Fat Diet-Induced Memory Impairment in Rats via Reducing Oxidative Stress and Glial Fibrillary Acidic Protein Expression in Brain. *Nutrients* **2021**, *13*, 10. https://dx.doi.org/10.3390/nu13010010

Received: 29 November 2020
Accepted: 18 December 2020
Published: 22 December 2020

1. Introduction

Widespread metabolic syndrome (MS) nowadays is a sign of many underlying health problems, which result mainly from consumption of a high-fat diet (HFD) with high energy input [1]. Metabolic syndrome is associated with body fat accumulation, hypertension, dyslipidemia, hyperglycemia and oxidative stress [2]. It seriously affects the brain, behavior, and memory [3] and raises the risk of dementia [4]. Memory impairment in MS appears to be due to the reduction in many factors including the cholinergic system, and signal transduction together with the reduction in hippocampal neuron density [4].

On the other hand, dietary restriction (DR), either by reduced energy intake or intermittent fasting (IF) has been proven to increase the quality and span of the life with reduction of the incidence of age-associated diseases [5]. Dietary restriction and physical exercise have been proven as an effective measure to reduce the risk of cardiovascular disease in obese humans [6]. Additionally, long-term DR has been reported to reduce

serum lipid concentrations and arterial blood pressure. Moreover, it has a neuroprotective effect as it can delay neuronal degeneration in Alzheimer's disease [7]. Initiation of DR early in the adulthood stage has been reported to be the only means of delaying the onset of the age associated diseases. Other studies reported that DR even initiated at late age or for a limited time can also have beneficial effects [8,9]. Dietary restriction has antioxidant and anti-inflammatory properties [10]. Intermittent fasting in animal models is a DR regimen in which food is allowed but only every other day [11]. It can prevent neuro inflammation and oxidative stress [6].

Thus, it is important to change the current feeding habits and to find a new easy applicable strategy to prevent these health hazards. Intermittent fasting is a new dietary restriction method that is proven to boost body metabolism [12], decrease body fat, and body weight [13], as well as cognitive impairment [14]. The current study aimed to assess the potential effects of both curative and prophylactic intermittent fasting against high-fat diet-induced metabolic syndrome in rats.

2. Material and Methods

The experimental protocol was approved by the local ethical committee of the Faculty of Medicine, Menoufia University with approval code 279/018 following the Guide for the Care and Use of Laboratory Animals (eighth edition, National Academies Press) [15].

2.1. Animals

Forty adult male Wister albino rats matched for weight and age between 150 and 200 g were used in this experiment. During the study, each 2 rats were kept in one cage at normal room temperature, humidity and normal light/dark cycle.

2.2. Experimental Design

Rats were randomly assigned into four experimental groups, 10 rats each.

Control group: rats were fed standard rat corn-based chow (Table 1) for 12 weeks [16].

Table 1. Chemical composition of basal standard diet.

Diet Constituents	Control Group
Fat	7–10%
Carbohydrates	68–70%
Protein	18–20%
Vitamins and minerals	1–2%
Kcal/100 g/day	341

High-fat diet (HFD) group: rats were fed HFD (Table 2) for 12 weeks [17].

Table 2. Chemical composition of high-fat diet.

Diet Constituents	HFD
Fat	30%
Carbohydrates	50–52%
Protein	18–20%
Vitamins and minerals	1–2%
Kcal/100 g/day	530

Curative intermittent fasting group (cur. IF): rats were fed HFD for 12 weeks and subjected to IF during the last 4 weeks alternating with HFD diet [11].

Prophylactic intermittent fasting group (pro. IF): rats were subjected to IF for 24 h and fed HFD in the other day from the beginning of the experiment until its end.

The experimental design is illustrated below (Figure 1).

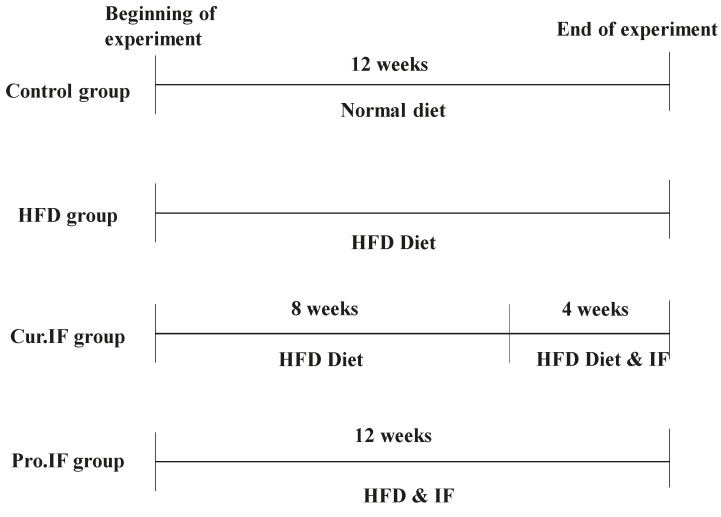

Figure 1. Diagram representing the experimental design. Rats were fed either basal (normal control group) diet; HFD; HFD and subjected to intermittent fasting (pro. IF) for 12 weeks, or HFD for 12 weeks and subjected to intermittent fasting (cur. IF) alternating with HFD during last 4 weeks. HFD means high-fat diet; pro. IF means prophylactic intermittent fasting while cur. IF means curative intermittent fasting.

2.3. Sampling

Rat body weights were recorded at the start of the experiment and at the end of the 4th and 8th weeks and at the end of the experiment (after 12 weeks from the beginning of the experiment) and the behavioral tests were performed as described below. Animals then were fasted overnight, and blood samples were collected, and sera samples were separated and used for measurements of fasting serum lipid profile. Then, rats were sacrificed by cervical decapitation and brains were removed and divided into two parts. One part was kept at −80 °C and used for estimation of malondialdehyde (MDA) and reduced glutathione (GSH) concentrations. The other half was kept in 10% neutral formalin and used for histopathological and immunohistochemical investigations.

2.4. Assessment of Behavioral Responses

All behavioral tests were performed between 9:00 a.m. and 2:00 p.m. in a calm observation room with normal day light. Rats were first adapted for 1 h before the beginning of the tests in the observation room. All tests were observed through video camera (Samsung ST93 Digital Camera, Suwon, South Korea). The equipment was cleaned with 70% ethanol to avoid odor cues for animals [18].

2.5. Assessment of Motor Function

Open Field Test

A wooden arena (100 × 100 × 60 cm height, with brown walls and floor) was divided into equal 25 squares. Rat was put in the center of the open field for 15 min and freely allowed to explore it [18]. The latency to move from the center was calculated, and the total distance moved by meter (m) was measured by calculating the numbers of crossed squares. The frequency of grooming was counted manually, time spent in the inner or outer zones also was calculated. After each test, the field was cleaned with 90% alcohol solution.

2.6. Assessment of Short-Term Spatial Memory

Y-Maze

The Y-maze consisted of three arms, each one 50 cm long, 10 cm wide and 20 cm high. It was used to evaluate the short-term spatial memory [19]. The Y-maze was made of wood and elevated 50 cm above the floor. This task was based on the innate behavior of animals to explore new areas. It consisted of two trials; a training phase and a test phase, each of them consisted of 5 min and was separated by a 90 min interval. During the training phase, the novel arm was blocked by a removable door then the rat was placed at the beginning of the start arm and left for 5 min to explore two arms. During the test phase, the "novel" arm was opened, and the rat could explore the available arms. Rats were observed by video camera. The number of the entries into the different arms and the time that rat spent in these arms were recorded.

2.7. Biochemical Investigations

Serum total cholesterol, triacylglycerol (TG) and high-density lipoprotein (HDL) levels were estimated by using an automatic analyzer 902 (Hitachi, Munich, Germany) and commercial kits (Bio-Med diagnostic, Cairo, Egypt). Serum levels of low-density lipoprotein (LDL) and very-low-density lipoprotein (VLDL) levels were analyzed according to the method of DeLong [20]. Serum level of VLDL was calculated by dividing serum level of TG by five [21]. Serum levels of low-density lipoprotein (LDL) were obtained by using the following equation [20]:

$$\text{LDL} - \text{C (mmol/L)} = \text{TC} - \text{HDL} - \text{C} - \text{TG}/2.2 \quad (1)$$

2.8. Measurement of Brain Tissues Malondialdehyde and Reduced Glutathione Concentrations

Brain tissues were homogenized in normal saline solution (1:9 w/v). The homogenate was centrifuged at 1800$\times$ g/min for 10 min. The supernatant was used for the measurements of lipid peroxidation and antioxidant enzyme activity via malondialdehyde (MDA). The concentration of malondialdehyde was quantified spectrophotometrically by using commercial kits (Biodiagnostic Company, Cairo, Egypt) according to [22]. The reduced glutathione (GSH) concentration was measured by using kits purchased from Biodiagnostic Company, Egypt, according to [23].

2.9. Histopathological Examination

Brain tissue samples of all groups were rapidly excised, cut into small pieces, and fixed in 10% neutral formalin. Then, tissue sections were processed and stained by hematoxylin and eosin stain according to [24].

2.10. Immunohistochemical Investigations

Glial fibrillary acidic protein (GFAP) was detected by using avidin–biotin complex (ABC) immunoperoxidase technique. After blocking the endogenous peroxidase, brain sections were incubated with anti-GFAP primary antibody at (1:100 dilution) for 20 min at room temperature. The primary GFAP antibody was mouse monoclonal antibody, (GFAP) Ab-1 (Clone GA-5), specific to the astrocytes obtained from Lab Vision Corporation, Medico Co., Egypt (Thermo Fisher, UK, Cat. #MS-280-R7). Then, the slides were incubated with the secondary anti-mouse antibody universal kits for 30 min in a humid chamber at room temperature after washing with diluted phosphate-buffered saline. All sections were stained by incubation with 3,3'-diaminobenzidine (DAB), a substrate chromogen, for 5–10 min resulting in brown-colored precipitate at the antigen sites. The Mayer's hematoxylin was used as a counter stain. Positive control was Cellosaurus cell line (IMR5) while for negative controls, incubation was without the primary antibody. The positive reactivity of GFAP was exhibited as different grades of reactivity (i.e., weak, moderate and strong), according to the intensity of staining. Positive reactivity was indicated by a brown-colored reaction [25].

H scoring: staining of the membrane was scored into four categories: 0 means no staining, 1 + means light staining visible only at high magnification, 2 + means intermediate staining, while 3 + means dark staining of linear membrane visible even at low magnification. The percentage of cells at different staining intensities was determined by visual assessment, with the score calculated using the formula 1 × (% of 1 + cells) + 2 × (% of 2 + cells) + 3 × (% of 3 + cells) [26]. Images were captured by using a colored video camera (Panasonic Color CCTV camera, Matsushita Communication, Industrial Co. Ltd., Tokyo, Japan) fixed on a light microscope (Olympus BX-40, Olympus Optical Co. Ltd., Tokyo, Japan). Images were taken at 400× magnification and 2.6 zoom. Photomicrographs were analyzed by using Software Image J program, a public domain image processing and analysis program (U.S. National Institutes of Health, Bethesda, MD, USA) (http://rsb.info.nih.gov/ij/) [27].

2.11. Statistical Analysis

Our data were expressed as mean ± standard error of the mean (SEM). The statistical analysis was carried out by using SPSS version 22 (IBM Corp., Armonk, NY, USA). Statistical analysis for behavior tests on open field and Y-mazes were performed by using Kruskal–Wallis and Mann–Whitney tests using all data sets to ensure normal distribution ($p > 0.5$). Other results were analyzed by using one-way ANOVA (analysis of variance), followed by (Tukey's) post hoc test for determination of significance of differences among groups. Differences were considered significant at $p < 0.05$.

3. Results

3.1. Intermittent Fasting Ameliorated HFD Increased Rats' Body Weight

Figure 2 showed rats' body weights of all experimental groups. High-fat diet significantly ($p < 0.001$) increased rats' body weight after 4, 8 and 12 weeks from the beginning of the experiment compared with the control rats fed standard diet. However, pro. IF significantly ($p < 0.001$) decreased rats' body weights after 4, 8 and 12 weeks from the beginning of the experiment compared to both HFD and cur. IF groups. Whereas cur. IF significantly ($p < 0.001$) decreased rats' body weight only after 12 weeks compared with HFD group.

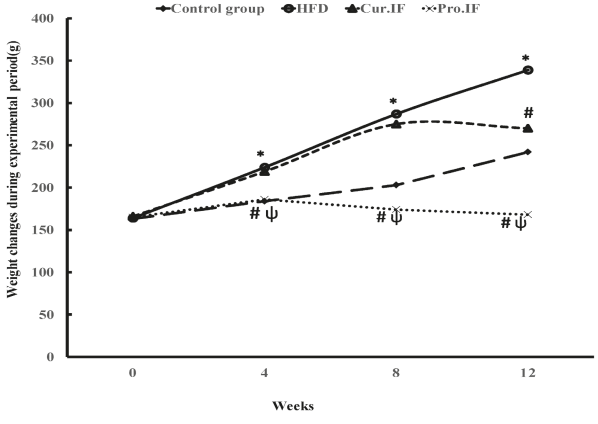

Figure 2. Effect of HFD and/or intermittent fasting on rats' body weights: Rats were fed either (a) basal (normal control group) diet; (b) HFD; (c) pro. IF; rats were subjected to both IF and HFD for 12 weeks; or (d) cur. IF; rats were subjected to HFD for 8 weeks then IF simultaneously with HFD during last 4 weeks. Rats' body weights were recorded after 4, 8 and 12 weeks from the beginning of the experiment. In all studied groups * HFD significant vis. control group, # pro. and cur. IF significant vis. HFD group, ψ pro. IF significant vise cur. IF.

3.2. Intermittent Fasting Improved the Behaviors of HFD Fed Rats

3.2.1. Open Field

Figure 3 showed the effects of HFD and/or IF on rats' motor functions and behavioral changes. High-fat diet significantly increased ($p < 0.001$) the length of time needed to move from the center of open field, time spent in the outer zone and the frequency of grooming compared with the control group. On the other hand, it significantly ($p < 0.001$) decreased total distance moved in open field and time spent in inner zone. Cur. IF significantly ($p < 0.001$) increased total distance moved while significantly ($p < 0.001$) decreased frequency of grooming compared with HFD group. Additionally, pro. IF significantly ($p < 0.001$) decreased latency to move from the center and the frequency of grooming while it significantly ($p < 0.001$) increased the total distance moved compared with HFD group. In addition, it significantly ($p < 0.001$) decreased latency to move from the center, time spent in the outer zone and the frequency of grooming with significant ($p < 0.001$) increase in the time spent in the inner zone compared with cur. IF group (Figure 3).

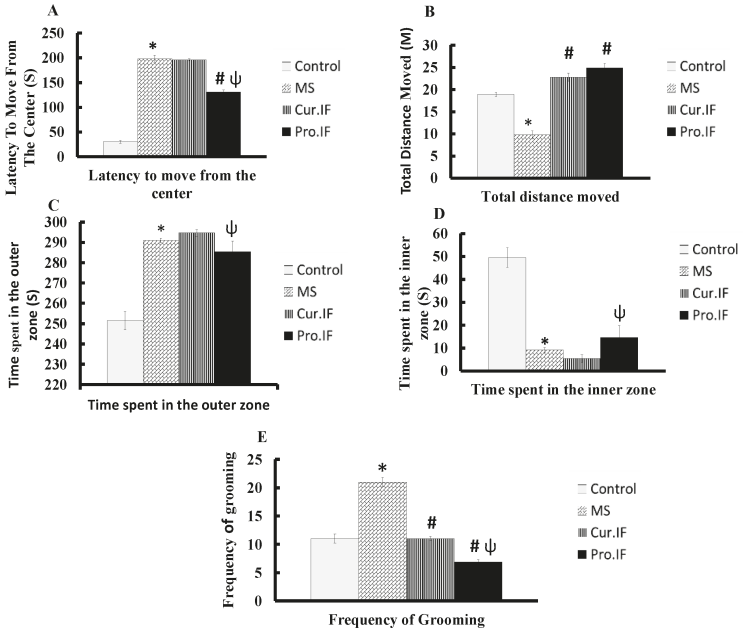

Figure 3. Effect of HFD and/or pro. and cur. IF on (**A**) latency to move from the center, (**B**) total distance moved, (**C**) time spent in the outer zone, (**D**) time spent in the inner zone, and (**E**) frequency of grooming in the open field test. Data are expressed as mean ± SEM ($n = 10$). * HFD significant vis. control group, # pro. and cur. IF significant vis. HFD group, ψ pro. IF significant vise cur. IF.

3.2.2. Y-Maze

Figure 4 shows the effect of HFD and/or IF on rats' behavior and short-term memory using Y-maze. Feeding rats HFD significantly ($p < 0.001$) decreased number of entries into all arms in training and test phases and the time spent in the other arm and novel arm in both phases compared with the control group. However, IF cur. and pro. IF significantly ($p < 0.001$) increased the number of the entries in both arms while it significantly ($p < 0.001$) decreased time spent in the start arm in the training phase compared with HFD group. Additionally, IF significantly ($p < 0.001$) increased the time spent in the novel arm in test phase compared with HFD group (Figure 4).

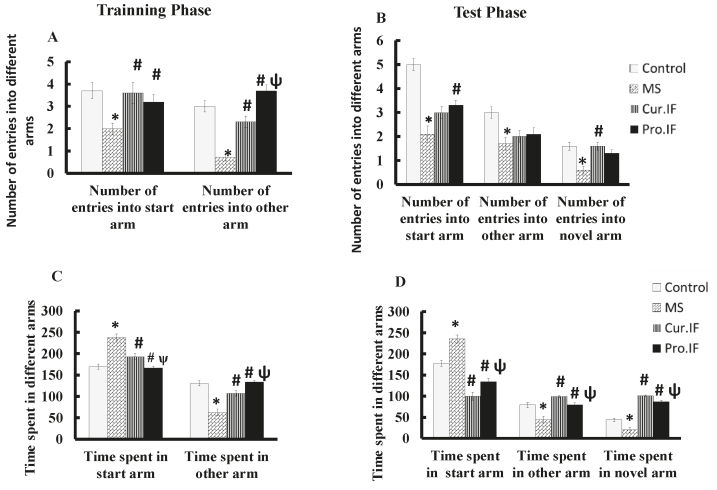

Figure 4. Effect of HFD and/or pro. and cur. IF on the short-term spatial memory tested by Y-maze in different studied groups: (**A**) the number of entries in the training phase; (**B**) the number of entries in the test phase; (**C**) the time spent in the training phase; (**D**) the time spent in the test phase. Data are expressed as mean ± SEM. (n = 10). * HFD significant vis. control group, # pro. and cur. IF significant vis. HFD group, ψ pro. IF significant vise cur. IF.

3.3. Intermittent Fasting Ameliorated HFD Altered Serum Lipid Profile in Rats

Table 3 shows that feeding rats HFD significantly ($p < 0.001$) increased serum cholesterol, triglycerides, LDL and VLDL levels while it significantly ($p < 0.001$) decreased serum HDL level compared with the control rats fed standard diet. Both the cur. and pro. IF significantly ($p < 0.001$) decreased serum cholesterol, triglycerides, LDL and VLDL levels compared with HFD group. In addition, pro. IF significantly ($p < 0.001$) increased serum HDL levels compared with those of HFD group. Moreover, pro. IF significantly ($p < 0.001$) decreased serum levels of cholesterol, triglycerides, LDL and VLDL while it significantly ($p < 0.001$) increased serum HDL level compared with curative IF group (Table 3).

Table 3. Effects of HFD and IF on serum lipid profile of all experimental groups.

Metabolite	Control	HFD	HFD & Cur IF	HFD & Pro IF
Cholesterol (mg/dL)	119.60 ± 1.88	277.10 ± 1.84 *	174.50 ± 2.37 #	129 ± 1.24 #ψ
Triglycerides (mg/dL)	122 ± 3.54	203.00 ± 7.20 *	174.70 ± 2.07 #	134.70 ± 2.54 #ψ
LDL (mg/dL)	43.60 ± 3.77	209.78 ± 2.22 *	109.06 ± 2.18 #	70.16 ± 1.94 #ψ
HDL(mg/dL)	51.60 ± 2.52	26.70 ± 0.97 *	31.50 ± 1.82	39.00 ± 1.52 #ψ
VLDL (mg/dL)	24.40 ± 0.70	40.62 ± 0.63 *	34.94 ± 0.41 #	26.94 ± 0.50 #ψ

Data are expressed as mean ± SEM (n = 10); * HFD significant vis. control group, # pro. and cur. IF significant vis. HFD group, ψ pro. IF significant vise cur. IF.

Data are expressed as mean ± SEM (n = 10); * HFD significant vis. control group, # pro. and cur. IF significant vis. HFD group, ψ pro. IF significant vise cur. IF.

3.4. Intermittent Fasting-Modulated HFD Altered Malondialdehyde and Reduced Glutathione Concentrations in the Brain Tissues

Feeding rats HFD significantly ($p < 0.001$) increased brain tissue MDA concentration while it significantly ($p < 0.001$) decreased brain tissue GSH concentration compared with the control group. However, both the cur. and pro. IF significantly ($p < 0.001$) decreased

brain tissue MDA concentration while it significantly ($p < 0.001$) increased brain tissue GSH concentration compared with HFD group. Moreover, pro. IF significantly ($p < 0.001$) reduced brain tissue contents of MDA while it significantly ($p < 0.001$) increased brain tissue content of GSH compared with cur. IF group (Figure 5A,B).

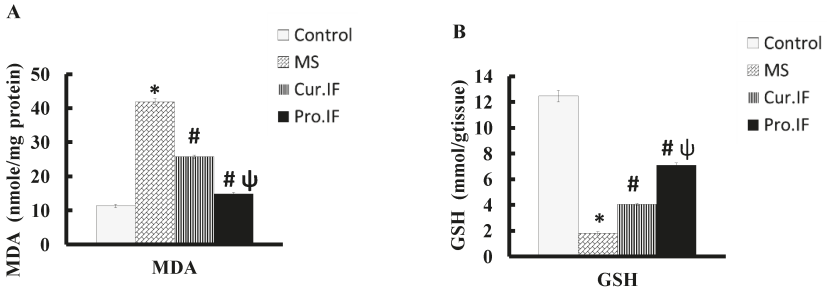

Figure 5. Effect of HFD and/or pro. and cur. IF on the brain tissue contents of MDA (**A**) and GSH (**B**) in all studied groups * HFD significant vis. control group, # pro. and cur. IF significant vis. HFD group, ψ pro. IF significant vise cur. IF.

3.5. Intermittent Fasting-Ameliorated HFD Induced Histopathological Changes in Brain Tissues of Rats

Figure 6 showed normal structure and morphology of the hippocampus of the control group with normal viability and thickness of the pyramidal cell layer and normal blood vessels with no apoptosis in both CA1 and CA3 areas. Dentate gyrus of the same group showed normal granular and polymorphic cell layers. Brain tissue sections of HFD group showed multiple degenerated cells, marked apoptosis with a decrease in the thickness of all layers of the hippocampus. Intermittent fasting significantly increased the thickness of all layers of the hippocampus while it decreased the number of apoptotic and degenerated cells compared with HFD group. The pro. IF group showed more significant increase in the thickness of all layers of the hippocampus with increase in the viability of pyramidal cell layer compared with cur. IF (Figure 6M,N).

3.6. Intermittent Fasting Reduced HFD Increased GFAP Protein Expression in Brain Tissues of Rats

Figure 7 illustrates that the hippocampal cells of the HFD group showed strong GFAP protein expression compared with that of the control group. However, hippocampus of both cur. and pro. IF groups showed weak and localized protein expression of GFAP compared with that of the control and HFD groups. Figure 7I shows that the H score was significantly increased in CA1 and CA3 areas of HFD group. Cur. and pro. IF groups significantly decreased H score in the same areas compared with HFD group. The pro. IF caused significant decrease in H score in CA3 area compared with that of the cur. IF group.

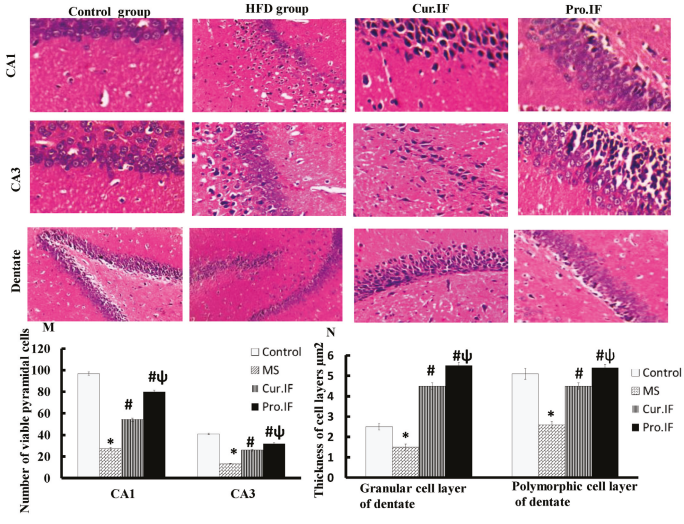

Figure 6. Effect of HFD and/or pro. and cur. IF on hippocampal structure. The figure showed normal morphology of CA1, CA3 and dentate gyrus in the control group with normal viable pyramidal cells, granular cells, absent apoptosis and normal blood vessels. The HFD group showed scattered degenerations, decrease in the viable pyramidal cells in both CA1 and CA3 areas of the hippocampus (**M**) together with decrease in the thickness of granular cells in dentate gyrus (**N**). The cur. IF group showed multiple degenerated cells, mild apoptosis while pro.IF group showed marked increase in the viable pyramidal cells with scattered degeneration in CA1 and CA3 regions dentate gyrus showed increase in thickness of its layers in both groups. * HFD significant vis. control group, # pro. and cur. IF significant vis. HFD group, ψ pro. IF significant vise cur. IF (**N**).

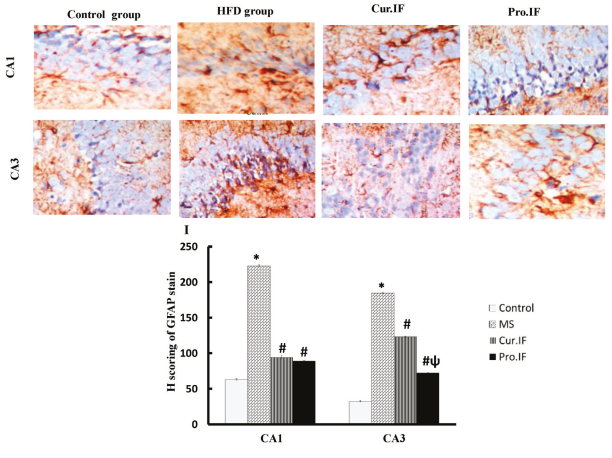

Figure 7. Effect of HFD and/or pro. and cur. IF on GFAP protein expression in the hippocampal sections in all studied groups. The figure shows significant increase in GFAP protein expression in CA1 and CA3 of HFD group. The cur. IF and pro. IF groups showed decreased GFAP protein expression in the same areas. The histogram (**I**) declares the changes in H score in these areas. * HFD significant vis. control group, # pro. and cur. IF significant vis. HFD group, ψ pro. IF significant vise cur. IF.

4. Discussion

The results of the current study revealed that the consumption of HFD increased rats' body weight while it decreased the short term-memory with abnormal behavior, dyslipidemia and oxidative stress in brain tissues. The HFD increased body weight was in line with the findings of Abd Eldaim et al., 2018 and Orabi et al., 2020 [28,29]. This may be due to HFD increasing food intake with excess energy intake and adiposity buildup as HFD creates more fat storage than fat oxidation in muscle. High-fat diet-induced abnormal behavior in rats was represented by decreased total distance moved in the open field and the time spent in the inner zone, increased the latency to move from the center, the time spent in the outer zone and the frequency of grooming. These findings may be due to HFD decreasing physical activity and physical efficacy with anxiety in rats [30]. In addition, HFD affected the normal behavior of rats in the Y maze, which is based on the natural preference of rodents to explore the novel environment rather than the previously known one. It increased the time spent in the start arm and decreased the frequency of entry and the total time spent in the novel arm. These data can be attributed to oxidative stress indicated by high level of MDA with low level of GSH in the brain tissues. Oxidative stress contributes to many neurodegenerative diseases and brain damage, and induces cell injury with impaired learning and memory. Additionally, one study relates Alzheimer's disease to consumption of HFD [31] while other studies attribute this cognitive impairment to other factors such as impaired glucoregulation [32], increased brain inflammation and alteration in blood brain barrier permeability [33]. It has been known that consumption of HFD is associated with significant weight gain and chronic low levels of inflammation together with brain insulin resistance with loss of synaptic plasticity [34]. Previous epidemiological data revealed an association between obesity, high-fat intake and cognitive dysfunctions [35]. This is in line with data revealed by Valladolid, who found that HFD impaired learning trials and spacial memory at the level of the hippocampus [36]. The effect of HFD occurs even after a short period of intake, as the memory deficit was detected after only one week [37]. Tran and Westbrook indicated that the cognitive dysfunction is reversible after stopping the HFD as they speculated that stopping HFD decreases the inflammatory condition induced by HFD and obesity [38]. Moreover, our data indicated hippocampal pyramidal cell affection with decreased viability, thickness and increased apoptosis with significant increase in the GFAP immunostaining in the HFD group, which might be attributable to inflammation of astrocytes due to consumption of HFD, which stimulates astrogliosis, as it has been shown that HFD causes hippocampal dysfunction and affects short-term memory [39].

Furthermore, the current study indicated that intermittent fasting improved brain structure and function by decreasing oxidative stress. This finding also can be explained by a significant decrease in oxidative stress in the brain tissue, which was indicated by significant decrease in MDA contents with significant increase in GSH contents in brain tissues. Caloric restriction by IF improves the brain redox state and increases GSH level as mentioned by Rebrin et al., 2007 [40], who found that 40% reduction in caloric intake improves oxidative stress in different brain areas in aged mice. Additionally, IF has a neuroprotective effect and increases the resistance of the hippocampus to excitotoxic stress, which may be due to mitochondrial reprogramming that decreases oxidant production [14]. According to Hu et al., short-term IF is a neuroprotective that can reduce the redox state and the neuro-inflammation. It has also been reported that post-operative IF reduces the concentration of MDA in brain tissues and increased GSH concentration in brain tissues [6]. Moreover, the current study indicated more significant decrease in oxidative stress and body weight with better performance of rats in behavioral tests of pro. IF compared to cur. IF. This may be due to the simultaneous neuroprotective action of IF that decreases the deleterious effect of HFD on brain oxidative stress and body weight. This was clear in the histological and immunohistochemical staining that showed significant increases in the thickness and viability of pyramidal cells and granular cells in the hippocampus. There were also significant decreases in the GFAP stain and H score in both IF groups. The pro. IF caused a more significant increase in the viability and thickness of pyramidal and

granular cell layers, with significant decrease in H score in the CA3 area compared to the cur. IF group.

Finally, the findings of the current study indicated that HFD induced significant dyslipidemia represented by significant increase in serum levels of TC, TG and LDL with significant decrease in HDL. This hyper-lipidemia might result from HFD-induced oxidative stress. Both pro. and cur. IF significantly decreased fasting serum lipids levels. These findings may be due to the fact that dietary restriction of calories can improve lipid profile parameters. It increases the activity of the lipoprotein lipase, resulting in increases of triglyceride clearance in the blood vessels. The activated LPL also increase the catabolism of lipoproteins rich in triglycerides, resulting in the transfer of esters, apoproteins and phospholipids to form HDL [41]. Moreover, IF decreases caloric intake, so the production of apolipoprotein A-1 may be optimal with subsequent increase in HDL concentrations in serum [42]. Our data were in line with Marbut et al. (2005) [43], as there was significant decrease in serum cholesterol, TGs and LDL levels with significant increase in HDL levels after IF for one month. Nurmasitoh et al. [44] also found higher HDL levels in rats subjected to IF.

5. Conclusions

Consumption of HFD increased rats' body weight while it decreased short term-memory with abnormal behavior, dyslipidemia and oxidative stress in brain tissues. In contrast, intermittent fasting significantly decreased body weight and oxidative stress, as well as improving short term-memory, behavior and dyslipidemia in HFD-fed rats. The pro. IF was more potent than cur. IF as it gave the brain a longer period of neuro-protection and resistance to oxidative stress and inflammation.

Author Contributions: Conceptualization, S.M.H.; data curation, M.A.A.E. and A.A.F.; formal analysis, S.M.H., A.A.F., A.S.E.D.M. and E.I.E.; funding acquisition, M.M.S.; investigation, M.A.A.E. and E.I.E.; methodology, A.A.F., A.S.E.D.M. and E.I.E.; resources, M.M.S.; software, E.I.E.; supervision, M.M.S.; visualization, A.S.E.D.M.; writing—original draft, S.M.H., A.A.F. and A.S.E.D.M.; writing—review & editing, M.A.A.E. All authors have read and agreed to the published version of the manuscript.

Funding: This study was supported by the Taif University Researchers Supporting Project (TURSP-2020/09), Taif University, Taif, Saudi Arabia.

Institutional Review Board Statement: The experimental protocol was approved by the local ethical committee of the Faculty of Medicine, Menoufia University with approval code 279/018, following the Guide for the Care and Use of Laboratory Animals (eighth edition, National Academies Press).

Informed Consent Statement: Not applicable as our study did not involve humans.

Data Availability Statement: The data presented in this study are available on request from the corresponding author.

Acknowledgments: The authors thank the technicians of Central Lab of Faculty of Medicine, Menoufia University, Egypt for their great help in performing the biochemical assays. Moreover, we appreciate and thank Taif University for the financial support of Taif University Researchers Supporting Project (TURSP-2020/09), Taif University, Taif, Saudi Arabia.

Conflicts of Interest: The authors declare that there is no conflict of interest among them concerning this manuscript.

References

1. Lasker, S.; Rahman, M.M.; Parvez, F.; Zamila, M.; Miah, P.; Nahar, K.; Kabir, F.; Sharmin, S.B.; Subhan, N.; Ahsan, G.U.; et al. High-fat diet-induced metabolic syndrome and oxidative stress in obese rats are ameliorated by yogurt supplementation. *Sci. Rep.* **2019**, *9*, 1–15. [CrossRef] [PubMed]
2. Freeman, L.R.; Haley-Zitlin, V.; Rosenberger, D.S.; Granholm, A.-C. Damaging effects of a high-fat diet to the brain and cognition: A review of proposed mechanisms. *Nutritional* **2014**, *17*, 241–251. [CrossRef] [PubMed]
3. Spencer, S.J.; D'Angelo, H.; Soch, A.; Watkins, L.R.; Maier, S.F.; Barrientos, R.M. High-fat diet and aging interact to produce neuroinflammation and impair hippocampal-and amygdalar-dependent memory. *Neurobiol. Aging* **2017**, *58*, 88–101. [CrossRef] [PubMed]

4. Forti, P.; Pisacane, N.; Rietti, E.; Lucicesare, A.; Olivelli, V.; Mariani, E.; Mecocci, P.; Ravaglia, G. Metabolic syndrome and risk of dementia in older adults. *J. Am. Geriatr. Soc.* **2010**, *58*, 487–492. [CrossRef] [PubMed]
5. Das, S.K.; Balasubramanian, P.; Weerasekara, Y.K. Nutrition modulation of human aging: The calorie restriction paradigm. *Mol. Cell. Endocrinol.* **2017**, *455*, 148–157. [CrossRef]
6. Hu, Y.; Zhang, M.; Chen, Y.; Yang, Y.; Zhang, J.-J. Postoperative intermittent fasting prevents hippocampal oxidative stress and memory deficits in a rat model of chronic cerebral hypoperfusion. *Eur. J. Nutr.* **2019**, *58*, 423–432. [CrossRef]
7. Qin, W.; Chachich, M.; Lane, M.; Roth, G.; Bryant, M.; de Cabo, R.; Ottinger, M.A.; Mattison, J.; Ingram, D.; Gandy, S.J. Calorie restriction attenuates Alzheimer's disease type brain amyloidosis in Squirrel monkeys (Saimiri sciureus). *J. Alzheimer's Dis.* **2006**, *10*, 417–422. [CrossRef]
8. Singh, R.; Lakhanpal, D.; Kumar, S.; Sharma, S.; Kataria, H.; Kaur, M.; Kaur, G. Late-onset intermittent fasting dietary restriction as a potential intervention to retard age-associated brain function impairments in male rats. *Age* **2012**, *34*, 917–933. [CrossRef]
9. Singh, R.; Manchanda, S.; Kaur, T.; Kumar, S.; Lakhanpal, D.; Lakhman, S.S.; Kaur, G. Middle age onset short-term intermittent fasting dietary restriction prevents brain function impairments in male Wistar rats. *Biogerontology* **2015**, *16*, 775–788. [CrossRef]
10. Morgan, T.; Wong, A.; Finch, C. Anti-inflammatory mechanisms of dietary restriction in slowing aging processes. In *Mechanisms of Dietary Restriction in Aging and Disease*; Karger Publishers: Los Angeles, CA, USA, 2007; Volume 35, pp. 83–97.
11. Wan, R.; Ahmet, I.; Brown, M.; Cheng, A.; Kamimura, N.; Talan, M.; Mattson, M.P. Cardioprotective effect of intermittent fasting is associated with an elevation of adiponectin levels in rats. *J. Nutr. Biochem.* **2010**, *21*, 413–417. [CrossRef]
12. Patterson, R.E.; Sears, D.D. Metabolic effects of intermittent fasting. *Annu. Rev. Nutr.* **2017**, *37*, 371–393. [CrossRef] [PubMed]
13. Liu, B.; Page, A.J.; Hatzinikolas, G.; Chen, M.; Wittert, G.A.; Heilbronn, L.K. Intermittent fasting improves glucose tolerance and promotes adipose tissue remodeling in male mice fed a high-fat diet. *Endocrinology* **2019**, *160*, 169–180. [CrossRef] [PubMed]
14. Li, L.; Wang, Z.; Zuo, Z.J. Chronic intermittent fasting improves cognitive functions and brain structures in mice. *PLoS ONE* **2013**, *8*, e66069. [CrossRef] [PubMed]
15. Albus, U. *Guide for the Care and Use of Laboratory Animals*, 8th ed.; SAGE Publications Sage: London, UK, 2012.
16. Ferragud, A.; Velázquez-Sánchez, C.; Abdullatif, A.A.; Sabino, V.; Cottone, P. Withdrawal from Extended, Intermittent Access to A Highly Palatable Diet Impairs Hippocampal Memory Function and Neurogenesis: Effects of Memantine. *Nutrients* **2020**, *12*, 1520. [CrossRef]
17. He, D.; Mustafi, D.; Fan, X.; Fernandez, S.; Markiewicz, E.; Zamora, M.; Mueller, J.; Sachleben, J.R.; Brady, M.J.; Conzen, S.D.; et al. Magnetic resonance spectroscopy detects differential lipid composition in mammary glands on low fat, high animal fat versus high fructose diets. *PLoS ONE* **2018**, *13*, e0190929. [CrossRef]
18. Matheus, F.C.; Rial, D.; Real, J.I.; Lemos, C.; Ben, J.; Guaita, G.O.; Pita, I.R.; Sequeira, A.C.; Pereira, F.C.; Walz, R.; et al. Decreased synaptic plasticity in the medial prefrontal cortex underlies short-term memory deficits in 6-OHDA-lesioned rats. *Behav. Brain Res.* **2016**, *301*, 43–54. [CrossRef]
19. Soares, E.; Prediger, R.D.; Nunes, S.; Castro, A.A.; Viana, S.D.; Lemos, C.; De Souza, C.M.; Agostinho, P.; Cunha, R.A.; Carvalho, E.; et al. Spatial memory impairments in a prediabetic rat model. *Neuroscience* **2013**, *250*, 565–577. [CrossRef]
20. DeLong, D.M.; DeLong, E.R.; Wood, P.D.; Lippel, K.; Rifkind, B.M. A comparison of methods for the estimation of plasma low-and very low-density lipoprotein cholesterol: The Lipid Research Clinics Prevalence Study. *JAMA* **1986**, *256*, 2372–2377. [CrossRef]
21. Wilson, P.W.; Abbott, R.D.; Garrison, R.J.; Castelli, W.P. Estimation of very-low-density lipoprotein cholesterol from data on triglyceride concentration in plasma. *Clin. Chem.* **1981**, *27*, 2008–2010. [CrossRef]
22. Draper, H.; Squires, E.; Mahmoodi, H.; Wu, J.; Agarwal, S.; Hadley, M. A comparative evaluation of thiobarbituric acid methods for the determination of malondialdehyde in biological materials. *Free Radic. Biol. Med.* **1993**, *15*, 353–363. [CrossRef]
23. Beutler, E.; Dubon, O.; Kelly, B.M. Improved method for the determination of blood glutathiones. *J. Lab. Clin. Med.* **1963**, *61*, 882–890. [PubMed]
24. Bancroft, J.D.; Gamble, M. *Theory and Practice of Histological Techniques*, 6th ed.; Churchill Livingstone, Elsevier Health Sciences: Beijing, China, 2008.
25. Kiernan, J.A. Histological and histochemical methods: Theory and practice. *Schock* **1999**, *12*, 479.
26. Pirker, R.; Pereira, J.R.; Von Pawel, J.; Krzakowski, M.; Ramlau, R.; Park, K.; De Marinis, F.; Eberhardt, W.E.; Paz-Ares, L.; Störkel, S.; et al. EGFR expression as a predictor of survival for first-line chemotherapy plus cetuximab in patients with advanced non-small-cell lung cancer: Analysis of data from the phase 3 FLEX study. *Lancet Oncol.* **2012**, *13*, 33–42. [CrossRef]
27. Schneider, C.A.; Rasband, W.S.; Eliceiri, K.W. NIH Image to ImageJ: 25 years of image analysis. *Nat. Methods* **2012**, *9*, 671–675. [CrossRef]
28. Abd Eldaim, M.A.; Ibrahim, F.M.; Orabi, S.H.; Hassan, A.; El Sabagh, H.S. l-Carnitine-induced amelioration of HFD-induced hepatic dysfunction is accompanied by a reduction in hepatic TNF-α and TGF-β1. Biochem. *Cell Biol.* **2018**, *96*, 713–725. [CrossRef]
29. Orabi, S.H.; Al-Sabbagh, E.S.; Khalifa, H.K.; Mohamed, M.A.E.G.; Elhamouly, M.; Gad-Allah, S.M.; Abdel-Daim, M.M.; Eldaim, M.A.A. Commiphora myrrha Resin Alcoholic Extract Ameliorates High Fat Diet Induced Obesity via Regulation of UCP1 and Adiponectin Proteins Expression in Rats. *Nutrients* **2020**, *12*, 803. [CrossRef]
30. Seibenhener, M.L.; Wooten, M.C. Use of the open field maze to measure locomotor and anxiety-like behavior in mice. *J. Vis. Exp.* **2015**, *96*, e52434. [CrossRef]

31. Xia, S.F.; Xie, Z.X.; Qiao, Y.; Li, L.R.; Cheng, X.R.; Tang, X.; Shi, Y.H.; Le, G.W. Differential effects of quercetin on hippocampus-dependent learning and memory in mice fed with different diets related with oxidative stress. *Physiol. Behav.* **2015**, *138*, 325–331. [CrossRef]
32. Mielke, J.G.; Nicolitch, K.; Avellaneda, V.; Earlam, K.; Ahuja, T.; Mealing, G.; Messier, C. Longitudinal study of the effects of a high-fat diet on glucose regulation, hippocampal function, and cerebral insulin sensitivity in C57BL/6 mice. *Behav. Brain Res.* **2006**, *175*, 374–382. [CrossRef]
33. Cordner, Z.A.; Tamashiro, K.L. Effects of high-fat diet exposure on learning & memory. *Physiol. Behav.* **2015**, *152*, 363–371.
34. Kothari, V.; Luo, Y.; Tornabene, T.; O'Neill, A.M.; Greene, M.W.; Geetha, T.; Babu, J.R. High fat diet induces brain insulin resistance and cognitive impairment in mice. *Biochim. Biophys. Acta (BBA)—Mol. Basis Dis.* **2017**, *1863*, 499–508. [CrossRef] [PubMed]
35. Luchsinger, J.A.; Tang, M.-X.; Shea, S.; Mayeux, R.J. Caloric intake and the risk of Alzheimer disease. *Arch. Neurol.* **2002**, *59*, 1258–1263. [CrossRef] [PubMed]
36. Valladolid-Acebes, I.; Stucchi, P.; Cano, V.; Fernández-Alfonso, M.S.; Merino, B.; Gil-Ortega, M.; Fole, A.; Morales, L.; Ruiz-Gayo, M.; Del Olmo, N. High-fat diets impair spatial learning in the radial-arm maze in mice. *Neurobiol. Learn.* **2011**, *95*, 80–85. [CrossRef] [PubMed]
37. Beilharz, J.E.; Maniam, J.; Morris, M.J. Short exposure to a diet rich in both fat and sugar or sugar alone impairs place, but not object recognition memory in rats. *Brain Behav. Immun.* **2014**, *37*, 134–141. [CrossRef] [PubMed]
38. Tran, D.M.; Westbrook, R.F. A high-fat high-sugar diet-induced impairment in place-recognition memory is reversible and training-dependent. *Appetite* **2017**, *110*, 61–71. [CrossRef] [PubMed]
39. Bondan, E.F.; Cardoso, C.V.; Martins, M.D.F.M.; Otton, R. Prejuízos de memória e expressão aumentada de GFAP em astrócitos hipocampais após dieta hipercalórica em ratos. *Arquivos de Neuro-Psiquiatria* **2019**, *77*, 601–608. [CrossRef] [PubMed]
40. Rebrin, I.; Forster, M.J.; Sohal, R.S. Effects of age and caloric intake on glutathione redox state in different brain regions of C57BL/6 and DBA/2 mice. *Brain Res.* **2007**, *1127*, 10–18. [CrossRef]
41. Chen, J.-H.; Ouyang, C.; Ding, Q.; Song, J.; Cao, W.; Mao, L. A moderate low-carbohydrate low-calorie diet improves lipid profile, insulin sensitivity and adiponectin expression in rats. *Nutrients* **2015**, *7*, 4724–4738. [CrossRef]
42. Das, B.; Mishra, T. Role of HDL-C in health and disease. *J. Indian Acad. Clin. Med.* **2012**, *13*, 218–222.
43. Marbut, M.M.; Al-Najjar, H.A.D.S.; Mustafa, A. Effect of Ramadan fasting on some physiological parameters. *Med. J. Tikrit Univ.* **2005**, *2*, 6–8.
44. Nurmasitoh, T.; Utami, S.Y.; Kusumawardani, E.; Najmuddin, A.A.; Fidianingsih, I. Intermittent fasting decreases oxidative stress parameters in Wistar rats (Rattus norvegicus). *Univ. Med.* **2018**, *37*, 31–38. [CrossRef]

nutrients

MDPI

Article

Effects of Three-Month Feeding High Fat Diets with Different Fatty Acid Composition on Myocardial Proteome in Mice

Adam Lepczyński [1,*], Małgorzata Ożgo [1], Katarzyna Michałek [1], Alicja Dratwa-Chałupnik [1], Marta Grabowska [2], Agnieszka Herosimczyk [1], Kamila P. Liput [3], Ewa Poławska [4], Andrzej Kram [5] and Mariusz Pierzchała [4]

[1] Department of Physiology, Cytobiology and Proteomics, West Pomeranian University of Technology, K. Janickiego 32 Str., 71-270 Szczecin, Poland; malgorzata.ozgo@zut.edu.pl (M.O.); katarzyna.michalek@zut.edu.pl (K.M.); alicja.dratwa-chalupnik@zut.edu.pl (A.D.-C.); agnieszka.herosimczyk@zut.edu.pl (A.H.)
[2] Department of Histology and Developmental Biology, Pomeranian Medical University, Żołnierska 48, 71-210 Szczecin, Poland; martag@pum.edu.pl
[3] Department of Molecular Biology, Institute of Genetics and Animal Biotechnology of the Polish Academy of Sciences, Postepu 36A Str., Jastrzebiec, 05-552 Magdalenka, Poland; k.stepanow@igbzpan.pl
[4] Department of Genomics and Biodiversity, Institute of Genetics and Animal Biotechnology of the Polish Academy of Sciences, Postepu 36A Str., Jastrzebiec, 05-552 Magdalenka, Poland; e.polawska@igbzpan.pl (E.P.); m.pierzchala@igbzpan.pl (M.P.)
[5] Department of Pathology, West Pomeranian Oncology Center, Strzałowska 22 Str., 71-730 Szczecin, Poland; akram@onkologia.szczecin.pl
* Correspondence: adam.lepczynski@zut.edu.pl

Citation: Lepczyński, A.; Ożgo, M.; Michałek, K.; Dratwa-Chałupnik, A.; Grabowska, M.; Herosimczyk, A.; Liput, K.P.; Poławska, E.; Kram, A.; Pierzchała, M. Effects of Three-Month Feeding High Fat Diets with Different Fatty Acid Composition on Myocardial Proteome in Mice. *Nutrients* **2021**, *13*, 330. https://doi.org/10.3390/nu13020330

Academic Editor: Frederic Capel
Received: 30 December 2020
Accepted: 20 January 2021
Published: 23 January 2021

Abstract: Westernized diet is characterized by a high content of saturated fatty acids (SFA) and a low level of omega-3 polyunsaturated fatty acids (PUFA), often accompanied by an imbalance in the omega-6/omega-3 PUFA ratio. Since increased intake of SFA and n-6 PUFA is considered as a cardiovascular disease risk factor, this study was conducted to determine whether a three-month dietary supplementation of high-fat diets (HFDs) with saturated fatty acids and a significant proportion of various n-6 and n-3 PUFA ratios would affect the architecture and protein expression patterns of the murine heart. Therefore, three HFD (n = 6) feeding groups: rich in SFA, dominated by PUFA with the n-6/n-3–14:1, and n-6/n-3–5:1, ratios were compared to animals fed standard mouse chow. For this purpose, we performed two-dimensional electrophoresis with MALDI-ToF mass spectrometry-based identification of differentially expressed cardiac proteins, and a histological examination of cardiac morphology. The results indicated that mice fed with all HFDs developed signs of hypertrophy and cardiac fibrosis. Animals fed SFA-rich HFD manifested the most severe cardiac hypertrophy and fibrosis lesions, whereas less pronounced changes were observed in the group of animals that ingested the highest amount of omega-3 FA. In general, all HFDs, regardless of FA composition, evoked a comparable pattern of cardiac protein changes and affected the following biological processes: lipid metabolism and FA β-oxidation, glycolysis, TCA cycle, respiratory chain, myocardium contractility, oxidative stress and PUFA eicosanoid metabolism. However, it should be noted that three proteins, namely IDH3A, LDHB, and AK1, were affected differently by various FA contents. High expression of these myocardial proteins found in the group of animals fed a HFD with the highest n-3 PUFA content could be closely related to the observed development of hypertrophy.

Keywords: proteomics; high fat diet; saturated fatty acids; polyunsaturated fatty acids; cardiac muscle; omega-6/omega-3 ratio

1. Introduction

Obesity has become a pandemic of the 21st century and is undoubtedly one of the greatest public health challenges for both humans and companion animals. It has been estimated that if the current trend continues, presumably up to 36.6% of men and 32.0% of women in Europe will be either overweight or obese by 2030 [1]. High prevalence of obesity

is one of the leading causes of elevated cardiovascular diseases (CVD), especially in Western societies [2,3]. It should be highlighted that CVD mortality is closely and directly related to the consumption of a nutrient-poor Western diet [4]. Westernized diet is generally defined as a high dietary intake of sugar, saturated fatty acids (SFA), and n-6 polyunsaturated fatty acids (PUFA), with associated reduced consumption of n-3 PUFA and fibre [5,6]. Polyunsaturated fatty acids (PUFA) belong to the group of the so-called essential fatty acids as mammals cannot synthesize n-3 and n-6, and thus they must be supplied with food [7]. N-6 and n-3 PUFA are bioactive compounds that exert a profound impact on various physiological processes [8]. Increased n-6 fatty acids intake, which is observed along with modified dietary patterns, induces changes in the n-6/n-3 ratio. Currently, this ratio is 15:1 in favor of n-6 acids, and it differs significantly from the diet of our ancestors, in which this ratio was close to one. Currently, the recommended dietary ratio of these fatty acids (FAs) is 2–5:1 [6,9]. This is based on the fact that there is a competition between fatty acids of n-6 and n-3 series as both of these FAs are metabolized by the same group of enzymes to their respective metabolites. Since n-6 acids are the most preferred substrates for those enzymes, their higher dietary content dramatically reduces the utilisation of n-3 acids. In addition, there is evidence suggesting that many gene-defined enzymes and receptors favor n-6 mediators and cause physiological and pathophysiological effects [10]. As a result of n-6 fatty acid intake, significant quantities of arachidonic acid (AA) and its active metabolites (PGE2 and PGI2 prostaglandins, TXA2 thromboxane, A4, B4, C4, D4, and E4 leukotrienes) are generated, which, unlike n-3 acid metabolites [11], induce inflammatory processes, show a thrombotic effect as well as enhance the synthesis of free radicals. The results of numerous in vivo and in vitro studies have clearly indicated that n-6 acids may also directly influence myocardial function. For example, AA-derived mediators have been shown to significantly affect cardiac arrhythmogenesis [12]. Furthermore, Fluri et al. (1990) and Schmilinsky-Fluri et al. (1997) found that AA had the ability to induce changes in the integrity of gap junctions between cardiac myocytes [13,14]. A higher ratio of dietary n-6/n-3 fatty acids (FAs) may also result in the activation of pro-inflammatory metabolic pathways in the myocardium, causing the generation of significant amounts of reactive nitrogen and oxygen species [15]. It has also been proven that dietary linoleic acid (LA) and its metabolites can induce collagen synthesis by cardiac fibroblasts, which can lead to fibrosis and increased stiffness of the left ventricle [16].

Considering the above, we hypothesized that feeding mice for three months high-fat diets with saturated fatty acids and a significant proportion of different ratios of unsaturated n-6 and n-3 fatty acids would affect the mouse heart architecture and the expression of proteins involved in cardiac muscle contraction, energetic metabolism, and stress response.

Therefore, the main purpose of this study was to (1) analyse the cardiac muscle histology, and (2) to screen for differences in protein expression patterns in the hearts of mice fed three high-fat diets with different fatty acid compositions, including SFA and PUFA with two different n-6 to n-3 ratios (14:1 and 5:1, respectively).

2. Materials and Methods

2.1. Animals, Diets, Housing Conditions, and Experiment Termination

The nutritional experiment was conducted in the vivarium of the Institute of Genetics and Animal Biotechnology of the Polish Academy of Sciences in Jastrzębiec. Experimental procedures were approved by the II Warsaw Local Ethics Committee for Animal Experimentation (WAW2_22/2016). Animals were maintained in standard cages under temperature- and humidity-controlled conditions with a 12-h light/dark cycle. Animals received water and food *ad libitum*.

Male Swiss-Webster mice ($n = 24$) were fed standard growth diets for 8 weeks after weaning. Next animals were randomly selected into four dietary groups ($n = 6$) that were fed with appropriate diet. Animals of the control group (STD) were fed with standard chow for mice Labofeed H (Morawski, Żurawia, Poland). Experimental groups were fed high fat diets. Animals of first experimental group (SFA group) were fed a diet rich in saturated

fatty acids (SFA group), which was composed with the addition of coconut virgin oil. Two other diets were dominated by the PUFA with different linoleic acid (LA) to α-linolenic acid (ALA) ratio. The diet with the high n-6 to n-3 FA ratio was prepared on the basis of the standard chow with addition of pumpkin seed oil. It allowed to obtain the diet with the n-6/n-3 ratio equal 13.76:1, which was used for feeding the 14:1 group. The last group of animals (5:1 group) were fed with a diet enriched with different vegetable oils that after the addition to the standard chow resulted in the n-6/n-3 ratio close to 5:1. Oil additives level in the experimental diets are given in Table 1. Confirmation of FA composition in used oils were estimated using a GC-7890 gas chromatograph (Agilent Technologies, Inc., Santa Clara, CA, USA) with a flame ionization detector (FID) and a 60 m capillary column, 0.25 mm internal diameter and 0.20 μm stationary layer thickness (Hewlett-Packard-88, Agilent J&W GC Columns, Santa Clara, CA, USA). Helium with a flow rate of 50 mL/min was used as a carrier gas. The dispenser and detector temperature was 260 °C. Temperature program: (1) from 140 °C to 190 °C (4 °C/min), (2) from 190 °C to 215 °C (0.8 °C/min). Supelco 37 Component FAME Mix, 47885-U (Sigma-Aldrich Co., St. Louis, MO, USA) standards were used for the FA determination. The total fat content in STD chow and SFA, 14:1 and 5:1 diets were about 2% and 22%, respectively. The diets were produced manually, divided in aliquots, vacuum packed, and stored in dark. Diets were given to the animals two times per day to avoid oxidation.

Table 1. Components of experimental diets.

Group	Components	(g)	LA/ALA	% SFA	% PUFA	% MUFA
SFA	Labofeed H	790	1.41	76.87	11.04	12.09
	virgin coconut oil	200				
	pumpkin seed oil	10				
14:1	Labofeed H	790	13.76	1.68	82.21	16.10
	pumpkin seed oil	210				
5:1	Labofeed H	790	5.00	9.91	79.69	10.40
	sunflower seed oil	80				
	pumpkin seed oil	65				
	avocado oil	20				
	virgin coconut oil	20				
	hemp seed oil	15				
	corn oil	10				

LA/ALA—linoleic acid (LA, 18:2 n–6) to α-linolenic acid (ALA, 18:3 n–3) ratio; SFA—saturated fatty acids; MUFA—monounsaturated fatty acids; PUFA—polyunsaturated fatty acids.

At the end of experiment after 12 h fasting period animals were euthanized in UNO Euthanasia Unit (Uno Roestvaststaal BV, Zevenaar, Netherlands) with 100% CO_2 gas after the saturation of the blood with O_2 by the exposition to carbogen. Immediately after the procedure the blood was collected via the heart puncture, and subsequently animal hearts were collected.

2.2. Plasma Biochemistry

Blood was collected into the EDTA coated tubes by cardiac puncture and mixed with and centrifuged at 3000 rcf for 10 min at 4 °C to obtain blood plasma. Blood plasma was stored at −70 °C. Biochemical analyses were performed using COBAS INTEGRA® 400 plus system (Roche Diagnostics Ltd., Rotkreuz, Switzerland) using ready prepared kits.

2.3. Histological Analyses

Hearts obtained during the section were fixed in 4% buffered paraformaldehyde and were then embedded in paraffin blocks. Next, 3 μm sections were cut using a microtome and then were placed on the poly-lysine-coated slides.

2.3.1. Hematoxylin and Eosin Staining (H&E)

Hematoxylin and eosin staining (H&E) was performed according to a protocol described in detail by Gamble (2008) [17]. The heart tissue sections were deparaffinized and rehydrated. Next, the sections were first stained with Mayer's hematoxylin for 5 min and washed in running water. Subsequently, the tissue sections were stained with eosin for 1 min and washed in distilled water. At the end, they were dehydrated and coverslipped.

2.3.2. Mallory Trichrome Staining

Hearts tissue sections after deparaffinization and rehydration were stained in 1% acid fuchsin solution (Sigma-Aldrich, St. Louis, MO, USA) in distilled water and next in 5% phosphotungstic acid solution for 20 min. At the next stage, the tissue sections were stained in a solution of 1% aniline blue (Sigma-Aldrich, St. Louis, MO, USA), 2% orange G (Sigma-Aldrich, St. Louis, MO, USA), and 2% oxalic acid (Sigma-Aldrich, St. Louis, MO, USA) in distilled water for 30 min. Afterwards, the slides were dehydrated and coverslipped.

2.3.3. Quantitative Analysis of Mallory's Trichrome Staining and Morphological Parameters

Using a ScanScope AT2 scanner (Leica Microsystems, Wetzlar, Germany) H&E-stained and Mallory's trichrome-stained hearts tissue sections were subjected scanning procedure at magnification of 400× (resolution of 0.25 µm/pixel). Subsequently, the obtained digital images of the tissue sections were analyzed on the computer screen with the use an ImageScope viewer software (v. 11.2.0.780; Aperio Technologies, Inc., Vista, CA, USA).

The cardiomyocytes diameter (µm) were assessed using ruler tool on the H&E-stained heart tissue sections. In each group, one hundred sixty longitudinally sectioned cells in the nucleus region were analyzed (16 cells in each mouse).

For the quantitative analysis of collagen on the Mallory's trichrome-stained hearts tissue sections, a positive pixel count v9 algorithm (v. 9.1; Aperio Technologies, Inc., Vista, CA, USA) was used. Other parameters have been set to get compliance with the visual assessment of color intensity. The areas of the analysis were manually determined. The percent of collagen that was positive for Mallory's trichrome staining were determined in 30 random fields for each group (5 in each mouse), with an average area of 1.25 mm^2 (for STD group), 1.60 mm^2 (for SFA group), 1.48 mm^2 (for 14:1 group), and 1.56 mm^2 (for 5:1 group).

2.4. Two-Dimensional Electrophoresis

2.4.1. Homogenization

After the collection hearts were washed in 0.9% NaCl solution and after that were weighted. Next, the hearts were frozen in the liquid nitrogen and stored in −80 °C until sample homogenisation. After defreezing in the presence of HEPES buffer, the hearts were opened using surgical blade and residual blood clots were washed out. Immediately after that whole hearts were pulverized using mortar in the presence of liquid nitrogen. Tissue powder was than homogenized using zircon beds (1.4 mm of diameter) using Tissue Lyser (Quiagene, Venlo, Netherlands) (20 min, 21 Hz) in lysis buffer containing 5 M urea, 2 M thiourea, 4% w/v CHAPS, and protease inhibitors (Protease Inhibitor Cocktail, Merc, St. Louis, MO, USA). Subsequently the homogenates were centrifuged at 20,800× g for 25 min at 4 °C. Harvested supernatants were stored at −80 °C.

2.4.2. Isoelectrofocusing (IEF)

In heart protein samples total protein concentration was determined by a modified Bradford assay (Protein Assay Dye Reagent Concentrate; Bio-Rad, Bio-Rad, CA, USA). Protein samples containing 350 µg of total protein, in 250 µL of lysis buffer (5 M urea, 2 M thiourea, 4% CHAPS, 1% (w/v) dithiothreitol (DTT), 0.5% (v/v) carrier ampholytes). Each sample was than subjected for IEF. Prior IEF samples were loaded in 11 cm IPG strips with non-linear 3–10 pH gradient by in-gel strips via rehydratation process (passive—5 h, 0 V

and active—12 h, 50 V). Subsequently isoelectric focusing was performed using Protean i12 IEF Cell (Bio-Rad, Hercules, CA, USA) in total of 37 kVh. Following IEF program was used: 250 V for 125 Vh, 500 V for 250 Vh, 1000 V for 500 Vh in rapid mode, linear voltage increase to 3500 V in 1:30 h, 3500 V for 35,000 Vh in rapid mode.

2.4.3. Second Dimension—SDS-PAGE

Immediately after IEF the IPG strips were equilibrated for 15 min in basal buffer (6 M urea, 0.5 M Tris/HCl, pH 6.8, 2% w/v SDS, 30% w/v glycerol) with 1% DTT addition. Next, strips were washed for 20 min in the basal equilibration buffer with addition of 2.5% iodoacetamide. Second dimension of electrophoresis was run at 40 V for 2.5 h and subsequently at 100 V for 16 h (15 °C) in 12% polyacrylamide gels in Protean Plus™ Dodeca Cell™ electrophoretic chamber (Bio-Rad, Hercules, CA, USA). To allow protein molecular masses comparison the samples were co-run with Precision Plus Protein™ Kaleidoscope™ Standard for SDS-PAGE (Bio-Rad, Hercules, CA, USA) as a reference

2.4.4. Image Staining and Analysis

After two dimensional electrophoresis (2-DE) separation, proteins in gels were detected with CBB G-250. The gels were placed in Dodeca™ Gel Stainer, large (Bio-Rad, Hercules, CA, USA) and washed with fixation buffer (50% ethanol, 5% phosphoric acid in ddH_2O) for 3 h. Than the buffer was replaced with the ready stock Bradford solution (Bio-Rad Protein Assay, Bio-Rad, Hercules, CA, USA) diluted 20 times in ddH_2O and gels were stain in that solution for 3 h. After staining, gels were washed in the ddH_2O 3 times for 15 min. After staining, gels images were digitalized using a GS-800™ Calibrated Densitometer (Bio-Rad, Hercules, CA, USA).

Obtained gel images of cardiac proteome were analyzed using PDQuest Analysis software 8.0.1, Advanced (Bio-Rad, Hercules, CA, USA). To measure the variability within the group, the coefficient of variation (CV) was calculated for each experimental group. Qualitative and quantitative comparisons between the replicate groups were performed to highlight the significant differences in the protein expression pattern. Experiment normalization was performed using a local regression model (LOESS). The experimental isoelectric points (pI) and molecular weight (kDa) values were computed for each identified differentially expressed protein spot.

2.4.5. Matrix-Assisted Laser Desorption Ionization—Time of Flight Mass Spectrometry (MALDI-ToF MS)

The protein spots that showed significantly differentiated expression were identified by peptide mass fingerprinting using MALDI-ToF mass spectrometer Microflex (Bruker, Brema, Germany). At least two biological replicates for each protein spots were manually excised from polyacrylamide gels. Then excised spots were destined in a buffer containing 25 mM NH4HCO3 in 5% v/v acetonitrile (ACN), followed by two washes with a solution of 25 mM NH4HCO3 in 50% v/v ACN. After each washing step protein spots were incubated at room temperature for 10 min in ultrasonic bath. Right after the decolorization, protein spots were dehydrated in 100% ACN for 20 min in ultrasonic bath and subsequently vacuum-dried for 15. The dry gel pieces were incubated with trypsin (20 µL/spot of 12.5 µg trypsin/mL in 25 mM NH4HCO3; Promega, Madison, WI, USA) at 37 °C as previously described by Ożgo et al. [18].

Resulting peptides were extracted with 100% CAN and combined using dry droplet method on the MALDI-MSP AnchorChip™ 600/96 plate (Bruker Daltonics, Brema, Germany) target with the matrix solution (5 mg/mL CHCA, 0.1% v/v TFA, 50% v/v ACN) in a final volume of 1 µL. The Microflex™ MALDI-TOF (matrix-assisted laser desorption/ionization time of flight) mass spectrometer (Bruker Daltonics, Brema, Germany) was operated in a positive ion reflector mode. External calibration was performed using Peptide Mass Standard II (Bruker Daltonics). The mass spectra were acquired with 150 shots of a nitrogen laser operating at 20 Hz and were internally calibrated using porcine tryptic autolytic products (842.51 and 2211.10 m/z). The mass spectra were acquired using the FlexControl

3.0 (Bruker, Brema, Germany) software and subsequently processed using the FlexAnalysis 3.0 (Bruker, Brema, Germany) software. Protein identification was performer using the Peptide Mass Fingerprinting (PMF) technique. Spectra were compared to mammalian SwissProt/NCBI databases using MASCOT search angine (http://www.matrixscience.com/). The following cryteria were used for database searches: (1) trypsin digestion with maximum one missed cleavage site; (2) cysteine carbamidomethylation as a fixed modification; (3) acetylation and methionine oxidation as variable modifications; (4) mass tolerance to 150 ppm.

2.4.6. Geneo Ontology Analyses

Cytoscape software presented biologic role specificity of most significantly differentially expressed gene products on the basis of their functional and pathway enrichment analyses including gene ontology databases: Genes in KEGG 08.05.2020-8024; Genes in WikiPathways 08.05.2020-293; Genes in INTERPRO_ProteinDomains 08.05.2020-12084; Genes in REACTOME_Reactions 08.05.2020-11188; Genes in GO_ImmuneSystemProcess-EBI-UniProt-GOA-ACAP-ARAP 08.05.2020_00h00-3426; Genes in REACTOME_Pathways 08.05.2020-10925; Genes in GO_MolecularFunction-EBI-UniProt-GOA-ACAP-ARAP 08.05.2020 00h00-17817; Genes in GO_CellularComponent-EBI-UniProt-GOA-ACAP-ARAP 08.05.2020 00h00-18937; Genes in GO_BiologicalProcess-EBI-UniProt-GOA-ACAP-ARAP 08.05.2020 00h00-17972. The *homo sapiens* was taken as an reference [19]. Differentially expressed gene products not involved in the CluGo analysis were categorized according to their biological functions and known pathways using STRING v. 11.0b [20]. Subcellular localisation of proteins were defined according to UniProtKB database (www.uniprot.org).

2.5. Western Blot

In the present study, the following primary antibodies were used to examine expression of selected proteins in the mouse heart: (1) mouse monoclonal anti- short-chain specific acyl-CoA dehydrogenase, ACADS (sc-365953, Santa Cruz Biotechnology, Santa Cruz, CA, USA); (2) mouse monoclonal anti- bifunctional epoxide hydrolase 2, sEH (sc-166961, Santa Cruz Biotechnology); (3) mouse monoclonal anti- superoxide dismutase 1, SOD1 (sc-101523, Santa Cruz Biotechnology, Santa Cruz, CA, USA); (4) mouse monoclonal anti-malate dehydrogenase, mitochondrial, MDH2 (sc-293474, Santa Cruz Biotechnology, Santa Cruz, CA, USA). Labeling of the antigen-antibody complexes were visualized with the use of secondary monoclonal goat anti-mouse (sc-516102, Santa Cruz Biotechnology, Santa Cruz, CA, USA) horseradish peroxidase-conjugated antibodies.

In the obtained supernatants the total protein was determined by the modified Bradford method (Protein Assay Dye Reagent Concentrate, Bio-Rad, Hercules, CA, USA). Subsequently, heart homogenates were mixed with the Leammli buffer in such proportions, so that after applying 10 μL of the sample to the wells, each of them contained 10 μg of total protein. The samples were warmed at 37 °C for 15 min and loaded on 12% polyacrylamide gels and run for 120 min at 100 V. Subsequently, the proteins were then electrotransfered (12 V, 14 min) from the gels to PVDF membranes. The membranes were blocked with 5% nonfat-milk in PBS-T (80 mM Na2HPO4, 20 mM NaH2PO4, 100 mM NaCl, and 0.1% Tween 20, pH 7.5) for 1 h and incubated overnight at 4 °C with the primary antibodies. In the current experiment, the following dilutions were used: anti-ACADS 1:500, anti-sHE 1:100, anti-SOD1 1:500, and anti-MDH2 1:100. The membranes were then incubated with a secondary anti-mouse horseradish peroxidase-conjugated antibody diluted 1:1000. The labeling was visualized by an enhanced chemiluminescence system (ECL Plus, Thermo Fisher Scientific, Waltham, MA, USA) and exposure to a CCD camera (Versadoc 4000MP, Bio-Rad, Hercules, CA, USA). The obtained images were recorded in a digital form and modified (auto-scale was used, speckles were removed and a representative band was cut out) using the Quantity One and PDQuest software (Bio-Rad, Hercules, CA, USA).

2.6. Statistic Analysis

The quantitative analysis of the differences in protein spot abundance, Student's t-test was used as integrated in the PDQuest 8.0.1 software (Bio-Rad, Hercules, CA, USA). Significance of the differences was set at the level of $p \leq 0.05$.

Biochemical data were analyzed by one-way analysis of variance. Differences between treatments were analysed by post hoc Tukey honestly significant. Differences at $p < 0.05$ were considered to be statistically significant.

The quantitative values for cardiomyocytes diameter and collagen were first analyzed for normality using the Shapiro–Wilk test. Because of the obtained values failed normal distribution assumption, the Kruskal–Wallis test with Dunn's multiple comparison test for post hoc analysis was applied to compare the difference between the groups. Differences at $p < 0.05$ were considered to be statistically significant.

3. Results

3.1. Morphometric and Histological Heart Parameters and Blood Plasma Biochemistry

None of HFDs affected murine heart masses. Histological analysis revealed cardiomyocyte hypertrophy in all mice receiving experimental diets (Table 2; Figure 1). An increase in cardiomyocyte diameter was statistically significant in mice fed a diet enriched with SFA ($p < 0.001$), 14:1 ($p < 0.001$), and 5:1 ($p < 0.001$), whereas a normal linear arrangement of myofibrils was found in all analyzed groups. Interstitial and perivascular fibrosis, as determined by the percentage of collagen, was statistically different between the SFA ($p = 0.017$) and 14:1 ($p = 0.022$) groups (Table 2; Figure 1). No significant statistical differences were demonstrated between the STD and experimental groups for blood plasma biochemical parameters (Table 2).

Table 2. Morphological, histological and plasma biochemical parameters after three-month diets—standard (STD), experimental high-fat diets rich in saturated fatty acids (SFA), and rich in PUFA with the 14:1 n-6/n-3 and 5:1 n-6/n-3 ratios—expressed in arithmetic mean values (SD).

Parameter	STD	SFA	14:1	5:1
body weight (g)	35.03 ^{A}	50.83 ^{B}	47.49 ^{B}	43.78 ^{B}
visceral fat (g)	0.201 ^{a}	0.311 ^{b}	0.317 ^{b}	0.306 ^{b}
heart weight (g)	0.1871	0.2671	0.2384	0.2281
cardiomyocyte diameter (μm) *	8.19 (1.37) ^{A}	14.46 ^{B} (3.36)	12.35 ^{C} (2.56)	10.03 ^{D} (1.64)
cardiomyocyte diameter range (μm)	4.95–13.21	8.01–19.81	7.35–16.98	6.13–16.84
collagenous tissue (%) *	5.42 ^{a} (1.48)	7.64 ^{c} (3.45)	7.32 ^{bc} (3.09)	5.92 ^{ab} (2.22)
lactate (mmol/l)	9.75 (2.48)	12.19 (3.13)	12.39 (3.42)	9.78 (1.79)
LDH (U/l)	1018.5 (451.9)	897.5 (229.7)	957.6 (444.8)	1021.1 (810)
CK (U/l)	233.7 (87.63)	150 (61.57)	183 (152)	289.1 (171)

With $^{A, B, C, D}$ significant differences ($p < 0.01$) between the groups are marked. The $^{a, b, c}$ was used to mark significant differences at $p < 0.05$ level. Values within the row marked with the different letters of alphabet differ significantly. With * the indices examined with Kruskal-Wallis test are marked. LDH -lactate dehydrogenase; CK—creatinine kinase.

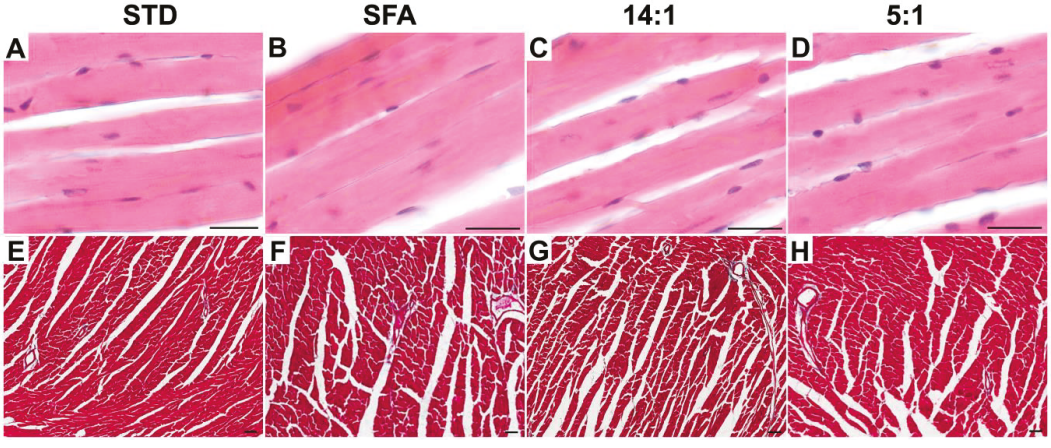

Figure 1. Representative light micrographs of H&E-stained (**A**–**D**) and Mallory's trichrome-stained (**E**–**H**) ventricle mid-region heart cross sections after STD (**A**,**E**), SFA (**B**,**F**), 14:1 (**C**,**G**) and 5:1 (**D**,**H**) diets. Scale bar—50 µm. STD – standard diet; SFA – high fat diet rich in saturated fatty acids; 14:1 – high fat diet rich in polyunsaturated fatty acids (PUFA) with LA/ALA ratio ~14:1; 5:1 – high fat diet rich in (PUFA) with LA/ALA ratio 5:1.

3.2. Analysis of Heart Proteome

Bioinformatic analysis revealed 365–404 protein spots per each analyzed 2-D gel, representing protein profiles of murine heart. The coefficient of variation (CV) was estimated at the level of 46.62%, 44.82%, 43.77%, and 46.30% for the STD, SFA, 14:1, and 5:1 group, respectively. Of the analyzed protein spots, 285 were common to all gel members.

Comparative analysis demonstrated that a HFD based on SFA caused significant ($p < 0.05$) differences in the expression of 17 protein spots of the cardiac muscle proteome in comparison to animals fed the STD diet. Of these, 11 were upregulated and 6 downregulated in the SFA group. A high-fat diet rich in PUFA with the n-6/n-3 ratio of 14:1 was shown to induce significant expression changes of 14 protein spots, of which 10 were upregulated and 4 were downregulated in comparison to the STD group. Seventeen protein spots were significantly altered in the group of animals fed a high-fat diet enriched with PUFA with the n-6/n-3 ratio of 5:1. Of these, 14 were found to be upregulated and 3 were downregulated when compared to the STD group. Detailed data concerning the differences in protein expression and protein identification are presented in Table 3. Significantly expressed proteins are shown in the representative protein profile of cardiac muscle—Figure 2. The heat map summarising the expression changes of significantly altered protein spots in animals fed different HFDs in comparison to the STD group are given in Figure 3.

Table 3. Differentially expressed protein spots between the standard (STD) and high-fat diet groups (SFA, 14:1, 5:1) in mouse cardiac muscle. Proteins were grouped according to their known biological processes. Spot numbers in the table correspond to the numbers in Figure 1 (2-DE proteome map) and Figure 3 (Heat Map).

Spot No	Protein Name	Gene Name	Seq. Cov. %	Mascot Score	STD	SFA	SFA/STD	14:1	14:1/ STD	5:1	5:1/ STD	Predicted pI/Mw	e\Estimated pI/Mw	SL
Cardiac Muscle Contraction														
1	Myosin regulatory light chain 2, ventricular/cardiac muscle isoform	MYL2	58	90	754.4	68.3 ^{ab}	**0.09**	339.5 ^{a}	0.45	392.3 ^{b}	0.52	4.86/18.9	4.5/16.6	C
2	Myosin light chain 3	MYL3	61	146	1585.6	460.3	**0.29**	588	**0.37**	734.3	0.46	5.03/22.5	4.4/25.9	C
3	Adenylate kinase isoenzyme 1	AK1	52	108	45.4	21.2 ^{ab}	**0.47**	48.3 ^{a}	1.06	65.2 ^{b}	**1.44**	5.67/21.6	4.6/24.8	C
4	Creatine kinase M-type	CKMM	36	101	264.5	390.5	1.48	494.6	**1.87**	506.2	**1.91**	6.58/43.2	7.6/41.60	C /MT
28	Fibrinogen beta chain	FGB	26	95	18.8	22 ^{a}	1.17	20 ^{b}	1.06	10 ^{ab}	**0.53**	6.68/55.4	6.1/58.4	EX
Glycolysis														
23	Triosephosphate isomerase	TPI1	33	85	152	169.1	1.11	188.3 ^{a}	1.24	134.7 ^{a}	0.89	5.56/32.7	7.6/25.0	C
24	L-lactate dehydrogenase B chain	LDHB	37	108	161.3	139.9 ^{a}	0.87	176.7 ^{b}	1.09	278.1 ^{ab}	**1.72**	5.70/36.8	5.3/36.3	C
TCA Cycle														
5	Isocitrate dehydrogenase (NAD) subunit alpha, mitochondrial	IDH3A	28	94	69.3	48.1 ^{ab}	0.69	93.1 ^{a}	1.34	108.9 ^{b}	1.57	5.86/35.0	4.8/39.4	MT
6			39	121	31.4	24.7 ^{a}	0.79	27.1 ^{b}	0.86	73.7 ^{ab}	**2.35**		5.0/39.6	
7			28	84	67	32 ^{ab}	**0.48**	73.3 ^{a}	1.09	78.5 ^{b}	1.17		5.3/39.3	
8	Succinate-CoA ligase (ADP-forming) subunit beta, mitochondrial	SUCLA2	34	87	303.8	151.5	**0.5**	158.9	**0.52**	172	**0.57**	4.94/36.3	4.8/44.7	MT
9	Malate dehydrogenase, mitochondrial	MDH2	30	63	106.1	117.7	1.11	95.9 ^{a}	0.9	144.8 ^{a}	**1.36**	6.16/36.7	5.7/34.4	MT
10	Pyruvate dehydrogenase E1 component subunit alpha, somatic form, mitochondrial	PDHA1	22	81	156.8	184.5 ^{a}	1.18	94.7 ^{ab}	0.6	232.1 ^{b}	**1.48**	8.49/43.9	7.4/42.2	MT
Respiratory Chain														
14	Electron transfer flavoprotein subunit alpha, mitochondrial	ETFA	40	96	92.8	140.4	**1.51**	107.9	1.16	125.4	**1.35**	8.62/35.3	7.2/30.6	MT
15			42	144	197	302.1	**1.53**	314.4	**1.6**	300	**1.52**		7.8/30.4	
22	Cytochrome b-c1 complex subunit 1, mitochondrial	UQCRC1	35	90	56.8	24.4 ^{a}	**0.43**	30.1 ^{b}	**0.53**	58.5 ^{ab}	1.03	5.81/53.4	4.9/48.5	MT

Table 3. *Cont.*

Spot No	Protein Name	Gene Name	Seq. Cov. %	Mascot Score	STD	SFA	SFA/STD	14:1	14:1/ STD	5:1	5:1/ STD	Predicted pI/Mw	e\Estimated pI/Mw	SL
Fatty Acid Metabolism and β-oxidation														
11	Short-chain specific acyl-CoA dehydrogenase, mitochondrial	ACADS	39	88	34.1	58.7	**1.72**	45.5	1.34	39.6	1.16	8.68/45.1	6.6/40.6	MT
12			49	156	53.7	145.6	**2.71**	134	**2.49**	133.2	**2.48**		7.2/39.7	
13	Long-chain specific acyl-CoA dehydrogenase, mitochondrial	ACADL	32	115	112.6	231.2	**2.05**	306.7	**2.72**	249.6	**2.22**	8.53/48.3	7.8/40.9	MT
16	Acyl-coenzyme A thioesterase 2, mitochondrial	ACOT2	40	142	87.2	173.2	**1.99**	157.7	**1.81**	182.9	**2.1**	6.88/49.9	6.6/43.7	MT
17			40	128	101.1	264.8	**2.62**	250.9	**2.48**	298.7	**2.95**		6.8/43.3	
18	Delta(3,5)-Delta(2,4)-dienoyl-CoA isomerase, mitochondrial	ECH1	34	74	21.6	35.3	1.64	23.9	1.11	32.9	**1.52**	7.6/36.4	5.9/31.7	MT/P
19			49	101	388.1	666.6	**1.72**	552.6	**1.42**	473	1.22		6.4/31.1	
20	Dihydrolipoyl dehydrogenase, mitochondrial	DLD	25	63	32.1	63.4	**1.98**	50.1	**1.56**	47.8	1.49	7.99/54.7	7.0/53.7	MT
21			28	90	104.4	166.9	**1.6**	186.4	**1.79**	161.9	1.55		7.6/56.3	
Oxidative Stress Prevention														
25	Superoxide dismutase (Cu-Zn)	SOD1	31	74	283.9	239.9	0.85	233	0.82	196.2	**0.69**	6.02/16.1	6.2/14.0	C/P
26/29	Peroxiredoxin-6	PRDX6	62	136	29.9	26.8	0.9	17.2	**0.57**	26.2	0.88	5.98/24.9	5.8/25.9	C
27/35	Bifunctional epoxide hydrolase 2	EPHX2	39	121	19.9	43.5	**2.18**	44.1	**2.22**	52.2	**2.62**	5.85/63.0	6.0/61.1	C/P

The results are the highest identification values from an average of two biological replicates. Statistically significant ($p < 0.05$) values of the average intensity of the SFA, 14:1 and 5:1 groups in relation to the STD group are marked in bold. With ^{a,b}—significant differences ($p < 0.05$) between the animal groups fed with experimental diets (SFA, 14:1 and 5:1 groups) are marked. Significantly different walues are marked with the same letters of the alphabet. SL—subcellular localisation; C—cytoplasm; MT—mitochondrion; P—peroxisome; EX—extracellular.

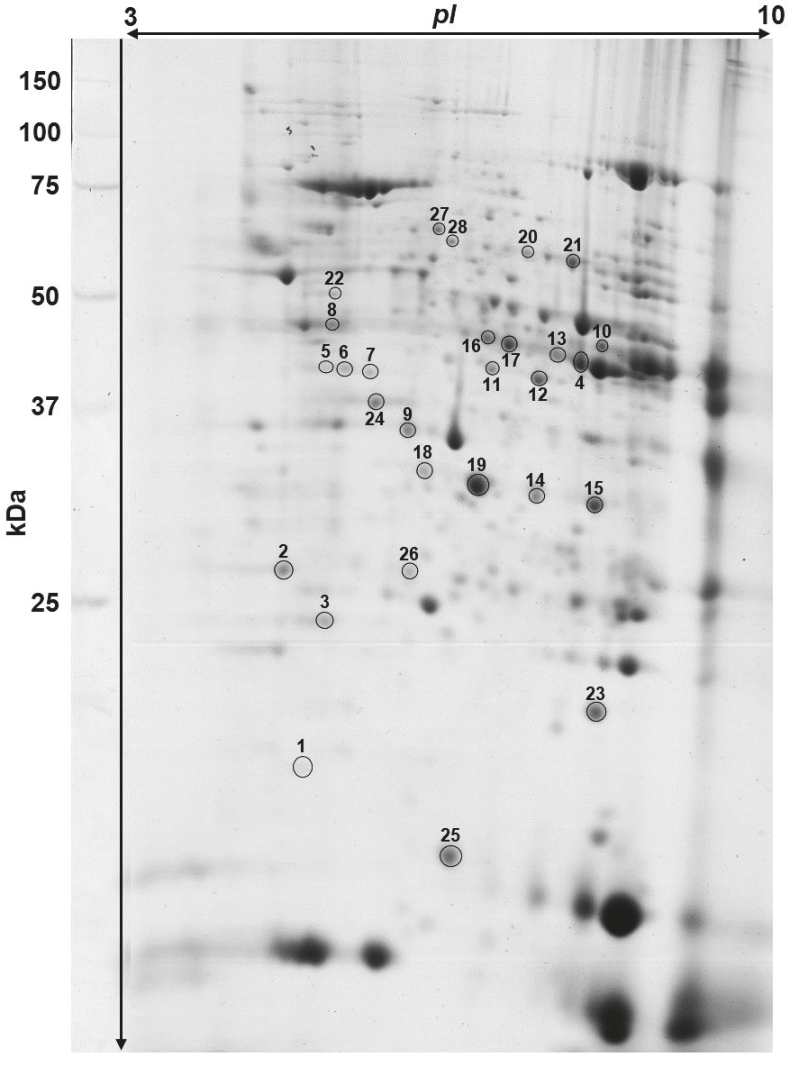

Figure 2. Representative two-dimensional electrophoresis gel image of the mouse heart proteome. Differentially expressed proteins between the animals fed standard diet (STD) and experimental high fat diets are indicated by numbers. Protein spot numbers refer to those presented in the heat map (Figure 3) and Table 3.

Significantly altered proteins were analysed using the Cystoscape software and the results of ClueGo enrichment are presented in Figure 4. Differentially expressed proteins were assigned to biological processes based on the aforementioned results as well as the data obtained from the STRING software analysis and uniport database. The groups of biological processes included: lipid metabolism and FA β-oxidation (ACADL, ACADS, ACOT2, ECH1, and DLD), glycolysis (TPI1 and LDHB), TCA cycle (IDH3A, SUCLA2, MDH2, and PDHA1), respiratory chain (ETFA and UQCRC1), myocardium contractility (MYL2, MYL3, AK1, CKMM, and FBG), oxidative stress (SOD1 and PRDX6), and PUFA eicosanoid metabolism (EPHX2). Contribution of the identified proteins to cardiomyocyte metabolism and contractile activity for each HFD is displayed in Figure 5.

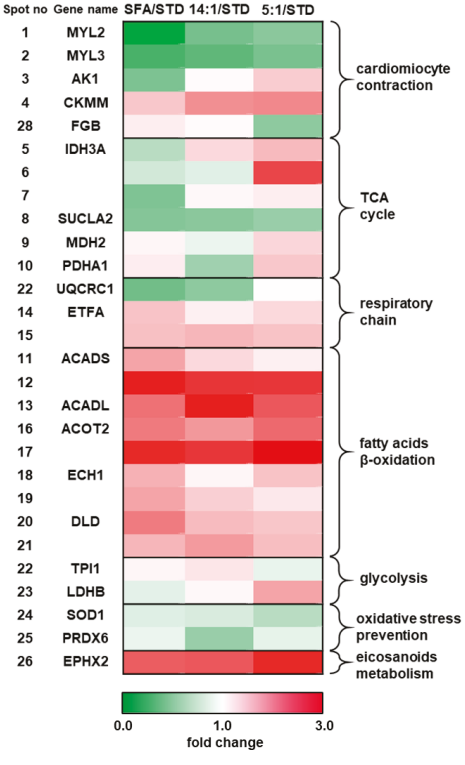

Figure 3. Heat map representing the identified proteins according to the magnitude of fold-change in the myocardium of mice fed high-fat diets with different fatty acid composition (SFA, n6/n3 PUFA 14:1, n6/n3 PUFA 14:1) compared to group of mice fed a standard diet (STD). Proteins were grouped according to their involvement in biological processes. Spot numbers refer to those presented on the 2-D proteome map (Figure 2) and Table 3. TCA - tricarboxylic acid cycle.

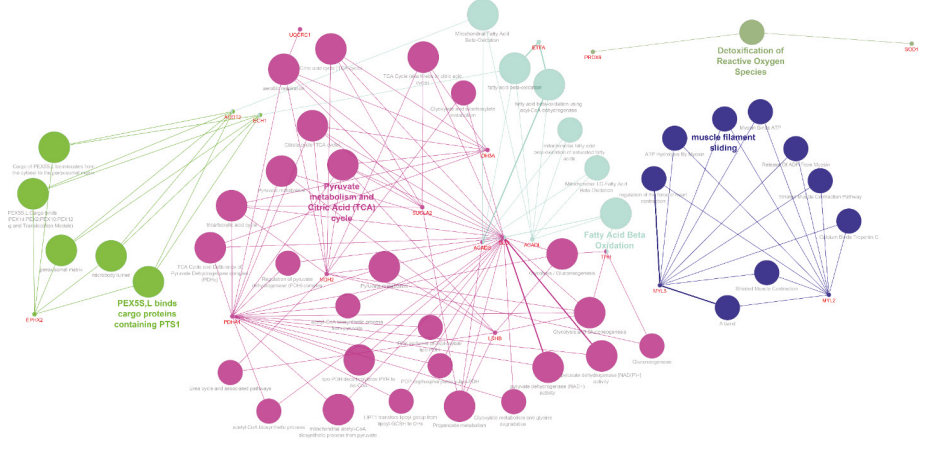

Figure 4. The ClueGO gene network of significantly altered pathways in cardiac muscle after 3 months of high-fat diets ingestion. Each node represents the Gene Ontology (GO) biological process/pathways and colors represent the GO group.

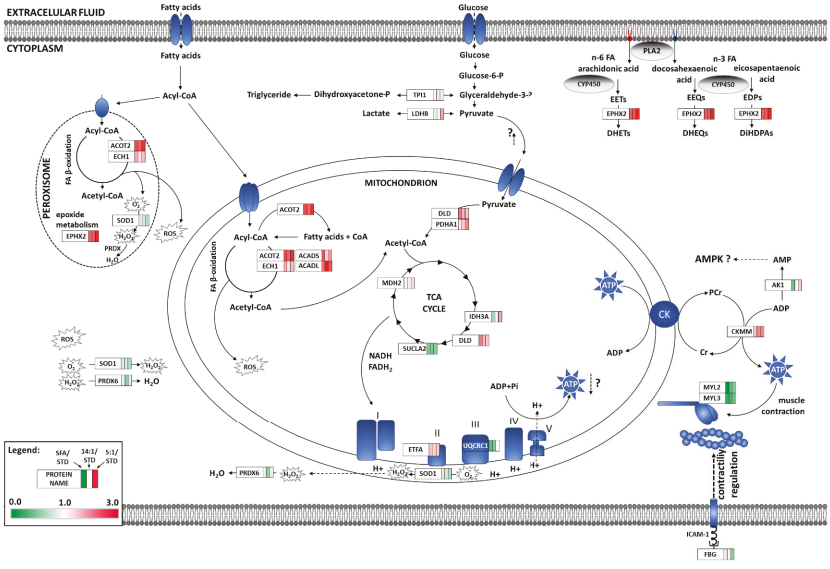

Figure 5. Overview of the effects of high-fat diets on the cardiomyocyte proteome. Identified proteins are shown according to the magnitude of fold-change in comparison to the STD group; red indicates upregulated proteins and green down-regulated proteins in the myocardium of mice. EETs—epoxyeicosatrienoic acids; DHETs—dihydroxyeicosatrienoic acids; EEQs—epoxyeicosatetraenoic acids; DHEQs—eicosatetraenoic acids; EDPs—epoxydocosapentaenoic acids; DiHDPAs—dihydroxydocosapentaenoic acids; AMPK—AMP-activated kinase.

Western-blot analysis was performed to verify the data concerning protein expression patterns based on 2-DE and subsequent identification using MALDI-ToF MS. We have selected proteins involved in fatty acid β-oxidation (ACADS), pyruvate metabolism and tricarboxylic acid cycle (MDH2), ROS detoxification (SOD1), and PUFA metabolism (EPHX2) for further validation based on the ClueGo analysis; the results of Western-blots are presented in Figure 6a–d, respectively. Expression patterns of selected murine heart proteins, confirmed by Western blot data, were consistent with 2-DE results.

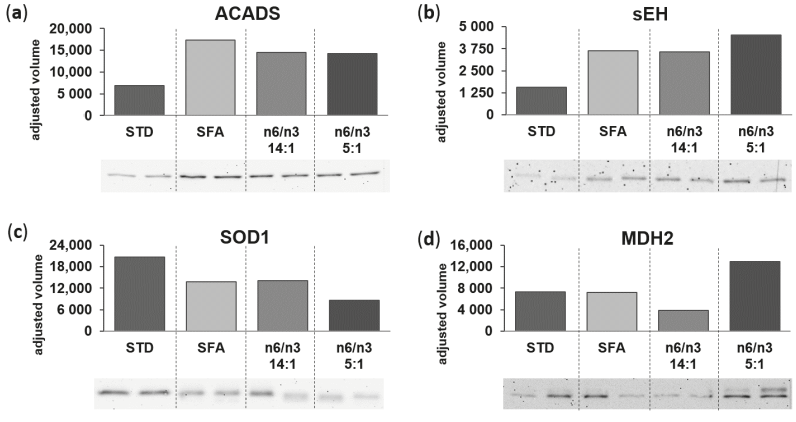

Figure 6. Validation of proteomic data obtained using 2-DE combined with MALDI-ToF MS. Protein expression levels of (**a**) short-chain specific acyl-CoA dehydrogenase, mitochondrial—ACADS (**b**) bifunctional epoxide hydrolase 2—sEH (**c**) superoxide dismutase 1—SOD1 (**d**) malate dehydrogenase, mitochondrial—MDH2. Western blots represent the murine myocardium from the control (STD) and experimental groups: SFA, 14:1 and 5:1.

4. Discussion

The present study aimed to analyse the effect of a three-month feeding with three types of high-fat diets (HFDs) containing different fatty acids (FAs) using proteomic and histological analysis of murine hearts. Our results clearly indicated that all HFDs, regardless of FA composition, promoted the development of obesity, as both weight gain and visceral fat mass were found to be significantly higher compared to control. It has been previously shown that diet-induced obesity is a key factor leading to histopathological myocardial changes associated with increased collagen deposition, which in turn may result in severe cardiac dysfunction [21]. This was in line with our findings as mice fed HFDs rich in SFA and PUFA with the n-3/n-6 ratio of 14:1 showed mild interstitial and perivascular collagen deposition. Furthermore, histological analyses of the heart also revealed signs of hypertrophy in response to all experimental diets. It should be noted that the highest hypertrophic lesions were observed in the SFA-fed animals, whereas the lowest were found in the group of mice fed a diet with the n-6/n-3 PUFA ratio of 5:1. As previously described and partially confirmed in our study, high fat diets rich in SFA [22–24] or diets based on equal proportions of SFA, MUFA, and PUFA [25] induced the development of cardiac hypertrophy and intravascular fibrosis. Additionally, excess dietary linoleic acid (LA) has also been related to increased collagen deposition in the left ventricle in C57BL/6 mice [16]. Collectively, our data may provide further evidence that high calorie intake triggers metabolic disorders, contributing to cardiac structure and function disorders [26]. The above-mentioned changes were also accompanied by cardiac protein expression alterations, including those related to cardiomyocyte contractility [27]. The results of the current study supported previous findings, as decreased expression of both isoforms of cardiac myosin light chains (MYL2 and MYL3), which are part of the cardiac contractile apparatus [28], was observed in all experimental groups. However, it should be emphasized that the most spectacular changes were observed in the SFA group, while the intake of HFD rich in PUFA led to less pronounced downregulation of MYL2 and MYL3 proteins. Myosin essential light chains play important roles in the regulation of cardiac myosin dynamics and crossbridge kinetics [29]. Attenuation of MYL2 phosphorylation is associated with the development of left ventricular hypertrophy resulting from depressed fractional shortening [30]. A marked reduction in MYL2 and MYL3 protein and mRNA levels was also observed in the hearts of rats with isoproterenol-induced cardiac hypertrophy [31]. Taking this into account, it can be assumed that HFDs, especially SFA-rich diet, led to impairments in the heart contractile apparatus, as indicated by decreased cardiac MYL expression, and could be one of the possible mechanisms for cardiac hypertrophy development.

There are some data that myocardial interstitial and perivascular fibrosis as well as cardiomyocyte hypertrophy may be related to increased expression of soluble epoxide hydrolase (sEH). Interestingly, our results demonstrated that mice fed all HFDs showed increased cardiac sEH protein expression compared to the STD diet. It should be pointed out that this protein plays a central role in the metabolism of bioactive lipid signalling molecules, as it is involved in the enzymatic conversion of omega-6 PUFA metabolites, epoxyeicosatrienoic acids (EETs) to less bioactive dihydroxyeicosatrienoic acids [32]. Accumulating evidence suggests that EETs display a broad spectrum of cardioprotective effects in the heart, including the impact on cardiac vasculature, heart fibroblasts and cardiomyocytes [33]. Recently, EETs have also been shown to cause coronary artery dilation, resulting in improved coronary blood flow [34], and to markedly limit collagen deposition [35]. A direct influence of EETs on cardiac myocytes have also been proposed, including the improvement of mitochondrial function, protection from angiotensin II-induced cardiac hypertrophy [36,37] and anti-arrhythmic effects [32]. Moreover, sEH is involved in the transformation of n-3 PUFA metabolites (epoxyeicosatetraenoic acids, EEQs, and epoxydocosapentaenoic acids, EDPs), exerting more potent anti-arrhythmogenic and anti-inflammatory effects than EETs to their biologically inactive forms [32,38]. Surprisingly, the highest expression of sEH in the present study was observed in animals fed a diet with the n-6/n-3 PUFA ratio of 5:1; however, this difference was not statistically significant.

Furthermore, the increased expression of cardiac sEH protein, recorded in all experimental groups, was not accompanied by severe hypertrophic and fibrotic lesions, which may be attributed to the higher synthesis of PUFA derivatives known to exert cardioprotective functions. This is particularly interesting in view of recent data suggesting that cytochrome P450 (CYP) enzymes more efficiently convert n-3 acids to epoxy and hydroxy metabolites that potentially mediate beneficial cardiovascular effects [32]. The increase of sHE in animals fed the SFA diet was not surprising and was consistent with the results of Pakiet et al. (2020), who have reported an increase in cardiac PUFA concentration in mice fed a HFD rich in SFA and MUFA [39].

Fibrinogen is a thrombin coagulable glycoprotein circulating in the blood, and its degradation products are involved in the regulation of cardiac muscle functions [40]. In the present study, we observed a significant decrease in FGB expression in the group of animals fed a HFD with n-6/n-3 PUFA 5:1. It was previously shown that fibrinogen gamma chain (FBG) could depress cardiac muscle contractility after binding to intercellular adhesion molecule-1 (ICAM-1) [40]. The expression of myocardial membrane-bound ICAM-1 has been shown to increase in response to stress and cardiac dysfunction [41], as well as after a high-fat diet intake [22]. However, as previously shown by Yamada et al. (2008), n-3 fatty acids decreased plasma concentrations of soluble ICAM-1 in patients with metabolic syndrome [42]. Therefore, the decreased cardiac FBG expression in the group of mice fed the PUFA-rich diet with the low n-6/n-3 ratio, observed in the current study, might be explained by reduced ICAM-1 expression. However, this remains speculative and requires further research.

The contractility of cardiac muscle is strictly dependent on proteins involved in ATP regeneration such as creatine kinase (CKM) and adenylate kinase 1 (AK1). The activity of those proteins is crucial for maintaining energy homeostasis and contractile activity of cardiomyocytes [43]. CKM is responsible for energy accumulation in the form of phosphocreatine (PCr) or reverse ATP regeneration from PCr. In the present study, a notable upregulation of CKM was observed in mice fed the HFD enriched with PUFA. An increasing trend of CKM expression was also observed in the group fed the SFA diet; however, this observation was not statistically confirmed. This was consistent with previous findings of Rayner et al. (2020), who demonstrated enhanced CKM activity in the heart of obese individuals, which was considered a compensatory mechanism to maintain ATP delivery despite a reduced phosphocreatine-to-ATP ratio [44]. Moreover, elevated CK activity is also considered as one of the risk factors of heart failure in mice [45]. Therefore, it seems that the compensatory increase in CKM expression, observed in the present study, could reflect a lower myocardial ATP synthesis. This was further supported by significant changes in the expression of adenylate kinase 1 (AK1), a protein known to catalyse ATP resynthesis from ADP particles. An increased synthesis of this signalling molecule regulates cellular energy balance, i.e., via the stimulation of AMP-activated protein kinase (AMPK), which is involved in the induction of fatty acid β-oxidation in cardiomyocytes [46,47]. It was previously shown that metabolic stress, e.g., fatty acid overload, increased adenylate kinase (AK1) activity [43]. Interestingly, the direction of AK1 expression differed significantly between the SFA and PUFA 5:1 groups. This protein in mice fed the SFA diet was downregulated, whereas cardiac AK1 overexpression was demonstrated in animals fed HFD with the n-6/n-3 ratio of 5:1 compared to the control group. This could suggest enhanced cardiac AMPK activation in animals fed with the highest amount of n-3 FA. This is particularly interesting due to the fact that AMPK is involved in the heart failure prevention via the activation of FA β-oxidation in the failing heart, mitochondrial biogenesis, improvement of glucose utilisation, prevention of autophagy, and improvement of heart contractility. Moreover, AMPK activation is one of the therapeutic targets in improving failing heart function [48]. However, this phenomenon needs to be better understood, and thus requires further research. Nevertheless, we have shown here that ingestion of diets rich in n-3 PUFA may potentially trigger changes in cardiac AMPK activity.

One of the metabolic consequences of dietary FA overload is increased activity of intracellular enzymes responsible for metabolization of these energetic substrates. Peroxisomal and mitochondrial β-oxidation are the major degradation pathways in fatty acid metabolism [26,49]. A recent study of Sikder et al. (2018) showed an increased rate of FA β-oxidation in the hearts of mice subjected to diet-induced obesity [50]. In addition, the results of the present study demonstrated higher expression of myocardial proteins involved in lipid metabolism and FA β-oxidation in response to all experimental HFDs, regardless of FA composition. On the other hand, previous studies demonstrated that intense FA β-oxidation, observed in response to dietary FA overload, resulted in suppressed glycolysis and pyruvate oxidation [49,51]. Our results, however, did not confirm the latter findings as we recorded a significant increase in the expression of cardiac L-lactate dehydrogenase B chain (LDHB) in mice fed a diet rich in PUFA with the n-6/n-3 ratio of 5:1. This could suggest a significant conversion of pyruvate to lactate in this group of animals. It has been previously reported that cardiomyocytes undergo hypertrophic changes due to elevated LDH activity, which stimulates NDRG3 expression by increasing lactate generation, followed by cell growth in animals with metabolic disorders [52]. These compensatory mechanisms are activated in order to prevent heart failure [52]. In our current study, less pronounced cardiac hypertrophy signs demonstrated in animals fed the 5:1 diet, which was characterized by a higher n-3 PUFA content, led to the assumption that this effect was due to the increased myocardial LDHB expression.

Our further analysis showed increased expression of enzymes engaged in FA β-oxidation, accompanied by significant changes in the relative abundance of proteins of the TCA cycle and electron transport chain (ETC) in the myocardium of mice fed all HFDs. This could indicate impairments in mitochondrial ATP production. Our data were consistent with the study of Vileigas et al. [26], who reported significant changes in the expression of many rat myocardial TCA enzymes and ETC proteins that contribute to disturbances in ATP synthesis in response to a high-calorie westernized diet. The decrease in the ATP synthesis rate in the heart of mice, as a metabolic response to the westernized diet was also confirmed by Luptak et al. [53]. Interestingly, our research revealed increased expression of isocitrate dehydrogenase [NAD] subunit alpha (IDH3a) in the hearts of animals fed the SFA-rich diet, whereas this protein was shown to be downregulated in mice fed the PUFA-diet with the n-6/n-3 ratio of 5:1 compared to the STD group. The studies aimed at identifying heart metabolic shifts in a diet-induced pre-diabetic mice model [54] and type 2 diabetes [55] showed significantly downregulated IDH3a expression. Moreover, the same effect was observed in the murine heart following the onset of the pressure overload heart failure [56] and in failing heart [57]. This could suggest that IDH3a protein expression pattern in animals fed different HFDs in our study could reflect increasing TCA impairments, which in turn was associated with the observed hypertrophic changes.

High-fat diets rich in PUFA with the n-6/n-3 ratios of 5:1 and 14:1 caused significant downregulation of enzymes preventing oxidative stress such as SOD1 and PRDX6. However, the remaining HFDs triggered an opposite trend in the expression of the aforementioned cardiac proteins. SOD1 and PRDX6 are proteins involved in ROS neutralization, thus their expression is induced in response to increased ROS generation. Based on this, downregulation of those proteins may reflect a possible mechanism of reduced antioxidant defence in murine hearts in response to HFD-feeding. In our opinion, this effect was probably caused by enhanced ROS generation, resulting from intensified fatty acid β-oxidation. Intracellular ROS increase, with a concomitant suppression of the mechanism involved in antioxidant defence, may be responsible for the development of cardiac hypertrophy, cardiac fibrosis and subsequent contractility impairments [53]. Rich (2010) [58] showed that feeding C57BL/6 mice with a high-fat diet may have contributed to the impairment of cardiac defence mechanisms against oxidative stress due to significant SOD1 downregulation. Disruption of the mechanisms preventing oxidative stress, manifested by decreased expression of SOD1, SOD2, catalase, and glutathione peroxidase, both at the transcript and protein levels, was also observed in the hearts of rats fed high-fat and low-carbohydrate

diets [59]. Moreover, a recent study of Vileigas et al. (2019) demonstrated that the expression of cardiac SOD1 was enhanced, while PRDX6 expression was decreased in mice fed a westernized diet [26].

5. Conclusions

Taken together, our data indicate that mice fed the HFD rich in SFA manifested the most severe cardiac hypertrophy and fibrosis lesions, whereas less pronounced changes were observed in the group of animals that ingested the highest amount of omega-3 FA. In general, all HFDs, regardless of FA composition, induced a comparable pattern of cardiac protein changes. However, it should be noted that three proteins, namely, IDH3A, LDHB, and AK1, were differently affected by different FA compositions. The high expression of these myocardial proteins found in the group of animals fed a HFD with the highest n-3 PUFA content could be closely related to the observed temporal delay in the development of hypertrophy. Future studies should pay particular attention to fully understand the role of AK1 and its potential involvement in AMPK activation in cardioprotection. In our opinion, soluble epoxide hydrolase (sEH) is another candidate protein for future functional analysis, as it is involved in the metabolism of cardioprotective n-6 and n-3 PUFA eicosanoids.

Author Contributions: Conceptualization, A.L., K.P.L., E.P., and M.P.; Data curation, A.L., M.O., K.M., M.G., and K.P.L.; Formal analysis, A.L., M.O., K.M., A.D.-C., M.G., and K.P.L.; Funding acquisition, A.L. and M.P.; Investigation, A.L. and A.H.; Methodology, A.L., M.O., K.M., M.G., K.P.L., and M.P.; Project administration, A.L., K.P.L., and M.P.; Resources, K.P.L., E.P., and M.P.; Software, A.L., M.G., A.K., and M.P.; Supervision, A.L. and M.P.; Validation, K.M.; Visualization, A.L.; Writing—original draft, A.L.; Writing—review and editing, A.L., M.O., K.M., A.D.-C., A.H., K.P.L., E.P., and M.P. All authors have read and agreed to the published version of the manuscript.

Funding: This research was funded by the National Science Centre of Poland MINIATURA1 grant No. 2017/01/X/NZ9/01173 and KNOW (Leading National Research Centre) Scientific Consortium "Healthy Animal—Safe Food", decision of the Ministry of Science and Higher Education No. 05-1/KNOW2/2015", grant No. KNOW2015/CB/PRO1/44.

Institutional Review Board Statement: The study design and animal handling was approved by the II Warsaw Local Ethics Committee for Animal Experimentation (WAW2_22/2016).

Informed Consent Statement: Not applicable

Data Availability Statement: The data presented in this study are available on the reasonable request from the corresponding author.

Conflicts of Interest: The authors declare no conflict of interest.

References

1. Krzysztoszek, J.; Laudańska-Krzemińska, I.; Bronikowski, M. Assessment of epidemiological obesity among adults in EU countries. *Ann. Agric. Environ. Med.* **2019**, *26*, 341–349. [CrossRef] [PubMed]
2. Timmis, A.; Townsend, N.; Gale, C.P.; Torbica, A.; Lettino, M.; Petersen, S.E.; Mossialos, E.A.; Maggioni, A.P.; Kazakiewicz, D.; May, H.T.; et al. European society of cardiology: Cardiovascular disease statistics 2019. *Eur. Heart J.* **2020**. [CrossRef] [PubMed]
3. Ortega, F.B.; Lavie, C.J.; Blair, S.N. Obesity and Cardiovascular Disease. *Circ. Res.* **2016**, *118*, 1752–1770. [CrossRef] [PubMed]
4. Tourlouki, E.; Matalas, A.-L.; Panagiotakos, D.B. Dietary habits and cardiovascular disease risk in middle-aged and elderly populations: A review of evidence. *Clin. Interv. Aging* **2009**, *4*, 319–330. [CrossRef] [PubMed]
5. Cordain, L.; Eaton, S.B.; Sebastian, A.; Mann, N.; Lindeberg, S.; Watkins, B.A.; O'Keefe, J.H.; Brand-Miller, J. Origins and evolution of the Western diet: Health implications for the 21st century. *Am. J. Clin. Nutr.* **2005**, *81*, 341–354. [CrossRef] [PubMed]
6. Simopoulos, A.P. Evolutionary Aspects of the Dietary Omega-6/Omega-3 Fatty Acid Ratio: Medical Implications. In *Evolutionary Thinking in Medicine*; Springer International Publishing: Cham, Swizterland, 2016; pp. 119–134.
7. Di Pasquale, M.G. The essentials of essential fatty acids. *J. Diet. Suppl.* **2009**, *6*, 143–161. [CrossRef] [PubMed]
8. Fats and fatty acids in human nutrition. Available online: https://www.who.int/nutrition/publications/nutrientrequirements/fatsandfattyacids_humannutrition/en/ (accessed on 30 December 2020).
9. Simopoulos, A.P.; Leaf, A.; Salem, N. Workshop Statement on the Essentiality of and Recommended Dietary Intakes for Omega-6 and Omega-3 Fatty Acids. *Prostaglandins Leukot. Essent. Fat. Acids* **2000**, *63*, 119–121. [CrossRef]
10. Lands, B. Consequences of Essential Fatty Acids. *Nutrients* **2012**, *4*, 1338–1357. [CrossRef]
11. Gillingham, B.L. The metabolic fate of alpha linolenic acid (ALA). *IHP Mag.* **2013**, *1*, 72–79.

12. Li, Y.; Kang, J.X.; Leaf, A. Differential Effects of Various Eicosanoids on the Production or Prevention of Arrhythmias in Cultured Neonatal Rat Cardiac Myocytes. *Prostaglandins* **1997**, *54*, 511–530. [CrossRef]
13. Schmilinsky-Fluri, G.; Valiunas, V.; Willi, M.; Weingart, R. Modulation of cardiac gap junctions: The mode of action of arachidonic acid. *J. Mol. Cell. Cardiol.* **1997**, *29*, 1703–1713. [CrossRef] [PubMed]
14. Fluri, G.S.; Rüdisüli, A.; Willi, M.; Rohr, S.; Weingart, R. Effects of arachidonic acid on the gap junctions of neonatal rat heart cells. *Pflügers Arch. Eur. J. Physiol.* **1990**, *417*, 149–156. [CrossRef]
15. Ghosh, S.; Novak, E.M.; Innis, S.M. Cardiac proinflammatory pathways are altered with different dietary n-6 linoleic to n-3 α-linolenic acid ratios in normal, fat-fed pigs. *Am. J. Physiol. Circ. Physiol.* **2007**, *293*, H2919–H2927. [CrossRef] [PubMed]
16. Beam, J.; Botta, A.; Ye, J.; Soliman, H.; Matier, B.J.; Forrest, M.; MacLeod, K.M.; Ghosh, S. Excess Linoleic Acid Increases Collagen I/III Ratio and "Stiffens" the Heart Muscle Following High Fat Diets. *J. Biol. Chem.* **2015**, *290*, 23371–23384. [CrossRef]
17. Gamble, M. The Hematoxylins and Eosin. In *Theory and Practice of Histological Techniques*; Elsevier: Amsterdam, The Netherlands, 2008; pp. 121–134.
18. Ozgo, M.; Lepczynski, A.; Robak, P.; Herosimczyk, A.; Marynowska, M. The current proteomic landscape of the porcine liver. *J. Physiol. Pharmacol.* **2019**. [CrossRef]
19. Shannon, P.; Markiel, A.; Ozier, O.; Baliga, N.S.; Wang, J.T.; Ramage, D.; Amin, N.; Schwikowski, B.; Ideker, T. Cytoscape: A software Environment for integrated models of biomolecular interaction networks. *Genome Res.* **2003**. [CrossRef]
20. Szklarczyk, D.; Gable, A.L.; Lyon, D.; Junge, A.; Wyder, S.; Huerta-Cepas, J.; Simonovic, M.; Doncheva, N.T.; Morris, J.H.; Bork, P.; et al. STRING v11: Protein–protein association networks with increased coverage, supporting functional discovery in genome-wide experimental datasets. *Nucleic Acids Res.* **2019**, *47*, D607–D613. [CrossRef]
21. Leopoldo, A.S.; Sugizaki, M.M.; Lima-Leopoldo, A.P.; do Nascimento, A.F.; Luvizotto, R.D.A.M.; de Campos, D.H.S.; Okoshi, K.; Pai-Silva, M.D.; Padovani, C.R.; Cicogna, A.C. Cardiac remodeling in a rat model of diet-induced obesity. *Can. J. Cardiol.* **2010**, *26*, 423–429. [CrossRef]
22. Sahraoui, A.; Dewachter, C.; de Medina, G.; Naeije, R.; Aouichat Bouguerra, S.; Dewachter, L. Myocardial Structural and Biological Anomalies Induced by High Fat Diet in Psammomys obesus Gerbils. *PLoS ONE* **2016**, *11*, e0148117. [CrossRef]
23. Sahraoui, A.; Dewachter, C.; Vegh, G.; Mc Entee, K.; Naeije, R.; Bouguerra, S.A.; Dewachter, L. High fat diet altered cardiac metabolic gene profile in Psammomys obesus gerbils. *Lipids Health Dis.* **2020**, *19*, 123. [CrossRef]
24. Oliveira Junior, S.A.; Padovani, C.R.; Rodrigues, S.A.; Silva, N.R.; Martinez, P.F.; Campos, D.H.S.; Okoshi, M.P.; Okoshi, K.; Dal-Pai, M.; Cicogna, A.C. Extensive impact of saturated fatty acids on metabolic and cardiovascular profile in rats with diet-induced obesity: A canonical analysis. *Cardiovasc. Diabetol.* **2013**, *12*, 65. [CrossRef] [PubMed]
25. Nguyen, S.; Shao, D.; Tomasi, L.C.; Braun, A.; de Mattos, A.B.M.; Choi, Y.S.; Villet, O.; Roe, N.; Halterman, C.R.; Tian, R.; et al. The effects of fatty acid composition on cardiac hypertrophy and function in mouse models of diet-induced obesity. *J. Nutr. Biochem.* **2017**, *46*, 137–142. [CrossRef] [PubMed]
26. Vileigas, D.F.; Harman, V.M.; Freire, P.P.; Marciano, C.L.C.; Sant'Ana, P.G.; de Souza, S.L.B.; Mota, G.A.F.; da Silva, V.L.; Campos, D.H.S.; Padovani, C.R.; et al. Landscape of heart proteome changes in a diet-induced obesity model. *Sci. Rep.* **2019**, *9*, 18050. [CrossRef] [PubMed]
27. Lyon, R.C.; Zanella, F.; Omens, J.H.; Sheikh, F. Mechanotransduction in Cardiac Hypertrophy and Failure. *Circ. Res.* **2015**, *116*, 1462–1476. [CrossRef]
28. Rayment, I.; Holden, H.; Whittaker, M.; Yohn, C.; Lorenz, M.; Holmes, K.; Milligan, R. Structure of the actin-myosin complex and its implications for muscle contraction. *Science* **1993**, *261*, 58–65. [CrossRef]
29. Sheikh, F.; Lyon, R.C.; Chen, J. Functions of myosin light chain-2 (MYL2) in cardiac muscle and disease. *Gene* **2015**, *569*, 14–20. [CrossRef]
30. Ding, P.; Huang, J.; Battiprolu, P.K.; Hill, J.A.; Kamm, K.E.; Stull, J.T. Cardiac Myosin Light Chain Kinase Is Necessary for Myosin Regulatory Light Chain Phosphorylation and Cardiac Performance In Vivo. *J. Biol. Chem.* **2010**, *285*, 40819–40829. [CrossRef]
31. Chowdhury, D.; Tangutur, A.D.; Khatua, T.N.; Saxena, P.; Banerjee, S.K.; Bhadra, M.P. A proteomic view of isoproterenol induced cardiac hypertrophy: Prohibitin identified as a potential biomarker in rats. *J. Transl. Med.* **2013**, *11*, 130. [CrossRef]
32. Arnold, C.; Markovic, M.; Blossey, K.; Wallukat, G.; Fischer, R.; Dechend, R.; Konkel, A.; von Schacky, C.; Luft, F.C.; Muller, D.N.; et al. Arachidonic Acid-metabolizing Cytochrome P450 Enzymes Are Targets of ω-3 Fatty Acids. *J. Biol. Chem.* **2010**, *285*, 32720–32733. [CrossRef]
33. Jamieson, K.L.; Endo, T.; Darwesh, A.M.; Samokhvalov, V.; Seubert, J.M. Cytochrome P450-derived eicosanoids and heart function. *Pharmacol. Ther.* **2017**, *179*, 47–83. [CrossRef]
34. Li, P.L.; Campbell, W.B. Epoxyeicosatrienoic acids activate K+ channels in coronary smooth muscle through a guanine nucleotide binding protein. *Circ. Res.* **1997**. [CrossRef] [PubMed]
35. He, Z.; Yang, Y.; Wen, Z.; Chen, C.; Xu, X.; Zhu, Y.; Wang, Y.; Wang, D.W. CYP2J2 metabolites, epoxyeicosatrienoic acids, attenuate Ang II-induced cardiac fibrotic response by targeting Gα 12/13. *J. Lipid Res.* **2017**, *58*, 1338–1353. [CrossRef] [PubMed]
36. Zhang, H.; Wang, T.; Zhang, K.; Liu, Y.; Huang, F.; Zhu, X.; Liu, Y.; Wang, M.H.; Tang, W.; Wang, J.; et al. Deletion of soluble epoxide hydrolase attenuates cardiac hypertrophy via down-regulation of cardiac fibroblasts-derived fibroblast growth factor-2. *Crit. Care Med.* **2014**. [CrossRef] [PubMed]

37. Ai, D.; Pang, W.; Li, N.; Xu, M.; Jones, P.D.; Yang, J.; Zhang, Y.; Chiamvimonvat, N.; Shyy, J.Y.J.; Hammock, B.D.; et al. Soluble epoxide hydrolase plays an essential role in angiotensin II-induced cardiac hypertrophy. *Proc. Natl. Acad. Sci. USA* **2009**, *106*, 564–569. [CrossRef]
38. Ye, D.; Zhang, D.; Oltman, C.; Dellsperger, K.; Lee, H.-C.; VanRollins, M. Cytochrome P-450 Epoxygenase Metabolites of Docosahexaenoate Potently Dilate Coronary Arterioles by Activating Large-Conductance Calcium-Activated Potassium Channels. *J. Pharmacol. Exp. Ther.* **2002**, *303*, 768–776. [CrossRef]
39. Pakiet, A.; Jakubiak, A.; Mierzejewska, P.; Zwara, A.; Liakh, I.; Sledzinski, T.; Mika, A. The Effect of a High-Fat Diet on the Fatty Acid Composition in the Hearts of Mice. *Nutrients* **2020**, *12*, 824. [CrossRef]
40. Boyd, J.H.; Chau, E.; Tokunanga, C.; Bateman, R.M.; Haljan, G.; Davani, E.Y.; Wang, Y.; Walley, K.R. Fibrinogen decreases cardiomyocyte contractility through an ICAM-1 dependent mechanism. *Crit. Care* **2008**, *12*, R2. [CrossRef]
41. Niessen, H. Upregulation of ICAM-1 on cardiomyocytes in jeopardized human myocardium during infarction. *Cardiovasc. Res.* **1999**, *41*, 603–610. [CrossRef]
42. Yamada, H.; Yoshida, M.; Nakano, Y.; Suganami, T.; Satoh, N.; Mita, T.; Azuma, K.; Itoh, M.; Yamamoto, Y.; Kamei, Y.; et al. In Vivo and In Vitro Inhibition of Monocyte Adhesion to Endothelial Cells and Endothelial Adhesion Molecules by Eicosapentaenoic Acid. *Arterioscler. Thromb. Vasc. Biol.* **2008**, *28*, 2173–2179. [CrossRef]
43. Dzeja, P.; Terzic, A. Adenylate kinase and AMP signaling networks: Metabolic monitoring, signal communication and body energy sensing. *Int. J. Mol. Sci.* **2009**, *10*, 1729–1772.
44. Rayner, J.J.; Peterzan, M.A.; Watson, W.D.; Clarke, W.T.; Neubauer, S.; Rodgers, C.T.; Rider, O.J. Myocardial Energetics in Obesity. *Circulation* **2020**, *141*, 1152–1163. [CrossRef] [PubMed]
45. Cao, F.; Maguire, M.L.; McAndrew, D.J.; Lake, H.A.; Neubauer, S.; Zervou, S.; Schneider, J.E.; Lygate, C.A. Overexpression of mitochondrial creatine kinase preserves cardiac energetics without ameliorating murine chronic heart failure. *Basic Res. Cardiol.* **2020**, *115*, 12. [CrossRef] [PubMed]
46. Dzeja, P.P.; Vitkevicius, K.T.; Redfield, M.M.; Burnett, J.C.; Terzic, A. Adenylate Kinase–Catalyzed Phosphotransfer in the Myocardium. *Circ. Res.* **1999**, *84*, 1137–1143. [CrossRef] [PubMed]
47. Hopkins, T.A.; Dyck, J.R.B.; Lopaschuk, G.D. AMP-activated protein kinase regulation of fatty acid oxidation in the ischaemic heart. *Biochem. Soc. Trans.* **2003**, *31*, 207–212. [CrossRef] [PubMed]
48. Li, X.; Liu, J.; Lu, Q.; Ren, D.; Sun, X.; Rousselle, T.; Tan, Y.; Li, J. AMPK: A therapeutic target of heart failure—not only metabolism regulation. *Biosci. Rep.* **2019**, *39*. [CrossRef] [PubMed]
49. Lopaschuk, G.D.; Ussher, J.R.; Folmes, C.D.L.; Jaswal, J.S.; Stanley, W.C. Myocardial Fatty Acid Metabolism in Health and Disease. *Physiol. Rev.* **2010**, *90*, 207–258. [CrossRef]
50. Sikder, K.; Shukla, S.K.; Patel, N.; Singh, H.; Rafiq, K. High Fat Diet Upregulates Fatty Acid Oxidation and Ketogenesis via Intervention of PPAR-γ. *Cell. Physiol. Biochem.* **2018**. [CrossRef]
51. Finck, B.N.; Lehman, J.J.; Leone, T.C.; Welch, M.J.; Bennett, M.J.; Kovacs, A.; Han, X.; Gross, R.W.; Kozak, R.; Lopaschuk, G.D.; et al. The cardiac phenotype induced by PPARα overexpression mimics that caused by diabetes mellitus. *J. Clin. Investig.* **2002**, *109*, 121–130. [CrossRef]
52. Dai, C.; Li, Q.; May, H.I.; Li, C.; Zhang, G.; Sharma, G.; Sherry, A.D.; Malloy, C.R.; Khemtong, C.; Zhang, Y.; et al. Lactate Dehydrogenase A Governs Cardiac Hypertrophic Growth in Response to Hemodynamic Stress. *Cell Rep.* **2020**, *32*, 108087. [CrossRef]
53. Luptak, I.; Sverdlov, A.L.; Panagia, M.; Qin, F.; Pimentel, D.R.; Croteau, D.; Siwik, D.A.; Ingwall, J.S.; Bachschmid, M.M.; Balschi, J.A.; et al. Decreased ATP production and myocardial contractile reserve in metabolic heart disease. *J. Mol. Cell. Cardiol.* **2018**, *116*, 106–114. [CrossRef]
54. Cruz-Topete, D.; List, E.O.; Okada, S.; Kelder, B.; Kopchick, J.J. Proteomic changes in the heart of diet-induced pre-diabetic mice. *J. Proteomics* **2011**, *74*, 716–727. [CrossRef] [PubMed]
55. Dabkowski, E.R.; Baseler, W.A.; Williamson, C.L.; Powell, M.; Razunguzwa, T.T.; Frisbee, J.C.; Hollander, J.M. Mitochondrial dysfunction in the type 2 diabetic heart is associated with alterations in spatially distinct mitochondrial proteomes. *Am. J. Physiol. Circ. Physiol.* **2010**, *299*, H529–H540. [CrossRef] [PubMed]
56. Abdurrachim, D.; Nabben, M.; Hoerr, V.; Kuhlmann, M.T.; Bovenkamp, P.; Ciapaite, J.; Geraets, I.M.E.; Coumans, W.; Luiken, J.J.F.P.; Glatz, J.F.C.; et al. Diabetic db/db mice do not develop heart failure upon pressure overload: A longitudinal in vivo PET, MRI, and MRS study on cardiac metabolic, structural, and functional adaptations. *Cardiovasc. Res.* **2017**, *113*, 1148–1160. [CrossRef] [PubMed]
57. Prévilon, M.; Le Gall, M.; Chafey, P.; Federeci, C.; Pezet, M.; Clary, G.; Broussard, C.; François, G.; Mercadier, J.-J.; Rouet-Benzineb, P. Comparative differential proteomic profiles of nonfailing and failing hearts after in vivo thoracic aortic constriction in mice overexpressing FKBP12.6. *Physiol. Rep.* **2013**, *1*. [CrossRef]
58. Rich, H.S. *Impact of High Fat Dietary Treatment and Nox2-Deficiency on Prooxidantand Antioxidant Enzyme Expression in the Heart*; University of Zurich: Zurich, Swizterland, 2010.
59. Liu, J.; Lloyd, S.G. High-fat, low-carbohydrate diet alters myocardial oxidative stress and impairs recovery of cardiac function after ischemia and reperfusion in obese rats. *Nutr. Res.* **2013**, *33*, 311–321. [CrossRef]

nutrients

MDPI

Article

Differential Deleterious Impact of Highly Saturated Versus Monounsaturated Fat Intake on Vascular Function, Structure, and Mechanics in Mice

Elena Vega-Martín [1,2,†], Marta Gil-Ortega [3,*,†], Raquel González-Blázquez [3], Sara Benedito [4], Jesús Fernández-Felipe [3], Mariano Ruiz-Gayo [3], Nuria del Olmo [3,5], Julie A. Chowen [6,7], Laura M. Frago [6,8], Beatriz Somoza [3,†] and María S. Fernández-Alfonso [1,2,9,†]

1 Instituto Pluridisciplinar, Universidad Complutense de Madrid, 28040 Madrid, Spain; elevega@ucm.es (E.V.-M.); marisolf@farm.ucm.es (M.S.F.-A.)
2 Departamento de Farmacología, Farmacognosia y Botánica, Facultad de Farmacia, Universidad Complutense de Madrid, 28040 Madrid, Spain
3 Departamento de Ciencias Farmacéuticas y de la Salud, Facultad de Farmacia, Universidad San Pablo-CEU, CEU Universities, 28925 Madrid, Spain; raquelgonzalezblazquez@gmail.com (R.G.-B.); jesus.fernandezfelipe@beca.ceu.es (J.F.-F.); ruigayo@ceu.es (M.R.-G.); nuriadelolmo@psi.uned.es (N.d.O.); bsomoza.fcex@ceu.es (B.S.)
4 Departamento de Fisiología, Facultad de Farmacia, Universidad Complutense de Madrid, 28040 Madrid, Spain; sbenedi@farm.ucm.es
5 Department of Psychobiology, School of Psychology, National Distance Education University (UNED), 28040 Madrid, Spain
6 Department of Pediatric Endocrinology, Hospital Infantil Universitario Niño Jesús, Instituto de Investigación la Princesa, Centro de Investigación Biomédica en Red Fisiopatología de la Obesidad y la Nutrición (CIBEROBN), Instituto de Salud Carlos III, 28009 Madrid, Spain; julieann.chowen@salud.madrid.org (J.A.C.); laura.frago@uam.es (L.M.F.)
7 IMDEA Food Institute, CEI UAM + CSIC, 28049 Madrid, Spain
8 Department of Pediatrics, Facultad de Medicina, Universidad Autónoma de Madrid, 28029 Madrid, Spain
9 Instituto de Investigación Sanitaria San Carlos (IdiSSC), 28040 Madrid, Spain
* Correspondence: mgortega@ceu.es
† These authors contributed equally to this work.

Citation: Vega-Martín, E.; Gil-Ortega, M.; González-Blázquez, R.; Benedito, S.; Fernández-Felipe, J.; Ruiz-Gayo, M.; del Olmo, N.; Chowen, J.A.; Frago, L.M.; Somoza, B.; et al. Differential Deleterious Impact of Highly Saturated Versus Monounsaturated Fat Intake on Vascular Function, Structure, and Mechanics in Mice. *Nutrients* **2021**, *13*, 1003. https://doi.org/10.3390/nu13031003

Academic Editor: Frederic Capel

Received: 30 January 2021
Accepted: 16 March 2021
Published: 19 March 2021

Abstract: Vegetable oils such as palm oil (enriched in saturated fatty acids, SFA) and high-oleic-acid sunflower oil (HOSO, containing mainly monounsaturated fatty acids, MUFA) have emerged as the most common replacements for trans-fats in the food industry. The aim of this study is to analyze the impact of SFA and MUFA-enriched high-fat (HF) diets on endothelial function, vascular remodeling, and arterial stiffness compared to commercial HF diets. Five-week-old male C57BL6J mice were fed a standard (SD), a HF diet enriched with SFA (saturated oil-enriched Food, SOLF), a HF diet enriched with MUFA (unsaturated oil-enriched Food, UOLF), or a commercial HF diet for 8 weeks. Vascular function was analyzed in the thoracic aorta. Structural and mechanical parameters were assessed in mesenteric arteries by pressure myography. SOLF, UOLF, and HF diet reduced contractile responses to phenylephrine and induced endothelial dysfunction in the thoracic aorta. A significant increase in the β-index, and thus in arterial stiffness, was also detected in mesenteric arteries from the three HF groups, due to enhanced deposition of collagen in the vascular wall. SOLF also induced hypotrophic inward remodeling. In conclusion, these data demonstrate a deleterious effect of HF feeding on obesity-related vascular alterations that is exacerbated by SFA.

Keywords: saturated fatty acids; monounsaturated fatty acids; purified high-fat diets; endothelial dysfunction; nitric oxide; vascular remodeling; arterial stiffness; collagen

1. Introduction

Obesity constitutes one of the major preventable risk factors for the development of several noncommunicable diseases including cardiovascular alterations, diabetes, mus-

culoskeletal disorders, and some cancers [1]. In fact, in both humans and mice models, increasing evidence has shown that obesity favors the development of vascular damage, such as endothelial dysfunction, that seems to be due, at least in part, to compromised nitric oxide (NO) availability [2,3] and/or increased oxidative stress [3,4]. In addition to endothelial dysfunction, the two other crucial mechanisms implicated in vascular alterations are arterial remodeling and stiffness. Indeed, chronic alterations in vascular structure may lead to significant changes in mechanical properties, such as compliance and distensibility [5], thus accounting for arterial stiffness, which has recently emerged as an independent risk factor for cardiovascular diseases [6,7]. Conversely, weight loss in overweight and obese individuals is associated with a reduction in arterial stiffness [8]. In addition, we have recently demonstrated that extracellular matrix remodeling, including an increase in collagen content and elastin fragmentation, plays a key role in the development of central arterial stiffness due to obesity [7].

For the last decades, the most common strategy to induce obesity in animal models has been the use of commercial high fat (HF) diets providing between 45 and 65% of energy from fat. However, despite being widely used, the purified commercial diets exhibit important nutritional differences compared to standard chow diets. In fact, whereas the main source of fat in chow diets is vegetable and fish oil, purified HF diets mainly contain lard, especially rich in saturated fatty acids (SFA) but very limited in monounsaturated (MUFA) and polyunsaturated fatty acids (PUFA). In addition, purified diets also provide a greater amount of easily metabolizable carbohydrates as compared to standard chow diets for rodents [9,10]. Therefore, commercial HF diets might not be fully representative of common diets ingested by the general population worldwide.

Despite the limited evidence concerning the specific impact of different fatty acids on vascular alterations, several studies performed on obese humans have shown that HF diets enriched in SFA impair flow-mediated dilation or endothelial function [11,12]. Similarly, a potential negative impact of SFA-enriched diets, but not of MUFA-enriched diets, on arterial stiffness has been also suggested [13]. However, a study performed by Sanders et al. [14] failed to show a beneficial effect of replacing SFA-enriched diets with MUFA-enriched diets elaborated from refined high-oleic-acid sunflower oil (HOSO) on endothelial function or arterial stiffness [14]. Contrarily, a study performed in spontaneously hypertensive rats evidenced a significant improvement in endothelial function in rats fed a MUFA-enriched diet elaborated from virgin olive oil [15].

Because the use of vegetable oils such as palm oil and HOSO has dramatically increased in food industry in the past decades in an attempt to replace trans fats [16], elucidating the precise effect of these oils on vascular alterations is of utmost importance. In this context, we hypothesized that HF diets enriched in SFA are more harmful than HF diets enriched in MUFA on the development of vascular alterations derived from obesity. Therefore, the main aim of this study was to analyze the differential impact of a SFA-enriched HF diet and a MUFA-enriched HF diet on endothelial function, vascular remodeling and the development of arterial stiffness as compared to commercial standard HF diets, as well as to characterize the mechanisms involved in these alterations.

2. Materials and Methods

2.1. Animals and Experimental Protocol

Four-week-old male C57BL/6J mice (Charles River, Écully, France) were housed under controlled dark-light cycles (12 h/12 h) and temperature (22 °C) and had access to food and water ad libitum. After one week of acclimation, animals were randomly divided into four groups (n = 7–10) with a similar average body weight (BW) and assigned to a standard diet (SD, 18% energy from fat; Harlan Laboratories, España, Spain), a HF diet enriched in saturated fat (saturated oil-enriched Food, SOLF, 70% energy from fat), a HF diet enriched in monounsaturated fat (unsaturated oil-enriched Food, UOLF, 70% energy from fat), or a commercially available high-fat diet (HF, 62% energy from fat, Test Diets, UK) for 8 weeks. UOLF and SOLF diets were elaborated by mixing standard chow diet (60%)

and 40% of either HOSO or palm kernel oil, respectively, as previously described [17]. BW and food intake were monitored weekly. Animals were euthanized and exsanguinated by decapitation. The thoracic aorta, the superior mesenteric artery and mesenteric resistance arteries were immediately dissected and used for vascular studies. Blood was collected in EDTA-coated tubes, centrifuged at 800× *g* for 10 min and plasma samples were stored at −80 °C until used for biochemical analysis.

The Institutional Animal Care and Use Committee approved all experimental procedures according with the European Union Laboratory Animal Care Rules (86/609/EEC) and were approved by the Animal Research Committee of San Pablo CEU University (PCD-CEU08-112-16 and PROEX 200/18). All efforts were made to avoid animal suffering in accordance with the ARRIVE guidelines for reporting experiments involving animals [18,19]. All experimental procedures were blinded.

2.2. Assessment of Biochemical Parameters

Glucose was assessed by a spectrophotometric method (Glucose Trinder Method, Roche Applied Science, Penzberg, Spain). Triglycerides and non-esterified fatty acids were analyzed using the GPO (Biolabo, Maizy, France) and the ACS-ACOD (Wako, Bioproducts, Germany) methods, respectively.

2.3. Functional Studies in the Thoracic Aorta Artery

The thoracic aorta was carefully isolated and placed in oxygenated, cold physiological Krebs Henseleit buffer (KH, 115 mM NaCl, 2.5 mM $CaCl_2$, 4.6 mM KCl, 25 mM $NaHCO_3$, 1.2 mM $MgSO_4$, 1.2 mM KH_2PO_4, 0.01 mM EDTA, and 11.1 mM glucose), deprived of perivascular adipose tissue and blood and cut into rings of 2–3 mm length. Vascular rings were then suspended around two intraluminal parallel wires and placed into an organ bath containing KH at pH = 7.4, 37 °C and bubbled with carbogen (95% O_2–5% CO_2) and connected to a force transducer. Isometric tension was recorded in a Power Lab system (AD Instruments, Oxford, UK). An optimal resting tension of 1 g was applied to aortic rings and was readjusted every 10 min. After 40 min period of equilibration, arterial contractility was assessed using a potassium chloride solution (KCl, 60 mM). Cumulative concentration-response curves in response to phenylephrine (Phe, 10^{-8}–10^{-6} M) were performed. Relaxation curves in response to acetylcholine (Ach, 10^{-9}–10^{-4} M) were also carried out in segments pre-contracted with Phe (from 10^{-6} to 10^{-5} M, as required to ensure a similar pre-contraction in all groups). The nitric oxide synthase inhibitor, NG-nitro-L-arginine methyl ester (L-NAME, 10^{-4} M), was added and the tissue was incubated 30 min prior to the addition of Phe. All reagents were provided by Sigma-Aldrich (Madrid, Spain).

2.4. Structural and Mechanical Properties in Mesenteric Resistance Arteries

Structural and mechanical properties were assessed in first-order branch mesenteric resistance arteries (MRA) by pressure myography (Model P100, Danish Myo-Tech, Hinnerup, Denmark), as previously described [20]. Briefly, intraluminal pressure was set at 70 mmHg for 30 min to stabilize MRA segments, which were incubated in calcium-free KH (0 Ca^{2+}-KH; 115 mM NaCl, 25 mM $NaHCO_3$, 4.6 mM KCl, 1.2 mM $MgSO_4$, 1.2 mM KH_2PO_4, 10 mM EGTA and 5.5 mM glucose) at 37 °C and bubbled with carbogen. External and internal diameters (D_{i0Ca} and D_{e0Ca}, respectively) were measured at increasing intraluminal pressures (5, 20, 40, 60, 80, 100, 120, and 140 mmHg). Thereafter, MRA segments were fixed with 4% paraformaldehyde (in 0.2 M phosphate buffer, pH 7.2–7.4) at 70 mmHg and 37 °C for 45 min and stored at 4 °C for confocal microscopy studies. Structural (lumen and vessel diameters, wall thickness, cross-sectional area (CSA) and wall-to-lumen ratio) and mechanical parameters (stress, strain, and incremental distensibility) were calculated from D_{e0Ca} and D_{i0Ca} values as previously described [21]. Arterial stiffness was assessed by the parameter β, the slope of the stress–strain relationship and a measure of intrinsic arterial stiffness [22].

2.5. Elastin Content and Organization in Mesenteric Resistance Arteries

Elastin content and organization were determined in the external (EEL) and internal elastic laminae (IEL) of previously fixed MRA by fluorescent confocal microscopy based on the auto fluorescent properties of elastin (excitation 488 nm/emission 500–560 nm). To avoid artery deformation, intact arterial segments were mounted with antifading solution (Citifluor) on a slide provided with a small well. MRA segments were visualized with a Leica TCS SP5 confocal microscope (Leica Microsystems, Wetzlar, Germany). Serial optical sections (stacks of images) from the adventitia to the lumen were captured with a 63× oil immersion objective at a wavelength of 488/515 nm. All images were captured under identical conditions of laser intensity, contrast, and brightness. Quantitative analyses were performed in three randomly selected regions of EEL and IEL of at least five independent experiments using Image J software [21]. From each stack of serial images, individual projections of IEL were reconstructed to measure total fenestra number and area. Elastin content was quantified from the mean fluorescence intensity values [23].

2.6. Collagen Content in Superior Mesenteric Arteries

Superior mesenteric arteries were homogenized in a lysis buffer containing (0.5 M NaCl, 0.1 M $Na_4P_2O_7$, 0.5 M dichloro diphenyl-trichloroethane, 0.5 M HEPES, 0.5 M NaF, 0.5 M Na_3VO_4, 0.1 M EDTA, 0.1 M EGTA, 20% glycerol, 0.2 M PMSF, 1 µL/mL leupeptin, 1 µL/mL N-α-p-tosyl-1-lysine in chloromethylketone [TLCK] and 1 µL/mL aprotinin) using a Tissue Lyser homogenizer (Qiagen, Hilden, Germany) and applying four cycles at 50 Hz for 5 min. Samples were subjected to thermal shocks (3x 37 °C/liquid nitrogen) and centrifuged at 10,000 rpm and 4 °C for 10 min. Supernatants were collected and protein concentration was assessed with the method described by Bradford [24].

Collagen content was quantified using a dot-blot-Sirius red-based assay, as previously described [25]. Briefly, 2 µL of samples were applied to PVDF membranes (BioRad, Spain), that were subsequently dried at 37 °C for 5 min to favor sample fixation and to reduce nonspecific binding of Sirius red (Sigma-Aldrich, Tres Cantos, Spain) to PVDF membranes. Membranes were incubated in 2.5×10^{-3}% *w*/*v* Sirius red dissolved in saturated picric acid for 30 min at 4 °C, washed in distilled water three times for 1 min and scanned with a Chemi Doc System (ChemiDoc XRS+ Imaging System BioRad, Alcobendas, Spain). Collagen staining was quantified using Image Lab 3.0 software (BioRad). Results were interpolated in a calibration curve (0.1 to 6 µg/µL) using gelatin from porcine skin, Type A and gel strength 300 (Sigma-Aldrich, Spain).

2.7. Statistical Analysis

Contractile responses to Phe are expressed in absolute values. Relaxation to Ach is expressed as the percentage of the previous contractile response to Phe. The maximal response (E_{max} values) and the potency (pD_2 values) were calculated by using nonlinear regression analyses of each individual concentration-response curve. The area under the curve (AUC) was determined from each individual concentration-response curve plot. All values are given as mean ± S.E.M. and n denotes the number of replicates used in each experiment. Student's *t* tests or ANOVA followed by Bonferroni or Tukey post-hoc test was used as appropriate. A value of $p < 0.05$ was considered statistically significant. Statistical analysis was performed using GraphPad Prism 7.0 (GraphPad Software, San Diego, CA, USA).

3. Results

3.1. SOLF, UOLF, and HF Diets Increase Body Weight and Glucose Levels But Differently Affect NEFA Concentrations

BW was significantly higher in SOLF, UOLF, and HF mice compared to the SD group (Figure 1a). However, the increase in BW was more pronounced in UOLF (14%) and especially in HF mice (36%) compared to SOLF mice (6%) ($p < 0.001$, BW_{SOLF} vs. BW_{HF}). In addition, whereas SOLF increased both glucose and NEFA plasma concentrations, the

UOLF and HD diet only increased glycemia (Figure 1b,c). The fat-enriched diets did not modify triglyceride levels (Figure 1d).

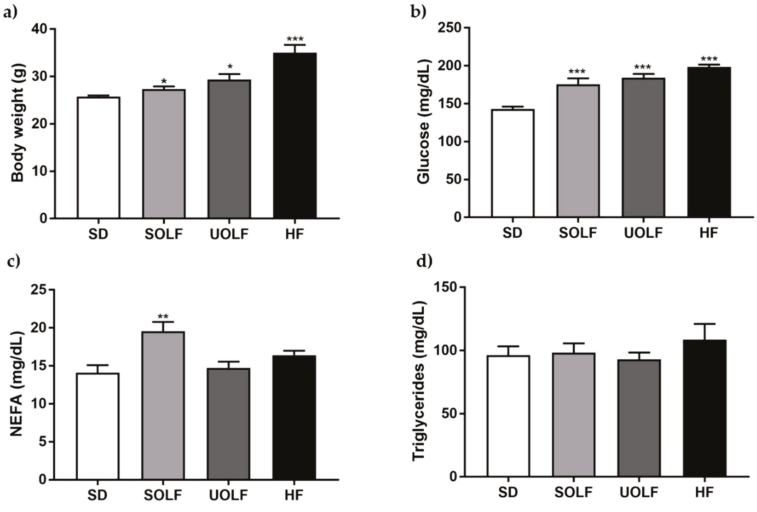

Figure 1. Body weight and biochemical parameters. Bar graphs showing body weight (**a**) and plasmatic concentrations of glucose (**b**), non-esterified free-fatty acids (NEFA); (**c**) and triglycerides (**d**). Data are shown as mean ± SEM of 7–10 animals per strain. * $p < 0.05$, ** $p < 0.01$, *** $p < 0.001$ vs. the control group SD.

3.2. SOLF, UOLF, and HF Diets Induce Endothelial Dysfunction and Reduce Contractile Responses to Phenylephrine in the Thoracic Aorta

Maximal contractions to KCl (60 mM) were significantly reduced in aortic rings from both SOLF and UOLF compared to SD (SD = 0.57 ± 0.02 g, SOLF = 0.38 ± 0.02 g and UOLF = 0.40 ± 0.02 g, $p < 0.001$), with no changes detected in the HF group (0.58 ± 0.03 g). Contractile responses to Phe (10^{-8}-10^{-6} M) were significantly diminished in arteries from SOLF, UOLF and HF animals compared to SD mice (Figure 2a), as evidenced by the maximal responses (E_{max}SD = 0.52 ± 0.04 g, E_{max}SOLF = 0.22 ± 0.04 g, E_{max}UOLF = 0.20 ± 0.04 g; E_{max}HF = 0.28 ± 0.1 g; $p < 0.05$ SOLF and HF and $p < 0.01$ UOLF *vs* SD). However, Phe potency was not modified by the diets (pD_2SD = 7.02 ± 0.06; pD_2SOLF = 6.89 ± 0.12; pD_2UOLF = 6.99 ± 0.13; pD_2HF = 6.92 ± 0.12). In addition, the functional integrity of the endothelium, as assessed by concentration-response curves to Ach (10^{-9} to 10^{-4} M), was also compromised in aortic rings from SOLF, UOLF, and HF mice as compared to the SD group (Figure 2b).

To determine whether these alterations were due to changes in NO contribution, basal NO availability was analyzed from the difference between response curves to Phe performed in the presence and absence of L-NAME (10^{-4} M). Pre-incubation with L-NAME significantly enhanced contractile responses to Phe in aortic rings from SD (Figure 2c), UOLF (Figure 2e) and HF (Figure 2f) mice. In contrast, L-NAME did not modify contractile responses to Phe in SOLF mice (Figure 2d). Therefore, and as evidenced by the difference between the AUC (Figure 2g), these data reveal that NO availability was significantly compromised by SOLF and to a lesser extent by UOLF, thus contributing to impair vascular functionality.

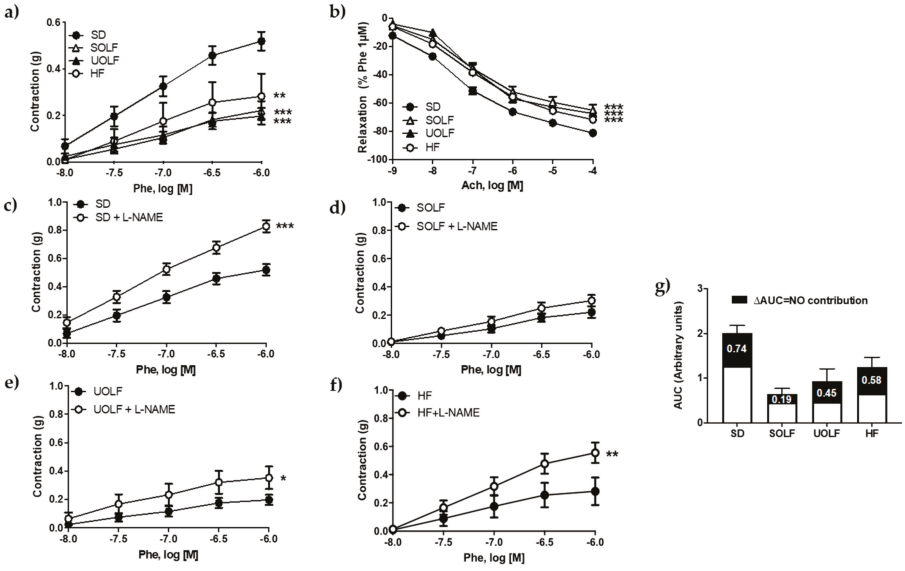

Figure 2. Characterization of vascular function. Concentration–response curves to (**a**) phenylephrine (Phe, 10^{-8} to 10^{-6} M) and (**b**) acetylcholine (Ach, 10^{-9} to 10^{-4} M) in aorta segments from standard (SD), unsaturated oil-enriched Food (UOLF), saturated oil-enriched Food (SOLF), and high-fat (HF) mice. Contractions are expressed in absolute values and relaxant responses are expressed as percentage of a previous contraction to Phe (10^{-6} M). Concentration–response curves to Phe (10^{-8} to 10^{-6} M) in aorta segments from SD (**c**), SOLF (**d**), UOLF (**e**), and HF mice (**f**) in absence and presence of L-NAME. (**g**) AUC in response to Phe in presence (full histogram) or absence (white bar) of L-NAME. The difference in AUC (black bar) represents NO bioavailability. Data are shown as mean ± SEM of 7–10 animals per group. * $p < 0.05$, ** $p < 0.01$, *** $p < 0.001$ vs. its corresponding control.

3.3. SOLF but Not UOLF or HF Diets Induced Hypotrophic Inward Remodeling in Mesenteric Resistance Arteries

The study of structural parameters revealed a significant reduction in the lumen diameter and CSA and, consequently, in the vessel diameter in MRA from SOLF mice compared to the SD without changes in the wall thickness and wall-to-lumen ratio (Figure 3a–e), thus demonstrating the development of hypotrophic inward remodeling. In contrast, HF mice exhibited a significant, though very mild, hypertrophic remodeling as evidenced by the increase in both the wall thickness and CSA together with a reduction in the wall-to-lumen ratio. Nevertheless, these alterations were not paralleled with changes either in the vessel or in the lumen diameter of HF mice' MRA. The UOLF diet did not exert any modification in MRA's structural parameters.

3.4. SOLF, UOLF, and HF Diets Induced Arterial Stiffness in Mesenteric Resistance Arteries

The study of mechanical parameters showed no significant alterations in stress (Figure 4a), strain (Figure 4b), or incremental distensibility (Figure 4c) from MRA, when analyzed independently. However, the stress/strain relationship was significantly shifted to the left in MRA from SOLF, UOLF, and HF mice compared to the SD group. In addition, MRA from SOLF, UOLF, and HF mice exhibited a significant increase in β-index as compared to the SD group, suggesting increased intrinsic arterial stiffness in these arteries (Figure 4d).

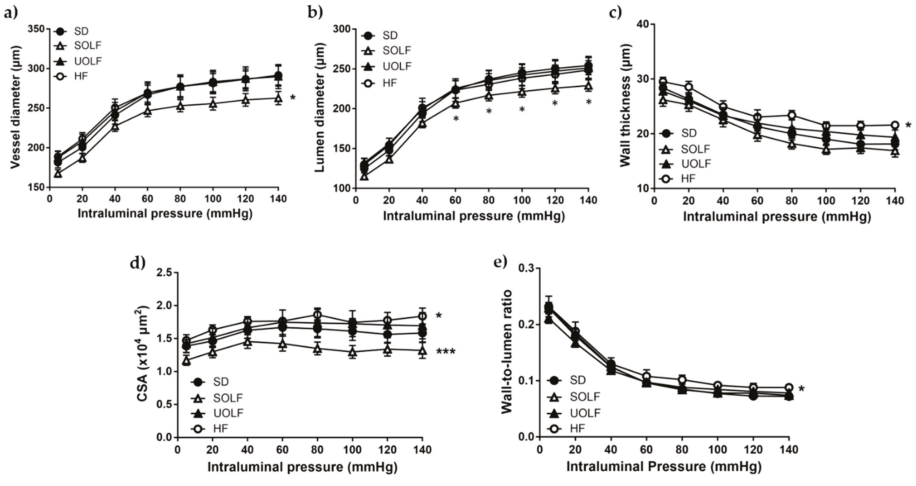

Figure 3. Characterization of structural parameters in first order mesenteric resistance arteries. (**a**) Vessel diameter–pressure, (**b**) lumen diameter–pressure, (**c**) wall thickness-pressure, (**d**) cross sectional area (CSA) pressure, and (**e**) media to lumen ratio-pressure of mesenteric resistance arteries (MRA) from SD, UOLF, SOLF, and HF mice. Results are expressed as mean ± SEM of n = 7–10. * $p < 0.05$ and *** $p < 0.001$ vs. the SD group.

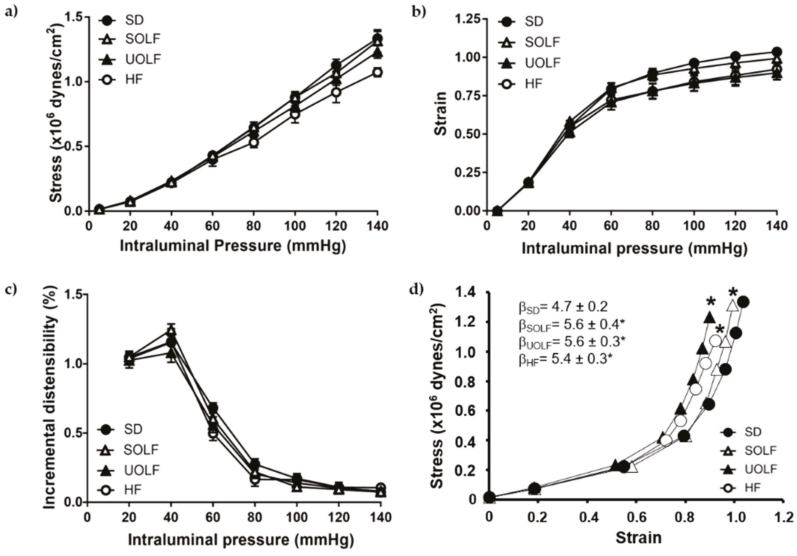

Figure 4. Characterization of mechanical parameters in first-order mesenteric resistance arteries. (**a**) Wall stress-pressure, (**b**) strain-pressure, (**c**) incremental distensibility-pressure curves and (**d**) stress-strain relationships with β values of MRA from SD, UOLF, SOLF, and HF mice. Results are expressed as mean ± SEM of n = 7–10. * $p < 0.05$ vs. the SD group.

3.5. SOLF, UOLF, and HF Diets Induced An Increase in Collagen Deposition but No Major Changes in Elastin Content or Organization

To determine the mechanisms involved in the development of arterial stiffness, we assessed the impact of fat-enriched diets on the two major proteins regulating arterial distensibility, elastin, and collagen. Elastin content was not modified by the diets either

in the external (EEL; Figure 5a,b) or in the internal elastic lamina (IEL; Figure 6a,b) from MRA. However, whereas SOLF and UOLF did not affect the fenestrae area or its number in the IEL, the HF diet significantly reduced the fenestrae number as compared to the SD group (Figure 6a,c), with no changes in the fenestrae area (Figure 6a,d).

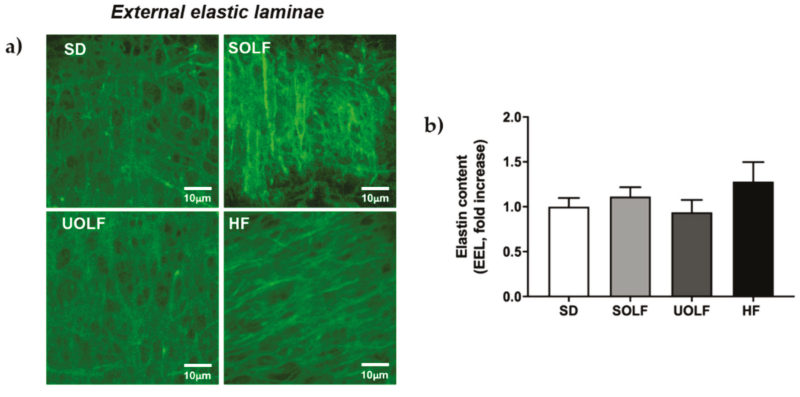

Figure 5. Elastin content and organization of external elastic laminae (EEL) in first-order MRA (**a**) Representative confocal microscopy images of projections of MRA's EEL from SD, UOLF, SOLF, and HF mice. Projections were obtained from serial optical sections captured with a fluorescence confocal microscope (x63 oil immersion objective, zoom 2). (**b**) Bar graphs show fluorescence intensity, indicative of elastin content in EEL from SD, UOLF, SOLF, and HF animals. Results are expressed as mean ± SEM of n = 4–10.

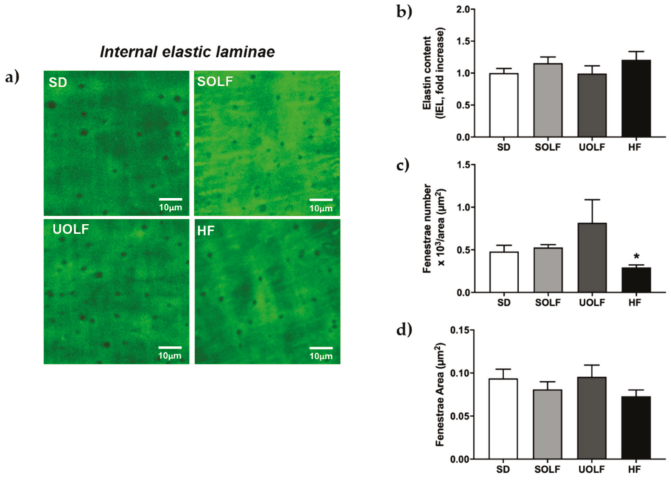

Figure 6. Elastin content and organization of internal elastic laminae (IEL) in first-order MRA. (**a**) Representative confocal microscopy images of projections of MRA's IEL from SD, UOLF, SOLF, and HF mice. Projections were obtained from serial optical sections captured with a fluorescence confocal microscope (x63 oil immersion objective, zoom 2). Bar graphs show (**b**) fluorescence intensity, indicative of elastin content in the IEL, (**c**) fenestrae number, and (**d**) fenestrae area in MRA from SD, UOLF, SOLF, and HF animals. Results are expressed as mean ± SEM of n = 4–10. * $p < 0.05$ vs. the SD group.

In contrast, MRA from SOLF, UOLF, and HF mice exhibited higher amounts of collagen than the arteries from SD mice (Figure 7). Together, these results suggest that arterial stiffness induced by fat-enriched diets results from enhanced collagen deposition in the vascular wall.

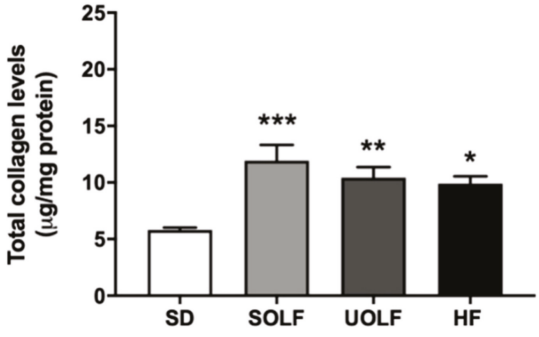

Figure 7. Collagen content in superior mesenteric arteries. Collagen content in the superior mesenteric artery from SD, UOLF, SOLF and HF mice. Results are expressed as mean ± SEM of n = 6. * $p < 0.05$, ** $p < 0.01$, *** $p < 0.001$ vs. the SD group.

4. Discussion

Numerous studies performed in mice/rat models of diet-induced obesity (DIO) [3,26–28] as well as in humans with obesity [29–31] have demonstrated a link between excessive energy intake and the development of endothelial dysfunction and arterial stiffness [7,32–36]. However, though most of these alterations have been generally attributed to an excessive intake of SFA [11,13,37,38], the net contribution of different fatty acid types to obesity-derived vascular alterations remains to be clarified. In this context, the novel findings of this study are that UOLF (enriched in vegetal-derived MUFA), as well as SOLF and HF diets (enriched in SFA from vegetal and animal sources, respectively) impair endothelial function and increase arterial stiffness as a result of enhanced collagen deposition in the arterial wall. SOLF also favors the development of hypotrophic inward remodeling.

As expected, the three fat-enriched diets induced an increase in BW as the result of an enhanced energy intake, as previously described [17]. However, BW increase was more evident in the HF group, what might be due to the fact that purified HF diets contain easily metabolizable carbohydrates, which might exacerbate weight gain [9]. In addition, and despite glucose levels being enhanced by SOLF, UOLF, and HF diet, only the SOLF group exhibited alterations in plasmatic concentrations of NEFA. It is important to note that a role for elevated NEFA on the development of endothelial dysfunction [2,27] and defective NO release [39] has been clearly demonstrated. In addition, a study performed in obese hypertensive patients revealed that elevated NEFA levels in plasma might also contribute to vascular growth and remodeling [40]. Therefore, the increase in NEFA observed exclusively in SOLF animals could contribute to the differential impact of SOLF vs. UOLF and HF diet on vascular alterations.

One of the major findings of this study is that UOLF, and not only SOLF and HF diet, impairs endothelial function after 8 weeks of diet. This result supports other studies showing a deleterious effect of SFA-enriched diets [37], manufactured either from animal (mainly lard) [3,26,27] or vegetable sources [13], on endothelial function. However, endothelial dysfunction displayed by UOLF animals was surprising, since a beneficial effect of olive oil-enriched diets has been reported by Herrera et al. [15]. It should be highlighted that this study also reported that the beneficial effects of olive oil were not observed in mice that consumed a HOSO-enriched diet, suggesting that the effect of olive oil is not linked to MUFA but to other olive oil components, like polyphenols, which are absent in

HOSO [15]. Therefore, our current data suggest that the intake of elevated amounts of fat exerts a deleterious impact on vascular function, independently of fatty acid composition.

Another interesting finding in the current study is the significant reduction of contractile responses to Phe detected in SOLF, UOLF, and HF mice, which has been previously described in mice fed a 62% fat HF diet for only 4 weeks [26]. This could be due to alterations in alpha-1 receptor function, as suggested by Juarez et al. [41], though further studies are required to better address this matter. In contrast, a commercial diet providing 45% energy content from fat was not able to alter NA-induced contractions after even 32 weeks of dietary treatment [3], which evidences that the diets used in our study (which provide 62–70% energy from fat) are much more aggressive than 45% commercial HF diets.

We also analyzed the contribution of NO to vascular responses. As expected, NO bioavailability was significantly compromised in SOLF mice. However, this effect was less pronounced in either HF or UOLF mice. These data point to the existence of additional mechanisms accounting for endothelial dysfunction, different from a reduction in NO release, that must take place in HF and UOLF mice. Unfortunately, the poor contractile response to Phe, together with the rapid desensitization to Phe detected in SOLF, UOLF, and HF mice, hindered a further characterization of such mechanisms. In any case, a role of contractile prostaglandins or oxidative stress, among others, cannot be discarded.

The development of hypotrophic inward remodeling was detected in MRA from SOLF mice. Vascular remodeling is another major vascular alteration that has been described in obesity. However, studies performed in DIO models [7], as well as in genetic models of obesity [42–44] and obese humans [45], have reported the development of hypertrophic outward remodeling instead of hypotrophic inward remodeling and independently of an elevation in blood pressure. Intriguingly, the vascular remodeling observed in arteries from SOLF mice has been also described in several models of hypertension such as the ouabain-induce hypertensive rat [46] or the MWF rat, also exhibiting albuminuria [20], and could be associated to enhanced collagen deposition compromising vascular distensibility and favoring the development of hypertension [46]. In this regard, a shift toward the left in the stress–strain relationship together with enhanced β-values were detected in SOLF, UOLF, and HF mice, thus evidencing increased arterial stiffness in the three experimental groups. Increasing evidence supports the association between obesity and arterial stiffness. In fact, numerous studies performed in obese humans have revealed an increase in pulse wave velocity (PWV) [36,47–49], indicative of systemic stiffness. Similarly, studies in models of genetic or DIO rodents have also described an increase in intrinsic arterial stiffness either in conduit [50,51] or in resistance arteries [7].

To better understand the mechanisms involved in the impairment of vascular distensibility induced by SOLF, UOLF, and HF diet, we assessed the content and organization of the two main proteins contained in the vascular extracellular matrix, which are responsible for vessels elasticity (elastin) and resistance to changes in blood pressure (collagen). In our model, no changes were detected in elastin content in the EEL or IEL nor in the fenestrae area and number, with the exception of the HF group that exhibited a reduction in fenestrae number. In this direction, we have previously showed a reduction in fenestrae area and number associated with increased arterial stiffness in mice fed a 45% HF diet for 32 weeks [7]. However, although it is known that IEL organization is more relevant than elastin content in the contribution to arterial stiffening [7,21], the present data discard a role for elastin in arterial stiffness induced by SOLF and UOLF, at least when administered for a short period of time (8 weeks). In contrast, a significant increase in total collagen content was detected in SOLF, UOLF, and HF mice. Numerous studies performed in different models of hypertension have stated a clear relationship between alterations in collagen turnover in favor of type I/III collagen synthesis and the development of arterial stiffness in resistance arteries from both obese humans and rodents [45,52,53]. Accordingly, we have previously reported enhanced deposition of type I collagen by long-term HF feeding [7] in murine MRA. Similar results were found in small mesenteric arteries from C57Bl6 mice fed a HF diet for 16 weeks [54] as well as in conduit arteries from a Wistar rat DIO model [55].

Together these results demonstrate that SOLF and UOLF favor the development of vascular alterations including endothelial dysfunction and arterial stiffness due to enhanced collagen deposition. Moreover, this study highlights the fact that the SOLF diet seems to be even more deleterious than the UOLF or even than commercial HF diets, since hypotrophic inward remodeling was also detected in this group.

In light of these findings, it is necessary to reassess the convenience of a massive use of palm or even HOSO in food industry and to identify the possible protective factors in oils such as olive oil in order to find potential healthier replacements. Nevertheless, and considering the high content of SFA and MUFA included in SOLF and UOLF, respectively, it would be of interest to elucidate the potential impact of these fatty acids when administered at lower doses.

Author Contributions: Conceptualization, E.V.-M., M.G.-O., B.S., and M.S.F.-A.; methodology, E.V.-M., M.G.-O., S.B., B.S., and M.S.F.-A.; validation E.V.-M., M.G.-O., M.R.-G., B.S., S.B., J.A.C., L.M.F., N.d.O., and M.S.F.-A.; formal analysis, E.V.-M., M.G.-O., R.G.-B., J.F.-F.; investigation, E.V.-M., M.G.-O., R.G.-B., J.F.-F., S.B., B.S.; resources, B.S., M.S.F.-A., M.R.-G., J.A.C., L.M.F., and N.d.O.; data curation, E.V.-M., M.G.-O., R.G.-B., M.R.-G., B.S., M.S.F.-A.; writing—original draft preparation, E.V.-M., M.G.-O., B.S., M.R.-G., and M.S.F.-A.; writing—review and editing, all authors; visualization, all authors; supervision, M.G.-O., B.S., and M.S.F.-A.; project administration, B.S. and M.S.F.-A.; funding acquisition, B.S., M.S.F.-A., M.R.-G., J.A.C., L.M.F., and N.d.O. All authors have read and agreed to the published version of the manuscript.

Funding: This research was funded by Ministerio de Economía y Competitividad (BFU2017-82565-C2-2-R, BFU2017-82565-C2-1-R and BFU2016-78556-R), FUSP-CEU and Grupos Universidad Complutense de Madrid (GR-921641).

Institutional Review Board Statement: The study was conducted according to the guidelines of the Declaration of Helsinki and approved by the Animal Research Committee of San Pablo CEU University and by the Ethics Board of the Regional Environment Committee of Comunidad Autónoma de Madrid (RD53/2013; Ref. PCD-CEU08-112-16 and PROEX 200/18).

Informed Consent Statement: Not applicable.

Data Availability Statement: The data presented in this study are available on request from the corresponding author.

Acknowledgments: We thank J. M. Garrido, J. Bravo, and I. Bordallo for skillful animal care during the experiment and Dolores Morales for her help with the confocal microscope.

Conflicts of Interest: The authors declare no conflict of interest.

References

1. WHO. *Obesity and Overweight*; World Health Organization: Geneva, Switzerland, 2020; Available online: https://www.who.int/news-room/fact-sheets/detail/obesity-and-overweight (accessed on 9 December 2020).
2. Li, H.; Bao, Y.; Zhang, X.; Yu, Y. Free fatty acids induce endothelial dysfunction and activate protein kinase C and nuclear factor-kappaB pathway in rat aorta. *Int. J. Cardiol.* **2011**, *152*, 218–224. [CrossRef] [PubMed]
3. Gil-Ortega, M.; Condezo-Hoyos, L.A.; García-Prieto, C.F.; Arribas, S.M.; González, M.C.; Aránguez, I.I.; Ruiz-Gayo, M.; Somoza, B.; Fernández-Alfonso, M.S. Imbalance between pro and anti-oxidant mechanisms in perivascular adipose tissue aggravates long-term high-fat diet-derived endothelial dysfunction. *PLoS ONE* **2014**, *9*, e95312. [CrossRef]
4. Inoguchi, T.; Li, P.; Umeda, F.; Yu, H.Y.; Kakimoto, M.; Imamura, M.; Aoki, T.; Etoh, T.; Hashimoto, T.; Naruse, M.; et al. High glucose level and free fatty acid stimulate reactive oxygen species production through protein kinase C–dependent activation of NAD(P)H oxidase in cultured vascular cells. *Diabetes* **2000**, *49*, 1939–1945. [CrossRef] [PubMed]
5. Crijns, F.R.L.; Wolffenbuttel, B.H.R.; De Mey, J.G.R.; Boudier, H.A.J.S. Mechanical properties of mesenteric arteries in diabetic rats: Consequences of outward remodeling. *Am. J. Physiol. Circ. Physiol.* **1999**, *276 Pt 2*, H1672–H1677. [CrossRef]
6. Sloboda, N.; Fève, B.; Thornton, S.N.; Nzietchueng, R.; Regnault, V.; Simon, G.; Labat, C.; Louis, H.; Max, J.-P.; Muscat, A.; et al. Fatty acids impair endothelium-dependent vasorelaxation: A link between obesity and arterial stiffness in very old Zucker rats. *J. Gerontol. Ser. A Biol. Sci. Med. Sci.* **2012**, *67*, 927–938. [CrossRef]
7. Gil-Ortega, M.; Martín-Ramos, M.; Arribas, S.M.; González, M.C.; Aránguez, I.; Ruiz-Gayo, M.; Somoza, B.; Fernández-Alfonso, M.S. Arterial stiffness is associated with adipokine dysregulation in non-hypertensive obese mice. *Vasc. Pharmacol.* **2016**, *77*, 38–47. [CrossRef] [PubMed]

8. Weisbrod, R.M.; Shiang, T.; Al Sayah, L.; Fry, J.L.; Bajpai, S.; Reinhart-King, C.A.; Lob, H.E.; Santhanam, L.; Mitchell, G.; Cohen, R.A.; et al. Arterial stiffening precedes systolic hypertension in diet-induced obesity. *Hypertension* **2013**, *62*, 1105–1110. [CrossRef] [PubMed]
9. Warden, C.H.; Fisler, J.S. Comparisons of diets used in animal models of high-fat feeding. *Cell Metab.* **2008**, *7*, 277. [CrossRef]
10. González-Blázquez, R.; Alcalá, M.; Fernández-Alfonso, M.S.; Villa-Valverde, P.; Viana, M.; Gil-Ortega, M.; Somoza, B. Relevance of control diet choice in metabolic studies: Impact in glucose homeostasis and vascular function. *Sci. Rep.* **2020**, *10*, 1–11. [CrossRef]
11. Keogh, J.B.; Grieger, J.A.; Noakes, M.; Clifton, P.M. Flow-mediated dilatation is impaired by a high-saturated fat diet but not by a high-carbohydrate diet. *Arterioscler. Thromb. Vasc. Biol.* **2005**, *25*, 1274–1279. [CrossRef] [PubMed]
12. Miller, M.; Beach, V.; Sorkin, J.D.; Mangano, C.; Dobmeier, C.; Novacic, D.; Rhyne, J.; Vogel, R.A. Comparative effects of three popular diets on lipids, endothelial function, and C-reactive protein during weight maintenance. *J. Am. Diet. Assoc.* **2009**, *109*, 713–717. [CrossRef] [PubMed]
13. Newens, K.J.; Thompson, A.K.; Jackson, K.G.; Wright, J.; Williams, C.M. Acute effects of elevated NEFA on vascular function: A comparison of SFA and MUFA. *Br. J. Nutr.* **2010**, *105*, 1343–1351. [CrossRef]
14. The RISCK Study Group; Sanders, T.A.B.; Lewis, F.J.; Goff, L.M.; Chowienczyk, P.J. SFAs do not impair endothelial function and arterial stiffness. *Am. J. Clin. Nutr.* **2013**, *98*, 677–683. [CrossRef]
15. Herrera, M.D.; Péerez-Guerrero, C.; Marhuenda, E.; Ruiz-Gutiéerrez, V. Effects of dietary oleic-rich oils (virgin olive and high-oleic-acid sunflower) on vascular reactivity in Wistar-Kyoto and spontaneously hypertensive rats. *Br. J. Nutr.* **2001**, *86*, 349–357. [CrossRef]
16. Huth, P.J.; Fulgoni, V.L., III; Larson, B.T. A systematic review of high-oleic vegetable oil substitutions for other fats and oils on cardiovascular disease risk factors: Implications for novel high-oleic soybean oils. *Adv. Nutr.* **2015**, *6*, 674–693. [CrossRef] [PubMed]
17. Plaza, A.; Antonazzi, M.; Blanco-Urgoiti, J.; Del Olmo, N.; Ruiz-Gayo, M. Potential Role of Leptin in Cardiac Steatosis Induced by Highly Saturated Fat Intake during Adolescence. *Mol. Nutr. Food Res.* **2019**, *63*, e1900110. [CrossRef]
18. Kilkenny, C.; Browne, W.; Cuthill, I.C.; Emerson, M.; Altman, D.G.; Group NCRRGW. Animal research: Reporting in vivo experiments: The ARRIVE guidelines. *Br. J. Pharmacol.* **2010**, *160*, 1577–1579. [CrossRef] [PubMed]
19. McGrath, J.C.; Drummond, G.B.; McLachlan, E.M.; Kilkenny, C.; Wainwright, C.L. Guidelines for reporting experiments involving animals: The ARRIVE guidelines. *Br. J. Pharmacol.* **2010**, *160*, 1573–1576. [CrossRef]
20. Gil-Ortega, M.; García-Prieto, C.F.; Ruiz-Hurtado, G.; Steireif, C.; González, M.C.; Schulz, A.; Kreutz, R.; Fernández-Alfonso, M.S.; Arribas, S.; Somoza, B. Genetic predisposition to albuminuria is associated with increased arterial stiffness: Role of elastin. *Br. J. Pharmacol.* **2015**, *172*, 4406–4418. [CrossRef]
21. Briones, A.M.; González, J.M.; Somoza, B.; Giraldo, J.; Daly, C.J.; Vila, E.; González, M.C.; McGrath, J.C.; Arribas, S.M. Role of elastin in spontaneously hypertensive rat small mesenteric artery remodelling. *J. Physiol.* **2003**, *552 Pt 1*, 185–195. [CrossRef]
22. Dobrin, P.B. Mechanical properties of arterises. *Physiol. Rev.* **1978**, *58*, 397–460. [CrossRef]
23. González, J.M.; Briones, A.M.; Starcher, B.; Conde, M.V.; Somoza, B.; Daly, C.; Vila, E.; McGrath, I.; González, M.C.; Arribas, S.M.; et al. Influence of elastin on rat small artery mechanical properties. *Exp. Physiol.* **2005**, *90*, 463–468. [CrossRef] [PubMed]
24. Bradford, M.M. A rapid and sensitive method for the quantitation of microgram quantities of protein utilizing the principle of protein-dye binding. *Anal. Biochem.* **1976**, *72*, 248–254. [CrossRef]
25. Rodríguez-Rodríguez, P.; Arribas, S.M.; De Pablo, A.L.L.; González, M.C.; Abderrahim, F.; Condezo-Hoyos, L. A simple dot-blot–Sirius red-based assay for collagen quantification. *Anal. Bioanal. Chem.* **2013**, *405*, 6863–6871. [CrossRef] [PubMed]
26. Arancibia-Radich, J.; González-Blázquez, R.; Alcalá, M.; Martín-Ramos, M.; Viana, M.; Arribas, S.; Delporte, C.; Fernández-Alfonso, M.S.; Somoza, B.; Gil-Ortega, M. Beneficial effects of murtilla extract and madecassic acid on insulin sensitivity and endothelial function in a model of diet-induced obesity. *Sci. Rep.* **2019**, *9*, 599. [CrossRef] [PubMed]
27. Garcia-Prieto, C.F.; Hernandez-Nuno, F.; Rio, D.D.; Ruiz-Hurtado, G.; Aranguez, I.; Ruiz-Gayo, M.; Somoza, B.; Fernández-Alfonso, M.S. High-fat diet induces endothelial dysfunction through a down-regulation of the endothelial AMPK-PI3K-Akt-eNOS pathway. *Mol. Nutr. Food Res.* **2015**, *59*, 520–532. [CrossRef] [PubMed]
28. Ketonen, J.; Shi, J.; Martonen, E.; Mervaala, E. Periadventitial Adipose Tissue Promotes Endothelial Dysfunction via Oxidative Stress in Diet-Induced Obese C57Bl/6 Mice. *Circ. J.* **2010**, *74*, 1479–1487. [CrossRef]
29. Virdis, A.; Colucci, R.; Bernardini, N.; Blandizzi, C.; Taddei, S.; Masi, S. Microvascular endothelial dysfunction in human obesity: Role of TNF-α. *J. Clin. Endocrinol. Metab.* **2019**, *104*, 341–348. [CrossRef]
30. Virdis, A.; Masi, S.; Colucci, R.; Chiriacò, M.; Uliana, M.; Puxeddu, I.; Bernardini, N.; Blandizzi, C.; Taddei, S. Microvascular endothelial dysfunction in patients with obesity. *Curr. Hypertens. Rep.* **2019**, *21*, 32. [CrossRef]
31. Steinberg, H.O.; Chaker, H.; Leaming, R.; Johnson, A.; Brechtel, G.; Baron, A.D. Obesity/insulin resistance is associated with endothelial dysfunction. Implications for the syndrome of insulin resistance. *J. Clin. Investig.* **1996**, *97*, 2601–2610. [CrossRef] [PubMed]
32. Strasser, B.; Arvandi, M.; Pasha, E.; Haley, A.; Stanforth, P.; Tanaka, H. Abdominal obesity is associated with arterial stiffness in middle-aged adults. *Nutr. Metab. Cardiovasc. Dis.* **2015**, *25*, 495–502. [CrossRef]
33. Manco, M.; Nobili, V.; Alisi, A.; Panera, N.; Handberg, A. Arterial stiffness, thickness and association to suitable novel markers of risk at the origin of cardiovascular disease in obese children. *Int. J. Med. Sci.* **2017**, *14*, 711–720. [CrossRef]

34. Aroor, A.R.; Jia, G.; Sowers, J.R. Cellular mechanisms underlying obesity-induced arterial stiffness. *Am. J. Physiol. Integr. Comp. Physiol.* **2018**, *314*, R387–R398. [CrossRef]
35. Kangas, P.; Tikkakoski, A.J.; Tahvanainen, A.M.; Leskinen, M.H.; Viitala, J.M.; Kähönen, M.; Kööbi, T.; Niemela, O.J.; Mustonen, J.T.; Pörsti, I.H. Metabolic syndrome may be associated with increased arterial stiffness even in the absence of hypertension: A study in 84 cases and 82 controls. *Metabolism* **2013**, *62*, 1114–1122. [CrossRef]
36. Zebekakis, P.E.; Nawrot, T.; Thijs, L.; Balkestein, E.J.; van der Heijden-Spek, J.; Van Bortel, L.M.; Struijker-Boudier, H.A.; Safar, M.E.; Staessen, J.A. Obesity is associated with increased arterial stiffness from adolescence until old age. *J. Hypertens.* **2005**, *23*, 1839–1846. [CrossRef] [PubMed]
37. Hall, W.L. Dietary saturated and unsaturated fats as determinants of blood pressure and vascular function. *Nutr. Res. Rev.* **2009**, *22*, 18–38. [CrossRef]
38. Vafeiadou, K.; Weech, M.; Sharma, V.; Yaqoob, P.; Todd, S.; Williams, C.M.; Jackson, K.G.; Lovegrove, J.A. A review of the evidence for the effects of total dietary fat, saturated, monounsaturated and n-6 polyunsaturated fatty acids on vascular function, endothelial progenitor cells and microparticles. *Br. J. Nutr.* **2012**, *107*, 303–324. [CrossRef] [PubMed]
39. Kim, F.; Tysseling, K.A.; Rice, J.; Pham, M.; Haji, L.; Gallis, B.M.; Baas, A.S.; Paramsothy, P.; Giachelli, C.M.; Corson, M.A.; et al. Free fatty acid impairment of nitric oxide production in endothelial cells is mediated by IKKbeta. *Arterioscler. Thromb. Vasc. Biol.* **2005**, *25*, 989–994. [CrossRef] [PubMed]
40. Lu, G.; Greene, E.L.; Nagai, T.; Egan, B.M. Reactive oxygen species are critical in the oleic acid–mediated mitogenic signaling pathway in vascular smooth muscle cells. *Hypertension* **1998**, *32*, 1003–1010. [CrossRef]
41. Juarez, E.; Tufiño, C.; Querejeta, E.; Bracho-Valdes, I.; Bobadilla-Lugo, R.A. Evidence of changes in alpha-1/AT1 receptor function generated by diet-induced obesity. *Diabetes Vasc. Dis. Res.* **2017**, *14*, 485–493. [CrossRef]
42. Bouvet, C.; De Chantemeèle, E.B.; Guihot, A.-L.; Vessieères, E.; Bocquet, A.; Dumont, O.; Jardel, A.; Loufrani, L.; Moreau, P.; Henrion, D. Flow-induced remodeling in resistance arteries from obese Zucker rats is associated with endothelial dysfunction. *Hypertension* **2007**, *50*, 248–254. [CrossRef]
43. Souza-Smith, F.M.; Katz, P.S.; Trask, A.J.; Stewart, J.A.; Lord, K.C.; Varner, K.J.; Vassallo, D.V.; Lucchesi, P.A. Mesenteric resistance arteries in type 2 diabetic db/db mice undergo outward remodeling. *PLoS ONE* **2011**, *6*, e23337. [CrossRef] [PubMed]
44. de Chantemele, E.J.B.; Vessieres, E.; Guihot, A.L.; Toutain, B.; Maquignau, M.; Loufrani, L.; Henrion, D. Type 2 diabetes severely impairs structural and functional adaptation of rat resistance arteries to chronic changes in blood flow. *Cardiovasc. Res.* **2009**, *81*, 788–796. [CrossRef]
45. Grassi, G.; Seravalle, G.; Scopelliti, F.; Dell'Oro, R.; Fattori, L.; Quarti-Trevano, F.; Brambilla, G.; Schiffrin, E.L.; Mancia, G. Structural and functional alterations of subcutaneous small resistance arteries in severe human obesity. *Obesity* **2010**, *18*, 92–98. [CrossRef] [PubMed]
46. Briones, A.M.; Xavier, F.E.; Arribas, S.M.; González, M.C.; Rossoni, L.V.; Alonso, M.J.; Salaices, M. Alterations in structure and mechanics of resistance arteries from ouabain-induced hypertensive rats. *Am. J. Physiol. Circ. Physiol.* **2006**, *291*, H193–H201. [CrossRef]
47. Dangardt, F.; Chen, Y.; Berggren, K.; Osika, W.; Friberg, P. Increased rate of arterial stiffening with obesity in adolescents: A five-year follow-up study. *PLoS ONE* **2013**, *8*, e57454. [CrossRef] [PubMed]
48. Nemes, A.; Gavallér, H.; Csajbók, É.; Forster, T.; Csanády, M. Obesity is associated with aortic enlargement and increased stiffness: An echocardiographic study. *Int. J. Cardiovasc. Imaging* **2007**, *24*, 165–171. [CrossRef]
49. Wildman, R.P.; Mackey, R.H.; Bostom, A.; Thompson, T.; Sutton-Tyrrell, K. Measures of obesity are associated with vascular stiffness in young and older adults. *Hypertension* **2003**, *42*, 468–473. [CrossRef]
50. Sista, A.K.; O'Connell, M.K.; Hinohara, T.; Oommen, S.S.; Fenster, B.E.; Glassford, A.J.; Schwartz, E.A.; Taylor, C.A.; Reaven, G.M.; Tsao, P.S. Increased aortic stiffness in the insulin-resistant Zucker fa/fa rat. *Am. J. Physiol. Circ. Physiol.* **2005**, *289*, H845–H851. [CrossRef]
51. Chen, J.-Y.; Tsai, P.-J.; Tai, H.-C.; Tsai, R.-L.; Chang, Y.-T.; Wang, M.-C.; Chiou, Y.-W.; Yeh, M.-L.; Tang, M.-J.; Lam, C.-F.; et al. Increased aortic stiffness and attenuated lysyl oxidase activity in obesity. *Arterioscler. Thromb. Vasc. Biol.* **2013**, *33*, 839–846. [CrossRef]
52. Briones, A.M.; Arribas, S.M.; Salaices, M. Role of extracellular matrix in vascular remodeling of hypertension. *Curr. Opin. Nephrol. Hypertens.* **2010**, *19*, 187–194. [CrossRef] [PubMed]
53. Stakos, D.A.; Tziakas, D.N.; Chalikias, G.K.; Mitrousi, K.; Tsigalou, C.; Boudoulas, H. Associations between collagen synthesis and degradation and aortic function in arterial hypertension. *Am. J. Hypertens.* **2010**, *23*, 488–494. [CrossRef] [PubMed]
54. Soares, A.G.; De Carvalho, M.H.C.; Akamine, E. Obesity induces artery-specific alterations: Evaluation of vascular function and inflammatory and smooth muscle phenotypic markers. *BioMed Res. Int.* **2017**, *2017*, 1–10. [CrossRef] [PubMed]
55. Martinez-Martinez, E.; Rodriguez, C.; Galan, M.; Miana, M.; Jurado-Lopez, R.; Bartolome, M.V.; Luaces, M.; Islas, F.; Martínez-González, J.; López-Andrés, N.; et al. The lysyl oxidase inhibitor (beta-aminopropionitrile) reduces leptin profibrotic effects and ameliorates cardiovascular remodeling in diet-induced obesity in rats. *J. Mol. Cell. Cardiol.* **2016**, *92*, 96–104. [CrossRef] [PubMed]

nutrients

MDPI

Article

Soluble Fiber Inulin Consumption Limits Alterations of the Gut Microbiota and Hepatic Fatty Acid Metabolism Caused by High-Fat Diet

Mayssa Albouery [1], Alexis Bretin [2], Bénédicte Buteau [1], Stéphane Grégoire [1], Lucy Martine [1], Ségolène Gambert [1,3], Alain M. Bron [1,4], Niyazi Acar [1], Benoit Chassaing [5,†] and Marie-Agnès Bringer [1,*,†]

[1] Centre des Sciences du Goût et de l'Alimentation, AgroSup Dijon, CNRS, INRAE, Université Bourgogne Franche-Comté, F-21000 Dijon, France; mayssa.albouery@gmail.com (M.A.); benedicte.buteau@inrae.fr (B.B.); stephane.gregoire@inrae.fr (S.G.); lucy.martine@inrae.fr (L.M.); segolene.gambert@chu-dijon.fr (S.G.); alain.bron@chu-dijon.fr (A.M.B.); niyazi.acar@inrae.fr (N.A.)
[2] Institute for Biomedical Sciences, Center for Inflammation, Immunity and Infection, Digestive Disease Research Group, Georgia State University, Atlanta, GA 30303, USA; abretin@gsu.edu
[3] Laboratoire de Biochimie Médicale, Plateforme de Biologie Hospitalo-Universitaire, F-21000 Dijon, France
[4] Department of Ophthalmology, University Hospital, F-21000 Dijon, France
[5] Inserm U1016, Team "Mucosal Microbiota in Chronic Inflammatory Diseases", CNRS UMR 8104, Université de Paris, F-75014 Paris, France; benoit.chassaing@inserm.fr
* Correspondence: marie-agnes.bringer@inrae.fr; Tel.: +33-380-69-31-11
† These authors contributed equally to this work.

Citation: Albouery, M.; Bretin, A.; Buteau, B.; Grégoire, S.; Martine, L.; Gambert, S.; Bron, A.M.; Acar, N.; Chassaing, B.; Bringer, M.-A. Soluble Fiber Inulin Consumption Limits Alterations of the Gut Microbiota and Hepatic Fatty Acid Metabolism Caused by High-Fat Diet. *Nutrients* **2021**, *13*, 1037. https://doi.org/10.3390/nu13031037

Academic Editor: Sara Ramos-Romero

Received: 9 March 2021
Accepted: 17 March 2021
Published: 23 March 2021

Abstract: Diet shapes the gut microbiota which impacts hepatic lipid metabolism. Modifications in liver fat content are associated with metabolic disorders. We investigated the extent of dietary fat and fiber-induced alterations in the composition of gut microbiota and hepatic fatty acids (FAs). Mice were fed a purified low-fat diet (LFD) or high-fat diet (HFD) containing non-soluble fiber cellulose or soluble fiber inulin. HFD induced hepatic decreases in the amounts of C14:0, C16:1n-7, C18:1n-7 and increases in the amounts of C17:0, C20:0, C16:1n-9, C22:5n-3, C20:2n-6, C20:3n-6, and C22:4n-6. When incorporated in a LFD, inulin poorly affected the profile of FAs. However, when incorporated in a HFD, it (i) specifically led to an increase in the amounts of hepatic C18:0, C22:0, total polyunsaturated FAs (PUFAs), total n-6 PUFAs, C18:3n-3, and C18:2n-6, (ii) exacerbated the HFD-induced increase in the amount of C17:0, and (iii) prevented the HFD-induced increases in C16:1n-9 and C20:3n-6. Importantly, the expression/activity of some elongases and desaturases, as well as the gut microbiota composition, were impacted by the dietary fat and fiber content. To conclude, inulin modulated gut microbiota and hepatic fatty acid composition, and further investigations will determine whether a causal relationship exists between these two parameters.

Keywords: fiber; inulin; high-fat diet; liver; metabolic syndrome; lipid; fatty acids; microbiota

1. Introduction

Long-term dietary habits influence the development of chronic diseases [1]. In particular, the adoption of Western dietary habits is strongly associated with the development of metabolic disorders [2–5]. This phenotype can be reproduced successfully and robustly in experimental models [6].

Although the molecular mechanisms involved are not fully understood, it is now well established that diet influences health partly through the pressure that the dietary nutrients exert on the gut microbiota. In addition to their exposure duration and to their dose in the diet, the nature of dietary macronutrients (proteins, carbohydrates, including fibers, and fat) is a factor that differentially influences the composition of the gut microbiota by selecting and supporting the growth of bacterial communities that harbor specific metabolic capacities. Studies in humans and in mice have shown that the fat and fiber content of the

diet deeply influences the composition of the gut microbiota and its function, which can, in turn, have profound impact on metabolic health [7–13].

The influence of fat intake as well as their source on gut microbial composition has been extensively studied [14]. Consumption of high-saturated fat diet, hereafter referred to as high-fat diet (HFD), generally results in important shifts in bacterial communities at the phylum level (e.g., decrease in Bacteroidetes and increase in Firmicutes, and Proteobacteria) as well as at the genus level (e.g., decrease in *Akkermansia muciniphila*). This reshaping of the gut microbiota modifies its functions towards higher capacities to harvest and store energy from the diet, and to induce metabolic endotoxemia and low-grade inflammation [14]. These properties make HDF-associated dysbiosis a necessary and sufficient factor to induce metabolic syndrome (MetS) and the subsequent chronic diseases [14]. Lack of soluble fiber is an important factor promoting HFD-induced metabolic disorders [15].

Dietary fibers are classified into two groups depending on their water solubility: soluble (e.g., gums, fructans, and pectins) and insoluble (e.g., cellulose, hemicellulose, and lignin). Whereas insoluble fibers resist bacterial fermentation in the colon, soluble fibers can be metabolized by the gut microbiota into bioactive molecules such as short-chain fatty acids (SCFAs), which can affect host health [16]. However, the composition and the physicochemical properties of the fibers (e.g., degree of polymerization for inulin-type fructans) are factors that can modulate their fermentation kinetics and their biological effects on the host, including on the composition of the gut microbiota [17–21]. Consumption of dietary soluble fibers has been shown to support the promotion of health beneficial bacteria (e.g., *Bifidobacterium* spp., *Lactobacillus* spp., *Akkermansia muciniphila*, and *Faecalibacterium prausnitzii*) and the suppression of bacteria with pathogenic potential (e.g., *Escherichia coli*) [22,23]. It is also associated with a decreased incidence of several metabolic disorders including hypertension, diabetes, obesity, as well as heart disease [13,24]. In particular, intake of inulin-type fructans has been shown to protect mice against HFD-induced MetS by modifying the composition and the functions of the gut microbiota [13,25–30].

A body of knowledge has accumulated and points to the gut microbiota as a key regulator of host lipid and fatty acid metabolism. Indeed, comparisons of germ-free (GF) mice with conventional or conventionalized mice have shown that gut microbes are required for proper digestion and absorption of dietary lipids and further fat storage [31,32]. The gut microbiota also plays an active role in controlling the hepatic expression of enzymes involved in lipid/fatty acid synthesis [33,34]. Fatty acids are a source of energy and are also fundamental constituents of membrane structure and functions. Depending on their nature, they can exert a panel of biological activities (e.g., regulation of signaling pathways, activation of transcription factors, and gene expression; precursors of bioactive lipid molecules) that influence health status [35]. In this study, we explored the impact of dietary fat and fiber content, individually and in combination, on the gut microbiota and hepatic fatty acid composition. Gut microbiota composition, hepatic fatty acid content, hepatic expression of enzymes involved in fatty acid biosynthesis, and their activities were analyzed in mice fed a purified low-fat or high-fat diet that were supplemented with insoluble (cellulose) or soluble (inulin) fibers.

2. Materials and Methods

2.1. Mice and Diets

C57BL/6J male mice (The Jackson Laboratory) were housed at Georgia State University, Atlanta, GA, USA (IACUC # 18006). At 6 weeks of age, mice were fed for 11 weeks a purified low-fat diet (LFD; 10% kcal fat, Research Diets Inc., New Brunswick, NJ, USA) or a purified high-fat diet (HFD; 60% kcal fat, Research Diets Inc.). As fiber source, LFD and HFD were containing either cellulose (LFDc, #D12450J and HFDc, #D12492) or inulin (LFDi, #D13081108 and HFDi #D13081106; source of inulin: chicory (Orafti®HP; BENEO-Orafti, Tienen, Belgium) with an average degree of polymerization $\geq$ 23) (Tables 1 and 2). The number of mice per group was n = 12 for LFDc, n = 11 for LFDi, n = 12 for HFDc and n = 12 for HFDi.

Table 1. Composition of diets used in this study.

Diets	LFDc [1] D12450J [5]	LFDi [2] D13081108 [5]	HFDc [3] D12492 [5]	HFDi [4] D13081106 [5]
Protein source	Casein	Casein	Casein	Casein
Fiber source	Cellulose	Inulin	Cellulose	Inulin
Protein (kcal%)	20	20	20	20
Carbohydrates (kcal%)	70	65	20	20
Fat (kcal%)	10	10	60	60
kcal/gm	3.8	3.5	5.24	4.6
Ingredients (g)				
Casein	200	200	200	200
L-Cystine	3	3	3	3
Corn Starch	506.2	456.2	0	0
Maltodextrin 10	125	125	125	75
Sucrose	63.8	63.8	68.8	68.8
Cellulose	50	0	50	0
Inulin	0	200	0	200
Soybean Oil	25	25	25	25
Lard	20	20	245	245
Mineral Mix, S10026	10	10	10	10
DiCalcium Phosphate	13	13	13	13
Calcium Carbonate	5.5	5.5	5.5	5.5
Potassium Citrate, 1 H_2O	16.5	16.5	16.5	16.5
Vitamin Mix, V10001	15	15	10	10
Choline Bitartrate	2	2	2	2

[1] LFDc: Low-fat diet supplemented with cellulose; [2] LFDi: Low-fat diet supplemented with inulin; [3] HFDc: High-fat diet supplemented with cellulose; [4] HFDi: High-fat diet supplemented with inulin; [5] Research Diets Inc.

At the end of the experimental period, feces were collected for microbiota analyses. Prior to euthanasia, mice were fasted for 15 h and mice were then weighted. Blood was collected by retrobulbar venous plexus puncture and hemolysis-free serum was generated by centrifugation using serum separator tubes for glucose determination (Becton Dickinson, Franklin Lakes, NJ, USA). Euthanasia was performed by cervical dislocation. After euthanasia, epididymal fat pad weights were measured. Livers were collected for fatty acid analyses.

2.2. Determination of Blood Glucose Concentration

Blood glucose concentration was measured using a glucometer (Nova Max, Waltham, MA, USA).

2.3. Quantification of Serum Lipids and Lipoproteins

Concentrations of plasma total cholesterol, HDL-cholesterol, LDL-cholesterol, and triglycerides were determined in samples having a suitable plasma volume ($n = 7$ for LFDc, $n = 8$ for LFDi, $n = 6$ for HFDc, and $n = 7$ for HFDi) to be analyzed using a Vista analyzer (Siemens Healthcare Diagnostics, Deerfield, IL, USA).

2.4. Lipid Extraction and Determination of Fatty Acid Profiles in Livers

Hepatic lipids were extracted using the Folch Procedure [36] and transmethylated using boron trifluoride in methanol [37]. The FA methyl esters (FAMEs) were analyzed by gas chromatography coupled with flame ionization detection (GC-FID) as previously described [33]. The data were processed using the ChromQuest software (Thermo Fisher Scientific Inc., Illkirch, France). They were expressed as a percentage relative to total FAMEs, defined as 100%.

Table 2. Fatty acid composition of the diets.

Fatty Acids [1]	Low-Fat Diet	High-Fat Diet
C10:0	0.0	0.0
C12:0	0.0	0.1
C14:0	0.5	1.1
C15:0	0.0	0.1
C16:0	14.9	19.6
C16:1	0.7	1.3
C17:0	0.2	0.4
C18:0	7.1	10.6
C18:1	28.8	34.0
C18:2n-6	41.9	28.7
C18:3n-3	5.0	2.0
C20:0	0.0	0.2
C20:1	0.2	0.6
C20:3n-6	0.0	0.1
C20:4n-6	0.2	0.3
C20:5n-3	0.0	0.0
C22:0	0.0	0.0
C22:1	0.0	0.0
C22:4n-6	0.0	0.0
C22:5n-3	0.0	0.1
C22:5n-6	0.0	0.0
C22:6n-3	0.0	0.0
C24:0	0.0	0.0
Total SFA	22.7	32.0
Total MUFA	29.7	36.0
Total PUFA	47.1	31.2
C18:2n-6/C18:3n-3	8.3	14.1
PUFA n-6/PUFA n-3	8.4	13.7

[1] g for 100 g.

Table 3. List of primers.

Genes	Forward Primers (5′-3′)	Reverse Primers (5′-3′)
Scd1	CAGGAGGGCAGGTTTCCAAG	CGTTCATTTCCGGAGGGAGG
Fads1	CGCCAAACGCGCTACTTTAC	CCACAAAAGGATCCGTGGCA
Fads2	CGTGGGCAAGTTCTTGAAGC	TCTGAGAGCTTTTGCCACGG
Elovl1	CCTGAAGCACTTCGGATGGT	TCACTTGCCCGTCCTTCTTC
Elovl2	GTGATGTCCGGGTAGCCAAG	GGACGCGTGGTGATAGACAT
Elovl3	TACTTCTTTGGCTCTCGCCC	AGCTTACCCAGTACTCCTCCA
Elovl5	TGATGAACTGGGTTCCCTGC	CAGCTGCCCTTGAGTGATGT
Elovl6	AGAACACGTAGCGACTCCGA	TCAGATGCCGACCACCAAAG

Scd1: Stearoyl-CoA desaturase 1; *Fads1* and 2: Fatty acid desaturase 1 and 2; *Elovl1*, *2*, *3*, *5*, and *6*: Elongation of very long chain fatty acids protein 1, 2, 3, 5 and 6.

2.5. Gene Expression

Gene expression was determined as previously described [38]. The mouse-specific primers used in this study are described in Table 3. Results were normalized to the housekeeping *Hprt* gene.

2.6. Microbiota Analysis by 16S rRNA Gene Sequencing Using Illumina Technology

For microbiota analysis, fresh feces were collected, snap-frozen in liquid nitrogen and stored at −80 °C. 16S rRNA gene amplification and sequencing were done using the Illumina MiSeq technology as previously extensively described [39].

2.7. Statistical Analyses

The data are presented as mean ± standard deviation (SD) or mean ± standard deviation of the mean (SEM). Statistical and correlation analyses were performed using

the GraphPad Prism software (GraphPad Software Inc., San Diego, CA, USA). Normality was tested by using D'Agostino and Pearson test and Shapiro–Wilk test. Data from the different groups were compared by using One-Way ANOVA Multiple comparison tests corrected with Bonferroni test. The p values of less than 0.05 were considered as statistically significant (* $p < 0.05$, ** $p < 0.01$, *** $p < 0.001$ and **** $p < 0.0001$).

3. Results

3.1. Enrichment of Diet with Inulin Impacts the Metabolic Parameters

In this study, we compared the impact of LFD and HFD supplementation with insoluble fiber (cellulose) or soluble fiber (inulin) on several metabolic parameters associated with MetS development (Figure 1).

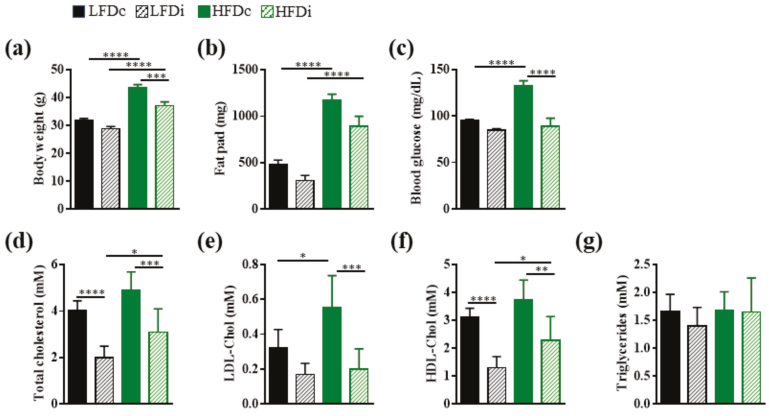

Figure 1. Metabolic parameters. Mice were fed low-fat diet (LFD) supplemented with cellulose (LFDc) or inulin (LFDi), or high-fat diet (HFD) supplemented with cellulose (HFDc) or inulin (HFDi) for 11 weeks. Mice were monitored for body weight (**a**), fat pad (**b**), 15h-fasting blood glucose (**c**) and serum concentration of total cholesterol (**d**), LDL-cholesterol (LDL-Chol; (**e**)), HDL-cholesterol (HDL-Chol; (**f**)) and triglycerides (**g**). Body weight, fat pad and blood glucose analyses are presented as mean ± SEM (n = 12 for the LFDc, HFDc and HFDi groups and n = 11 for the LFDi group). Lipid and lipoprotein concentrations are presented as mean ± SD (n = 8 for the LFDi group, n = 7 for the LFDc and HFDi groups, and n = 6 for the HFDc group). * $p < 0.05$, ** $p < 0.01$, *** $p < 0.001$ and **** $p < 0.0001$.

When added to a purified low-fat diet, inulin did not alter neither the body weight of mice, their adiposity, as assessed by fat pad mass measurement, nor their blood glucose concentration, as assessed by measuring blood glucose concentration in a fasting state (Figure 1a–c). However, the level of cholesterol, and particularly that of HDL-cholesterol, was significantly ($p < 0.0001$) decreased in LFDi-fed mice compared to LFDc-fed mice (HDL-cholesterol, LFDi: 1.31 ± 0.14 mM and LFDc: 3.10 ± 0.12 mM; Figure 1d–f).

We previously reported that mice fed HFD compared to those fed LFD develop MetS features (Figure 1a–f; [38]). We showed that the body weight of mice fed HFDi was significantly ($p < 0.001$) decreased compared to those fed HFDc (HFDi: 37.12 ± 0.39 g and HFDc: 43.67 ± 0.29 g; Figure 1a). This phenotype was associated with a decrease in fat deposition in HFDi-fed mice compared to HFDc-fed mice but the difference in fat pad mass between these two groups did not reach statistical significance (Figure 1b). Moreover, inulin significantly prevented HFD-associated dysglycemia and hypercholesterolemia (Figure 1c–f). Blood glucose concentration and levels of LDL, HDL, as well as total cholesterol in HFDi-fed mice were similar to those of LFDc-fed mice (Figure 1c–f). It should be noted that we did not observe any effect of the diets on the serum triglyceride levels of mice (Figure 1g).

All of these results show that inulin has a cholesterol-lowering effect and is effective in preventing metabolic disturbances induced by HFD.

3.2. Inulin Supplementation Induces Specific Changes in the Gut Microbiota of Mice Fed LFD or HFD

As diet is a major modulator of the gut microbiota, we examined next the modifications in microbiota composition according to the fat and fiber content of the diet (Figure 2 and Appendix A, Figure A1). As presented in Figure 2a, beta diversity analysis importantly revealed profound alterations of microbiota composition in HFD-fed mice compared with LFD-fed mice, along the PC1 axis, both for cellulose- and inulin-supplemented diets. Furthermore, a fiber effect was observed for both LFD- and HFD-fed mice along the PC2 axis, demonstrating that both fat and fiber, to a lesser extent, impact the fecal microbiota composition. Investigation of alpha diversity demonstrated a fat effect in decreasing microbiota alpha diversity, without any beneficial effect associated with soluble fiber supplementation (Figure 2b). Taxonomic analysis demonstrated, among numerous modifications, a decrease in the abundance of *Akkermansia muciniphila* induced by HFD when compared with LFD (Figures 2c and A1), as previously described [40,41], while inulin supplementation failed to prevent such loss, further demonstrating the profound impact of dietary component in regulating this microbiota member. Moreover, Linear discriminant analysis Effect Size (LEfSe) approach demonstrated that inulin supplementation had a specific impact on the intestinal microbiota based on diet fat content, with for example, an impact on *Ruminococcus gnavus* under LFD diet and an impact on the Bacteroidetes phylum under HFD diet (Figure A1). Altogether, this microbiota composition analysis demonstrated that both fat content and fiber content have profound impacts on microbiota composition.

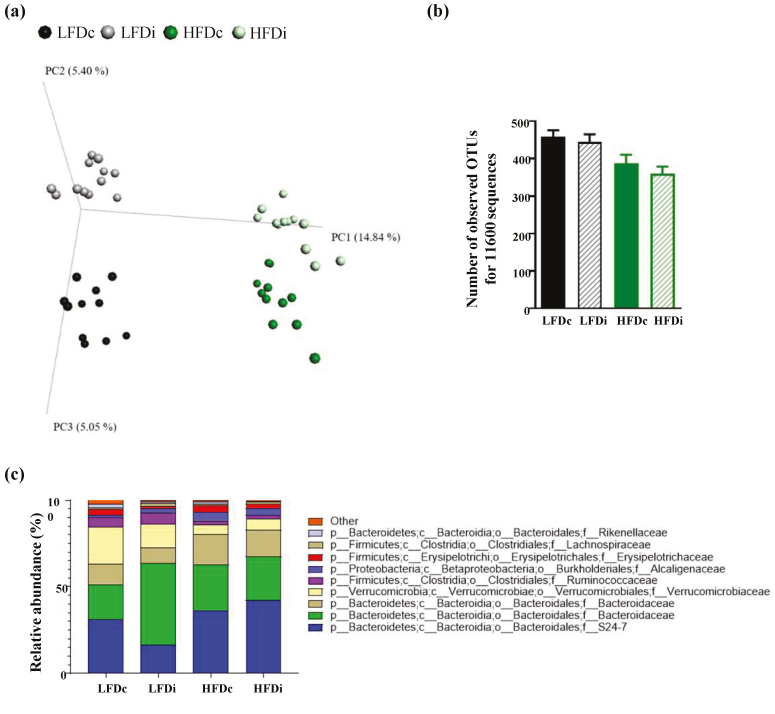

Figure 2. Microbiota composition analysis. Mice were fed low-fat diet (LFD) supplemented with cellulose (LFDc) or inulin (LFDi), or high-fat diet (HFD) supplemented with cellulose (HFDc) or inulin (HFDi) for 11 weeks. (**a**) Microbiota composition was analyzed at the final time point, and principal coordinate analysis of the unweighted Unifrac distance was plotted. (**b**) Alpha rarefaction was analyzed using the number of observed OTUs, and (**c**) microbiota was taxonomically summarized at the family level. For alpha diversity analyses, data are presented as mean ± SEM (n = 12 for the LFDc, HFDc and HFDi groups and n = 11 for the LFDi group).

3.3. Inulin Supplementation Modulates Hepatic Fatty Acid Profile

Given the roles of the gut microbiota in the regulation of the hepatic fatty acid metabolism, together with the diet-induced modifications of the gut microbiota composition, we sought to determine and compare hepatic fatty acid profiles of mice exposed to LFD and HFD supplemented with cellulose or inulin. Analyses of fatty acids were performed by GC-FID and the amount of each fatty acid was determined relative to total fatty acid content (Figures 3–5).

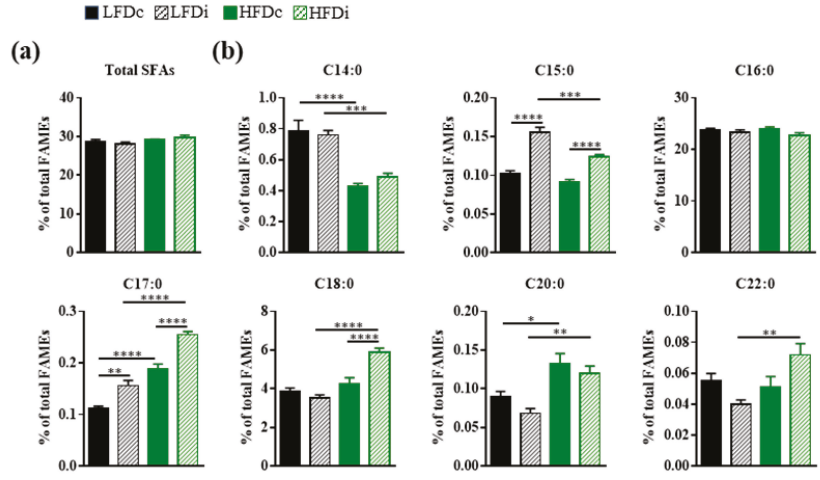

Figure 3. Hepatic content in saturated fatty acids. Mice were fed low-fat diet (LFD) supplemented with cellulose (LFDc) or inulin (LFDi), or high-fat diet (HFD) supplemented with cellulose (HFDc) or inulin (HFDi) for 11 weeks. Percentages of (**a**) total saturated fatty acids (SFAs) or (**b**) individual SFAs relative to total FAMEs. Data are presented as mean ± SEM (n = 12 for the LFDc and HFDc groups and n = 11 for the LFDi and HFDi groups). * $p < 0.05$, ** $p < 0.01$, *** $p < 0.001$ and **** $p < 0.0001$.

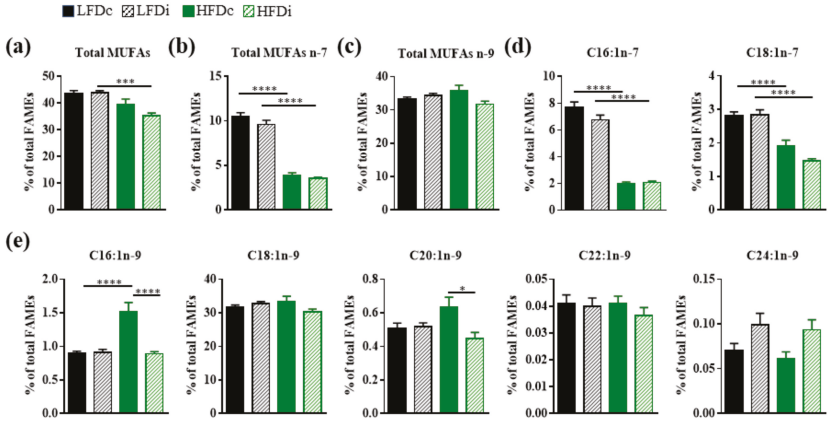

Figure 4. Impact of fat and inulin on the hepatic abundance of monounsaturated fatty acids. Mice were fed low-fat diet (LFD) supplemented with cellulose (LFDc, black bars) or inulin (LFDi, hatched black bars), or high-fat diet (HFD) supplemented with cellulose (HFDc, green bars) or inulin (HFDi, hatched green bars) for 11 weeks. Percentages of (**a**) total monounsaturated fatty acids (MUFAs), (**b**) total omega-7 MUFAs, (**c**) total omega-9 MUFAs, (**d**) individual omega-7 MUFAs or (**e**) individual omega-9 MUFAs relative to total FAMEs. Data are presented as mean ± SEM (n = 12 for the LFDc and HFDc groups and n = 11 for the LFDi and HFDi groups). * $p < 0.05$, *** $p < 0.001$ and **** $p < 0.0001$.

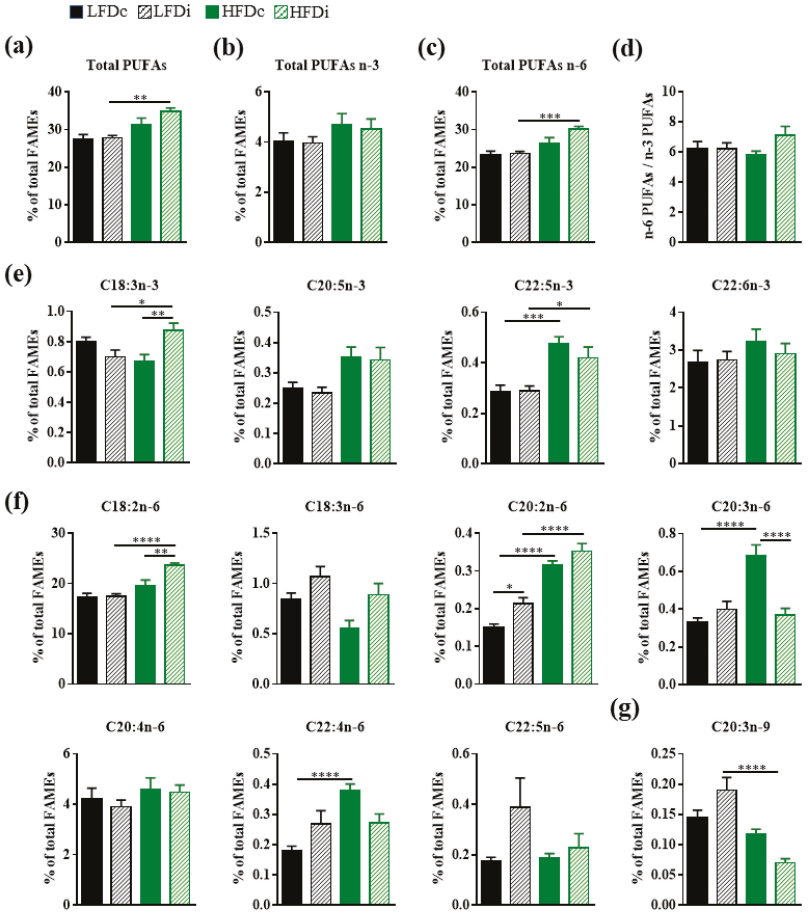

Figure 5. Impact of fat and inulin on the hepatic abundance of polyunsaturated fatty acids. Mice were fed low-fat diet (LFD) supplemented with cellulose (LFDc, black bars) or inulin (LFDi, hatched black bars), or high-fat diet (HFD) supplemented with cellulose (HFDc, green bars) or inulin (HFDi, hatched green bars) for 11 weeks. Percentages of (**a**) total polyunsaturated fatty acids (PUFAs), (**b**) total omega-3 (n-3) PUFAs, (**c**) total omega-6 (n-6) PUFAs, (**d**) overall n-6 PUFAs/n-3 PUFAs ratio, (**e**) individual n-3 PUFAs, (**f**) individual n-6 PUFAs or (**g**) individual omega-9 (n-9) PUFA relative to total FAMEs. Data are presented as mean ± SEM (n = 12 for the LFDc and HFDc groups and n = 11 for the LFDi and HFDi groups). * $p < 0.05$, ** $p < 0.01$, *** $p < 0.001$ and **** $p < 0.0001$.

3.3.1. Saturated Fatty Acids

Regardless of the diet, no changes were observed neither in the hepatic abundance of total saturated fatty acids (SFAs; Figure 3a) nor in that of palmitic acid (C16:0), the most abundant SFA in the liver (Figure 3b). However, there were several diet-related modifications among other SFA species. Compared to LFD-fed mice, the livers of HFD-fed mice had significantly decreased amounts of C14:0, both in condition of supplementation with cellulose (LFDc vs. HFDc; $p < 0.0001$) and inulin (LFDi vs. HFDi, $p < 0.001$), and C15:0 but only in condition of inulin supplementation (LFDi vs. HFDi; $p < 0.001$; Figure 3b). In contrast, the amounts of C17:0 and C20:0 were increased in the livers of HFD-fed mice compared to those of LFD-fed mice in condition of supplementation with cellulose (LFDc vs. HFDc; C17:0, $p < 0.0001$ and C20:0, $p < 0.05$) and inulin (LFDi vs. HFDi; C17:0, $p < 0.0001$ and C20:0, $p < 0.01$). However, the amounts of C18:0 and C22:0

were increased only in condition of supplementation with inulin (LFDi vs. HFDi; C18:0, $p < 0.0001$ and C22:0, $p < 0.01$; Figure 3b).

In addition to the effect of fat, the type of fiber incorporated in the diet modulated the hepatic content in SFAs. Indeed, hepatic amounts of C15:0 and C17:0 were significantly increased in the livers of mice fed inulin-supplemented LFD (C15:0, $p < 0.0001$ and C17:0, $p < 0.05$) and HFD ($p < 0.0001$) compared to those fed with cellulose-supplemented diets (Figure 3b). Similarly, the level of C18:0 was significantly ($p < 0.0001$) increased in the livers of HFDi-fed mice compared to those of HFDc-fed mice (Figure 3b). No effect of inulin was observed on the hepatic amounts of C14:0, C20:0, and C22:0.

3.3.2. Monounsaturated Fatty Acids

The fat and fiber contents of the diets also impacted the hepatic content in monounsaturated fatty acids (MUFAs; Figure 4). The livers of HFD-fed mice had significantly decreased amounts of total MUFAs in condition of supplementation with inulin when compared to LFD-fed mice ($p < 0.001$; Figure 4a). HFD was associated with significant ($p < 0.0001$) decreases in the amount of MUFAs from the omega-7 (n-7) series regardless of its fiber content (Figure 4b,d). A significant ($p < 0.0001$) increase in the hepatic amount of C16:1n-9 was also observed in mice fed HFDc compared to those fed LFDc (Figure 4e). Whereas this fiber had no effect on the hepatic amounts of MUFAs n-7 in both LFD and HFD-fed mice, inulin significantly ($p < 0.0001$) prevented the HFD-related increase in the hepatic amount of C16:1n-9 and ($p < 0.05$) decrease in the amount of hepatic C20:1n-9 in HFD-fed mice (Figure 4d,e).

3.3.3. Polyunsaturated Fatty Acids

Several diet-related changes were also observed in the hepatic content in polyunsaturated fatty acids (PUFAs; Figure 5). Whereas the hepatic amount of total polyunsaturated fatty acids (PUFAs) was similar in mice fed LFDc and HFDc, it was significantly increased in the livers of mice fed HFDi compared to those fed LFDi ($p < 0.01$; Figure 5a). These results may be ensued from modifications affecting PUFAs from the omega-6 (n-6) series. Indeed, significant increases in the amounts of total n-6 PUFAs ($p < 0.001$) and particularly those of C18:2n-6 ($p < 0.0001$), which is the most abundant n-6 PUFA and is the precursor of the fatty acids from the n-6 series, and C20:2n-6 ($p < 0.0001$) were observed in the livers of HFDi-fed mice compared to LFDi-fed mice (Figure 5c,f). Amongst PUFAs from the omega-3 (n-3) series, the hepatic levels of C18:3n-3 ($p < 0.05$) and C22:5n-3 ($p < 0.05$) were also significantly increased in mice fed HFDi compared to LFDi but these changes did not lead to significant modification in the hepatic content of total n-3 PUFAs (Figure 5e). In contrast, the amount of the only PUFA from the omega-9 (n-9) series detected in the liver, C20:3n-9, was significantly ($p < 0.0001$) decreased in mice fed HFDi compared to those fed LFDi (Figure 5g). Fat-related modifications in several PUFAs were also observed in condition of diet supplementation with cellulose. We previously reported that HFD induced an increase in the hepatic amounts of C20:2n-6 and C20:3n-6 [38]. Here we showed that C22:5n-3 and C22:4n-6 amounts were also significantly increased in the liver of HFDc-fed mice compared to LFDc-fed mice (Figure 5e,f).

Except for the C20:2n-6 whose level was significantly ($p < 0.05$) increased in LFDi-fed mice compared to LFDc mice, inulin supplementation of the LFD did not modify the hepatic PUFA content (Figure 5). In contrast, the amounts of C18:3n-3 and C18:2n-6 were significantly increased in the livers of HFDi-fed mice compared to HFDc-fed mice ($p < 0.01$, Figure 5e,f). In addition, we showed that inulin supplementation of HFD enabled to prevent the increase in the amount of C20:3n-6 caused by this diet ($p < 0.0001$, Figure 5f).

Of note, the fat and fiber content of the diets did not impact the overall hepatic ratio of n-6 PUFAs to n-3 PUFAs (Figure 5d).

Altogether, these results showed that the hepatic composition in fatty acids is modulated by both the fat and the fiber content of the diet. In addition, inulin is effective

in preventing several changes affecting the hepatic fatty acid composition induced by HFD consumption.

3.4. Fatty Acid Elongase and Desaturase Expressions in the Liver Are Modulated by the Fat and Fiber Content of the Diet

Several studies support the role of gut microbes in the regulation of the hepatic fatty acid metabolism [34,42,43]. In view of the changes in gut microbiota and the hepatic modifications in the fatty acid content that we observed in mice fed different diets, we sought to examine the expression of several enzymes involved in the desaturation and elongation of fatty acids in the liver (Figure 6).

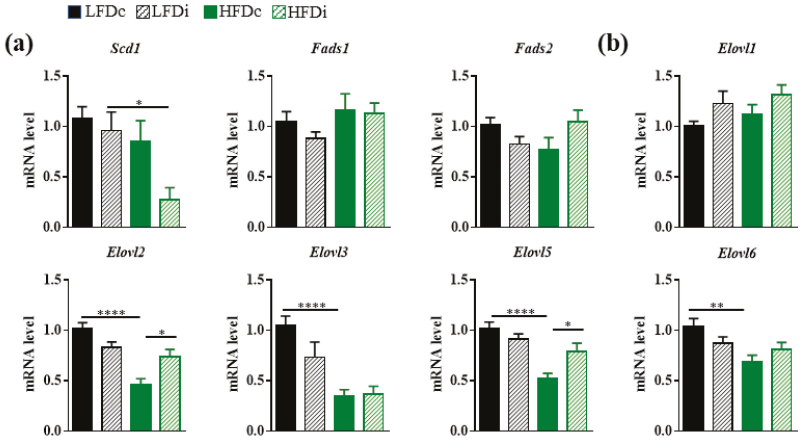

Figure 6. Modulation of hepatic gene expressions involved in lipid biosynthesis by the diet. Mice were fed low-fat diet (LFD) supplemented with cellulose (LFDc, black bars) or inulin (LFDi, hatched black bars), or high-fat diet (HFD) supplemented with cellulose (HFDc, green bars) or inulin (HFDi, hatched green bars) for 11 weeks. (**a**) Hepatic expression of genes encoding enzymes involved in the desaturation of fatty acids: acyl-CoA desaturase 1 (Scd1), acyl-CoA (8-3)-desaturase (Fads1) and acyl-CoA 6-desaturase (Fads2). (**b**) Hepatic expression of genes encoding enzymes involved in the elongation of fatty acids: elongation of very long chain fatty acids proteins 1, 2, 3, 5 and 6 (Elovl1, Elovl2, Elovl3, Elovl5 and Elovl6). The levels of mRNA were normalized to Hprt mRNA level for calculation of the relative levels of transcripts. mRNA levels are illustrated as fold change. Data are presented as mean ± SEM (n = 10-12 in each group). * $p < 0.05$, ** $p < 0.01$ and **** $p < 0.0001$.

The expression levels of the genes encoding the desaturases FADS1 (acyl-CoA (8-3)-desaturase) and FADS2 (acyl-CoA 6-desaturase) and the elongase ELOVL1 (elongation of very long chain fatty acids protein 1) remained similar in the livers of mice regardless of the diets they were exposed to (Figure 6a,b). However, we showed that the expression level of Scd1 that encodes a delta-9 desaturase and is the rate limiting enzyme that catalyzes the biosynthesis of MUFAs, was significantly ($p < 0.05$) decreased by 3.6-fold in the livers of HFDi-fed mice compared to LFDi-fed mice (Figure 6a). We previously reported that HFD induced a decrease in the expression levels of Elovl2 and Elovl5 [38]. Here, chronic exposure to HFD also induced significant decreases in the hepatic expression levels of other elongases (Figure 6b). Indeed, the mRNA levels of Elovl3 and Elovl6 where significantly decreased by 3.0-fold ($p < 0.0001$) and 1.5-fold ($p < 0.01$), respectively, in the livers of mice fed HFDc compared to those fed LFDc. Interestingly, supplementation of the HFD with inulin limited the dysregulation of the hepatic Elovl2 and Elovl5 expression (Figure 6b). Interestingly, correlation analysis revealed some positive and negative correlations between the relative abundance of microbiota members and the expression of these hepatic genes involved in lipid biosynthesis, suggesting that direct interaction between the intestinal microbiota and hepatic gene expression could exist (Appendix A, Figure A2).

These results show that the fat content of the diet modulates the saturation and desaturation program of fatty acids in the liver. Inulin was efficient in limiting some of the HFD-induced dysregulations that affected the expression of elongases.

3.5. The Hepatic Activity of Enzymes Involved in the Biosynthesis of Fatty Acids Is Modulated by the Fat and Fiber Content of the Diet

The fatty acid content of the liver depends on several factors that include the amounts of precursors provided by the diet, the expression of enzymes that regulate the length and the unsaturation of the fatty acids but also the degree of activity of these enzymes. Based on the amounts of precursors and specific fatty acids, we estimated, when possible, the hepatic activity of several desaturases and elongases (Figure 7). Our results showed that HFD induced a decrease of the SCD1 activity for the production of MUFAs (C16:1n-7 and C18:1n-9). However, we observed that the production of C16:1n-7 from C16:0 was impaired regardless of the fiber content of the HFD whereas the production of C18:1n-9 from C18:0 was only decreased in mice fed with the inulin-supplemented HFD (Figure 7a). The activity of FADS1 was not modulated by the diet (Figure 7b). Nevertheless, we showed that FADS2 activity was decreased in HFD-fed mice compared to LFD-fed mice when the diets were supplemented with cellulose and that addition of inulin to HFD enabled to protect against this loss of activity (Figure 7c). Regarding elongase activities, we showed that the fat or fiber content of the diet had no impact on ELOVL3 activity (Figure 7d). In addition, ELOVL2 and ELOVL5 activities were increased in the liver of HFD-fed mice compared to LFD-fed mice (Figure 7e). Supplementation of HFD with inulin prevented this effect (Figure 7e). In addition, supplementing HFD with inulin also increased ELOVL6 activity (Figure 7g).

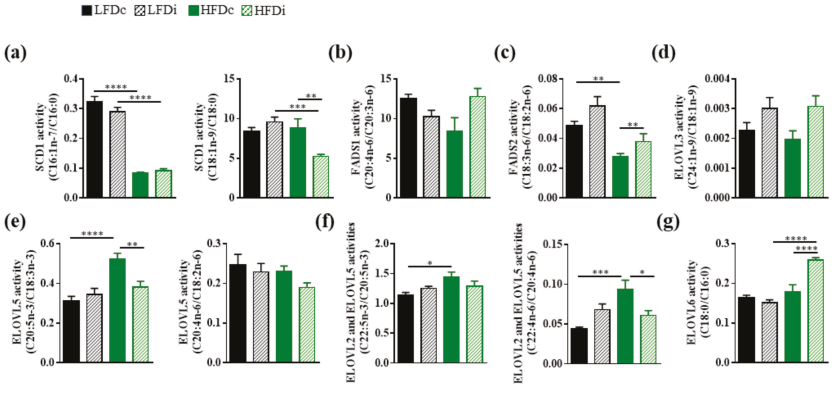

Figure 7. Modulation of the hepatic activities of enzymes involved in fatty acid biosynthesis by the diet. Mice were fed low-fat diet (LFD) supplemented with cellulose (LFDc, black bars) or inulin (LFDi, hatched black bars), or high-fat diet (HFD) supplemented with cellulose (HFDc, green bars) or inulin (HFDi, hatched green bars) for 11 weeks. (**a**) SCD1 activity corresponding to the ratio "product" (C16:1n-7 or C18:1n-9)/"precursor" (C16:0 or C18:0). (**b**) FADS1 activity corresponding to the ratio "product" (C20:4n-6)/"precursor" (C20:3n-6). (**c**) FADS2 activity corresponding to the ratio "product" (C18:3n-6)/"precursor" (C18:2n-6). (**d**) ELOVL3 activity corresponding to the ratio "product" (C24:1n-9)/"precursor" (C18:1n-9). (**e**) ELOVL5 activity corresponding to the ratio "product" (C20:5n-3 or C20:4n-6)/"precursor" (C18:3n-3 or C18:2n-6). (**f**) ELOVL2 and ELOVL5 activities corresponding to the ratio "product" (C22:5n-3 or C22:4n-6)/"precursor" (C20:5n-3 or C20:4n-6). (**g**) ELOVL6 activity corresponding to the ratio "product" (C18:0)/"precursor" (C16:0). Data are presented as mean ± SEM (n = 11–12 in each group). * $p < 0.05$, ** $p < 0.01$, *** $p < 0.001$ and **** $p < 0.0001$.

Altogether, these results showed that the fat content of the diet modulated the hepatic activity of several enzymes involved in the fatty acid biosynthesis and that supplementation of HFD with inulin enabled to partly prevent these changes. However, inulin had no effect on the activity of these enzymes in a standard diet.

4. Discussion

Quality, quantity, as well as the origin of the ingested food are factors that can deeply influence human health. Among other roles, nutrition plays a significant part in the maintenance of the symbiotic interplay between gut microbes and the host, which are essential for the proper operation of the host's biological functions. Composition of the diet, dietary patterns, as well as dietary habits are factors that shape the gut microbiota, and destabilization of the latter can affect the health status, particularly by influencing liver metabolism [1,3]. In this study, we aimed at investigating the impact of dietary fat and fiber contents on the gut microbiota composition and lipid metabolism in the liver.

Chronic exposure to HFD is known to induce an abnormal hepatic accumulation of lipids, including fatty acids [44]. These lipid dysregulations may have deleterious consequences, such as the promotion of hepatotoxicity and chronic inflammation, as well as the exacerbation of insulin resistance [45]. In this study, we have chosen to focus on the qualitative modifications that occur in the hepatic fatty acid profile after a chronic exposure to HFD. Indeed, both the quantity and the nature of the fatty acids can influence biological processes [46,47]. We found that a chronic exposure to HFD did not modify the relative abundance of total SFAs, MUFAs, and PUFAs in the liver. This result was in disagreement with previous studies showing an increase in the amount of SFAs and a decrease in that of PUFAs in the livers of HFD-fed mice compared to those of LFD-fed mice [44,48]. However, this discrepancy could ensue from variations in different parameters such as the fatty acid content of the diets, the duration of exposure to the diets, the type of targeted lipids for the fatty acid analysis, and the differences in the genetic background of the used mouse strains [49]. However, when considering the qualitative composition of hepatic lipids, several changes in the fatty acids profile were observed. Among SFAs, HFD impaired only the relative abundance of a few species that are poorly represented in the liver. These modifications concerned the C14:0, whose hepatic amount was decreased, and the C17:0 and C20:0, whose hepatic amounts were increased in HFD-fed mice. In addition, we showed that HFD feeding led to substantial modifications among hepatic MUFAs. In particular, the amount of the MUFAs from the n-7 series (C16:1n-7 and C18:1n-7), which represent 10% of total fatty acids in the liver of LFD-fed mice, was twofold decreased in the livers of HFD-fed mice. Moreover, the amount of C16:1n-9 was increased in the liver of HFD-fed mice. However, the amount of C18:1n-9, the most abundant MUFA in the liver, was unaffected by the diet. Finally, the hepatic amounts of several PUFAs (C22:5n-3, C20:2n-6, C20:3n-6 and C22:4n-6) were increased in the livers of HFD-fed mice. Although some parameters were not similar (e.g., mouse strain, and formulation of the HFD), it is interesting to note that some of these alterations (decreases in the amounts of C14:0, C16:1n-7 and increases in the amounts of C16:1n-9 and C22:4n-6) were similar to those reported by others in the liver of mice [44]. Some of the alterations we highlighted could have biological consequences. Myristic acid (C14:0) can be transferred to proteins by processes named N-myristoylation and lysine myristoylation [50]. These posttranslational modifications influence several physiological processes (e.g., immune responses, cell proliferation, differentiation, survival, and cell death) by modifying or stabilizing protein conformation, influencing protein–protein interactions, enhancing subcellular targeting endomembranes and plasma membranes, and to receptors. In addition, several immune-metabolic effects have been reported for palmitoleic acid (C16:1n-7) and vaccenic acid (C18:1n-7). In particular, they exert beneficial effects on MetS by reducing inflammation and improving some of its features such as hepatic lipid deposition and insulin sensitivity [51]. Finally, high levels of dihomo-gamma-linolenic acid (DGLA, C20:3n-6) have been reported in the plasma of obese subjects and in patients with liver steatosis [52,53].

These changes in the fatty acid content of the liver may have different origins. Indeed, we cannot exclude that they are directly related to the fatty acid formulation of the diet. Indeed, the amounts of C17:0, C20:0, C16:1, C22:5n-3, and C20:3n-6 and some precursors such as C20:4n-6 were higher in HFD compared to LFD. Another hypothesis is that the

changes in the fatty acid content of the liver result from modulation of host lipid metabolism. Indeed, HFD-associated changes in the fatty acid content of the liver could also be related to modifications in the expression levels or activity of the enzymes involved in their biosynthesis. The biosynthesis of MUFAs from SFAs is catalyzed by SCD-1, also known as delta-9 desaturase. Its substrates are C16:0 and C18:0, which yield 16:1n-7 and 18:1n-9, respectively. Conflicting results have been reported in the literature regarding expression of *Scd1* in mice exposed to HFD and/or in mouse models of MetS [42,43,54]. In our study, we showed that the hepatic expression level of *Scd1* was unchanged by the diet. Moreover, when looking at the hepatic SCD-1 activity towards its different substrates, we observed that, while the conversion of C18:0 into C18:1n-9 was unchanged, the conversion C16:0 into C16:1n-7 was a 3.9-fold decrease in the liver of HFD-fed mice. Others have already described such ambivalence in the SCD1 activity regarding its substrate to produce preferentially n-7 or n-9 MUFAs in mice fed with HFD [44]. Regarding the biosynthesis of PUFAs, their degree of unsaturation and their length are regulated by desaturases in conjunction with elongases. In agreement with previous studies, the livers of HFD-fed mice had no modifications in the expression levels of *Fads1* and *Fads2* mRNAs, which encode a delta-5 desaturase and a delta-6 desaturase respectively but had a decrease in the activity of FADS2 [43,44,55]. In addition, while a decrease in the expression levels of several genes involved in the elongation of fatty acids (*Elovl2*, *Elovl3*, *Elovl5*, and *Elovl6*) was observed as already reported by others [43], the activity of ELOVL5 and ELOVL2 were increased in the liver of mice fed a HFD. Such results could explain, at least in part, the increase of the hepatic amounts that we observed for some PUFAs. Finally, in accordance with a previous study, we found that ELOVL6 activity was not modified in the liver of mice fed with a HFD [44].

Inulin is a non-digestible functional polysaccharide that belongs to the fructan carbohydrate subgroup. It is composed of β-D-fructosyl units (from 2 to 60 monomers) that are linked together by (2→1) glycosidic bonds and it usually ends with a (1→2) D-glucosyl moiety. It is present in some plants such as chicory roots, Jerusalem artichoke tubers, salsify roots, garlic bulbs and leek bulbs. The daily intake of inulin is estimated to be between 1 and 10 g in Western countries with a higher consumption by Europeans than North Americans [56–59]. So far, no toxicity has been reported for inulin consumption neither in animals nor in humans. However, gastrointestinal intolerance can be observed when inulin is consumed at high levels, with the daily dietary fiber recommendations for humans being a dose of up to 20 g. In this study, diet was supplemented with a relatively high dose of 200 g of inulin/kg of food for 11 weeks. Follow up studies appear warranted to study the impact of lower dose on a longer period in order to mimic humans' exposure. A limitation of this study is that the food intake has not been measured so the daily dietary inulin intake cannot be estimated.

Insoluble fibers, such as cellulose, are generally poorly fermented by gut microbes. Cellulose is used as a core constituent of HFD to prevent diarrhea. We previously reported that the amount of cellulose present in the HFD (50 g/kg compare to 200 g/kg) only modestly impact the microbiota composition compared to inulin supplementation [13]. Inulin transits along the upper gastrointestinal tract without being neither absorbed nor degraded until it reaches the colon, where it is fermented by specific bacterial groups of the microbiota that will generate SCFAs. The ability of inulin to prevent MetS through gut microbiota alterations has been convincingly shown in several experimental models [13,25,26,60]. We showed that mice fed HFDi gained less weight compared to those fed HFDc. The origin of this phenotype remains to be determined. However, in the context of our study we could not exclude that it could also be due to the difference of energetic value of the diets even if it is slight (HFDc: 5.24 kcal/g and HFDi: 4.6 kcal/g) or to a different food intake between the two groups of mice, a parameter that we have not evaluated. Indeed, it has been already reported that food intake is reduced in mice fed with compositionally defined diet supplemented with inulin [15]. However, other studies showed that there is no impact of inulin supplementation of HFD on food intake [25] while others reported that food intake in mice fed HFD plus long-chain

inulin was higher than those of mice fed HFD and HFD plus short-chain inulin [19]. Several studies suggest that the anti-obesogenic effects of inulin depend on the dietary dosage or the degree of polymerization, which are factors that could influence its fermentation into SCFA by the gut microbiota [18,61,62].

In this study, we did not observe any effect of inulin supplementation to the LFD or the HFD on the amount of plasma triglycerides in a fasting state. The effect of inulin on triglyceridemia is not yet clearly established. Indeed, some discrepancies have been reported according to factors such as the fasting state of the mice at the time of the analysis, the diet in which the fiber is incorporated or its degree of polymerization [13,63,64]. Inulin consumption was also associated with a decrease in plasma cholesterol levels in mice fed LFD. Several hypotheses have been proposed to explain the cholesterol-lowering effect of inulin such as modifications of the bile acid metabolism and modulation of the hepatic lipogenesis [65].

Here, we focused on the effect of diet supplementation with inulin on liver fatty acids. We showed that supplementation of a standard mouse diet with inulin only led to slight changes in the fatty acid profile, concerning exclusively the poorly represented fatty acids (C15:0, C17:0, and C20:2n-6). In addition, in such a diet, inulin had no impact neither on the expression of desaturases and elongases at the transcript level nor on the activity of these enzymes. However, we found that supplementation of HFD with inulin led to substantial modifications of the fatty acid profile in the liver. In fact, in this diet, several effects of inulin can be distinguished. First, supplementation of HFD with inulin, as for LFD, induced an increase in the amount of C15:0. A second effect of inulin was the modification of the amounts of several fatty acids (e.g., increases in the amounts of C18:0, C22:0, total PUFA, total PUFA n-6, C18:3n-3, and C18:2n-6) in the liver when this fiber was combined to HFD. A third effect of inulin was the exacerbation of some of the modifications induced by the HFD (e.g., increase in the amount of C17:0). A last effect of inulin was a preventive one. Indeed, we showed that supplementation of HFD with inulin prevented the hepatic increases in the amounts of C16:1n-9 and C20:3n-6.

Modifications of the fatty acid profile in the liver of mice fed with diets supplemented with inulin could result from the modulation of the expression of desaturases and elongases and/or of their activity. We observed that supplementation of HFD with inulin highly reduced the amount of *Scd1* mRNA and impaired the activity of SCD1 for the production of C18:1n-9 from C18:0. Interestingly, inulin also prevented the dysregulation of ELOVL2 and ELOVL5 at both the transcript and the activity levels.

Diet is an important modulator of the composition and the function of the gut microbiota. Depending on its composition, diet exerts selective pressures on the gut microbes and allows the growth of specific bacteria species that are genetically equipped to metabolize dietary substrates or their derivative products. There is accumulating evidence pointing out to the gut microbiota as a key factor linking long-term dietary habits to host metabolic status. A role of gut microbes in the absorption and storage of lipids and in the regulation of hepatic lipogenesis has been highlighted by several studies [31–34]. Chronic consumption of a diet high in fat and low in fiber is known to promote profound changes in the composition of the gut microbiota, including in microbes identified as major triggers of metabolic dysregulations [66].

As expected, chronic exposure to a HFD led to profound alterations in microbiota composition. Interestingly, both "fat" and "fiber" effects were observed, demonstrating that both of these diet components impact the fecal microbiota composition. Among numerous microbiota alterations, taxonomic analysis demonstrated a decrease in *Akkermansia muciniphila* induced by HFD when compared with LFD, as previously described [25,40,41]. Such reduction in *A. muciniphila* abundance has also been reported in patients with metabolic disorders [67,68], while supplementation with *A. muciniphila* has been shown to improve metabolic parameters of overweight and obese patients [69]. Interestingly, our data identified that inulin supplementation was not sufficient to prevent HFD-induced loss of *A. muciniphila.* Hence, both fat content and fiber content have profound effects on

microbiota composition, in a way that can impact the observed hepatic phenotypes. Among the molecules produced by gut bacteria, short-chain fatty acids (SCFAs) have been identified as factors involved in the regulation of the hepatic fatty acid metabolism and in the promotion of the beneficial effects of inulin on host metabolism and inflammation [27,34]. However, inulin does not seem to act solely by modulating SCFAs through microbiota shaping. Indeed, inulin also protects against HFD-induced MetS through the elicitation of IL-22 expression in a microbiota-dependent manner [13].

Inulin is a widely used ingredient in foods for multiple applications (as prebiotic, source of dietary fiber, sweetener, etc.). However, several studies indicate that purified inulin could also have deleterious effect on health, with the promotion of colitis as well as hepatocellular carcinoma in mice models [70,71]. Thus, the nutritional and health claims related to the use of purified inulin should be accompanied with caution on its possible harmful effects under specific contexts such as genetical susceptibility or pre-existing microbial dysbiosis.

5. Conclusions

A high proportion of fat in the diet modified the composition of the gut microbiota and this phenotype was associated with changes of the fatty acid profile in the liver. We showed that the modifications in liver fatty acids could result, at least in part, from dysregulations of the expression levels of enzymes involved in fatty acid elongation and desaturation and/or of their activities. When added to a standard diet, inulin poorly affects the gut microbiota composition and the hepatic profile in fatty acids. In combination with HFD, inulin prevented some of the modifications induced by the HFD but also exacerbated others. Our results show that inulin might act by partly rescuing the growth of bacterial species that are impaired in condition of HFD and by regulating the expression and the activity of desaturases and elongases. In addition to bringing new insights to the molecular mechanisms linking diet to the hepatic metabolism of fatty acids, this study sheds the light on the precautions that should be taken regarding the use of inulin for the design of dietary interventions due to the ambivalence of this fiber in preventing or exacerbating potential deleterious effect of HFD.

Author Contributions: Conceptualization, M.-A.B. and B.C.; Methodology, M.A., A.B., B.C., M.-A.B., S.G. (Stéphane Grégoire), S.G. (Ségolène Gambert), L.M., and B.B.; Validation, M.-A.B. and B.C.; Formal Analysis, M.A., A.B., A.M.B., N.A., B.C., and M.-A.B.; Investigation, M.A., A.B., B.C., S.G. (Stéphane Grégoire), S.G. (Ségolène Gambert), L.M., B.B., and M.-A.B.; Writing—Original Draft Preparation, M.-A.B. and B.C.; Writing—Review and Editing, M.A., A.B., A.M.B., and N.A.; Supervision, M.-A.B. and B.C.; Project Administration, M.-A.B. and B.C.; Funding Acquisition, M.-A.B. and B.C. All authors have read and agreed to the published version of the manuscript.

Funding: This research was funded by Agence Nationale de la Recherche (ANR-11-LABX-0021-01); INRAE; the Conseil Régional de Bourgogne, Franche-Comté (PARI grant); the FEDER (European Funding for Regional Economic Development); and the Fondation de France/Fondation de l'œil. BC's laboratory is supported by a Starting Grant from the European Research Council (ERC) under the European Union's Horizon 2020 research and innovation programme (grant agreement No. ERC-2018-StG-804135), a Chaire d'Excellence from IdEx Université de Paris—ANR-18-IDEX-0001, and an Innovator Award from the Kenneth Rainin Foundation.

Institutional Review Board Statement: All mice were housed at Georgia State University, Atlanta, Georgia, USA, under institutionally approved protocols (IACUC #A18006).

Data Availability Statement: The data presented in this study are available on request from the corresponding author.

Conflicts of Interest: The authors declare no conflict of interest. The funders had no role in the design of the study; in the collection, analyses, or interpretation of data; in the writing of the manuscript, or in the decision to publish the results.

Appendix A

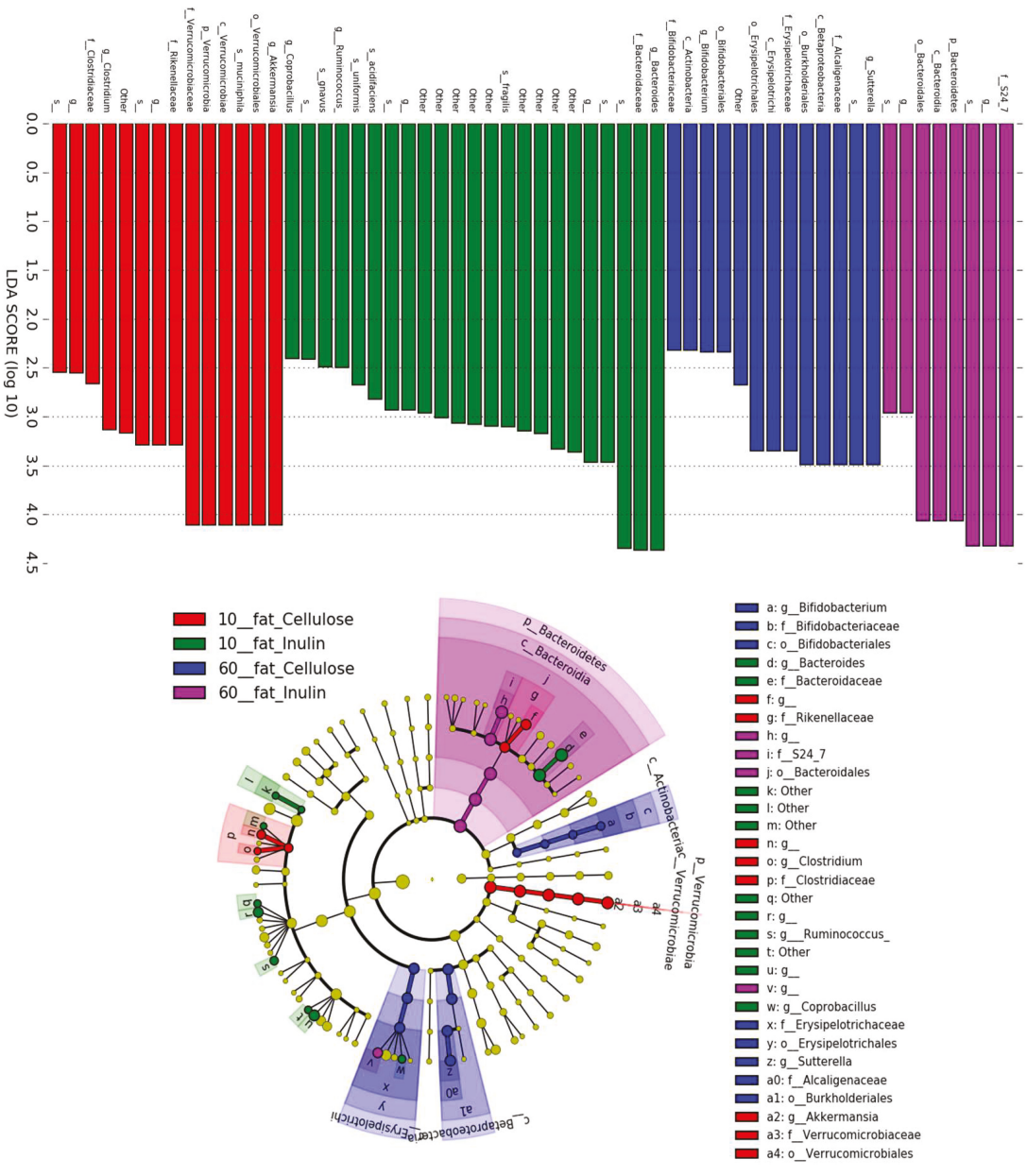

Figure A1. Microbiota composition analysis. Mice were fed LFD supplemented with cellulose (LFDc) or inulin (LFDi), or HFD supplemented with cellulose (HFDc) or inulin (HFDi) for 11 weeks. Microbiota composition was analyzed at the final time point, and LEFSE analysis was performed to identify taxa significantly altered in one group compared to another.

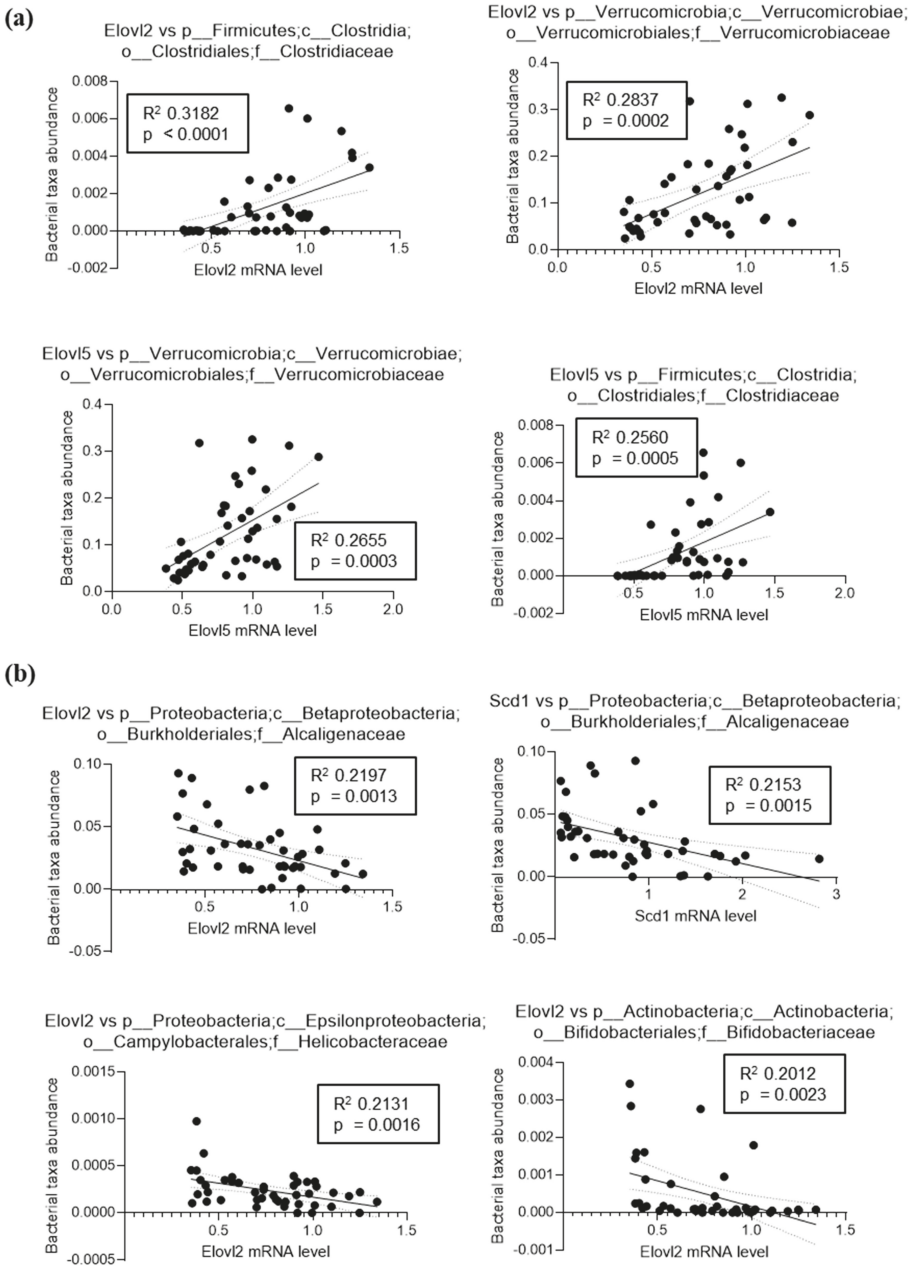

Figure A2. Correlation analysis between the relative abundance of selected microbiota members and the expression of hepatic gene involved in lipid biosynthesis. (**a**) Strongest and most significant positive correlations. (**b**) Strongest and most significant negative correlations.

References

1. Sonnenburg, J.L.; Backhed, F. Diet-microbiota interactions as moderators of human metabolism. *Nature* **2016**, *535*, 56–64. [CrossRef]
2. Cani, P.D.; Delzenne, N.M. The role of the gut microbiota in energy metabolism and metabolic disease. *Curr. Pharm. Des.* **2009**, *15*, 1546–1558. [CrossRef]
3. Moszak, M.; Szulinska, M.; Bogdanski, P. You Are What You Eat-The Relationship between Diet, Microbiota, and Metabolic Disorders-A Review. *Nutrients* **2020**, *12*, 1096. [CrossRef]
4. Saklayen, M.G. The Global Epidemic of the Metabolic Syndrome. *Curr. Hypertens. Rep.* **2018**, *20*, 12. [CrossRef] [PubMed]
5. Santos-Marcos, J.A.; Perez-Jimenez, F.; Camargo, A. The role of diet and intestinal microbiota in the development of metabolic syndrome. *J. Nutr. Biochem.* **2019**, *70*, 1–27. [CrossRef]
6. Winzell, M.S.; Ahren, B. The high-fat diet-fed mouse: A model for studying mechanisms and treatment of impaired glucose tolerance and type 2 diabetes. *Diabetes* **2004**, *53* (Suppl. 3), S215–S219. [CrossRef]
7. Alcock, J.; Lin, H.C. Fatty acids from diet and microbiota regulate energy metabolism. *F1000Res* **2015**, *4*, 738. [CrossRef] [PubMed]
8. Cani, P.D.; Amar, J.; Iglesias, M.A.; Poggi, M.; Knauf, C.; Bastelica, D.; Neyrinck, A.M.; Fava, F.; Tuohy, K.M.; Chabo, C.; et al. Metabolic endotoxemia initiates obesity and insulin resistance. *Diabetes* **2007**, *56*, 1761–1772. [CrossRef] [PubMed]
9. Daniel, H.; Gholami, A.M.; Berry, D.; Desmarchelier, C.; Hahne, H.; Loh, G.; Mondot, S.; Lepage, P.; Rothballer, M.; Walker, A.; et al. High-fat diet alters gut microbiota physiology in mice. *ISME J.* **2014**, *8*, 295–308. [CrossRef] [PubMed]
10. Desai, M.S.; Seekatz, A.M.; Koropatkin, N.M.; Kamada, N.; Hickey, C.A.; Wolter, M.; Pudlo, N.A.; Kitamoto, S.; Terrapon, N.; Muller, A.; et al. A Dietary Fiber-Deprived Gut Microbiota Degrades the Colonic Mucus Barrier and Enhances Pathogen Susceptibility. *Cell* **2016**, *167*, 1339–1353.e1321. [CrossRef] [PubMed]
11. Holscher, H.D. Dietary fiber and prebiotics and the gastrointestinal microbiota. *Gut Microbes* **2017**, *8*, 172–184. [CrossRef]
12. Vandeputte, D.; Falony, G.; Vieira-Silva, S.; Wang, J.; Sailer, M.; Theis, S.; Verbeke, K.; Raes, J. Prebiotic inulin-type fructans induce specific changes in the human gut microbiota. *Gut* **2017**, *66*, 1968–1974. [CrossRef] [PubMed]
13. Zou, J.; Chassaing, B.; Singh, V.; Pellizzon, M.; Ricci, M.; Fythe, M.D.; Kumar, M.V.; Gewirtz, A.T. Fiber-Mediated Nourishment of Gut Microbiota Protects against Diet-Induced Obesity by Restoring IL-22-Mediated Colonic Health. *Cell Host Microbe* **2018**, *23*, 41–53.e44. [CrossRef] [PubMed]
14. Murphy, E.A.; Velazquez, K.T.; Herbert, K.M. Influence of high-fat diet on gut microbiota: A driving force for chronic disease risk. *Curr. Opin. Clin. Nutr. Metab. Care* **2015**, *18*, 515–520. [CrossRef]
15. Chassaing, B.; Miles-Brown, J.; Pellizzon, M.; Ulman, E.; Ricci, M.; Zhang, L.; Patterson, A.D.; Vijay-Kumar, M.; Gewirtz, A.T. Lack of soluble fiber drives diet-induced adiposity in mice. *Am. J. Physiol. Gastrointest. Liver Physiol.* **2015**, *309*, G528–G541. [CrossRef] [PubMed]
16. Makki, K.; Deehan, E.C.; Walter, J.; Backhed, F. The Impact of Dietary Fiber on Gut Microbiota in Host Health and Disease. *Cell Host Microbe* **2018**, *23*, 705–715. [CrossRef]
17. Han, K.H.; Kobayashi, Y.; Nakamura, Y.; Shimada, K.; Aritsuka, T.; Ohba, K.; Morita, T.; Fukushima, M. Comparison of the effects of longer chain inulins with different degrees of polymerization on colonic fermentation in a mixed culture of Swine fecal bacteria. *J. Nutr. Sci. Vitaminol.* **2014**, *60*, 206–212. [CrossRef]
18. Du, H.; Zhao, A.; Wang, Q.; Yang, X.; Ren, D. Supplementation of Inulin with Various Degree of Polymerization Ameliorates Liver Injury and Gut Microbiota Dysbiosis in High Fat-Fed Obese Mice. *J. Agric. Food Chem.* **2020**, *68*, 779–787. [CrossRef]
19. Li, L.L.; Wang, Y.T.; Zhu, L.M.; Liu, Z.Y.; Ye, C.Q.; Qin, S. Inulin with different degrees of polymerization protects against diet-induced endotoxemia and inflammation in association with gut microbiota regulation in mice. *Sci. Rep.* **2020**, *10*, 978. [CrossRef] [PubMed]
20. Pompei, A.; Cordisco, L.; Raimondi, S.; Amaretti, A.; Pagnoni, U.M.; Matteuzzi, D.; Rossi, M. In vitro comparison of the prebiotic effects of two inulin-type fructans. *Anaerobe* **2008**, *14*, 280–286. [CrossRef]
21. Zhu, L.; Qin, S.; Zhai, S.; Gao, Y.; Li, L. Inulin with different degrees of polymerization modulates composition of intestinal microbiota in mice. *FEMS Microbiol. Lett.* **2017**, *364*. [CrossRef] [PubMed]
22. Le Bastard, Q.; Chapelet, G.; Javaudin, F.; Lepelletier, D.; Batard, E.; Montassier, E. The effects of inulin on gut microbial composition: A systematic review of evidence from human studies. *Eur. J. Clin. Microbiol. Infect. Dis.* **2020**, *39*, 403–413. [CrossRef] [PubMed]
23. Myhrstad, M.C.W.; Tunsjo, H.; Charnock, C.; Telle-Hansen, V.H. Dietary Fiber, Gut Microbiota, and Metabolic Regulation-Current Status in Human Randomized Trials. *Nutrients* **2020**, *12*, 859. [CrossRef] [PubMed]
24. Bozzetto, L.; Costabile, G.; Della Pepa, G.; Ciciola, P.; Vetrani, C.; Vitale, M.; Rivellese, A.A.; Annuzzi, G. Dietary Fibre as a Unifying Remedy for the Whole Spectrum of Obesity-Associated Cardiovascular Risk. *Nutrients* **2018**, *10*, 943. [CrossRef] [PubMed]
25. Bao, T.; He, F.; Zhang, X.; Zhu, L.; Wang, Z.; Lu, H.; Wang, T.; Li, Y.; Yang, S.; Wang, H. Inulin Exerts Beneficial Effects on Non-Alcoholic Fatty Liver Disease via Modulating gut Microbiome and Suppressing the Lipopolysaccharide-Toll-Like Receptor 4-Mpsi-Nuclear Factor-kappaB-Nod-Like Receptor Protein 3 Pathway via gut-Liver Axis in Mice. *Front. Pharmacol.* **2020**, *11*, 558525. [CrossRef] [PubMed]
26. Tan, S.; Caparros-Martin, J.A.; Matthews, V.B.; Koch, H.; O'Gara, F.; Croft, K.D.; Ward, N.C. Isoquercetin and inulin synergistically modulate the gut microbiome to prevent development of the metabolic syndrome in mice fed a high fat diet. *Sci. Rep.* **2018**, *8*, 10100. [CrossRef]

27. Brooks, L.; Viardot, A.; Tsakmaki, A.; Stolarczyk, E.; Howard, J.K.; Cani, P.D.; Everard, A.; Sleeth, M.L.; Psichas, A.; Anastasovskaj, J.; et al. Fermentable carbohydrate stimulates FFAR2-dependent colonic PYY cell expansion to increase satiety. *Mol. Metab.* **2017**, *6*, 48–60. [CrossRef]
28. Dewulf, E.M.; Cani, P.D.; Neyrinck, A.M.; Possemiers, S.; Van Holle, A.; Muccioli, G.G.; Deldicque, L.; Bindels, L.B.; Pachikian, B.D.; Sohet, F.M.; et al. Inulin-type fructans with prebiotic properties counteract GPR43 overexpression and PPARgamma-related adipogenesis in the white adipose tissue of high-fat diet-fed mice. *J. Nutr. Biochem.* **2011**, *22*, 712–722. [CrossRef]
29. Jakobsdottir, G.; Nyman, M.; Fak, F. Designing future prebiotic fiber to target metabolic syndrome. *Nutrition* **2014**, *30*, 497–502. [CrossRef] [PubMed]
30. Salazar, N.; Dewulf, E.M.; Neyrinck, A.M.; Bindels, L.B.; Cani, P.D.; Mahillon, J.; de Vos, W.M.; Thissen, J.P.; Gueimonde, M.; de Los Reyes-Gavilan, C.G.; et al. Inulin-type fructans modulate intestinal *Bifidobacterium* species populations and decrease fecal short-chain fatty acids in obese women. *Clin. Nutr.* **2015**, *34*, 501–507. [CrossRef]
31. Backhed, F.; Ding, H.; Wang, T.; Hooper, L.V.; Koh, G.Y.; Nagy, A.; Semenkovich, C.F.; Gordon, J.I. The gut microbiota as an environmental factor that regulates fat storage. *Proc. Natl. Acad. Sci. USA* **2004**, *101*, 15718–15723. [CrossRef]
32. Martinez-Guryn, K.; Hubert, N.; Frazier, K.; Urlass, S.; Musch, M.W.; Ojeda, P.; Pierre, J.F.; Miyoshi, J.; Sontag, T.J.; Cham, C.M.; et al. Small Intestine Microbiota Regulate Host Digestive and Absorptive Adaptive Responses to Dietary Lipids. *Cell Host Microbe* **2018**, *23*, 458–469.e455. [CrossRef]
33. Albouery, M.; Buteau, B.; Gregoire, S.; Cherbuy, C.; Pais de Barros, J.P.; Martine, L.; Chain, F.; Cabaret, S.; Berdeaux, O.; Bron, A.M.; et al. Age-Related Changes in the Gut Microbiota Modify Brain Lipid Composition. *Front. Cell. Infect. Microbiol.* **2019**, *9*, 444. [CrossRef] [PubMed]
34. Kindt, A.; Liebisch, G.; Clavel, T.; Haller, D.; Hormannsperger, G.; Yoon, H.; Kolmeder, D.; Sigruener, A.; Krautbauer, S.; Seeliger, C.; et al. The gut microbiota promotes hepatic fatty acid desaturation and elongation in mice. *Nat. Commun.* **2018**, *9*, 3760. [CrossRef] [PubMed]
35. Kremmyda, L.S.; Tvrzicka, E.; Stankova, B.; Zak, A. Fatty acids as biocompounds: Their role in human metabolism, health and disease: A review. part 2: Fatty acid physiological roles and applications in human health and disease. *Biomed. Pap. Med. Fac. Univ. Palacky Olomouc Czech Repub.* **2011**, *155*, 195–218. [CrossRef]
36. Folch, J.; Lees, M.; Sloane Stanley, G.H. A simple method for the isolation and purification of total lipides from animal tissues. *J. Biol. Chem.* **1957**, *226*, 497–509. [CrossRef]
37. Morrison, W.R.; Smith, L.M. Preparation of Fatty Acid Methyl Esters and Dimethylacetals from Lipids with Boron Fluoride—Methanol. *J. Lipid Res.* **1964**, *5*, 600–608. [CrossRef]
38. Albouery, M.; Buteau, B.; Gregoire, S.; Martine, L.; Gambert, S.; Bron, A.M.; Acar, N.; Chassaing, B.; Bringer, M.A. Impact of a high-fat diet on the fatty acid composition of the retina. *Exp. Eye Res.* **2020**, *196*, 108059. [CrossRef] [PubMed]
39. Viennois, E.; Bretin, A.; Dube, P.E.; Maue, A.C.; Dauriat, C.J.G.; Barnich, N.; Gewirtz, A.T.; Chassaing, B. Dietary Emulsifiers Directly Impact Adherent-Invasive E. coli Gene Expression to Drive Chronic Intestinal Inflammation. *Cell Rep.* **2020**, *33*, 108229. [CrossRef]
40. Schneeberger, M.; Everard, A.; Gomez-Valades, A.G.; Matamoros, S.; Ramirez, S.; Delzenne, N.M.; Gomis, R.; Claret, M.; Cani, P.D. *Akkermansia muciniphila* inversely correlates with the onset of inflammation, altered adipose tissue metabolism and metabolic disorders during obesity in mice. *Sci. Rep.* **2015**, *5*, 16643. [CrossRef]
41. Shin, N.R.; Lee, J.C.; Lee, H.Y.; Kim, M.S.; Whon, T.W.; Lee, M.S.; Bae, J.W. An increase in the *Akkermansia* spp. population induced by metformin treatment improves glucose homeostasis in diet-induced obese mice. *Gut* **2014**, *63*, 727–735. [CrossRef] [PubMed]
42. Singh, V.; Chassaing, B.; Zhang, L.; San Yeoh, B.; Xiao, X.; Kumar, M.; Baker, M.T.; Cai, J.; Walker, R.; Borkowski, K.; et al. Microbiota-Dependent Hepatic Lipogenesis Mediated by Stearoyl CoA Desaturase 1 (SCD1) Promotes Metabolic Syndrome in TLR5-Deficient Mice. *Cell Metab.* **2015**, *22*, 983–996. [CrossRef]
43. Wang, Y.; Botolin, D.; Xu, J.; Christian, B.; Mitchell, E.; Jayaprakasam, B.; Nair, M.G.; Peters, J.M.; Busik, J.V.; Olson, L.K.; et al. Regulation of hepatic fatty acid elongase and desaturase expression in diabetes and obesity. *J. Lipid Res.* **2006**, *47*, 2028–2041. [CrossRef] [PubMed]
44. Da Silva-Santi, L.G.; Antunes, M.M.; Caparroz-Assef, S.M.; Carbonera, F.; Masi, L.N.; Curi, R.; Visentainer, J.V.; Bazotte, R.B. Liver Fatty Acid Composition and Inflammation in Mice Fed with High-Carbohydrate Diet or High-Fat Diet. *Nutrients* **2016**, *8*, 682. [CrossRef]
45. Ipsen, D.H.; Lykkesfeldt, J.; Tveden-Nyborg, P. Molecular mechanisms of hepatic lipid accumulation in non-alcoholic fatty liver disease. *Cell. Mol. Life Sci.* **2018**, *75*, 3313–3327. [CrossRef] [PubMed]
46. Calder, P.C. Functional Roles of Fatty Acids and Their Effects on Human Health. *JPEN J. Parenter. Enter. Nutr.* **2015**, *39*, 18S–32S. [CrossRef]
47. De Carvalho, C.; Caramujo, M.J. The Various Roles of Fatty Acids. *Molecules* **2018**, *23*, 2583. [CrossRef]
48. Echeverria, F.; Valenzuela, R.; Bustamante, A.; Alvarez, D.; Ortiz, M.; Espinosa, A.; Illesca, P.; Gonzalez-Manan, D.; Videla, L.A. High-fat diet induces mouse liver steatosis with a concomitant decline in energy metabolism: Attenuation by eicosapentaenoic acid (EPA) or hydroxytyrosol (HT) supplementation and the additive effects upon EPA and HT co-administration. *Food Funct.* **2019**, *10*, 6170–6183. [CrossRef]

49. Montgomery, M.K.; Hallahan, N.L.; Brown, S.H.; Liu, M.; Mitchell, T.W.; Cooney, G.J.; Turner, N. Mouse strain-dependent variation in obesity and glucose homeostasis in response to high-fat feeding. *Diabetologia* **2013**, *56*, 1129–1139. [CrossRef] [PubMed]
50. Yuan, M.; Song, Z.H.; Ying, M.D.; Zhu, H.; He, Q.J.; Yang, B.; Cao, J. N-myristoylation: From cell biology to translational medicine. *Acta Pharmacol. Sin.* **2020**, *41*, 1005–1015. [CrossRef]
51. De Souza, C.O.; Vannice, G.K.; Rosa Neto, J.C.; Calder, P.C. Is Palmitoleic Acid a Plausible Nonpharmacological Strategy to Prevent or Control Chronic Metabolic and Inflammatory Disorders? *Mol. Nutr. Food Res.* **2018**, *62*. [CrossRef]
52. Jiang, Z.; Hayashi, T.; Kashima, K.; Kurotani, K.; Shirouchi, B.; Mizoue, T.; Sato, M. Alteration of Serum Phospholipid n-6 Polyunsaturated Fatty Acid Compositions in Nonalcoholic Fatty Liver Disease in the Japanese Population: A Cross-Sectional Study. *Lipids* **2020**, *55*, 599–614. [CrossRef]
53. Matsuda, M.; Kawamoto, T.; Tamura, R. Predictive value of serum dihomo-gamma-linolenic acid level and estimated Delta-5 desaturase activity in patients with hepatic steatosis. *Obes. Res. Clin. Pract.* **2017**, *11*, 34–43. [CrossRef] [PubMed]
54. Hu, C.C.; Qing, K.; Chen, Y. Diet-induced changes in stearoyl-CoA desaturase 1 expression in obesity-prone and-resistant mice. *Obes. Res.* **2004**, *12*, 1264–1270. [CrossRef] [PubMed]
55. Valenzuela, R.; Barrera, C.; Espinosa, A.; Llanos, P.; Orellana, P.; Videla, L.A. Reduction in the desaturation capacity of the liver in mice subjected to high fat diet: Relation to LCPUFA depletion in liver and extrahepatic tissues. *Prostaglandins Leukot. Essent. Fat. Acids* **2015**, *98*, 7–14. [CrossRef] [PubMed]
56. Bonnema, A.L.; Kolberg, L.W.; Thomas, W.; Slavin, J.L. Gastrointestinal tolerance of chicory inulin products. *J. Am. Diet. Assoc.* **2010**, *110*, 865–868. [CrossRef] [PubMed]
57. Carabin, I.G.; Flamm, W.G. Evaluation of safety of inulin and oligofructose as dietary fiber. *Regul. Toxicol. Pharmacol.* **1999**, *30*, 268–282. [CrossRef]
58. Coussement, P.A. Inulin and oligofructose: Safe intakes and legal status. *J. Nutr.* **1999**, *129*, 1412S–1417S. [CrossRef]
59. Van Loo, J.; Coussement, P.; de Leenheer, L.; Hoebregs, H.; Smits, G. On the presence of inulin and oligofructose as natural ingredients in the western diet. *Crit. Rev. Food Sci. Nutr.* **1995**, *35*, 525–552. [CrossRef] [PubMed]
60. Kumar, S.A.; Ward, L.C.; Brown, L. Inulin oligofructose attenuates metabolic syndrome in high-carbohydrate, high-fat diet-fed rats. *Br. J. Nutr.* **2016**, *116*, 1502–1511. [CrossRef] [PubMed]
61. Asto, E.; Mendez, I.; Rodriguez-Prado, M.; Cune, J.; Espadaler, J.; Farran-Codina, A. Effect of the Degree of Polymerization of Fructans on Ex Vivo Fermented Human Gut Microbiome. *Nutrients* **2019**, *11*, 1293. [CrossRef]
62. Stewart, M.L.; Timm, D.A.; Slavin, J.L. Fructooligosaccharides exhibit more rapid fermentation than long-chain inulin in an in vitro fermentation system. *Nutr. Res.* **2008**, *28*, 329–334. [CrossRef]
63. Delzenne, N.M.; Daubioul, C.; Neyrinck, A.; Lasa, M.; Taper, H.S. Inulin and oligofructose modulate lipid metabolism in animals: Review of biochemical events and future prospects. *Br. J. Nutr.* **2002**, *87* (Suppl. 2), S255–S259. [CrossRef]
64. Zhu, Z.; Huang, Y.; Luo, X.; Wu, Q.; He, J.; Li, S.; Barba, F.J. Modulation of lipid metabolism and colonic microbial diversity of high-fat-diet C57BL/6 mice by inulin with different chain lengths. *Food Res. Int.* **2019**, *123*, 355–363. [CrossRef]
65. Reis, S.A.; Conceicao, L.L.; Rosa, D.D.; Dias, M.M.; Peluzio Mdo, C. Mechanisms used by inulin-type fructans to improve the lipid profile. *Nutr. Hosp.* **2014**, *31*, 528–534. [CrossRef] [PubMed]
66. Velasquez, M.T. Altered Gut Microbiota: A Link Between Diet and the Metabolic Syndrome. *Metab. Syndr. Relat. Disord.* **2018**, *16*, 321–328. [CrossRef]
67. Dao, M.C.; Everard, A.; Aron-Wisnewsky, J.; Sokolovska, N.; Prifti, E.; Verger, E.O.; Kayser, B.D.; Levenez, F.; Chilloux, J.; Hoyles, L.; et al. *Akkermansia muciniphila* and improved metabolic health during a dietary intervention in obesity: Relationship with gut microbiome richness and ecology. *Gut* **2016**, *65*, 426–436. [CrossRef] [PubMed]
68. Zhou, Q.; Zhang, Y.; Wang, X.; Yang, R.; Zhu, X.; Zhang, Y.; Chen, C.; Yuan, H.; Yang, Z.; Sun, L. Gut bacteria *Akkermansia* is associated with reduced risk of obesity: Evidence from the American Gut Project. *Nutr. Metab.* **2020**, *17*, 90. [CrossRef]
69. Depommier, C.; Everard, A.; Druart, C.; Plovier, H.; Van Hul, M.; Vieira-Silva, S.; Falony, G.; Raes, J.; Maiter, D.; Delzenne, N.M.; et al. Supplementation with *Akkermansia muciniphila* in overweight and obese human volunteers: A proof-of-concept exploratory study. *Nat. Med.* **2019**, *25*, 1096–1103. [CrossRef]
70. Miles, J.P.; Zou, J.; Kumar, M.V.; Pellizzon, M.; Ulman, E.; Ricci, M.; Gewirtz, A.T.; Chassaing, B. Supplementation of Low- and High-fat Diets with Fermentable Fiber Exacerbates Severity of DSS-induced Acute Colitis. *Inflamm. Bowel Dis.* **2017**, *23*, 1133–1143. [CrossRef] [PubMed]
71. Singh, V.; Yeoh, B.S.; Chassaing, B.; Xiao, X.; Saha, P.; Aguilera Olvera, R.; Lapek, J.D., Jr.; Zhang, L.; Wang, W.B.; Hao, S.; et al. Dysregulated Microbial Fermentation of Soluble Fiber Induces Cholestatic Liver Cancer. *Cell* **2018**, *175*, 679–694.e622. [CrossRef] [PubMed]

nutrients

MDPI

Article

Effects of Three-Month Administration of High-Saturated Fat Diet and High-Polyunsaturated Fat Diets with Different Linoleic Acid (LA, C18:2n–6) to α-Linolenic Acid (ALA, C18:3n–3) Ratio on the Mouse Liver Proteome

Kamila P. Liput [1,2], Adam Lepczyński [3], Agata Nawrocka [1,4], Ewa Poławska [1], Magdalena Ogłuszka [1], Aneta Jończy [2], Weronika Grzybek [5], Michał Liput [6], Agnieszka Szostak [1], Paweł Urbański [1], Agnieszka Roszczyk [1], Chandra S. Pareek [7,8] and Mariusz Pierzchała [1,*]

1 Department of Genomics and Biodiversity, Institute of Genetics and Animal Biotechnology of the Polish Academy of Sciences, ul. Postepu 36A, Jastrzebiec, 05-552 Magdalenka, Poland; k.liput@igbzpan.pl (K.P.L.); a.nawrocka@igbzpan.pl (A.N.); e.polawska@igbzpan.pl (E.P.); m.ogluszka@igbzpan.pl (M.O.); a.szostak@igbzpan.pl (A.S.); p.urbanski@igbzpan.pl (P.U.); a.roszczyk@igbzpan.pl (A.R.)
2 Department of Molecular Biology, Institute of Genetics and Animal Biotechnology of the Polish Academy of Sciences, ul. Postepu 36A, Jastrzebiec, 05-552 Magdalenka, Poland; a.jonczy@igbzpan.pl
3 Department of Physiology, Cytobiology and Proteomics, West Pomeranian University of Technology, K. Janickiego 32 Str., 71-270 Szczecin, Poland; Adam.Lepczynski@zut.edu.pl
4 Department of Experimental Genomics, Institute of Genetics and Animal Biotechnology of the Polish Academy of Sciences, ul. Postepu 36A, Jastrzebiec, 05-552 Magdalenka, Poland
5 Department of Biotechnology and Nutrigenomics, Institute of Genetics and Animal Biotechnology of the Polish Academy of Sciences, ul. Postepu 36A, Jastrzebiec, 05-552 Magdalenka, Poland; w.grzybek@igbzpan.pl
6 Department of Stem Cell Bioengineering, Mossakowski Medical Research Institute of the Polish Academy of Sciences, 02-106 Warsaw, Poland; mliput@imdik.pan.pl
7 Institute of Veterinary Medicine, Faculty of Biological and Veterinary Sciences, Nicolaus Copernicus University, 87-100 Toruń, Poland; pareekcs@umk.pl
8 Division of Functional Genomics in Biological and Biomedical Research, Centre for Modern Interdisciplinary Technologies, Nicolaus Copernicus University, 87-100 Torun, Poland
* Correspondence: m.pierzchala@igbzpan.pl; Tel.: +48-22-736-70-28

Citation: Liput, K.P.; Lepczyński, A.; Nawrocka, A.; Poławska, E.; Ogłuszka, M.; Jończy, A.; Grzybek, W.; Liput, M.; Szostak, A.; Urbański, P.; et al. Effects of Three-Month Administration of High-Saturated Fat Diet and High-Polyunsaturated Fat Diets with Different Linoleic Acid (LA, C18:2n–6) to α-Linolenic Acid (ALA, C18:3n–3) Ratio on the Mouse Liver Proteome. *Nutrients* **2021**, *13*, 1678. https://doi.org/10.3390/nu13051678

Academic Editor: Frederic Capel

Received: 25 April 2021
Accepted: 12 May 2021
Published: 15 May 2021

Abstract: The aim of the study was to evaluate the effect of different types of high-fat diets (HFDs) on the proteomic profile of mouse liver. The analysis included four dietary groups of mice fed a standard diet (STD group), a high-fat diet rich in SFAs (SFA group), and high-fat diets dominated by PUFAs with linoleic acid (LA, C18:2n–6) to α-linolenic acid (ALA, C18:3n–3) ratios of 14:1 (14:1 group) and 5:1 (5:1 group). After three months of diets, liver proteins were resolved by two-dimensional gel electrophoresis (2DE) using 17 cm non-linear 3–10 pH gradient strips. Protein spots with different expression were identified by MALDI-TOF/TOF. The expression of 13 liver proteins was changed in the SFA group compared to the STD group (↓: ALB, APOA1, IVD, MAT1A, OAT and PHB; ↑: ALDH1L1, UniProtKB—Q91V76, GALK1, GPD1, HMGCS2, KHK and TKFC). Eleven proteins with altered expression were recorded in the 14:1 group compared to the SFA group (↓: ARG1, FTL1, GPD1, HGD, HMGCS2 and MAT1A; ↑: APOA1, CA3, GLO1, HDHD3 and IVD). The expression of 11 proteins was altered in the 5:1 group compared to the SFA group (↓: ATP5F1B, FTL1, GALK1, HGD, HSPA9, HSPD1, PC and TKFC; ↑: ACAT2, CA3 and GSTP1). High-PUFA diets significantly affected the expression of proteins involved in, e.g., carbohydrate metabolism, and had varying effects on plasma total cholesterol and glucose levels. The outcomes of this study revealed crucial liver proteins affected by different high-fat diets.

Keywords: HFD; SFA; omega-3 PUFA; omega-6 PUFA; nutriproteomics; 2DE; MALDI TOF/TOF

1. Introduction

Saturated fatty acids (SFAs) are mainly found in dairy foods, lards, processed meats—e.g., salami, sausage and bacon—manufactured foods—including snacks, cakes and biscuits—and deep-fried foods. Plant-derived oils like palm and coconut oils are also sources of SFAs [1]. In recent years, interest in coconut oil consumption has increased. For instance, this oil consumption in the USA increased by 34% in 2014 compared to 2004. The reason for such a popularity of coconut oil, particularly cold-pressed, was mostly due to information about its health-promoting properties, such as anti-proliferative and pro-apoptotic effects on breast cancer cells of the dominant SFA in coconut oil—lauric acid (12:0) [2]. Additionally, the high content of medium-chain triacylglycerols (MCTs) was mentioned as one of the arguments for coconut oil consumption [3]. Scientific reports have indicated that MCTs induced thermogenesis and reduced food consumption [4,5]. However, this evidence was insufficient to attribute MCT properties to coconut oil in weight loss support.

The highly publicized issue of coconut oil properties, which assist in reducing body weight, was not supported by scientific evidence [6]. Moreover, dietary recommendations encourage limiting SFA intake and replacing them with polyunsaturated fatty acids (PUFAs) to decrease the risk of metabolic disorders, for example, the World Health Organization and American Dietary Guidelines 2015–2020 recommend reducing SFA intake to less than 10 percent of calories per day [7]. The American Heart Association stated that reducing SFAs intake to 5–6% of daily calories had a beneficial effect on adults by lowering LDL-C [8]. An epidemiological study by Kromhout et al. found a positive correlation between SFA consumption and coronary heart disease incidence (CHD) [9]. In contrast, a diet rich in high-unsaturated fatty acids may decrease risk factors, morbidity, and mortality related to coronary vascular disease (CVD) [10]. The recommendations for replacing saturated and trans fats with unsaturated fats were also supported by the results describing a reduction in total mortality associated with replacing 5% of energy from saturated fats with equivalent energy derived from polyunsaturated and monounsaturated fats [11]. According to Gouaref et al., increased pro-inflammatory cytokine concentrations (TNFα, IL-6, IL1β) were associated with elevated levels of saturated non-esterified fatty acids (NEFAs) and decreased plasma PUFAs. A positive correlation was also found between the plasma PUFA/SFA and HDL-c/LDL-c ratios ($r = +66$, $p < 0.01$) in the group of patients with type 2 diabetes mellitus (T2DM) and hypertension [12]. Additionally, female mortality caused by breast cancer was the highest in the group characterized by high saturated fat intake [1,13].

The Mediterranean dietary pattern (MedDiet) and Dietary Approaches to Stop Hypertension (DASH) dietary pattern are the most frequently studied dietary recommendations for preventing and treating heart failure. Both share the common characteristic of restricting saturated fatty acids than the Westernized dietary pattern, specifically to a diet with high saturated fatty acids. Additionally, the MedDiet emphasized increased consumption of unsaturated fatty acids (UFA), which are composed of both monounsaturated (MUFA) and polyunsaturated fatty acids (PUFA) found in fatty fish and plant oils [14].

However, recommendations to reduce saturated fatty acid consumption are currently questioned because of inconclusive evidence that dietary saturated fats are associated with an increased risk of CHD or CVD [15]. Despite many studies, the role of dietary SFAs and PUFAs in metabolic disturbances remains unclear. According to Uger at al. consolidation all dietary SFAs into a single group was an oversimplification and the SFAs effects on health should be considered regarding the chemical structure and dietary source [16].

Thus, the present work aimed to identify key hepatic protein mediators involved in biological mechanisms of action of different high-fat diets based on plant-derived oils with varying SFA and PUFA contents.

2. Materials and Methods

2.1. Animals, Diets and Sampling

The nutritional experiment was carried out in the animal house of the Institute of Genetics and Animal Biotechnology of the Polish Academy of Sciences in Jastrzębiec. Experimental procedures were approved by the Second Warsaw Local Ethics Committee for Animal Experimentation (WAW2_22/2016). Animals were kept in standard cages under temperature- and humidity-controlled conditions with a 12-h light/dark cycle.

Male Swiss-Webster mice (n = 32) were fed standard growth diets for eight weeks after weaning. Next, animals were separated into four groups (8 mice per group). Mice were fed one of the four types of feed. The first group (STD group) were mice fed complete chow for laboratory animals containing 22% crude protein, 4.2% crude fat, 3.5% crude fiber, 5.7% crude ash (Labofeed H, "Morawski" Feed Factory, Kcynia, Poland). The second group (SFA group) were mice fed Labofeed H with coconut virgin oil. The third and the fourth groups were mixtures of Labofeed H feed with the addition of vegetable oils with high PUFAs content, varying in the ratio of linoleic acid (18:2n–6, LA) to α-linolenic acid (18:3n–3, ALA), in details, the first group ratio omega-6/3 was 13.76:1 (14:1 group) and in the second was 5:1 (5:1 group). The composition and the fatty acid contents in each diet were varied using different oils addition according to Table 1.

The prepared diets were vacuum packed, stored in the dark and given to the animals two times per day to avoid fatty acid oxidation. The mice had ad libitum access to water and food and were weighed every two weeks. After three months of feeding with specific diets, animals were sacrificed, livers were dissected out, and median lobes were frozen in liquid nitrogen and then stored at −70 °C for further analysis.

The amounts of added vegetable oils were determined based on the analysis of the fatty acid content of individual oils using a GC-7890 gas chromatograph (Agilent Technologies, Inc., Santa Clara, CA, USA) with a flame ionization detector (FID) and a 60 m capillary column, 0.25 mm internal diameter and 0.20 μm stationary layer thickness (Hewlett-Packard-88, Agilent J&W GC Columns, Santa Clara, CA, USA). The carrier gas was helium with a flow rate of 50 mL/min. The dispenser and detector temperatures were 260 °C. Temperature program: (1) from 140 °C to 190 °C (4 °C/min), (2) from 190 °C to 215 °C (0.8 °C/min). The results were compared to the external standard Supelco 37 Component FAME Mix, 47885-U, (Sigma-Aldrich Sp. z o.o., Poznan, Polandrimental diets according to [17].

Table 1. Gas Chromatography Parameters.

Group	Components	[g]	LA/ALA	% SFA	% PUFA	% MUFA
SFA	Labofeed H	790	1.41	76.87	11.04	12.09
	virgin coconut oil	200				
	pumpkin seed oil	10				
14:1	Labofeed H	790	13.76	1.68	82.21	16.10
	pumpkin seed oil	210				
5:1	Labofeed H	790	5.00	9.91	79.69	10.40
	sunflower seed oil	80				
	pumpkin seed oil	65				
	avocado oil	20				
	virgin coconut oil	20				
	hemp seed oil	15				
	corn oil	10				

LA/ALA, linoleic acid (LA, 18:2n–6) to α-linolenic acid (ALA, 18:3n–3) ratio; SFA, saturated fatty acids; MUFA, monounsaturated fatty acids; PUFA, polyunsaturated fatty acids.

2.2. Plasma Biochemical Parameters

Blood was collected after death by cardiac puncture and mixed with 10 μL 0.5M EDTA and centrifuged at 3000× g for 10 min at 4 °C. Next, plasma was collected and frozen at

−70 °C. Biochemical analyses were performed using COBAS INTEGRA® 400 plus system (Roche Diagnostics Ltd., Rotkreuz, Switzerland). Following biochemical tests were used: ALB2 (albumin); ALTL (alanine aminotransferase), ASTL (aspartate aminotransferase), BILT3 (total bilirubin), CHE2 (cholinesterase), CHOL2 (total cholesterol), GLUC3 (glucose), HDLC3 (high-density lipoprotein-cholesterol), IRON2 (iron), LDL_C (low-density lipoprotein-cholesterol), LIPC (lipase), TP2 (total protein), and TRIGL (triacylglycerols).

2.3. Two-Dimensional Electrophoresis

2.3.1. Homogenization

Livers were dissected out and perfused by ice-cold PBS and stored at −70 °C. About 100 mg of the medial lobe of mouse liver was added to 2 mL vials containing ceramic beads (1.4 mm of diameter) and lysis buffer: 7 M urea, 2 M thiourea, 4% w/v CHAPS and protease inhibitors (cOmplete™, Mini Protease Inhibitor Cocktail, Roche Diagnostics GmbH, Mannheim, Germany) and then homogenized using MagNA Lyser Instrument (Roche Diagnostics GmbH, Mannheim, Germany). The homogenization conditions were as follows: two runs of 20 s at 4000 rpm and one run of 20 s at 5000 rpm (between each run samples were put in the cooling block for 3 min). Subsequently, the homogenates were centrifuged at 12,000× g for 25 min at 4 °C. Supernatants were collected and stored at −70 °C.

2.3.2. First Dimension—Isoelectrofocusing (IEF)

A modified Bradford assay was used to determine the protein extract's concentration according to the manufacturer's instructions (Protein Assay Dye Reagent Concentrate; Bio-Rad Laboratories, Inc., Hercules, CA, USA). The standard curve was determined from the series standard dilution of bovine serum albumin (BSA). Samples containing 660 µg of total protein were mixed with lysis buffer (7 M urea, 2 M thiourea, 4% CHAPS, 1% (w/v) dithiothreitol (DTT) and 0.5% (v/v) ampholytes (40% BioLyte® 3/10 Ampholyte, Bio-Rad Laboratories, Inc., Hercules, CA, USA) to adjust to a final volume of 330 µL per sample. Each liver sample was analyzed in two technical replicates. The precast immobilized pH gradient strips (non-linear pH 3–10, 17-cm length) were loaded with 600 µg of proteins by in-gel rehydration (passive—5 h, 0 V and active—12 h, 50 V). After rehydration, one electrode wick with 20 µL 0.01% DTT was placed in the cathode, and the other electrode wick with water was placed in the anode. Focusing began at 250 V for 125 Vh, 500 V for 250 Vh, 1000 V for 500 Vh in rapid mode, 5000 V for 1.5 h in linear mode and 5000 V for 90,000 Vh in rapid mode. During rehydration and IEF IPG strips were overlaid with mineral oil. Rehydration and isoelectrofocusing were carried in Protean i12 IEF Cell (Bio-Rad Laboratories, Inc., Hercules, CA, USA) at 20 °C. The separation of proteins in the non-linear range of pH 3–10 was assessed using the two-dimensional standard (2-D SDS-PAGE Standards, Bio-Rad Laboratories, Inc., Hercules, CA, USA). The mixture contained the following proteins with different molecular masses and isoelectric points conalbumin (76 kDa, pI 6.0, 6.3, 6.6), bovine serum albumin (66.2 kDa, pI 5.4, 5.6), actin (43 kDa, pI 5.0, 5.1), GAPDH (36 kDa, pI 8.3, 8.5), carbonic anhydrase (31 kDa, pI 5.9, 6.0), trypsin inhibitor (21.5 kDa, pI 4.5) and myoglobin (17.5 kDa, pI 7.0).

2.3.3. Second Dimension—SDS-PAGE

After IEF, the IPG strips were stored at −70 °C and prior to separation on the second dimension were transferred into equilibration buffer (6 M urea, 2% w/v SDS, 30% v/v glycerol, 17 mM Tris-HCl pH 6.8) for 15 min with additional 1% (w/v) DTT. For the next 20 min, IPG strips were incubated with equilibration buffer with 2.5% (w/v) iodoacetamide at room temperature. Finally, the strip was placed in 12% SDS-PAGE gel (aqueous acrylamide and bisacrylamide solution at a ratio of 29:1, 18 cm × 20 cm × 1.00 mm) and was fixed in place with a 0.5% (w/v) low-melting agarose overlay containing a trace amount of bromophenol blue to track electrophoresis. Gels were run in PROTEAN xi cell (Bio-Rad Laboratories, Inc., Hercules, CA, USA) 40 V for 2.5 h and 100 V for 18 h. The running buffer

(25 mM Tris, 192 mM glycine, 0.1% SDS) was cooled externally to 10 °C. The size standard used to determine the molecular weight on 2DE gels contained the following masses of proteins: 250 kDa, 150 kDa, 100 kDa, 75 kDa, 50 kDa, 37 kDa, 25 kDa, 20 kDa, 15 kDa and 10 kDa (Precision Plus Protein™ Standard Plugs, Unstained, Bio-Rad Laboratories, Inc., Hercules, CA, USA).

2.3.4. Image Staining and Analysis

After SDS-PAGE, the gels were washed in 500 mL distilled water three times. The gels were stained according to protocols described by [18,19]. Gels were fixed three hours in 750 mL buffer containing: 28.8% ethanol, 2.6% phosphoric acid and distilled water. Next, gels were incubated in staining buffer composed of 5% ammonium sulfate-18-hydrate, 10% ethanol, 0.02% Coomassie G-250 and 8.5% phosphoric acid for three hours. Gels were washed in 200 mL distilled water and destained using a solution of 10% ethanol and 2% phosphoric acid.

After staining, gels were scanned on a GelDoc XR+ (Bio-Rad Laboratories, Inc., Hercules, CA, USA). Protein spots were assigned automatically and manually verified. Protein spots densitometric analyses were performed by the PDQuest™ Advanced 8.0.1 software (Bio-Rad Laboratories, Inc., Hercules, CA, USA), applying the local regression model (LOESS) to normalize spot intensity.

The average value of the protein spot's densitometric intensity was applied to estimate changes between the groups. The fold of change below 1.00 means a decrease, whereas above 1.00 means the protein level increase. Based on the fold change value, a heat map was prepared in GraphPad Prism 7.04 (GraphPad Software, San Diego, CA, USA). Assignments of differentially expressed proteins according to their participation in metabolic pathways were performed using STRING 11.0 and the following databases: KEGG, REACTOME and Gene Ontology [20].

2.4. Matrix-Assisted Laser Desorption Ionization–Time of Flight Mass Spectrometry (MALDI-TOF MS)

The significantly differentiated protein spots have been analyzed using matrix-assisted laser desorption/ionization time-of-flight mass spectrometry (MALDI-TOF MS) to determine protein mass fingerprint and identify the specific protein. Biological replicates of each protein spots were manually excised from the average three polyacrylamide gels. Then, excised spots were destained with a solution of 200 mM NH_4HCO_3 in 40% acetonitrile and incubated at 37 °C for 30 min. Next, spots were vacuum-dried for 15–25 min. The dry gel piece was incubated for 16 h in 20 µL 20 µg/mL trypsin (0.4 µg trypsin in 40 mM NH_4HCO_3, 9% acetonitrile, 1 mM HCl per one spot) at 37 °C. Digestion was terminated by the addition of 2 µL of 5% trifluoroacetic acid (TFA). Peptide-matrix crystal layer was obtained on 800 µm AnchorChip 384 BC target plate (Bruker Daltonik GmbH, Bremen, Germany). Briefly, 1 µL of peptides from the in-gel digestions supernatant was loaded on the target plate and left to dry completely. Then, 1 µL of 5 µg/µL CHCA matrix solution (α-cyano-4-hydroxycinnamic acid in 70% acetonitrile and 0.1% TFA) was applied to the same spot and left to dry completely. Mass spectra were acquired in positive-ion reflector mode using the ultrafleXtreme™ spectrometer (Bruker Daltonik GmbH, Bremen, Germany). Peptide Calibration Standards Mix II (Bruker Daltonik GmbH, Bremen, Germany) was used for external calibration of the mass scale. Typically, 2000 shots were accumulated for mass spectrum generation in MS mode. The peak lists were cleared from all background peaks (such as matrix peaks—generated from CHCA crystallines, keratin contamination or polyacrylamide—from gel piece digestion without visible spot). The spectra were processed using the FlexAnalysis 3.4 and BioTools 3.2. Peptide alignment and protein identification was performed using the Peptide Mass Fingerprinting (PMF) technique. Data were compared to the mammalian SwissProt database using MASCOT software (http://www.matrixscience.com/ (accessed on 13 May 2021)). The following parameters were used for database searches: (1) trypsin digestion; (2) cysteine carbamidomethylation (Carbamidomethyl (C)) as a fixed modification; (3) acetylation (Acetyl (Protein N-term)

and methionine oxidation (Oxidation (M) as variable modifications; (4) mass tolerance to 150 ppm; and (5) maximum one missed cleavage site. The theoretical molecular mass and theoretical isoelectric point of statistically significant hits were compared with the localization of their protein spots in 2DE gel following two protein standards: one-dimensional Precision Plus Protein^{TM} Standard Plug (Bio-Rad Laboratories, Inc., Hercules, CA, USA) and two-dimensional 2-D SDS-PAGE Standards (Bio-Rad Laboratories, Inc., Hercules, CA, USA). UniProt [21], Gene Ontology [22,23] and pLoc-mEuk [24] were used to determine the cellular location of identified proteins.

2.5. Protein Expression Analysis by Western Blotting

Total protein was extracted from approximately 30 mg of liver samples using AllPrep RNA/DNA/PROTEIN (QIAGEN) according to the manufacturer's instructions. The protein pellet was dissolved in lysis buffer containing 7 M urea, 2 M thiourea and 4% CHAPS. Samples were boiled in Laemmli reducing sample buffer (62.5 mM Tris-HCl pH 6.8, 20% glycerol, 2% SDS, 5% β-mercaptoethanol, bromophenol blue), separated by 12% SDS-PAGE and transferred to a PVDF membrane. Specific antibodies are listed in Table S1 in the Supplementary Materials Chemiluminescence signals were detected using Clarity Western ECL Substrate (Bio-Rad Laboratories, Inc.) and ChemiDoc XRS+ Gel Imaging System (Bio-Rad Laboratories, Inc., Hercules, CA, USA).

The band lane's intensity value was quantified using Quantity One 1-D Analysis Software in Optical Density units (Bio-Rad Laboratories, Inc., Hercules, CA, USA). The experimental intensity values of target proteins (OAT and PRDX6) were normalized using the lane normalization factor, the value of the observed signal for GAPDH in each lane divided by the highest observed GAPDH signal on the blot. The normalized signal of each experimental target band was calculated by dividing each experimental target band's observed signal intensities by the determined lane normalization factor.

2.6. RNA Extraction and Quantitative RT-PCR

2.6.1. RNA Isolation

Total RNA was extracted from approximately 30 mg of liver samples from 6 samples per group using AllPrep RNA/DNA/PROTEIN (QIAGEN) according to manufacturer's instructions with the following modifications: (1) flow-through with 96% ethanol was added to RNeasy spin column into two parts (each time 430 µL) and (2) only 680 µL RW1 was used. The yield and purity of extracted total RNA were determined by NanoDrop ND-1000 spectrophotometer (Thermo Fisher Scientific Inc., Waltham, MA, USA) RNA samples were diluted to a concentration of approx. 640.28 ng/µL. RNA samples with an absorbance ratio OD 260/280 between 2.01–2.11 (average 2.05) and OD 260/230 between 2.01–2.31 (average 2.13) were used for RT reaction. RNA integrity was confirmed using 1% agarose gel electrophoresis with 0.002% ethidium bromide in TBE buffer (0.089 M Tris base, 0.089 M boric acid, 0.0025 M EDTA). Extracted RNA mixed with gel loading solution contained 60 mM Tris-HCl (pH 7.6), 60 mM EDTA, 0.003% bromophenol blue, 0.03% xylene cyanol FF, 60% glycerol (BLIRT S.A., Gdansk, Poland) and heated for 10 min in 70 °C. The gels were run for 60 min with constant voltage (90 V) before imaging under UV transillumination using UV Gel Doc XR+ (Bio-Rad Laboratories, Inc., Hercules, CA, USA).

2.6.2. Reverse Transcription (RT)

The first-strand cDNA synthesis was done using the Transcriptor First Strand cDNA Synthesis Kit (Roche Diagnostics GmbH, Mannheim, Germany). Reaction mix preparation: 1.5 µg of total RNA was reverse-transcribed using 2.5 µM anchored-oligo $d(T)_{18}$ primers and 60 µmol random hexamers and 10 U transcriptor reverse transcriptase in a final volume 20 µL. Stages of reverse transcription: denaturation of the template-primer mix at 65 °C for 10 min, reverse transcription at 25 °C for 10 min and 50 °C for 60 min, inactivation of transcriptor reverse transcriptase at 85 °C for 5 min. In each qPCR run, non-reverse transcriptase controls (NRT) were included.

2.6.3. Primers Design

Sequences of primers for reference and target genes were designed using Primer-BLAST (https://www.ncbi.nlm.nih.gov/tools/primer-blast/ (accessed on 13 May 2021)) on the genes mRNA nucleotide sequences from Gene database (https://www.ncbi.nlm.nih.gov/gene (accessed on 13 May 2021)), based on the following parameters: (1) primer length: 19–23 bp, (2) GC content—50–60%, (3) Tm—50–65 °C, (4) Max Tm difference = 3 °C, (5) Primer must span an exon-exon junction and (6) amplicon length 50–210 bp. All primers used in this study were synthesized in the Genomed S. A. The reference gene candidates were selected from the literature [25,26]. NormFinder was used to determine expression stability of selected candidate reference genes—beta-2 microglobulin (*B2m*), peptidylprolyl isomerase (*Ppia*) and cyclin G associated kinase (*Gak*) [27]. NormFinder identified *Gak* as the optimal reference gene, with the stability value equals 0.106. Sequences of all primers are provided in Supplementary Materials in Table S2.

2.6.4. Amplified Products Verification and Real-Time PCR Analysis

Six biological replicates for each group and three technical replicates for *Prdx6* and *Oat* of each biological replicate were analyzed for qPCR analysis. No-template controls (with water) were run for every reaction. Real-time PCRs were conducted in the 20 µL mixture contained 5 µL of diluted cDNA (dilution factor 25), 200 nM each of the forward and reverse primers and 10 µL of LightCycler® 480 SYBR Green I Mater (Roche Diagnostics GmbH, Germany). The qPCR was performed in LightCycler 480 Thermocycler (Roche Diagnostics GmbH, Germany) using the following cycle parameters: initial denaturation 95 °C, 5 min, amplification in 45 cycles of 95 °C for 10 s, 59 °C for 10 s and 72 °C for 20 s. Post-amplification melting-curve analysis was performed under conditions: 95 °C for 5 s, 65 °C for 1 min, and the temperature was increased to 97 °C.

All primer sets were tested for specificity in 2.5% agarose gel electrophoresis stained with SYBR™ Safe DNA Gel Stain (Thermo Fisher Scientific Inc., Waltham, MA, USA). Amplification specificity of each reaction was done by melting curve analysis.

The quantification of gene expression by cycle (Cq) values of every sample were done by LightCycler 480 Software ver. 1.5.1.62 qPCR efficiencies in the exponential phase were calculated for each primer pair for each amplification plate using LinRegPCR version 2018.0 [28]. The relative expression levels for each mRNA transcript were based on the method described by Pfaffl M.W. (2001) [29,30]. Calibrator was the average value of the SFA group. All target genes were normalized to a reference gene (*Gak*).

2.7. Statistical Analysis

Alterations in mass body weights during the experiment were analyzed by Two-Way ANOVA and Tukey's multiple comparisons test using GraphPad Prism 7.04 (GraphPad Software, San Diego, CA, USA).

The comparative densitometric analysis of protein spots included liver samples isolated from 32 mice fed a 3-month diet consisted of a set of 510 spots that occurred on each of 2DE gels. The values of each spot's intensity in the four groups in two technical replications for individuals were used to analyze the multiple regression function recorded in the form of a model (1). The same model (1) was used to analyze biochemical and relative expression levels of selected target genes. The analysis was performed in the SAS 9.4 system. (SAS Institute Inc., Cary, NC, USA). The differences between diet groups were estimated using Tukey's test. For the observations that presented the data distribution were non-normal, the Wilcoxon Mann–Whitney test was used to compare the differences between diet groups. The levels of significance in this model were marked as follows: *—$p < 0.05$; **—$p < 0.01$; ***—$p < 0.001$.

$$y_{ijkl} = \mu + O_i + M_j(O_i) + G_k + e_{ijkl} \quad (1)$$

y—response variable; O_i—i-paternal genetic effect; $M_j(O_i)$—j-maternal genetic effects nested into i—paternal genetic effect; G_k—effect of diet type; and e—the error term.

Mean values, standard deviations (SD), standard error of the mean (SEM) and bar plots were made in GraphPad Prism 7.04 (GraphPad Software, San Diego, CA, USA).

3. Results

3.1. Total Fat Content in Diets

The total fat content in the STD was about 2.11%. Whereas the SFA and 14:1 and 5:1 diets contained 22.54%, 21.56% and 21.86% fat, respectively (Figure 1). A more than 10 times higher fat content in the SFA, 14:1 and 5:1 diets than in the STD diet resulted from the addition of vegetable oils.

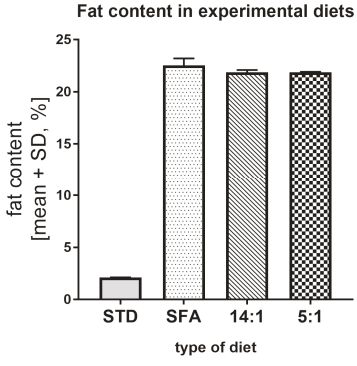

Figure 1. Amount of total fat content in the experimental diets.

Body weights of mice initially did not differ. Body weights of the STD and SFA groups varied after 14 days (^{AB}—$p < 0.05$), and mice from the SFA group were significantly heavier than corresponding animals from the STD group after 28 and 42 days of the experiment (^{CD}—$p < 0.01$ and ^{EF}—$p < 0.001$, respectively). The latter trend continued until the end of diet treatment. After 42 days of the SFA diet, the mice weighed more than the 5:1 group (^{CD}—$p < 0.01$), and they gained proportionally more weight after 85 days (^{gh}—$p < 0.001$). Body weights in the 14:1 group after 56 days of the experiment were greater than in the STD group (^{cd}—$p < 0.01$). Similarly, after another two weeks, body weights of mice from the 14:1 group were higher than the STD group (^{ef}—$p < 0.001$). This trend was maintained after 85 days of feeding with respective diets (Figure 2).

3.2. Biochemical Blood Parameters

Changes in blood plasma parameters in mice fed the STD diet, SFA diet, 14:1 diet and 5:1 diet for three months were presented in Table 2. There were no significant statistical differences between the experimental groups in any of the parameters measured except for total cholesterol and glucose concentrations. The total cholesterol levels in mice fed the SFA and 14:1 diets were significantly higher than in animals fed the STD diet. Moreover, high-fat diets (SFA, 14:1, and 5:1 diets) caused a significant increase in glucose concentration compared to the STD diet.

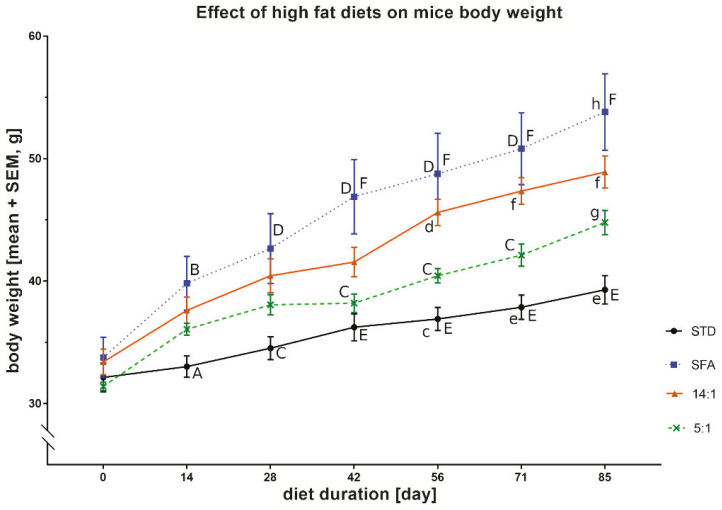

Figure 2. Body weights of mice fed standard (STD), high-fat high-saturated (SFA) diets and high-fat high-polyunsaturated diets with LA/ALA equal 14:1 and 5:1 (14:1 and 5:1, respectively) during approximately 3 months of the experiment. Values are means ± SEM, n = 8. Values with a different letter differ significantly at the same diet duration time point: ^{AB}—$p < 0.05$; ^{CD} or ^{cd}—$p < 0.01$; ^{EF} or ^{ef} or ^{gh}—$p < 0.001$.

Table 2. Plasma biochemical parameters after three-month diets—the standard (STD), the experimental diets (SFA, 14:1 and 5:1)—expressed in arithmetic mean values (SD) (8 per group).

Parameter	STD	SFA	14:1	5:1
albumin [g/L]	33.34 (1.51)	32.39 (1.74)	34.01 (1.91)	31.54 (1.36)
total protein [g/L]	53.61 (4.19)	57.09 (7.38)	59.01 (8.48)	49.80 (2.21)
total bilirubin [µmol/L]	1.58 (0.65)	1.65 (0.34)	1.09 (0.54)	1.49 (0.59)
alanine aminotransferase [U/L]	41.00 (17.78)	36.25 (10.31)	38.25 (16.00)	32.75 (6.02)
aspartate aminotransferase [U/L]	138.13 (62.66)	93.00 (21.84)	106.50 (47.88)	109.13 (65.12)
cholinesterase [U/L]	8219.75 (2215.14)	6931.88 (981.76)	6659.50 (1134.28)	6563.75 (488.00)
lipase [U/L]	13.66 (1.15)	21.04 (2.95)	23.39 (6.48)	18.49 (2.97)
iron [µmol/L]	19.99 (4.52)	26.33 (5.22)	26.14 (4.50)	25.84 (4.42)
glucose [mmol/L]	**5.29 ^{C,E} (1.66)**	**12.01 ^{D} (1.32)**	**10.60 ^{D} (1.68)**	**11.40 ^{F} (1.44)**
total cholesterol [mmol/L]	**2.83 ^{A,C} (0.31)**	**3.98 ^{B} (0.48)**	**4.44 ^{D} (0.63)**	3.60 (0.58)
high-density lipoprotein-cholesterol [mmol/L]	2.79 (0.33)	3.81 (0.64)	4.12 (0.86)	3.53 (0.58)
low-density lipoprotein-cholesterol [mmol/L]	0.12 (0.13)	0.39 (0.18)	0.37 (0.27)	0.31 (0.20)
triacylglycerols [mmol/L]	0.91 (0.28)	1.39 (0.38)	1.13 (0.17)	1.17 (0.31)

Significant differences between means were determined using the statistical model (1). Results were considered significant at ^{AB}—$p < 0.05$; ^{CD}—$p < 0.01$; ^{EF}—$p < 0.001$ and highlighted in bold.

3.3. Analysis of Liver Proteome Differences

Approximately 977 spots were recorded in one 2DE gel with 510 spots overlapping in each of 64 2DE gels. The mean coefficient of variation (CV) of the STD group was 46.47%, 42.04% in the SFA group, 43.29% in the 14:1 group and 42.83% in the 5:1 group.

Thirty-seven gel spots showed a significant change in abundance. The results are shown in representative images in Figures 3–5.

The list of gel spots whose densitometric intensity varied between the groups and the results of MALDI-TOF protein identification associated with each spot are presented in Table 3. Comparative mass spectrometric analysis of mouse liver extracts identified a total of 35 proteins. Mitochondrial ATP synthase subunit beta (ATP5F1B) and carbonic anhydrase 3 (CA3) were identified in two spots. MASCOT scores of the protein assignments ranged from 61 to 346 (average MASCOT score—161). Proteins were identified with an average of 46% sequence coverage based on 5 to 32 matching peptides. The median number of peptides matches was 13. Median E-values ranged from 1.70×10^{-30} to 4.90×10^{-2}.

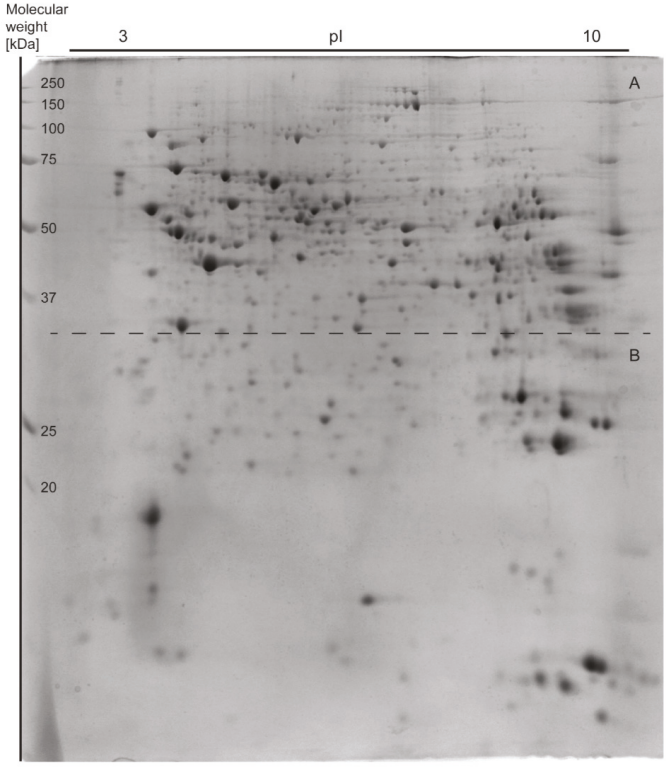

Figure 3. The representative two-dimensional electrophoresis gel image of mouse liver proteins. A total of 600 µg of whole liver proteins was applied to the IPG strip (non-linear pH 3–10, 17-cm length) for the first dimension and then the second dimension was performed on 12% SDS-PAGE gels. The 2DE gel (18 cm × 20 cm × 1.00 mm) was stained with Coomassie Brilliant Blue G-250. The figure was divided into two parts (A and B) according to the dashed line.

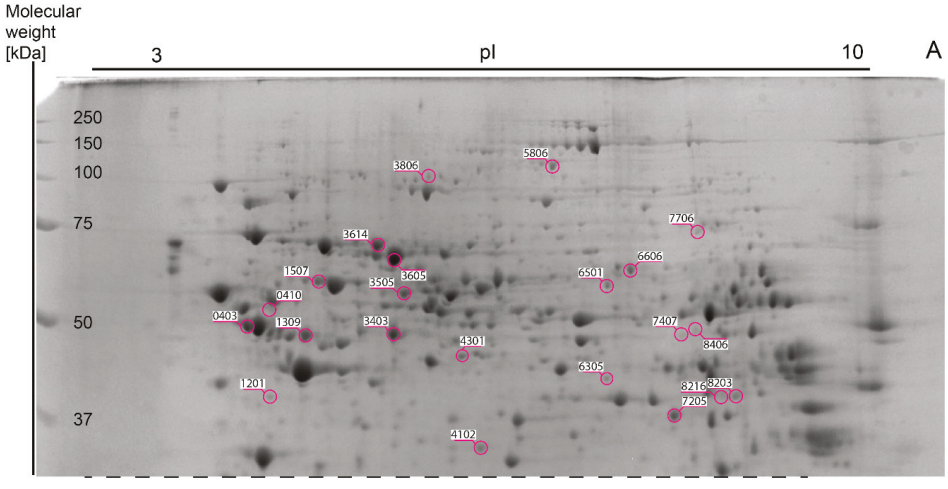

Figure 4. Part A of Figure 3 eresentative 2DE map of liver proteins stained with Coomassie Brilliant Blue G-250). Spot numbers (SSP) and areas of differential spots in the figure correspond to the SSP number in Table 3.

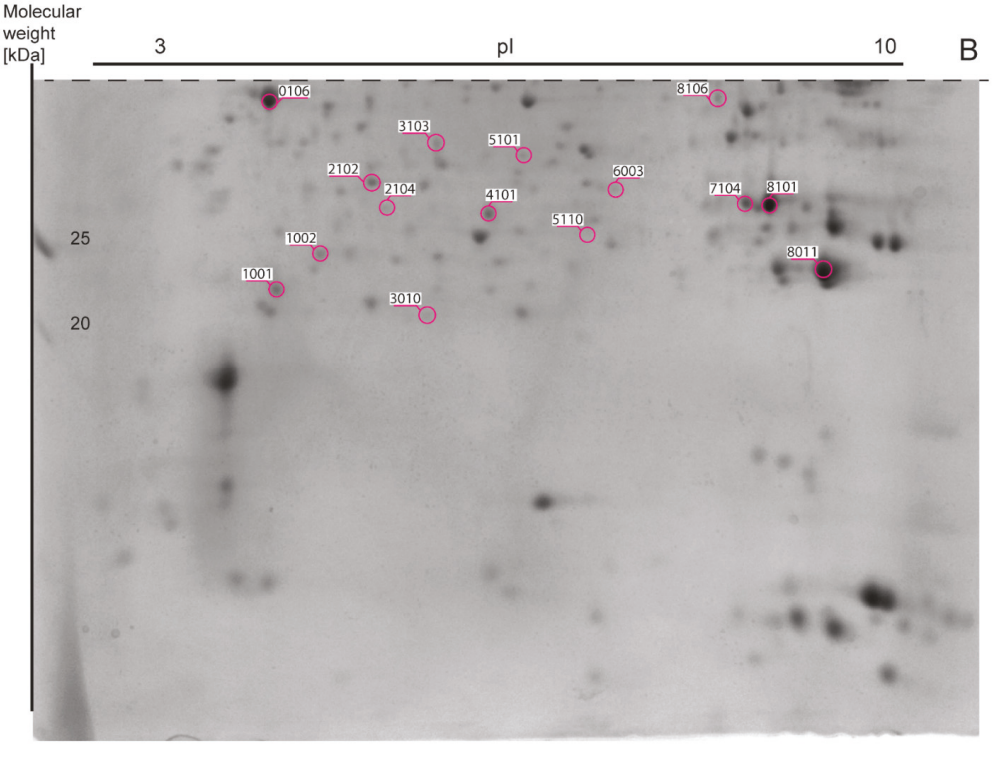

Figure 5. Part B of Figure 3 (representative 2DE map of liver proteins stained with Coomassie Brilliant Blue G-250). Spot numbers (SSP) and areas of differential spots in the figure correspond to the SSP number in Table 3.

Table 3. Differentially expressed protein spots between the standard (STD) and the high-fat diet groups (SFA, 14:1, 5:1) in mouse liver.

Spot Number (SSP)	Protein Name	Accession Number UniProtKB/NCBI	Gene Symbol	*MASCOT Score*	E-Value	Sequence Coverage	Peptides Matched /Peptides Searched	Theoretical pI/MW (Da)	Fold Change					
									SFA/STD	14:1/STD	5:1/STD	14:1/SFA	5:1/SFA	5:1/14:1
0106	Regucalcin	Q64374/NP_033086.1	*Rgn*	188	1.1e-14	61%	16/28	5.15/ 33,899	1.13	1.34 (**)	1.20	1.19	1.07	0.90
0403	ATP synthase subunit beta, mitochondrial	P56480/NP_058054.2	*Atp5f1b*	346	1.7e-30	70%	32/49	5.19/ 56,265	1.39	1.29	0.78	0.92	0.56 (**)	0.61 (*)
0410	ATP synthase subunit beta, mitochondrial	P56480/NP_058054.2	*Atp5f1b*	298	1.1e-25	59%	28/37	5.19/ 56,265	0.79	0.72	1.58	0.91	2.00	2.21 (*)
1001	Lactoylglutathione lyase	Q9CPU0/NP_001107032.1	*Glo1*	72	3.90e-03	30%	5/13	5.24/ 20,967	1.12	1.48 (***)	1.24	1.32 (**)	1.11	0.84
1002	Apolipoprotein A-I	Q00623/NP_033822.2	*Apoa1*	168	1.1e-12	48%	18/46	5.51/ 30,597	0.65 (*)	0.96	0.44 (***)	1.47 (*)	0.67	0.46 (***)
1201	Galactokinase	Q9R0N0/NP_058601.2	*Galk1*	95	2.1e-05	33%	11/40	5.17/ 42,668	1.36 (**)	1.36 (**)	1.05	1.00	0.78 (*)	0.77 (*)
1309	Keratin, type I cytoskeletal 18	P05784/NP_034794.2	*Krt18*	256	1.7e-21	66%	27/61	5.22/ 47,509	0.86	0.88	0.73 (**)	1.03	0.86	0.83
1507	60 kDa heat shock protein, mitochondrial	P63038/NP_034607.3	*Hspd1*	213	3.4e-17	42%	22/38	5.91/ 61,088	1.15	0.94	0.82	0.82	0.71 (**)	0.87
2102	Prohibitin	P67778/NP_032857.1	*Phb*	184	2.7e-14	65%	13/26	5.57/ 29,859	0.80 (***)	0.78 (***)	0.79 (***)	0.98	1.00	1.02
2104	NADH dehydrogenase [ubiquinone] iron-sulfur protein 3, mitochondrial	Q9DCT2/NP_080964.1	*Ndufs3*	155	2.1e-11	47%	11/20	6.67/ 30,302	0.89	0.85 (*)	0.81 (**)	0.95	0.91	0.96
3010	Ferritin light chain 1	P29391/NP_034370.2	*Ftl1*	108	1.1e-06	53%	8/23	5.66/ 20,847	1.16	0.87	0.79	0.75 (*)	0.69 (**)	0.92
3103	Ketohexokinase	P97328/NP_032465.2	*Khk*	61	4.90e-02	26%	5/14	5.59/ 33,300	1.44 (**)	1.29	1.32	0.89	0.91	1.02
3403	S-adenosylmethionine synthase isoform type-1	Q91X83/NP_598414.1	*Mat1a*	179	8.5e-14	50%	20/43	5.51/ 44,051	0.66 (*)	0.53 (***)	0.62 (***)	0.80 (*)	0.93	1.16
3505	Sulfite oxidase, mitochondrial	Q8R086/NP_776094.2	*Suox*	215	2.1e-17	45%	16/26	6.07/ 61,231	1.15	1.20 (**)	1.09	1.04	0.94	0.90
3605	Albumin	P07724/NP_033784.2	*Alb*	288	1.1e-24	54%	29/55	5.75/ 70,700	0.45 (**)	0.47 (**)	0.41 (**)	1.06	0.93	0.87
3614	Stress-70 protein, mitochondrial	P38647/NP_034611.2	*Hspa9*	245	2.1e-20	48%	29/46	5.81/ 73,701	1.07	1.01	0.73	0.94	0.69 (*)	0.73
3806	Cytosolic 10-formyltetrahydrofolate dehydrogenase	Q8R0Y6/NP_081682.1	*Aldh1l1*	114	2.7e-07	21%	13/23	5.64/ 99,502	1.57 (*)	1.88 (***)	1.37	1.19	0.87	0.73 (*)
4101	Indolethylamine N-methyltransferase	P40936/NP_033375.1	*Inmt*	113	3.4e-07	51%	10/23	5.75/ 30,068	0.88	0.87	0.82 (*)	0.98	0.93	0.94
4102	ester hydrolase C11orf54 homolog	Q91V76/NP_001186413.1	N/A	120	6.7e-08	46%	13/40	5.86/ 35,430	1.30 (**)	1.35 (**)	1.51 (***)	1.04	1.16	1.12

Table 3. *Cont.*

Spot Number (SSP)	Protein Name	Accession Number UniProtKB/NCBI	Gene Symbol	*MASCOT Score*	E-Value	Sequence Coverage	Peptides Matched /Peptides Searched	Theoretical pI/MW (Da)	Fold Change					
									SFA/STD	14:1/STD	5:1/STD	14:1/SFA	5:1/SFA	5:1/14:1
4301	Ornithine aminotransferase, mitochondrial	P29758/NP_058674.1	*Oat*	205	2.1e-16	53%	20/36	6.19/48,723	0.62 (***)	0.60 (***)	0.68 (***)	0.97	1.09	1.13 (*)
5101	Endoribonuclease LACTB2	Q99KR3/NP_663356.1	*Lactb2*	86	1.80e-04	26%	8/17	5.89/33,019	1.09	1.00	1.26 (*)	0.92	1.16	1.27 (*)
5110	Peroxiredoxin-6	O08709/NP_031479.1	*Prdx6*	189	8.5e-15	72%	15/33	5.71/24,969	1.17	1.45 (***)	1.44 (***)	1.25	1.24	0.99
5806	Pyruvate carboxylase, mitochondrial	Q05920/NP_001156418.1	*Pc*	101	5.3e-06	15%	13/22	6.25/130,344	1.27	1.19	0.91	0.94	0.71 (**)	0.76
6003	Haloacid dehalogenase-like hydrolase domain–containing protein 3	Q9CYW4/NP_077219.1	*Hdhd3*	117	1.3e-07	35%	10/24	6.31/28,237	1.01	1.21 (*)	1.11	1.20 (*)	1.10	0.92
6305	Isovaleryl-CoA dehydrogenase, mitochondrial	Q9JHI5/NP_062800.1	*Ivd*	95	2.2e-05	34%	12/38	8.53/46,695	0.74 (***)	1.02	0.97	1.39 (***)	1.32	0.95
6501	Carboxylesterase 1D	Q8VCT4/NP_444430.2	*Ces1d*	124	2.7e-08	33%	15/31	6.17/62,034	1.12	1.34 (*)	0.81	1.20	0.73	0.60 (**)
6606	Triokinase/FMN cyclase	Q8VC30/NP_663471.1	*Tkfc*	249	8.5e-21	55%	27/40	6.44/59,938	1.45 (***)	1.28	1.15	0.88	0.79 (*)	0.90
7104	Carbonic anhydrase 3	P16015/NP_031632.2	*Ca3*	231	5.3e-19	81%	16/34	6.89/29,633	1.13	1.41 (*)	1.56 (***)	1.25 (*)	1.39 (*)	1.11
7205	Arginase-1	Q61176/NP_031508.1	*Arg1*	225	2.1e-18	72%	19/52	6.51/34,957	0.95	0.73 (***)	0.86	0.77 (**)	0.91	1.18
7407	Hydroxymethylglutaryl-CoA synthase, mitochondrial	P54869/NP_032282.2	*Hmgcs2*	97	1.4e-05	25%	13/32	8.65/57,300	1.39 (**)	0.92	1.02	0.66 (*)	0.73	1.10
7706	long-chain–fatty-acid–CoA ligase 1	P41216/NP_032007.2	*Acsl1*	116	1.7e-07	24%	14/31	6.81/78,928	0.78	0.65 (**)	0.75	0.83	0.97	1.16
8011	Glutathione S-transferase P 1	P19157/NP_038569.1	*Gstp1*	86	1.90e-04	48%	13/53	7.68/23,765	0.86	1.05	1.24	1.22	1.44 (*)	1.18
8101	Carbonic anhydrase 3	P16015/NP_031632.2	*Ca3*	237	1.3e-19	81%	18/81	6.89/29,633	0.97	1.14	1.33 (*)	1.18	1.37 (**)	1.16
8106	Glycerol-3-phosphate dehydrogenase [NAD(+)], cytoplasmic	P13707/NP_034401.1	*Gpd1*	119	8.5e-08	40%	12/32	6.75/38,176	1.42 (**)	1.06	1.42 (**)	0.75 (*)	1.00	1.33 (*)
8203	Acetyl-CoA acetyltransferase, cytosolic	Q8CAY6/NP_033364.2	*Acat2*	83	3.40e-04	27%	8/30	7.16/41,727	1.00	1.30 (*)	1.55 (**)	1.31	1.55 (**)	1.19
8216	Serine–pyruvate aminotransferase, mitochondrial	O35423/NP_057911.2	*Agxt*	92	4.1e-05	33%	11/44	8.37/46,282	1.20	1.24	1.93 (*)	1.03	1.61	1.56
8406	Homogentisate 1,2-dioxygenase	O09173/NP_038575.2	*Hgd*	103	3.4e-06	28%	11/28	6.86/50,726	1.18	0.62 (*)	0.77	0.52 (***)	0.65 (**)	1.25

The results show the highest identification values of proteins from an average of three biological replicates. The statistically significant ($p < 0.05$) value of the average intensity of the SFA, 14:1, 5:1 groups compared to the STD group, as well as the 14:1 and 5:1 groups compared to the SFA, and the 5:1 group compared to the 14:1 group. The significance of differences estimated using the model (1). *—$p < 0.05$; **—$p < 0.01$; ***—$p < 0.001$.

The altered liver proteins were grouped into functional sets based on the STRING database, which was presented with a green–white–red fold of change value scale.

Changes in the expression of hepatic proteins involved in lipid metabolism were presented in Figure 6. Significantly higher values of protein abundance were obtained for fatty acid β-oxidation proteins—ACAT2 in the 5:1 group compared to the SFA group ($p < 0.01$) and IVD in the 14:1 group relative to the SFA group ($p < 0.001$). Moreover, ACAT2 intensity was increased in the 14:1 and 5:1 groups compared to the STD group ($p < 0.05$ and $p < 0.01$, respectively). There was a significantly lower protein abundance of IVD in the SFA group than in the STD group ($p < 0.001$). Significantly lower values (more than 2-fold lower) were obtained for albumin after high-fat diets (SFA, 14:1 and 5:1) in comparison to the STD group ($p < 0.01$). The mean values for APOA1 abundance were lower for the SFA and 5:1 diets in comparison to the STD group ($p < 0.05$ and $p < 0.001$, respectively). Statistically significant differences in APOA1 abundance were also found between the 5:1 and 14:1 groups ($p < 0.001$). Expression of other proteins involved in lipid biosynthesis was also decreased, inter alia ACSL1, whose expression was reduced in the 14:1 compared to the STD group, and CES1D, whose expression was lower in the 5:1 versus the 14:1 group ($p < 0.01$).

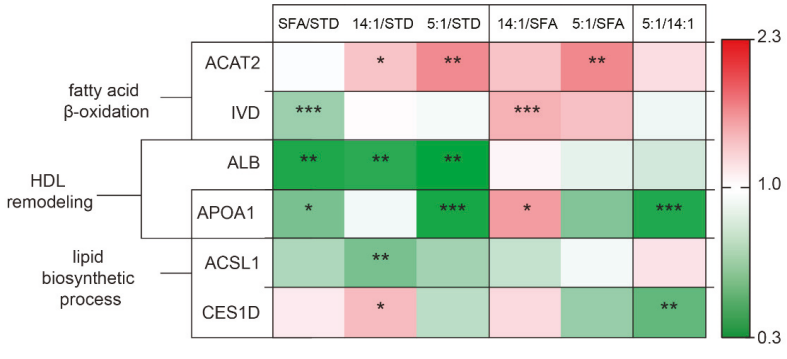

Figure 6. Changes in the abundance of proteins involved in lipid metabolism. The statistically significant ($p < 0.05$) value of the average intensity of the SFA, 14:1 and 5:1 groups compared to the STD group; the 14:1 and 5:1 groups compared to the SFA group; the 5:1 group compared to the 14:1 group. The significance of differences estimated using the model (1). *—$p < 0.05$; **—$p < 0.01$; ***—$p < 0.001$.

Diets enriched with PUFAs or SFAs affected hepatic proteins involved in amino acid metabolism (Figure 7). In the 14:1 group, the quantity of ARG1 was reduced in comparison to the STD ($p < 0.001$) and SFA groups ($p < 0.01$). In the SFA, 14:1, and 5:1 groups, reductions were observed in the level of MAT1A ($p < 0.05$, $p < 0.001$, $p < 0.001$, respectively) and OAT (all—$p < 0.001$) in comparison to the STD group. After three months of diet, AGXT levels significantly increased in the 5:1 group compared to the STD group ($p < 0.05$). The level of SUOX was increased in the 14:1 group compared to the STD group ($p < 0.01$). Moreover, increased abundance of IVD was determined in the 14:1 group compared to the SFA group ($p < 0.001$); similarly lower levels of HGD were also found in the 14:1 and 5:1 groups versus the SFA group ($p < 0.001$ and $p < 0.01$, respectively). There were significant reductions in the abundance of IVD, HGD and INMT in the SFA, 14:1 and 5:1 groups, respectively, in comparison to the STD group ($p < 0.001$, $p < 0.05$ and $p < 0.05$, respectively).

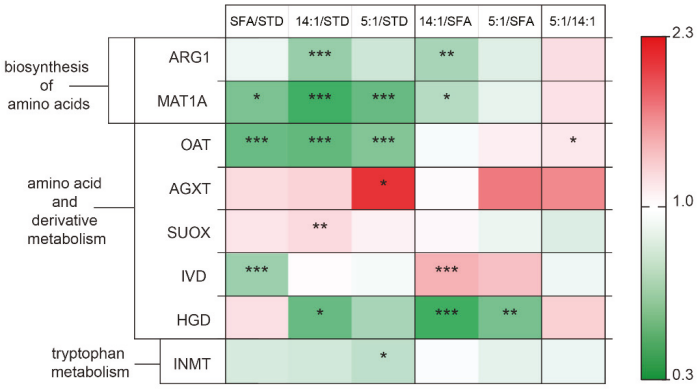

Figure 7. Changes in the abundance of proteins involved in amino acid metabolism. The statistically significant ($p < 0.05$) value of the average intensity of the SFA, 14:1 and 5:1 groups compared to the STD group; the 14:1 and 5:1 groups compared to the SFA group; the 5:1 group compared to the 14:1 group. The significance of differences estimated using the model (1). *—$p < 0.05$; **—$p < 0.01$; ***—$p < 0.001$.

Liver proteome analyses showed an influence of the treatment with different diets enriched with PUFAs or SFAs on several proteins responsible for carbohydrate metabolism and ATP synthesis (Figure 8). The level of hepatic PC decreased successively in the 5:1 group in comparison to the SFA group ($p < 0.01$). Levels of proteins involved in glycolytic processes, such as TKFC, KHK and GALK1, were all significantly increased in the SFA group in relation to the STD group ($p < 0.01$). GALK1 level was also increased in the 14:1 group compared to the STD group ($p < 0.01$). In contrast, TKFC and GALK1 expression was decreased in the 5:1 compared to the SFA group ($p < 0.05$). Additionally, GALK1 abundance was also decreased in the LA/ALA 5:1 group compared to the 14:1 group ($p < 0.05$). Two isoforms of ATP5F1B, including SSP 0403 and SSP 0410, showed differentiated changes in mouse livers, ATP5F1B SSP 0403 from the 5:1 group was decreased compared to the 14:1 group ($p < 0.05$), while expression level of ATP5F1B SSP 0410 in the 5:1 group was more highly expressed compared to the 14:1 group ($p < 0.05$). Additionally, ATP5F1B SSP 0403 expression was shown to be reduced in the 5:1 group versus the SFA group ($p < 0.01$).

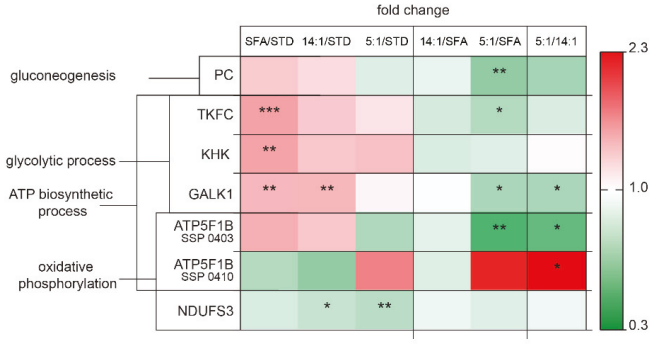

Figure 8. Changes in the abundance of proteins involved in carbohydrate metabolism and ATP synthesis. The statistically significant ($p < 0.05$) value of the average intensity of the SFA, 14:1 and 5:1 groups compared to the STD group; the 14:1 and 5:1 groups compared to the SFA group; the 5:1 group compared to the 14:1 group. The significance of differences estimated using the model (1). *—$p < 0.05$; **—$p < 0.01$; ***—$p < 0.001$.

The heat map in Figure 9 demonstrates the clustering of significantly increased versus significantly decreased expression of proteins involved in oxidative stress in liver tissue in mice fed with high-polyunsaturated fatty acid diets compared to tissues of mice fed with the standard diet or high-saturated fatty acid diet. Endoribonuclease LACTB2 levels were markedly elevated in the 5:1 samples in comparison to the STD and 14:1 samples ($p < 0.05$). The expression of HSPD1 was down-regulated in the 5:1 group compared to the SFA group ($p < 0.01$). ARG1 was identified as a down-regulated protein in the 14:1 group relative to the STD and SFA groups ($p < 0.001$ and $p < 0.01$, respectively). Two up-regulated proteins found in the 5:1 group in comparison to the SFA group included CA3 and GSTP1. High levels of PRDX6 were found in the liver of mice fed the 14:1 and 5:1 diets compared to the STD group ($p < 0.001$).

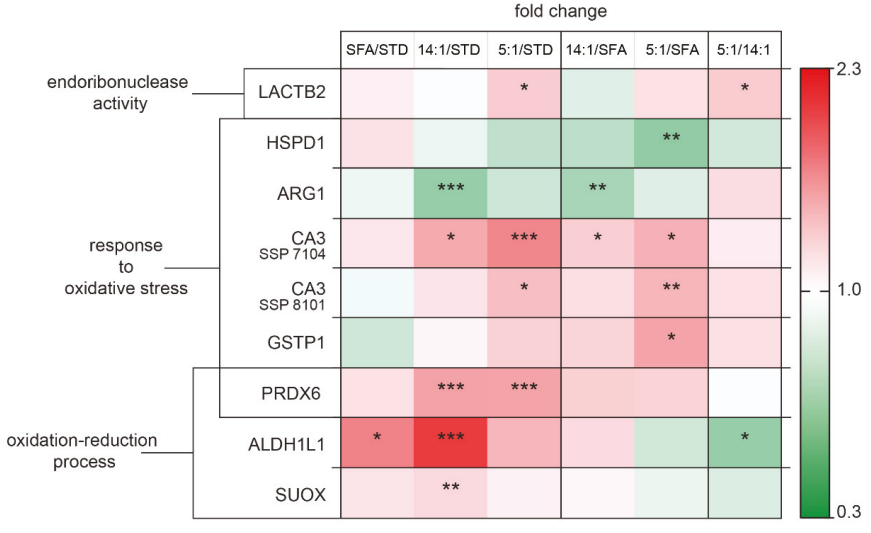

Figure 9. Changes in the abundance of proteins involved in oxidative stress regulation. The statistically significant ($p < 0.05$) value of the average intensity of the SFA, 14:1 and 5:1 groups compared to the STD group; the 14:1 and 5:1 groups compared to the SFA group; the 5:1 group compared to the 14:1 group. The significance of differences estimated using the model (1). *—$p < 0.05$; **—$p < 0.01$; ***—$p < 0.001$.

Our results of proteomic screening provided a list of proteins involved in cell death processes (Figure 10). RGN and GLO1 levels were increased in the 14:1 group in comparison to the STD group ($p < 0.01$ and $p < 0.001$, respectively). The animals fed the 14:1 diet had significantly increased GLO1 level compared to the SFA group ($p < 0.01$). In contrast, GSTP1 expression was markedly decreased in the 5:1 group compared to the SFA group ($p < 0.05$).

PHB levels were decreased following the HFD treatment (SFA/STD, 14:1/STD and 5:1/STD, $p < 0.001$). KRT18 protein expression changed significantly following 3 months of feeding the PUFA diet (LA/ALA ratio—5:1) in comparison to the STD group ($p < 0.01$). The levels of HSPA9 and HSPD1 proteins in the 5:1 group were significantly lower in relation to the SFA group ($p < 0.05$ and $p < 0.01$, respectively). FTL1 expression was decreased in the groups of mice fed the high-PUFA diets compared to the group fed the high-saturated diet (14:1/SFA $p < 0.05$ and 5:1/SFA $p < 0.01$, respectively). We observed a lower level of ACSL1 in mice treated with the 14:1 diet compared to the group fed the standard diet ($p < 0.01$).

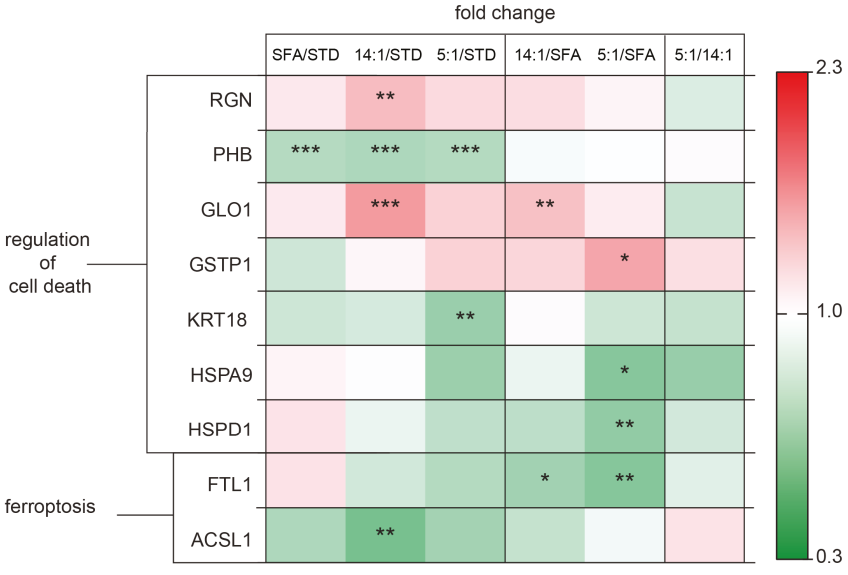

Figure 10. Changes in proteins involved in cell death processes. The statistically significant ($p < 0.05$) value of the average intensity of the SFA, 14:1 and 5:1 groups compared to the STD group; the 14:1 and 5:1 groups compared to the SFA group; the 5:1 group compared to the 14:1 group. The significance of differences estimated using the model (1). *—$p < 0.05$; **—$p < 0.01$; ***—$p < 0.001$.

After three months of the STD diet, the expression of 13 proteins was different in comparison to the SFA group, including elevated levels of six proteins: ALB (SSP 3605), APOA1 (SSP 1002), IVD (SSP 6305), MAT1A (SSP 3403), OAT (SSP 4301) and PHB (SSP 2102) as well as reduced levels of seven proteins: ALDH1L1 (SSP 3806), GALK1 (SSP 1201), GPD1 (SSP 8106), HMGCS2 (SSP7407), KHK (SSP 3103), TKFC (SSP 6606) and UniProtKB: Q91V76 (SSP 4102).

The differences in the expression of 11 protein between the 14:1 and SFA diets were identified, involving higher levels of the following five proteins: APOA1 (SSP 1002), GLO1 (SSP 1001), HDHD3 (SSP 6003), IVD (SSP 6305) and CA3 (SSP 7104). Expression downregulation was observed the case of six proteins in the 14:1 group in comparison to the SFA group: ARG1 (SSP 7205), FTL1 (SSP 3010), GPD1 (SSP 8106), HGD (SSP 8406), HMGCS2 (SSP 7407) and MAT1A (SSP 3403).

The level of eleven proteins was altered in the 5:1 group compared to the SFA group. The expression of three proteins was elevated in the 5:1 group: ACAT2 (SSP 8203), CA3 (SSP 7104 and SSP 8101) and GSTP1 (SSP 8011). The level of eight proteins in the 5:1 group was decreased in comparison to the SFA group: ATP5F1B (SSP 403), GALK1 (SSP 1201), HSPD1 (SSP 1507), FTL1 (SSP 3010), HSPA9 (SSP 3614), PC (SSP 5806), TKFC (SSP 6606) and HGD (SSP 8406).

After three months of feeding the high-PUFA diets (14:1 and 5:1) the level of CA3 was increased in comparison to the SFA group. Two protein spots—FTL1 and HGD—were identified that were consistently reduced in the liver proteome of mice fed high PUFA diets in comparison to the SFA diet.

The present proteomic study also revealed differences between groups fed high-PUFA diets in the levels of hepatic proteins, including downregulated proteins in the 5:1 group (ALDH1L1, APOA1, CES1D, GALK1) and three upregulated proteins in the 5:1 group (GPD1, LACTB2, OAT) in comparison to the 14:1 group.

A detailed comparison of increased and decreased protein expressions between experimental groups is presented in Figure 11A,B.

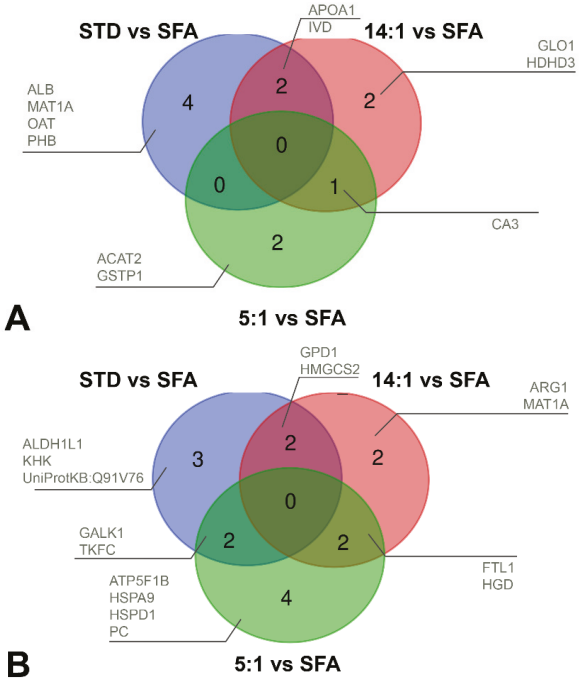

Figure 11. Venn diagram of differentially expressed proteins after three-months diets. (**A**) The number and list of proteins with increased expression in the STD (blue), 14:1 (red) and 5:1 (green) groups compared to the SFA. (**B**) The number and list of proteins with decreased expression in the STD (blue), 14:1 (red) and 5:1 (green) groups compared to the SFA.

3.4. Controlling mRNA and Protein Expression Levels by High-Fat Diets

OAT and PRDX6 were further analyzed as representatives of amino acid metabolism and oxidative stress regulation processes, respectively. The mRNA and protein expression levels of these proteins were measured using real-time PCR and immunoblotting. The specificity of primary antibodies and primers were confirmed. Only one amplification product was detected for each of the primer pairs. The PCR reaction specificity was ensured by post-amplification melting-curve analysis. Uncropped Western blots, amplicon products and melting curves were available in the Supplementary Materials (Figures S1–S3).

No significant differences were observed in OAT and PRDX6 protein levels (Figures 12a and 13a). As shown in Figure 12b, OAT expression was insignificantly reduced in the high-fat diet groups (SFA and 5:1) in comparison to the STD group, but the reduction pattern was consistent with 2DE data. The expression of OAT gene at the mRNA level was not significantly increased in animals fed with the STD diet compared to the other experimental groups (Figure 12c).

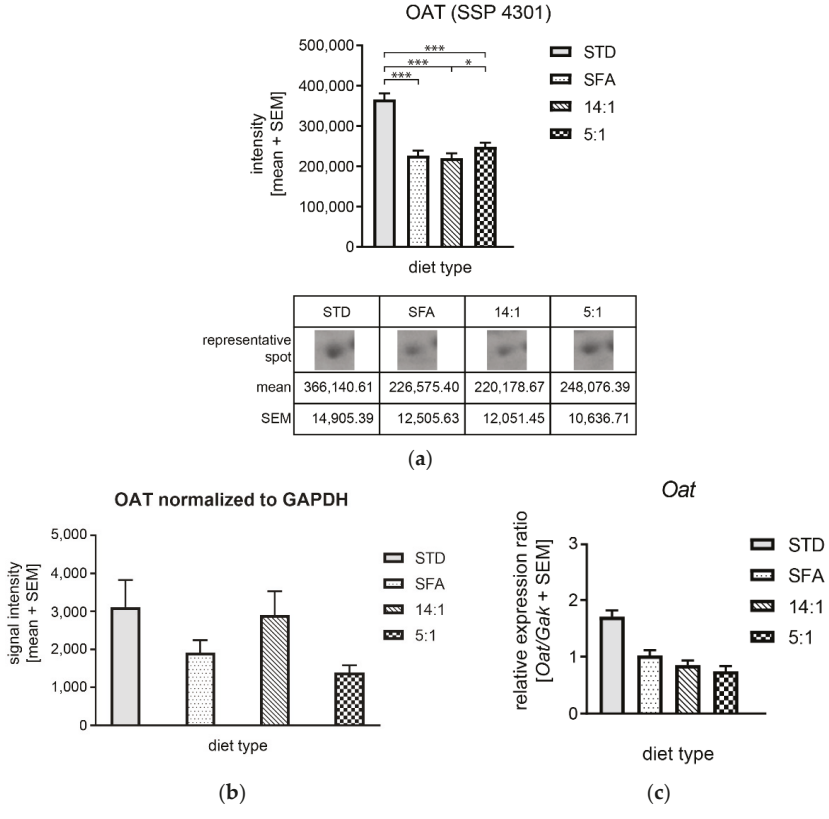

Figure 12. Alterations of OAT expression in response to different high-fat diets. (**a**) Protein levels based on 2DE; (**b**) Western blotting analysis using anti-OAT and anti-GAPDH antibodies and six mouse liver samples per group; signal intensities of OAT were normalized to GAPDH signal intensities. Graphs presented a mean intensity with a standard error of the mean (SEM); (**c**) *Oat* mRNA level normalized to *Gak*. *—$p < 0.05$; ***—$p < 0.001$.

Real-time PCR results were consistent with the 2DE results showing the increased PRDX6 mRNA level in the 14:1 group compared to the STD group, while increased *Prdx6* expression in the 5:1 group was not confirmed. The immunoblot analysis did not confirm changes in PRDX6 levels between groups (Figure 13b).

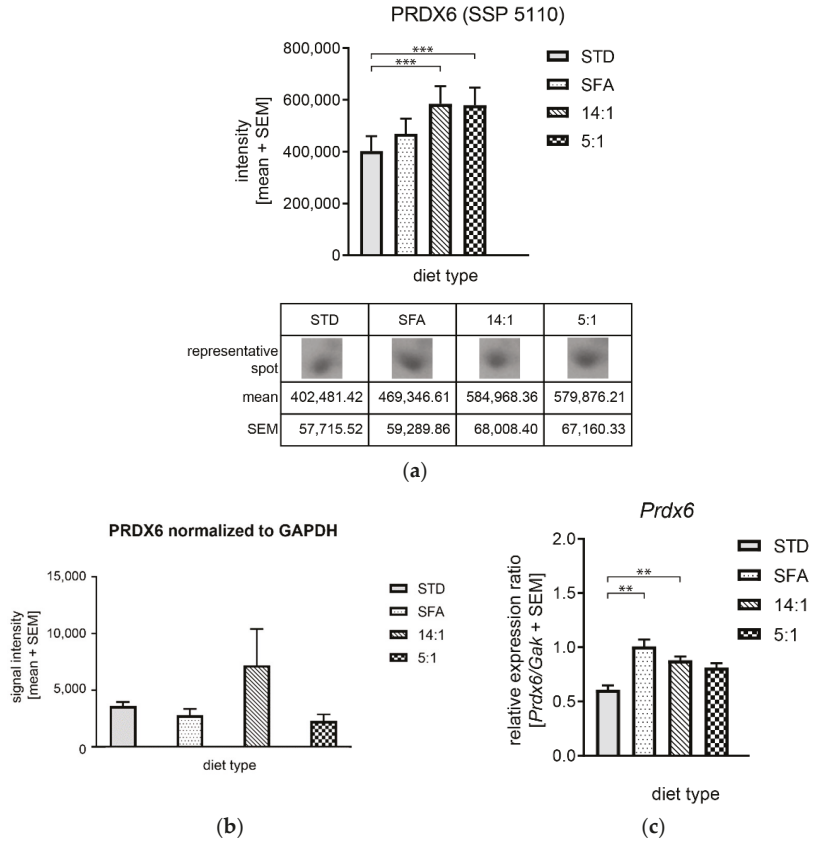

Figure 13. Alterations of PRDX6 expression in response to different high-fat diets. (**a**) Protein levels based on 2DE; (**b**) Western blotting analysis using anti-PRDX6 and anti-GAPDH antibodies and six mouse liver samples per group; signal intensities of PRDX6 were normalized to GAPDH signal intensities. Graphs presented a mean intensity with a standard error of the mean (SEM); (**c**) *Prdx6* mRNA level normalized to *Gak*. **—$p < 0.01$; ***—$p < 0.001$.

4. Discussion

The study presented the influence of HFDs with different fatty acid composition on the mouse liver proteome. In the experiment, we assigned two control groups. Animals of the control group (STD) received standard chow for laboratory mice. The SFA group was used as a negative control in comparisons between high-fat diet groups, according to a high content of saturated fatty acids with a chain length of 12–18 carbons and a low PUFA content in coconut oil. We compared the effects of a high LA/ALA ratio (14:1) with the effects induced by a lower ratio (5:1) to investigate the impact of high-fat diets with different n–6/n–3 polyunsaturated fatty acids contents on liver metabolism. These two LA/ALA proportions mimic the high ratio of these fatty acids (14:1) specific to a Western-type diet, and the low ratio of these acids (5:1) is considered a healthy diet.

It was shown that the composition of consumed fat and the content of individual fatty acids had a different effect on weight gain [31]. In the present study, we noticed differences in weight gain between the experimental groups, as body weight gain was higher in the SFA group in comparison to the STD group after the first two weeks of the experiment. Body weights in the SFA group were significantly increased when compared to the STD group and the group fed the high-fat diet with the recommended n–6/n–3 (5:1) ratio.

These results were consistent with the study of Beulen et al. who showed that replacing SFAs with PUFAs in the diet resulted in body weight loss [32]. One possible explanation could be a different fat accumulation, as shown in the studies by Rosqvist et al. where the group consuming SFAs was characterized by an increased fat accumulation in the liver and viscera compared to the group ingesting more PUFAs [33]. Increased uptake of this feed due to its attractive aroma, which was caused by a characteristic flavor of virgin coconut oil, could be another factor affecting body weight of the SFA mouse group. In addition, after 56 days of the diet, body weights of mice from the 14:1 group were elevated compared to the STD group, and this difference increased during the following four weeks of the experiment. However, the current study showed that the SFA diet was more obesogenic than the 14:1 and 5:1 PUFA diets.

In this study, high-fat diets (SFA and 14:1) increased total cholesterol levels compared to the standard low-fat diet, which was consistent with the results of Li et al. who reported that total plasma cholesterol levels were significantly higher in mice fed a high-fat diet after 12 and 16 weeks of the experiment compared to a low-fat diet group [34,35]. However, supplementation with a high-fat diet enriched in n–3 acids (5:1 diet) did not significantly change total cholesterol content in comparison to a standard diet. This could indicate that a high-saturated fat diet and a diet high in n–6 FAs disturbed cholesterol homeostasis to a higher extent than the high-PUFA 5:1 diet. This was partially in line with the findings of Kralova Lesna et al. who confirmed that PUFA diet consumption resulted in a substantially lower concentration of total cholesterol than in the SFA diet [36]. A similar result was also obtained by Gaundal et al. as these authors demonstrated that replacing products rich in SFAs with high amounts of PUFAs for only three days in young but adult men and women, resulted in a reduction of total cholesterol levels in blood serum [37].

We also found that feeding HFDs rich in PUFAs for three months did not change blood plasma biochemical parameters, including albumin, triglycerides, LDL and HDL lipoproteins. This observation differed slightly from the study by Diniz et al. who reported that albumin and HDL cholesterol levels were higher in PUFA-fed rats than in SFA-fed rats, however triacylglycerol and LDL cholesterol levels were lower after the administration of PUFA diets compared to the SFA diet [38]. These differences could be due to the shorter treatment period (5 weeks in the study of Diniz vs. 12 weeks in the present study).

4.1. Differences in the Expression of Proteins Related to Lipid Metabolism

Soltis et al. showed that a high-fat diet caused liver dysfunction, including abnormal hepatocyte morphology and apoptosis rate [39]. Liver steatosis may lead to its dysfunction, inflammation, fibrosis, and consequently, to cirrhosis and hepatocellular carcinoma. Previous studies demonstrated that fat accumulation in the liver caused by a high-fat diet was associated with increased lipogenesis and inhibition of lipolysis [40]. Similar results were not obtained in the present study. The expression of proteins related to lipid biosynthesis processes, such as APOA1 and ACSL, was reduced following the high-fat diet. Moreover, none of the altered proteins was related to lipolysis.

Our results clearly showed that all high-fat diets reduced ALB protein level compared to the STD diet. Additionally, concentrations of two other proteins related to lipid metabolism—ACAT and IVD—were increased after PUFA-rich diets compared to the SFA diet. We also identified proteins whose expression was altered between PUFA-rich diets: APOA1 and CES1D levels were decreased in the 5:1 group compared to the 14:1 group.

Proteomic studies performed here indicated that different types of high-fat diets also altered the abundance of proteins associated with lipid metabolism, such as ACAT2. This protein is mainly expressed in the liver, but also in the small intestine [41]. ACAT2 is an endoplasmic reticulum transmembrane protein that is responsible for transferring the fatty acyl moiety of acyl-CoA to free cholesterol by producing cholesteryl esters (CE), mainly cholesteryl oleate and palmitate. ACAT2-derived CE can be packaged directly into apoB-containing lipoproteins or stored as neutral lipid droplets in the cytosol [42]. A significantly higher abundance of ACAT2 protein was observed in the 14:1 and 5:1 groups than in the

control group, and in the 5:1 group compared to the SFA group. This result has confirmed that PUFAs are preferred fatty acid substrates for ACAT2 in the liver and may stimulate ACAT activity as opposed to SFAs. The consequence of increased hepatic ACAT2 activity was a higher secretion of cholesteryl ester from the liver and subsequent enrichment of LDL with cholesteryl oleate [43]. Bell et al. fed ACAT2$^{-/-}$ mice with diets enriched in either n–3 or n–6 PUFAs, saturated FAs and *cis* or *trans* monounsaturated FAs. After 20 weeks of the diet, the control group showed signs of atherosclerosis signs, whereas ACAT2$^{-/-}$ mice were protected against atherosclerosis regardless of the administered fat [43]. On the other hand, ACAT2$^{-/-}$ mice were shown to be more susceptible to insulin resistance caused by a high-fat diet [41]. It is interesting because animals fed PUFA-rich HFDs with the highest expression of ACAT2, simultaneously showed slightly lower plasma glucose level. Moreover, ACAT2 expression was shown to be stabilized by saturated fatty acids and sterols through the ROS formation, which prevented its degradation via ubiquitin-proteasome pathway [41]. It has indicated that different expression pattern may be observed for this protein depending on its particular modifications.

IVD was another protein associated with lipid metabolism differentially expressed in response to 3 months feeding with high-fat diets. This protein level was higher in the 14:1 than in the SFA group ($p < 0.001$). Additionally, IVD expression was decreased in the SFA group compared to the STD group ($p < 0.001$). A contrasting result was obtained by Guo et al. who showed that mice fed a high fat died had elevated IVD levels in the liver compared to mice fed a normal diet, which was suggested as enhanced branched-chain amino acid (BCAA) degradation in liver mitochondria of mice fed the high-fat diet [44]. It should be emphasized, however, that IVD downregulation may lead to the accumulation of isovaleryl-CoA derivatives, including isovaleric acid (IVA), and reduced production of acetyl-CoA and acetoacetate [45]. The consequences of IVA accumulation may be the induction of oxidative stress and protein oxidative damage due to significantly elevated carbonyl formation [46]. This suggested that a marked downregulation of IVD could induce oxidative stress in the livers of animals fed the SFA diet.

APOA1 is the main protein forming HDL particles. The highest HDL concentration in blood plasma was recorded in the 14:1 group. Chylomicrons enriched in n–6 PUFAs, such as linoleic acid, are enzymatically removed from circulation faster than chylomicrons enriched in SFAs or n–3 PUFAs [47]. Reduced fat mass was observed in mice overexpressing APOA1 [48]. Similarly, ApoA-I$^{-/-}$ mice showed increased body weight compared to wild type mice fed an obesogenic diet [49]. In this study, increased APOA1 levels in the liver of 14:1 mice, compared to the SFA group ($p < 0.05$), could be a reason for lower weight gains by 14:1 mice compared to SFA mice. It may also be the reason why 14:1 mice exhibited increased circulating cholesterol levels compared to the SFA and 5:1 groups (but results were not significant). Han et al. reported that Pepck and G6Pase mRNA levels were significantly elevated in the livers of Apoa-I-deficient mice (ApoA-I$^{-/-}$). Plasma glucose concentrations in the latter animals were significantly increased compared to wild-type controls. This suggests that APOA-I decrease can modulate critical gluconeogenic enzymes [50]. This observation was consistent with our results, where the level of APOA1 protein was lower in the livers of mice from the SFA and 5:1 groups compared to the STD group, and could also be the reason for increased plasma glucose levels. An in-depth analysis of the detected change in the expression of apolipoprotein A1 at the protein level under the influence of diets with a different LA to ALA ratio ($p < 0.001$) should be the direction of further research.

CES1D was another identified protein whose expression differed between mice fed different LA/ALA diets, as it was decreased in the 5:1 group versus the 14:1 group ($p < 0.01$); murine CES1D is also annotated as triacylglycerol hydrolase (TGH) or CES3. Lian et al. showed that CES1D deficiency attenuated both simple hepatic steatosis and irreversible NASH [51]. Mice deficient in CES1D expression ameliorated high-fat diet-induced hepatic steatosis by reducing of de novo lipogenesis [51]. In addition, hepatic CES1D is involved in the supply of substrates for VLDL assembly. CES1D inhibition decreased VLDL secre-

tion both in vitro and in vivo [51]. Moreover, fatty acid oxidation was also significantly increased in hepatocytes isolated from Ces1d-deficient mice [52]. VLDL level and steatosis and fibrosis markers were not determined in the present study, but a high-PUFA diet with 5:1 LA/ALA ratio has the potential to alleviate fatty liver disease and prevent steatohepatitis in comparison to a high-PUFA diet with LA/ALA of 14:1.

4.2. Changes in the Expression of Proteins Involved in Carbohydrate Metabolism

Our study showed increased blood glucose levels after 12-week feeding of all types of high-fat diets compared to the standard diet; the highest glucose level was recorded after the SFA diet treatment. Our results were consistent with the work of He et al. [34]. Almost all circulating glucose is derived from hepatic glycogenolysis (breakdown of stored glycogen) and de novo production of glucose from precursors such as pyruvate and galactose (i.e., gluconeogenesis, which is stimulated by glucagon and inhibited by insulin) [53].

The present study showed that the liver proteome after three months of the SFA diet was characterized by an increased level of TKFC, KHK and GALK1 proteins in comparison to the STD diet. These proteins are involved in the glycolytic process. Hepatic fructose metabolism, represented by two enzymes (KHK and TKFC) was changed following the high-fat-high-saturated diet (SFA group) in comparison to the standard diet (STD group). Nevertheless, these alterations did not occur after high-fat-high-PUFA diets in contrast to the STD group. KHK, the first enzyme of fructose metabolism, provides substrates for fatty-acid synthesis and enhances de novo lipogenesis. In this way, the SFA diet could lead to fatty liver disease and insulin resistance pathogenesis, as elevated KHK protein levels were found in liver biopsies of obese adolescent humans with NAFLD [54]. Alterations in the second step of hepatic fructolysis were also observed in the form of changed TKFC protein levels. The SFA diet significantly increased the level of TKFC protein compared to the STD group ($p < 0.001$). However, TKFC expression in the 5:1 group was reduced compared to the SFA group ($p < 0.05$).

We found a set of 3 proteins involved in glucose metabolism that were down-regulated in mice liver by the high-PUFA 5:1 diet compared to the SFA diet. This category included proteins involved in gluconeogenesis (PC, $p < 0.01$) and glycolysis (GALK1 and TKFC, $p < 0.05$). Increased hepatic gluconeogenesis is a critical step in the pathogenesis of type 2 diabetes. PC protein regulates hepatic glucose production. Chronically decreased PC expression in liver and adipose tissue was demonstrated to reduce plasma glucose concentrations, the rate of endogenous glucose production, adiposity, plasma lipid concentrations, hepatic steatosis and improved hepatic insulin sensitivity [55]. Thus, the 5:1 diet may be more therapeutic in reducing fasting hyperglycemia in humans with type 2 diabetes than the 14:1 and SFA diets. Additionally, two high-fat diets (SFA and 14:1) increased GALK1 levels in the liver in comparison to the STD group ($p < 0.01$). The human body metabolizes galactose through the Leloir pathway, and in the first step, GALK, which phosphorylates α-D-galactose to galactose-1-phosphate (gal-1-P), is the rate-limiting enzyme in the clearance of galactose from the blood [56,57]. Increased expression of GALK may result in the accumulation of toxic galactose-1-phosphate. On the other hand, the SFA and 14:1 diets may be beneficial in the management of galactokinase deficiency (galactosemia type II) to avoid blocking the Leloir pathway leading to galactitol accumulation in the lens [58].

4.3. Changes in the Expression of Proteins Associated with Amino Acid Metabolism.

The present proteomic study revealed alterations between the levels of proteins involved in amino acid metabolism in the liver, as a result of different types of high-fat diet digestion. The expression of MAT1A and OAT was decreased in all experimental high-fat groups compared to the STD group. There were also proteomic alterations in ARG1, HGD and MAT1 hepatic levels between the high-PUFA 14:1 group and SFA group. Moreover, one protein was upregulated in the group of mice fed a diet with a 5:1 n–6/n–3 PUFA ratio compared to mice fed a diet with a 14:1 ratio.

ARG1 expression was decreased in the liver of mice fed the 14:1 diet in comparison to mice fed the SFA diet ($p < 0.01$). A downregulation of ARG1 expression was observed in the 14:1 group as opposed to the STD group ($p < 0.001$). Similar results were obtained in the study of Bashir et al. where ARG1 protein and mRNA levels were reduced in murine macrophages in adipose tissue of the group fed an HFD in comparison to the lean group fed standard chow [59]. L-Arginine (Arg), hydrolyzed by arginase, is considered an important amino acid in homeostasis maintenance, and its metabolism is altered in various diseases [60]. Arginase I (ARG1) is the most abundantly expressed isoform in hepatocytes. Furthermore, liver damage was shown to increase plasma arginase activity in obese rodents [61,62]. A study by Romero et al. in diabetic rats revealed significantly increased arginase I levels in the aorta and liver, as well as elevated vascular and hepatic arginase activity [63]. A diet rich in PUFA with LA/ALA of 14:1 has been found to be an effective therapeutic strategy to reduce the level of this protein. In addition, this is because arginase inhibition may be a treatment option for obesity-induced vascular endothelial dysfunction, hepatic lipid abnormalities, whole-body adiposity and obesity-related hypertension [61,64,65].

The current work showed a reduced level of OAT protein in the groups fed high-fat diets compared to the group fed the STD diet. A reduction in OAT expression at the protein level was observed in the livers of mice fed with PUFA-rich feed (14:1 and 5:1) compared to mice fed with SFAs. There were also differences in the level of this protein between the groups fed with different PUFA proportions (14:1 and 5:1). Animals fed the 5:1 diet showed higher OAT gene expression at the protein level. This result was consistent with similar analyses using two-dimensional electrophoresis, in which a diet rich in PUFA n–3 with a lower n–6/n–3 ratio (5:1) increased the level of OAT expression and its activity in the liver compared to animals receiving a diet with an n–6/n–3 ratio of 30:1 [66]. Our results differed from those obtained by Luo et al. [67], as the latter authors demonstrated increased expression of the *Oat* gene at the protein level in the livers of mice fed a high-fat diet compared to the group of animals fed a standard-fat diet. However, disparate results between the studies could be due to different total fat contents in the feeds (10% and 60%) used by Luo et al. [67]. OAT is a key enzyme in the urea cycle that metabolizes ornithine to glutamate semialdehyde in the liver. Nevertheless, its overexpression in transgenic mice did not alter amino acid homeostasis [68]. *Oat* is a PPARα-regulated gene [69] and its activation by PUFA induces the expression of genes with the PPRE sequence, including ACOX and CPT-I [70]. High expression of the *Oat* gene is characteristic of hepatocellular carcinoma (HCC); for this reason, it is supposed to be involved in carcinogenesis. The ability of OAT inhibitors to limit HCC growth makes OAT a potential therapeutic target for inhibiting the growth of this tumor [71]. For this reason, higher fatty acid contents in the diet, in particular *n*–6 PUFAs, may inhibit tumorigenesis in the liver and act similarly to synthetic OAT inhibitors.

Twelve-week interventions with the 14:1 and 5:1 high-PUFA diets led to reduced HGD levels compared to the high-saturated fat diet ($p < 0.001$ and $p < 0.01$, respectively). Similar results were obtained by Mendez et al. who reported that fish oil mixture supplementation of a high-fat high-sucrose (HFHS) diet significantly downregulated HGD level in rat liver compared to a control diet [72]. According to these results, dietary fat restriction should be considered to avoid adverse homogentisic acid (HGA) accumulation, for instance in alkaptonuria patients with residual HGD enzymatic activity caused by missense mutations in the *HGD* gene.

4.4. Changes in the Expression of Proteins Involved in Oxidative Stress Regulation

Previous research has shown that long-term feeding with a high-fat diet increases oxidative stress [73]. Among the experimental high-fat diets, the 14:1 and 5:1 groups exhibited altered levels of proteins mainly involved in the response to oxidative stress, including PRDX6, when compared to standard dietary fat levels. However, it should be mentioned that these results were only partially validated at the mRNA level and using

immunoblotting at the protein level. PUFAs undergo peroxidation after reacting with free radicals and are converted into reactive free radicals, and their chain reaction products display high biological activity [74]. PRDX6 is known as a bifunctional protein with both glutathione peroxidase and phospholipase A2 activity. Oxidant stress is a potent inducer of PRDX6 expression [75] that reduces H_2O_2 and phospholipid hydroperoxides. Lack of PRDX6 is associated with pro-inflammatory gene upregulation in the liver [76]. Overexpression of PRDX6 reduced reactive oxygen species levels and improved cell viability [77]. Moreover, PRDX6 has been shown to maintain mitochondria integrity under oxidative stress and protect against insulin resistance and non-alcoholic fatty liver disease induced by a high-fat diet [78]. Thus, increased hepatic PRDX6 expression in animals fed PUFA-rich HFDs may indicate the contribution of PUFAs to liver protection against oxidative stress caused by high-fat diet administration. Consequently, the lack of a protective effect of PRDX6 overexpression may lead to the development of metabolic disorders.

Extensive hepatic proteomic changes induced by feeding PUFAs revealed proteins associated with oxidative stress response, including HSPD1, CA3 and GSTP1. HSPD1/HSp60 was downregulated in the 5:1 group compared to the SFA group ($p < 0.01$). However, no alterations were observed between HFDs and STD. Our data were not consistent with the results obtained by Guo et al. who showed HSP60 upregulation in liver mitochondria isolated from mice fed an HFD compared to a regular diet [44]. Hsp60 forms a large homo-oligomeric protein complex that assists in folding proteins and protein domains [79]. CA3 belongs to a family of enzymes that catalyze the reversible condensation of water and carbon dioxide to carbonic acid, which further dissociates to bicarbonate. Bicarbonate is considered a necessary precursor for fatty acid synthesis and storage. Thus, CA3 is abundant in tissues that synthesize and store lipids, such as liver and adipose tissue [80]. Zimmerman provided information on the role and mechanism of action of CA3 as an antioxidant by assessing S-glutathionylation and irreversible oxidation of two protein-reactive cysteines in the presence of increasing intensity of oxidative stress damage [81]. In the present study, CA3 level was increased in the livers of animals from the 14:1 and 5:1 groups compared to the STD group. Increased CA3 can exert adverse effects because it is involved in hepatic steatosis development induced by a Western diet containing high fructose corn syrup; CA3 inhibition resulted in a decrease in hepatic steatosis and weight gain [82].

4.5. Changes in the Expression of Proteins Involved in Cell Death Processes

Another set of altered hepatic proteins has been associated with cell death processes. In the present study, PHB levels were lower in the livers of mice fed all types of high-fat diets compared to the standard-fat diet ($p < 0.001$). Such results indicate that three-month diets rich in fat may initiate liver dysfunctions, because PHB is known to be a highly conserved, ubiquitously expressed protein that participates in diverse processes, including mitochondrial chaperoning activity, growth and apoptosis. PHB exhibits antioxidant properties in the liver [83,84]. Ko et al. demonstrated that knockout mice lacking PHB1 had impaired mitochondrial function, upregulated expression of genes involved in malignant transformation and liver fibrosis, as well as multiple liver lesions between 35–46 weeks of age [85].

Our results also revealed changes in the expression of other proteins related to cell death processes, including RGN, GLO1 and KRT18, whose levels were increased in the PUFA groups compared to the STD group, while HSPA9, HSPD1 and FTL1 levels were decreased in the 5:1 group compared to the SFA group. RGN is known as a calcium-binding protein that plays a significant role in maintaining intracellular calcium signaling and lipid metabolism [86]. A proteomic study by Ahmed et al. found that mice fed a high n–3 PUFA diet showed lower RGN expression compared to mice fed a low *n*–3 PUFA diet [66]. This result was not confirmed in the current experiments, where the RGN level was elevated in mice fed the 14:1 diet in comparison to the STD group (a low n–3-PUFA diet) ($p < 0.01$). RGN overexpression was shown to induce hepatic insulin resistance and

hyperlipidemia in rats [87]. Yamaguchi et al. showed increased serum RGN levels, whereas liver mRNA levels decreased after carbon tetrachloride administration, suggesting a role of this protein in cellular response in chronic liver damage [88]. KRT18 levels markedly decreased following 3 months of feeding the PUFA LA/ALA 5:1 diet in comparison to the STD group (0.73-fold change, $p < 0.01$). KRT18 encodes type I intermediate filament chain keratin 18. Ubiquitinated KRT18, KRT8, and sequestosome 1/p62 are the main components of Mallory–Denk bodies (MDB) specific for alcoholic steatohepatitis and NASH [89]. The major molecular processes involved in MDB formation are associated with an elevated ratio of keratin 8 to keratin 18 [90]. Imbalance in KRT8/KRT18 expression occurs in alcoholic liver disease (ALD) and promotes MDB formation [91]. Harada et al. proved that KRT18 overexpression inhibited MDB formation and protected against inflammatory infiltration [92]. Betterman et al. showed that KRT18 deficiency in hepatocytes led to steatosis, which increased with age, and ultimately to steatohepatitis [93]. This study indicated that a PUFA-rich diet with an LA/ALA ratio of 5:1 could disturb hepatocellular type I and type II keratin homeostasis and promote liver steatosis.

HSPA9 is a member of the heat shock protein 70 (Hsp70) family [94]. This protein expression was downregulated in the livers of animals from the 5:1 group when compared to the SFA group. HSPA9 plays a significant role in chaperoning misfolded proteins, mitochondrial import and assistance in iron-sulfur cluster (ISC) biogenesis [95,96]. HSPA9 is overexpressed in numerous types of tumors and is involved in carcinogenesis and progression processes [97], including hepatocellular carcinoma metastasis. Reduced HSPA9 expression in immortalized cells causes growth arrest. Thus, HSPA9 is a potential target for HCC cancer therapy [98]. The decreased HSPA9 expression in the group of animals fed the high-PUFA diet with an LA/ALA ratio of 5:1 could be caused by n–3 PUFA administration, which partially prevented liver damage caused by excessive amounts of FAs.

5. Conclusions

Our study revealed differential regulation of metabolic processes in the livers of mice fed high-fat diets with qualitative differences in fatty acids composition. Moreover, the results showed that high-fat diets increased, to varying degrees, plasma biochemical parameters, including total cholesterol and glucose concentrations. The replacement of saturated fatty acids with PUFAs resulted in many changes in the liver protein expression profiles. These changes could result in alterations in various processes, e.g., increased fatty acid β-oxidation, reduced glucose synthesis and glycolysis or redox balance changes. These distinct changes in liver metabolism could potentially explain differences in mortality and metabolic disorders disclosed in epidemiological studies on the type and amount of consumed fat.

The current study could not distinguish which dietary LA/ALA ratio was less destructive for the liver. Nevertheless, the results provided strong evidence for the different influence of low and high LA/ALA dietary ratios on liver metabolism, as two proteins were upregulated in the 5:1 group (OAT, LACTB2) and four proteins were downregulated (APOA1, CES1D, GALK1, ALDH1L1) in comparison to the 14:1 group. Thus, these results led us to the conclusion that the dietary recommendation of replacing SFAs with PUFAs is too general and should be investigated in more detail.

Solving the problem of an improperly balanced diet in terms of fatty acids is a matter of alleviating adverse metabolic changes, including overweight, obesity, hyperglycemia and hyperlipidemia, which is particularly important in the 21st century. Appropriate recommendations regarding dietary fat content and quality can prevent the development of chronic diseases causing disability, death and increased health care expenditure.

Supplementary Materials: The following are available online at https://www.mdpi.com/article/10.3390/nu13051678/s1, Table S1: List of immunoblot antibodies; Table S2: List of reference and target genes investigated in the analysis; Figure S1a,b: Western blot replicates as uncropped images; Figure S2: Amplicon products lengths; Figure S3a,b: Amplicon products melting curves.

Author Contributions: Conceptualization, M.P., A.L. and E.P.; methodology, M.P., A.L., E.P., K.P.L., A.N., A.J. and W.G.; software, M.P., A.L., K.P.L. and A.J.; validation, K.P.L. and A.J.; formal analysis, M.P.; investigation, K.P.L., A.N., M.O., A.S., A.J., W.G., M.L., P.U. and A.R.; resources, M.P. and A.J.; data curation, M.P. and K.P.L.; writing—original draft preparation, K.P.L., A.L. and M.P.; writing—review and editing, K.P.L., M.O., E.P., A.J., A.N., P.U., M.L., A.L., C.S.P. and M.P.; visualization, K.P.L.; supervision, M.P., A.L.; project administration, K.P.L., A.N. and M.P.; funding acquisition, M.P. All authors have read and agreed to the published version of the manuscript.

Funding: This research was funded by KNOW (Leading National Research Centre) Scientific Consortium "Healthy Animal—Safe Food", the decision of Ministry of Science and Higher Education No. 05-1/KNOW2/2015", grant no. KNOW2015/CB/PRO1/44.

Institutional Review Board Statement: The study design and animal handling were approved by the II Warsaw Local Ethics Committee for Animal Experimentation (WAW2_22/2016).

Informed Consent Statement: Not applicable.

Conflicts of Interest: The authors declare no conflict of interest.

References

1. Diao, P.; Wang, X.; Jia, F.; Kimura, T.; Hu, X.; Shirotori, S.; Nakamura, I.; Sato, Y.; Nakayama, J.; Moriya, K.; et al. A saturated fatty acid-rich diet enhances hepatic lipogenesis and tumorigenesis in HCV core gene transgenic mice. *J. Nutr. Biochem.* **2020**, *85*, 108460. [CrossRef]
2. Lappano, R.; Sebastiani, A.; Cirillo, F.; Rigiracciolo, D.C.; Galli, G.R.; Curcio, R.; Malaguarnera, R.; Belfiore, A.; Cappello, A.R.; Maggiolini, M. The lauric acid-activated signaling prompts apoptosis in cancer cells. *Cell Death Discov.* **2017**, *3*, 17063. [CrossRef]
3. Lima, R.D.S.; Block, J.M. Coconut oil: What do we really know about it so far? *Food Qual. Saf.* **2019**, *3*, 61–72. [CrossRef]
4. Rothwell, N.J.; Stock, M.J. Stimulation of thermogenesis and brown fat activity in rats fed medium chain triglyceride. *Metabolism* **1987**, *36*, 128–130. [CrossRef]
5. Van Wymelbeke, V.; Louis-Sylvestre, J.; Fantino, M. Substrate oxidation and control of food intake in men after a fat-substitute meal compared with meals supplemented with an isoenergetic load of carbohydrate, long-chain triacylglycerols, or medium-chain triacylglycerols. *Am. J. Clin. Nutr.* **2001**, *74*, 620–630. [CrossRef]
6. Clegg, M.E. They say coconut oil can aid weight loss, but can it really? *Eur. J. Clin. Nutr.* **2017**, *71*, 1139–1143. [CrossRef]
7. Department of Health and Human Services and U.S. Department of Agriculture (HHS) and (USDA). *Dietary Guidelines for Americans*, 8th ed.; US Department of Health and Human Services: Washington, DC, USA, 2015. Available online: http://health.gov/dietaryguidelines/2015/guidelines/ (accessed on 13 May 2021).
8. Eckel, R.H.; Jakicic, J.M.; Ard, J.D.; de Jesus, J.M.; Houston Miller, N.; Hubbard, V.S.; Lee, I.M.; Lichtenstein, A.H.; Loria, C.M.; Millen, B.E.; et al. 2013 AHA/ACC guideline on lifestyle management to reduce cardiovascular risk: A report of the American College of Cardiology/American Heart Association Task Force on Practice Guidelines. *Circulation* **2014**, *129*, S76–S99. [CrossRef]
9. Kromhout, D.; Menotti, A.; Bloemberg, B.; Aravanis, C.; Blackburn, H.; Buzina, R.; Dontas, A.S.; Fidanza, F.; Giampaoli, S.; Jansen, A.; et al. Dietary saturated and trans fatty acids and cholesterol and 25-year mortality from coronary heart disease: The Seven Countries Study. *Prev. Med.* **1995**, *24*, 308–315. [CrossRef]
10. Billingsley, H.E.; Carbone, S.; Lavie, C.J. Dietary Fats and Chronic Noncommunicable Diseases. *Nutrients* **2018**, *10*, 1385. [CrossRef]
11. Wang, D.D.; Li, Y.; Chiuve, S.E.; Stampfer, M.J.; Manson, J.E.; Rimm, E.B.; Willett, W.C.; Hu, F.B. Association of Specific Dietary Fats With Total and Cause-Specific Mortality. *JAMA Intern. Med.* **2016**, *176*, 1134–1145. [CrossRef] [PubMed]
12. Gouaref, I.; Bouazza, A.; Abderrhmane, S.A.; Koceir, E.-A. Lipid Profile Modulates Cardiometabolic Risk Biomarkers Including Hypertension in People with Type-2 Diabetes: A Focus on Unbalanced Ratio of Plasma Polyunsaturated/Saturated Fatty Acids. *Molecules* **2020**, *25*, 4315. [CrossRef]
13. Brennan, S.F.; Woodside, J.V.; Lunny, P.M.; Cardwell, C.R.; Cantwell, M.M. Dietary fat and breast cancer mortality: A systematic review and meta-analysis. *Crit. Rev. Food Sci. Nutr.* **2017**, *57*, 1999–2008. [CrossRef] [PubMed]
14. Billingsley, H.E.; Hummel, S.L.; Carbone, S. The role of diet and nutrition in heart failure: A state-of-the-art narrative review. *Prog. Cardiovasc. Dis.* **2020**, *63*, 538–551. [CrossRef]
15. Siri-Tarino, P.W.; Sun, Q.; Hu, F.B.; Krauss, R.M. Meta-analysis of prospective cohort studies evaluating the association of saturated fat with cardiovascular disease. *Am. J. Clin. Nutr.* **2010**, *91*, 535–546. [CrossRef]
16. Unger, A.L.; Torres-Gonzalez, M.; Kraft, J. Dairy Fat Consumption and the Risk of Metabolic Syndrome: An Examination of the Saturated Fatty Acids in Dairy. *Nutrients* **2019**, *11*, 2200. [CrossRef] [PubMed]
17. Lepczyński, A.; Ożgo, M.; Michałek, K.; Dratwa-Chałupnik, A.; Grabowska, M.; Herosimczyk, A.; Liput, K.P.; Poławska, E.; Kram, A.; Pierzchała, M. Effects of Three-Month Feeding High Fat Diets with Different Fatty Acid Composition on Myocardial Proteome in Mice. *Nutrients* **2021**, *13*, 330. [CrossRef]
18. Pink, M.; Verma, N.; Rettenmeier, A.W.; Schmitz-Spanke, S. CBB staining protocol with higher sensitivity and mass spectrometric compatibility. *Electrophoresis* **2010**, *31*, 593–598. [CrossRef]

19. Dratwa-Chałupnik, A.; Lepczyński, A.; Ożgo, M.; Herosimczyk, A.; Michałek, K.; Niemcewicz, M.; Pałyszka, A.; Skrzypczak, W. Analysis of the efficiency of post-electrophoretic protein staining using Colloidal Coomassie Blue G-250. *Acta Sci. Pol. Zootechnica* **2015**, *14*, 67–76.
20. Szklarczyk, D.; Gable, A.L.; Lyon, D.; Junge, A.; Wyder, S.; Huerta-Cepas, J.; Simonovic, M.; Doncheva, N.T.; Morris, J.H.; Bork, P.; et al. STRING v11: Protein-protein association networks with increased coverage, supporting functional discovery in genome-wide experimental datasets. *Nucleic Acids Res.* **2019**, *47*, D607–D613. [CrossRef]
21. UniProt, C. UniProt: A worldwide hub of protein knowledge. *Nucleic Acids Res.* **2018**, *47*, D506–D515.
22. Ashburner, M.; Ball, C.A.; Blake, J.A.; Botstein, D.; Butler, H.; Cherry, J.M.; Davis, A.P.; Dolinski, K.; Dwight, S.S.; Eppig, J.T.; et al. Gene Ontology: Tool for the unification of biology. *Nat. Genet.* **2000**, *25*, 25–29. [CrossRef] [PubMed]
23. Carbon, S.; Douglass, E.; Dunn, N.; Good, B.; Harris, N.L.; Lewis, S.E.; Mungall, C.J.; Basu, S.; Chisholm, R.L.; Dodson, R.J.; et al. The Gene Ontology Resource: 20 years and still GOing strong. *Nucleic Acids Res.* **2018**, *47*, D330–D338.
24. Cheng, X.; Xiao, X.; Chou, K.-C. pLoc-mEuk: Predict subcellular localization of multi-label eukaryotic proteins by extracting the key GO information into general PseAAC. *Genomics* **2018**, *110*, 50–58. [CrossRef]
25. Gong, H.; Sun, L.; Chen, B.; Han, Y.; Pang, J.; Wu, W.; Qi, R.; Zhang, T.-M. Evaluation of candidate reference genes for RT-qPCR studies in three metabolism related tissues of mice after caloric restriction. *Sci. Rep.* **2016**, *6*, 38513. [CrossRef] [PubMed]
26. Hruz, T.; Wyss, M.; Docquier, M.; Pfaffl, M.W.; Masanetz, S.; Borghi, L.; Verbrugghe, P.; Kalaydjieva, L.; Bleuler, S.; Laule, O.; et al. RefGenes: Identification of reliable and condition specific reference genes for RT-qPCR data normalization. *BMC Genom.* **2011**, *12*, 156. [CrossRef]
27. Andersen, C.L.; Jensen, J.L.; Ørntoft, T.F. Normalization of Real-Time Quantitative Reverse Transcription-PCR Data: A Model-Based Variance Estimation Approach to Identify Genes Suited for Normalization, Applied to Bladder and Colon Cancer Data Sets. *Cancer Res.* **2004**, *64*, 5245. [CrossRef]
28. Ruijter, J.M.; Ramakers, C.; Hoogaars, W.M.H.; Karlen, Y.; Bakker, O.; van den Hoff, M.J.B.; Moorman, A.F.M. Amplification efficiency: Linking baseline and bias in the analysis of quantitative PCR data. *Nucleic Acids Res.* **2009**, *37*, e45. [CrossRef]
29. Pfaffl, M.W. A new mathematical model for relative quantification in real-time RT-PCR. *Nucleic Acids Res.* **2001**, *29*, e45. [CrossRef]
30. Tyburski, J.; Studzińska, A.; Daca, P.; Tretyn, A. PCR w czasie rzeczywistym. Metody analizy danych. *Biotechnologia* **2008**, *1*, 86–96.
31. Timmers, S.; de Vogel-van den Bosch, J.; de Wit, N.; Schaart, G.; van Beurden, D.; Hesselink, M.; van der Meer, R.; Schrauwen, P. Differential effects of saturated versus unsaturated dietary fatty acids on weight gain and myocellular lipid profiles in mice. *Nutr. Diabetes* **2011**, *1*, e11. [CrossRef]
32. Beulen, Y.; Martínez-González, M.A.; van de Rest, O.; Salas-Salvadó, J.; Sorlí, J.V.; Gómez-Gracia, E.; Fiol, M.; Estruch, R.; Santos-Lozano, J.M.; Schröder, H.; et al. Quality of Dietary Fat Intake and Body Weight and Obesity in a Mediterranean Population: Secondary Analyses within the PREDIMED Trial. *Nutrients* **2018**, *10*, 2011. [CrossRef] [PubMed]
33. Rosqvist, F.; Iggman, D.; Kullberg, J.; Cedernaes, J.; Johansson, H.E.; Larsson, A.; Johansson, L.; Ahlström, H.; Arner, P.; Dahlman, I.; et al. Overfeeding polyunsaturated and saturated fat causes distinct effects on liver and visceral fat accumulation in humans. *Diabetes* **2014**, *63*, 2356–2368. [CrossRef] [PubMed]
34. He, Y.; Yang, T.; Du, Y.; Qin, L.; Ma, F.; Wu, Z.; Ling, H.; Yang, L.; Wang, Z.; Zhou, Q.; et al. High fat diet significantly changed the global gene expression profile involved in hepatic drug metabolism and pharmacokinetic system in mice. *Nutr. Metab.* **2020**, *17*, 37. [CrossRef] [PubMed]
35. Li, Y.; Li, J.; Cao, P.; Liu, Y. Sinapine-enriched rapeseed oils reduced fatty liver formation in high-fat diet-fed C57BL/6J mice. *RSC Adv.* **2020**, *10*, 21248–21258. [CrossRef]
36. Kralova Lesna, I.; Suchanek, P.; Kovar, J.; Stavek, P.; Poledne, R. Replacement of dietary saturated FAs by PUFAs in diet and reverse cholesterol transport. *J. Lipid Res.* **2008**, *49*, 2414–2418. [CrossRef]
37. Gaundal, L.; Myhrstad, M.C.W.; Leder, L.; Byfuglien, M.G.; Gjøvaag, T.; Rud, I.; Retterstøl, K.; Holven, K.B.; Ulven, S.M.; Telle-Hansen, V.H. Beneficial effect on serum cholesterol levels, but not glycaemic regulation, after replacing SFA with PUFA for 3 d: A randomised crossover trial. *Br. J. Nutr.* **2021**, *125*, 915–925. [CrossRef]
38. Diniz, Y.S.A.; Cicogna, A.C.; Padovani, C.R.; Santana, L.S.; Faine, L.A.; Novelli, E.L.B. Diets rich in saturated and polyunsaturated fatty acids: Metabolic shifting and cardiac health. *Nutrition* **2004**, *20*, 230–234. [CrossRef]
39. Soltis, A.R.; Kennedy, N.J.; Xin, X.; Zhou, F.; Ficarro, S.B.; Yap, Y.S.; Matthews, B.J.; Lauffenburger, D.A.; White, F.M.; Marto, J.A.; et al. Hepatic Dysfunction Caused by Consumption of a High-Fat Diet. *Cell Rep.* **2017**, *21*, 3317–3328. [CrossRef]
40. Yoshimura, S.; Nakashima, S.; Tomiga, Y.; Kawakami, S.; Uehara, Y.; Higaki, Y. Short- and long-term effects of high-fat diet feeding and voluntary exercise on hepatic lipid metabolism in mice. *Biochem. Biophys. Res. Commun.* **2018**, *507*, 291–296. [CrossRef]
41. Wang, Y.-J.; Bian, Y.; Luo, J.; Lu, M.; Xiong, Y.; Guo, S.-Y.; Yin, H.-Y.; Lin, X.; Li, Q.; Chang, C.C.Y.; et al. Cholesterol and fatty acids regulate cysteine ubiquitylation of ACAT2 through competitive oxidation. *Nat. Cell Biol.* **2017**, *19*, 808–819. [CrossRef]
42. Temel, R.E.; Hou, L.; Rudel, L.L.; Shelness, G.S. ACAT2 stimulates cholesteryl ester secretion in apoB-containing lipoproteins. *J. Lipid Res.* **2007**, *48*, 1618–1627. [CrossRef]
43. Bell, T.A.; Kelley, K.; Wilson, M.D.; Sawyer, J.K.; Rudel, L.L. Dietary Fat–Induced Alterations in Atherosclerosis Are Abolished by ACAT2-Deficiency in ApoB100 Only, LDLr−/− Mice. *Arterioscler. Thromb. Vasc. Biol.* **2007**, *27*, 1396–1402. [CrossRef]

44. Guo, Y.; Darshi, M.; Ma, Y.; Perkins, G.A.; Shen, Z.; Haushalter, K.J.; Saito, R.; Chen, A.; Lee, Y.S.; Patel, H.H.; et al. Quantitative proteomic and functional analysis of liver mitochondria from high fat diet (HFD) diabetic mice. *Mol. Cell Proteom.* **2013**, *12*, 3744–3758. [CrossRef]
45. Schlune, A.; Riederer, A.; Mayatepek, E.; Ensenauer, R. Aspects of Newborn Screening in Isovaleric Acidemia. *Int. J. Neonatal Screen.* **2018**, *4*, 7. [CrossRef]
46. Solano, A.F.; Leipnitz, G.; De Bortoli, G.M.; Seminotti, B.; Amaral, A.U.; Fernandes, C.G.; Latini, A.S.; Dutra-Filho, C.S.; Wajner, M. Induction of oxidative stress by the metabolites accumulating in isovaleric acidemia in brain cortex of young rats. *Free Radic. Res.* **2008**, *42*, 707–715. [CrossRef]
47. Botham, K.M.; Avella, M.; Cantafora, A.; Bravo, E. The lipolysis of chylomicrons derived from different dietary fats by lipoprotein lipase in vitro. *Biochim. Biophys. Acta Lipids Lipid Metab.* **1997**, *1349*, 257–263. [CrossRef]
48. Ruan, X.; Li, Z.; Zhang, Y.; Yang, L.; Pan, Y.; Wang, Z.; Feng, G.-S.; Chen, Y. Apolipoprotein A-I possesses an anti-obesity effect associated with increase of energy expenditure and up-regulation of UCP1 in brown fat. *J. Cell Mol. Med.* **2011**, *15*, 763–772. [CrossRef]
49. Wei, H.; Averill, M.M.; McMillen, T.S.; Dastvan, F.; Mitra, P.; Subramanian, S.; Tang, C.; Chait, A.; LeBoeuf, R.C. Modulation of adipose tissue lipolysis and body weight by high-density lipoproteins in mice. *Nutr. Diabetes* **2014**, *4*, e108. [CrossRef]
50. Han, R.; Lai, R.; Ding, Q.; Wang, Z.; Luo, X.; Zhang, Y.; Cui, G.; He, J.; Liu, W.; Chen, Y. Apolipoprotein A-I stimulates AMP-activated protein kinase and improves glucose metabolism. *Diabetologia* **2007**, *50*, 1960–1968. [CrossRef]
51. Lian, J.; Wei, E.; Groenendyk, J.; Das, S.K.; Hermansson, M.; Li, L.; Watts, R.; Thiesen, A.; Oudit, G.Y.; Michalak, M.; et al. Ces3/TGH Deficiency Attenuates Steatohepatitis. *Sci. Rep.* **2016**, *6*, 25747. [CrossRef]
52. Lian, J.; Wei, E.; Wang, S.P.; Quiroga, A.D.; Li, L.; Di Pardo, A.; van der Veen, J.; Sipione, S.; Mitchell, G.A.; Lehner, R. Liver specific inactivation of carboxylesterase 3/triacylglycerol hydrolase decreases blood lipids without causing severe steatosis in mice. *Hepatology* **2012**, *56*, 2154–2162. [CrossRef] [PubMed]
53. Gonzalez, J.T.; Betts, J.A. Dietary sugars, exercise and hepatic carbohydrate metabolism. *Proc. Nutr. Soc.* **2018**, *78*, 246–256. [CrossRef]
54. Softic, S.; Gupta, M.K.; Wang, G.-X.; Fujisaka, S.; O'Neill, B.T.; Rao, T.N.; Willoughby, J.; Harbison, C.; Fitzgerald, K.; Ilkayeva, O.; et al. Divergent effects of glucose and fructose on hepatic lipogenesis and insulin signaling. *J. Clin. Investig.* **2017**, *127*, 4059–4074. [CrossRef]
55. Kumashiro, N.; Beddow, S.A.; Vatner, D.F.; Majumdar, S.K.; Cantley, J.L.; Guebre-Egziabher, F.; Fat, I.; Guigni, B.; Jurczak, M.J.; Birkenfeld, A.L.; et al. Targeting pyruvate carboxylase reduces gluconeogenesis and adiposity and improves insulin resistance. *Diabetes* **2013**, *62*, 2183–2194. [CrossRef] [PubMed]
56. Cai, D.; Yuan, M.; Liu, H.; Han, Z.; Pan, S.; Yang, Y.; Zhao, R. Epigenetic and SP1-mediated regulation is involved in the repression of galactokinase 1 gene in the liver of neonatal piglets born to betaine-supplemented sows. *Eur. J. Nutr.* **2017**, *56*, 1899–1909. [CrossRef]
57. Coelho, A.I.; Berry, G.T.; Rubio-Gozalbo, M.E. Galactose metabolism and health. *Curr. Opin. Clin. Nutr. Metab. Care* **2015**, *18*, 422–427. [CrossRef]
58. Ramani, P.; Arya, K. Galactokinase Deficiency. StatPearls [Internet]. Treasure Island (FL): StatPearls Publishing. Available online: https://www.ncbi.nlm.nih.gov/books/NBK560683/ (accessed on 13 May 2021).
59. Bashir, S.; Sharma, Y.; Jairajpuri, D.; Rashid, F.; Nematullah, M.; Khan, F. Alteration of adipose tissue immune cell milieu towards the suppression of inflammation in high fat diet fed mice by flaxseed oil supplementation. *PLoS ONE* **2019**, *14*, e0223070. [CrossRef]
60. Ito, T.; Kubo, M.; Nagaoka, K.; Funakubo, N.; Setiawan, H.; Takemoto, K.; Eguchi, E.; Fujikura, Y.; Ogino, K. Early obesity leads to increases in hepatic arginase I and related systemic changes in nitric oxide and l-arginine metabolism in mice. *J. Physiol. Biochem.* **2018**, *74*, 9–16. [CrossRef]
61. Johnson, F.K.; Peyton, K.J.; Liu, X.-M.; Azam, M.A.; Shebib, A.R.; Johnson, R.A.; Durante, W. Arginase promotes endothelial dysfunction and hypertension in obese rats. *Obesity* **2015**, *23*, 383–390. [CrossRef]
62. Erdely, A.; Kepka-Lenhart, D.; Salmen-Muniz, R.; Chapman, R.; Hulderman, T.; Kashon, M.; Simeonova, P.P.; Morris, S.M., Jr. Arginase activities and global arginine bioavailability in wild-type and ApoE-deficient mice: Responses to high fat and high cholesterol diets. *PLoS ONE* **2010**, *5*, e15253. [CrossRef]
63. Romero, M.J.; Platt, D.H.; Tawfik, H.E.; Labazi, M.; El-Remessy, A.B.; Bartoli, M.; Caldwell, R.B.; Caldwell, R.W. Diabetes-induced coronary vascular dysfunction involves increased arginase activity. *Circ. Res.* **2008**, *102*, 95–102. [CrossRef]
64. Chung, J.H.; Moon, J.; Lee, Y.S.; Chung, H.-K.; Lee, S.-M.; Shin, M.-J. Arginase inhibition restores endothelial function in diet-induced obesity. *Biochem. Biophys. Res. Commun.* **2014**, *451*, 179–183. [CrossRef]
65. Moon, J.; Do, H.J.; Cho, Y.; Shin, M.-J. Arginase inhibition ameliorates hepatic metabolic abnormalities in obese mice. *PLoS ONE* **2014**, *9*, e103048. [CrossRef]
66. Ahmed, A.A.; Balogun, K.A.; Bykova, N.V.; Cheema, S.K. Novel regulatory roles of omega-3 fatty acids in metabolic pathways: A proteomics approach. *Nutr. Metab.* **2014**, *11*, 6. [CrossRef]
67. Luo, M.; Mengos, A.E.; Stubblefield, T.M.; Mandarino, L.J. High fat diet-induced changes in hepatic protein abundance in mice. *J. Proteom. Bioinform.* **2012**, *5*, 60–66. [CrossRef]

68. Ventura, G.; De Bandt, J.-P.; Segaud, F.; Perret, C.; Robic, D.; Levillain, O.; Le Plenier, S.; Godard, C.; Cynober, L.; Moinard, C. Overexpression of ornithine aminotransferase: Consequences on amino acid homeostasis. *Br. J. Nutr.* **2008**, *101*, 843–851. [CrossRef]
69. Rakhshandehroo, M.; Knoch, B.; Müller, M.; Kersten, S. Peroxisome Proliferator-Activated Receptor Alpha Target Genes. *PPAR Res.* **2010**, *2010*, 612089. [CrossRef]
70. Zúñiga, J.; Cancino, M.; Medina, F.; Varela, P.; Vargas, R.; Tapia, G.; Videla, L.A.; Fernández, V. N-3 PUFA supplementation triggers PPAR-α activation and PPAR-α/NF-κB interaction: Anti-inflammatory implications in liver ischemia-reperfusion injury. *PLoS ONE* **2011**, *6*, e28502. [CrossRef]
71. Zigmond, E.; Ben Ya'acov, A.; Lee, H.; Lichtenstein, Y.; Shalev, Z.; Smith, Y.; Zolotarov, L.; Ziv, E.; Kalman, R.; Le, H.V.; et al. Suppression of Hepatocellular Carcinoma by Inhibition of Overexpressed Ornithine Aminotransferase. *ACS Med. Chem. Lett.* **2015**, *6*, 840–844. [CrossRef]
72. Méndez, L.; Ciordia, S.; Fernández, M.S.; Juárez, S.; Ramos, A.; Pazos, M.; Gallardo, J.M.; Torres, J.L.; Nogués, M.R.; Medina, I. Changes in liver proteins of rats fed standard and high-fat and sucrose diets induced by fish omega-3 PUFAs and their combination with grape polyphenols according to quantitative proteomics. *J. Nutr. Biochem.* **2017**, *41*, 84–97. [CrossRef]
73. Ciapaite, J.; van den Broek, N.M.; te Brinke, H.; Nicolay, K.; Jeneson, J.A.; Houten, S.M.; Prompers, J.J. Differential effects of short- and long-term high-fat diet feeding on hepatic fatty acid metabolism in rats. *Biochim. Biophys. Acta Mol. Cell Biol. Lipids.* **2011**, *1811*, 441–451. [CrossRef]
74. Su, L.-J.; Zhang, J.-H.; Gomez, H.; Murugan, R.; Hong, X.; Xu, D.; Jiang, F.; Peng, Z.-Y. Reactive Oxygen Species-Induced Lipid Peroxidation in Apoptosis, Autophagy, and Ferroptosis. *Oxid. Med. Cell Longev.* **2019**, *2019*, 5080843. [CrossRef]
75. Fisher, A.B. Peroxiredoxin 6: A bifunctional enzyme with glutathione peroxidase and phospholipase A_2 activities. *Antioxid. Redox Signal.* **2011**, *15*, 831–844. [CrossRef]
76. Arriga, R.; Pacifici, F.; Capuani, B.; Coppola, A.; Orlandi, A.; Scioli, M.G.; Pastore, D.; Andreadi, A.; Sbraccia, P.; Tesauro, M.; et al. Peroxiredoxin 6 Is a Key Antioxidant Enzyme in Modulating the Link between Glycemic and Lipogenic Metabolism. *Oxid. Med. Cell Longev.* **2019**, *2019*, 9685607. [CrossRef] [PubMed]
77. Tu, Q.; Xiong, Y.; Fan, L.; Qiao, B.; Xia, Z.; Hu, L.; Wang, Y.; Peng, G.; Ye, Q. Peroxiredoxin 6 attenuates ischemia- and hypoxia-induced liver damage of brain-dead donors. *Mol. Med. Rep.* **2016**, *13*, 753–761. [CrossRef]
78. Lee, D.H.; Jung, Y.Y.; Park, M.H.; Jo, M.R.; Han, S.B.; Yoon, D.Y.; Roh, Y.S.; Hong, J.T. Peroxiredoxin 6 Confers Protection Against Nonalcoholic Fatty Liver Disease Through Maintaining Mitochondrial Function. *Antioxid. Redox Signal.* **2019**, *31*, 387–402. [CrossRef]
79. Voos, W.; Röttgers, K. Molecular chaperones as essential mediators of mitochondrial biogenesis. *Biochim. Biophys. Acta Mol. Cell Res.* **2002**, *1592*, 51–62. [CrossRef]
80. Renner, S.W.; Walker, L.M.; Forsberg, L.J.; Sexton, J.Z.; Brenman, J.E. Carbonic anhydrase III (Car3) is not required for fatty acid synthesis and does not protect against high-fat diet induced obesity in mice. *PLoS ONE* **2017**, *12*, e0176502. [CrossRef]
81. Zimmerman, U.-J.P.; Wang, P.; Zhang, X.; Bogdanovich, S.; Forster, R.E. Anti-Oxidative Response of Carbonic Anhydrase III in Skeletal Muscle. *IUBMB Life* **2004**, *56*, 343–347.
82. Malcolm, T.; Aroor, A.; Bivin, W.; Sowers, J.; Woodman, R.; Lockette, W. Carbonic anhydrase mediates hepatic steatosis and vascular stiffness induced by a Western diet. *FASEB J. Off. Publ. Fed. of Am. Soc. Exp. Biol.* **2016**, *30*, 956.958.
83. Xia, L.; Liu, Y.; Zhang, S.; Yang, Y.; Zhou, Z.; Tu, J. Can Prohibitin 1 be a Safeguard against liver disease? *Ann. Hepatol.* **2019**, *18*, 790–795. [CrossRef]
84. Peng, Y.-T.; Chen, P.; Ouyang, R.-Y.; Song, L. Multifaceted role of prohibitin in cell survival and apoptosis. *Apoptosis* **2015**, *20*, 1135–1149. [CrossRef] [PubMed]
85. Ko, K.S.; Tomasi, M.L.; Iglesias-Ara, A.; French, B.A.; French, S.W.; Ramani, K.; Lozano, J.J.; Oh, P.; He, L.; Stiles, B.L.; et al. Liver-specific deletion of prohibitin 1 results in spontaneous liver injury, fibrosis, and hepatocellular carcinoma in mice. *Hepatology* **2010**, *52*, 2096–2108. [CrossRef] [PubMed]
86. Yamaguchi, M. The role of regucalcin in nuclear regulation of regenerating liver. *Biochem. Biophys. Res. Commun.* **2000**, *276*, 1–6. [CrossRef] [PubMed]
87. Yamaguchi, M. Regucalcin, a novel regulatory protein implicated in obesity and diabetes. *Integr. Mol. Med.* **2014**, *1*, 7–10. [CrossRef]
88. Yamaguchi, M.; Tsurusaki, Y.; Misawa, H.; Inagaki, S.; Ma, Z.J.; Takahashi, H. Potential role of regucalcin as a specific biochemical marker of chronic liver injury with carbon tetrachloride administration in rats. *Mol. Cell Biochem.* **2002**, *241*, 61–67. [CrossRef]
89. Kucukoglu, O.; Guldiken, N.; Chen, Y.; Usachov, V.; El-Heliebi, A.; Haybaeck, J.; Denk, H.; Trautwein, C.; Strnad, P. High-fat diet triggers Mallory-Denk body formation through misfolding and crosslinking of excess keratin 8. *Hepatology* **2014**, *60*, 169–178. [CrossRef] [PubMed]
90. Singla, A.; Moons, D.S.; Snider, N.T.; Wagenmaker, E.R.; Jayasundera, V.B.; Omary, M.B. Oxidative stress, Nrf2 and keratin up-regulation associate with Mallory-Denk body formation in mouse erythropoietic protoporphyria. *Hepatology* **2012**, *56*, 322–331. [CrossRef]
91. Guldiken, N.; Usachov, V.; Levada, K.; Trautwein, C.; Ziol, M.; Nahon, P.; Strnad, P. Keratins 8 and 18 are type II acute-phase responsive genes overexpressed in human liver disease. *Liver Int.* **2015**, *35*, 1203–1212. [CrossRef]

92. Harada, M.; Strnad, P.; Resurreccion, E.Z.; Ku, N.-O.; Omary, M.B. Keratin 18 overexpression but not phosphorylation or filament organization blocks mouse Mallory body formation. *Hepatology* **2007**, *45*, 88–96. [CrossRef]
93. Bettermann, K.; Mehta, A.K.; Hofer, E.M.; Wohlrab, C.; Golob-Schwarzl, N.; Svendova, V.; Schimek, M.G.; Stumptner, C.; Thüringer, A.; Speicher, M.R.; et al. Keratin 18-deficiency results in steatohepatitis and liver tumors in old mice: A model of steatohepatitis-associated liver carcinogenesis. *Oncotarget* **2016**, *7*, 73309–73322. [CrossRef] [PubMed]
94. Wolf, J.H.; Bhatti, T.R.; Fouraschen, S.; Chakravorty, S.; Wang, L.; Kurian, S.; Salomon, D.; Olthoff, K.M.; Hancock, W.W.; Levine, M.H. Heat shock protein 70 is required for optimal liver regeneration after partial hepatectomy in mice. *Liver Transpl.* **2014**, *20*, 376–385. [CrossRef] [PubMed]
95. Bondia-Pons, I.; Boqué, N.; Paternain, L.; Santamaría, E.; Fernández, J.; Campión, J.; Milagro, F.; Corrales, F.; Martínez, J.A. Liver proteome changes induced by a short-term high-fat sucrose diet in wistar rats. *J. Nutrigenet Nutrigenomics* **2011**, *4*, 344–353. [CrossRef]
96. Maio, N.; Rouault, T.A. Outlining the Complex Pathway of Mammalian Fe-S Cluster Biogenesis. *Trends Biochem. Sci.* **2020**, *45*, 411–426. [CrossRef] [PubMed]
97. Kang, Q.; Zou, H.; Yang, X.; Cai, J.-B.; Liu, L.-X.; Xie, N.; Wang, L.-M.; Li, Y.-H.; Zhang, X.-W. Characterization and prognostic significance of mortalin, Bcl-2 and Bax in intrahepatic cholangiocarcinoma. *Oncol. Lett.* **2018**, *15*, 2161–2168. [CrossRef]
98. Yi, X.; Luk, J.M.; Lee, N.P.; Peng, J.; Leng, X.; Guan, X.-Y.; Lau, G.K.; Beretta, L.; Fan, S.-T. Association of Mortalin (HSPA9) with Liver Cancer Metastasis and Prediction for Early Tumor Recurrence. *Mol. Cell Proteomics* **2008**, *7*, 315–325. [CrossRef]

MDPI
St. Alban-Anlage 66
4052 Basel
Switzerland
Tel. +41 61 683 77 34
Fax +41 61 302 89 18
www.mdpi.com

Nutrients Editorial Office
E-mail: nutrients@mdpi.com
www.mdpi.com/journal/nutrients

MDPI
St. Alban-Anlage 66
4052 Basel
Switzerland

Tel: +41 61 683 77 34

www.mdpi.com

ISBN 978-3-0365-5304-7